INTER

International Network on Timber Engineering Research

INTER - International Network on Timber Engineering Research

2014 the International Network on Timber Engineering Research (INTER) was founded.

Scope

Presentation, discussion and documentation of research results in timber engineering and development of application rules for timber design codes or standards related to timber engineering.

Approach

Annual meetings in different countries/places hosted by meeting participants

Presentation and discussion of papers

Peer review of the abstracts before the meeting and of the papers during the meeting

Decision of the acceptance of the abstracts before the meeting by a well-defined review process

Decision of the acceptance of the papers for the proceedings during the meeting

Publication of the papers and the discussion in proceedings

Rules

All decisions including the appointment of the chairperson or the location of annual meetings are made by the participants attending a meeting.

Membership

Persons contributing to or being interested in research related to timber engineering.

INTER PROCEEDINGS MEETING FIFTY-TWO 2019

MEETING FIFTY-TWO

TACOMA WA, USA

AUGUST 2019

INTER

International Network on Timber Engineering Research

Proceedings

Meeting 52

26 - 29 August 2019

Tacoma WA, USA

Edited by Rainer Görlacher

Table of Contents

1   List of participants

AUSTRIA
M Augustin   holz.bau forschungs gmbh
R Brandner   Graz University of Technology
K Bratulic   Holz.bau forschungs gmbh
A Ringhofer   Graz University of Technology

BELGIUM
D Sonck   BuildSoft, Merelbeke

CANADA
Y H Chui   University of Alberta
H Daneshvar   University of Alberta
L Epp   StructureCraft Builders
F Lam   University of British Columbia, Vancouver
H Mpidi Bita   Katerra
Md Shahnewaz   UNBC Prince George
B Sullivan   StructureCraft Builders
T Tannert   UNBC Prince George
L Zhou   University of Victoria

CHINA
X Sun   Tongji University
H Dong   Tongji University
J Luo   Tongji University
X Wang   Tongji University
H Xiong   Tongji University

CROATIA
J Barbalic   University of Zagreb

ESTONIA
A Just   Tallinn University of Technology
K N Mäger   Tallinn University of Technology

GERMANY
S Aicher   MPA University Stuttgart
H J Blaß   Karlsruhe Institute of Technology (KIT)
P Dietsch   Technical University of Munich
M Frese   Karlsruhe Institute of Technology (KIT)
R Görlacher   Karlsruhe Institute of Technology (KIT)
U Kuhlmann   University fo Stuttgart
K-U Schober   Mainz University of App. Sc.
M Westermayr   Technical University of Munich
S Winter   Technical University of Munich

JAPAN
K Kobayashi   Shizuoka University
T Nagashima   Sumitomo Forestry CO.,LTD., Tsukuba
K Tachibana   Sumitomo forestry Co., Ltd., Tsukuba
T Tsuchimoto   Building Research Institute, Tsukuba

NEW ZEALAND
J Brown   University of Canterbury
M Li   University of Canterbury
P Quenneville   The University of Auckland

SPAIN
J M Cabrero   Universidad de Navarra, Pamplona
M Yurrita   Universidad de Navarra, Pamplona

SWEDEN
R Atashipour   Chalmers University of Technology
H Danielsson   Lund University
K Forsman   Lund University
R Jockwer   Chalmers Technical University
M Schweigler   Linnaeus University
E Serrano   Lund University

SWITZERLAND
T Ehrhart   ETH Zurich
R Fahrni   ETH Zurich

A Frangi   ETH Zurich
S Franke   Berner Fachhochschule, Biel
K Mueller   ETH Zurich
P Palma   EMPA
K Voulpiotis   ETH Zurich

TURKEY
A Ceccotti   Bogazici University, Istanbul

USA
H-E Blomgren   Katerra
S Breneman   WoodWorks - Wood Products Council
A Busch   Colorado School of Mines
J Chen   APA - The Engineered Wood Association, Tacoma
J Dolan   Washington State University
E Elias   APA - The Engineered Wood Association, Tacoma
T Lim   Mississippi State University
E McDonnell   Holmes Structures
G Montgomery   Swinerton Builders
A Sinha   Oregon State University
M Stoner   Swinerton Builders
B Yeh   APA - The Engineered Wood Association, Tacoma

2   Minutes of the Meeting

by F Lam, Canada

CHAIRMAN'S INTRODUCTION

Dr. P Dietsch welcomed the delegates to the 6th International Network of Timber Engineering Research (INTER) which constitutes the 52nd meeting of the group including the series of former CIB-W18 meetings. INTER continues our tradition of yearly meetings to discuss research results related to timber structures with the aim of transferring them into practical applications. P Dietsch offered his appreciation for the significant contribution of the past Chair H Blass towards the goals of CIB W18 and INTER. H Blass Chairmanship was marked by clarity and structure, motivating critical thinking and questioning in the search for quality and validity within an open and friendly atmosphere. P Dietsch also thanked F Lam and R Görlacher for their long-time services to CIB-W18 and INTER and for agreeing to continue their roles in recording of the meeting discussions and preparation of the proceedings, respectively.

The Chair thanked BJ Yeh and his team from APA Engineered Wood Association for hosting this meeting.

This meeting also constitutes the 3rd meeting in the USA, after a meeting in Athens/Georgia in 1993 and a meeting in Colorado in 2003.

There were 68 delegates from 15 countries participating in this meeting with 10 delegates from USA. Twenty-seven papers were accepted for this meeting with 55 submitted abstracts. The papers were selected based on a review process for the abstracts with 4 acceptance criteria (state of the art, originality, assumed content, and relation to standards or codes). 19 long-time members of INTER had served as reviewers, each abstract was reviewed by at least 7 reviewers. The Chair thanked all reviewers for their service to INTER and all authors for their interest in presenting their results at INTER.

Papers to be presented at INTER shall be submitted at least one month before the meeting to enable all participants to read the papers beforehand. Therefore papers brought directly to the meeting were not accepted for presentation, discussions, or publication. Same rule applied to papers where none of the authors was present or papers which were not defended by one of the authors. In the second case, a onetime exception was made as the first author of Paper 52-12-6 had to cancel his participation, hence the paper would be presented by A Busch.

The presentations were limited to 20 minutes each, allowing time for meaningful discussions after each presentation. The Chair asked the presenters to conclude the presentation with a general proposal or statements concerning impact of the

research results on existing or future potential applications and development in codes and standards.

The topics covered in this meeting were: Timber joints and fasteners (11), Duration of load (1), Laminated members (6), Structural stability (3), Fire (2), Glued Joints (1), Robustness (3). Numbers in parentheses are the number of papers presented in each topic based on initial allocation.

The Chair invited all authors to amend their papers according to the comments and recommendations received during the discussion. The proceedings will be produced by R Görlacher. Finalized papers must be sent to R Görlacher until end of September.

The participants could present notes towards the end of the technical session. R Görlacher brought a list of intended note presentations. Participants intending to present notes that were not on the list would need to notify R Görlacher accordingly. The presentation of notes is limited to 10 minutes, no discussion of notes is foreseen.

An address list of the participants was circulated for verification of accuracy.

E Elias, President of APA Engineered Wood Association, gave a welcoming address. BJ Yeh welcomed the participants and made housekeeping announcements.

INFORMATION FROM OTHER ORGANISATIONS

The Chair recalled the main objective of INTER which is to discuss research results related to timber structures with the aim of transferring them into practical applications, meaning codes and standards. INTER is an independent body with strong links to standardization, hence the Chair welcomed all delegates that also represent standardization committees and the Chairmen of ISO TC165, YH Chui and CEN/TC 250/SC 5, S Winter.

ISO TC165 Timber structures: YH Chui presented information on the background of TC165 and their activities.

CEN/TC 250/SC 5 Design of timber structures: S Winter provided background and updates on SC5 activities. S Winter also mentioned the possibility to share, present and discuss at INTER the final drafts developed by the six Project Teams. P Dietsch added that the work of SC5 towards harmonization of standards is important and is appreciated. P Dietsch also mentioned the background documents for the next generation of EC5 that were developed within COST Action FP1402 (www.costfp1402.tum.de) and COST FP1404 (https://costfp1404.ethz.ch).

TIMBER JOINTS AND FASTENERS

52 - 7 - 1   Product Characteristics of Self-Tapping Timber Screws - A Ringhofer,
                   G Schickhofer

Presented by A Ringhofer

P Quenneville asked how many cycles can the screws sustain before breakage. A Ringhofer responded that this would depend on the load level and their experience is that the number of cycles before failure is not that high. More work will be done in this area.

D Dolan commented that one might want to put these screws in situations where they are designed not to take cyclic loads. A Ringhofer agreed and said that there are cases where for example fatigue and corrosion effects are important.

R Jockwer commented that the distribution of properties along screw length might be an issue. A Ringhofer and H Blass agreed on this point based on their experience on screw performance.

YH Chui asked about the actual aim of the research. A Ringhofer said that the theoretical approach was intended for quality control and guidance for product development.

A Frangi stated that he was not concerned about difference between different products but more concerned with differences within a product.

H Daneshvar discussed his experience regarding the importance of screw behavior during cyclic tests. H Blass commented that these screws can be used in seismic situation especially if they are designed to behave elastically with appropriate q values.

U Kuhlmann asked and received clarification that the definition of ductility was based on ASTM approach.

D Dolan discussed fatigue versus seismic response in terms of energy dissipated by the connector in earthquakes.

P Dietsch and A Ringhofer discussed why the mechanical model assumed the screws thread would be activated completely and uniformly under axial loads.

R Jockwer commented that it would make sense for designers to use capacity rather than strength.

T Tannert commented that CSA O86 requires knowledge of 95th percentile for capacity design in seismic situation. A Ringhofer responded that this can be obtained based on COV information and there seemed to be no real difference amongst producers.

M Li commented about the verification of results where good match can be obtained based on average values but this may not be achievable based on the tails.

52 - 7 - 2   Withdrawal Strength of Screws and Screw Groups in European Beech (Fagus s.) Parallel to the Grain - M Westermayr, J W G van de Kuilen

Presented by M Westermayr

A Frangi asked whether you would get the same results from pull-push compared to pull-pull tests. M Westermayr agreed that pull-pull test results might be lower than pull-push tests. R Brandner said that results from TU Graz indicated that there was no difference in strength but there was a difference in the measured stiffness.

H Blass questioned whether one could get the same increase without considering unbonded length but just increase the inserted length of the screws. M Westermayr agreed but stated that the unbonded length consideration prevented splitting at the free surface and was the intention of this part of the investigation. R Brandner mentioned that even with unbonded length one would get splitting.

S Franke found similar influence when dealing with glued-in rods and asked whether they tried different unbonded lengths. M Westermayr said no only 50 mm was used successfully.

J Brown asked about the influence of unbonded length on post peak behavior and if an analytical model will be considered. M Westermayr said that this aspect has not been studied.

R Jockwer asked whether the consideration of unbonded length could lead to reduced fastener spacing. M Westermayr said that for practical purposes the spacing used in the study is already very small.

BJ Yeh received clarification that the use of unbonded length was not intended for natural checking.

A Ringhofer and M Westermayr discussed shear analogy issues, the shear area of the 8 mm diameter screws in comparison with the shear area of the parallel to grain shear tests and uniformity of the distribution of shear stresses along the length of the members.

52 - 7 - 3   Density Variations in Beech LVL - Influence on Insertion Moment and Withdrawal Capacity of Screws - M Frese

Presented by M Frese

F Lam asked whether the difference in the observed withdrawal capacities between face and edge applications would be due to differences in density only. M Frese responded that there could be other effects but density effects were important. Natural material such as timber would also have issues with density variation from knots. M Frese also stated different approach could be used to consider different material.

R Brandner asked what about the different approach. M Frese stated that mean value of the insertion moment could be considered. R Brandner said that such approach is already in use. M Frese said maximum values could also be considered when more data is available. R Brandner said that higher quantile would be more appropriate than maximum values.

S Franke asked about overlapping of veneer in production process that could increase the density. M Frese agreed but overlaps did not occur frequently and he did not specifically test their influence.

S Aicher questioned the large increase in torsional moment for depth greater than 80 mm. M Frese stated that after this depth rough thread would start to penetrate the wood causing the increase.

YH Chui commented that based on density one would expect 10% increase but the results indicated 20% increase. M Frese said that there are contributions from the glue also.

52 - 7 - 4   Steel Dowel Connections in Beech Hardwood - S Franke, B Franke

Presented by S Franke

S Winter asked why a_{3t} was chosen smaller than a_1 and received clarification that increasing a_1 or a_2 can also lead to higher ductility.

S Winter questioned why the proposed factor of 1.2 in mode 3 only applied for hardwood and not softwood. S Franke said this could also be applied if one was sure of the rope effect of the dowel.

H Blass commented that you are proposing the rope effect in mode 3 and asked would you also propose rope effect for the plastic hinge forming in the outside steel plate. He also questioned about how to design for the full shear capacity of the fastener. S Franke said that more work needed to be done.

JM Cabrero received clarification that only 5 replicates were used and that comparison between reinforced and not reinforced cases was done only for the 5d case. Also load deformation data indicated mostly yielding failure mode.

R Jockwer questioned that $n_{ef}=n$ for mode 3 can be applied to other modes if minimum spacing and other conditions are met. He asked about the regression

coefficient as it is done for data showing two distinct groupings. S Franke agreed and said that the regression coefficient for individual groups would be much lower.

P Quenneville mentioned that the results for 7d are as good as the results for 9d because the tests were stopped at 15 mm displacement. P Quenneville also discussed whether one could see two wood-steel-wood connections where mode 1 might be approached. S Franke said that they all failed before 15 mm. The displacement shown in the load deformation curves includes machine movements and connection deformations.

U Kuhlmann asked about stiffness information and stated that they would be useful.

P Dietsch said that information to support the statements made in the conclusions is missing (e.g. how the connections were reinforced and illustration of the prSIA splitting model) and that this should be included for further clarification. S Franke will update the paper.

52 - 7 - 5   Effective Thickness of the Wood Member in a Timber-to-steel Connection with Large Diameter under Brittle Failure - M Yurrita, J M Cabrero

Presented by M Yurrita

P Quenneville commented that the proposal was well done to take care of the outliers in the NZ code.

R Jockwer questioned whether wood-steel-wood connections also saw brittle failure modes. H Blass commented that in timber to timber connections capacity is less compared to steel-timber connections hence less prone to brittle failures.

R Brandner commented that species would also make a difference and inclusion of mean values rather than median values would be useful.

52 - 7 - 6   Row Shear and Block Shear Failure of Connections with Axially Loaded Screws - H J Blass, M Flaig, N Meyer

Presented by H Blass

S Franke asked what rolling shear strength was used. H Blass responded 1 MPa per EN480.

S Franke stated that the paper assumed the screws all have the same forces and asked if this was fine. H Blass stated that this was an assumption that seemed to work fine.

B Sullivan asked about diagonal rows on block shear effect. H Blass said this is not with the scope of the study and will find out later.

JM Cabrero received definition of the outer perimeter and asked if one could use this as a parameter. H Blass explained that if tension failure perpendicular to grain occurred first this would lead to dynamic effect to row shear failure. T Tannert followed up and asked whether tension or row shear governed. H Blass said both would govern and confirmed that small specimens for rolling shear testing was used.

S Winter commented about rolling shear strength being 1.2 to 1.3 MPa.

S Aicher stated that from mechanics point of view inclusion of stiffness would be important. H Blass responded that this is still being discussed as the spring stiffness would be dependent on the geometrical arrangements of the screws and the parameters to establish spring stiffness are not clear.

R Brandner agreed that more discussion on this issue would be needed. He agreed that n_{ef} should not be used to consider brittle failure.

H Xiong and H Blass discussed the use of screws in tension perpendicular to grain applications.

P Quenneville asked what if stiffness of the shear spring were made much higher than the outer two springs. H Blass stated the actual failure plane seemed to be much larger than assumed. F Lam commented that the observed failure plane or failure area would be determined after the fact and might be much different from that at time of failure. H Blass agreed.

J Chen and H Blass discussed the expected capacity based on ETA and test results with the test results of screw groups being lower. There is a direct correlation between the characteristic values in ETA to test results of the screw group.

52 - 7 - 7   New Analytical Model for Brittle Failure in the Parallel-to-grain Direction of Timber Connections with Large Diameter Fasteners - M Yurrita, J M Cabrero

Presented by M Yurrita

M Li and M Yurrita discussed how to interpret the load capacity results where mix failure mode occurred with yielding happening first and then brittle failure.

H Blass asked for explanation of the motivation behind using tension strength parallel to grain in the ratio. M Yurrita responded that this was based on fitting process.

D Dolan stated this paper dealt with nice symmetrical connections and asked what would happen for unsymmetrical cases where for example one side steel plate

leading to rolling shear failure being dominate. M Yurrita responded that this was covered in a previous paper but did not have data.

P Dietsch stated that strength values would be needed in the model and asked how they were obtained.   M Yurrita stated that they used values in timber design codes and converted characteristic values to mean values.   S Winter asked if there was any real tested material properties. M Yurrita responded that yes in some cases there was real test data for material properties in other cases properties were taken from the code.

M Li asked if there was a capacity hierarchy between different timber failure modes in the test data. M Yurrita responded yes with a factor of ~ 0.8 to 0.9.

52 - 7 _ 8   Embedment Test Analysis and Data in the Context of Phenomenological Modeling for Dowelled Timber Joint Design - M Schweigler, T K Bader, J-F Bocquet, R Lemaître, C Sandhaas

Presented by M Schweigler

R Jockwer asked about fitting curves to reflect the high nonlinear behavior. M Schweigler responded that this approach is more practical for use in standards.

S Franke asked about the ½ hole tests with uniformly loaded dowel versus the model and discussed the difference between ½ hole and full hole tests with up to 30% difference. M Schweigler confirmed that all the data considered was based on full hole tests.

YH Chui commented that the poor correlation was surprising and asked whether they looked into the breaking up the data into individual groups for regression analysis. M Schweigler responded that this was done and there was no correlation.

M Li stated the one would expect significant bending in the fastener when loaded up to 15 mm. The ASTM recommended ½ hole test may be more realistic and suggested loading up to 1d rather than 15 mm. M Schweigler agreed.

JM Cabrero discussed where to put the reinforcement. M Schweigler responded that reinforcement was needed to get ductile failure mode. H Blass added that sometimes reinforcement would be needed especially in modified wood.

A Frangi asked whether one could work with this level of high variability.   M Schweigler responded that some of this variability came from how the testing was conducted and agreed that one would need to control the influencing parameters better to reduce the variability.

P Palma commented that embedment tests might not be the right way to do this and single fastener tests might be more appropriate.

S Winter asked if there is a proposal for EC test procedure TC 124 WG1. M Schweigler stated they are working on it.

P Quenneville stated if the quality of the dowel cannot be controlled on site, what would be the purpose of tracking this in tests. M Schweigler responded the collected information may lead to more on site quality control.

52 - 7 - 9   Beam-on-Foundation Modelling as an Alternative Design Method for Timber Joints with Dowel-Type Fasteners – Part 2: Modelling Techniques for Multiple Fastener Joint or Connection - R Lemaître, J-F Bocquet, M Schweigler, T K Bader

Presented by M Schweigler

JM Cabreo received confirmation that zero length springs were used and received clarification of the connection analogy.

R Jockwer and M Schweigler discussed the slenderness of the dowel and the stiffness definition of the dowels with different behaviour. They discussed the highly non-linear behaviour of nail connections and the distinction between nail versus large diameter dowels.

P Palma asked how brittle failure modes were accounted for. M Schweigler responded that this is for ductile failure mode. At least this method would allow the load distribution to be estimated which can then be used in the next step for brittle failure prediction.

M Li asked whether this method could capture the uneven distribution of loads between the dowels. M Schweigler stated that this method could do so as non-rigid link elements were used.

S Aicher commented that Figure 7 in the paper indicated EC5 seemed to be 2.5 times larger than the predictions and this is alarming.   M Schweigler responded that EC5 did not consider multiple dowel effects, e.g. n_{ef}. H Blass confirmed this and that EC5 has not been fully tested for such cases as extrapolation was used in EC5.

D Dolan received confirmation that shear lag effect was considered in the model.

52 - 7 - 10 Transmission of perpendicular to grain forces using self-tapping screws - P Dietsch, S Rodemeier, H J Blass

Presented by P Dietsch

A Frangi asked if deformations could be calculated and would this method be recommended for tall buildings. P Dietsch responded that deformation could be calculated with this method of reinforcement and this method could be used multi-storey buildings but should be critically analysed for tall timber buildings. A Frangi commented that 3 to 4 mm of deformation x 10 storeys might be too much.

T Tannert commented that only small number of replicates was used and asked if one would be confident to make code recommendations for only 10d overlap. P Dietsch stated that essentially screw failure was tested one could rely on longer screws which would then fail at the same buckling loads due to their high slenderness.

R Jockwer mentioned that this detail has already been used in practice. He mentioned that load transfer via the overlap zone and screw head load transfer would happen early. P Dietsch agreed and stated that this might be the reason why 10d is sufficient.

B Sullivan and H Blass discussed about using large diameter threaded rod and its practicality.

YH Chui asked for comments about plate size. P Dietsch responded plate size was not varied.

S Breneman asked about the use of this technique in CLT structures with local loads. H Blass stated a PTEC 2019 paper covers this aspect.

52 - 7 - 11 Component Method in Timber Construction – Experimental and Numerical Research - U Kuhlmann, J Gauss

Presented by U Kuhlmann

F Lam asked about the number of replicates. U Kuhlmann said in some cases two replicates were used.

S Winter asked why K_{ser} is so low. U Kuhlmann responded that this could be due to the differences between single fasteners and a group of fasteners S Winter received confirmation that the blue line in slide 23 was based on EC5 with 50% reduction of stiffness and that n_{ef} was not applied because of the reinforcement.

A Frangi commented on the 5d or 7d cases, mentioning that more spacing and less dowels would get better ductility in unreinforced cases. U Kuhlmann will look into this further.

A Frangi asked if both moment and shear were present and if one would consider using a shear key. U Kuhlmann responded that in the design of steel joints one would

reserve some of the connections for shear the rest for bending. U Kuhlmann will consider this in future.

JM Cabrero received confirmation that the brittle failures had 2 replicates and one had net section failure and the other case was splitting.

R Jockwer received clarification that the doubling of K_{ser}, allowed by EC5 for steel-timber connections, was not used, i.e. the stiffness from EC5 was actually ¼ not ½.

P Quenneville did not agree that the net tension failure was due to group effect. He agreed that EC5 overestimated the stiffness in multiple dowel case grossly. He asked if higher stiffness could be achieved by using inclined screws rather than dowels. U Kuhlmann agreed.

M Schweigler asked about the rotational springs and received clarification that they were uncoupled.

S Aicher stated that to get the spring stiffness you tested a joint with multiple fasteners and asked how many dowels in a joint to determine the spring stiffness. U Kuhlmann responded that in so called component method one already tested the component of interest. S Aicher questioned how could this method deal with cases with more dowels. U Kuhlmann responded that the number of dowels did not have much influence on stiffness as shown in slide 12 (Figure 3.2). S Aicher stated that size of the connection would have an influence. F Lam and U Kuhlmann further discussed whether slide 12 (Figure 3.2) showed a difference in stiffness between groups.

A Frangi received clarification that the rotational spring properties were determined by tests. He stated that glued in rods may have better stiffness characteristics.

P Quenneville commented that slide 12 (Figure 3.2) is a normalized graph so it did not show the stiffness difference well. He agreed with S Aicher that there would be a test configuration effect.

M Li received confirmation that both sides of the beam had similar bending stiffness.

DURATION OF LOAD

52 - 9 - 1   Duration of Load Effect on Axially-Loaded Self-Tapping Screws Inserted Parallel to Grain in Soft- and Hardwood - R Brandner, A Ringhofer, R Sieder

Presented by R Brandner

A Frangi commented that parallel to end grain application is allowed in Swiss code with strength adjustment factor since 30 years. R Brandner confirmed that groups of fasteners will be studied.

R Jockwer commented that moisture content might have an effect. R Brandner agreed and responded that DOL effect will be much higher with cyclical conditions.

H Blass stated that variable climate would lead to more severe load duration effects. He also questioned the influence on withdrawal capacity when fasteners were loaded in shear for rope effect.   R Brandner responded that this cannot be answered now. A Ringhofer stated that some of the results (Pirnbacher) had open climate conditions and moisture content did not seem to play a significant role. It would be useful to examine the open climate condition by itself.

T Tannert questioned if there would be more effect for groups of fasteners. R Brandner discussed that block shear failure would be expected in short term and change of failure mode might be experienced in long term.

S Winter questioned the starting point of the moisture in the specimens. R Brandner stated that the moisture did not change and provided clarification of DOL factors in EC5. S Winter and R Brandner discussed brittle failure would occur for variable climate and group of fasteners.

F Lam received clarification that the specimens were not predrilled.

YH Chui received clarification that there were 3 specimens loaded in series and when a failure occurred the failed specimen was replaced and the series was reloaded.

R Jockwer received clarification that perpendicular to grain results were only available in Pirnbacher's study.

S Aicher questioned the use of linear interpolation of data in slide 19 compared to the nonlinear case. One would get more significant load duration effect at longer time to failure and Foschi model might be more appropriate.   R Brandner explained the linearity of data around the regression line and large uncertainties existed at longer time to failure.

LAMINATED MEMBERS

52 - 12 - 1 Compressive Strength and Buckling Resistance of GLT Columns Made of European Beech - T Ehrhart, R Steiger, P Palma, E Gehri, A Frangi

Presented by T Ehrhart

H Blass stated that he has no preference of including eccentricity explicitly in buckling curves or just giving guidance that designers should consider eccentricity in design. T Ehrhart responded since we never have zero eccentricity, we should include some considerations in standard.

S Winter discussed second order analysis and mentioned that eccentricity of L/400 included geometric and structural imperfection. Also production process can lead to geometric imperfection. How to distinguish and include both is difficult. Furthermore EC5 is only an execution rule. In tests you need to measure the real deviations and then add the additional eccentricities. T Ehrhart responded that curvatures were measured and load application was the only way. 2/3 of the members had L/2000 deviation.

H Blass commented that in his work he did not have any structural eccentricity but the code considered eccentricity via simulations.

S Winter commented that proposal for a code would need buckling results from other buckling directions also. T Ehrhart said that this was done via simulations. S Winter said you would not be able to consider structural imperfections in simulations. A Frangi said that the code is allowing this level of eccentricity in production. H Blass said that this is only a limit but this limit is not observed in production. A Frangi felt that one should still consider this eccentricity level in simulations. P Dietsch said that changes of moisture content could also lead to additional eccentricity.

H Blass commented that in real structures you never have hinged supports; hence, there would be inherent safety.

M Westermayr added beech column tests were also conducted at TUM with consideration of both buckling directions and that they did not see an influence of buckling direction.

H Daneshvar commented that in practice we do not have columns but beam-columns. He questioned what type of failure modes were observed. T Ehrhart responded that at ultimate load compression failure were observed first.

52 - 12 - 2 Cross Laminated Timber at In-Plane Shear Loading – Comparison of Model Predictions - H Danielsson, E Serrano

Presented by H Danielsson

R Brandner commented that the Austrian code model is not the same as that considered in EC5 as there was an error in transfer of the model from Bogenspergers work.

A Frangi commented that this is important to EC5. One should be looking into the lastest draft of the Austrian code and the EC5 draft and check if the assumptions were correct.

P Dietsch asked if torsional strength can be included based on laminate thickness. H Danielsson responded that may be this is possible.

52 - 12 - 3 Net-section Tension and Shear Strength of In-plane Loaded CLT Panels -
     T Tannert, C Loss, M Popovski, H Mpidi Bita

Presented by T Tannert

F Lam stated that one should not add the capacity of individual failure mode together to estimate the total capacity of the connection. Although it seemed to work here, it is only fortuitous and cannot be generalized.   F Lam further commented that Weibull approach should be based on stressed volume integral and simple area ratio approach would only be valid for uniform stress cases. Also using Weibull approach with combinations of failure is tricky. T Tannert agreed.

BJ Yeh commented that fasteners have concentrated stress condition and volume effect may not be appropriate.

YH Chui agreed with F Lam's comments. Results of small scale test and large specimen test will be different.

H Blass commented that EC5 split ring design includes size effect considerations.

M Li asked about size effect for longitudinal shear and received confirmation that similar shape factors were used for all three strengths. Also f[MPa] are average values.

P Quenneville stated that the testing matrix is not large enough to have a reliable model and in reality there would be more complication with sharing of loads between loaded surfaces. T Tannert said that there were more data available and will try to include them in the revised paper. Also there is interest from designers to look at this type of hold-downs.

R Brandner stated that block shear tests do not represent real shear strengths. T Tannert said that based on past results there was agreements between ASTM block shear tests and EC5 approach. R Brandner said that this type of hold down is not new and there are existing information.

E Serrano agreed that Weibull theory would not work without considering stress distribution. K= Cov-1.085 is from statistics.

52 - 12 - 4 Prediction of Load-Bearing Capacity of Notched Cross Laminated Timber
     Plates - E Serrano, P J Gustafsson, H Danielsson

Presented by E Serrano

R Jockwer asked if clamping effect was included, would the capacity decrease. E Serrano responded that it could play a big role and should be considered in future.

M Li commented that FEM used cohesive element and crack propagation was considered at inclined angle. Would the model consider the crack propagation later along the glue line. E Serrano responded that this is done.

J Chen asked about the E/G ratio of 15.6 and Rs value of 2 MPa. E Serrano responded that the E/G ratio was referenced to a 1988 CIB W18 paper and it is an assumption with strength class data indicating a value of 16. E Serrano also said that Rs value was not important for fracture energy in tension perpendicular to grain.

S Winter said in EC5 the limit of Alpha is to 0.5 as larger notches are not right because it could lead to vibration and other issues; therefore, higher values for Alpha are not meaningful. S Winter suggests to limit at 0.5, setting a range for which the formula was applicable. E Serrano confirmed that the beam width is 100mm.

52 - 12 - 5 Compressive Strength and Stiffness of End Grain Contact Joints in Softwood Glulam and CLT - M Flaig, T Schmidt, H J Blaß

Presented by H Blass

P Quenneville received confirmation that the 20% reduction was due to wetting effects.   He wondered what would happen if further cuts were made. H Blass responded that the weak link is not location dependent.

S Winter received confirmation that the reduction values were provided for both the mean and characteristic values. Also recovery from drying was not considered as this deals with structural safety during construction.

R Brandner asked whether a flexible layer rather than a rigid steel plate was tried. H Blass said no this was not done.

A Frangi said he would expect even more damage in practice and that we are lucky that at even 40% reduction is no major issue since we do not have full design load during construction. H Blass said design for construction phase may be one consideration in design for Service Class 3.

R Jockwer said in Swiss standard there is a 20% reduction factor considered for timber to timber contact joint without steel plate.   A Frangi stated that this reduction in Switzerland is not for moisture content but for uneven contact surfaces.

YH Chui received confirmation that the specimens were tested wet without drying. H Blass also clarified that the specimens were rotated 180 degrees after cutting to make sure their end grains were different.

52 - 12 - 6 From Testing to Codification: Post-Tensioned Cross Laminated Timber
           Rocking Walls - S Pei, J D Dolan, R B Zimmerman, E McDonnel, A Busch,
           P Line, M Popovski

Presented by A Busch

A Frangi asked about design considerations for diaphragm and wall connection. D Dolan responded that special details were made to transfer only lateral forces and shear key was also made available to ensure compatibility.

F Lam received confirmation that 3 D shaking will be available.

M Li stated that 10 storey structures will be wind governed and asked how to achieve both the stiffness demand from wind and rocking motions in earthquake. R Zimmerman said that in a 6 storey situation seismic drift demand would govern. In US there is no code requirement for wind design for serviceability at this building height.

M Li asked about the connectivity between multiple panels along the building height. A Busch responded that rigid splines that are stronger than the wood would be used.

L Epp asked under 12 storeys there is no code requirements for wind loads in US but will the design guide consider wind design. R Zimmerman said that the design guide will only reference other standard.

J Brown asked about aspect ratio for walls and coupled walls.   R Zimmerman responded that there will be some limitations in the design guide for coupled walls, for example, modeling box types are not included. D Dolan said that the aspect ratio of walls will be governed by transportation.

P Quenneville asked what level of acceleration would be expected at the top level. R Zimmerman said no information yet.

T Tannert asked if only one rocking plane will be expected. A Busch responded yes. T Tannert asked if this design method goes into NDS only how would designers design this type of systems without ASCE7. A Busch responded that this is just the starting point and will aim to go into ASCE 7 down the road and it will be a long road.

A Ceccotti asked about the floor plan. D Dolan commented that there could be torsional issues. S Aicher agreed that torsional response might result as wall elements may have different stiffness. D Dolan agreed as ongoing 2 D testing will help guide this aspect of the program.

STRUCTURAL STABILITY

52 - 15 - 1 Seismic Performance of End Brace Connections in Ductile Braced Timber Frame - H Daneshvar, J Niederwestberg, C Dickof, J Spencer, J-P Letarte, Y H Chui

Presented by H Daneshvar

F Lam questioned whether shaping of the steel plate is a better option compared to a perforated plate. H Daneshvar agreed that it is possible. F Lam commented that this paper described only a proposed test program of a new connection system aiming to quantify Rd Ro factors for seismic design; the work is incomplete and not suitable for INTER. H Daneshvar responded that the experimental work was delayed. F Lam said that the FEM work is also incomplete as it deals with monotonic loading only and shows large difference to codes.

P Quenneville asked about the amount of deformation for these types of plates and how many cycles can the plates sustain. H Daneshavr responded 10 mm for 3 rows and will look into the number of cycles. P Quenneville asked about capacity design factor for these connectors. H Daneshavr responded this is not clear yet as there is no guideline. P Quenneville said it would depend on variability and should be >1.5.

A Frangi asked whether ductile timber frame can be combined with shear walls. H Daneshvar responded this is common in concrete systems. D Dolan disagreed and said that ASCE does not allow combining concrete shearwalls with ductile frames.

M Li asked why there is such a big difference in initial stiffness between model and code. H Daneshvar said that the design case is based on two points and the FEM should be more accurate. As material was assumed to be linear and perfectly plastic, real material properties input should be used.

T Tannert said that your work seems to aim to combine two lateral load resistance systems which necessitates to achieve the same ductility. H Daneshvar said that the work aims to study how these two systems can act together. T Tannert and H Daneshvar discussed the difference between mean fy values and the expect fy.

A Ceccotti received confirmation that the dowel diameter was 16 mm.

52 - 15 - 2 Lateral Resistance and Deflection of CLT Shear Walls - Md Shahnewaz, M Popovski, T Tannert

Presented by Md Shahnewaz

H Blass commented that if acoustic insulation layer was not considered in the research, there would be large difference in deformation with acoustic insulation layer considered. M Shahnewaz said the work was based on modeling and may be able to add this as part of the model in future.

BJ Yeh received confirmation that there were 19 wall tests results presented with a test result/equation prediction factor of 2. M Li asked if this information included corner walls. MD Shahnewaz said no and that in the model the corner wall was assumed rigid but this is not reality. T Tannert said there is no data with perpendicular walls and that they need data for confirmation.

M Li said that there is good agreement between model and test results for ultimate capacity of wall. He questioned if a wrong guess was made for the ultimate capacity of the hold-down component of the model. MD Shahnewaz responded that how you calculate ultimate capacity of the connection made the difference. Even if we had test data, they are not the same connections used.

D Dolan and MD Shahnewaz discussed the FBD of the connection in relation to the boundary conditions including the gravity load and the connectivity of the components. T Tannert said gravity load was ignored.

H Mpidi Bita asked about the combination of shear and rotation in the connection. MD Shahnewaz said interaction was ignored in model.

52 - 15 - 3   Development of Timber Buckling-Restrained Braces for Mass Timber Braced Frames - C Murphy, C P Pantelides, H-E Blomgren, D R Rammer

Presented by H-E Blomgren

D Dolan asked at this level of drift what would be the rotation requirement of the beam column. HE Blomgren agreed that there would be a need to get commercially available systems and joints and detailing to handle this as needed. More work is being done.

K Voulpiotis asked about the performance of the brace after effect of long term loading. HE Blomgren said this is an interesting question but do not have an answer. He added that there would not be gravity load for this brace.

H Daneshvar received clarification that the load protocol followed ASCE chapter K load protocol. He asked if the use of this brace open to public. HE Blomgren said there is a provisional patent filed.

M Li commented that there are lots of interest in New Zealand to use this type of system and asked what would be overstrength factor on the components of BRB for capacity design. HE Blomgren said factors would be defined by practitioners.

M Li commented that NZ tested glulam frames with steel BRB. They performed well but how to connect the BRB to the frame was critical. He said the overstrength factor used was 1.5.

H Blass asked regarding the bolted connections, if self-tapping screws would be an alternative. HE Blomgren said this would be possible but have not done this.

FIRE

52 - 16 - 1 Preliminary Design Model for Wooden I-Joists in Fire - K N Mäger, A Just

Presented by KN Mäger

A Frangi commented that the flange size of the I joist was small and asked if one should consider the full cross section rather than symmetry as there would be heat accumulation from both sides. KN Mäger agreed and will check later.

A Frangi commented that at temperature of 300C how would it be possible for the profile to exist. KN Mäger responded that the image was just an illustration.

H Blass and KN Mäger discussion the possibility of insulation falling off the protection layer. H Blass mentioned that the possibility of the insulation layer falling off would necessitate prescriptive rules.

P Palma commented that the results would depend on workmanship. KN Mäger agreed that this was possible.

BJ Yeh asked if the model would always assume the failure occur in the flange. KN Mäger responded that if charring occurred in the web, the failure would be governed by the web. BJ Yeh responded that based on N.A. fire test experience web would govern and the profile shown has not been seen in N.A. fire tests. S Winter said that this was because glass wool was used and not rock wool.

S Winter asked about the cases of having another layer for acoustic profile and partially insulated cavity. This situation would be helpful. KN Mäger responded that acoustic profile case would need to be tested. Also having a cavity should equalize the temperature a little bit. Partially insulated cases would need further investigation and the web should be fully insulated as a minimum.

A Frangi commented that one should limit the contribution to 15 minutes after the gypsum layer was compromised regardless of the fact that modelling results are conservative.

52 - 16 - 2   Code Calibration for Timber in Fire – On the Use of 20% Fractiles for the Strength - R Fahrni, G De Sanctis, A Frangi

Presented by R Fahrni

F Lam commented that the errors were based on sum of squares and it would be interesting to separate the errors into conservative versus non-conservative cases. R Fahrni agreed and said it would be interesting to study the cases where large errors occurred.

P Palma commented the structures did not take into consideration the behaviour of connections.   R Fahrni said that a method to calculate the reliability of connections in fires would be needed.

U Kuhlmann appreciated the basic assumptions leading to the bias solution. It would be important to hold up the calibration process with relative code calibration to avoid making gross errors. R Fahrni agreed and said that there are always bias in models and true reliability would not be possible.

BJ Yeh was amazed by the difference between N. American and European approaches, especially in terms of reliabilities in fire. In N. America codes are calibrated to mean values rather than 20th percentile. R Fahrni responded that in N America the full load would be used but in Europe a reduced live load would be used. It seemed that making a reduction to live load would make more sense as the full design live load would be unlikely to occur in fire.

GLUED JOINTS

52 - 18 - 1   Investigations Concerning Screw-Press Gluing of Assemblies with CLT -- K Bratulic, M Augustin, G Schickhofer

Presented by K Bratulic

M Li received confirmation that the screws were for pressure and most manufacturers would not take them out after. He commented that as clamping forces were important how were they measured. K Bratulic responded that the pull through test method for flat head screws were conducted and from the results one could establish the clamping forces based on the deformation of the press-in depth. M Augustin added that the clamping force could be measured with strain gauges in screws and also under the screw head; this was done.

S Franke asked would one get 5 mm insertion in timber in press screwing. K Bratulic responded that the 5 mm was used as an example only. The absolute deformation value was defined as screw head height + 2 mm as press in depth.

S Franke and K Bratulic discussed the dependence of clamping force on bond quality.

S Franke asked why only small specimens and not full width specimens were extracted. K Bratulic responded that this was done to check local effects.

T Lim commented about the pressure film technique and received confirmation on where they were applied.

H Blass asked whether the self weight of the beam was considered. K Bratulic said no.

H Blass commented that if the webs do not have the same depth one would need to pull up the web which would further reduce the pressure.

S Aicher agreed that the pull through strength of individual screws would be important in screw press application. He commented about the dense spacing of screws and the graph of shear strength. He asked what was the explanation for the low values of shear strength. He also stated that the German code was amended to take care of the influence of thicker plates.

K Bratulic responded on the relationship between bond line thickness versus shear strength, mentioning that in some cases even though bond line thickness was small, failure was observed. S Aicher said may be one should not allow screws with countersunk head as it would provide localized deformation. M Augustin commented that they were not happy with the shear tests for CLT and there were issues with the delamination tests.

S Aicher commented that the normalized pull through capacity should be equal for all types of screws but washer head screws seemed to be better.

S Franke asked if the mean values were checked. K Bratulic said no. S. Franke received clarification of the amount of PU glue applied and that it was not dependent on glueline thickness at this range.

ROBUSTNESS
52 - 22 - 1 Catenary Action for Cross-laminated Timber Floor Systems - H Mpidi Bita,
             T Tannert

Presented by H Mpidi Bita

P Dietsch asked why the screws were not applied at inclined angle and how would this system be adapted for outer walls. H Mpdi Bita responded that given the limitation of the number of specimens available for the project, self tapping screws could not be used, also the lap joint considered would be commonly used in Canada. Also the case of outer wall would be a good topic for a future project.

S Winter commented that such connection would create channels in crossing walls which would create issues for fire and acoustic performance.

H Daneshvan and H Mpdi Bita discussed the relationship between the catenary and shear forces and that the boundary condition in the test might not be realistic as it would be driven by the anchorage forces allowed. The clamping force would depend on the surrounding structure which would also influence the end wall stiffness.

D Dolan commented on robustness in terms of earthquake safety.

E Toumpanaki received clarification of the boundary conditions that would represent the bracket connection. E Toumpanaki stated as the bracket was installed below, this would act differently compared to reality. H Mpidi Bita mentioned that testing slabs supported on three edges was not possible. T Tannert responded that FEM will be developed to address boundary conditions issues. He commented that concrete and steel industry developing similar guidelines would give little details.

S Aicher asked do you really intend to use platform type construction for 15 storeys buildings. H Mpdi Bita mentioned that compression perpendicular to grain issues would be problematic. S Aicher said such systems could be use with modifications.

P Quenneville asked how would this system act compared to a continuous CLT panel and would such large catenary forces be needed if similar actions could be developed via some continuous structural system. H Mpdi Bita responded LVL floor plates could offer continuity and develop high forces; however, their behaviour would be brittle. He added the focus of the work was to study how catenary action could be developed. Such forces would not be available in a system that was not continuous and also not available in continuous systems that were brittle.

U Kuhlmann commented that she was not too convinced that the joint could take rotational demand at centre point and ends of member. She agreed that continuous plates could help with catenary action at high deformations also joints would need to take moments. H Mpdi Bita agreed but stated that availability of moment resisting joints would be critical.

M Li commented on dynamic effects, e.g. from removal of columns. H Mpdi Bita said that the current study only dealt with the linear static case. In design, factors would be applied to amplify forces to account for nonlinear dynamic effects. F Lam commented that this work represented a good starting point but many issues still exit as indicated by the questions raised by the delegates. The issue of dynamics would be critical as it would deal not only with amplified loads but also dynamic effects on capacity including rate of loading effect on strengths and low cycle fatigue behaviour.

52 - 22 - 2 Addressing robustness in the 2nd-generation EN 1995-1-1 Eurocode 5 - P
            Palma, R Steiger , R Jockwer

Presented by P Palma

P Dietsch stated that the statement that typical hall structures are inherently segmented is not true as lap-jointed purlins can lead to considerable load-distribution. He mentioned that the post-tensioning of vertical systems could be connected to robustness in term of vertical ties. P Palma responded that 11 to 12 degree rotation might be a requirement for catenary action and agreed that vertical ties could be a good option.

K Voulpiotis commented that rocking wall systems with post tensioning would be very beneficial to robustness and resiliency. P Dietsch commented that stiffness of CLT cores using post tensioning to resist wind load would be a good application.

D Dolan commented that in the US seismic codes for timber systems featuring over-strength requirements might push designers to make high strength connections which could be brittle.

H Mpidi Bita commented that post-tensioned systems are good but still would need horizontal catenary actions. Also segmentation would imply damage was allowed. How to control and design for damage development would be critical for segmentation consideration. P Palma agreed.

H Daneshvar commented that progressive collapse consideration should follow the approaches of concrete and steel where conventional systems would be used and additional systems would be added for catenary action. He asked if progressive collapse has to be considered in building design in Europe. P Palma responded that this would not be mandated and there was not an actual guide but that a motherhood statement is given, stating that damage should be limited.

P Dietsch and H Mpidi Bita discussed the importance of segmentation for tall buildings. In wide and horizontal cases segmentation would be important. In tall timber it would be hard to achieve. P Palma said in Europe there is a large number of structures where progressive collapse considerations would be required. In US there are progressive collapse consideration requirements for government and military buildings. They are working on similar approaches for civilian buildings.

S Winter commented that it is necessary to give guidance so that progressive collapse situations are avoided. However with so many available systems, we must not make the design guidelines too strict. In addition, S Winter does not agree with the requirement of calculating probabilistic numbers as correct structural design has much larger effect.

52 - 22 - 3   Robustness in Tall Timber Buildings - An Improved Framework - K Voulpiotis, J Köhler, R Jockwer, A Frangi

Presented by K Voulpiotos

P Quenneville asked would you look at requiring reduction of forces. K Voulpiotis said this might be needed.

E Toumpanaki commented construction and site inspection would be another set of issues that would need consideration.

U Kuhlmann commented that connection to probability needed lots of assumptions that could influence results. A more deterministic approach would be preferred. The probabilistic method connected with cost would be even more problematic. Consequence in view of safety would be better . K Voulpiotis responded that component design is already based on probability in the background. He agreed that many assumptions were needed but the approach could be used to guide the conceptual design phase. Finally the concept of cost would be tied to safety and not to monetary values. U Kuhlmann responded that focus on consequence would be better than cost. R Jockwer agreed and they discussed the relationship between I_{Rob} vs C_{Ind}/C_{Dir} in terms of good and bad conceptual design for robustness.

P Dietsch discussed the proposed framework. What else would be needed in terms of robustness on the level of connections, components, and materials in addition to good design practice? E Voulpiotis agreed and said that if connectors were needed for robustness as a conceptual point, one would need to provide additional considerations to achieve this.

P Palma asked about the robustness index. How to assure that apples are not compared to pears, what kind of consequences would be needed for consideration and how a designer could determine this. E Voulpiotis responded that there are many I_{Rob} definitions and the I_{Rob} in this paper could be referenced to Baker's work as a relative term. P Palma said a better way is to simply state a building is safe if a certain index is reached.

H Daneshvar commented that the framework is not timber focus and how could you bring this toward timber. E Voulpiotis responded by discussing compartment design for timber as we are moving towards more tall timber structures. P Quenneville agreed that this work is completely material independent. E Voulpiotis responded that this is a valid concern but timber design might have different consequences per ductility, size effects etc. P Quenneville discussed cost or consequence for timber and mentioned that the structural concept will have a larger influence on robustness than the lower steps in the framewpork. E Voulpiotis responded that they will be working on this.

NOTES

Five notes were presented

ANY OTHER BUSINESS

G Schickhofer TU Graz will receive the Wallenberg prize this year for his and his institutes outstanding work on CLT. The INTER group expresses our congratulations to G Schickhofer and his team.

VENUE AND PROGRAMME FOR NEXT MEETING

D Dolan presented an invitation to Concepcion Chile for INTER 2020 during August 17-20, 2020.

Host will be Universidad de Concepcion and Universidad del Bio Bio

S Winter and S Aicher will host the 2021 meeting Munich Germany August 23-26, 2021

Future INTER meeting sites will be Biel 2022, Shanghai 2023, Padua 2024, and Turkey 2025

CLOSE

BJ Yeh thanked the delegates for coming to Tacoma for the 2019 INTER meeting.

The Chair thanked BJ Yeh and the team from APA for having organized an excellent meeting. The Chair also thanked R Görlacher and F Lam for their work.

3 INTER Papers, Tacoma WA, USA 2019

52 - 7 - 1   Product Characteristics of Self-Tapping Timber Screws - A Ringhofer, G Schickhofer

52 - 7 - 2   Withdrawal Strength of Screws and Screw Groups in European Beech (Fagus s.) Parallel to the Grain - M Westermayr, J W G. van de Kuilen

52 - 7 - 3   Density Variations in Beech LVL - Influence on Insertion Moment and Withdrawal Capacity of Screws - M Frese

52 - 7 - 4   Steel Dowel Connections in Beech Hardwood - S Franke, B Franke

52 - 7 - 5   Effective Thickness of the Wood Member in a Timber-to-steel Connection with Large Diameter under Brittle Failure - M Yurrita, J M Cabrero

52 - 7 - 6   Row Shear and Block Shear Failure of Connections with Axially Loaded Screws - H J Blass, M Flaig, N Meyer

52 - 7 - 7   New Analytical Model for Brittle Failure in the Parallel-to-grain Direction of Timber Connections with Large Diameter Fasteners - M Yurrita, J M Cabrero

52 - 7 - 8   Embedment Test Analysis and Data in the Context of Phenomenological Modeling for Dowelled Timber Joint Design - M Schweigler, T K Bader, J-F Bocquet, R Lemaître, C Sandhaas

52 - 7 - 9   Beam-on-Foundation Modelling as an Alternative Design Method for Timber Joints with Dowel-Type Fasteners – Part 2: Modelling Techniques for Multiple Fastener Joint or Connection - R Lemaître, J-F Bocquet, M Schweigler, T K Bader

52 - 7 - 10   Transmission of Perpendicular to Grain Forces Using Self-tapping Screws - P Dietsch, S Rodemeier, H J Blaß

52 - 7 - 11   Component Method in Timber Construction – Experimental and Numerical Research - U Kuhlmann, J Gauß

52 - 9 - 1   Duration of Load Effect on Axially-Loaded Self-Tapping Screws Inserted Parallel to Grain in Soft- and Hardwood - R Brandner, A Ringhofer, R Sieder

52 - 12 - 1   Compressive Strength and Buckling Resistance of GLT Columns Made of European Beech - T Ehrhart, R Steiger, P Palma, E Gehri, A Frangi

52 - 12 - 2   Cross Laminated Timber at In-Plane Shear Loading – Comparison of Model Predictions - H Danielsson, E Serrano

Product Characteristics of Self-Tapping Timber Screws

Andreas Ringhofer[*], Gerhard Schickhofer

Graz University of Technology, Institute of Timber Engineering and Wood Technology, [*] andreas.ringhofer@tugraz.at

Keywords: self-tapping timber screws; steel tensile capacity; yield strength; yield moment; torsional resistance; analytical approach

1   Introduction

Due to their simple and economic installation without predrilling as well as their high axial load bearing capacity, self-tapping screws have become probably the most relevant fasteners in contemporary timber engineering. Following the provisions given in Eurocode 5, certain product properties are required for the design of connections or reinforcements, which are assembled with self-tapping screws: Their yield moment M_y serves as an input variable for the design of single shear connections with laterally loaded screws, while their tensile capacity f_{tens} limits their performance in terms of axial loading. When inserting them in timber, the occurring torque R_{tor} (times a factor) must not exceed their torsional capacity f_{tor}. This verification is not part of Eurocode 5 but has to be fulfilled for obtaining a CE-mark for the screw product.

In order to gain a better understanding about self-tapping timber screws, the information given in 65 European Technical Assessments (ETAs) was collected and compared (Ringhofer 2017). Considerable differences could be observed for the characteristic properties $f_{tens,k}$, $M_{y,k}$ and $f_{tor,k}$. For instance, $f_{tens,k}$ of a reference screw (made of carbon steel, nominal outer thread diameter d_{nom} = 8 mm) is between 17 kN and 33 kN. This range of approx. 90 % even exceeds the one of the withdrawal parameter $f_{ax,k}$ (37 %, for ρ_k = 350 kg/m³), which was assessed for the same screw type. Timber is a natural building material with a large variability in mechanical properties while structural steel is commonly regarded to behave rather homogenously, i.e. isotropic on the macroscopic level. Thus, the opposite was assumed in advance.

It is worth mentioning that the reported bandwidth of $f_{tens,k}$ is valid for standardised loading and environmental conditions, as they are applied to determine f_{tens}, M_y and f_{tor}. Furthermore, only screws made of carbon steel were considered and steel tensile failure was assumed having been occurred in the threaded section of the screw. Consequently, two main product characteristics, namely (i) the thread geometry and (ii) the production process, may be responsible for this observed high variability of the mechanical properties.

With regard to (i), the geometry of a common screw thread is defined by d, d_c, p and v as the outer and inner thread diameter, the thread pitch and the flank inclination angle. In addition, $\eta = d_c / d$ as the ratio of the inner and outer thread diameter and $\psi = v / 2$ as the half flank inclination angle are introduced.

Pöll (2017) analysed 34 ETAs of self-tapping screws (as part of the aforementioned database) regarding the declared bandwidths of d, η, p and v for nominal screw diameters $d_{nom} = \{5, 8, 10, 12\}$ mm. In case of $d_{nom} = 8$ mm, especially for both parameters η and p, a remarkable difference between the declared minima and maxima can be observed (η: $\Delta = 27$ %, p: $\Delta = 82$ %). Approximating the screw thread as a prismatic member with circular cross-section ($d_{cylinder} = d_c$, Bejtka and Blaß 2006, ETA-11/0190 2018), the ratio η has a quadratic or cubic influence on the size of f_{tens} or M_y and f_{tor}. Thus, the given %-difference of η (powered by 2) serves as a first explanation for the observed bandwidth of $f_{tens,k}$. Since this state-of-the-art approach does not consider the remaining thread parameters p and v, a related assessment of their impact on f_{tens}, M_y and f_{tor} is not possible.

With regard to (ii) and concentrating on screws made of carbon steel, hardened after forming the thread, the five main production steps are: the pre-treatment of the raw material, the forming of the screw (thread) geometry, the hardening process, the adding of protective coats, and the final treatment of the screw.

Taking the findings made by Ringhofer (2017) into account, the thread forming and the hardening are responsible for the final material composition and thus the size of the screw's steel tensile strength f_u, its yield strength f_y and its ductility D. Besides the geometrical parameters, these material properties govern the size of f_{tens}, M_y, and f_{tor}. The thread geometry is commonly rolled on a steel rod with cylindrical cross-section. In dependence of the scheduled thread length l_{thread}, different kinds of rolling facilities are applied. Short threads with $l_{thread} \leq 300$ mm (partially threaded screws and short fully threaded screws) are formed by flat die rollers, while for longer ones (except the start thread, again formed by flat die rollers) thread die rollers are used. On the one hand, both rolling methods are cold working, increase the steel hardness (und thus strength) and decrease the viscosity and the deformability due to an irreversible (plastic) material deformation. On the other hand, they differ remarkably regarding the final thread quality; i.e. the process-inherent engraving of notches and cracks is far more pronounced when flat die rolling is applied, see Figure 1. As the tool wear has a crucial (negative) impact on the dimension of these surface discontinuities, an exact quantification of their influence on f_{tens}, M_y and f_{tor} is quite sophisticated. This causes a residual uncertainty regarding the explanation of the outlined variability of the mechanical screw properties.
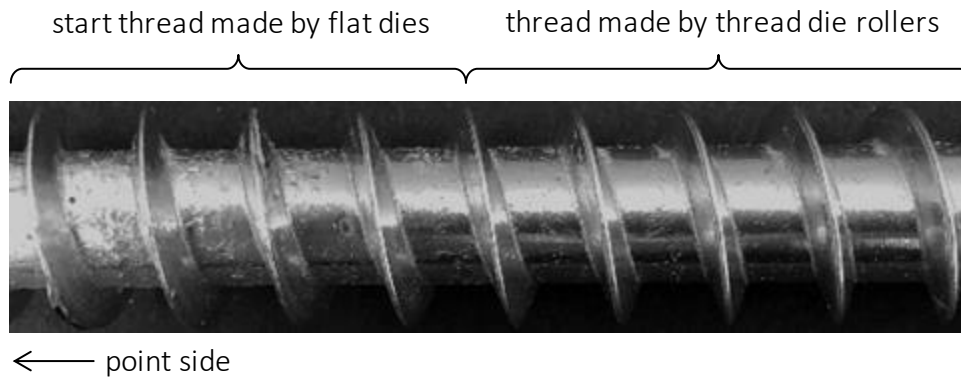
start thread made by flat dies　　　　thread made by thread die rollers

point side

Figure 1. Detail photo of a screw thread (d_{nom} = 14 mm) with transition from flat die to thread die rolling.

After cold-forming the screws are hardened. This takes place in form of three main phases: warming up to roughly 900 °C (at least above the GSK-line in the iron-carbon diagram), austeniting under constant temperature ≈ 900 °C and cooling-down below at least 300 C (quenching). Since the final screw hardness (and thus f_y, f_u and D) significantly depends on the diffusivity of the carbon atoms, the quenching time is seen as a key parameter of hardening, governing the size of the mechanical screw properties. To increase the torsional resistance of the screw, "carbonitriding" can be additionally applied. Hereby, the screw's surface gets additionally enriched by carbon, increasing the hardness of this outer thread zone. One possibility to reverse negative (but also positive) effects of hardening (and carbonitriding) is "tempering", where the screw is again warmed up to roughly 300 °C, partially re-organising the crystal lattice and decreasing its inner lattice stress.

Back to the content of those ETAs, which were analysed by Ringhofer (2017), information about or even indicators for the chosen hardening procedure in form of declared surface and core hardness values, steel tensile strength f_u and ductility D is missing. Currently, it is consequently not possible to quantify the influence of the production process on the variability of the declared mechanical properties. Note: $f_{tens,k}$ of screws with d_{nom} = 8 mm from different manufacturers but with more or less equal thread geometry varies between 17 and 24 kN, compare for instance ETA-12/0114 (2017) with ETA-12/0373 (2017). Thus, the production process is assumed being predominately responsible for this difference.

Aiming to fill this lack of knowledge, i.e. to quantify the influence especially of the production process (thread rolling, screw hardening) on the mechanical screw properties f_{tens}, M_y and f_{tor}, several experimental programmes were conducted at Graz University of Technology. An overview of the executed tests and the related configurations as well as a discussion of the gained results is presented hereafter. Furthermore, the focus of this contribution is on a new analytical model for the description of and the relationship between f_{tens}, M_y and f_{tor}, aimed to improve the state-of-the-art approach of approximating the screw thread profile by an ideal cylinder ($d_{cylinder}$ = {d_c, 1.1 · d_c, d}; Bejtka and Blaß 2006, EN 1995-1-1 2014, Blaß et al. 2017).

The motivation behind as well as brief summary of the model derivation are presented in Section 2 while a verification with the related test results is given in Section 5.

2   Analytical approach

2.1   General comments

The new analytical model was derived for one main reason: Currently, each of the mechanical screw properties, which are necessary to CE-label the product, has to be determined by experimental testing. Therefore, different configurations are applied, c.f. EN 14592 (2012) or EAD 130118-00-0603 (2016). The test results are subsequently used to declare characteristic properties, which serve as basic parameters for the design process. A theoretical relationship between $\{f_y, f_u\}$ and $\{M_y, f_{tens}\}$, as it is e.g. applied to determine the yield moment of dowels, is missing for screws.

This is in fact surprisingly since steel and therewith manufactured products, such as self-tapping timber screws, are commonly assumed as isotropic material with an elastic-plastic stress-strain relationship. In principle, this mechanical constitution should enable the theoretical determination of all different design properties by a few material parameters, namely the modulus of elasticity, the yield and tensile strength and the ductility, combined with a stress hypothesis. Thus, the prevalent aim of modelling was to consistently theoretically describe f_{tens}, M_y and f_{tor} for the threaded part of a screw. The main characteristics, the novel approach bases on, are:

- The real thread profile, defined by the parameters d, η, p and v, is considered instead of a circular cross-section,

- equal to the approximation by an ideal cylinder, the screw is assumed as a prismatic beam,

- the material is homogeneous and behaves in an ideal-plastic way. Thus, only the yield strength f_y remains as necessary mechanical property for the determination of M_y and f_{tor}, and

- the von-Mises criterion for isotropic materials serves as a stress hypothesis to determine the bearable torsional shear stress in case of yielding, $\tau_{T,y}$.

2.2   3D-model of the thread geometry

For a parametrisation of the screw thread profile by the parameters $\{d, \eta, p, v\}$, it was necessary to formulate a three-dimensional model of the thread geometry. Therefore, two mathematical functions, namely a cone line and a helicoid function were applied, see Figure 2 (left). Combining these functions leads to the formulae for the upper and lower thread surface functions. Exemplarily, the upper one is given in Equation (1):

$$\begin{bmatrix} x_1 \\ y_1 \\ z_1 \end{bmatrix} = \begin{bmatrix} \left[d \cdot (1-\eta)/2 - r \right] \cdot \tan\psi \\ -r \cdot \sin\varphi \\ r \cdot \cos\varphi \end{bmatrix} + \begin{bmatrix} p \cdot \varphi / (2\pi) \\ -\eta \cdot d / 2 \cdot \sin\varphi \\ \eta \cdot d / 2 \cdot \cos\varphi \end{bmatrix}. \tag{1}$$

In addition, the inner thread cylinder is defined by Equation (2):

$$\begin{bmatrix} x_3 \\ y_3 \\ z_3 \end{bmatrix} = \begin{bmatrix} x \\ -\eta \cdot d / 2 \cdot \sin\varphi \\ \eta \cdot d / 2 \cdot \cos\varphi \end{bmatrix}. \tag{2}$$

In a second step, these three-dimensional functions are converted into two-dimensional ones. This is done by expressing r by x, the gained section curves for a given x are as follows:

$$\begin{bmatrix} y_{1,2} \\ z_{1,2} \end{bmatrix} = \begin{bmatrix} -\chi_{1,2} \cdot \sin\varphi \\ \chi_{1,2} \cdot \cos\varphi \end{bmatrix}, \text{ with } \chi_{1,2} = \frac{d}{2} \pm \left(\frac{p \cdot \varphi}{2\pi} - x \right) \cdot \frac{1}{\tan\psi}. \tag{3}$$

The intersections (as functions of x and φ) of the upper (1) and lower (2) section curves with the inner thread cylinder (3) are denoted as $\varphi_{1,2}$ and result by equalising Equations (2) and (3), see Equation (4) and Figure 2 (right).

$$\varphi_{1,2} = \omega \cdot \pi \text{ and } \omega = \left[x \mp \frac{d}{2} \cdot (1-\eta) \cdot \tan\psi \right] \cdot \frac{2}{p}. \tag{4}$$
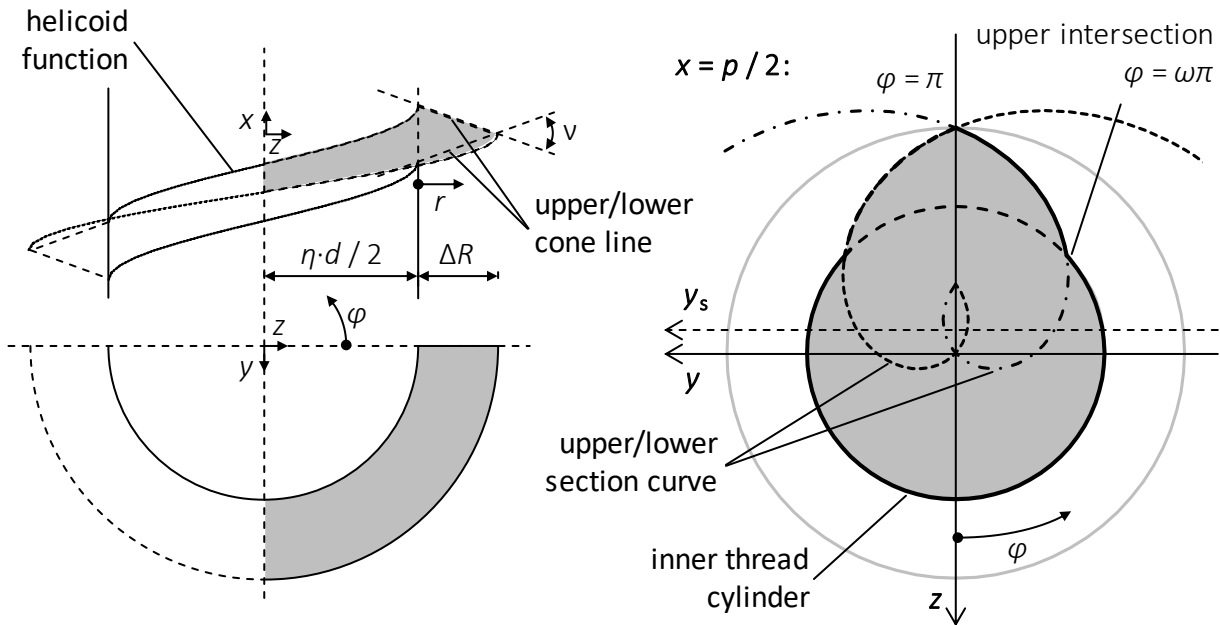

Figure 2. Illustration of mathematical functions describing the three-dimensional screw thread profile (left), cross-sectional shape of an example screw's threaded part at x = p / 2 (right).

Presupposing a given x (here $x = p / 2$ is applied), the thread profile, defined by Equations (3) and (4) serves as a basis for the determination of elastic and plastic cross-

sectional properties. For instance, the cross-sectional area A_s results in form of Equation (5), while the formulae for determining the gravity centre are outlined in Section 9.1.

$$A_s = 2 \cdot \left(A_{dc} + A_2 \right) = 2 \cdot \left(\int_0^{\omega\pi} \int_0^{r(\varphi)} r \, dr d\varphi + \int_{\omega\pi}^{\pi} \int_0^{\chi(\varphi)} \chi \, d\chi d\varphi \right) =$$
$$= \frac{\eta^2 \cdot d^2}{4} \cdot \omega\pi + \frac{\pi \cdot \tan\psi}{12 \cdot p} \cdot \left[d^3 - \left(d + (\omega - 1) \cdot p \cdot \cot\psi \right)^3 \right] \tag{5}$$

Regarding the determination of further elastic cross-sectional properties, such as the moments of inertia, the interested reader is kindly referred to Ringhofer (2017).

2.3   Principles for the determination of plastic cross-sectional screw properties

The approximation of an ideal-plastic material behaviour constitutes that the normal stress of all fibres of the cross-section has equalled the yield strength f_y. In case of pure bending, the bearable moment at this theoretical limit of full plasticity is further denoted as plastic moment M_{pl}. For the determination of $M_{pl,z}$ of the given screw thread profile, the force and moment equilibriums are considered:

$$N_c = N_t \rightarrow A_c \cdot f_y = A_t \cdot f_y \rightarrow A_c = A_t \overset{!}{=} \frac{A}{2}, \text{ and} \tag{6}$$

$$M_{pl,z} = N_c \cdot y_{s,c} + N_t \cdot y_{s,t}, \text{ with} \tag{7}$$

N_c and N_t as the plastic normal forces due to a bending moment $M_z = M_{pl,z}$, A_c and A_t as the partial areas under full yield stress in compression and tension and $y_{s,c}$ and $y_{s,t}$ as the distances of the gravity centres of A_c and A_t to the total one; see Figure 3.
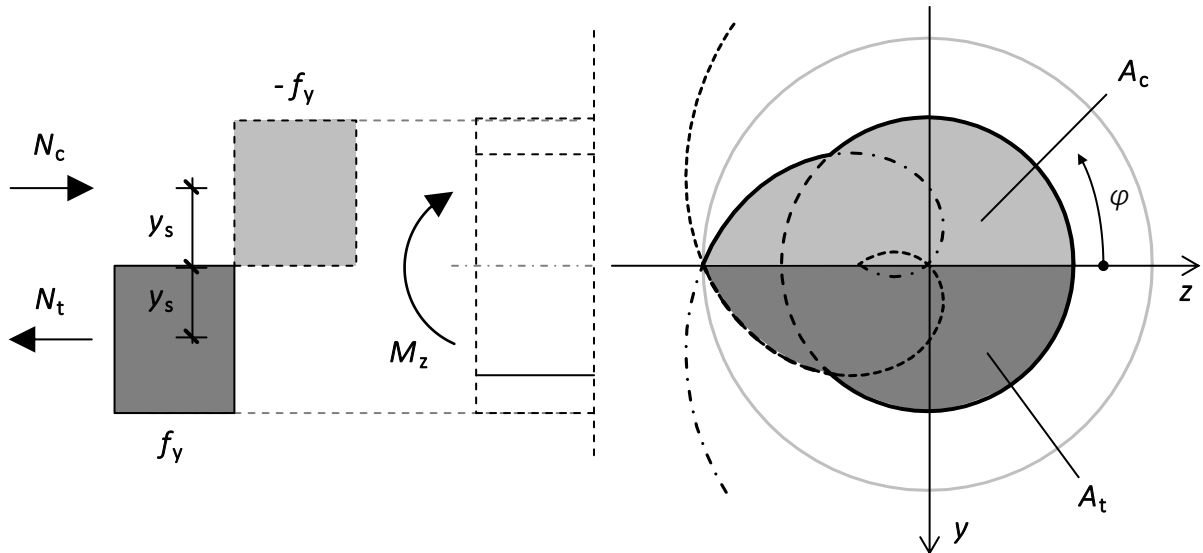
Figure 3. Stress distribution in the thread profile loaded in pure bending with assumed ideal-plastic material behaviour.

For the given thread profile, cross-sectional symmetry about the z-axis leads to

$$y_{s,c} = y_{s,t} = y_s, \text{ and } M_{pl,z} = \left(N_c + N_t \right) \cdot y_s = A_s \cdot f_y \cdot y_s \tag{8}$$

$$M_{pl,z} = (N_c + N_t) \cdot y_s = A_s \cdot f_y \cdot y_s. \tag{9}$$

The determination of y_s as the only unknown property is solvable in closed form and given in Section 9.2. Now concentrating on the screw thread profile, loaded by a normal force N. Due to the given eccentricity z_s between the screw axis (coordinate origin, where N applies) and the centre of gravity, not only N but also a bending moment $M_y = N \cdot z_s$ has to be considered, see Figure 4.
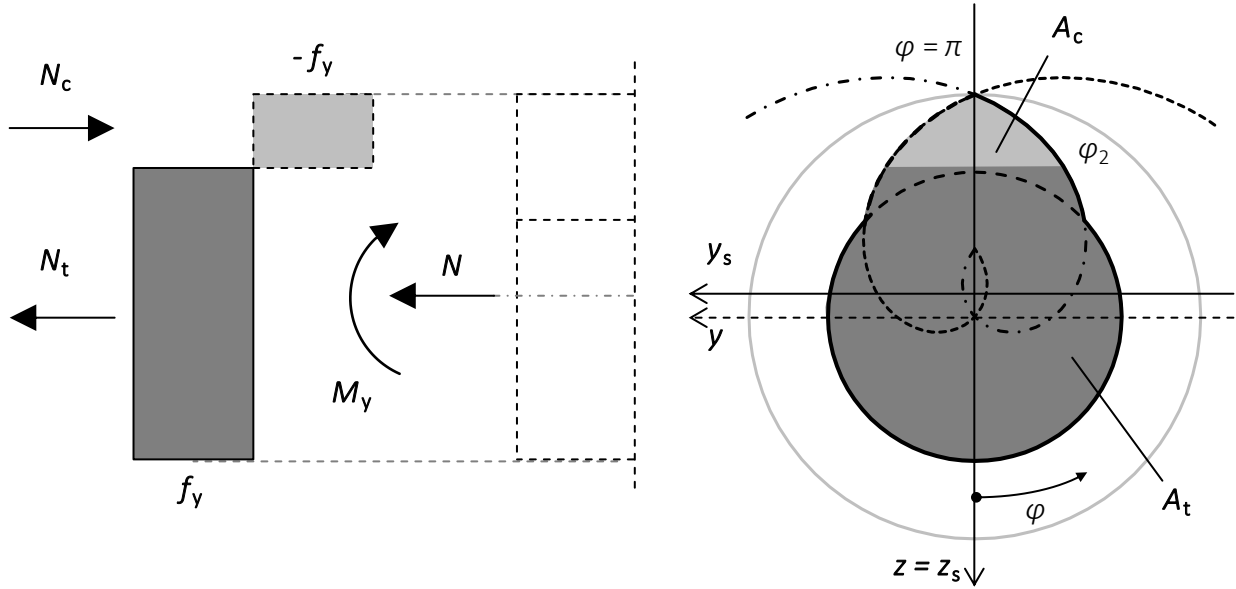
Figure 4. Stress distribution in the axially loaded screw thread profile with assumed ideal plastic material behaviour.

For this $N+M$ interaction, force and moment equilibrium result as follows:

$$N = N_t + N_c = A_t \cdot f_y + A_c \cdot (-f_y) = f_y \cdot (A_t - A_c), \text{ and} \tag{10}$$

$$M_y = N \cdot z_s = M_t + M_c = N_t \cdot z_{s,t} + N_c \cdot z_{s,c} = f_y \cdot (A_t \cdot z_{s,t} - A_c \cdot z_{s,c}). \tag{11}$$

Subsequently, $A_{pl,N}$ as the cross-section's area reserved for the normal force N is defined by

$$A_{pl,N} = A_t - A_c, \text{ which leads to } N = N_{pl} = A_{pl,N} \cdot f_y. \tag{12}$$

In contrast to the procedure described for $M_{pl,z}$, the determination of φ_2 (transition between A_t and A_c, Figure 4) disables a solution of N_{pl} in a closed form. Consequently, $A_{pl,N}$ was determined by means of numerical integration for the geometrical parameter set $p = \{0.4, 0.7, 1.0\} \cdot d$, $v = \{20, 40, 60\}°$ and $\eta = \{0.5, 0.7, 0.9\}$. The gained results served for deriving an empirical approach to determine $A_{pl,N}$, which is presented in Section 2.4.

To avoid overextending the scope of this paper, for the determination of the bearable torsional moment in case of full plasticity, $M_{T,pl}$ the interested reader is kindly referred to Ringhofer (2017).

2.4   Summary

Based on the content of Sections 2.1 to 2.3 and the considerations given in Ringhofer (2017), the proposed way of how to determine the mechanical properties M_y and f_{tor} by the results gained from screw tensile testing ($\rightarrow f_{tens,exp} = F_{u,exp}$, and $F_{y,exp}$ according to Section 3.2) can be summarised as follows:

$$\{f_{y,pred}, f_{u,pred}\} = \frac{\{F_{y,exp}, F_{u,exp}\}}{A_{pl,N,emp}}, \text{ with } A_{pl,N,emp} = A_{dc} \cdot \omega^{\left(\frac{-0.015}{\eta^{3.95}}\right)}. \tag{13}$$

Here, A_{dc} is defined as cross-sectional area of the complete inner thread cylinder.

$$M_{y,pred} \overset{!}{=} M_{z,pl,pred} = W_{pl,z} \cdot f_{y,pred} = A_s \cdot y_s \cdot f_{y,pred}, \text{ with} \tag{14}$$

y_s as closed-form solution according to Section 9.2. Note: the bending resistance about the z-axis is weaker than the one about the y-axis (Figure 3).

$$f_{tor,pred} \overset{!}{=} f_{tor,pl,pred} = W_{T,pl,emp} \cdot \tau_{T,y,pred}, \text{ with} \tag{15}$$

$$W_{T,pl,emp} = \left(-\frac{2}{3} \cdot \eta + 1.93\right) \cdot W_{T,el,dc} \cdot \omega^{\left(\frac{-0.2108}{\eta^{1.7105}}\right)}, \text{ and} \tag{16}$$

$$W_{T,el,dc} = \frac{\eta^3 \cdot d^3}{16} \cdot \pi, \text{ and } \tau_{T,y,pred} = \frac{f_{y,pred}}{\sqrt{3}}. \tag{17}$$

3   Materials and methods

3.1   Overview

An overview of the test programmes, which were conducted (a) to quantify the influence of the production process and (b) to verify the novel approach, is given in Table 1. The following parameters have been investigated:

- The screw manufacturer: A, B and C,

- the hardening of screws from manufacturer A, with (II) as standard procedure, (I) additionally carbonitrided, (IV) tempered after hardening and (III), carbonitrided and tempered afterwards,

- the fastener type, screws (s) and wire rods (r), the latter to verify Equation (13),

- the nominal diameter $d_{nom} = \{8, 10, 12\}$ mm,

- the inner thread diameter d_c for $d_{nom} = 8$ mm; A_s_II_08_240_hw had a significantly higher η than the other screws and

- the thread forming method; the tested thread sections of A_s_II_08_650 and C_s_II_14_800 were made by flat die (start thread) and thread die rollers. The other tested screw thread sections were made by flat die rolling.

Table 1. Overview of the experimental programme.

product ID	manufacturer	product	hardening	nominal diameter d_{nom} [mm]	total length l_{screw} [mm]
A_s_I-V_08_240	A	screw	I-V	8	240
A_r_I-V_08_240	A	wire rod	I-V	8	240
A_s_II_08_240_hw*	A	screw	II	8	240
A_s_II_08/10_500	A	screw	II	8, 10	500
A_s_II_08_650*	A	screw	II	8	650
A_s_II_08/10_1000	A	screw	II	8, 10	1000
A_s_II_12_450	A	screw	II	12	450
B_s_II_08/10/12_300	B	screw	II	8, 10, 12	300
C_s_II_08_200	C	screw	II	8	200
C_s_II_14_800	C	screw	II	14	800

* partially threaded screw

3.2 Methods

3.2.1 Tensile, bending and torsional testing

To determine the screw's steel tensile capacity f_{tens}, the test set-up was arranged on the basis of EN 14592 (2012), which implies a fixed support at the screw's point side and (hinged) head embedment in a steel plate with adequate dimensions, see Figure 5 (a). The load was thereby applied monotonically by a vertical movement of the head's hinged support. The loading velocity varied between 0.3 ÷ 0.7 mm/min (but stayed constant for each test) in order to reach the force maximum in the timeframe of 10 ± 5 s as proposed in EN 14592 (2012). All related experiments were performed on the test rig LIGNUM-UNI-275 (universal testing device, Zwick GmbH & Co. KG) at Graz University of Technology.

For determining the yield moment M_y, the applied test configuration deviated from that proposed in EN 409 (2009), see Figure 5 (b). The screw thread sections, cut with certain lengths and clamped by inner steel cylinders (dimensions varied in dependence of the fastener diameter), served as the weakest part of this two-span beam system. Since the outer steel cylinder's moment of inertia is several times bigger than that of the screw cross-section, beam rotation $\Delta\varphi$, enforced by removing the dowel and pushing down the handle, solely occurred along the free span length of the screw thread (commonly 3 d). The moment-rotation relationship M-φ, subsequently used for determining M_y, was gained by deriving M according to Equation (18) and φ by recording the beam rotation.

$$M = F \cdot a \cdot \left(1 - \frac{c}{b} \right) \qquad (18)$$

43

Following EN 14592 (2012) and EN ISO 10666 (2000) the test set-up to determine f_{tor} was realised by fixing the screws at their point side by clamping jaws, while the torsional moment was applied and recorded by an insertion engine. The static system is hereby assumed as a one-dimensional torsional bar, the load application as a support rotation about the product's x-axis, c.f. Figure 5 (c).
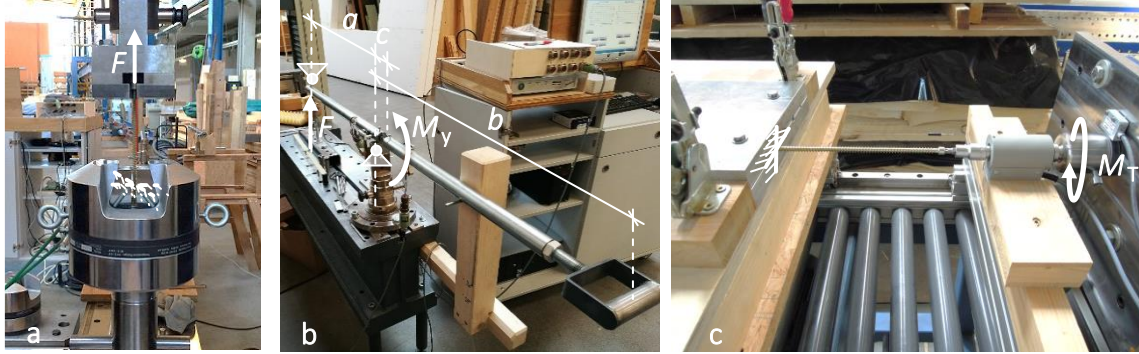
Figure 5. Setups for testing the steel tensile capacity (a), the yield moment (b) and the torsional capacity (c).

3.2.2 Determination of mechanical screw properties

Both, f_{tens} and f_{tor}, were set equal to the maximum values of the force-time history of each tensile and torsional test. The applied procedure to determine F_y and D based on the standard ASTM E2126 (2002) and presupposes an elastic-ideal plastic material behaviour in form of the so-called equivalent energy elastic-plastic (EEEP) curve (Figure 6). Considering the boundary condition of equal areas A_i below both, the recorded and the ideal force-deformation relationship, F_y can be derived as follows:

$$F_y = K_{ser} \cdot \left(v_u - \sqrt{v_u^2 - \frac{2 \cdot A_{real}}{K_{ser}}} \right),$$

(19)

with v_u as the deformation at F_u and K_{ser}, here defined as the (spring) stiffness of the (assumed) linear-elastic part ($F = 0.1 \div 0.4 \cdot F_{max}$) of the experimentally determined force-deformation relationship, calculated by means of the linear regression analysis. Subsequently, D results as ratio between v_y and v_u, the former as the deformation at F_y. Note: since no local way measurement set-up was applied, only the determined ductility for screws with the same length is considered for discussion hereafter.

The gained values of M_y, which are presented in this contribution (Section 4.2), were determined equal to F_y according to Equation (19). This procedure deviated from the one recommended by EAD 130118-00-0603 (2016). A comparison between the present values of M_y and ones determined in accordance to EAD 130118-00-0603 (2016) can be found in Ringhofer (2017), showing that the differences are kept in a limit of about 5 %.
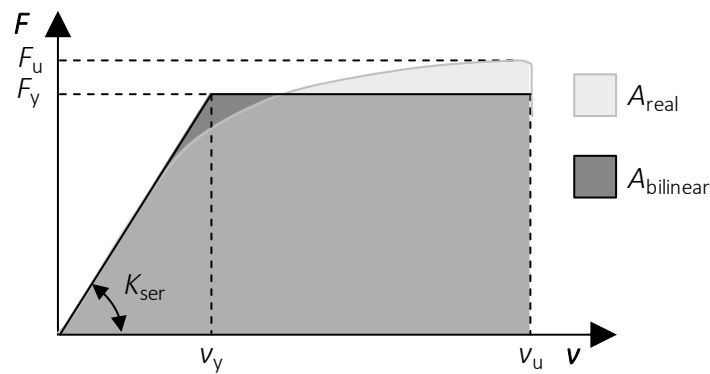
Figure 6. Definition of K_{ser}, F_u, F_y, v_y and v_u according to ASTM E2126 (2002).

4 Test results and discussion

4.1 Geometrical screw properties

The thread parameters d, d_c and p were determined for the majority of investigated screws and are given in Table 2. Products, where the corresponding values have been taken out from related ETAs instead, are outlined herein. This especially concerns the flank inclination angle v, which was not measured at all. These geometrical parameters, subsequently serving as input values for the model estimations (Section 5), represent the observed bandwidths of d, d_c, p and v. While for the ratio η a significant difference between the product A_s_II_08_240_hw and the other ones with d_{nom} = 8 mm is given, both further thread parameters p and v vary either to a limited extent (p) or not at all (v).

Table 2. Geometrical properties (mean values) of the investigated products.

product ID	type	d_{nom} [mm]	d [mm]	d_c [mm]	η [-]	v*** [°]	p [mm]
A_s_I-V_08_240	thread*	8	8.00	5.15	0.64	40	3.66
A_r_I-V_08_240	wire rod	8	5.76	-	-	-	-
A_s_II_08_240_hw	thread*	8	8.13	6.15	0.76	40	4.02
A_s_II_08_500	thread*	8	7.99	4.98	0.62	40	3.59
A_s_II_10_500	thread*	10	10.3	6.29	0.61	40	4.68
A_s_II_08_650	thread*	8	7.97	5.25	0.66	40	4.01
A_s_II_08_650	thread**	8	8.10	4.99	0.62	40	3.99
A_s_II_08_1000	thread*	8	8.07	5.05	0.63	40	3.59
A_s_II_10_1000	thread*	10	10.3	6.28	0.61	40	4.65
A_s_II_12_450	thread*	12	12.0	7.00	0.58	40	6.00
B_s_II_08_300	thread*	8	8.15	5.02	0.62	40	4.16
B_s_II_10_300	thread*	10	9.77	6.12	0.63	40	5.17
B_s_II_12_300	thread*	12	12.0	7.29	0.61	40	6.20
C_s_II_08_200***	thread*	8	8.00	5.00	0.63	40	3.70
C_s_II_14_800	thread*	14	13.9	8.70	0.63	40	6.60
C_s_II_14_800	thread**	14	13.9	8.49	0.61	40	6.58

* section formed by flat die rolling, ** section formed by thread die rolling, *** properties adopted from the ETAs

4.2 Overview of mechanical screw properties

The mean values and coefficients of variation of f_{tens}, F_y, f_y (according to Equation 13) and D per product ID for screw tensile testing are shown in Table 3, while Table 4 includes the results for bending and torsion. As it was well-known already and irrespective of the screw manufacturer, f_{tens}, M_y and f_{tor} significantly increase with increasing d_c. Since this is more pronounced for M_y and f_{tor} than for f_{tens} it serves as an indicator for the different impact of the inner thread diameter on these properties.

Excluding the products A_s_I-V_08_240, which were specifically hardened, and comparing screw thread sections with similar geometry and made by flat die rolling, remarkable differences in f_{tens} (and direct proportional in M_y and f_{tor}) between the manufacturers A, B and C can be observed. This again underlines the impact of the specifically applied hardening process on the mechanical screw properties.

With regard to the related dispersion, the corresponding values of CV[X] for f_{tens} are consistently low and don't seem to be influenced by the screw manufacturer. In general, CV[f_{tens}] < CV[f_{tor}] < CV[F_y] < CV[M_y] < CV[D], which is caused on the one hand by a given uncertainty in measuring deformations and rotations (F_y, M_y, D) and on the other hand by a higher impact of surface discontinuities on bending and torsional than on tensile properties.

Table 3. Mean values and coefficients of variation of screw tensile properties.

product ID	d_{nom} [mm]	η [-]	n [-]	f_{tens} [kN]	CV[f_{tens}] [%]	F_y [kN]	CV[F_y] [%]	f_y [N/mm²]	D [-]	CV[D] [%]
A_s_I_08_240	8	0.64	15	29.0	0.56	26.4	0.75	1,232	3.00	4.01
A_s_II_08_240	8	0.64	10	30.5	0.45	28.0	1.01	1,305	3.45	5.13
A_s_III_08_240	8	0.64	5	19.9	0.44	19.5	0.93	908	2.48	8.30
A_s_IV_08_240	8	0.64	15	19.6	0.48	18.9	0.71	880	4.55	8.42
A_s_V_08_240	8	0.64	5	11.9	3.64	11.3	3.68	528	6.61	10.4
A_s_II_08_240_hw	8	0.76	10	36.5	0.50	33.2	0.68	1,108	3.83	1.71
A_s_II_08_500	8	0.62	11	26.8	0.75	24.9	1.07	1,232	2.44	8.66
A_s_II_08_650*	8	0.66	10	25,8	0.89	23.5	1.29	1,061	3.58	2.85
A_s_II_08_650**	8	0.62	10	27.4	0.79	25.4	1.32	1,257	5.65	6.42
A_s_II_10_500	10	0.61	11	45.3	0.16	40.4	0.49	1,251	3.38	1.47
A_s_II_12_450	12	0.58	12	51.9	0.91	45.6	1.17	1,132	2.39	4.17
B_s_II_08_300	8	0.62	11	23.7	1.45	22.1	1.48	1,080	1.96	11.6
B_s_II_10_300	10	0.63	6	30.9	1.10	30.0	2.66	990	1.55	4.49
B_s_II_12_300	12	0.61	3	53.9	0.57	51.8	1.57	1,199	1.70	6.62
C_s_II_08_200	8	0.63	5	23.4	0.94	22.4	1.40	1,101	2.80	8.05

* section formed by flat die rolling, ** section formed by thread die rolling

Table 4. Mean values and coefficients of variation of screw bending and torsional properties.

product ID	d_{nom} [mm]	η [-]	n [-]	M_y [Nm]	CV[M_y] [%]	n [-]	f_{tor} [Nm]	CV[f_{tor}] [%]
A_s_I _08_240	8	0.64	3	33.7	2.17	5	35.7	0.48
A_s_II_08_240	8	0.64	3	30.3	1.55	10	32.9	1.47
A_s_III_08_240	8	0.64	3	25.0	3.74	5	23.0	1.32
A_s_IV_08_240	8	0.64	3	20.9	7.64	5	21.4	0.22
A_s_V_08_240	8	0.64	3	13.8	5.57	-	-	-
A_s_II_08_240_hw	8	0.76	-	-	-	10	43.8	0.78
A_s_II_08_500	8	0.62	-	-	-	10	28.7	0.95
A_s_II_08_650*	8	0.66	10	28.0	5.56	-	-	-
A_s_II_08_1000	8	0.63	12	32.1	6.02	-	-	-
A_s_II_10_500	10	0.61	-	-	-	12	61.6	0.75
A_s_II_10_1000	10	0.61	12	57.8	3.48	-	-	-
A_s_II_12_450	12	0.58	14	83.0	2.76	12	85.5	0.98
B_s_II_08_300	8	0.62	3	27.6	1.06	10	26.9	3.04
B_s_II_10_300	10	0.63	3	45.1	2.19	10	44.1	1.57
B_s_II_12_300	12	0.61	3	79.7	5.81	10	79.2	13.8

* section formed by thread die rolling

4.3   Impact of the hardness

Concentrating now on the influence of screw hardening, the results of hardness tests for product ID A_s_I-IV_08_240 are introduced in Figure 7. It is worth mentioning that they were determined by Toblier (2014) by means of macro-hardness testing (Emco Test M4C 025 G3M) according to EN ISO 6507-1 (2004) at the Institute of Materials Science, Joining and Forming at Graz University of Technology. As illustrated in Figure 7 (left), hardness according to Vickers (HV1) was measured point-wisely over the half thread profile. Considering this additional information and the mechanical properties given in Table 3 and Table 4 for product ID A_s_I-V_08_240 the following observations are made:

- Screw hardening is responsible for the final size of f_{tens}, M_y and f_{tor}, while the impact of cold working due to thread rolling is negligible, compare A_s_I-IV_08_240 with A_s_V_08_240. In fact, the austeniting under high temperature during the hardening removes all prior embossed steel modifications.

- As expected and shown on the illustrations, tempering and carbonitriding have a significant impact on the steel hardness. Thereby, the influence of tempering can be observed in form of a constant negative shift of the (more or less) homogenous hardness distribution of sample A_s_II_08_240. With regard to the mechanical properties, tempering somehow downscales f_{tens}, M_y and f_{tor} by a factor of approx. 1.50, compare A_s_I_08_240 with A_s_III_08_240 and A_s_II_08_240 with A_s_IV_08_240. In contrast, the carbonitriding has no effect on the profile's inner

zones, but significantly modifies the surface hardness, leading to a progressive increase with an increasing distance to the cross section's gravity centre. Interestingly, the steel tensile capacity does not seem to be affected by this measure. Both bending and torsional capacities, which benefit from this increase in hardness in the profile's outer zones, are upscaled by the factors of approx. 1.08 and 1.15 respectively, compare A_s_I_08_240 with A_s_II_08_240 and A_s_III_08_240 with A_s_IV_08_240.

- However, the positive effect of carbonitriding and the negative effect of tempering on f_{tens}, M_y and f_{tor} goes along with an oppositional behaviour of the ductility D. Comparing A_s_II_08_240 with A_s_IV_08_240, tempering increases D by the factor of approx. 1.30, while carbonitriding even halves D in case of A_s_III_08_240 vs. A_s_IV_08_240. The main reason therefore is an increase of brittleness in the cross-section's outer zones as a consequence of an enrichment of carbon in this area.

- With regard to the dispersion of the mechanical properties, an impact of carbonitriding or tempering on CV[X] is not observed at all. Comparing A_s_I-IV_08_240 with A_s_V_08_240, significantly higher CV[f_{tens}] can be observed for unhardened screws. The hardening is thus expected to homogenise the material.
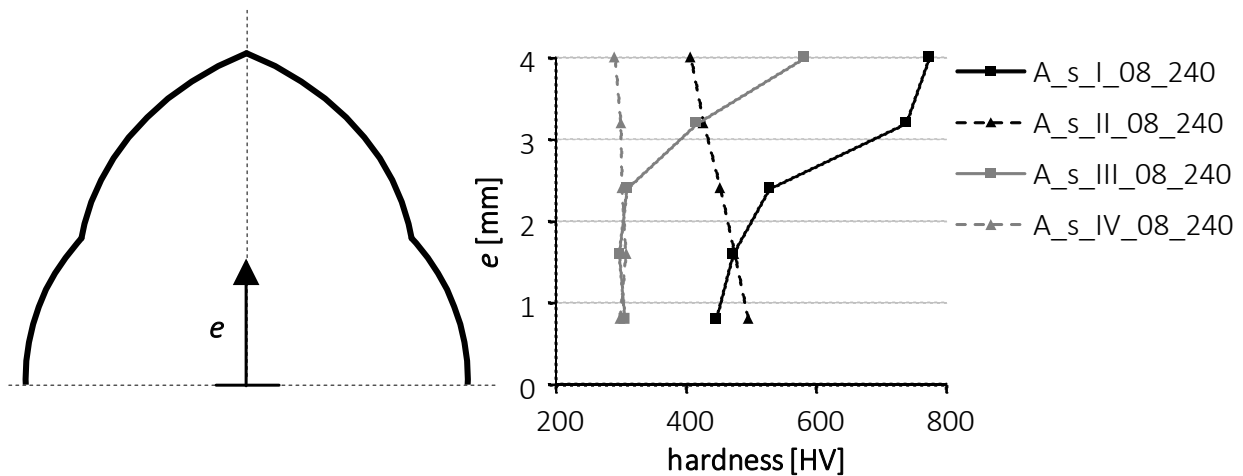
Figure 7. Varying hardness distributions over the screw thread profile determined by Toblier (2014) for product ID A_s_I-IV_08_240.

4.4 Impact of the thread forming process

In Table 5 the mechanical properties of the two differently produced thread sections along one and the same screw are shown. With regard to the size of f_{tens}, only small deviations between flat die rolling and thread die rolling can be observed for both screw products. Considering the results given in Table 2, flat and thread die rolling obviously leads to a slightly different thread geometry. Thus, it is reasonable to evaluate on the level of stresses instead of forces. Presupposing that the novel approach leads to an appropriate prediction of f_y (Equation 13 was applied for determination) a

far more pronounced, significant difference between flat die rolling and thread die rolling is given for the yield strength. Since an equal hardness of both thread sections can be expected, these deviations are probably caused by the difference in the thread quality, see Figure 1. A similar relationship given for the ductility D supports this statement.

Table 5. Comparison of main mechanical properties of two differently produced thread sections along one screw (mean values, n = 10 per screw type and thread section)

product ID	d_{nom} [mm]	thread type	f_{tens} [kN]	CV[f_{tens}] [%]	Δf_{tens}* [%]	f_y [N/mm²]	CV[f_y] [%]	Δf_y* [%]	D [-]	CV[D] [%]
A_s_II_08_650	8	flat die	25.8	0.89	1.06	1,061	1.29	1.18	3.58	2.85
		thread die	27.4	0.79		1,257	1.32		5.65	6.42
C_s_II_14_800	14	flat die	68.9	1.15	1.05	1,022	1.23	1.10	4.56	4.37
		thread die	72.2	0.51		1,129	2.01		6.40	3.92

* referred to flat die rolling

5   Model verification

In a first step Equation (13) is assessed regarding the suitability in determining the steel tensile and yield strength by testing the screw thread in axial tension. Therefore, both mechanical properties given in Table 3 for product ID A_s_I-V_08_240 shall be compared with the ones gained for the wire rods A_r_I-V_08_240, which were hardened with the same configurations. Thus, equal strength properties can be expected. In contrast to the thread profile, their circular cross section enables a simple determination of f_u and f_y as the ratios between F_u and F_y and their cross-sectional area A_{dc} according to Section 2.4 (with d = 5.76 mm, Table 2). As shown in Table 6, the differences between experimental and predicted values are comparatively small for hardened screws (A_s_I-IV_08_240). Interestingly, a consistent underestimation of the test results by the model is given. One reason therefore could be the negative influence of thread surface discontinuities, decreasing f_{tens} and F_y of thread sections to some extent. The significant deviation between experimental and predicted values, which can be observed for unhardened screws (A_s_V_08_240) can be explained by the impact of cold forming the screw thread.

Table 6. Comparison of experimentally determined and predicted values for f_y and f_u.

product ID	$f_{u,exp}$ [N/mm²]	$f_{u,pred}$ [N/mm²]	Δ* [%]	$f_{y,exp}$ [N/mm²]	$f_{y,pred}$ [N/mm²]	Δ* [%]
A_s_I _08_240	1,398	1,353	-3.22	1,299	1,232	-5.16
A_s_II_08_240	1,490	1,421	-4.63	1,394	1,305	-6.38
A_s_III_08_240	980	927	-5.41	944	908	-3.81
A_s_IV_08_240	947	914	-3.48	916	880	-3.93
A_s_V_08_240	471	553	17.4	441	528	19.7

* referred to experimental values, ** section formed by flat die rolling

In a second step, the experimentally determined bending and torsional properties M_y and f_{tor} are compared with model predictions, determined by Equation (14) and

Equation (15). In addition, two approaches, which approximate the screw by an ideal cylinder ($d_{cylinder} = \{d_c, d\}$) are considered as well. Therefore, the plastic bending and torsional properties were determined as follows:

$$M_{y,pred} \overset{!}{=} W_{pl} \cdot f_{y,pred} = \frac{d^3_{cylinder}}{6} \cdot f_{y,pred}, \text{ and } f_{tor,pred} \overset{!}{=} W_{T,pl} \cdot \tau_{T,y,pred} = \frac{2}{3} \cdot r^3_{cylinder} \cdot \pi \cdot \tau_{T,y}, \text{ (20)}$$

with $f_{y,pred}$ according to Equation (13), but with $A_{cylinder}$ instead of $A_{pl,N,emp}$. As illustrated in Figure 8 (left), a comparatively high agreement between tests results and values predicted by the novel approach can be observed. Test results of A_s_I_08_240 and A_s_III_08_240 are slightly underestimated and the ones of A_s_II_08_240 and A_s_IV_08_240 are slightly overestimated. Possible explanations are the quantified impact of carbonitriding (Section 4.3) and the probable one of thread surface discontinuities. Comparing the predictive quality of all three approaches, the best agreement can be observed for the novel approach, which considers the real thread geometry. In case of M_y, the model with $d_{cylinder} = d_c$ is closely located to the test results as well, while the model with $d_{cylinder} = d$ significantly overestimates the bending and torsional properties.
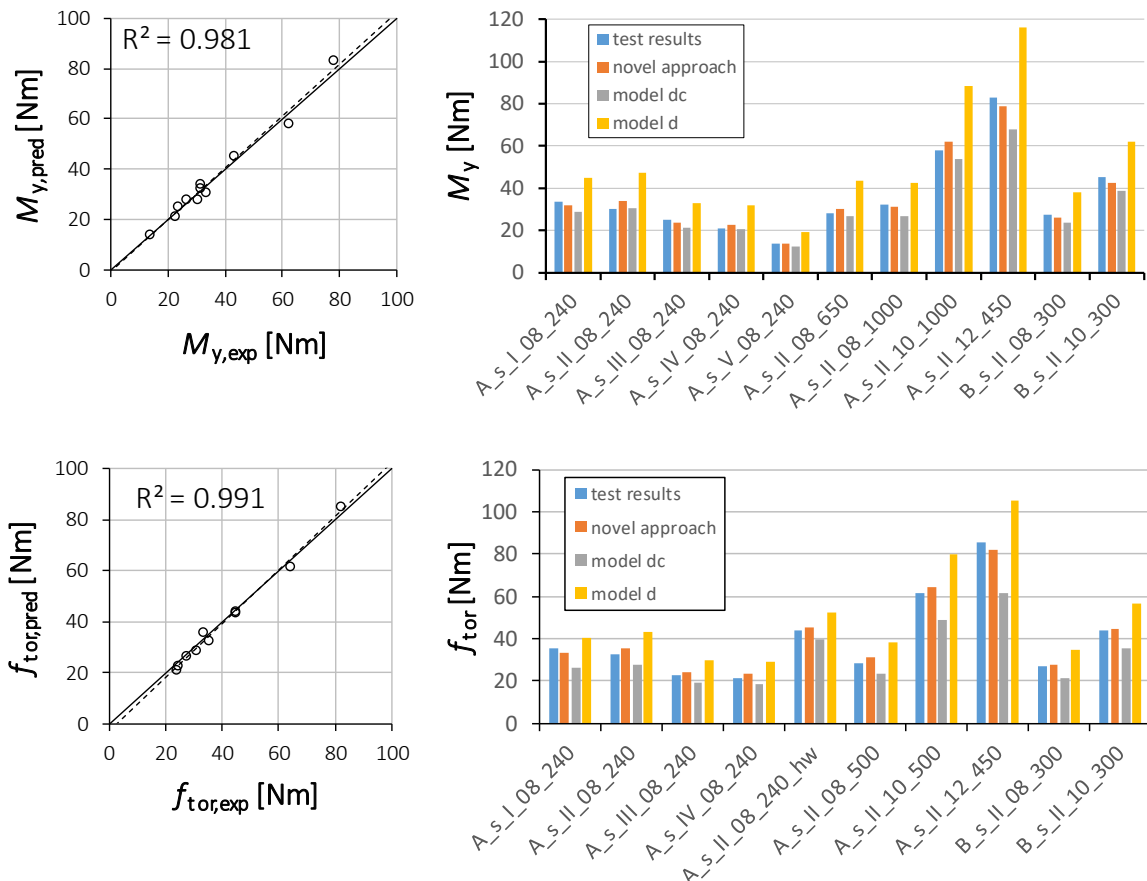

Figure 8. Comparison of test results (mean values) with predicted values of M_y (above) and f_{tor} (below) by the novel approach (left) and additionally by both cylindrical approaches with d_c and d (right).

6   Summary, conclusion and outlook

The focus of this contribution was set on the product characteristics of self-tapping timber screws. The aim was to discuss and quantify the influence of the screw thread geometry and the production process on f_{tens}, M_y and f_{tor}, as the relevant parameters for screw application and design. The experimental results presented in this paper confirm the significant, progressive impact of the inner thread diameter on these mechanical properties. With regard to the screw production process, the investigated thread forming methods, flat die and thread die rolling, differ remarkably in the final thread quality. On the level of stresses, a decrease in strength of about 15 % can be observed for flat die if compared to thread die rolling. Thus, different mechanical properties along the thread of long fully threaded screws can be expected in practise. If the screw has a thread-free shank as well, three main sections with significantly different values for $f_{tens,k}$, $M_{y,k}$ and $f_{tor,k}$ are given. Especially for laterally loaded screws, the inhomogeneous distribution of M_y should be considered, at least when high-sophisticated models are applied for determining the load-slip behaviour.

Summarising the impact of different hardening methods, carbonitriding was observed to increase both bending and torsional resistances to some extent, but remarkably decreases the ductility. A more brittle failure behaviour of the screw when loaded in tension and/or bending can be expected. Hardening the outer thread zones combined with surface discontinuities caused by thread forming should be seen critical especially in terms of cyclic loading with a certain demand of ductility (seismic actions) or a pronounced dependence on crack propagation (high-cycle fatigue, stress corrosion cracking). To face this problem, i.e. to allow screw application beyond static and quasi-static loading, e.g. the surface hardness could be restricted in the frame of CE-labelling.

With regard to the suitability of the novel approach for predicting strength values as well as bending and torsional properties on the basis of screw tensile tests, a comparatively high agreement between model estimations and test results is given. Thus, a related application is recommended not only for improving current design provisions (Eurocode 5, ETAs) but also prospective regulations, dealing with the interaction of bending moments, normal and shear forces (MNV), occurring simultaneously in the fastener.

Consequently, further studies will focus on an advancement of the present approach regarding MNV-interaction. In addition, a more detailed quantification of the impact of thread surface discontinuities on the mechanical properties is scheduled.

7   References

ASTM E2126 (2002): Standard Test Methods for Cyclic (Reversed) Load Test for Shear Resistance of Walls for Buildings. ASTM International.

Bejtka, I; Blaß, HJ (2006): Self-tapping screws as reinforcements in beam supports. In: Proceeding of the 39th CIB W18 Meeting, Florence (Italy), CIB-paper 39-07-2.

Blaß, HJ; Sandhaas, C; Meyer, N (2017): Steel-to-timber connections: Failure of laterally loaded dowel-type fasteners. In: Proceeding of the 4th INTER Meeting, Kyoto (Japan), INTER-paper 50-07-1.

EAD 130118-00-0603 (2016): Screws for use in timber constructions. EOTA.

EN 409 (2009): Timber structures – Test methods – Determination of the yield moment of dowel type fasteners. CEN.

EN 1995-1-1:2004 + AC:2006 + A1:2008 + A2:2014 (2014): Eurocode 5: Design of timber structures – Part 1-1: General – Common rules and rules for buildings. CEN.

EN 14592:2008 + A1:2012 (2012): Timber structures – Dowel-type fasteners – Requirements. CEN.

ETA-11/0190 (2018): Würth self-tapping screws. European Technical Assessment (ETA), Deutsches Institut für Bautechnik (DIBt), Berlin (Germany).

ETA-12/0114 (2017): SPAX self-tapping screws. European Technical Assessment (ETA), ETA Danmark, Göteborg (Danmark).

ETA-12/0373 (2017): Schmid screws RAPID, STARDRIVE and SP. European Technical Assessment (ETA), Österreichisches Institut für Bautechnik (OIB), Vienna (Austria).

EN ISO 6507-1 (2004): Metallic materials – Vickers hardness test – Part 1: Test method. CEN.

EN ISO 10666 (2000): Drilling screws with tapping screw thread – Mechanical and functional properties. CEN

Pöll, M (2017): Entwicklung einer Hartlaubholzschraube: Optimierung der Gewindegeometrie für die Beanspruchung auf Herausziehen. Master's Thesis, Graz University of Technology (in German).

Ringhofer, A (2017): Axially Loaded Self-Tapping Screws in Solid Timber and Laminated Timber Products. In: Schickhofer, G; Brandner, R (eds.) Timber Engineering & Technology, TET 5, Verlag der Technischen Universität Graz.

Toblier, L (2014): Untersuchung der wasserstoffinduzierten Versprödung von verzinkten, hochfesten Holzschrauben. Bachelor's Thesis, Graz University of Technology.

8   Acknowledgements

9 Annex

9.1 Position of the gravity centre

Cross-sectional symmetry in case of $x = p \, / \, 2$ leads to $y_s = 0$.

$$z_s = \frac{A_{dc} \cdot z_{s,dc} + A_2 \cdot z_{s,2}}{0.50 \cdot A_s} , \text{ with } z_{s,i} = \frac{\displaystyle\int_{\varphi_1}^{\varphi_1} \int_0^{r(\varphi)} \left[r(\varphi) \right]^2 \cdot \cos\varphi \, dr \, d\varphi}{\displaystyle\int_{\varphi_1}^{\varphi_1} \int_0^{r(\varphi)} r \, dr \, d\varphi} \tag{21}$$

$$z_{s,2} = \frac{-p \cdot \left[a + b \cdot \cos(\omega\pi) + c \cdot \sin(\omega\pi) \right]}{\tan\psi \cdot \pi^4 \cdot \left[\tan^3\psi \cdot d^3 - \left(\tan\psi \cdot d + (\omega-1) \cdot p \right)^3 \right]} , \text{ with} \tag{22}$$

$$a = -6 \cdot p^3 + 3 \cdot \tan^2\psi \cdot d^2 \cdot p \cdot \pi^2 , \tag{23}$$

$$b = 3p \cdot \left[-2p^2 + \left(\tan\psi \cdot d + (\omega-1) \cdot p \right)^2 \cdot \pi^2 \right] , \tag{24}$$

$$c = \left[\tan\psi \cdot d + (\omega-1) \cdot p \right] \cdot \pi \cdot \left[-6p^2 + \left(\tan\psi \cdot d + (\omega-1) \cdot p \right)^2 \cdot \pi^2 \right], \text{ and} \tag{25}$$

$$z_{s,dc} = \frac{\eta \cdot d \cdot \sin(\omega\pi)}{3 \cdot \omega\pi} . \tag{26}$$

9.2 Coordinate y_s in terms of pure bending about the z-axis

$$y_s = \frac{A_2 \cdot y_{s,2} + A_{dc} \cdot y_{s,dc}}{0.50 \cdot A_s} , \text{ with} \tag{27}$$

$$y_{s,2} = \frac{p \cdot \left[a + b \cdot \cos(\omega\pi) - c \cdot \sin(\omega\pi) \right]}{\tan\psi \cdot \pi^4 \cdot \left[\tan^3\psi \cdot d^3 - \left(\tan\psi \cdot d + (\omega-1) \cdot p \right)^3 \right]} , \text{ and} \tag{28}$$

$$a = -6 \cdot \tan\psi \cdot d \cdot p^2 \cdot \pi + \tan^3\psi \cdot d^3 \cdot \pi^3 , \tag{29}$$

$$b = \left[\tan\psi \cdot d + (\omega-1) \cdot p \right] \cdot \pi \cdot \left[-6p^2 + \left(\tan\psi \cdot d + (\omega-1) \cdot p \right)^2 \cdot \pi^2 \right] , \tag{30}$$

$$c = 3p \cdot \left[-2p^2 + \left(\tan\psi \cdot d + (\omega - 1) \cdot p \right)^2 \cdot \pi^2 \right], \text{ and} \tag{31}$$

$$y_{s,dc} = \frac{\eta \cdot d \cdot \left[1 - \cos(\omega\pi) \right]}{3 \cdot \omega\pi}. \tag{32}$$

Discussion

The paper was presented by A Ringhofer

P Quenneville asked how many cycles can the screws sustain before breakage. A Ringhofer responded that this would depend on the load level and their experience is that the number of cycles before failure is not that high. More work will be done in this area.

D Dolan commented that one might want to put these screws in situations where they are designed not to take cyclic loads. A Ringhofer agreed and said that there are cases where for example fatigue and corrosion effects are important.

R Jockwer commented that the distribution of properties along screw length might be an issue. A Ringhofer and H Blass agreed on this point based on their experience on screw performance.

YH Chui asked about the actual aim of the research. A Ringhofer said that the theoretical approach was intended for quality control and guidance for product development.

A Frangi stated that he was not concerned about difference between different products but more concerned with differences within a product.

H Daneshvar discussed his experience regarding the importance of screw behavior during cyclic tests. H Blass commented that these screws can be used in seismic situation especially if they are designed to behave elastically with appropriate q values.

U Kuhlmann asked and received clarification that the definition of ductility was based on ASTM approach.

D Dolan discussed fatigue versus seismic response in terms of energy dissipated by the connector in earthquakes.

P Dietsch and A Ringhofer discussed why the mechanical model assumed the screws thread would be activated completely and uniformly under axial loads.

R Jockwer commented that it would make sense for designers to use capacity rather than strength.

T Tannert commented that CSA 086 requires knowledge of 95th percentile for capacity design in seismic situation. A Ringhofer responded that this can be obtained based on COV information and there seemed to be no real difference amongst producers.

M Li commented about the verification of results where good match can be obtained based on average values but this may not be achievable based on the tails.

Withdrawal strength of screws and screw groups in European beech (*Fagus s.)* parallel to the grain

Maximilian Westermayr, Technical University of Munich, Professorship of Wood Technology, Munich, Germany

Jan Willem van de Kuilen, Technical University of Munich, Professorship of Wood Technology, Munich, Germany; Biobased Structures and Materials, Delft University of Technology

1   Introduction

The hardwood species beech (*Fagus sylvatica)* is widely spread all over Europe, reaching from Western France to the Black Sea and from Southern Sweden to Southern Italy. The national forest inventories in Germany, Austria and Switzerland register an increase in hardwood species and especially in the species beech, as monoculture softwood stands are steadily transformed to more stable mixed deciduous and coniferous forests. The good availability of beech timber on the European market could thus benefit the growing timber construction sector and the resulting higher demand of the resource wood.

But not only the good availability of beech timber, also the favourable mechanical properties of the species may lead to beech structural elements complementing conventional softwood components in future timber construction. Many studies are available proofing the high mechanical potential of beech components, mainly for beech glulam (e.g. Frühwald et al., 2003; Glos et al., 2004; Ehrhart et al., 2018; Westermayr et al., 2018). To make full use of the high mechanical performance of beech components, safe and efficient connections are a key requirement to transfer loads. One of the most frequently used fasteners in timber construction are screws.

Their easy application in practice, high load bearing capacity as well as affordability are some of the benefits intelligent screw connections can provide.

The load bearing capacity of an axially loaded screw is governed by its withdrawal capacity or by tensile failure of the screw. Withdrawal is a combination of different overlapping stresses, depending on the angle between screw axis and grain direction, like shear around the outer screw diameter as well as rolling shear and tension perpendicular to the grain.

Extensive investigations on the withdrawal capacity of modern screws in softwood species were performed e.g. by Bejtka (2005), Blaß et al. (2006), Frese and Blaß (2009), Ringhofer et al. (2014) and Ringhofer (2017). Concerning hardwood species, Hübner et al. (2010) and Hübner (2013) carried out withdrawal tests of structural screws in European ash (*Fraxinus e.*), beech and black locust (*Robinia p.*) and found high withdrawal capacities for those species. So did Meyer (2016) in beech laminated veneer lumber (LVL) and confirmed the high performance of structural screws for beech LVL.

However, there is a lack of knowledge on the mechanical behaviour of structural screws in solid beech and beech glulam, especially concerning screws applied parallel to the grain. The knowledge gaps result from the large variety of parameters, which potentially influence the withdrawal strength of screws in timber.

In the first part of this work, the effects of testing time, insertion length and screw diameter on the withdrawal strength in grain direction are investigated using a single screw type. Further, possible influences on the withdrawal strength resulting from different screw types with varying thread and tip geometries are presented. The relation between withdrawal strength of screws applied in grain direction and shear strength of timber determined by EN 408:2012 is discussed. Required minimum spacing of screws to the edge and minimum spacing between two screws were examined in push-pull tests. Finally, the possibilities and limitations of end-grain connections using multiple axially loaded screws parallel to the grain in beech glulam are discussed. Different screw configurations were applied to optimize the load bearing capacity and to avoid splitting of the glulam members.

2 Materials and Methods

2.1 Materials

Beech boards from Central Germany were used for the production of all specimens. The boards originated from two collectives. Collective A consisted of slightly steamed beech boards of low and middle quality, which partly included numerous wood defects like knots and knot clusters, pith and bark inclusions. The beech boards of collective B were not steamed and of middle and high quality. For production of the

specimens, the MUF adhesive *Kauramin 683+688* of *BASF* was processed with a mixing ratio of 100:30 according to the manufacturers' specifications.

For all tests except the investigation concerning possible influences caused by different thread and tip geometries, the same screw *type1* was used. The self-drilling screw *type 1* is considered to be representative for common structural screws applied in timber construction. Table 1 shows mean geometrical characteristics of the applied screw types, which were provided by four different manufacturers.

Table 1. Geometrical characteristics of the screws applied in this study.

	Type 1	Type2	Type3	Type4	Type5	Type6
d_o	11.0/9.0/7.0	10.0	10.0	10.0	10.0	10.0
d_c	6.6/5.9/4.6	6.4	6.5	6.3	6.2	6.0
d_c/d_o	0.60/0.66/0.66	0.64	0.65	0.63	0.62	0.60
p	5.8/4.7/3.7	5.5	4.8	6.6	4.6	5.1
p/d_o	0.53/0.52/0.53	0.55	0.48	0.66	0.46	0.51
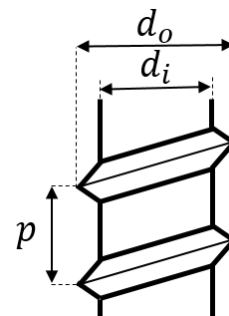
The geometrical characteristics are not taken from the manufacturer specifications but were determined on five measuring points of 10 randomly selected screws of each screw type.

2.2 Methods

2.2.1 Glulam members

All specimens consisted of four-layer beech glulam members with cross sections of 80x80 mm² and 110x80 mm², as described in Westermayr et al. (2018) plus some additionally produced screw withdrawal specimens. The four 20 mm thick lamellas within each glulam member were arranged according to their dynamic Modulus of Elasticity (dyn. MoE), which resulted in two different glulam built-ups. These two glulam built-ups, namely homogeneous and combined, are illustrated in Figure 1, showing the data of the glulam members for the end-grain connection specimens.
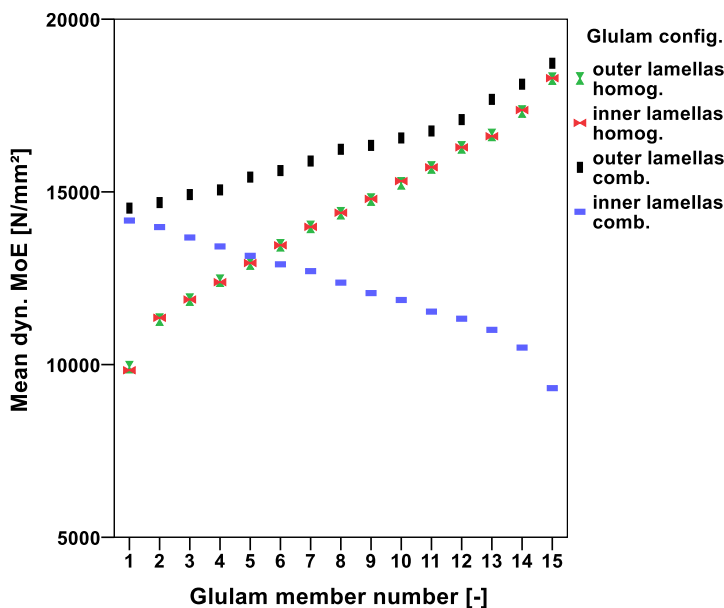

Figure 1. Mean dyn. MoE of inner/outer lamellas of the homogeneous/combined glulam members.

All four lamellas within one glulam member of the homogeneous built-ups had similar dyn. MoE, ranging from ~8.000 to ~18.000 N/mm². In contrast, the mean dyn. MoE of the two outer lamellas increased as the mean dyn. MoE of the two inner lamellas decreased regarding the combined built-ups. The subsequent process of specimen selection is illustrated in Figure 2.
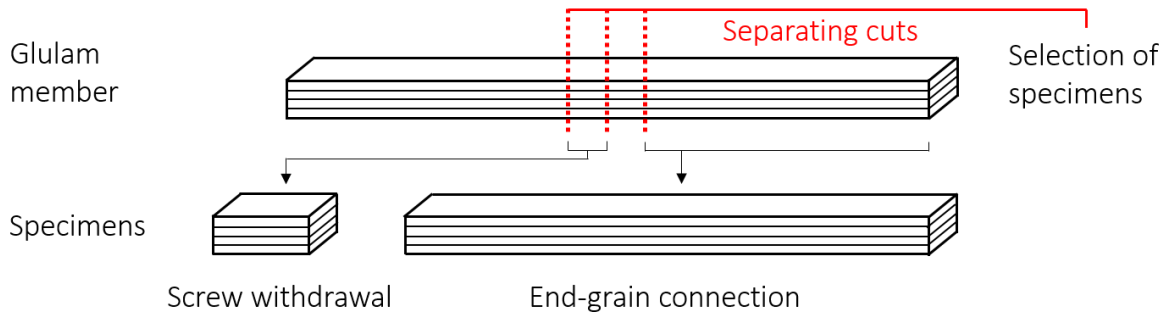

Figure 2. Selection and separation of specimens from the glulam members.

The 30 glulam members with lengths of ~3.100 mm were finally cut into screw withdrawal specimens as well as end-grain connection specimens. All specimens were stored in normal climate at 20 °C and 65 %rh before testing.

2.2.2 Screw withdrawal

The screw withdrawal specimens were not solely cut from the glulam members intended for the end-grain connection specimens as shown in figure 2, but additionally also from similar glulam members, which were produced for further examinations, like tensile testing (e.g. Westermayr et al., 2018).

As far as wood quality allowed, a maximum of six screw withdrawal specimens were cut from the same glulam member. Two of the six specimens were used for centric insertion of the screw in one of the two inner lamellas (red dots in figure 3, left) to examine the influences of d_o, the length of the threaded part of the screw penetrating the timber minus the tip l_{eff} and different screw types on the withdrawal capacity. This means each withdrawal test was performed into another lamella. The remaining four specimens per glulam member were divided in two specimens each for the examination of the influence of the testing time and for the examination of the tip influence. Each of the two varying parameters (testing time=60 or 240 s and tip=inside or outside specimen) were examined into the same lamella, as the red and green dots in figure 3 illustrate, performing the two tests immediately one after another to reduce effects related to varying timber properties.

As the number of specimens gained from the glulam members was not sufficient, some more additional screw withdrawal specimens were produced from the same material. Furthermore, three-layer specimens were produced using the same material but 40 mm thick lamellas for the examination of minimum spacing to the edge and between two screws. The specimens and their positioning of the screws on the cross section are illustrated in figure 3.
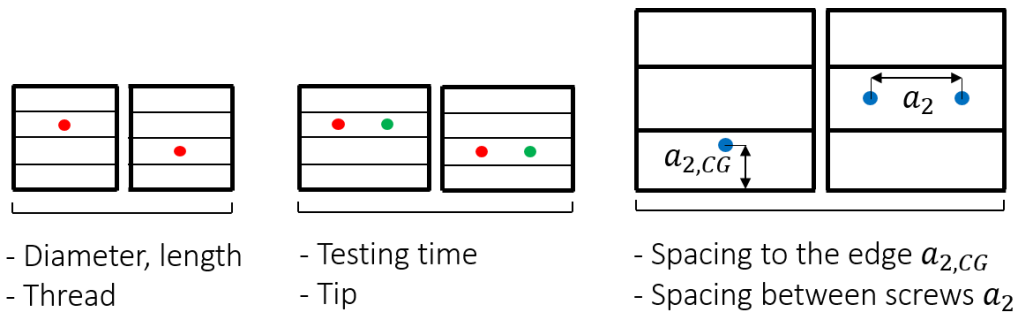
- Diameter, length
- Thread
- Testing time
- Tip
- Spacing to the edge $a_{2,CG}$
- Spacing between screws a_2

Figure 3. Positioning of the screws on the cross section for the different objectives of investigation.

All specimens were pre-drilled with d_c and 75 % of l_{nom}. The withdrawal load was determined in push-pull tests following EN 1382:2016. After testing, each specimen was sawed open along the screw channel in order to check for wood defects around the screw and to remove a piece directly beside the screw channel for the determination of density and moisture content according to EN 13183-1:2002. Density was adjusted to 12 % moisture content according to EN 384:2016. Withdrawal strength was calculated according to equation 1. (1)

$$f_{ax} = \frac{F_{max}}{d_o \times \pi \times l_{eff}}$$

2.2.3 End-grain connection

Two end-grain connection specimens were selected from each glulam member in a way, that the area of screw insertion was preferably free of obvious wood defects. The end-grain connection specimens had a length of ~1.200 mm, divided into 600 mm free testing length and 600 mm clamping length for the tensile testing device. All end-grain connection specimens were planed to the final cross section of 78x78 mm² immediately before drilling the lead-holes to ensure parallel surfaces and thus symmetrical screw spacing. Length of the lead-holes was 75 % of l_{eff}. The embedment length l_{emb} was drilled with $\boldsymbol{d_o}$ preventing the screw thread to penetrate into the timber. The positioning of the screws on the cross section and the fully assembled specimens' side view are shown in figure 4.
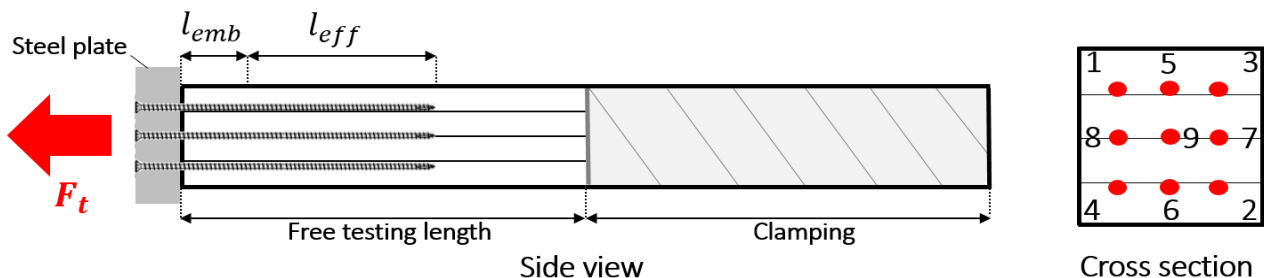

Figure 4. Side view of the end-grain connection specimen and screw positioning on the cross section.

In each end-grain connection specimen, nine screws *type1* with d_o=11 mm were inserted to mount a 50 mm thick steel plate, which induced the force in the subsequent tensile test. The spacing between the centerlines of the screws a_2 were

22 mm=2d, the spacing to the edge $a_{2,CG}$ were 17 mm~1.5d. The screws were tightened crosswise in the order as shown in figure 4 by applying a torque wrench in two steps with torques of initially 19 Nm and finally 23 Nm to ensure even fit of the screw heads onto the steel plate. The seven configurations given in table 2 were tested.

Table 2. Connection configurations and resulting configuration coding for the following analysis.

l_{emb}	l_{eff}	d_c	Config. Code	n	Glulam nr.
0	70	7	0_70_7	8	1,5,9,13
50	70	7	50_70_7	8	1,5,9,13
0	70	9	0_70_9	8	2,6,10,14
0+50	70	7	0+50_70_7	8	2,6,10,14
50	90	7	50_90_7	6	4,8,12
50	110	7	50_110_7	8	3,7,11,15
50	150	7	50_150_7	8	3,7,11,15

The center and corner screws number 1,2,3,4 and 9 (see figure 4) of configuration 0+50_70_7 were inserted with l_{emb}=50 mm and the screws number 5,6,7 and 8 with l_{emb}=0 mm. The column on the right in table 2 allocates the glulam member numbers given in figure 1 with the end-grain connection configurations. Thus it appears, that all connection configurations are evenly represented by the different glulam built-ups.

To avoid bending moments during testing, a hinge was mounted between specimen and load application. The load increased steadily over a period of 300 s ± 120 s until failure occurred. Density and moisture content of each specimen were determined on a cut piece of the full cross section around the screw tips directly after testing. Density was adjusted to 12 % moisture content according to EN 384:2016, moisture content was calculated according to EN 13183-1:2002. The withdrawal strength of the end-grain connection was calculated dividing equation (1) by nine.

3 Results and Discussion

3.1 Density and moisture content

The density distributions are given in figure 5. The overall mean density of all beech specimens was 737 kg/m³ with a COV of 3.9 %. The performed Kolmogorov-Smirnov test yields a normally distributed population. As it can be seen in figure 5 on the right, the densities in the different test subgroups are comparable with slightly higher densities of the spacing specimens and slightly lower densities of the end-grain connection specimens. Thus, no density correction of the withdrawal strength was conducted.
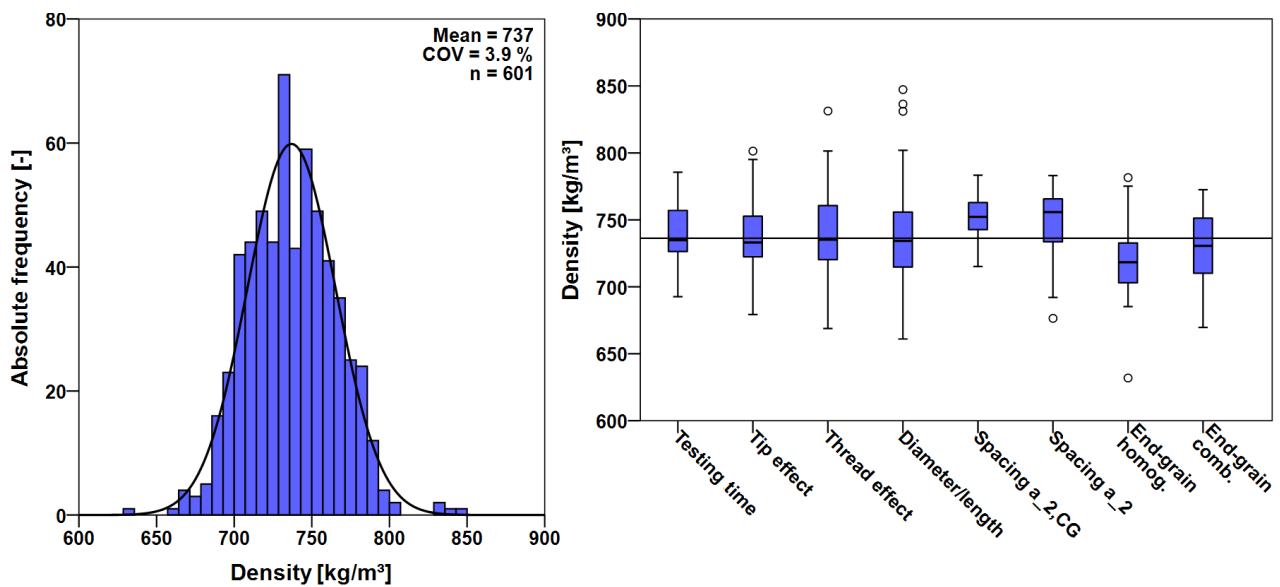
Figure 5. Density distribution of all specimens (left) and of the different test subgroups (right).

Mean moisture content of the material was 10.6 % with a COV of 10 %, showing an even distribution in all test subgroups. The withdrawal strength of specimens with moisture contents between 8 and 12 % (≙94.5 % of all specimens) were not adjusted, the remaining specimens with moisture contents above 12 % (≙5.5 % of all specimens) were adjusted with equation 2 according to Ringhofer et al. (2014).

$$(2)$$

$$f_{ax} = f_{ax,u} \times (1 - 0{,}036 \times (u - 12))$$

3.2 Withdrawal capacity of screws parallel to grain

3.2.1 Influence of testing time

To examine the influence of testing time on the withdrawal strength in beech timber parallel to the grain, screws of *type1* with d_o=11 mm were applied over a length of 90 mm. The results are given in figure 6 showing the single values and boxplots.
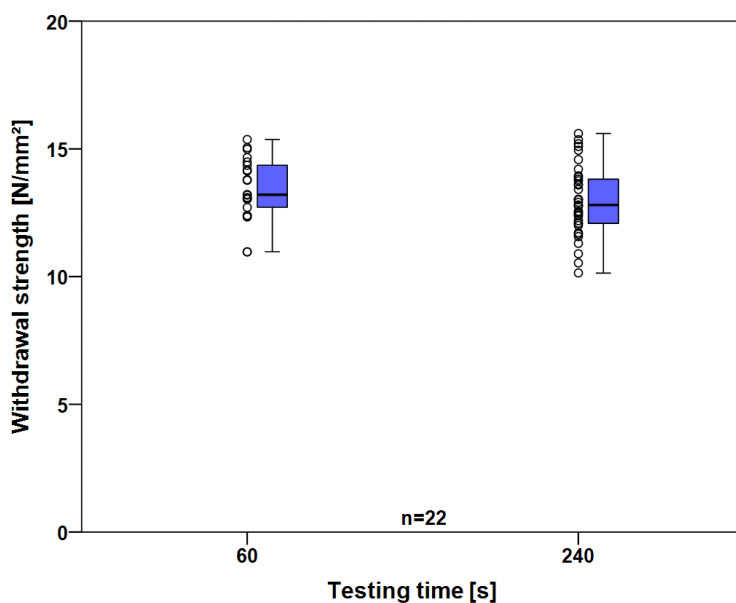
Figure 6. Withdrawal strengths of 22 specimens each tested within 60 s and 240 s.

The withdrawal tests were performed in a way, that F_{max} was reached initially within a testing time of ~60 s. Subsequently, the tests were repeated aiming to reach F_{max} within ~240 s. The mean values and COVs of both testing times are almost congruent with mean withdrawal strengths of 13.4 and 13.3 N/mm² for testing times of 60 and 240 s. A T-test confirmed, that no significant differences in withdrawal strength exist on mean level between the two different testing time groups, although scatter in the 240 s-group was slightly higher. This finding is in good accordance with Ringhofer (2017), who also found no significant impact of the testing time on the withdrawal strength for testing times between 45 and 450 s of screws applied 90° to grain direction in softwood.

3.2.2 Influence of screw type

This subchapter deals with the influences resulting from different tip and thread geometries on the withdrawal strength. The tested screws exhibited very different kinds of tips, as it can be seen in figure 7.
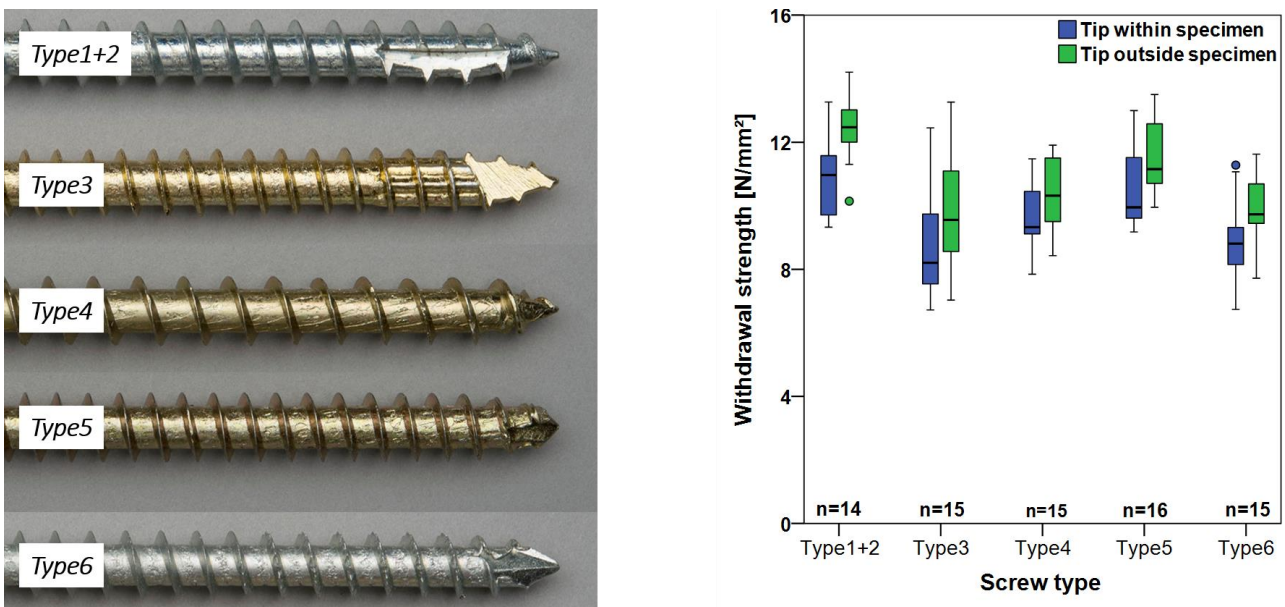
Figure 7. Tips of the screws tested in this study (left) and withdrawal strengths of the screw types depending on their tip placed within and outside the specimen (right).

The tips of screw *type1-4* were threaded, whereas screw *type5* had a drill and screw *type6* had a cut tip. The screws *type 1-3* had partial tips with an additional compactor regarding screw *type3*. The tip of screw *type 4* had a mating thread.

All screws were initially inserted over a length of 90 mm with their tips embedded into the timber and loaded until withdrawal failure occurred. Subsequently, the screws were removed and the specimens were cut to a length of 90 mm. Then, the screws were inserted again into the same lamellas in a way, that the tip protrudes the specimens. The resulting withdrawal strengths for the different screw types and the tips within and outside the specimens are shown in figure 7 on the right. Applying

equation 3, the tip influence x on the withdrawal strength is taken into account calculating the effective screw insertion length l_{eff} by adjusting the total screw insertion length l_{nom}.

$$(3)$$

$$l_{eff} = l_{nom} - xd$$

The following mean withdrawal strength values for specimens with embedded or external tip as well as the corresponding values for x are given in table 3.

Table 3. Withdrawal strength depending on screw tip embedded in specimens or not and x values.

Screw	$\overline{f_{ax}}$ tip embedded [N/mm²]	$\overline{f_{ax}}$ tip external [N/mm²]	Δf_{ax} [%]	x
Type1+2	11.0	12.4	11	0.94
Type 3	8.7	9.8	12	1.06
Type4	9.6	10.4	11	0.70
Type5	10.5	11.6	8	0.82
Type6	8.9	10.0	9	0.97
All types	9.7	10.8	**10**	**0.91**

For all screw types, withdrawal strength is around 10 % lower, when the tip is embedded into the timber, compared to the tip being outside of the specimen. The effect on the withdrawal strength caused by different tips is very similar concerning the different screw types. The calculated values for x range from 0.7 to 1.06, showing a mean value of 0.91 independent of the screw type. This implies subtracting one time d_o from l_{nom} allows a good estimation of l_{eff}.

Eckelman (1975) tested the withdrawal capacity perpendicular to the grain in different hardwoods and came to the same conclusion of subtracting $1d_o$ from l_{nom} to calculate l_{eff}. This approach is also status quo for the withdrawal design of screws 0° to grain direction in SIA 265:2012. For modern screws inserted parallel to the grain in Sitka spruce, Pirnbacher et al. (2009) determined a correction of l_{nom} with a x value of 1.21. Hübner (2013) found a value for x=1.19 for screws in ash applied 0° to grain direction. Both studies (Pirnbacher et al., 2009; Hübner, 2013) mentioned a slightly higher x value for screws inserted 0° to grain direction in contrast to 90° application.

Besides examining the effects resulting from the different screw types' tips, possible influences of the thread geometries on the withdrawal strength were analysed. To isolate possible thread effects on the withdrawal strength, the screw types 2-6 were tested as all of these screw types exhibited the same d_o=10 mm. Further, all tests in this chapter were performed with the same l_{nom}=90 mm and the withdrawal strength values were adjusted with the x values of each specific screw type to respect the different tip types. The resulting withdrawal strength values for each screw type are shown in form of scatter- and boxplots in figure 8.
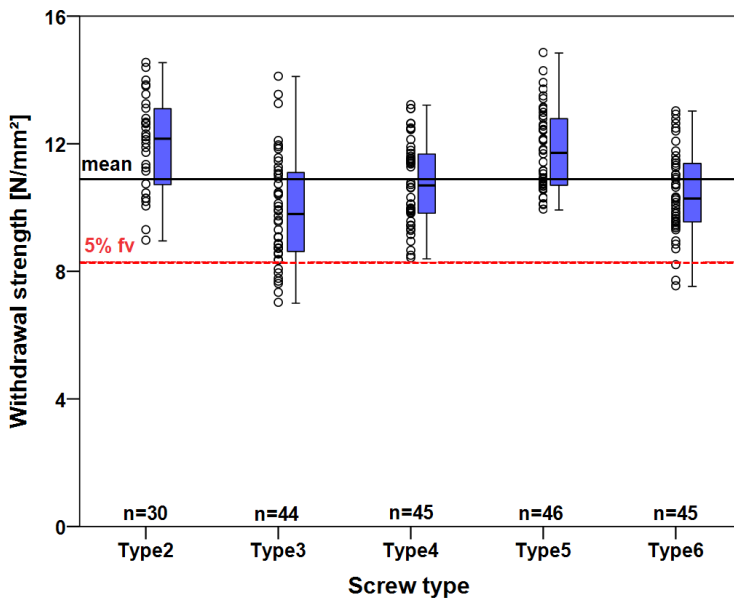
Figure 8. Withdrawal strength values of each screw type and overall mean/5% fractile values.

Mean withdrawal strength of the 210 tests was 10.9 N/mm² with a COV of 15 %. The variabilities within the different groups were on comparable level with COVs around 13 %. ANOVA analysis confirmed significant differences in the mean withdrawal strength values between the five different screw types, although specimen densities within the screw type groups were comparable. However, statistical tests yield three groups with similar withdrawal strength consisting of *type2+type5, type4+type6* and *type3.*

Analysing the thread characteristics d_c/d_o, p and p/d_o given in table 1 did not allow any relation between the mentioned geometrical thread properties and the withdrawal strength. For example, the mean withdrawal strength of *type3* screws was 16 % lower than the corresponding values of the *type5* screws, although the mentioned thread characteristics were almost congruent.

Apart from the thread characteristics given in table 1, it was especially noticeable, that the two screws *type3* and *6* with the lowest withdrawal strength values differentiated from the other screw types in terms of the shape of d_o. The flanks of screw *type3* were of the lowest sharpness with a small notch on d_o. The screw *type6* had a wave-shaped contour on the first ~50 mm of the thread. During the experiments, it was remarkable, that both screw *types3* and *6* showed a rather ductile behaviour in withdrawal after F_{max} was reached. In most cases, the screws *type3* and *6* did not fail brittle with an immediate break out of the timber surrounding the screw, but load decreased slowly after F_{max} over a long period of time. It is further assumed, that possibly the different tip characteristics led to varying withdrawal strength values by causing different degrees of initial damages during screw insertion process and/or during withdrawal loading. The compactor on the tip of screw *type3* as well as the wave-shaped contour on the first ~50 mm of the thread regarding screw *type6* (see figure 7) may additionally explain the lowest withdrawal strengths and the highest scatter of these two screw types. The higher density and more brittle behaviour of

the species beech may lead to higher affinity concerning crack initiation and thus greater differentiation in withdrawal strength for varying screw types, as for example Pirnbacher and Schickhofer (2007) found for six different screw types applied 0° to grain direction in softwood. Finally, the varying withdrawal strength values observed for the different screw types could not be explained entirely by the identified parameters of the screws and the wood material.

3.2.3 Influence of screw length and diameter

In most of the studies dealing with the withdrawal properties of contemporary screws types (Pirnbacher and Schickhofer, 2009; Hübner, 2013; Ringhofer, 2017), the effective screw insertion length l_{eff} is reported to not significantly influence the withdrawal strength, although the mentioned studies focused mainly on softwood and/or withdrawal perpendicular to the grain. To examine possible influences of l_{eff} on the withdrawal strength of parallel to grain applied screws in beech timber, tests with *type1* screws of d_o=9 and 11 mm were performed. For reasons of better transferability of the results, the slenderness $\lambda=\frac{l_{eff}}{d_o}$ is used in the following instead of l_{eff}.

It might seem, that the examined slenderness between ~2 and ~8 did not cover a wide range, but as screws parallel to grain in beech gain very high withdrawal strength, slenderness above λ=9 already mainly led to steel tensile failure of the screws. Figure 9 shows the tip corrected withdrawal strength values of both screw diameters with a detailed section of the slenderness between λ=3-8.

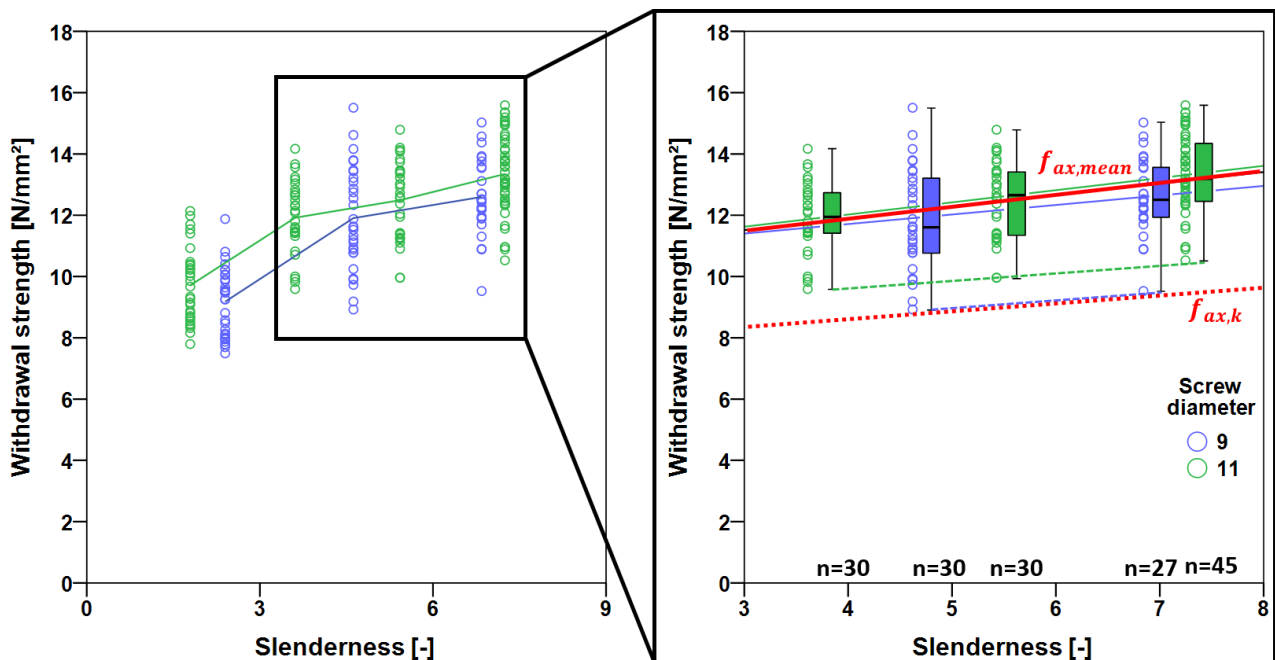Figure 9. Relation between withdrawal capacity and screws'slenderness.

For insertion lengths ~<3.5d_o, the withdrawal strength values are lower, than test data indicate for higher insertion lengths. Between slenderness of ~3.5 and ~7.5, a linear increase of the withdrawal strength can be observed regarding both screw diameters. The linear functions of mean and characteristic withdrawal strength values

of both screw diameters show similar slope and can be described by the following expressions: (4)

$$f_{ax,mean} = 10.35 + 0.39\lambda; \qquad f_{ax,k} = 8.44 + 0.23\lambda; \qquad \lambda = \frac{l_{eff}}{d_o}$$

In contrast to the results given in most literature, no influence of the screw diameter on the withdrawal strength was found for screws with d_o of 7, 9, 10 and 11 mm, which exhibited almost congruent withdrawal strength and scatter for the same l_{eff}.

3.2.4 Shear model

After reaching F_{max}, the withdrawal of an even wooden cylinder was observed around the outer thread flanks, as it can be seen in figure 10, left. This indicated a very local shear failure in longitudinal direction along the outer screw diameter. Figure 10 on the right compares the withdrawal strength values of screws inserted parallel to the grain in beech and ash with shear strength values in longitudinal direction (LR and LT) determined according to EN 408:2012 by Van de Kuilen et al. (2017). Concerning the withdrawal test data, results from specimens with d_o of 7, 9 and 11 mm and slenderness between 3.5 and 8 were considered to represent different screw insertion configurations. For both tests according to EN 408:2012 and EN 1382:2016, the same material was used as explained in chapter 2.1.
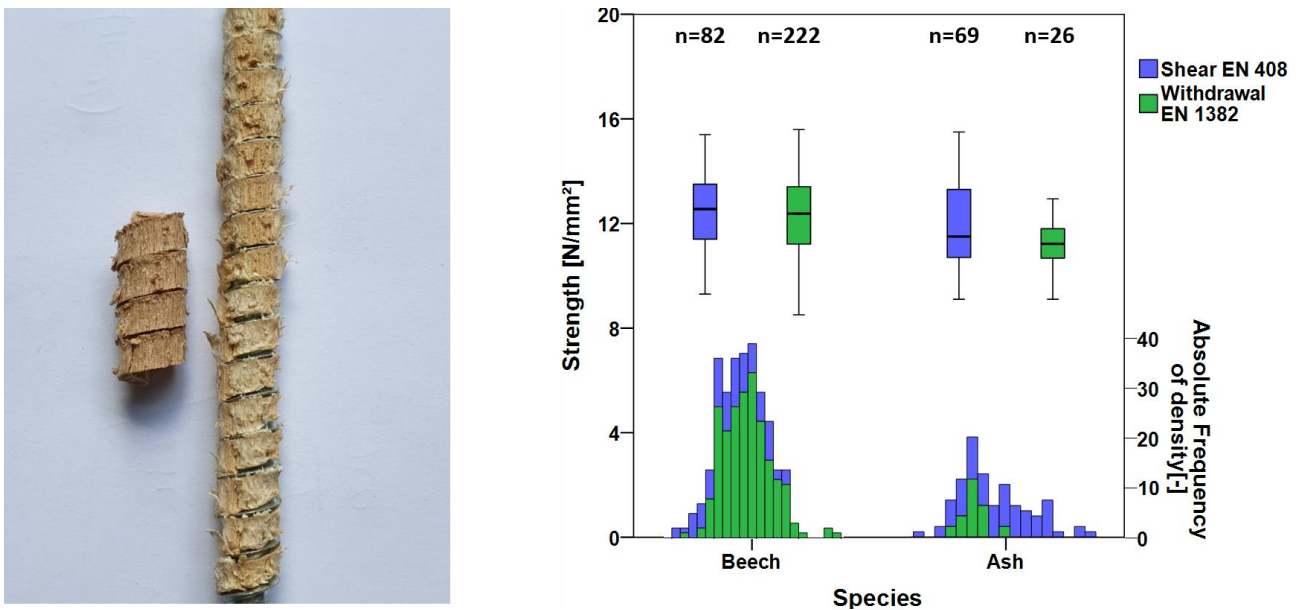
Figure 10. Shear cylinders along the outer screw diameter (left) and strength/denisty for beech and ash determined by shear test according to EN 408 and withdrawal test according to EN 1382 (right).

The density distributions are similar for both tests within each species, although the number of ash specimens tested in withdrawal was comparably low. It becomes obvious, that the mean strength values determined by withdrawal testing and by shear testing are almost congruent, leading to quotients for $\frac{f_{mean,EN408}}{f_{mean,EN1382}}$ of 1.02 (beech) and 1.06 (ash). Already Eckelman (1975) proposed the application of shear strength for

the prediction of the withdrawal of screws, which seems to be a good predictor for the withdrawal strength of parallel to grain applied screws.

3.3 Spacing

For the design of the end-grain connection with multiple screws, the required minimum spacing of screws to the edge $a_{2,CG}$ as well as spacing between screws a_2 were examined in push-pull tests applying screws with d_o=11 mm and l_{nom}=70 mm. The corresponding results are illustrated in figure 11.
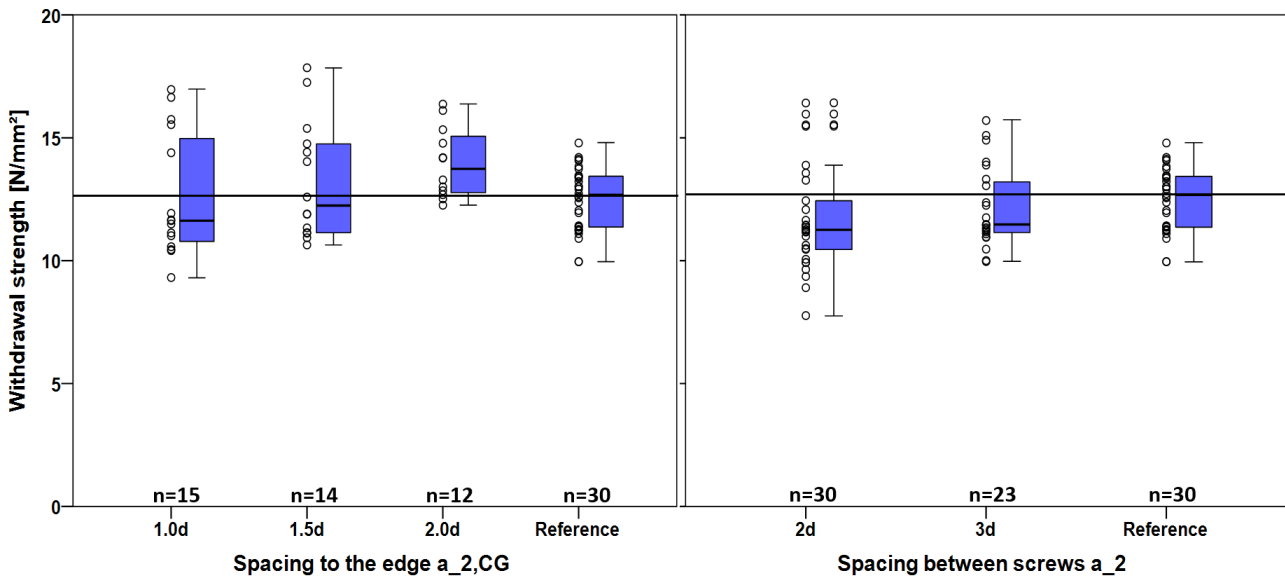
Figure 11. Withdrawal strength of screws for different edge spacing and spacing between screws.

The results are put into context with the "reference" withdrawal strength values of the same screw with d_o=11 mm and l_{nom}=70 mm, but placed in the centre of the specimens, where no effects from the edge were expected. As always two screws were tested examining the spacing between two screws, their withdrawal strength was calculated by dividing F_{max} by two to allow the relation to the reference.

In total, parallel to grain inserted screws in beech allow very low minimum spacing when it comes to short-term withdrawal loading, as the load transmission from the screw thread into the timber is mainly limited to a very local shear cylinder around the outer screw diameter. Low minimum spacing result in a higher variability of strength values, although mean withdrawal strength of the reference was reached with a minimum spacing of 1.0d for $a_{2,CG}$ and 3.0d for a_2. For minimum spacing $a_{2,CG}$≤1.5d and a_2=2d, radial cracks occurred mainly along the wood rays during screw insertion or during loading in ~40 % of the specimens, although these cracks often did not lead to significant decrease in withdrawal strength. With regard to long-term loading, higher minimum spacing may be crucial.

3.4 End-grain connection

As always nine screws were inserted per specimen in the seven end-grain connection configurations given in table 2. The F_{max} values of the end-grain connection specimens were divided by nine to allow a comparison with the reference. The reference

values consist of withdrawal strength values of the same screw insertion configuration determined on a single screw with d_o=11 mm and l_{nom}=70 mm. As the end-grain connection specimens with configuration 50_110_7 and 50_150_7 partly failed due to steel failure of the screws and not withdrawal, the strength values given in figure 12 are maximum shear stress values around the outer screw diameter instead of withdrawal strength values for the two mentioned configurations.

Config.	n	$\overline{f_{ax}}$ [N/mm²]	COV [%]
Reference	30	12.5	10
0_70_7	8	7.4	9
0_70_9	8	6.8	16
50_70_7	8	9.1	9
0+50_70_7	8	9.5	9
50_90_7	6	8.8	8
50_110_7	8	8.9	11
50_150_7	8	7.4	6
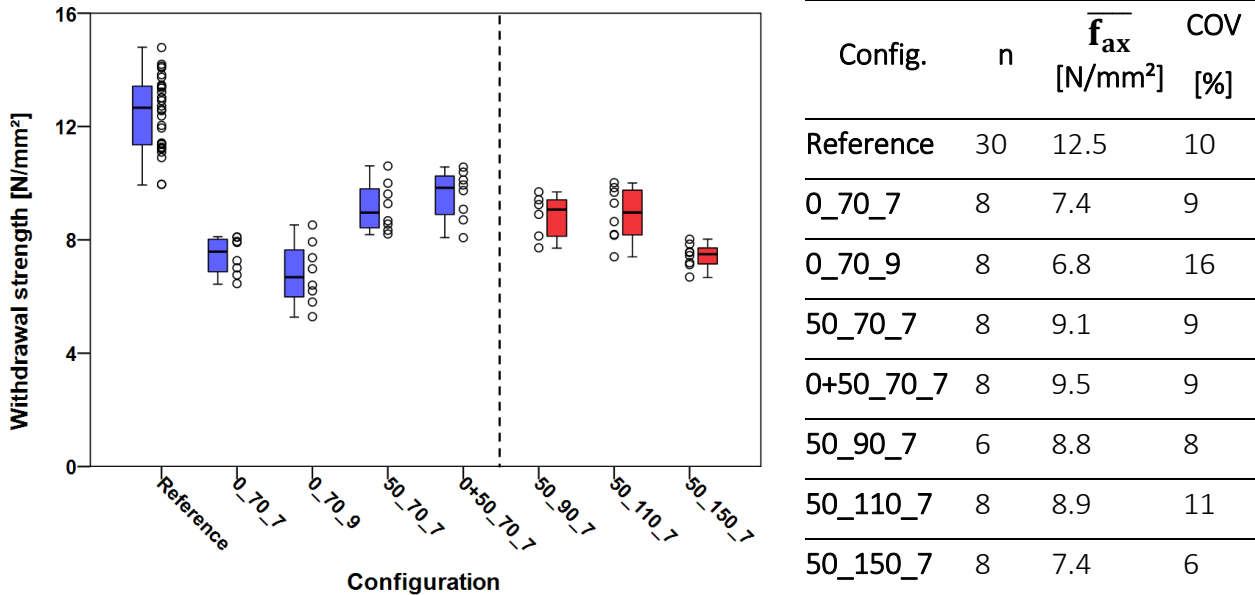
Figure 12. Withdrawal strength of the end-grain connection configurations and the reference.

The data on the left of the dashed line show approaches to increase withdrawal strength of the end-grain connection aiming to approximate the mean reference withdrawal strength of 12.5 N/mm².

Starting point is configuration 0_70_7, which is corresponding to the reference configuration. Configuration 0_70_7 exhibited in the mean 59 % of the reference withdrawal strength, showing numerous cracks between the single screws and towards the edges, as figure 13 illustrates. To reduce stresses perpendicular to the grain, the lead holes of configuration 0_70_9 were predrilled 2 mm wider than d_i =7 mm of the screw. This led to even lower f_{ax} and higher scatter with on average 54 % of the reference withdrawal strength. The application of l_{emb}=50 mm concerning configuration 50_70_7 and a depth decoupling of the screw threads regarding configuration 0+50_70_7 led to a similar increase in f_{ax} with 73 % and 76 % of the reference withdrawal strength. In none of the last mentioned configurations, cracking was observed any more.

Increasing l_{nom} to 90 mm and 110 mm led to constant f_{ax}, although two specimens of the configuration 50_110_7 already failed due to tensile failure of the screws. This explains also the decrease of f_{ax} for configuration 50_150_7, as steel tensile strength of the screws was limiting in all cases and thus no real withdrawal strength could be determined. Comparing the f_{ax} values of the configurations 50_70_7 and 50_90_7, where all screws failed in withdrawal, to the corresponding reference withdrawal strength values determined on single screws, a n_{ef} of ~0.7 was calculated.

Finally, figure 13 puts the load-bearing capacity of the connection in relation to the tensile strength of the homogeneous and combined beech glulam members described in Westermayr et al. (2018), which were produced of the same material. Their load-bearing capacity was calculated with the tensile strength data of Westermayr et al. (2018) and a cross section of 78x78 mm².
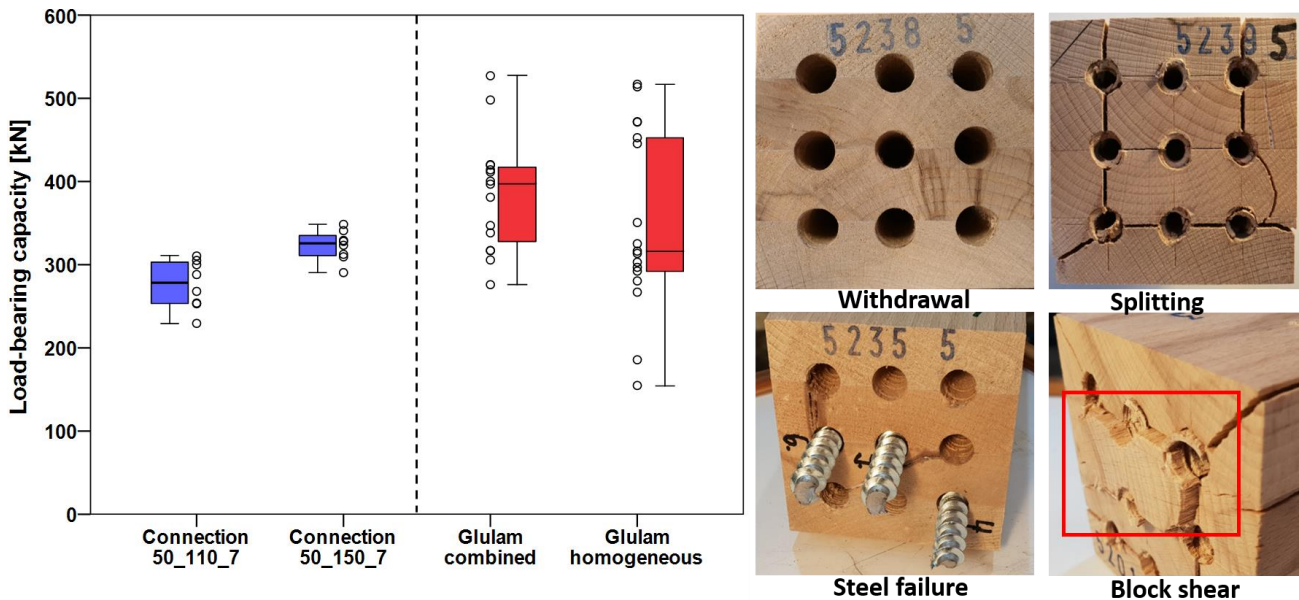
Figure 13. Tensile performance of the end-grain connection compared to the tensile load-bearing capacity of homogeneous and combined beech glulam members (left) and failure modes (right).

The end-grain connection with configuration 50_150_7 reaches around 88 % of the mean tensile load-bearing capacity of the homogeneous and 80 % of the combined glulam members. An even higher load-bearing capacity of the connection in comparison to the wooden cross section was observed on characteristic level. In summary, a good short-term performance of the connection was found in relation to the load-bearing capacity of the wooden cross section.

4 Conclusions and Outlook

Screw applied parallel to the grain in beech show high withdrawal strength. Different testing times of 60 and 240 s did not affect the withdrawal strength. The tip influence can be taken into account subtracting one time the screw outer diameter from the total screw insertion length. Different screw types showed slightly different withdrawal strength values, which may be a result of the threads' sharpness and drilling modifications of the screw tips. Increasing screw insertion length led to slightly increasing withdrawal strength, as screw diameter did not show any significant impact on withdrawal properties. Shear strength shows a good correlation with withdrawal strength parallel to the grain for beech and ash. Low required minimum spacing were found in push-pull tests, although there is a need of further investigation concerning crack initiation, as Blaß and Uibel (2009) performed. The end-grain connection

showed good performance with a load-bearing capacity, which almost exceeds the tensile load-bearing capacity of the wooden cross section of similar beech glulam members. Further investigations are necessary concerning crack initiation and propagation, especially under varying climate and long-term loading, although Mayr (2018) found good long-term performance of screws applied in beech parallel to the grain. A long-term test stand is initiated at TU Munich to determine long-term strength and creep of screws applied parallel to the grain in beech. Further, works on the stiffness of the end-grain connection are in progress.

5 Acknowledgements

6 References

Bejtka, I. (2005): Verstärkung von Bauteilen aus Holz mit Vollgewindeschrauben. In German. Karlsruher Berichte zum Ingenieurholzbau, Band 2. Universitätsverlag Karlsruhe, ISSN 1860-093X, ISBN 3-937300-54-6.

Blaß, H. J.; Bejtka, I.; Uibel, T. (2006): Tragfähigkeit von Verbindungen mit selbstbohrenden Holzschrauben mit Vollgewinde. In German. Karlsruher Berichte, Band 4. Universitätsverlag Karlsruhe, ISBN 3-86644-034-0.

Blaß, H. J.; Uibel, T. (2009): Spaltversagen von Holz in Verbindungen. Ein Rechenmodell für die Rissbildung beim Eindrehen von Holzschrauben. Karlsruher Berichte, Band 12. Universitätsverlag Karlsruhe, ISBN 978-3-86644-312-9.

Ehrhart, T.; Steiger, R.; Palma, P.; Frangi, A. (2018): Mechanical properties of European beech glued laminated timber. Conference paper 51-12-4, INTER-Meeting 5, Tallinn, Estonia.

Eckelman, C. A. (1975): Screwholding performance in hardwoods and particleboard. Forest Products Journal Vol.25, 6, p. 30-35.

Frese, M.; Blaß, H. J. (2009): Models for the calculation of the withdrawal capacity of self-tapping screws. Conference paper 42-7-3, CIB-Meeting 42, Dübendorf, Switzerland.

Frühwald, A., Ressel, J. B., Bernasconi, A. (2013): Hochwertiges Brettschichtholz aus Buchenholz. In German. Institut für Holzphysik und mechanische Technologie des Holzes, Bundesforschungsanstalt für Forst- und Holzwirtschaft, Hamburg, Germany.

Glos, P.; Denzler, J. K.; Linsenmann, P. (2004): Strength and stiffness behaviour of beech laminations for high strength glulam. Conference paper 37-6-3, CIB-Meeting 37, Edinburgh, Scotland.

Hübner, U.; Rasser, M.; Schickhofer G. (2010): Withdrawal capacity of screws in European ash (Fraxinus excelsior L.). Conference paper, 11. World Conference on Timber Engineering 2010, Riva del Garda, Italy.

Hübner, U. (2013): Withdrawal strength of self-tapping screws in hardwoods. Conference paper 46-7-4, CIB-Meeting 46, Vancouver, Canada.

Mayr, P. (2018): Einfluss konstanter Langzeitbeanspruchung auf die Tragfähigkeit selbstbohrender Holzschrauben appliziert in Faserrichtung in Fichte, Buche und BauBuche. Masters Thesis, Institute of Timber Engineering and Wood Technology, TU Graz.

Meyer, N. (2016): Zugbeanspruchte Verbindungen in Buchenfurnierschichtholz. In German. Conference paper, Karlsruher Tage 2016 – Holzbau. KIT Scientific Publishing, DOI 10.5445/KSP/1000058398.

Pirnbacher, G.; Schickhofer, G. (2007): Schrauben im Vergleich – eine empirische Betrachtung. Conference paper, 6.Grazer Holzbau-Fachtagung, Graz, Austria.

Pirnbacher, G.; Brandner, R.; Schickhofer, G. (2009): Base parameters of self-tapping screws. Conference paper 42-7-1, CIB-Meeting 42, Dübendorf, Switzerland.

Ringhofer, A.; Grabner, M.; Silva, C.; Branco, J.; Schickhofer, A. (2014): The influence of moisture content variation on the withdrawal capacity of self-tapping screws. Holztechnologie 55 3 p.33-40.

Ringhofer, A. (2017): Axially loaded self-tapping screws in solid timber and laminated timber products. Monographic series TU Graz, Timber Engineering & Technology, Volume 5, DOI 10.3217/978-3-85125-555-3.

Van de Kuilen, J. W.; Gard, W.; Ravenshorst, G.; Antonelli, V.; Kovryga, A. (2017): Shear strength values for soft- and hardwoods. Conference paper 50-6-1, INTER-Meeting 4, Kyoto, Japan.

Westermayr, M.; Stapel, P.; Van de Kuilen, J. W. (2018): Tensile and compression strength of small cross section beech (*Fagus s.*) glulam members. Conference paper 51-12-2, INTER-Meeting 5, Tallinn, Estonia.

EN 384:2016: Structural timber – Determination of characteristic values of mechanical properties and density. CEN.

EN 408:2012: Timber structures – Structural timber and glued laminated timber– Determination of some physical and mechanical properties. CEN.

EN 1382:2016: Timber structures – Test methods – Withdrawal capacity of timber fasteners. CEN.

EN 13183-1:2002: Moisture content of a piece of sawn timber - Part 1: Determination by oven dry method. CEN.

SIA 265:2012: Timber Structures. Swiss Standard. Schweizerischer Ingenieur- und Architektenverein.

Discussion

The paper was presented by M Westermayr

A Frangi asked whether you would get the same results from pull-push compared to pull-pull tests. M Westermayr agreed that pull-pull test results might be lower than pull-push tests. R Brandner said that results from TU Graz indicated that there was no difference in strength but there was a difference in the measured stiffness.

H Blass questioned whether one could get the same increase without considering unbonded length but just increase the inserted length of the screws. M Westermayr agreed but stated that the unbonded length consideration prevented splitting at the free surface and was the intention of this part of the investigation. R Brandner mentioned that even with unbonded length one would get splitting.

S Franke found similar influence when dealing with glued-in rods and asked whether they tried different unbonded lengths. M Westermayr said no only 50 mm was used successfully.

J Brown asked about the influence of unbonded length on post peak behavior and if an analytical model will be considered. M Westermayr said that this aspect has not been studied.

R Jockwer asked whether the consideration of unbonded length could lead to reduced fastener spacing. M Westermayr said that for practical purposes the spacing used in the study is already very small.

BJ Yeh received clarification that the use of unbonded length was not intended for natural checking.

A Ringhofer and M Westermayr discussed shear analogy issues, the shear area of the 8 mm diameter screws in comparison with the shear area of the parallel to grain shear tests and uniformity of the distribution of shear stresses along the length of the members.

Density variations in beech LVL: influence on insertion moment and withdrawal capacity of screws

Matthias Frese
Karlsruhe Institute of Technology, Timber Structures and Building Construction

1   Introduction

1.1   Motivation and objective

The manufacturing process of beech LVL panels causes panel to panel and inherent density variations. Unlike panel to panel variation, where the density changes from one panel to another, inherent variations arise perpendicular to the veneer layers in the cross-section of a single panel in a narrow area. If panels are processed to glulam-like products, inherent variations repeat in every lamination. Density variations in turn influence amongst others the insertion moment and the withdrawal capacity of self-tapping or self-drilling wood screws.

prEN 14592 provides EN 15737 for testing the insertion moment and EN 1382 for testing the withdrawal capacity. Both testing standards apply to engineered wood products too. In both of them, it is generally stipulated that the density of the provided specimens has to be representative for that of the material actually used. However, there is no further reference how to account for specific density variations in wood-based products as beech LVL launched in the market of building materials in 2014 (Hassan and Eisele 2015).

For that reason, the paper aims at looking into the correlation between such density variations in beech LVL and these parameters. In a broader sense, the findings may contribute to a more purposive and better application of the preceding testing standards in terms of both parameters and LVL-based products.

The results presented and discussed hereafter were gained in a research project on the development of self-drilling screws for high dense wood products (Frese and Blaß 2018).

1.2   Causes of density variations in beech LVL

In asking about the causes of density variations in beech LVL, one has to differentiate between panel to panel and inherent variations. A natural reason for both types of variations is the density variation of the beech wood itself or the veneers thereof. Further causes lie in the manufacturing process as illustrated in Fig. 1. In order to manufacture a beech LVL standard panel with a nominal thickness of 40 mm, 14 rotary peeled veneers are fed into a continuous hot press. Prior to the feeding, glue is applied on one of the adjacent veneer faces. At this stage of manufacture, the uncompressed stack is called veneer fan. The veneers are ideally 3.35 mm in thickness resulting in a 47 mm thick unit at the beginning of densification. The following densification process is accompanied by controlled heat supply and compression in radial direction (of the veneers) to achieve a 10% densification of the veneer fan and, finally, a constant panel thickness of 42 mm prior to sanding of both surfaces.

If the averaged thickness of all the veneers in the fan is significantly thinner than 3.35 mm, the fan is less densified compared to densification under ideal conditions. If it is significantly thicker, the fan is more densified. Such changes cause the density variations from panel to panel. This variation is hereafter referred to as V1. Maximum densification takes place at a certain combination of temperature and compression. However, since temperature is not constant both in thickness and manufacturing direction and since compression decreases in manufacturing direction, outer veneers are more strongly densified compared to inner ones. This effect is known as surface densification of wood as described for example by Tarkow and Seborg 1968, Sandberg et al. 2013 and Wang et al. 2018. As a consequence, the local density systematically varies along the thickness direction of the panel. The manufacturing process causes, therefore, higher local density in the outer layers than in the inner ones. This variation is hereafter referred to as V2. Such a variation is also known from particle board manufacture with continuous hot presses where maximum density is intended in the outer faces in order to improve the bending strength, cf. Soiné 1984 and 1986 and Krüzner 1985.
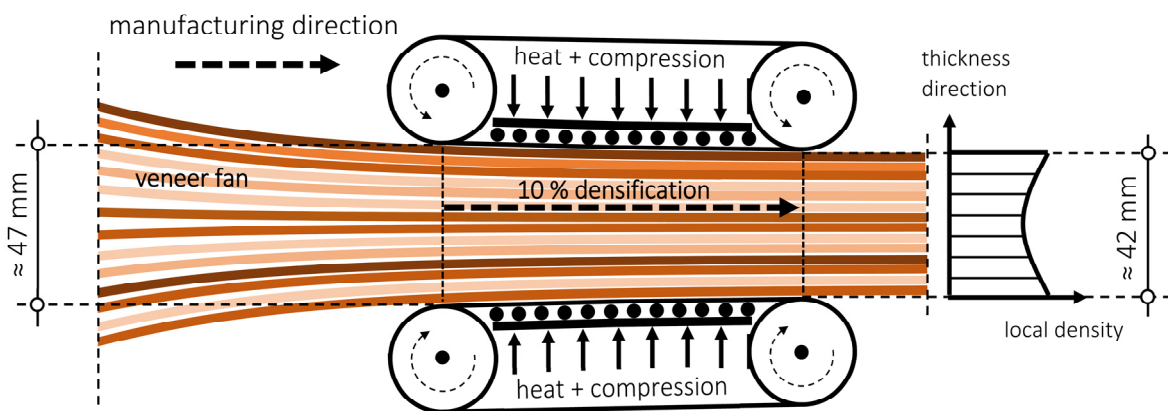

Figure 1. Simplified schematic of the manufacturing process: a veneer fan with glue in the relative interfaces is continuously moved in manufacturing direction under heat supply and compression.

It is to be expected that the density variations V1 and V2 influence mechanical resistances of the material. Depending on the location where a screw is inserted and depending on the direction of insertion one has to be aware of systematic differences in the values of insertion moment and withdrawal capacity of screws.

2 Material and methods

2.1 Preceding examination of the density variations

The density variations V1 and V2 were examined. In case of V1, the densities of 160 small cross-sectional slices were determined. The slices originated from different panels or spatially separated panel regions. Each slice was 40 mm thick and, therefore, encompassed 14 veneers. One half of these slices contained two cross layers and was 100 mm wide the other half had no cross layers and was quadratic. Examples of the slices are illustrated in Fig. 2 (top). The single values of the V1 specimens describe a density averaged over the nominal panel thickness $t_{\ell am}$ with 14 veneers. In case of V2, seven large cross-sectional slices as exemplified in Fig. 2 (bottom left) were sawn off from glulam-like beams (240 mm in depth) composed of six beech LVL laminations. These slices contained, therefore, five secondary glue lines. The laminations originated from panels with nominal thickness. The slices were separated parallel to the veneer layers into 24 times 6.8 mm thick stripes each (t_{stripe}) as illustrated in Fig. 2 (bottom right). During separation by sawing, the secondary glue lines were carefully preserved in the relative stripes. Afterwards their densities were determined. Hence, the values describe a local density which reflects an average over approximately 7 mm with 2-3 veneer layers.

density specimens for V1

≈ 40 mm

density specimens for V2
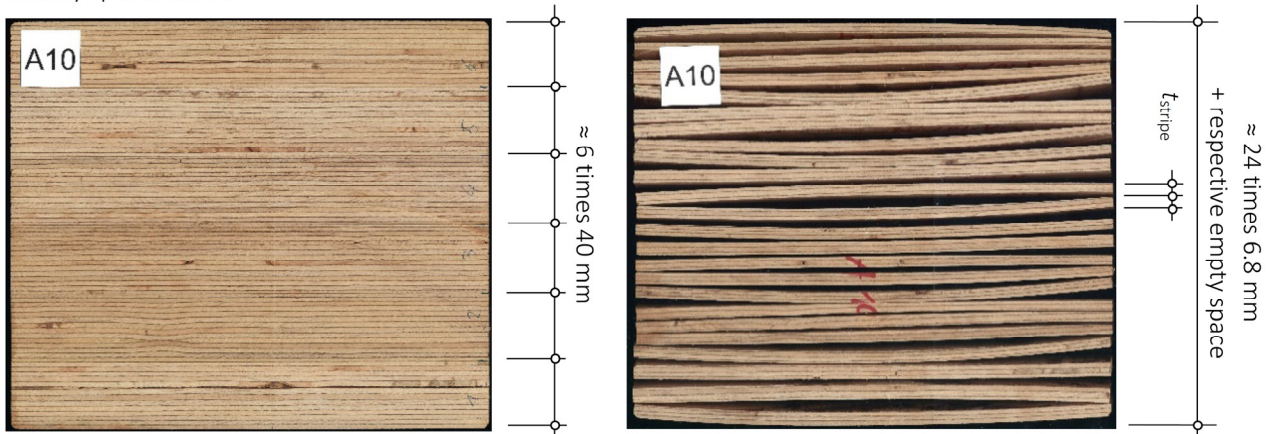
Figure 2. Two different small cross-sectional slices and slice cut from glulam-like beams and respective stripes for the density profile.

Fig. 3 shows the probability distributions of the values for V1 and V2. While means are almost similar (816/802=1,017), the COV and the span between minimum and maximum values increase with decreasing quantity of veneer layers in the respective unit. In Fig. 4, the local density values are plotted against the respective stripe number in ascending order. Hence, this representation exemplifies the density profiles perpendicular to the veneer layers or along the glulam beam depth of 240 mm for each of the seven slices. The connecting lines make clear that the typical density profile shown in Fig. 1 (right) actually repeat in every lamination.
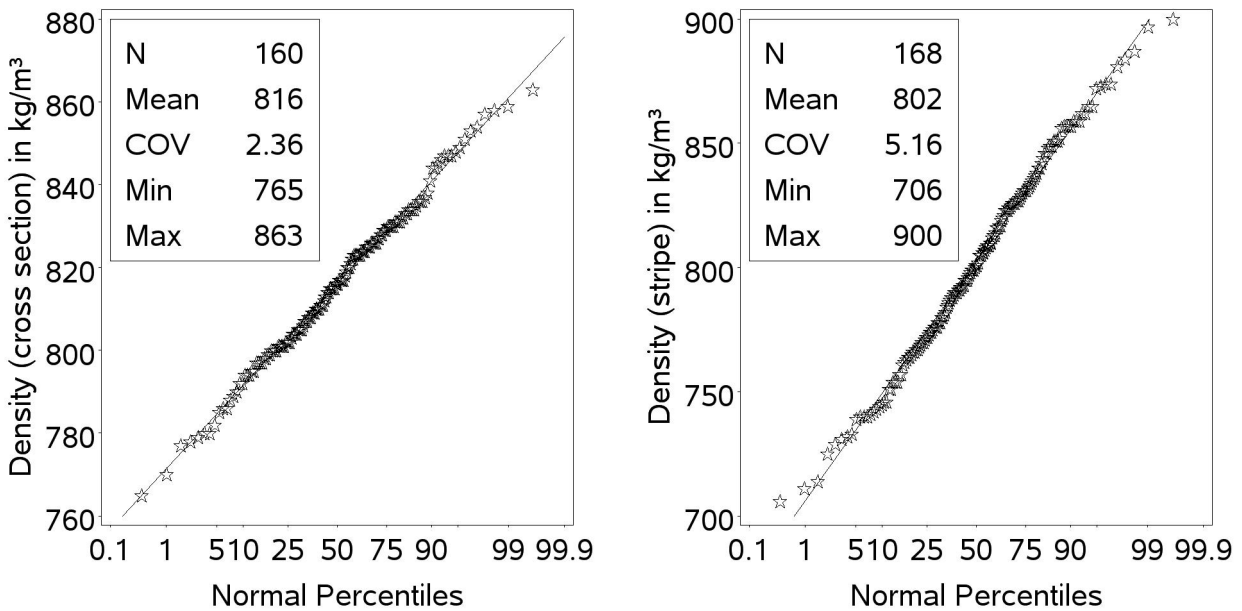
Figure 3. Density variation: panel to panel by small cross-sections (V1) and inherent by stripes (V2).
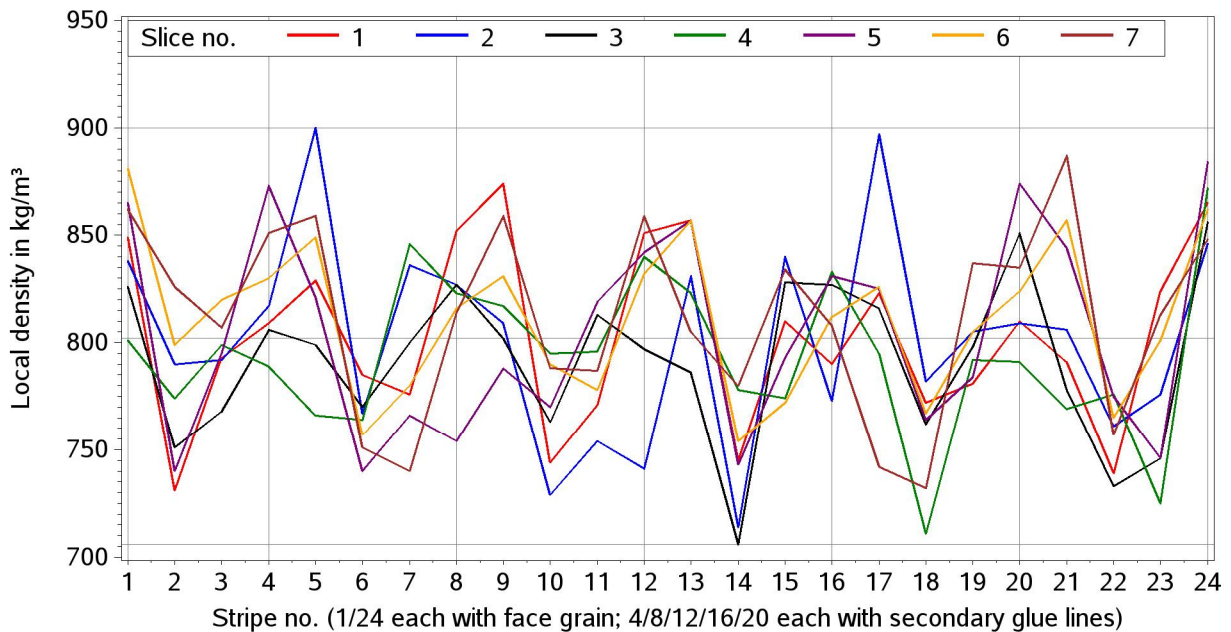
Figure 4. Density profile perpendicular to the veneer layers in glulam-like beech LVL.

2.2   Insertion tests

In total, 664 self-drilling screws (ASSY 3.0) were driven in beech LVL specimens while the torsional moment during insertion (torsional moment) was recorded. The experimental work was carried out by Stieger 2016. Table 1 contains the detailed information on nominal diameter (d) of the screws, their total length, thread length, tip shape and rough thread. The last two columns contain definitions of the examined global insertion directions and positions. In order to figure out any differences between the insertion moments related to the three possible global insertion directions (s. Fig. 5 left) extensive comparative tests were carried out with 7-mm screws. Additionally to that, differences were examined between insertion moments of the two global directions perpendicular to the face and edge grain with 5-mm and 10-mm screws. Using all the screw diameters, insertion tests with staggered positions in the edge grain (as illustrated in Fig. 5 right) were conducted. Thereby, the influence of the inherent density variation between the secondary glue lines were considered.

Table 1. Wood screws and test programme.

d	Screw length	Thread length	Tip shape	Rough thread	Global insertion direction	Staggered insertion in edge grain
mm	mm	mm				
5	120	60			face/ - /edge	yes
6	110	70			- / - /edge	yes
7	160	80			face/end/edge	yes
8	220	100			- / - /edge	yes
10	320	120			face/ - /edge	yes
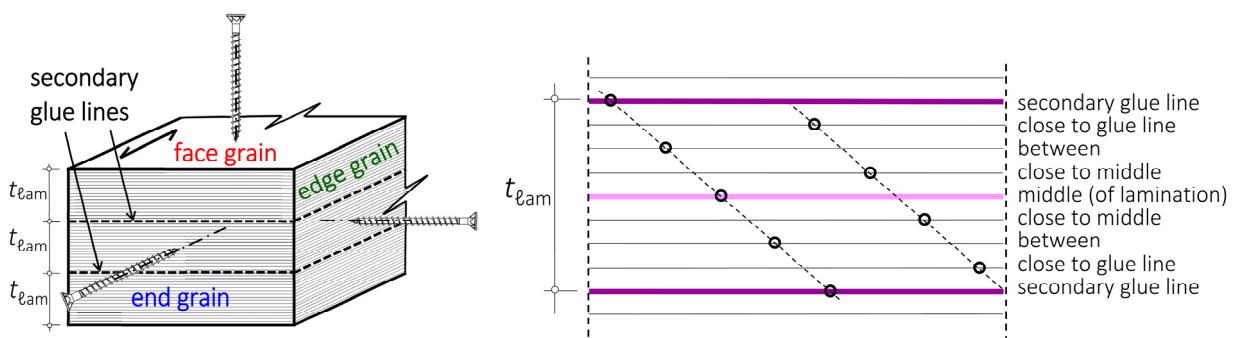
Figure 5. Global insertion directions and staggered insertion positions in the edge grain

2.3   Withdrawal tests

160 withdrawal tests were performed. The experimental work was carried out by Walter 2016. The nominal diameter (d) of the screws varied between 7.2 and 8.5 mm. The pitch and the ratio of core to nominal diameter were also varied. Prior to insertion of the screws, the specimens were predrilled with the core diameter. One half of the screws was inserted perpendicular to the face grain and the other half perpendicular to the

edge grain as illustrated in Fig. 6 on the left and right side, respectively. The penetration length was constant and corresponded to 40 mm. In the face grain, both higher and lower densified veneers proportionally contributed to the withdrawal capacity. In the edge grain, the position of the screw axis was exclusively in the middle of a lamination. Thus, their screw channel was in an area where the density of the veneers exhibits the lowest values. The withdrawal parameter (f_{ax}) was evaluated using the maximum testing load and the product of nominal diameter and penetration length.
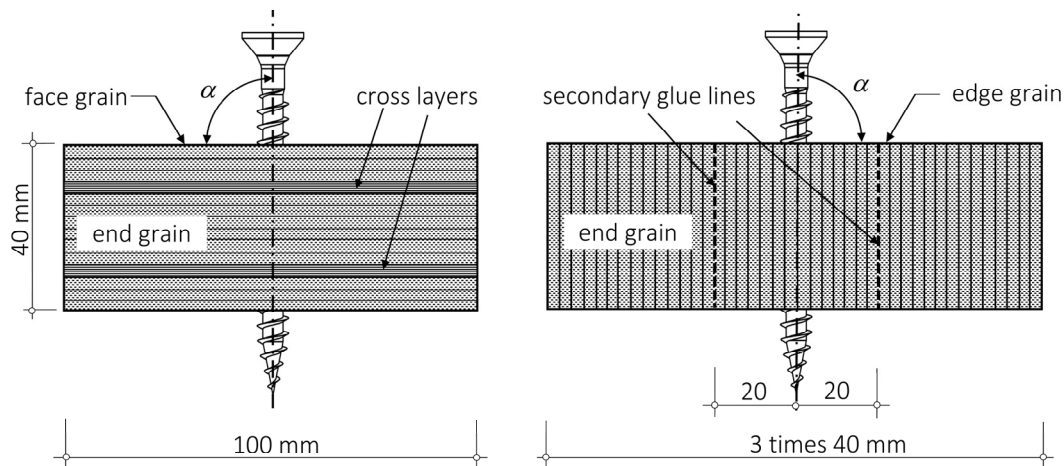
Figure 6. Specimens for the withdrawal tests.

3 Results

3.1   Insertion tests

Fig. 9 in the appendix is composed of three diagrams and shows the evaluation of 276 insertion tests with 7-mm screws. Since the insertion tests with these screws included all the three global directions, unlike the other diameters, this representation is taken as example for the subsequent explanations and information. The diagram at the top makes clear the span of torsional moments depending on the insertion depth and the global insertion direction. For each of the three global directions, the data of the respective curves were put together and were represented by a high low plot procedure where vertical lines show the span and the continuous lines the mean value. The diagram in the middle exemplifies the maximum torsional moments depending on the insertion depth and the global direction. The curves of the maximum torsional moments are not necessarily related to a single insertion test but represent an upper envelope curve. The diagram at the bottom describes the maximum torsional moments depending on insertion depth and the examined staggered positions in the edge grain. In detail, the diagram exemplifies the respective upper envelope curves which were obtained for the five different positions.

The respective diagrams for the screw diameters 5, 6, 8 and 10 mm are arranged according to the same structure as in Fig. 9. They are represented in the appendix in Fig. 7, 8, 10 and 11.

The insertion tests with 5-mm, 7-mm and 10-mm screws give evidence that the largest span of torsional moments arise in the edge grain and the lowest in the face grain. This is in particular evident by Fig. 9 and 11 (top). Furthermore, Fig. 9 (top) makes clear that the span of torsional moments in the end grain is larger than that in the face grain, but smaller than that in the edge grain.

Independently of the insertion depth, the maximum torsional moments develop in the edge grain. This is proved by the insertion tests with 5-mm, 7-mm and 10-mm screws as illustrated in Fig. 7, 9 and 11 (middle). The differences between the maximum values in the edge grain and those in the face and end grain are very pronounced (Fig. 9 middle). The evaluation in Table 2 (upper part) exemplifies these differences in numbers for 7-mm screws and the insertion depths 40 and 80 mm.

Screws systematically driven in the staggered positions in the edge grain exhibit their maximum torsional moments in the following positions: glue line, close to glue line and between. This applies for all examined diameters as illustrated in Fig. 7-11 (bottom). Thus, the torsional moments are correlated with the inherent density variation V2 to some extent. An evaluation in numbers is shown in Table 2 (lower part). Herein, the differences amount to more than 30%.

Since the respective rough threads become effective after an insertion depth deeper than the thread length, the curves show a steeper gradient after that depth. This is in particular evident for the 8-mm and 10-mm screws, see Fig. 10 and 11 (middle and bottom).

Table 2: Evaluation of maximum torsional moments for 7-mm screws

Direction/position	Depth in mm	$M_{t,max}$ in Nm		Depth in mm	$M_{t,max}$ in Nm	
⊥ face grain		9.04	(79%)		12.3	(77%)
⊥ end grain	40	8.46	(74%)	80	12.7	(79%)
⊥ edge grain		11.4	(100%)		16.0	(100%)
middle		8.70	(88%)		11.7	(83%)
close to middle		8.55	(86%)		12.0	(85%)
between	40	9.41	(95%)	80	12.6	(89%)
close to glue line		11.4	(115%)		16.0	(113%)
glue line		9.93	(100%)		14.1	(100%)

3.2 Withdrawal tests

There are significant differences between the withdrawal parameters which relate to the two insertion directions, cf. Table 3. In agreement with the correlation found between the torsional moments and faces, the lowest 5th percentile (37.2 N/mm²) was determined for the edge grain in the middle of a lamination. This value amounts to 80% of that found for the face grain (47.3 N/mm²).

Table 3: Statistics of results for withdrawal tests

| Withdrawal perp. to | N | f_{ax} in N/mm² | | | Density in kg/m³ | | |
		Mean	COV	5th P.	N	Mean	COV
face grain	77	55.4	8.29	47.3	80	819	25.2
edge grain, middle	77	43.3	9.26	37.2	80	813*	21.4

* Averaged over 14 veneer layers. The mean does, therefore, not reflect the local density directly around the screw channel.

4 Conclusions and consequences

Findings concerning density variations and consequences in terms of insertion and withdrawal tests are:

- The accuracy in describing density variations in beech LVL depends on the size of the unit used for the density determination. Outer layers in beech LVL panels exhibit the highest density (about 900 kg/m³), inner ones the lowest (about 700 kg/m³). This is in line with findings of surface densification in engineered wood products manufactured in continuous hot presses.

- In order to obtain the highest torsional moments in beech LVL, screws should be tested in or close to the secondary glue lines in the edge grain of glulam made of beech LVL. In case of new types of LVL products, all faces should be subject of the insertion tests and staggered insertion positions should be examined in the edge grain.

- Screw failure during insertion must not occur. Therefore, a comparison between the actual maximum torsional moments and the characteristic torsional strength may be used to adapt and improve the safety margin in terms of screw failure, cf. EN 14592. Unlike softwoods where high-dense knot clusters randomly occur, influences on the torsional moments in beech LVL and comparable LVL products made of other wood species are more predictable.

- The influence of the inherent density variation on the withdrawal capacity is comparable to that on the torsional moment. Assuming α = 90°, the lowest withdrawal capacities are to be expected in the middle of a lamination in the edge grain. Nevertheless, withdrawal tests should be performed in all relevant faces to figure out potential differences between the respective withdrawal parameter. It should be noted that locally slight splitting could also have had an influence on the lower withdrawal capacities of screws inserted in the middle of the lamination.

- Consequences of screw failure during insertion are seen to be critical, since screw failure means total loss of a screw. The withdrawal capacity of a screwed connection is usually based on more than two screws. Hence, a common withdrawal capacity in the edge grain is seen to be less sensitive to inherent density variations.

5 References

prEN 14592:2017 Timber structures - Dowel-type fasteners - Requirements

EN 15737:2009 Timber structures - Test methods - Torsional resistance of driving in screws

EN 1382:2016 Timber structures - Test methods - Withdrawal capacity of timber fasteners

Hassan J, Eisele M: BauBuche - Der nachhaltige Hochleistungswerkstoff. Bautechnik 92 (2015) 1, 40-45

Frese M, Blaß HJ: Entwicklung von selbstbohrenden Schrauben für Laubholz höherer Dichte. Schlussbericht für die Öffentlichkeit (FKZ 031A437J), KIT 2018

Tarkow H, Seborg R: Surface Densification Of Wood. Forest Products Journal 18 (1968) 9, 104-107

Sandberg D, Haller P, Navi P: Thermo-hydro and thermo-hydro-mechanical wood processing: An opportunity for future environmentally friendly wood products. Wood Material Science & Engineering 8 (2013) 1, 64-88

Wang J, Wang X, Zhan T, Zhang Y, Lv C, He Q, Fang L, Lu X: Preparation of hydro-thermal surface-densified plywood inspired by the stiffness difference in "sandwich structure" of wood. Construction and Building Materials 177 (2018) 83-90

Soiné, H: Kontinuierliche Preßverfahren in der Spanplattenindustrie - Bison Hydro-Dyn-Presse und Siempelkamp Stabteppich-Presse. Holz als Roh- und Werkstoff 42 (1984) 93-98

Soiné, H: ContiRoll-Doppelbandpresse zur kontinuierlichen Herstellung von Spanplatten. Holz als Roh- und Werkstoff 44 (1986) 371-378

Krüzner, M: Form- und Preßstraßen für Holzwerkstoffplatten - Das Band-Formstraßensystem und die kontinuierliche Contiroll Heißpresse. Holz als Roh- und Werkstoff 43 (1985) 379-402

Stieger J: Experimentelle Arbeiten, theoretische Untersuchungen und statistische Betrachtungen zur Entwicklung einer selbstbohrenden Hartholzschraube. Masterarbeit, KIT 2016 (unpublished)

Walter R: Analyse von unterschiedlichen Gewindeformen für selbstbohrende Hartholzschrauben. Bachelorarbeit, KIT 2016 (unpublished)

6 Appendix
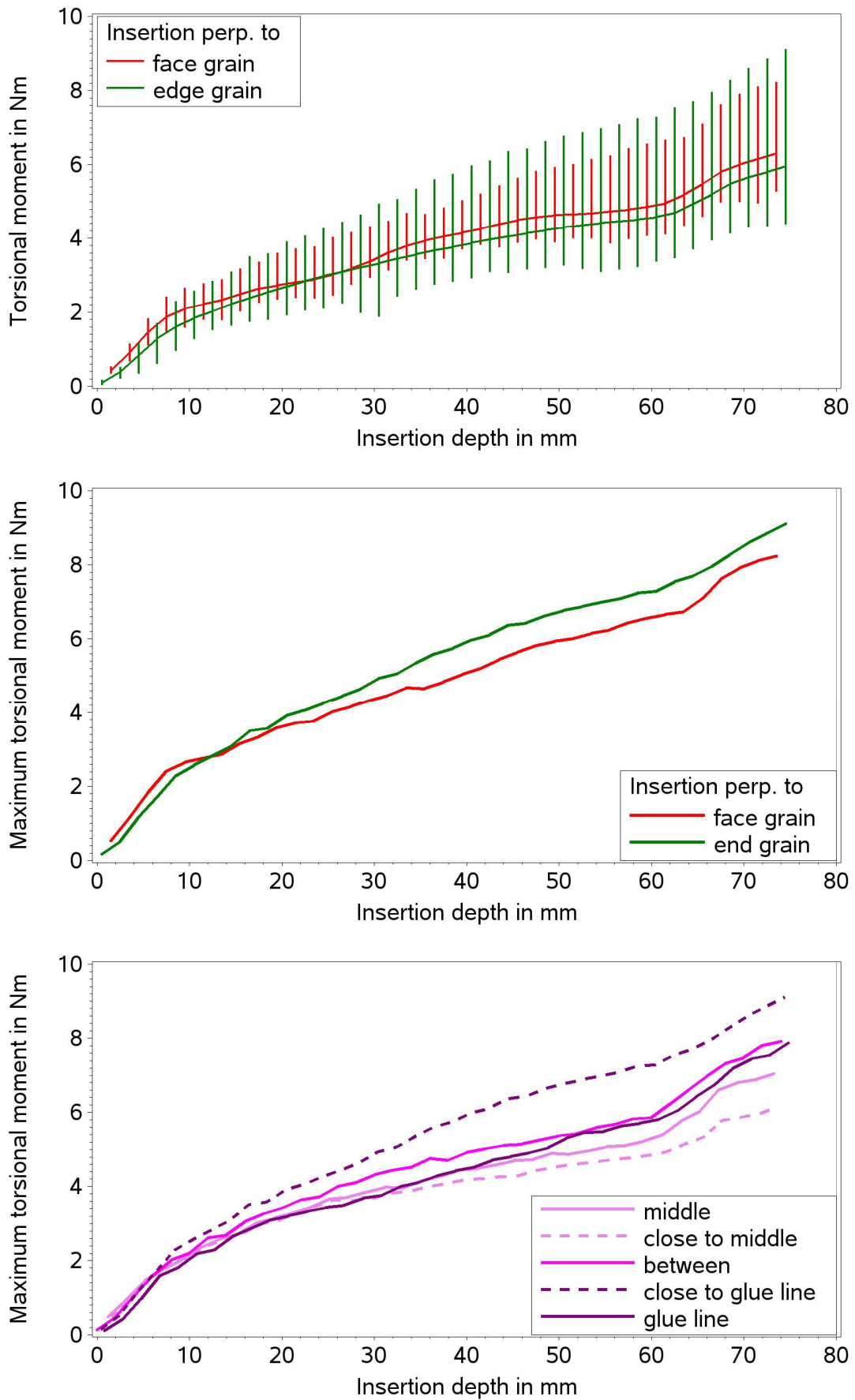
Figure 7. Results for 5-mm screws.
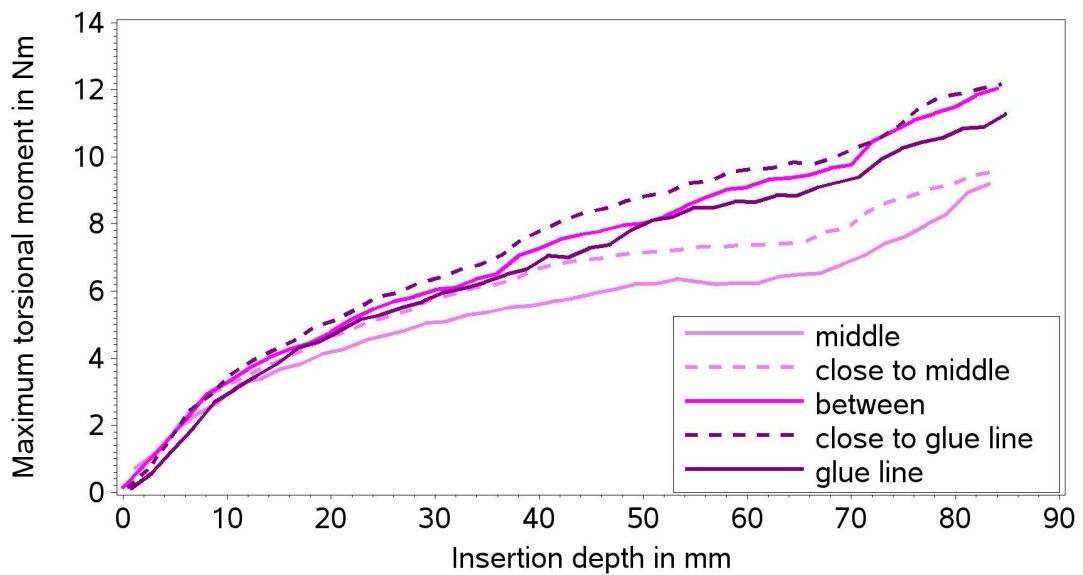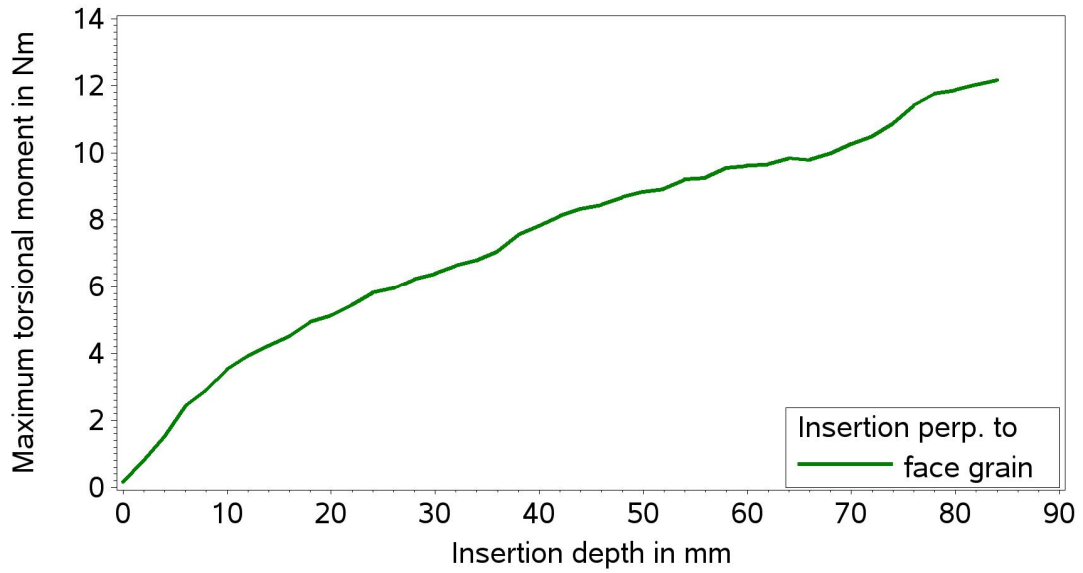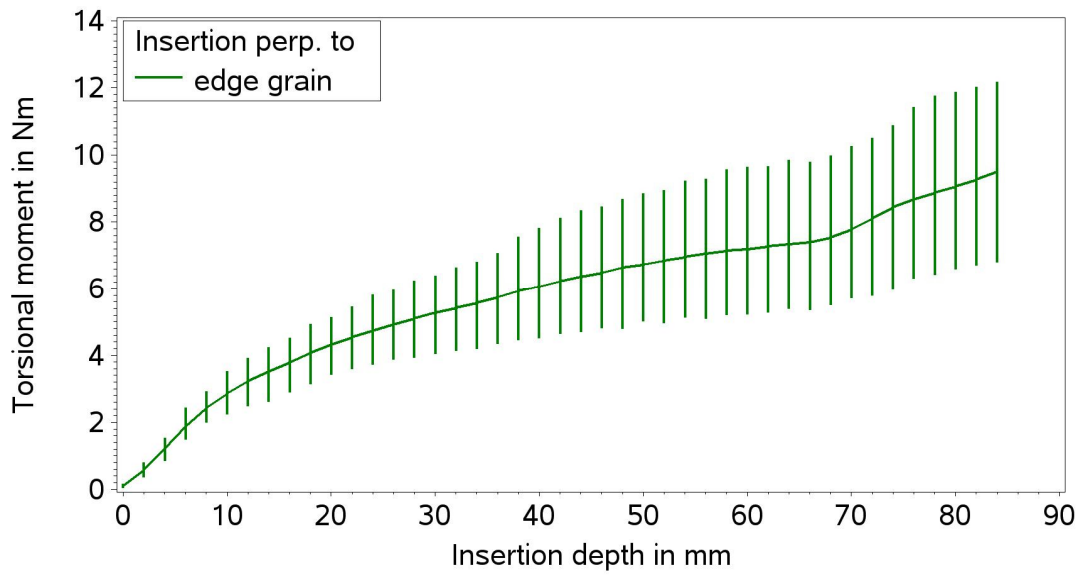
Figure 8. Results for 6-mm screws.
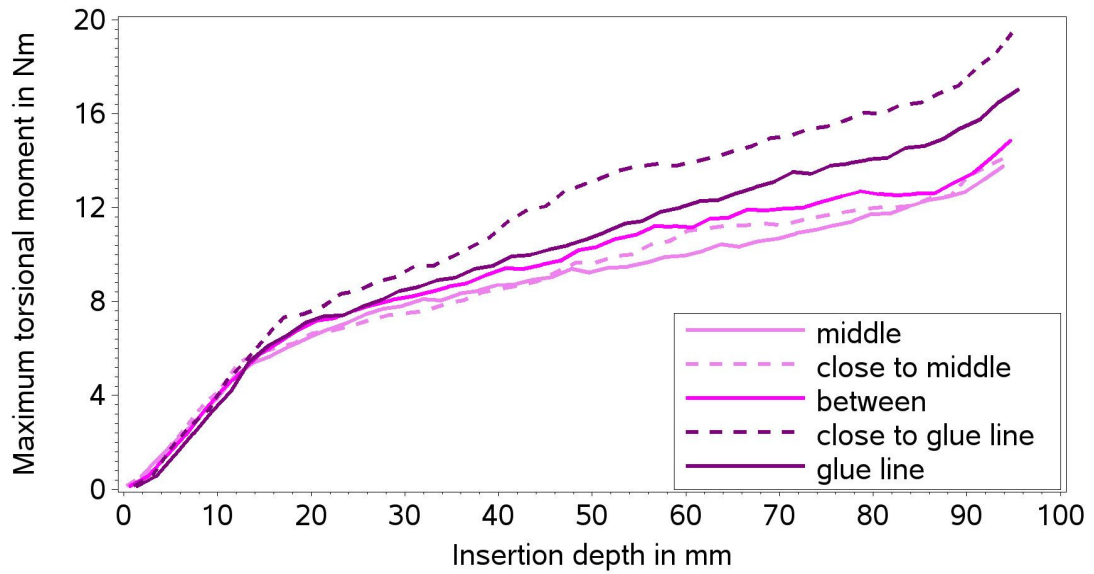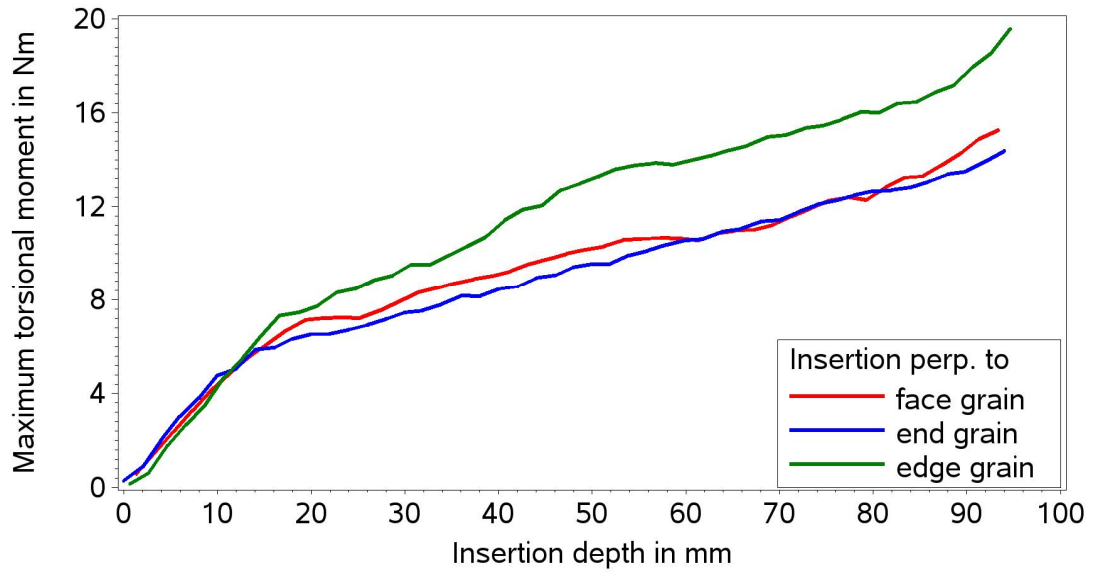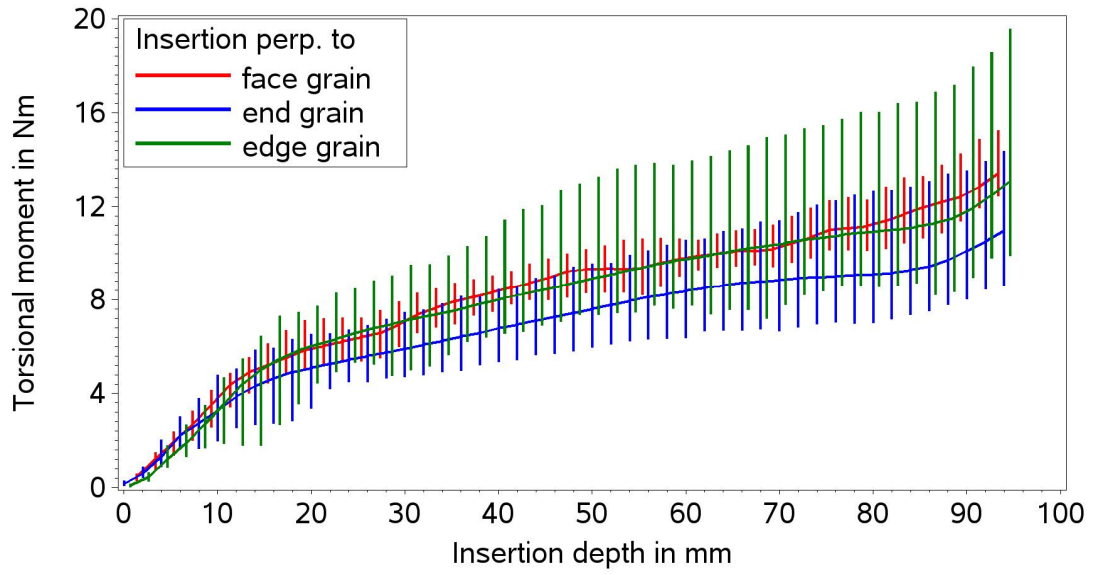
Figure 9. Results for 7-mm screws.
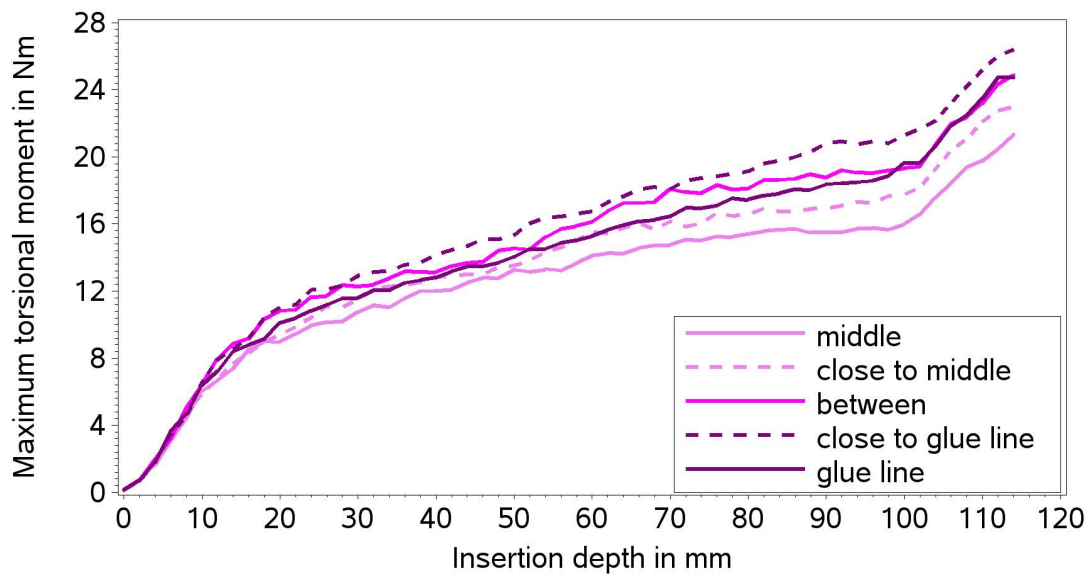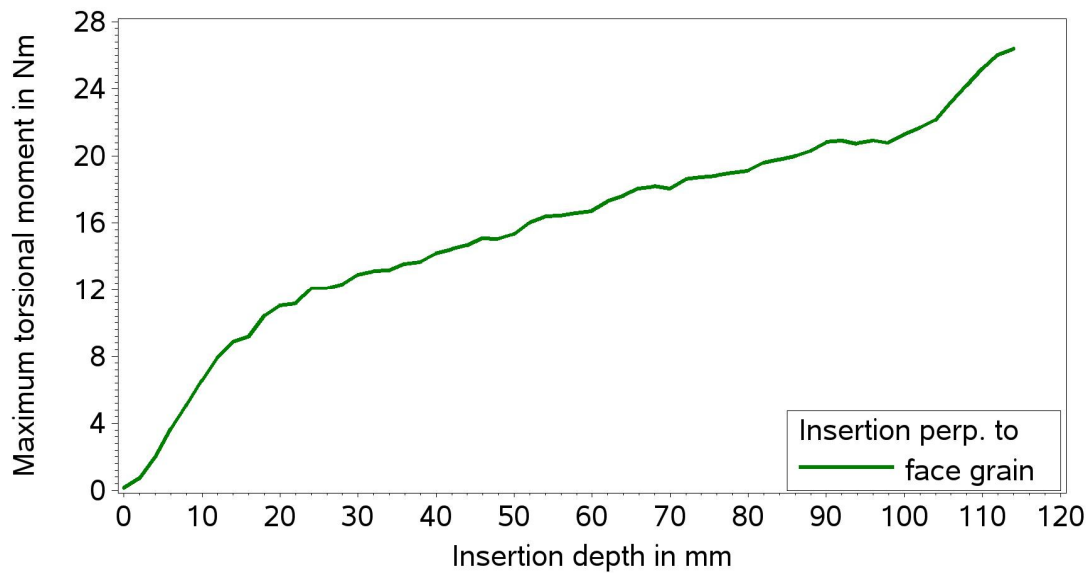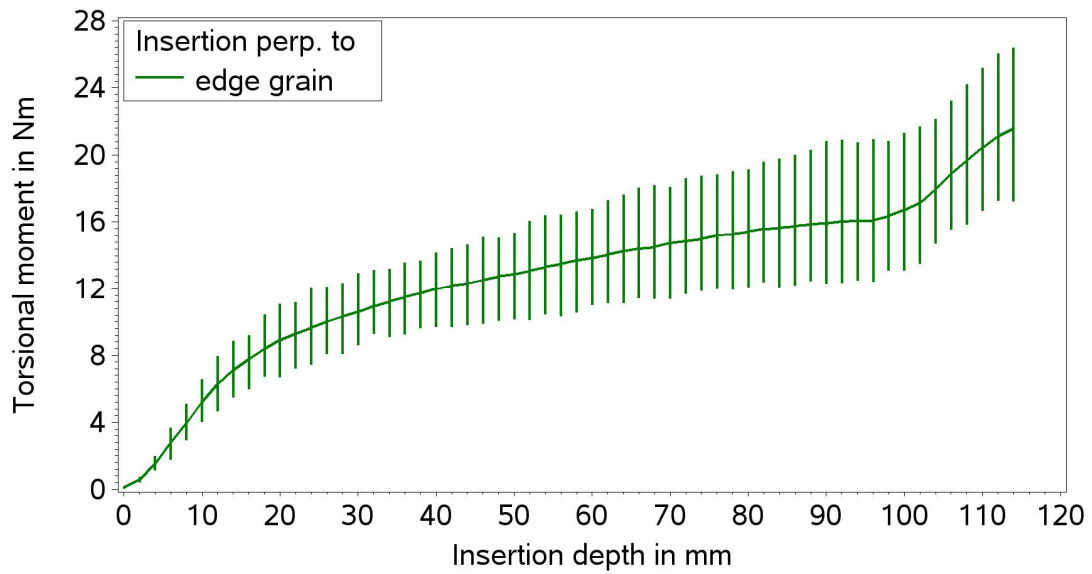
Figure 10. Results for 8-mm screws.
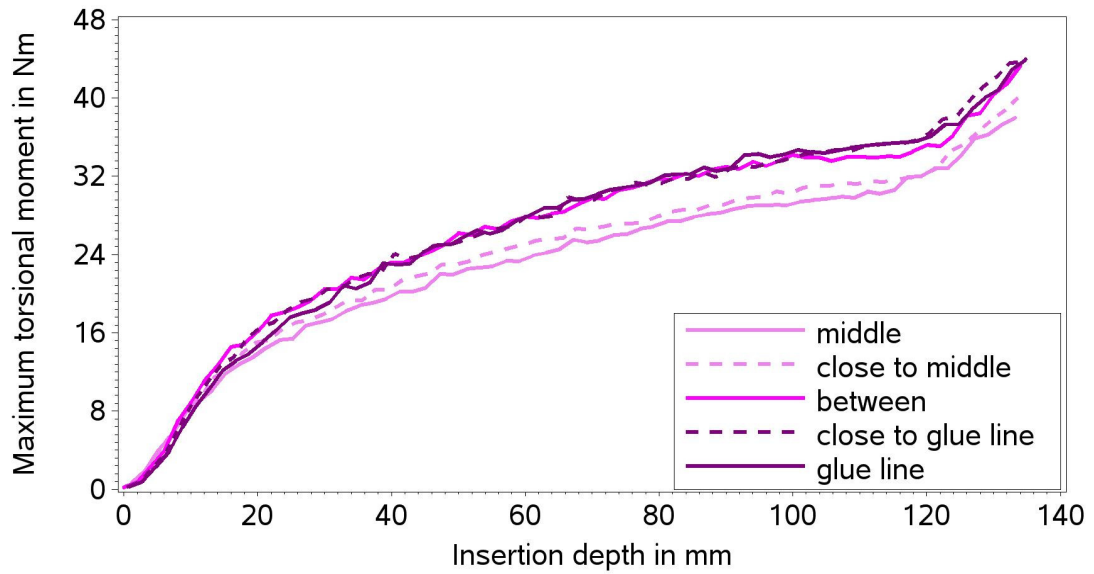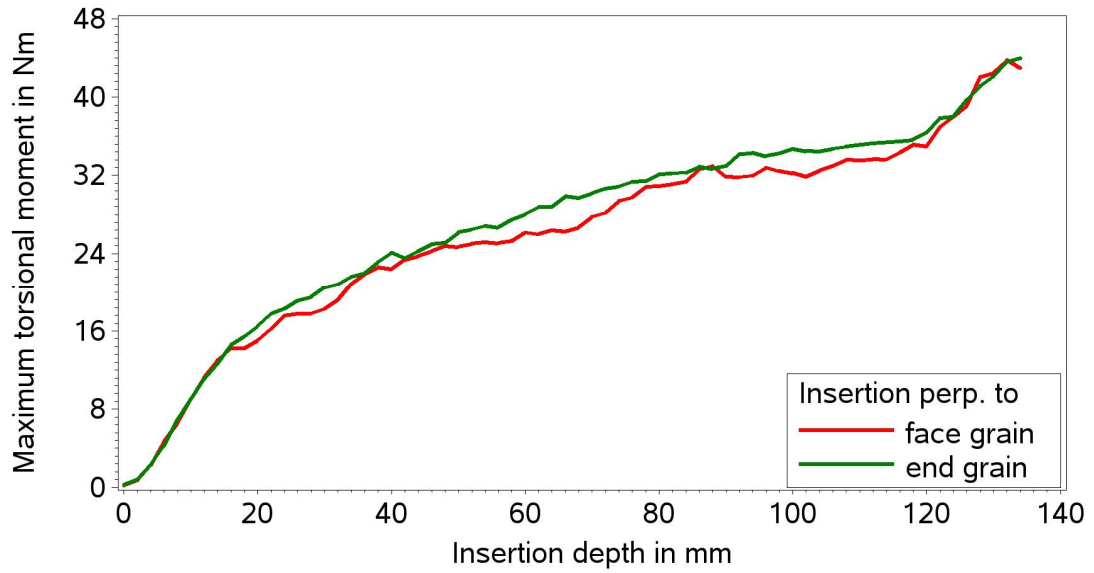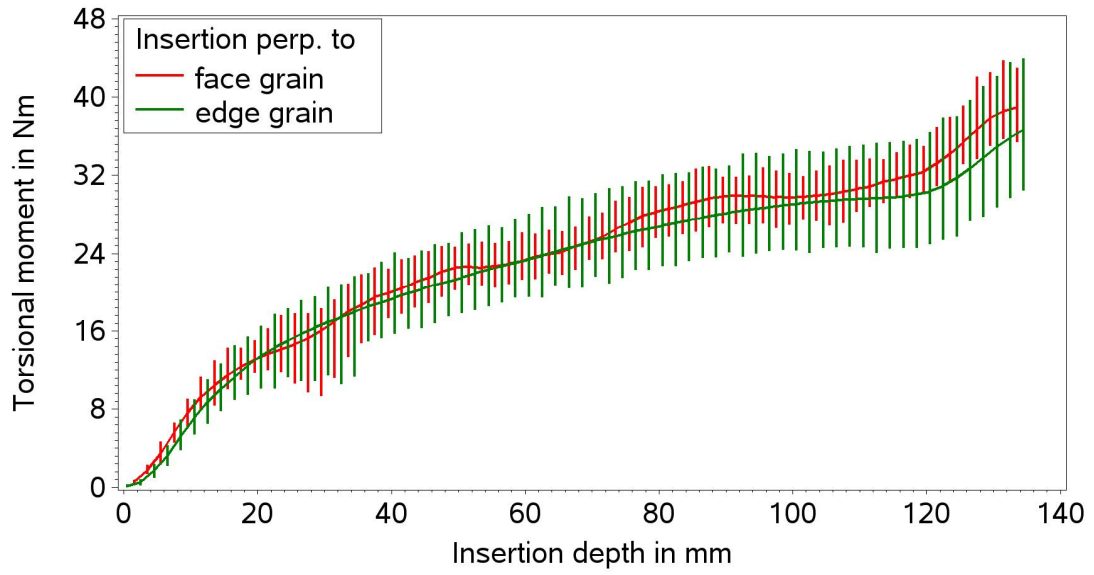
Figure 11. Results for 10-mm screws.

Discussion

The paper was presented by M Frese

F Lam asked whether the difference in the observed withdrawal capacities between face and edge applications would be due to differences in density only. M Frese responded that there could be other effects but density effects were important.   Natural material such as timber would also have issues with density variation from knots. M Frese also stated different approach could be used to consider different material.

R Brandner asked what about the different approach.   M Frese stated that mean value of the insertion moment could be considered. R Brandner said that such approach is already in use. M Frese said maximum values could also be considered when more data is available. R Brandner said that higher quantile would be more appropriate than maximum values.

S Franke asked about overlapping of veneer in production process that could increase the density. M Frese agreed but overlaps did not occur frequently and he did not specifically test their influence.

S Aicher questioned the large increase in torsional moment for depth greater than 80 mm. M Frese stated that after this depth rough thread would start to penetrate the wood causing the increase.

YH Chui commented that based on density one would expect 10% increase but the results indicated 20% increase. M Frese said that there are contributions from the glue also.

Steel dowel connections in beech hardwood

Steffen Franke, Bern University of Applied Sciences

Bettina Franke, Bern University of Applied Sciences

Keywords: hardwood, beech, connections, steel dowel type, design

1 Introduction

Discussion and ambition in Europe about the use of hardwood as construction material are currently present. In Switzerland, 31 % of the entire wood stock is hardwood, where the biggest part with 18 % counts for beech wood, (Eid. Forschungsanstalt für Wald 2018). On the one hand, hardwood provides excellent mechanical strength properties but on the other hand, the strength parameters are less investigated and standardized for the design of connections with mechanical fasteners. The current design equations are mainly developed and valid for softwood. Details and explanations for hardwood are missing. The performances of connections in modern hardwood timber constructions must be determined with high reliability. The behaviour of connections is exhaustively characterized by its stiffness and its capacity. The European Yield Model (EYM) is widely accepted and used in many standards for the calculation of the load-bearing capacities of dowel-type shear connections based on specific material properties and joint dimensions and layout. For hardwood connections, the research shows still open queries even if partly comprehensive investigations are carried out, e.g. Hübner et al. (2008), Gehri (2010), Hübner (2013), and Sandhaas et al. (2013).

The embedment strength is one key parameter in the design of connections. The European standard EN 1995-1-1:2004 (Eurocode 5, EC 5) provides values for embedment strength in dependency on the density, dowel diameter and load-to-grain angle. The empirical equations for embedment strength was proposed by Whale & Smith (1986) based on tests on softwood and tropical hardwood. Various researchers (e.g. Whale, Smith, Hilson (1987), Whale, Smith, Larsen (1987), Ehlbeck, Werner
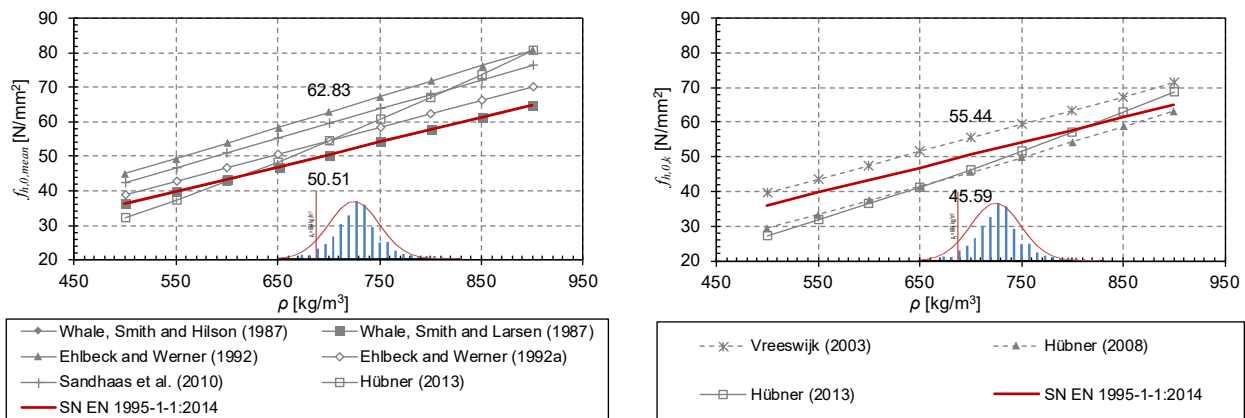
Figure 1 Embedment strengths for dowels parallel to the grain for hardwood as mean values $f_{h,0,mean}$ (left) and characteristic values $f_{h,0,k}$(right), including density of tests as distribution function

(1992a,b), Vreeswijk (2003), Hübner (2008 and 2013), Sandhaas et al. (2010)) investigated again the embedment strength for European hardwoods e.g. ash, beech or oak and derived further equations. The embedment strength between these equations shows a variation of about 12 MPa depending on the density and fastener diameter as shown in Figure 1. Some of the approaches are derived differently for the mean level and characteristic level. The values according to the standard are on the lower bound for the mean embedment strength and in the middle of the range of the characteristic values.

2   Experimental test program

2.1   Material

For both, assembling/insertion tests and load carrying capacity tests glulam of GL40h of European Beech (Fagus sylvatica) from Swiss forests with an average density of about 723 kg/m³ (CoV = 3.5%) was used. The characteristic density was calculated to 684 kg/m³. The specimens were climatized at 20 °C and 65% relative humidity prior testing which resulted in a moisture content of 9.5 M% (CoV = 10.3 M%). For the investigation of the influence of moisture changes some groups of the specimen have been dried to about 8 M% respectively moistened to 14 -15 M% as given in the specific chapters.

Standard galvanized steel dowels with diameters of 8, 10, 12 and 14 mm, ordered as grade S235JR, were used. The effective dowel mean tensile strength of $f_{u,mean} = 610 \text{ MPa}$ was determined in tests according to SN EN ISO 6892-1:2016 without section reduction.

2.2   Assembling of steel dowel type connections in beech wood

According to Eurocode 5, the holes for dowel fasteners in hardwood must be predrilled, but information about the predrilling diameter is not given. On the other hand, predrilling diameters slightly smaller than the nominal dowel diameter are being used for softwood, but in question for using in hardwood. Therefore, small test
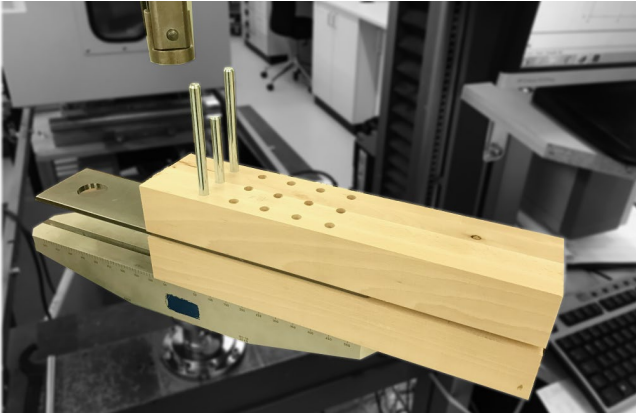
Figure 2 Test setup of double part specimens for connection with slotted in steel plates
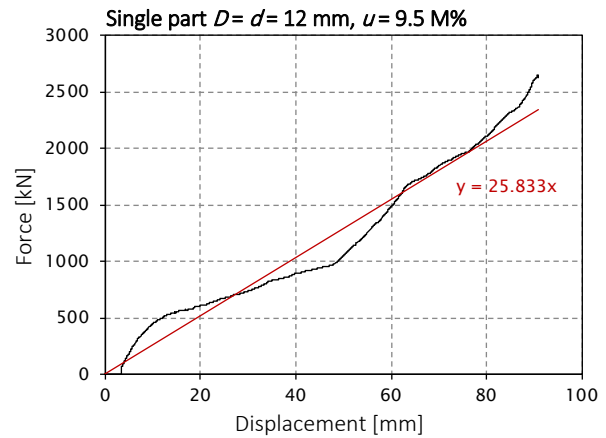
Figure 3 Load displacement curve for a single part specimen with regression line for analyses

series with single- and double-part specimens and different predrilling diameters were carried out firstly under practical conditions with manual insertion and secondly by using a testing machine to quantify the insertion force and for further evaluations of more diameters and moisture influences where specimens have been dried to 8 M% or moistened to 15 M% after assembling.

The manual insertion was carried out with a carpenter as specialist who inserted the dowels with common hand tools (hammer, axe) in a board of 80 mm thickness with predrilling diameters D of d - 0.1 mm to d + 0.6 mm in steps of 0.1 mm, where d is the nominal diameter of the dowel. According to the results of the manual investigations, further investigations and quantifications of the force needed for insertion by using a compression testing machine were carried out with the two predrilling diameters D of d (already strong) and d + 0.1 mm (practically good) for dowels with diameters of 8 and 12 mm. The predrilling diameters $D < d$ was characterised as too strong and $D \geq d$ + 0.2 mm as too loose (dowels are even falling through).

For the insertion force tests, single part specimens of 80 mm and double part specimens of 70 mm each (both separately drilled by CNC machines) with a steel plate in between representing a slotted in steel plate connection, Figure 2, were used. The steel dowels were inserted displacement controlled with a speed of 80 mm/min while the insertion force was measured and analysed by regression as shown in Figure 3 for easy of comparison and further analytical analyses.

2.3   Investigations of the load carrying capacity

The investigations on the load carrying capacity of steel dowel type connection in beech started with a principle connection - a double shear dowel connection with steel dowels of 8 mm diameter, one slotted in steel plate and a dowel layout of m x n = 2 x 3, as shown in Figure 4 and Figure 5. The tests are divided in smaller dimension tests for validation of single parameters and test with practical dimension for the validation of design concepts. Ductile failure with a ductility factor of at least 3 (according to SIA 265:2012) as yielding of the fasteners was aspired as this is one

requirement for high performing connection. For providing design parameters for hardwood, the testing program with dowels in beech glulam members carried out considers a variation of:

- load to grain angle (parallel and perpendicular to grain)

- fastener spacings and edge/end distances

- number of fasteners perpendicular and in load direction

- timber member thickness

- number of shear planes

- dowel diameter

- moisture influence

The complete and detailed test program is comprised in the research report, Franke et al. (2019). The tests were carried out according to EN 26891:1991 as symmetric pull-pull configuration for connection loaded parallel to grain and as back hold test for connections loaded perpendicular to grain, compare Figure 4 and Figure 5. Mostly five repetitions have been carried out per series (parameter). The load and relative deformation between the steel plate and the timber member in front of the first dowels was measured during the test.
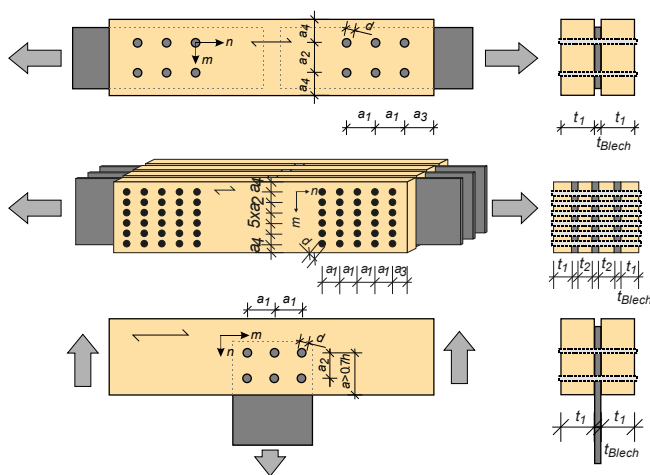
Figure 4 Principle sketch of test specimens including declaration of variables
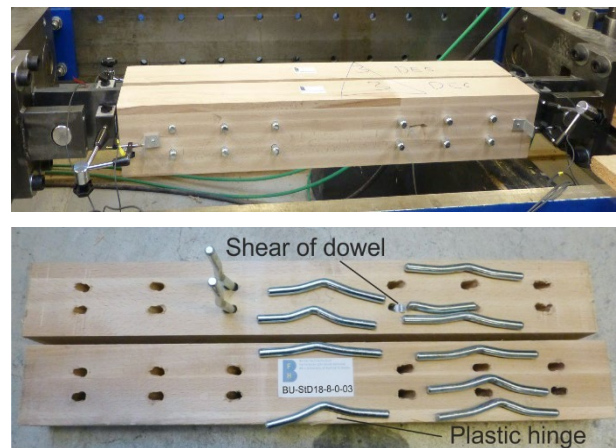
Figure 5 Test setup for connections loaded parallel to grain and perpendicular to grain

3   Discussion of experimental test results

3.1   Assembling of steel dowel type connections in beech wood

The characterization of the manual insertion of the steel dowels was obviously with criteria from too loose (for $D > d + 0.1$ mm) up to too strong or even not possible (for $D \leq d$) by the practical experiences of the specialist. Crack initiations were not observed in all insertion cases. For all insertion tests using a mechanical testing machine; a relatively linear increase in force over the specimen thickness/penetration depth
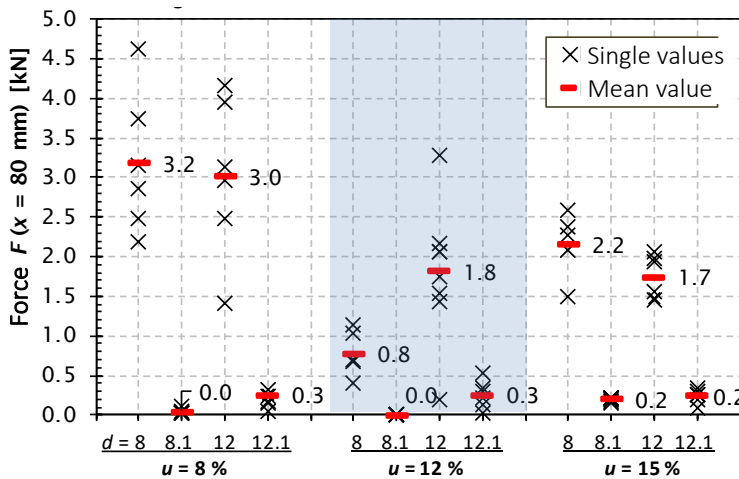
Figure 6 Analyses of the insertion forces depending on the diameter and moisture content given for an insertion depth of 80 mm

could be observed, as seen in Figure 3. The smaller the predrilling hole diameter, the greater the forces and the variation of the force, see Figure 6. Insertion forces of 0.8 and 1.8 kN are determined without impact of moisture content for pre-drilling with the nominal diameter and member thickness of 80 mm. Insertion forces up to 3.0 kN are observed for the lower moisture content of 8 M%. For pre-drilling with $d +$ 0.1 mm, maximum forces of 0.3 kN are achieved regardless of the moisture change.

The insertion forces observed confirm the in practice instinctively determined assessments "too loose" ($d + 0.2$ mm), "good" ($d + 0.1$ mm) and "too strong" ($d + 0.0$ mm). The predrilling diameter which require too much effort, may already lead to early damage and/or preventing the mounting on site. For practical use, a difference of 0.1 mm between dowel diameter and borehole is recommended for dowel joints in hardwood. This can be done by an additional pulling the dowel from the factory or an adjustment of the drill diameter.

3.2   Load carrying capacity

The tests performed in general ductile where mostly two plastic hinges per shear plane were reached, as shown in Figure 5. Steel dowel shear failure was even observed as well. The tests were analysed according to EN 26891:1991. The load capacities in the diagrams are given as per fastener per steel plate (including two shear planes) without considering the effective number of fasteners per row. The results are grouped per diagram according to the fastener spacings a_1, a_2, a_3, and the member thickness t, as shown in Figure 7 for parallel to grain and in Figure 8 for perpendicular to grain loaded connections.

For connections loaded parallel to grain:

The load capacities per fastener ($F_{max/15mm}$) observed show an increase with increasing spacing parallel to grain a_1 between the dowels from 5d to 9d, and with increasing spacing perpendicular to grain a_2 from 2d to 3d. A minimum spacing a_2 of 3d
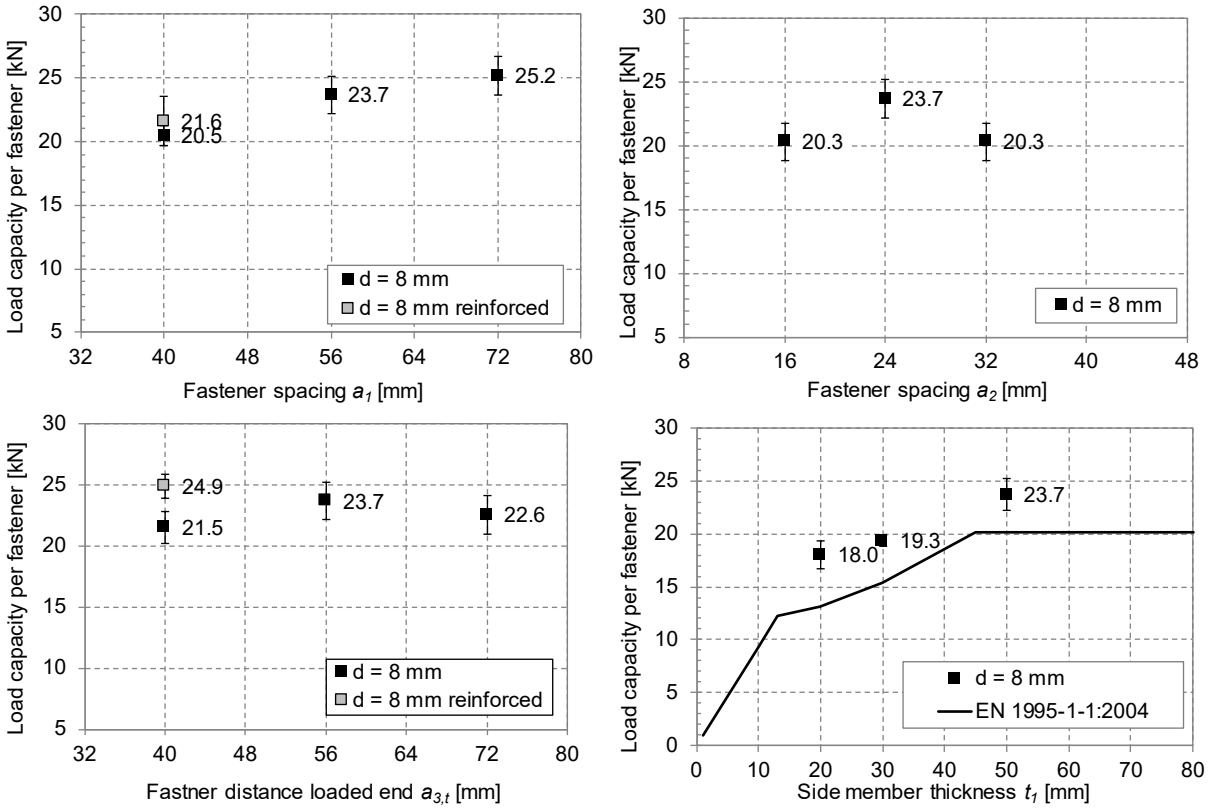
Figure 7 Experimental capacities depending on distance a_1 (top, left), a_2 (top, right), $a_{3,t}$ (bottom left), and side member thickness t_1 (bottom right) for parallel to grain connections m x n = 2 x 3
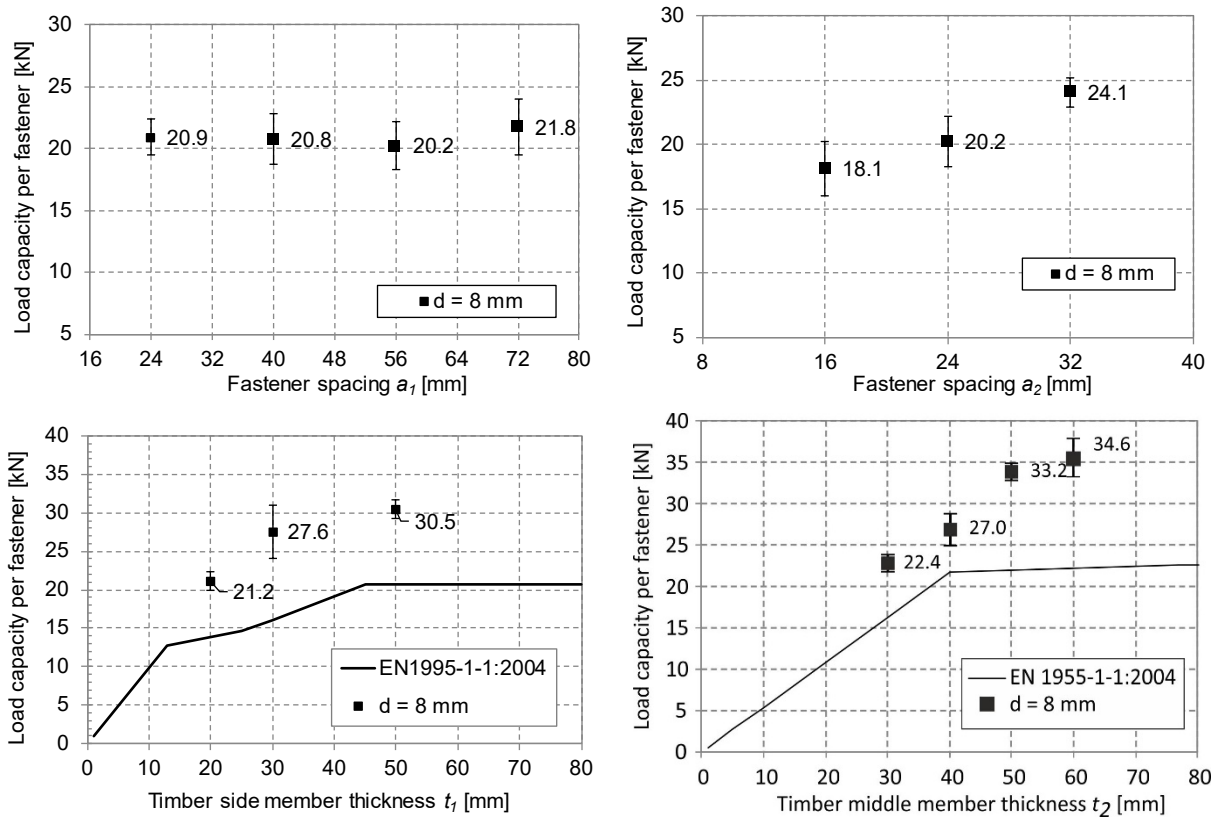
Figure 8 Experimental capacities (incl. standard derivation) depending on spacing a_1 (top, left), a_2 (top, right), side member thickness t_1 (bottom left), and middle member thickness t_2 for perpendicular to grain connections m x n = 2 x 3

98

perpendicular to the grain is recommended since the smaller spacing of $2d$ shows a reduced load capacity. The load capacities according to the side member thickness t_1 follow the trend of the capacities according to the EYM and are in the range of mode 2 (one plastic hinge) and mode 3 (two plastic hinges) and correspond with the failure observed in the tests. However, they show higher capacities than the calculated "mean" values according to EC5. The approximation of the EYM was calculated using the EC5 design equations considering the mean density for beech glulam with $\rho_{mean} = 700 \text{ kg/m}^3$ and mean steel dowel strength of $f_{u,mean} = 610 \text{ MPa}$ based on the nominal diameter. No rope effect is considered.

For connections loaded perpendicular to grain:

The load capacities per fastener ($F_{max/15\text{mm}}$) observed show no dependency on the spacing parallel to grain between the dowels a_1 from $3d$ up to $9d$. With each increasing distance perpendicular to grain a_2 from $2d$ to $4d$, the load capacities increase by about 20%. Likewise, the parallel to grain tests, the load capacities depending on different side or middle member thickness t_1 or t_2 can be assigned to the three EYM failure modes but are higher than the calculated "mean" values according to EC5.

4   Recommendations for the design

4.1   Spacings – edge and end distances, effective number of fasteners

For steel dowel type connections in beech wood, the recommended minimum spacings and edge and end distances are defined slightly different to EC 5 with regard to ductile load bearing connections ($D \geq 3$), compare Table 1. For steel dowel type connections loaded parallel to grain, there are three constellations which fulfill the criterion on ductility regarding the test results:

- $a_1 \geq 9d$ if $a_1 \geq 3d$

- $a_1 \geq 7d$ if $a_1 \geq 4d$ or reinforcement to prevent splitting

- $a_1 \geq 5d$ including reinforcement to prevent splitting.
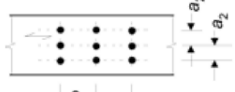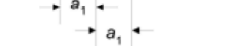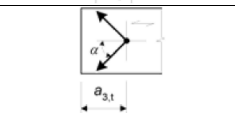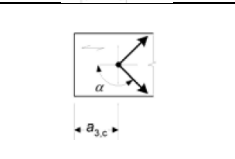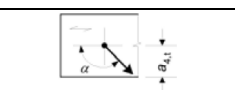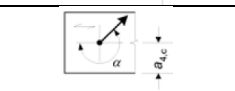
By meeting the minimum timber member thicknesses according to EN 1995-1-1, ductile failure was observed, and the design can be done without considering the effective number of fasteners n_{ef} respectively by $n_{ef} = n$.

4.2   Load capacities for connections loaded parallel to the grain

The comparison of the load carrying capacities of the experimental tests and the prediction of the standards EC5 shows a underprediction of about 33%, but with a clear linear trend and high correlation independent of using the reduction by n_{ef}, see Figure 9. Formulas (1) to (3) have been used for the prediction:

$$M_{y,R,mean} = 0.3 f_{u,mean} d^{2.6} \tag{1}$$

Table 1 Requirements to distances and spacings for beech wood in relation to SIA 265:2012 and EN 1995-1-1:2014 by meeting the minimum timber member thickness for modus 3 of EYM

		SIA 265:2012	EN 1995-1-1:2014	Beech (No. of tests)
a_1 parallel to grain		$7d$	$(3+2|\cos\alpha|)d$	$9d$ [1),2),3)] (15)
a_2 perpendicular to grain		$3d$	$3d$	$3d$ [1)] (15)
$a_{3,t}$ loaded end $-90° \leq \alpha \leq 90°$		$\max\{7d; 80\,\text{mm}\}$	$\max\{7d; 80\,\text{mm}\}$	$9d$ [1),2)] (15)
$a_{3,c}$ unloaded end $90° \leq \alpha \leq 150°$ $150° \leq \alpha \leq 210°$ $210° \leq \alpha \leq 270°$		$5d$	$a_{3,t}\|\sin\alpha\|$ $\max\{3,5d; 40\,\text{mm}\}$ $a_{3,t}\|\sin\alpha\|$	$5d$ (-)
$a_{4,t}$ loaded edge $0° \leq \alpha \leq 180°$		$4d$	$\max\{(2+2\sin\alpha)d; 3d\}$	$4d$ (-)
$a_{4,c}$ unloaded edge $180° \leq \alpha \leq 360°$		$3d$	$3d$	$3d$ (-)

[1)] recommendations according to test results
[2)] $7d$ if $a_2 \geq 4d$
[3)] $5d$ if reinforcements against splitting are used
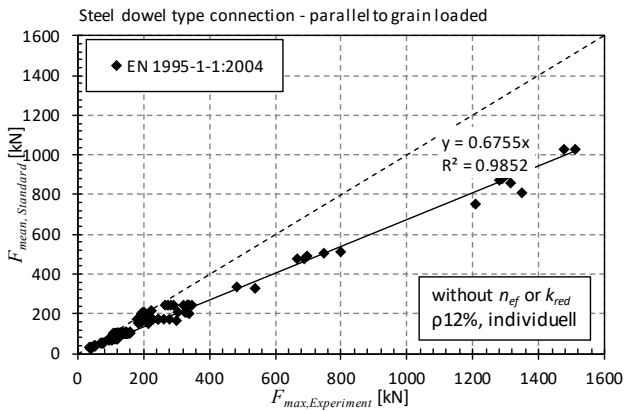
Figure 9 The observed capacities versus the estimated capacities according to the EC5
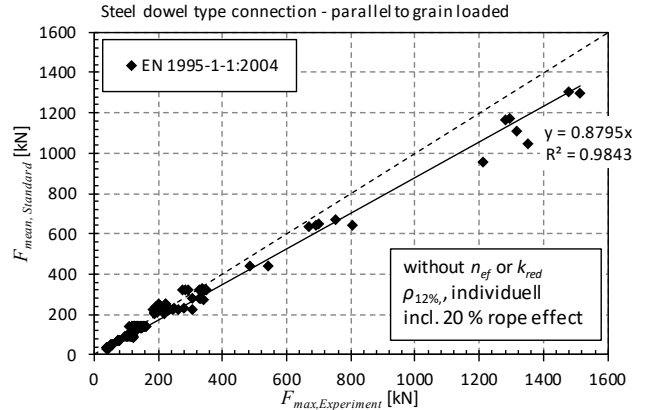
Figure 10 The observed capacities versus the new recommended estimated capacities according to the EC5

$$f_{h,0,mean} = 0.082(1-0.01d)\rho_{mean}$$

$$f_{h,90,mean} = \frac{f_{h,0,mean}}{0.9+0.015d} \tag{2}$$

$$R_{Verb,EC5} = (n_{ef})\min\begin{cases} f_{h,mean}t_1 d \\ f_{h,mean}t_1 d\left(\sqrt{2+\frac{4M_{y,mean}}{f_{h,mean}d\,t_1^2}}-1\right) \\ 2,0\sqrt{M_{y,mean}f_{h,mean}d} \end{cases} \tag{3}$$

Due to the underprediction, the maximum embedment strength as shown in Figure 1 according to Ehlbeck and Werner (1992), as shown in Figure 1, was used in a second step and a rope effect of 20 % for the shear planes where failure occurred in modus 3 in a third step. The estimation of the capacities could therefore be increased to 88%, see Figure 10.

4.3   Load capacities for connections loaded perpendicular to grain

The comparison of the tests perpendicular to the grain does not show the same good correlation. This is because the design formulas do not consider all layout parameters which influence the capacities. This can be seen in Figure 9 at the values on the plateau at 100 kN where the connections layout varies manly in the spacings. Likewise, to the parallel to grain tests, the standard generally underestimates the results. A clear difference could be seen between the tests failing in splitting (marked as triangles) resp. bending of the dowels (marked as dots). Therefore, splitting and ductile failures have further been evaluated separately.
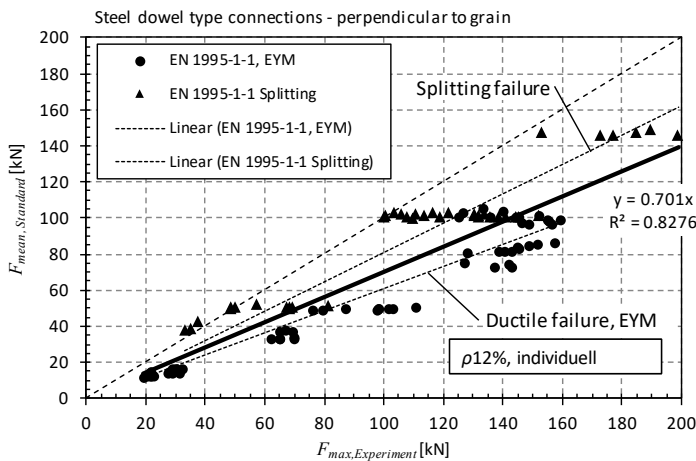
Figure 11 The observed capacities versus estimated capacities according to the EC5 with differentiation of the failure bending of the dowels (dots) or splitting (triangles)
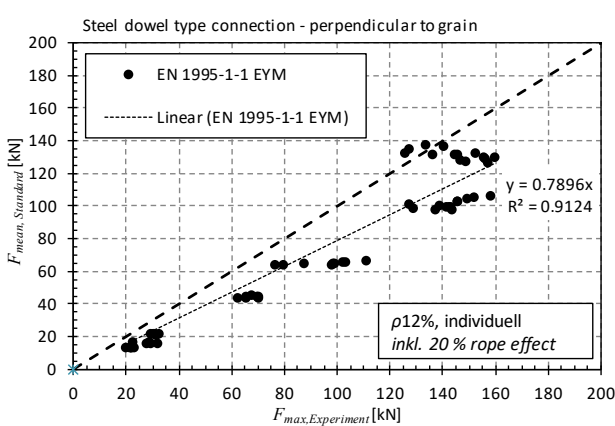
Figure 12 The observed capacities versus the new recommended estimated capacities according to the EC5 for ductile failure modes
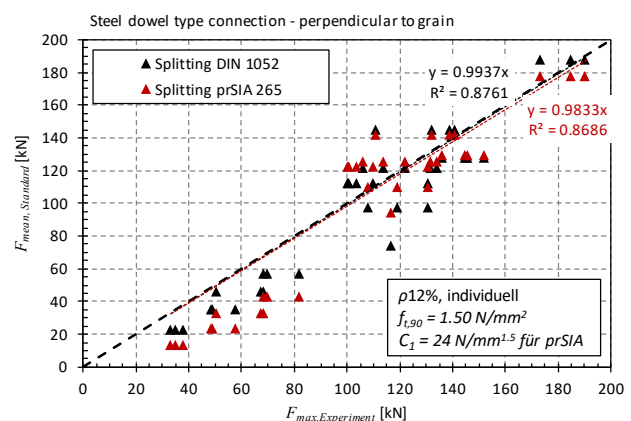
Figure 13 The observed capacities versus the new recommended estimated capacities according to the DIN 1052:2008 or prSIA265:2012 for the splitting failure

With the same principle as the parallel to the grain tests by increasing embedment strength and introduction of the rope effect of 20% for modus 3 failures, the capacities could be estimated up to 79%, see Figure 12. For the splitting prediction, the model of the DIN 1052:2004 and the prSIA265 was used. 100% estimation could be achieved by using a mean tensile strength perpendicular to the grain of 1.5 N/mm² and C_1 of 24 N/mm$^{1.5}$ respectively.

4.4   Design formulas

As shown before, the formulas of the EC5 can be used as basis to predict the load carrying capacities of dowel connections in hardwood using following modifications and results in the formulas (4) to (6):

- No effective number of fasteners can be used

- Higher embedment strength values according to Ehlbeck and Werner (1992a)

- Considering of 20% of the EYM capacity as rope effect for mode 3 cases

- Splitting can be predicted by the concept of DIN 1052 or prSIA 265 with design values of 0.3 N/mm² for the tensile strength perpendicular to grain and 11.7 N/mm$^{1.5}$ as $C_{1,d.}$

$$M_{y,Rk} = 0.3 f_u d^{2.6} \tag{4}$$

$$f_{h,0,k} = 0.102(1-0.01d)\rho_k$$
$$f_{h,90,k} = 0.102(1-0.016d)\rho_k \tag{5}$$

$$R_{v,Rk,(EC5)} = \min \begin{cases} f_{h,k} t_1 d \\ f_{h,k} t_1 d \left(\sqrt{2 + \dfrac{4 M_{y,Rk}}{f_{h,k} d\, t_1^2}} - 1 \right) \\ 1,2 \cdot 2,3 \sqrt{M_{y,Rk} f_{h,k} d} \end{cases} \tag{6}$$

5   Summaries and view

The load-carrying capacity and failure behaviour of dowel connections are described by ductile failures as embedment failure, yielding of fastener, shear of fasteners or brittle failures as e.g. splitting of timber members which depends on the connection layout. To provide design formulas for dowel connections in hardwood experimental investigation for parallel and perpendicular to grain tests have been carried out. The tests performed in general ductile where mostly two plastic hinges per shear plane were reached and the impact on spacings, member thickness and effective number of dowels could be clarified and recommendations for the design are given. The results show:

- A pre-drilling diameter 0.1 mm greater as the nominal dowel diameter should be used for ease of assembling.

- Ductile failure by bending of the dowels according to mode 3 of the EYM can be achieved by meeting the minimum thicknesses according to the EC5 definitions.

- The effective number of fasteners in loading direction does not have to be used.

- Adjusted spacings and distances are defined according to the different comparisons.

- The design formulas of Eurocode 5 can be used as basis but underpredict the load carrying capacities.

- By using higher embedment strengths according to Ehlbeck and Werner (1992a) and a contribution of the rope effect, predictions of 79% and 88% can be achieved for the perpendicular and parallel to grain tests respectively.

- The design formulas of DIN 1052 and prSIA 265 can be used to predict the splitting by using the given strength parameters.

There are still some explanations missing about the underestimation of the EYM equations, which will be further investigated. Also, further investigations will be done regarding the more accurate definition and use of the rope effect. Analyses regarding the stiffness of the dowel connections in hardwood will be done and provided since the deformations at the connections have been measured.

6   Acknowledgements

7   References

DIN 1052:2008 Entwurf, Berechnung und Bemessung von Holzbauwerken, Deutsches Institut für Normung e.V., Berlin.

Ehlbeck J., Werner H. (1992a): Softwood and Hardwood Embedding Strength for dowel-type fastener. In: Proceedings CIB-W18, Ahus, Sweden, Paper 25-7-2.

Ehlbeck J., Werner H. (1992b): Tragfähigkeit von Laubholzverbindungen mit stabförmigen Verbindungsmitteln. Technical Report. Versuchsanstalt für Stahl, Holz und Steine, Universität Karlsruhe

Eid. Forschungsanstalt für Wald Schnee u. Landschaft (2018): Schweizerisches Landesforstinventar, 4. Landesforstinventar 2009 –2013, Switzerland

EN 1995-1-1:2014 Eurocode 5: Design of timber structures - Part 1-1: General and rules for buildings. CEN.

EN 26891:1991, European Standard, Timber Structures; Joints with mechanical fasteners, General principles for the determination of strength and deformation characteristics. Brussels, Belgium.

Franke, S., Magnière, N. 2014. Discussion of Testing and Evaluation Methods for the Embedment Behaviour of Connections, In: INTER, Paper 47-7-1, Bath, UK

Franke S., Franke B., Jockwer R., Heubuch S. (2019): Entwicklung von bemessungs- und ausführungsrelevanten Grundlagen für hochleistungsfähige Anschlüsse in Laubholz, Research report, ISBN 978-3-906878-06-5, Publishing Sept 2019

Gehri E. (2010): Screw connections in hardwood structures. In: 16. Internationales Holzbau-Forum, Garmisch-Partenkirchen, Germany.

Hübner U. (2013): Mechanische Kenngrößen von Buchen-, Eschen- und Robinienholz für lastabtragende Bauteile. Thesis (PhD). Technische Universität Graz.

Hübner, U., Bogensperger, T., Schickhofer, G., 2008. Embedding strength of European hardwoods. In: CIB-W18 Meeting 41, 41-7-5, St. Andrews, Canada.

prSIA 265:2012, *Holzbau.* (in German), in preparation, Schweizerischer Ingenieur- und Architektenverein, Zürich.

Sandhaas C., Ravenshorst G.J.P., Blass H.J., van de Kuilen J.W.G. (2013): Embedment tests parallel-to-grain and ductility aspects using various wood species. Eur. J. Wood Prod. 71, 599–608.

SN EN ISO 6892-1:2016 Metallische Werkstoffe – Zugversuch - Teil 1: Prüfverfahren bei Raumtemperatur (in German)

SIA 265:2012, *Holzbau.* (in German), Schweizerischer Ingenieur- und Architektenverein, Zürich.

Vreeswijk, B., 2003. Timber joints using hardwood species. Thesis (Master), Faculty of Civil Engineering, Delft University of Technology, Delft, The Netherlands.

Whale L.R.J. , Smith I., Hilson B.O. (1986): Behaviour of nailed and bolted joints under short-term lateral load – conclusions from some recent research. In: Proceedings of CIBW18, Bd. 1. Florence, Italy, Paper 19-7-1.

Whale L.R.J., Smith I., Hilson B.O. (1987): Characteristic properties of nailed and bolted joints under short-term lateral load. Part 4 – The influence of testing mode and fastener diameter upon embedment test data. In: Journal of the Institute of Wood Science 11 (1987), Nr. 5, S. 156–161.

Whale L.R.J., Smith I., Larsen H.J. (1987): Design of nailed and bolted joints – Proposal for the revision of existing formulae in draft Eurocode 5 and the CIB code. In: Proceedings of CIB-W18 Meeting, 20-7-1, Ireland.

Discussion

The paper was presented by S Franke

S Winter asked why a_{3t} was chosen smaller than a_1 and received clarification that increasing a_1 or a_2 can also lead to higher ductility.

S Winter questioned why the proposed factor of 1.2 in mode 3 only applied for hardwood and not softwood. S Franke said this could also be applied if one was sure of the rope effect of the dowel.

H Blass commented that you are proposing the rope effect in mode 3 and asked would you also propose rope effect for the plastic hinge forming in the outside steel plate. He also questioned about how to design for the full shear capacity of the fastener. S Franke said that more work needed to be done.

JM Cabrero received clarification that only 5 replicates were used and that comparison between reinforced and not reinforced cases was done only for the 5d case. Also load deformation data indicated mostly yielding failure mode.

R Jockwer questioned that $n_{ef}=n$ for mode 3 can be applied to other modes if minimum spacing and other conditions are met. He asked about the regression coefficient as it is done for data showing two distinct groupings. S Franke agreed and said that the regression coefficient for individual groups would be much lower.

P Quenneville mentioned that the results for 7d are as good as the results for 9d because the tests were stopped at 15 mm displacement. P Quenneville also discussed whether one could see two wood-steel-wood connections where mode 1 might be approached. S Franke said that they all failed before 15 mm. The displacement shown in the load deformation curves includes machine movements and connection deformations.

U Kuhlmann asked about stiffness information and stated that they would be useful.

P Dietsch said that information to support the statements made in the conclusions is missing (e.g. how the connections were reinforced and illustration of the prSIA splitting model) and that this should be included for further clarification. S Franke will update the paper.

Effective thickness of the wood member in a timber-to-steel connection with large diameter fastener under brittle failure

Miguel Yurrita. Wood Chair. Department of Building Construction, Services and Structures. University of Navarra. 31009 Pamplona, Spain. myurrital@alumni.unav.es

José Manuel Cabrero. Wood Chair. Department of Building Construction, Services and Structures. University of Navarra. 31009 Pamplona, Spain. jcabrero@unav.es

Keywords: Effective thickness , Brittle failure , Elastic range , Large diameter fastener , Beam on elastic foundation

1   Introduction

Timber connections have been usually designed considering only the ductile failure mode. Brittle failure modes have not been normally considered, as they are expected to be avoided by respecting minimum spacing between fasteners, which is not always the case. Therefore, the study of brittle failure modes for timber connections with large diameter fasteners is of utmost importance. Brittle failure modes of connections with large diameter fasteners can be simply explained in relation to the failure planes generated in the wood member:the head tensile planes H that are activated in block shear (Fig. 1b) and net tension (Fig. 1c), and the lateral shear planes L, which appear in row shear (Fig. 1a) and block shear (Fig. 1b).

In the case of lateral shear plane L, for design purposes, its area is defined by its length (namely the length of the connection L_c) multiplied by the effective thickness t_{ef} of the wood member.

(a) Row shear   (b) Block shear   (c) Net tension
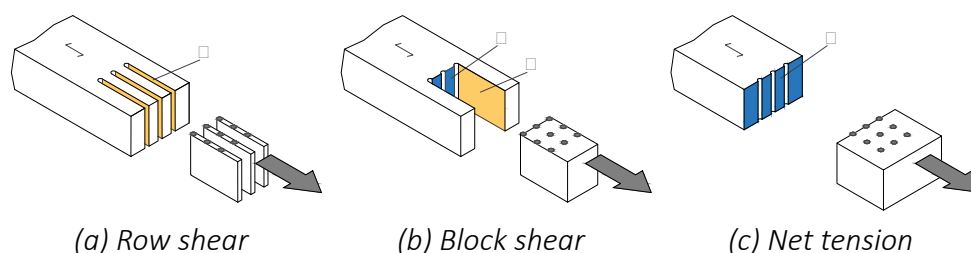
Figure 1. Failure planes (lateral shear L, and head tensile H) related to each brittle failure mode.

(a) ws side view   *(b) wsw side view*   *(c) sws side view*   *(d) msp side view*
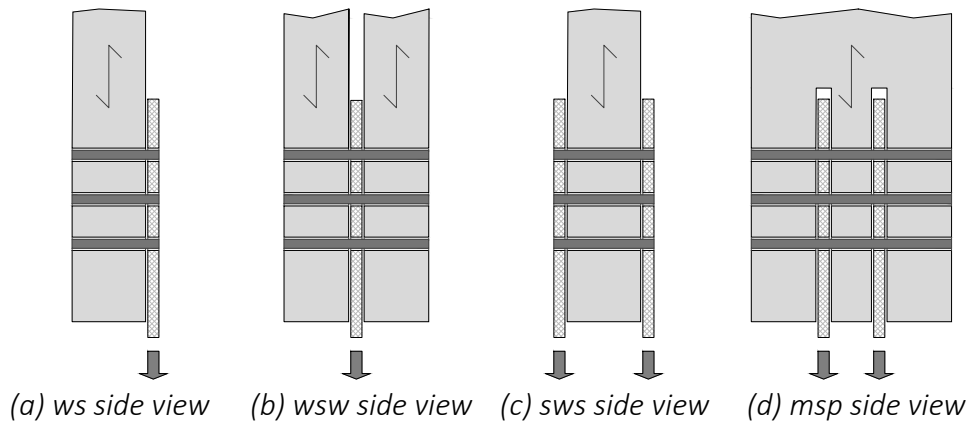
Figure 2. Side views of the possible configurations of a timber-to-steel connection with large diameter fasteners.

The definition of this effective thickness t_{ef} is of utmost importance for a safe design of timber connections. Most of the existing proposals define it as the distance between the plastic hinges in the fastener. However, brittle failure usually happens before the fastener yields, so the fastener still remains within its elastic range. Therefore, the t_{ef} calculation should be based on the elastic behaviour of the fastener before yielding.

In addition, the effective thickness t_{ef} depends on the position of the wood member in a connection: in wood-steel (*ws*) -Fig. 2a- and wood-steel-wood (*wsw*) -Fig. 2b- the wood member is considered as an outer member of the connection, whereas in the case of steel-wood-steel (*sws*) -Fig. 2c- it is an inner member of the joint. Finally, in the case of connections with multiple shear planes (*msp*) -Fig. 2d- there are two outer timber elements, and one or more inner elements depending on the number of shear planes.

2 State of the art

2.1 Early approaches

Early proposals focused in the post-elastic range of the fastener. *Kangas and Vesa* (1998) and *Johnsson and Parida* (2013) studied nailed connections, and provided a formula considering the distance between two plastic hinges (equivalent to mode *e* from Table 1):
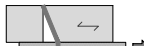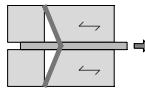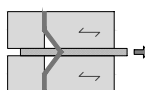
$$t_{ef} = 2\sqrt{\frac{M_{y,R}}{f_{h,0}d}}, \tag{1}$$

where d is the dowel diameter, $f_{h,0}$ is the embedment strength and $M_{y,R}$ is the plastic bending moment of the fastener.

2.2 Eurocode 5

The Eurocode 5 (2004) in its Annex A uses a similar approach to determine the effective thickness. The effective thickness depends on the yielding mode of the connection, as

Table 1. Effective thickness t_{ef} and its corresponding yielding modes, as provided by Annex A of Eurocode 5 (2004).

Effective thickness t_{ef}	Fastener yielding modes (Eurocode 5, 2004)		
$0.4t$		Mode a	
$1.4\sqrt{\dfrac{M_{y,R}}{f_{h,0}d}}$		Mode b	
$t\left(\sqrt{2+\dfrac{M_{y,R}}{f_{h,0}dt^2}}-1\right)$	Mode d		Mode g
$2\sqrt{\dfrac{M_{y,Rk}}{f_{h,0}d}}$	Mode e		Mode h
t	For the rest of modes		

can be seen in Table 1. Relating brittle failure to the fastener yielding (ductile mode) is an error of concept. In addition, it only provides an approach for timber-to-steel connections with one or two shear planes. No consideration is done regarding timber-to-timber connections or multiple shear planes connections.

2.3 Hanhijärvi and Kevarinmäki

Hanhijärvi and Kevarinmäki (2007) proposed a formula for the elastic range, which is different for outer and inner timber members.

$$t_{ef} = \begin{cases} \min\left(1, \dfrac{d}{0.6\sqrt{\dfrac{1.5f_{h,0}}{f_y}}2.45t}\right)t & \text{(outer members)} \\[4ex] \min\left(1, \dfrac{d}{0.5\sqrt{\dfrac{1.5f_{h,0}}{f_y}}1.23t}\right)t & \text{(inner members)} \end{cases} \tag{2}$$

This proposal was developed for large diameter fasteners (the previous ones seem to have been developed for small diameter fasteners). It is quite cumbersome, and it requires several geometrical and material parameters, such as the thickness of the timber element t, the fastener diameter d, the embedment strength in the parallel-to-grain direction $f_{h,0}$ of the timber product, and the yield strength f_y of the steel fastener.

2.4 Quenneville and Zarnani

As the previous one, the model from *Quenneville and Zarnani* (2017) is valid for large diameter fasteners and also distinguishes between outer and inner timber members. It

is very simple, and provides just two values (3), depending on the relative position of the timber element in the connection:

$$t_{ef} = K_{LS}\, t, \quad \text{where} \begin{cases} K_{LS} = 1.00 & \text{(inner members)} \\ K_{LS} = 0.65 & \text{(outer members)} \end{cases} \tag{3}$$

2.5 Zarnani and Quenneville

Although this proposal by *Zarnani and Quenneville* (2014) is only valid for rivets, a particular case of small diameter fasteners, it is worthwhile including it in this overview. Their proposal includes a different analysis for the plastic range (considering none, one or two plastic hinges) and another one that considers the elastic behaviour of the fastener before yielding. For the elastic range, a simple linear fitting based on a beam on elastic foundation is given. As rivets are a standard product, this fitting is further simplified to fixed values depending on the rivet penetration length L_p:

$$t_{ef} = \begin{cases} 0.95 L_p & \text{for } L_p = 28.5 \text{ mm} \\ 0.85 L_p & \text{for } L_p = 53.5 \text{ mm} \\ 0.75 L_p & \text{for } L_p = 78.5 \text{ mm} \end{cases} \tag{4}$$

3 Beam on elastic foundation model (BOEF)

As done by *Zarnani and Quenneville* (2014) for the case of rivets, a beam on elastic foundation (BOEF) model (*Celigüeta*, 1998), is used to determine the effective thickness of the lateral failure planes L of timber members in connections with large diameter fasteners in the elastic range. The BOEF model is used to study the two possible relative positions of the timber member within the connection. For the case of an outer member (Fig. 3b) the load is applied in one side, while for an inner timber member (Fig. 3a) the load is symmetrically applied at both sides. In addition, for each case, two situations have been considered depending on the steel plate thickness: a thin plate which allows a free rotation of the fastener, and a thick plate that clamp the fastener, restricting its rotation.

Three main parameters are involved in the development of the BOEF model (*Celigüeta*, 1998): the modulus of elasticity of the fastener E_y; the timber product by means of the modulus of elasticity parallel-to-grain E_0; and the slenderness of the fastener (beam), defined as the ratio between its length (equal to the timber thickness t) and its diameter d. Since the modulus of elasticity E_0 is quite similar for any type of steel, only the timber product and the slenderness t/d should be considered.

<table>
<tr><td>(a) Interior members</td><td>(b) Exterior members</td></tr>
</table>
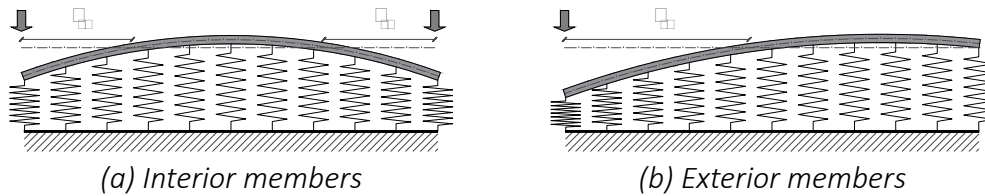
Figure 3. Simulation of a fastener in contact with wood as a beam on elastic foundation.

3.1 Parametric study of the BOEF model

A parametric study taking as a basis a C24 timber member with a thickness $t = 75\text{mm}$ and a fastener of $d = 25\text{mm}$ (stocky slenderness, $t/d = 3$) has been used in order to study the influence of the timber product and the slenderness of the fastener. The results from the BOEF model(thick and thin plates) are compared with those obtained by applying the approach of the Eurocode 5 (2004), *Hanhijärvi and Kevarinmäki* (2007) and *Quenneville and Zarnani* (2017), which are the three models that consistently consider all the possible brittle failure modes in connections with large diameter fasteners. The cases where the timber element is an outer or an inner member of the connection are considered separately. The results are given in Fig. 4.

3.1.1 Influence of the timber product

Fig. 4a and Fig. 4b provide the obtained results from the parametric study considering the variation of the timber product for inner an outer timber members, respectively. The variation of the timber product is given by means of the timber density ρ (abscissas axis), which is more or less related to the modulus of elasticity parallel-to-grain E_0. Some specific timber products are plotted for reference by means of vertical dashed lines.

For the case of inner members (Fig. 4a) a total agreement between all the proposals is shown, with a constant ratio $t_{ef}/t = 1$. However, the differences in the case of outer members (Fig. 4b) are noticeable: the BOEF model (both for thin and thick plates) remains constant, with a value very close to the one from *Quenneville and Zarnani* (2017) for thin plates, and a value equal to the timber thickness for thick plates. The other two models depict a decreasing trend, higher in the case of *Hanhijärvi and Kevarinmäki* (2007). Therefore, according to the BOEF model, the timber product does not have a main role in the determination of the effective thickness t_{ef} in the elastic range. The model from *Quenneville and Zarnani* (2017) seems to be the most similar.

3.1.2 Influence of the fastener slenderness

Fig. 4c and Fig. 4d provide the obtained results from the parametric study considering the variation of the fastener slenderness t/d.

For inner members, (Fig. 4c) the BOEF remains with the $t_{ef}/t = 1$ for slow slenderness. When the slenderness increases, at some point ($t/d = 7$ and $t/d = 11.5$ for thin and
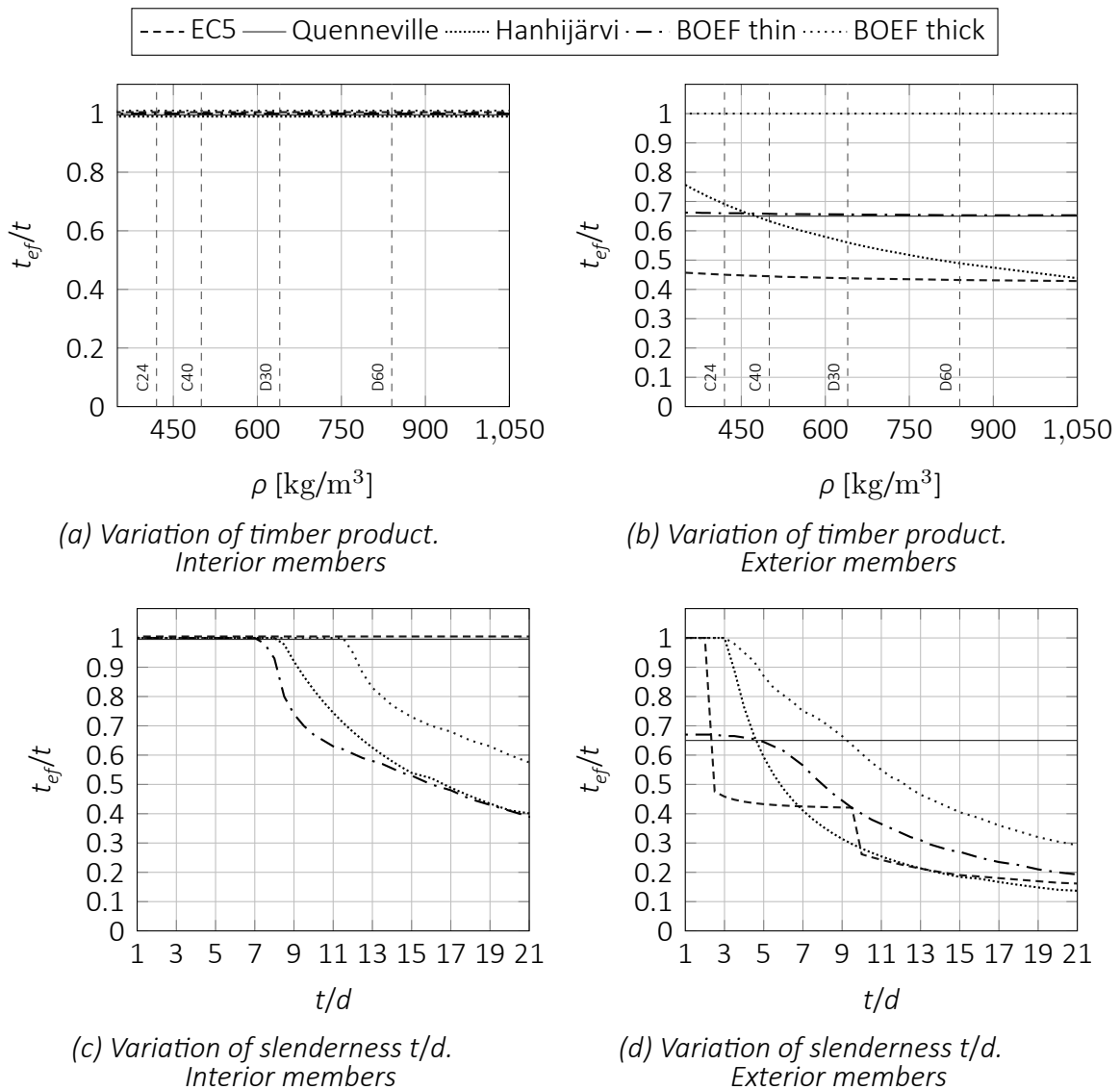
Figure 4. Parametric study of the BOEF model (Celigüeta, 1998) considering the variation of the timber product and the slenderness of the fastener

thick plates, respectively) the effective thickness start to decrease. A similar tendency, in between the thin and thick plates cases is shown by *Hanhijärvi and Kevarinmäki* (2007).

In the case of outer members, very different trends among the different proposals are noticed. In cases of low slenderness (until $t/d = 3$) the BOEF model is quite similar to *Quenneville and Zarnani* (2017). As the slenderness increases, the t_{ef} of the BOEF model decreases, as done by the proposal from *Hanhijärvi and Kevarinmäki* (2007), which conversely proposes $t_{ef}/t = 1$ for stocky fasteners. The Eurocode 5 (2004) results in a confusing behaviour with three parts related to the different yielding modes (none, one and two plastic hinges).

4   Proposal for determining the effective thickness

A new approach to obtain the effective thickness t_{ef} of the timber member in the elastic range of the fastener in connections with large diameter fasteners is proposed. Considering the slenderness t/d as the only main parameter, it is based on a fitting of the al-

(a) Interior members *(b) Exterior members*
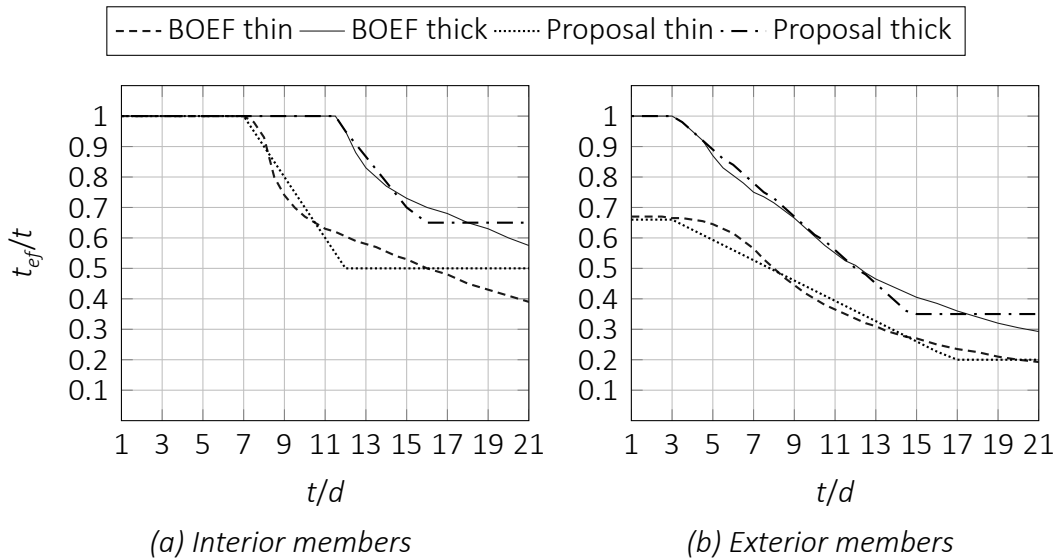
Figure 5. Fitting of the proposed formulae to the analytic results from the BOEF model.

ready explained BOEF model for both inner and outer timber members combined with thick and thin steel plates:

- Thin plates:

$$\text{Outer members:} \quad t_{ef} = \begin{cases} 0.66t & \text{if } \frac{t}{d} \leq 3 \\ \max\left(0.76 - \frac{t}{30d}; 0.2\right) t & \text{if } \frac{t}{d} > 3 \end{cases} \tag{5}$$

$$\text{Inner members:} \quad t_{ef} = \begin{cases} t & \text{if } \frac{t}{d} \leq 7 \\ \max\left(1.7 - \frac{t}{10d}; 0.5\right) t & \text{if } \frac{t}{d} > 7 \end{cases} \tag{6}$$

- Thick plates:

$$\text{Outer members:} \quad t_{ef} = \begin{cases} t & \text{if } \frac{t}{d} \leq 3 \\ \max\left(1.17 - \frac{t}{18d}\right); 0.35t & \text{if } \frac{t}{d} > 3 \end{cases} \tag{7}$$

$$\text{Inner members:} \quad t_{ef} = \begin{cases} t & \text{if } \frac{t}{d} \leq 11.5 \\ \max\left(1.95 - \frac{t}{12d}\right); 0.65t & \text{if } \frac{t}{d} > 11.5 \end{cases} \tag{8}$$

The correlation between the fitting formulae and the BOEF model is given in Fig. 5. For *msp* connections, outer and inner members are studied separately. Due to this simplification, a factor of 0.85 should be applied for the obtained t_{ef} in these case of joints.

5 Validation of the proposal

An extensive database of tests has been gathered and studied in order to compare the prediction ability of the different approaches and the proposal. The works from 16 authors, with a total of 160 different connection configurations and 926 single tests were

compiled. The sample of tests includes three main connection configurations (*sws*, *wsw* and *msp*, using mainly glulam and LVL as timber products and bolts and dowels as fasteners. More data about all the studied set of tests is given in Table 2.

Due to the reduced number of test per each configuration, the mean level is considered more adequate than the characteristic one in order to compare the prediction ability of the calculation models with the test results. Mean material properties have been obtained from the characteristic ones following the work from *Jockwer et al.* (2018).

In order to isolate the effective thickness parameter, it has been decided to use only one model - the one from *Quenneville and Zarnani* (2017)- in combination with the effective thickness values provided by the four studied approaches. The choice of the model from *Quenneville and Zarnani* (2017) as the basis is due to previous works -*J. Cabrero and Yurrita* (2018), *Yurrita, J. M. Cabrero, et al.* (2019)- where this model has been considered as the one with the best balance between accuracy and simplicity.

Fig. 6 depicts the obtained results. The predicted load capacities (ordinates axis) are compared with the experimental results (abscissas axis). The tests have been divided in three groups, according to the three main positions of the timber members in the connection: *sws*, *wsw* and *msp*. For each of the three cases, a linear fitting passing through the origin of coordinates with its corresponding slope m and the coefficient of correlation R^2 is provided. The ideal correlation 1:1 is given by a dashed line for reference.

However, as the target of this analysis is not to evaluate the accuracy of the model from *Quenneville and Zarnani* (2017), slopes m close to 1 are of minor importance. What matters in this case is to obtain coefficients of correlation R^2 close to 1, and similar slopes m between the three joint configurations (no matter if they are close to 1 or not). Such results are proof of a good performance of the effective thickness t_{ef} parameter.

As expected, the least accurate results are obtained by the Eurocode 5 (2004) (Fig. 6a), where higher differences in slope are noticed (with a quite conservative slope for the case of *wsw* connections). The proposal from *Quenneville and Zarnani* (2017) (Fig. 6b) works very well for *sws* and *msp*, but provides the worst R^2 for *wsw*, possibly due to its excessive simplification. For this type of connections, the effective thickness t_{ef} for slenderness $t/d > 3$ tends to diminish, and this trend is not considered here, leading to a very risky overestimation of the load capacity of the connection. *Hanhijärvi and Kevarinmäki* (2007) overestimate the results for *msp* configurations. In addition, it should be reminded the difficulty and the amount of data needed for this particular model. Finally, the new proposal provides the best results (slopes with differences lower to 1.5% and good R^2 values).

The influence of the slenderness is clearly demonstrated in Fig. 7. Here, the ratio between the predicted F_P and the tested load capacities F_T (ordinates axis) is evaluated by

Table 2. Summary of the tests used for the validation.

Author	Number of		Joint scheme					Fastener		Timber product				Failure mode	
	Config.	Tests	sws	ws[a]	ww[a]	wsw	mult.[b]	Bolt	Dowel	Glulam	LVL	CLT	Solid	Ductile	Brittle
Massé et al. (1998)[c]	5	15	5	-	-	-	-	-	5	5	-	-	-	1	4
Quenneville and Mohammad (2000)[c]	37	370	37	-	-	-	-	37	-	36	-	-	1	6	31
Mohammad and Quenneville (2001)[c]	13	130	-	1	-	12	-	13	-	13	-	-	-	-	13
Anderson (2001)[c]	3	9	-	1	2	.	-	3	-	3	-	-	-	-	3
Dodson (2003)	6	27	6	-	-	-	-	6	-	6	-	-	-	-	6
Reid (2004)[c]	4	40	4	-	-	-	-	-	4	4	-	-	-	-	4
Sjödin and Johansson (2007)	6	30	-	-	-	6	-	-	6	6	-	-	-	-	6
Leivo et al. (2000)[d]	4	12	-	-	-	4	-	-	4	4	-	-	-	-	4
SP (1992)[d]	2	4	-	-	-	-	2	-	2	2	-	-	-	-	2
Kevarinmäki (1997)[d]	1	3	1	-	-	-	-	1	-	1	-	-	-	-	1
VTT (2003)[d]	1	3	-	-	-	-	1	-	1	1	-	-	-	-	1
Hanhijärvi and Kevarinmäki (2008)[e]	39	118	16	-	-	13	10	-	39	23	16	-	-	-	39
Hübner (2013)[c]	3	15	-	-	-	3	-	-	3	-	-	-	3	3	-
Misconel et al. (2016)[c]	2	10	-	-	-	2	-	1	1	-	2	-	-	2	-
Ottenhaus et al. (2018)	6	30	-	-	-	6	-	-	6	-	3	3	-	2	4
Yurrita, J. M. Cabrero, et al. (2019)	28	110	-	-	-	-	28	-	28	16	12	-	-	-	28
Total	160	926	69	2	2	46	41	61	99	120	33	3	4	14	146
%	-	-	43.1%	1.3%	1.3%	28.8%	25.6%	38.1%	61.9%	75.0%	20.6%	1.9%	2.5%	8.7%	91.3%

[a] As there are only two configurations of *ww* and *ws*, they have been gathered with the *wsw* configurations.
[b] All the multiple shear connections have 4 shear planes, except three configurations with 6 and one with 8 shear planes.
[c] Only the tests with two or more rows of fastener have been considered.
[d] Part of the results gathered by Kevarinmäki, A. (2009).
[e] One configuration has been dismissed as the properties of the timber were not provided.
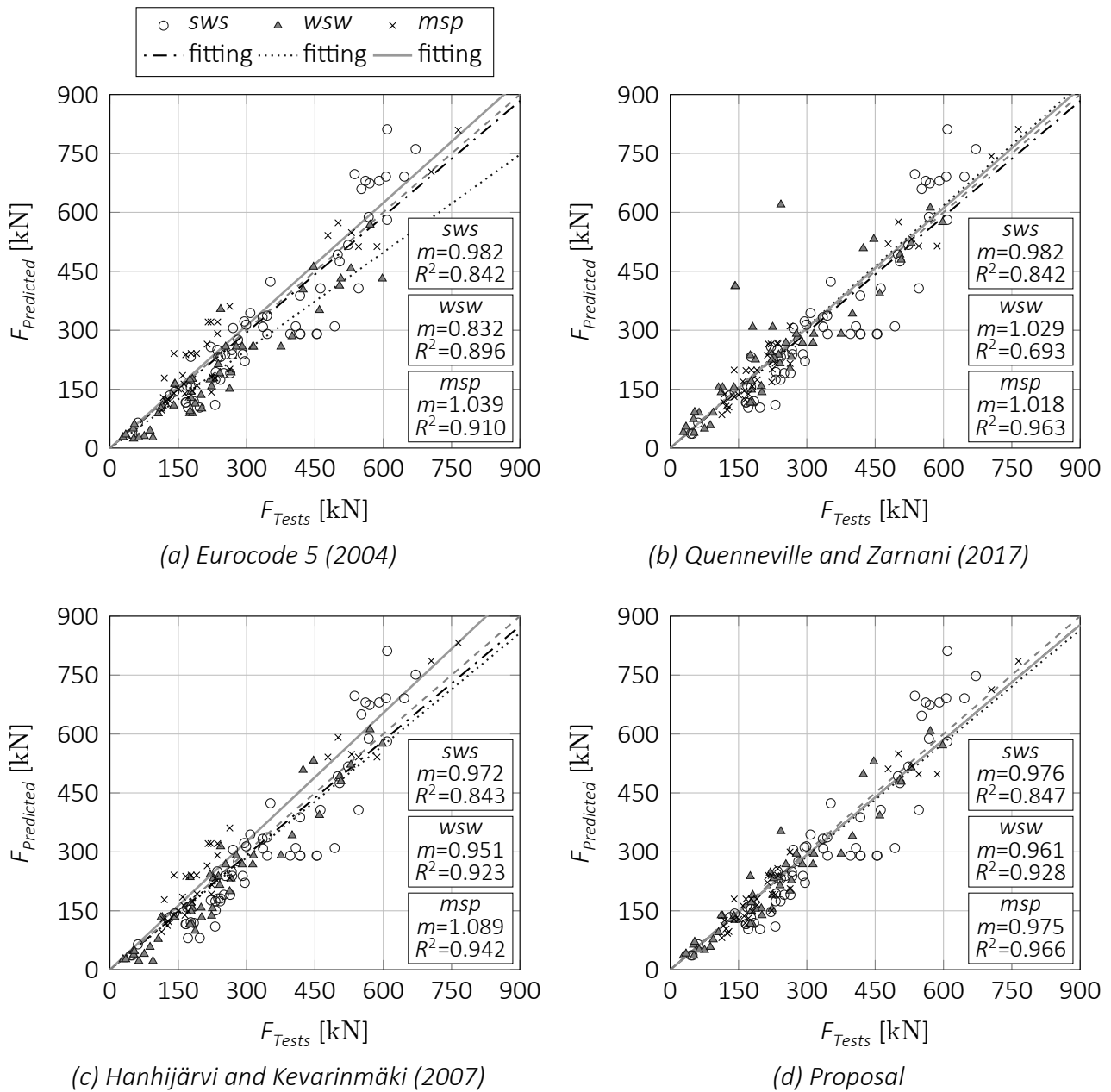
Figure 6. Comparison between the values obtained from the tests and the corresponding theoretical values predicted by the model of Quenneville and Zarnani (2017), combined with the four proposals for the effective thickness.

classifying the results according to the fastener slenderness *t/d* (abscissas axis). A horizontal fitting line for each type of joint configuration would be desirable, as it would mean that the prediction ability does not change with the variation of the slenderness.

The Eurocode 5 (2004) (Fig. 7a) provides the most chaotic behaviour, with different slopes for each joint configuration. *Hanhijärvi and Kevarinmäki* (2007) (Fig. 7c) shows a slight trend to underestimate the capacity as the slenderness increases. The opposite happens in the case of *Quenneville and Zarnani* (2017) (Fig. 7b) which, due to its oversimplification, leads to several problems when the slenderness increases. An almost even behaviour is reached by the proposal (Fig. 7d), independently of the slenderness.

A statistical analysis considering the results from all the joint configurations together
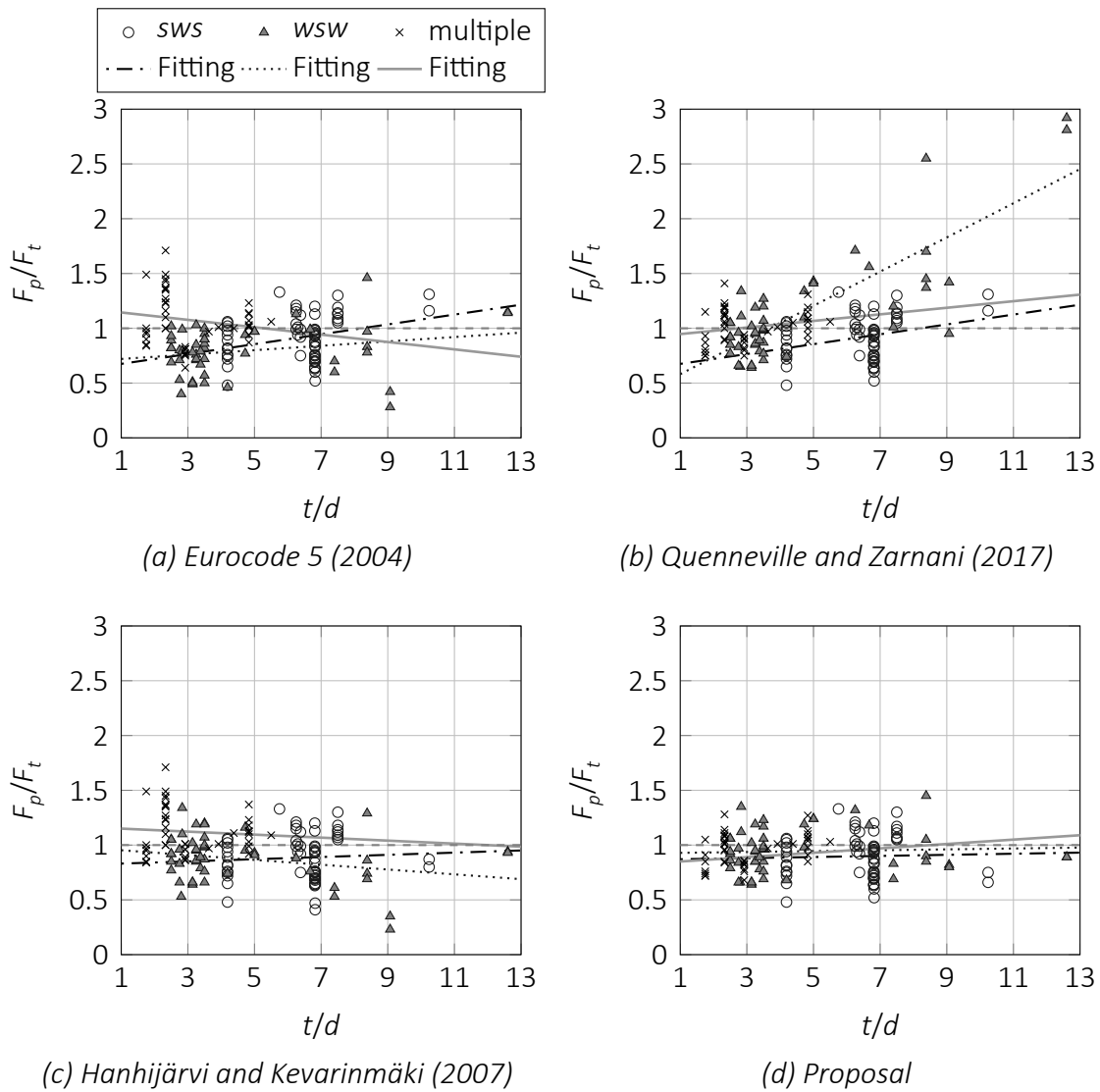
Figure 7. Comparison of the prediction accuracy of the four proposals for the effective thickness, combined with the model of Quenneville and Zarnani (2017), considering the slenderness of the fastener.

has been additionally performed (see Table 3). Several metrics were used to assess the four approaches: the coefficient of determination Q^2 (best values are the closest to 1), the mean square error *MRE* and its corresponding standard deviation *SD* (lower values are the best ones), the slope *m*, the correlation coefficient *c* (values closer to 1 are the best) and, finally, the concordance correlation coefficient *CCC* metric (another time values closer to 1 are the best ones, with a recommended threshold value of 0.85). All these metrics were already used and explained in more detail by *J. Cabrero and Yurrita* (2018). The statistical analysis confirms the proposal as the most accurate approach: it obtains the best results for all the metrics, except the slope *m* (which, as previously explained, it is of minor importance in this case). *Hanhijärvi and Kevarinmäki* (2007) ranks the second place and, due to the lack of accuracy from *Quenneville and Zarnani* (2017) in the case of *wsw*, this model and the Eurocode 5 (2004) are quite even in the last positions.

In the boxplot graphic in Fig. 8 the ratio between the predicted load F_P of each approach combined with the model from *Quenneville and Zarnani* (2017) and the load capacity

Table 3. Comparison of the results of combining the model from Quenneville and Zarnani (2017) with the anlyzed effective thickness proposals.

Model	Q^2	MRE (SD)	m	c	CCC
Eurocode 5 (2004)	0.832	0.184 (0.151)	0.981	0.915	0.924
Quenneville and Zarnani (2017)	0.802	0.176 (0.190)	1.029	0.900	0.911
Hanhijärvi and Kevarinmäki (2007)	0.854	0.169 (0.145)	1.031	0.919	0.936
Proposal	**0.877**	**0.150 (0.139)**	**0.972**	**0.951**	**0.944**
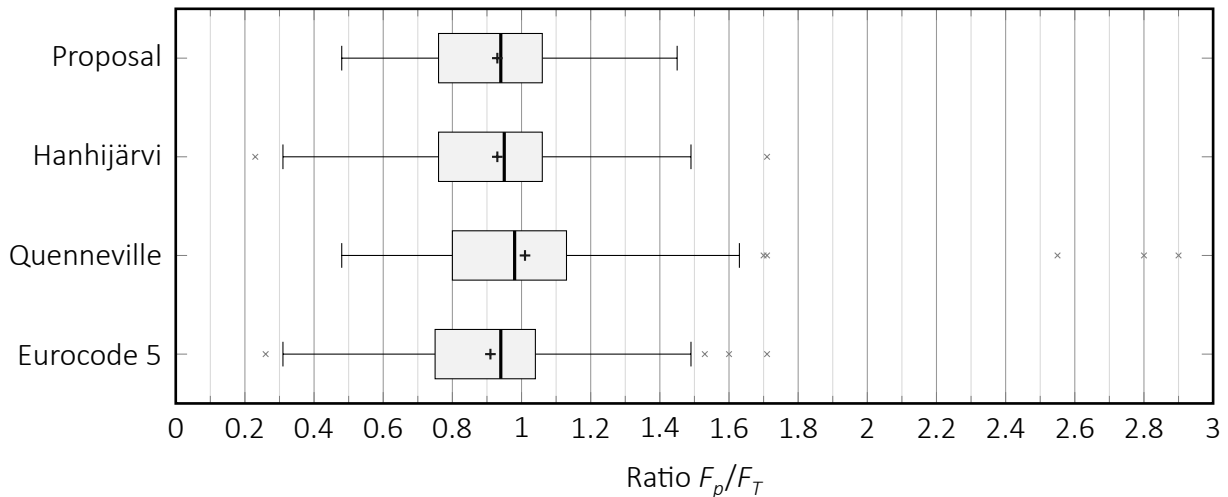
Figure 8. Boxplot considering the accuracy of the predicted ratio between the predicted failure load F_P and the tested failure load F_T. Mean value is depicted with a cross.

F_T from the test results is used as the main parameter. The new proposal provides the least scatter with no outliers. It is, therefore, confirmed as the most accurate approach. The length of the whiskers is similar in the rest of proposals, and all of them get several outliers. Some of these outliers obtained by *Quenneville and Zarnani* (2017) are quite remarkable, since they are close to $F_P/F_T = 3$.

6   Conclusions and future work

A correct determination of the effective thickness t_{ef} in the elastic range is necessary for a safe calculation of the capacity of brittle failure modes. A new approach for timber-to-steel connections with large diameter fasteners is proposed. It is derived from a fitting based on a beam on elastic foundation model, and it only requires the slenderness of the fastener as the main parameter. An extensive database of test results proves its superior accuracy in comparison to the existing approaches. This parameter is the first step to provide a whole new model dealing with brittle failure modes of timber connections with large diameter fasteners loaded parallel-to-grain, which is explained in the companion paper (*Yurrita and J. Cabrero*, 2019).

The model is expected to work for timber-to-timber connections as well. However, due to the lack of enough available tests in the literature it is not possible to validate it. As a future work, an experimental campaign studying this kind of connections is needed.

7   Acknowledgements

8   References

Anderson, G. T. (2001). "Experimental Investigation of Group Action Factor for Bolted Wood Connections". MA thesis. Virginia Polytechnic Institute and State University. ISBN: 9835103658.

Cabrero, J. and M. Yurrita (2018). "Performance assessment of existing models to predict brittle failure modes of steel-to-timber connections loaded parallel-to-grain with dowel-type fasteners." In: *Engineering Struct.* 171. doi:10.1016/j.engstruct.2018.03.037, pp. 895–910.

Celigüeta, J. T. (1998). *Curso de Análisis Estructural*. Pamplona (Spain): EUNSA. ISBN: 84-313-1612-8.

Dodson, M. A. (2003). "The Effects of Row Spacing and Bolt Spacing in 6-Bolt and 4-Bolt Wood-to-Steel Connections". MA thesis. Washington State University.

Eurocode 5 (2004). *Design of timber structures – Part 1-1: General and rules for buildings.* EN 1995-1-1:2004. Brussels, Belgium: Comité Européen de Normalisation (CTN).

Hanhijärvi, A. and A. Kevarinmäki (2008). "VTT PUBLICATIONS 677: Timber Failure Mechanisms in High-Capacity Dowelled Connections of Timber to Steel.ISBN 9789513870904". In:

Hanhijärvi, A. and A. Kevarinmäki (2007). "Design method against timber failure mechanisms of dowelled steel-to-timber connections". In: *CIB-W18 Timber Structures*. Bled, Slovenia, Paper 40-7-3.

Hübner, U. (2013). "Mechanische Kenngrößen von Buchen, Eschen und Robinienholz für lastabtragende Bauteile". PhD thesis. Technische Universität Graz, p. 425.

Jockwer, R., G. Fink, and J. Köhler (2018). "Assessment of the failure behaviour and reliability of timber connections with multiple dowel-type fasteners". In: *Engineering Structures* 172. doi:10.1016/j.engstruct.2018.05.081, pp. 76–84.

Johnsson, H. and G. Parida (2013). "Prediction model for the load-carrying capacity of nailed timber joints subjected to plug shear". In: *Materials and Structures* 46.12. doi:10.1617/s11527-013-0030-8, pp. 1973–1985. ISSN: 1359-5997.

Kangas, J. and J. Vesa (1998). "Design on timber capacity in nailed steel-to-timber joints". In: *CIB-W18 Timber Structures*. Savonlinna, Finland, Paper 31-7-4.

Kevarinmäki, A. (2009). *Design method for timber failure capacity of dowelled and bolted glulam connections. Research report number VTT-S-07046-09*. Helsinki: VTT Technical Research Center of Finland.

Kevarinmäki, A. (1997). *Ristipultilla vahvistetut puurakenteiden liitokset (Cross-bolt Reinforced Joints of Timber Structures). HUT/LSEBP Publication 64*. Tech. rep. Helsinki: Helsinki University of Technology.

Leivo, M., V. M. Westman, and M. Viinikainen (2000). *Teräslevyinen tappivaarnaliitos - liitoskokeet (Dowelled Steel-to-Timber Connection - Joint Tests)*. Tech. rep. University of Applied Sciences.

Massé, D., J. Salinas, and J. Turnbull (1998). *Lateral strength and stiffness of single and multiple bolts in gluelaminatedtimber loaded parallel to grain*. Tech. rep. Ottawa, Canada: Engineering and Statistical Research Centre, Research Branch, Agriculture.

Misconel, M., M. Ballerini, and V. de Kuilen J W G (2016). "Steel-to-timber joints of beech-lvl with very high strength steel dowels". In: *Proceedings of the Wolrd Conference on Timber Engineering, WCTE*. Vienna, pp. 269–276. ISBN: 978-3-903024-35-9.

Mohammad, M. and P. Quenneville (2001). "Bolted wood-steel and wood-steel-wood connections: verification of a new design approach". In: *Canadian Journal of Civil Engineering* 28.2. doi:10.1139/l00-105, pp. 254–263. ISSN: 0315-1468.

Ottenhaus, L.-M., M. Li, T. Smith, and P. Quenneville (2018). "Mode cross over and ductility of dowelled LVL and CLT connections under monotonic and cyclic loading". In: *Journal of Structural Engineering* 144.7. doi:10.1061/(ASCE)ST.1943-541X.0002074.

Quenneville, P. and M. Mohammad (2000). "On the Failure Modes and Strength of Steel-Wood-Steel Bolted Timber Connections Loaded Parallel to Grain". In: *Canadian Journal of Civil Engineering* 27.4, pp. 761–773.

Quenneville, P. and P. Zarnani (2017). *Proposal for the Connection Chapter of the New Zealand Design of Timber Structures*. Unpublished.

Reid, M. S. (2004). "Predictions of Two-Row Multi-Bolted Connections Resistance Subjected to Parallel-to-Grain Loading". MA thesis. Royal Military College of Canada.

Sjödin, J. and C.-J. Johansson (2007). "Influence of initial moisture induced stresses in multiple steel-to-timber dowel joints". In: *Holz als Roh- und Werkstoff* 65.1. doi:10.1007/s00107-006-0136-6, pp. 71–77. ISSN: 0018-3768.

SP (1992). *Dragprovning av limträbalkar. Research report number SP 91B1. Ordered by Moelven Limträ A/S*. Tech. rep. Swedish National Testing and Research Intitute.

VTT (2003). *Monileikkeisten tappivaarnaliitosten kuormituskokeet (Loading Tests of Multiple Shear Dowelled Connections). Research report no RTE 1583/03. Ordered by Wood Focus Oy*. Tech. rep. Technical Research Center of Finland.

Yurrita, M. and J. Cabrero (2019). "52 - 7 - 7. New analytic model for brittle failure in the parallel-to-grain direction of timber connections with large diameter fasteners". In: *6th Meeting of the International Network on Timber Engineering Research (INTER)*. Tacoma, USA.

Yurrita, M., J. M. Cabrero, and P. Quenneville (2019). "Brittle failure in the parallel-to-grain direction of multiple shear softwood timber connections with slotted-in steel plates and dowel-type fasteners". In: *Construction and Building Materials* 216. doi:10.1016/j.conbuildmat.2019.04.100, pp. 296–313.

Zarnani, P. and P. Quenneville (2014a). "Wood Block Tear-Out Resistance and Failure Modes of Timber Rivet Connections: A Stiffness-Based Approach". In: *Journal of Structural Engineering* 140.2. doi:10.1061/(ASCE)ST.1943-541X.0000840, p. 04013055. ISSN: 0733-9445.

Zarnani, P. and P. Quenneville (2014b). "Strength of timber connections under potential failure modes: An improved design procedure". In: *Construction and Building Materials* 60. doi:10.1016/j.conbuildmat.2014.02.049, pp. 81–90. ISSN: 09500618.

Discussion

The paper was presented by M Yurrita

P Quenneville commented that the proposal was well done to take care of the outliers in the NZ code.

R Jockwer questioned whether wood-steel-wood connections also saw brittle failure modes. H Blass commented that in timber to timber connections capacity is less compared to steel-timber connections hence less prone to brittle failures.

R Brandner commented that species would also make a difference and inclusion of mean values rather than median values would be useful.

Row shear and block shear failure of connections with axially loaded screws

Hans Joachim Blass[1,2], Marcus Flaig[2] and Nico Meyer[1]

[1]Timber Structures and Building Construction, Karlsruhe Institute of Technology

[2]Blaß und Eberhart GmbH, Karlsruhe

1 Introduction

The failure mode of an axially loaded screw generally is governed by the withdrawal capacity of the threaded part of the screw in the timber member (Figure 1 (a)), the tensile capacity of the screw itself and for partially threaded screws in timber-to-timber connections the head pull-through capacity of the screw. In connections with groups of axially loaded screws, also brittle timber failure modes are observed as e.g. row shear failure for reduced fastener spacing a_1 (Figure 1 (d)) or timber splitting for low ratios of penetration length of the screw to the depth of the timber member (Figure 1 (e)).
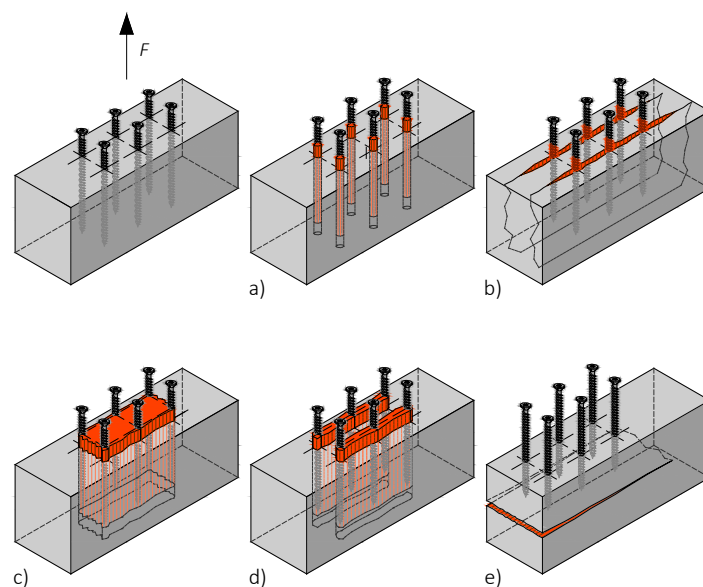
Figure 1: Timber failure modes in connections with axially loaded screws perp. to grain, (a) Withdrawal, (b) Splitting, (c) Block shear, (d) Row shear, (e) Tensile perp. to grain.

In the design of timber connections with groups of axially loaded fasteners, an effective number of fasteners $n_{ef} < n$ is used, where n is the number of axially loaded fasteners. n_{ef} takes into account the uneven load distribution between fasteners for withdrawal or tensile failure, but also brittle failure modes. Only for failure mode (e) in Figure 1 specific design models are available in codes.

Mahlknecht and Brandner (2016) published a model describing block shear failure in timber members around groups of axially loaded screws perpendicular to grain. Their model takes into account the stiffness as well as the load-carrying capacity of the contributing planes around the group of screws, where tensile stresses perp. to grain, shear or rolling shear stresses are transferred. Carradine et al. (2009) presented test results with single and groups of axially loaded screws and for the latter often observed row shear failure (Figure 2).

Figure 2: Row shear failure (mode (d) in Figure 1) in connections with axially loaded screws perpendicular to grain in LVL from Carradine et al. 2009 [2].

Meyer and Blass (2018) describe row shear failure of glued-in rods as a combination of rolling shear capacity in the timber member and withdrawal capacity of the first and last rod in the row, respectively.

Koch (2018) performed tests with axially loaded screws in softwood glulam. He confirmed the row shear model in Meyer and Blass also for screws and observed block shear as well as row shear failures. In his tests and contrary to Figure (3), the block often only comprised a part of the penetration length of the screws close to the screw heads while the lower screw parts were withdrawn from the timber member.

Fig. 3: Block shear failure (mode (c) in Figure 1) with rolling shear failure over the complete beam depth caused by axially loaded screws perpendicular to grain in glulam.

2 Row shear

Meyer und Blass (2018) studied the behaviour of connections with axially loaded glued-in rods in Beech LVL. Connections with axially loaded metric steel rods arranged between 0° and 90° between rod axis and grain direction were tested to failure. Connections consisting of a group of rods showed lower load-carrying capacities per rod compared to single rod connections. This apparent loss in load-carrying capacity in connections with rods arranged perpendicular to grain was caused by row shear failure: a small block of timber between two consecutive rods arranged in a row parallel to grain is withdrawn together with the glued-in rods (see Figure 4).
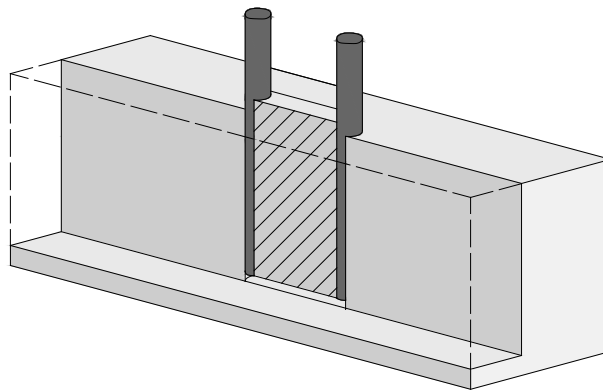
Fig. 4:   Rolling shear failure (mode (d) in Figure 1) between two axially loaded fasteners.

The load-carrying capacity $F_{90,R}$ for failure mode row shear is derived from the sum of the contributions of rolling shear in two planes and half of the axial withdrawal capacity of the two outer fasteners:

$$F_{90,R} = 2 \cdot (r-1) \cdot f_{v,r} \cdot \ell_{ef} \cdot a_1 + f_{ax} \cdot \ell_{ef} \cdot d \qquad (1)$$

where:

r is the number of fasteners arranged parallel to grain;

$f_{v,r}$ is the rolling shear strength in N/mm²;

ℓ_{ef} is the fastener penetration depth in mm;

a_1 is the fastener spacing parallel to grain in mm;

f_{ax} is the fastener withdrawal parameter in N/mm²;

d is the fastener diameter in mm.

The tensile perp to grain resistance of the plane formed by the fastener tips is disregarded.

Tests with rows of axially loaded screws in the edge face of LVL (Pinus Radiata) performed by Carradine at al. (2009) often showed row shear failure. The rolling shear strength of the LVL used in the tests is not provided, a comparison of the ultimate

test loads with equation (1) is hence hardly possible. Subsequently, Koch (2018) performed row shear tests with screws in glulam. All test results are documented in detail in Koch (2018).

In order to trigger row shear failure, the screw holes were predrilled allowing a minimum spacing $a_1 = 4\,d$ parallel to grain. Self-tapping screws with diameters $d = 6$ mm and $d = 8$ mm were used with a penetration depth of the thread of $\ell_{ef} = 10\,d$. Both, radial and tangential screw arrangement was used in the tests. Screw tensile and withdrawal capacity were determined for single screws as a basis for the test evaluation. The test results were compared with equation (1) using the following parameters:

- Expected screw's tensile capacity:
  $f_{tens} = 15$ kN for $d = 6$ mm and $f_{tens} = 26$ kN for $d = 8$ mm
- Characteristic tensile capacity of the screws:
  $f_{tens,k} = 12{,}5$ kN for $d = 6$ mm and $f_{tens,k} = 23$ kN for $d = 8$ mm
- Expected withdrawal parameter: $f_{ax} = 1{,}25 \cdot f_{ax,k} \cdot \left(\rho / 350 \right)^{0,8}$
- Characteristic withdrawal parameter:
  $f_{ax,k} = 11{,}5$ N/mm² for $d = 6$ mm and $f_{ax,k} = 11{,}0$ N/mm² for $d = 8$ mm
- Characteristic glulam density: $\rho_k = 385$ kg/m³
- Expected rolling shear strength: $f_{v,r} = 2$ N/mm²
- Characteristic rolling shear strength: $f_{v,r,k} = 1$ N/mm²

Table 1 shows the comparison between the test results and the expected and characteristic capacities $F_{90,R}$ and $F_{90,Rk}$ according to equation (1) and, additionally, the expected and characteristic capacities according to the screws' ETAs without a specific row shear design.

The **average** ratio between ultimate test load and expected load-carrying capacity is $F_{max}/F_{90,R} = 0{,}93$ or $F_{max}/F_{ETA,R} = 0{,}98$, respectively. The design according to the screws' ETAs with $n_{ef} = n^{0,9}$ hence represents the average test results better than the row shear model according to equation (1).

The **characteristic** ratio determined according to EN 14358 is $F_{max}/F_{90,Rk} = 1{,}14$ and $F_{max}/F_{ETA,Rk} = 1{,}03$, the **minimum** ratios from 28 tests $F_{max}/F_{90,Rk} = 1{,}19$ and $F_{max}/F_{ETA,Rk} = 1{,}01$. The required characteristic ratio is 1,0. Both, the row shear model as well as the design of the screws taking into account the effective number of screws, n_{ef}, lead to an adequate load-carrying capacity of axially loaded screws arranged in rows parallel to grain. Here, the row shear model is more conservative.

Table 1: *Comparison between ultimate test loads and load-carrying capacities $F_{90,R}$ according to equation (1) and according to the ETAs of the screws, respectively.*

Test	F_{max} in kN	ρ in kg/m³	$F_{90,R}$ in kN	$F_{90,Rk}$ in kN	$F_{ETA,R}$ in kN	$F_{ETA,Rk}$ in kN
RS1.1V1	18,1	470	18,6	10,2	19,0	12,0
RS1.1V2	19,4	491	18,8	10,2	19,7	12,0
RS1.1V3	13,4	434	18,2	10,2	17,8	12,0
RS1.1V4	26,0	435	18,2	10,2	17,9	12,0
RS1.1V5	12,2	371	17,4	10,2	15,7	12,0
RS1.2V1	17,8	445	18,3	10,2	18,2	12,0
RS1.2V2	16,4	476	18,7	10,2	19,2	12,0
RS1.2V3	17,5	418	18,0	10,2	17,3	12,0
RS1.2V4	13,1	446	18,3	10,2	18,2	12,0
RS1.2V5	15,5	473	18,6	10,2	19,1	12,0
RS2.1V1	36,4	440	31,9	17,8	30,7	20,4
RS2.1V2	42,1	426	31,6	17,8	29,9	20,4
RS2.1V3	26,5	393	30,9	17,8	28,0	20,4
RS2.1V4	28,2	393	30,9	17,8	28,0	20,4
RS2.1V5	27,9	467	32,4	17,8	32,2	20,4
RS2.1V6	24,2	378	30,6	17,8	27,1	20,4
RS2.2V1	28,0	455	32,2	17,8	31,5	20,4
RS2.2V2	32,0	412	31,3	17,8	29,1	20,4
RS2.2V3	30,4	432	31,7	17,8	30,2	20,4
RS2.2V4	28,6	408	31,2	17,8	28,9	20,4
RS2.2V5	34,8	437	31,8	17,8	30,5	20,4
RS2.2V6	37,0	422	31,5	17,8	29,6	20,4
RS3.1V1	16,2	456	21,3	11,7	18,6	12,0
RS3.1V2	20,3	376	20,3	11,7	15,9	12,0
RS3.1V3	15,3	407	20,7	11,7	16,9	12,0
RS3.1V4	16,7	445	21,2	11,7	18,2	12,0
RS3.1V5	15,7	405	20,7	11,7	16,9	12,0
RS3.1V6	15,5	458	21,3	11,7	18,6	12,0

3   Block shear

3.1   Design model

The only block shear model for axially loaded fasteners with force components perpendicular to grain was published by Mahlknecht and Brandner (2016). They studied the behaviour of axially loaded groups of screws in glulam and cross laminated timber loaded under 45° (only glulam) or 90° to the grain direction. Their model is similar to the model of Zarnani (2013) for block shear failure caused by loads parallel to grain. The stiffnesses of the shear, tensile and rolling shear planes (see Fig. 5) are determined as linear springs. In a first step the area with minimum ratio of load-carrying capacity to stiffness – or minimum failure deformation – is identified. The loads carried by the remaining planes are added to the load-carrying capacity of the plane failing first. The sum of the loads of the three planes just before failure of the first plane is the load-carrying capacity of the connection, unless after failure of the first plane the load-carrying capacities of the remaining planes are higher. This is checked by an iterative calculation where the planes fail progressively in the order of their respective failure deformations.
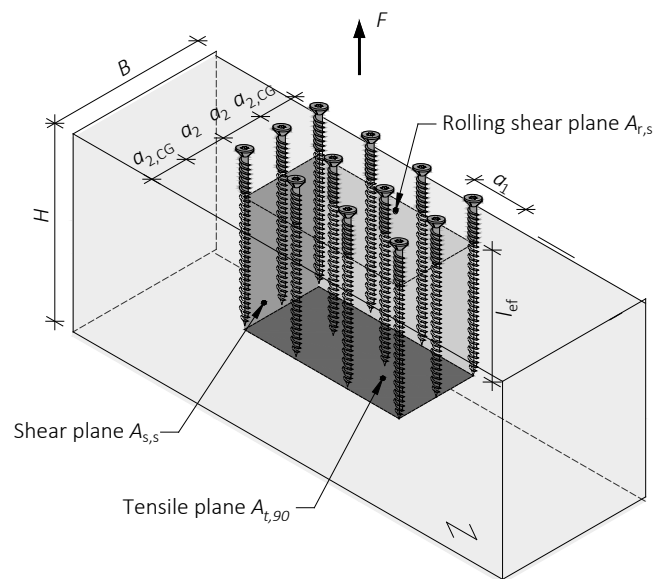
Fig. 5:   Failure planes loaded in shear, tension perp. to grain or rolling shear according to Mahlknecht and Brandner (2016).

However, shear failure in the planes $A_{s,s}$ was not observed in tests. The block shear failure was rather characterised by rolling shear planes exceeding the actual length of the connection. Another ambiguity of the model is that the spring stiffnesses of the possible failure planes are independent of the edge distance perpendicular to the grain, $a_{2,CG}$, and of the ratio ℓ_{ef}/H. For small edge distance $a_{2,CG}$ and low ratio ℓ_{ef}/H the failure will rather be tensile perpendicular to grain failure over the complete member width B without rolling shear failure, see e.g. Ehlbeck and Görlacher (1995). On the other hand, for high ratio ℓ_{ef}/H and not to small an edge distance $a_{2,CG}$, the rolling shear failure planes will cover the complete member depth H and no tensile perp. to grain failure is going to occur. Obviously, the model of Mahlknecht and Brandner

could be extended to take into account alternative failure plane patterns, however, this would further complicate the application of the already complex model.

As an alternative to the model by Mahlknecht and Brandner, Blass and Flaig (2019) proposed a simplified design model taking into account block shear failure. The modifications related to the model of Mahlknecht and Brandner are as follows:

- Shear failure in planes perpendicular to the grain is not considered,
- Brittle failure is either caused by tension perpendicular to the grain in a plane defined by the screw tips or by rolling shear in planes defined by the outer screw rows, simultaneous load transfers via rolling shear and tension perpendicular to the grain are not taken into account,
- The tension perpendicular to the grain capacity is determined according to the German national annex to Eurocode 5 (DIN EN 1995-1-1/NA),
- Rolling shear failure planes exceed the length of the connection parallel to the grain on each end by 0,75 ℓ_{ef},
- It is considered that only a part of the load component perpendicular to the grain causes tension perp. to grain stresses or rolling shear stresses.

If rolling shear initiates failure, only part of the force component perpendicular to grain causes rolling shear stresses. This is illustrated using a connection where $\ell_{ef} = h$ (see Fig. 6).
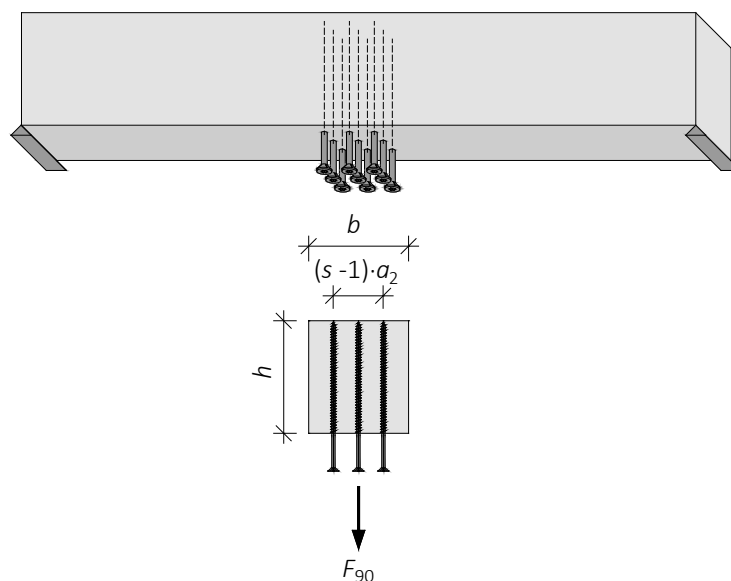
Fig. 6:   Bending member with axially loaded screws.

The beam in Fig. 6 is loaded by a concentrated force introduced over the complete beam depth using screws. In the case of rolling shear failure, the central part of the cross-section between the two outermost rows of screws is pulled down over a certain beam length (see also Fig. 3). Before rolling shear failure occurs, the load F_{90} causes a deformation of the complete beam width b. For this purpose, the cross-sectional parts outside the connection width $(s - 1) \cdot a_2$ are also pulled downwards.

The load F_{90} may be subdivided into two parts: the first part causes the deformation of the central beam part with the width $(s - 1) \cdot a_2$, the second part the deformation of the two outer beam segments with the accumulated width $b - (s - 1) \cdot a_2$. Only the second part is transferred via rolling shear stresses into the outer beam segments and consequently, only this part causes rolling shear stresses.

Assuming an extended length of the rolling shear areas $\ell_r = (r - 1) \cdot a_1 + 1{,}5 \cdot \ell_{ef}$, the average rolling shear stress over this length results as:

$$\tau_r = \frac{F_{90} \cdot \left(b - (s-1) \cdot a_2\right)}{2 \cdot b \cdot \ell_{ef} \cdot \left(1{,}5 \cdot \ell_{ef} + (r-1) \cdot a_1\right)} \tag{2}$$

The characteristic load-carrying capacity for the failure mode rolling shear follows as:

$$F_{r,90,Rk} = \frac{f_{v,r,k} \cdot 2 \cdot b \cdot \ell_{ef} \cdot \left(1{,}5 \cdot \ell_{ef} + (r-1) \cdot a_1\right)}{\left(b - (s-1) \cdot a_2\right)} \tag{3}$$

where:

$f_{v,r,k}$ is the characteristic rolling shear strength in N/mm²;

b is the beam width in mm;

r is the number of screws parallel to grain;

s is the number of screws perpendicular to grain;

a_1 is the screw spacing parallel to grain in mm;

a_2 is the screw spacing perpendicular to grain in mm in mm;

ℓ_{ef} is the screw penetration depth perpendicular to grain in mm.

The characteristic load-carrying capacity of a group of axially loaded screws hence is the minimum of the load-carrying capacities associated to the failure modes "screw tensile failure", "withdrawal failure", "tensile failure perpendicular to grain" and "rolling shear failure":

$$F_{90,Rk} = \min\left\{n_{ef} \cdot f_{tens,k}\,; n_{ef} \cdot F_{ax,Rk}\,; F_{t,90,Rk}\,; F_{r,90,Rk}\right\} \tag{4}$$

where:

$f_{tens,k}$ is the characteristic screw tensile capacity in N

$F_{ax,Rk}$ is the characteristic screw withdrawal capacity according to ETA or EN 1995-1-1 in N

n_{ef} is the effective number of screws according to EN 1995-1-1, equation (8.41)

$F_{t,90,Rk}$ is the characteristic tensile perp. to grain capacity according to DIN EN 1995-1-1/NA (2013) or equation (5) in N

$$F_{t,90,Rk} = \frac{k_s \cdot h}{h - \ell_{ef}} \cdot \left(6{,}5 + \frac{18 \cdot \ell_{ef}^2}{h^2}\right) \cdot \left(t_{ef} \cdot h\right)^{0,8} \cdot f_{t,90,k} \tag{5}$$

$$k_s = \max\left\{1; 0,7 + \frac{1,4 \cdot (r-1) \cdot a_1}{h}\right\} \tag{6}$$

where:

h is the beam depth in mm

t_{ef} is the effective width of tensile area A_t,

         $t_{ef} = \min \{b; (s-1) \cdot a_2 + 6\,d; 6 \cdot s \cdot d\}$ in mm

$f_{t,90,k}$ is the characteristic tensile perp. to grain strength in N/mm²

$F_{r,90,Rk}$ is the characteristic rolling shear capacity according to equation (3) in N

3.2 Test results

Tests with groups of axially loaded screws in spruce glulam were performed by Mahlknecht and Brandner (2016), Ringhofer and Schickhofer (2015) and Koch (2018). Mahlknecht and Brandner only give average load-carrying capacities of the test series, Ringhofer and Schickhofer as well as Koch provide single test results.

The tests by Mahlknecht and Brandner showed different failure modes depending on the joint configuration. Test series A to E were performed with screws arranged under 45° to the grain, series H to I with screws perpendicular to the grain. Screw tensile and withdrawal capacity were determined for single screws as a basis for the test evaluation. The test results were compared with equation (4) using the following parameters:

- Average ultimate load per series perpendicular to member axis: F_{max}
- Expected screw's tensile capacity:
  $f_{tens} = 15,6$ kN for $d = 6$ mm and $f_{tens} = 27,8$ kN for $d = 8$ mm
- Expected withdrawal parameter: $f_{ax} = 1,25 \cdot f_{ax,k} \cdot (\rho/350)^{0,8}$
- Characteristic withdrawal parameter:
  $f_{ax,k} = 12,1$ N/mm² for $d = 6$ mm and $f_{ax,k} = 10,9$ N/mm² for $d = 8$ mm
- Characteristic glulam density: $\rho_k = 385$ kg/m³
- Expected rolling shear strength: $f_{v,r} = 2$ N/mm²
- Expected tensile strength perpendicular to grain: $f_{t,90} = 1$ N/mm²

Table 2 shows the comparison between the test results and the expected capacities $F_{90,R}$ according to equation (4) for the different failure modes. A significant difference between the test results for load directions 45° and 90°, respectively, could not be found. The simultaneous occurrence of rolling shear and shear stresses in the rolling shear planes for load direction 45° obviously did not influence the test results. This does not prove, however, that there is no shear/rolling shear interaction since the rolling shear capacity did not govern the design.

Table 2:   Comparison between ultimate test loads and load-carrying capacities according to equation (4) for the different failure modes.

Test series	F_{max} in kN	ρ in kg/m³	$n_{ef} \cdot F_{ax,R}$ in kN	$n_{ef} \cdot f_{tens}$ in kN	$F_{t,90,R}$ in kN	$F_{r,90,R}$ in kN
A	155	486	177	119	393	366
B	155	486	177	119	393	366
C	145	486	141	119	212	259
D	120	486	105	119	128	177
E	127	486	105	119	128	274
H	275	428	252	221	1061	675
N	179	428	123	181	166	315
K	171	428	150	221	144	282
O	184	461	160	221	548	372
J	191	461	160	221	548	282
I	183	461	131	181	543	280

The **average** ratio between ultimate test load and expected load-carrying capacity is $F_{max}/F_{90,R}$ = 1,25. Since the calculated rolling shear failure was not governing in any of the test series, the design according to the screws' ETAs also represents the average test results well. Even though the single test results are not given, the research report shows that for all 103 single tests F_{max} was higher the characteristic load-carrying capacity according to the screws' ETAs.

The ultimate loads of the single tests by Ringhofer and Schickhofer (2015) and Koch (2018) were also compared with the results of equation (4). The comparison was performed for **expected** values of the load-carrying capacity as for the tests by Mahlknecht and Brandner but also on a **characteristic** level. For the latter, the characteristic load-carrying capacity was calculated according to equation (4) and the ratio $F_{max}/F_{90,Rk}$ was calculated for each one of the 64 tests. For 28 out of the 64 tests the rolling shear capacity was governing. Subsequently, the characteristic ratio according to EN 14358 was calculated. The characteristic load-carrying capacity of the connections is seen as sufficient, if the characteristic ratio according to EN 14358 does not fall below 1,0.

The **average** ratio between ultimate test load and expected load-carrying capacity is $F_{max}/F_{90,R}$ = 1,49. The calculation model underestimates the expected load-carrying capacity of the connections.

The **characteristic** ratio determined according to EN 14358 is $F_{max}/F_{90,Rk}$ = 1,20, the **minimum** ratio $F_{max}/F_{90,Rk}$ = 1,10 and the COV of the ratio $F_{max}/F_{90,Rk}$ is 11%. The required characteristic ratio is 1,0. The block shear model according to equation (4) hence leads to an adequate load-carrying capacity of groups of axially loaded screws with a load component perpendicular to grain.

4 Conclusions

The present paper considers brittle failure modes in connections with screws loaded axially perpendicular to grain. The available test data are evaluated and compared with design proposals from Mahlknecht and Brandner (2016) for block shear, Meyer and Blass (2018) for row shear as well as with the approach only based on an effective number of fasteners n_{ef}. Even if an effective number of fasteners n_{ef} primarily incorporates the influence of uneven load distribution between the single screws in a connection, it obviously also at least partly compensates for brittle failure modes as block shear failure or row shear failure.

The analytical model derived for glued-in rods taking into account row shear failure in connections with axially loaded fasteners arranged in rows parallel to grain and loaded perpendicular to grain also very well predicts the load-carrying capacity of similar connections with screws. This model may also be used for groups with several rows of screws, if the spacing a_2 perpendicular to grain is large.

The analytical model proposed by Mahlknecht and Brandner for block shear failure in connections with groups of axially loaded screws and load components perpendicular to grain was modified as follows:

- Shear planes perpendicular to the grain are not considered,
- Brittle failure is either caused by tension perpendicular to the grain in a plane defined by the screw tips or by rolling shear in planes defined by the outer screw rows, simultaneous load transfers via rolling shear and tension perpendicular to the grain are disregarded,
- The tension perpendicular to the grain capacity is determined according to the German national annex to Eurocode 5 (DIN EN 1995-1-1/NA),
- Rolling shear failure planes exceed the length of the connection parallel to the grain on each end by 0,75 ℓ_{ef},
- It is considered that only a part of the load component perpendicular to the grain causes tension perp. to grain stresses or rolling shear stresses.

In order to verify the modified analytical model, ultimate test loads of axially loaded screwed connections are compared with the results of the model. The ultimate loads from the tests agree well with the model predictions. For the comparison, the model parameters screw tensile strength and withdrawal capacity were determined separately by tests. If block shear design is disregarded, the design of axially loaded screwed connections according to the screws' ETAs still leads to an adequate load-carrying capacity.

5 References

Blass, H.J. and Flaig, M. (2019). "Block shear failure in the connection area of timber members with axially loaded screws" (in German). Research report, Karlsruher Berichte zum Ingenieurholzbau (submitted for publication).

Carradine, D.M., Newcombe, M.P. and Buchanan, A.H. (2009). "Using Screws for Structural Applications in Laminated Veneer Lumber." Proc., International council for research and innovation in building and construction, CIB-W18, Switzerland, paper 42-7-7.

Ehlbeck, J., Görlacher R. and Werner, H. (1989). „Determination of Perpendicular-to-Grain Tensile Stresses in Joints with Dowel-Type Fasteners - A draft proposal for design rules" Proc., International council for research and innovation in building and construction, CIB-W18, German Democratic Republic, paper 22-7-2.

Ehlbeck, J. and Görlacher R. (1995) „Tension perpendicular to the grain in joints". In: Timber Engineering STEP 1, Basis of design, material properties, structural components and joints. Lecture C2. Centrum Hout, The Netherlands, ISBN 90-5645-001-8.

DIN EN 1995-1-1/NA (2013). National Annex – Nationally determined parameters – Eurocode 5 – Design of timber structures – Part 1-1: General – Common rules and rules for buildings.

Koch, E. (2018). "Block shear failure in connections with axially loaded screws" (in German). Master's Thesis, KIT Timber structures and building construction, 157 pp.

Mahlknecht, U., Brandner, R. and Augustin M. (2016). „Block shear failure mode of axially loaded groups of screws." Proc., World Conference on Timber Engineering WCTE 2016, Vienna, Austria.

Meyer, N. and Blass H.J. (2018). „Connections with glued-in rods in trusses made of Beech-LVL". Proc., World Conference on Timber Engineering WCTE 2018, Seoul, Korea.

Ringhofer, A. and Schickhofer, G. (2015). „Ausziehprüfungen von Schraubengruppen in Anlehnung an das EAD 130015-00-0603, Abschnitt 2.2.1.10 zur Bestimmung der Mindestabstände a_1 und a_2". Prüfbericht NR. PB15-471-1-01, Lignum Test Center (LTC), TU Graz, 42 S.

Zarnani, P. (2013). "Load-Carrying Capacity and Failure Mode Analysis of Timber Rivet Connections" Dissertation, Department of Civil and Environmental Engineering, The University of Auckland, New Zealand.

Discussion

The paper was presented by H Blass

S Franke asked what rolling shear strength was used. H Blass responded 1 MPa per EN480.

S Franke stated that the paper assumed the screws all have the same forces and asked if this was fine. H Blass stated that this was an assumption that seemed to work fine.

B Sullivan asked about diagonal rows on block shear effect. H Blass said this is not with the scope of the study and will find out later.

JM Cabrero received definition of the outer perimeter and asked if one could use this as a parameter. H Blass explained that if tension failure perpendicular to grain occurred first this would lead to dynamic effect to row shear failure. T Tannert followed up and asked whether tension or row shear governed. H Blass said both would govern and confirmed that small specimens for rolling shear testing was used.

S Winter commented about rolling shear strength being 1.2 to 1.3 MPa.

S Aicher stated that from mechanics point of view inclusion of stiffness would be important. H Blass responded that this is still being discussed as the spring stiffness would be dependent on the geometrical arrangements of the screws and the parameters to establish spring stiffness are not clear.

R Brandner agreed that more discussion on this issue would be needed. He agreed that n_{ef} should not be used to consider brittle failure.

H Xiong and H Blass discussed the use of screws in tension perpendicular to grain applications.

P Quenneville asked what if stiffness of the shear spring were made much higher than the outer two springs. H Blass stated the actual failure plane seemed to be much larger than assumed. F Lam commented that the observed failure plane or failure area would be determined after the fact and might be much different from that at time of failure. H Blass agreed.

J Chen and H Blass discussed the expected capacity based on ETA and test results with the test results of screw groups being lower. There is a direct correlation between the characteristic values in ETA to test results of the screw group.

New analytic model for brittle failure in the parallel-to-grain direction of timber connections with large diameter fasteners

Miguel Yurrita. Wood Chair. Department of Building Construction, Services and Structures. University of Navarra. 31009 Pamplona, Spain. myurrital@alumni.unav.es

José Manuel Cabrero. Wood Chair. Department of Building Construction, Services and Structures. University of Navarra. 31009 Pamplona, Spain. jcabrero@unav.es

1   Introduction

Timber connections with steel fasteners are nowadays the most widespread type of joint applied in timber engineering. Fig. 1a depicts a typical timber-to-steel connection, with a total of 9 large diameter fasteners (such as dowels or bolts) which protrude the whole timber thickness, distributed in 3 columns and 3 rows loaded parallel-to-grain. All the main geometrical parameters and the used nomenclature within this paper are included in Fig. 1.

There are several types of connections depending on the number and relative position of the timber elements and steel plates: wood steel-wood or *sws* connection (two side timber members and a central steel plate, Fig. 1c); wood-steel (*ws*, Fig. 1b), steel-wood-steel (*sws*, Fig. 1d), steel-wood-steel (*sws*, Fig. 1d) or the multiple shear plane connections (*msp*, Fig. 1e) that combine several timber and steel elements. All of them may be also designed with only wood, by replacing the steel plates with another timber element.

Traditionally, the design of timber connections with steel fasteners has been focused on assuring a ductile failure mode, being the European Yield Model (EYM) the usual calculation procedure. The ductile failure mode, namely embedment of timber and yielding of the fastener (Fig. 2a) is the only possible ductile failure mode for a timber connection with large diameter fasteners loaded in the parallel-to-grain direction. The
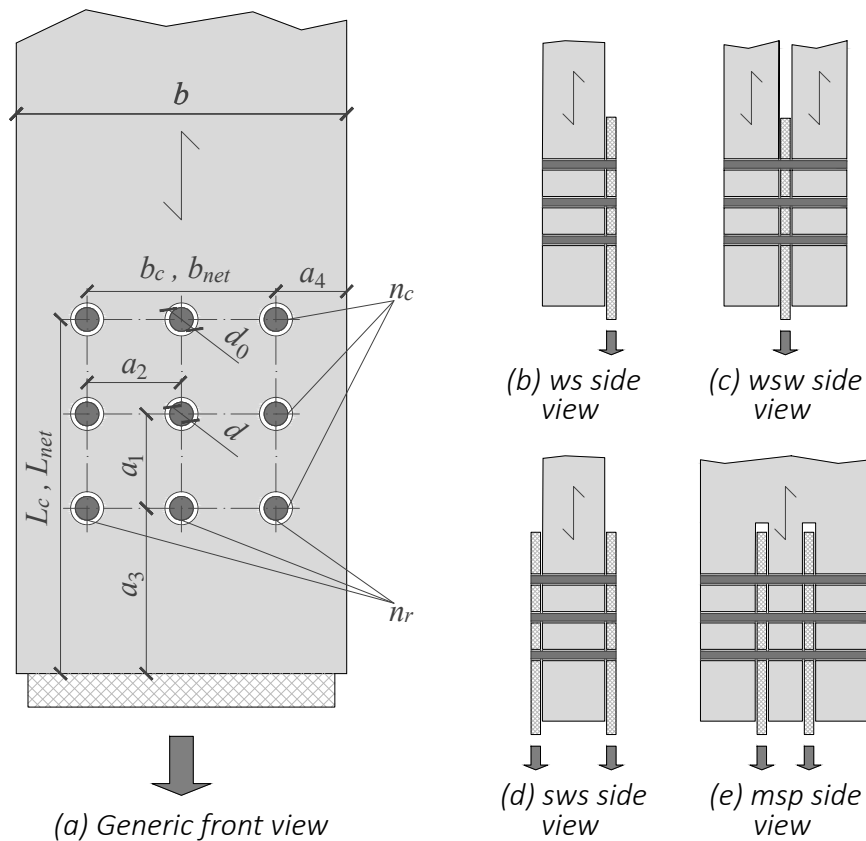
Figure 1. Basic geometry of a generic timber-to-steel connection with large diameter fasteners. Front view and possible side views configurations are given.

rest of them, all represented in Fig. 2, are brittle failure modes: splitting (Fig. 2b), row shear (Fig. 2c), block shear (Fig. 2d) and net tension (Fig. 2e).

Even though these brittle failure modes may lead to a sudden collapse of the building (with the human and material damages associated) they were omitted until the 1980s, when some authors such as *Nozynski* (1980) started to consider them. Since then, many proposals appeared dealing with one or more of this failure modes. Some of them were included in codes such as the Eurocode 5 (2004), the *CSA Standard O86-09* (2009) or in the connection chapter of the future version of the New Zealand standard (*Quenneville and Zarnani*, 2017), which is an evolution from the Canadian proposal. For a detailed analysis and comparison among all of them, the reader is referred to *J. Cabrero and Yurrita* (2018).

2 Existing proposals

Only three of the existing proposals consider in a consistent way all the possible brittle failure modes: the Eurocode 5 (2004), the model from *Hanhijärvi and Kevarinmäki* (2008) and the one from *Quenneville and Zarnani* (2017). All of them are intended as design models which allow to determine the capacity of the failure planes involved in each failure mode. Such capacity is based on the area of the load planes where the failure may occur: the shear lateral planes (related to row shear -Fig. 3a- and block shear

(a) Embedment   (b) Splitting   (c) Row shear   (d) Block shear   (e) Net tension
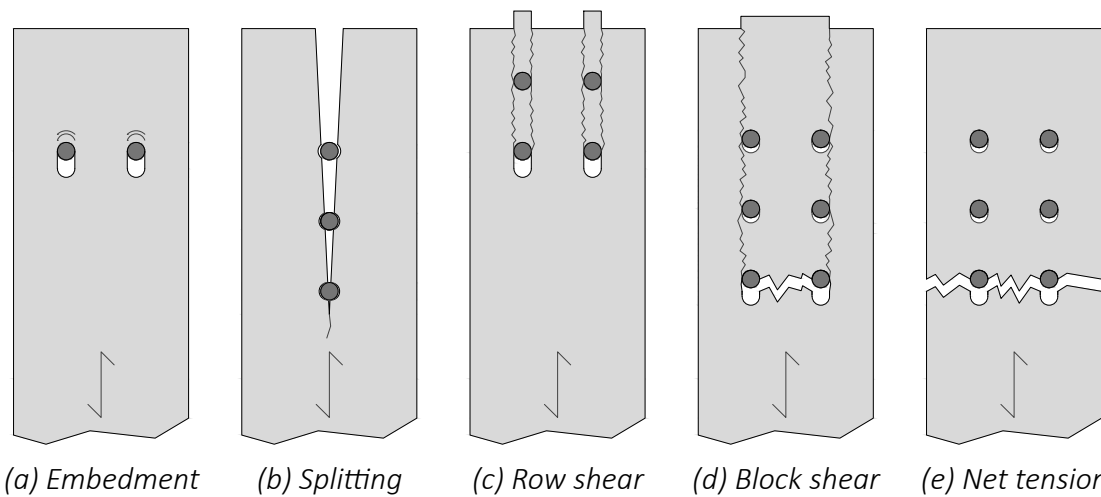
Figure 2. Possible failure modes of a timber connection with dowel-type fasteners: (a) embedment is the only ductile failure mode, the rest are brittle.

-Fig. 3b-) and the head tension plane (related to block shear -Fig. 3b- and net tension -Fig. 3c-). The obtained area is then multiplied by corresponding strength, either tensile strength parallel-to-grain $f_{t,0}$ (head plane H) or the shear strength f_v (lateral planes L).

The Eurocode 5 (2004) is the only which to obtains some of the brittle capacities by means of the ductile model (EYM), reduced with the effective number of fasteners n_{ef}. This parameter, derived from the work from *Jorissen* (1998), can be assumed to include both row shear and splitting failures, although the designer is not informed of such brittle failures. Block shear for connections with steel plates was included in its informative Annex A.

The model from *Hanhijärvi and Kevarinmäki* (2008) considers all the possible failure modes at once in a single calculation procedure. The method may lead to an inconsistent failure mode that could be a mixture of many of them.

Quenneville and Zarnani (2017) analyse each failure mode separately. Only splitting is not considered, as it is unexpected to be the case in connections with more than one row of fasteners and this is the case of most of the connections used in practice.

In *Yurrita and J. M. Cabrero* (2018) the prediction ability of these three models was compared. The comparison demonstrated that the Eurocode 5 (2004) obtained the worst accuracy, and was deemed as too conservative. Meanwhile, the other two models reached similar results, but the model from *Quenneville and Zarnani* (2017) performed slightly better. Its accuracy, in addition to its superior simplicity, positioned this latter model as the most convenient one.

The performed analysis allowed to detect several weak points in the three models such as the effective thickness of the fastener -the new proposal for this parameter is presented in the companion paper (*Yurrita and J. Cabrero*, 2019)-, the length of the shear planes, or the relation between the head tensile and lateral shear planes.

(a) Row shear   *(b) Block shear*   *(c) Net tension*
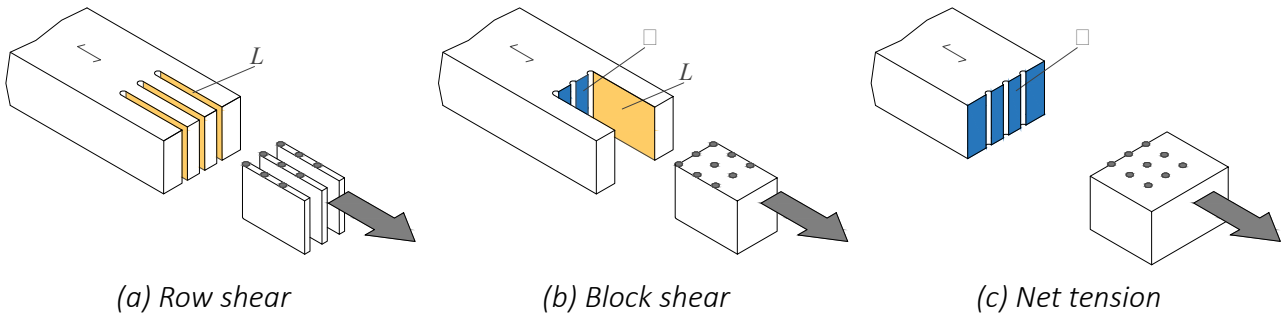
Figure 3. Loading planes (lateral shear L, and head tensile H) related to each failure mode.

3   Proposal of a new model

Taking as a basis the simplicity reached by the model from *Quenneville and Zarnani* (2017) a new design model that analyses separately each failure mode and incorporates the newly included considerations is proposed. A complete summary of the proposal for brittle failure of connections with large diameter fastener is given below.

3.1   General considerations

The brittle load capacity F_B of a connection may be obtained as:

$$F_B = \sum_1^n F_{B,i} \tag{1}$$

where $F_{B,i}$ is the brittle load capacity of each timber member i.

In the case of a multiple shear plane connection of any number of shear planes n_s, the predicted load capacity may be improved by means of a stiffness model (*Yurrita, J. M. Cabrero, and Quenneville*, 2019) which leads to the following expression:

$$F_B = \min \begin{cases} F_{b,1}\left(2 + \frac{n_s-2}{2}\frac{t_2}{t_1}\right) & \text{(outer members),} \\ F_{b,2}\left(\frac{n_s-2}{2} + 2\frac{t_1}{t_2}\right) & \text{(inner members),} \end{cases} \tag{2}$$

where the subscripts 1 and 2 refer to the outer and inner timber members respectively, and t_i is their thickness. The equation (2) assumes a symmetrical joint configuration, where the outer members are equal, and so are the inner members.

The brittle capacity $F_{B,i}$ of a single timber element i is obtained as the minimum of the different brittle failure modes:

$$F_{B,i} = \min \begin{cases} F_{B,rs,i} & \text{(row shear failure),} \\ F_{B,bs,i} & \text{(block shear failure),} \\ F_{B,nt,i} & \text{(net tension failure).} \end{cases} \tag{3}$$

As previously done by *Quenneville and Zarnani* (2017), splitting is not considered in this model, as it is not an expected failure mode for connections with more than a row of fasteners.

3.2 Brittle load capacity of a timber member

3.2.1 Row shear

The row shear capacity $F_{B,rs}$ of a timber member i is defined by the load capacity $F_{L,i}$ of the two lateral shear planes L generated by each row of fasteners of the connection, as shown in Fig. 3a:

$$F_{B,rs,i} = 2n_r F_{L,i}, \tag{4}$$

where n_r is the number of rows and $F_{L,i}$ is the shear capacity of the lateral plane given in (6).

3.2.2 Block shear

The block shear is defined by the failure of two lateral shear planes L and a head tensile plane H, as depicted in Fig. 3b. The block shear capacity $F_{B,bs,i}$ of a timber element i is thus defined as:

$$F_{B,bs,i} = 2F_{L,i} + F_{T,i}, \tag{5}$$

where $F_{L,i}$ is the shear capacity of the lateral shear planes L given in (6) and $F_{T,i}$ is the tension capacity of the head plane H given in (11).

3.2.3 Net tension

The net tension capacity $F_{T,net}$ of a timber member i is determined by the capacity of the net cross sectional area of the timber element, defined in (12) and shown in Fig. 3c.

3.3 Plane capacities

3.3.1 Lateral shear plane

The capacity of each lateral shear plane $F_{L,i}$ is defined as:

$$F_{L,i} = k_v t_{ef} L_c f_v, \tag{6}$$

where k_v is the shear factor ($k_v = 0.4 + \sqrt{\frac{f_v}{f_{t,0}}}$); L_c is the length of the shear plane ($L_c = a_1(n_c-1)+a_3$); and t_{ef} is the effective depth of the lateral plane along the timber element, defined as:

- Thin plates:

Outer members: $t_{ef} = \begin{cases} 0.66t & \text{if } \frac{t}{d} \leq 3 \\ \max\left(0.76 - \frac{t}{30d}; 0.2\right)t & \text{if } \frac{t}{d} > 3 \end{cases}$ (7)

Inner members: $t_{ef} = \begin{cases} t & \text{if } \frac{t}{d} \leq 7 \\ \max\left(1.7 - \frac{t}{10d}; 0.5\right)t & \text{if } \frac{t}{d} > 7 \end{cases}$ (8)

- Thick plates:

Outer members: $t_{ef} = \begin{cases} t & \text{if } \frac{t}{d} \leq 3 \\ \max\left(1.17 - \frac{t}{18d}\right); 0.35t & \text{if } \frac{t}{d} > 3 \end{cases}$ (9)

Inner members: $t_{ef} = \begin{cases} t & \text{if } \frac{t}{d} \leq 11.5 \\ \max\left(1.95 - \frac{t}{12d}\right); 0.65t & \text{if } \frac{t}{d} > 11.5 \end{cases}$ (10)

where t is the thickness of the corresponding timber member and d is the diameter of the fastener.

Same formulae may be applied to obtain the effective depth in connections with multiple shear planes. However, as the influence of the adjacent parts is not considered, a reduction factor of 0.85 of the obtained effective thickness is recommended as a simplification.

3.3.2 Head tensile plane

The capacity of the head tensile plane $F_{T,i}$ of the timber member i is obtained as:

$$F_{T,i} = k_t A_{T,b} f_{t,0},$$ (11)

where k_t is the tensile factor ($k_t = 0.9 + \sqrt{\frac{f_v}{f_{t,0}}}$) and $A_{T,b}$ is the head tensile plane area ($A_{T,b} = (a_2 - d_0)(n_r - 1)t$, where d_0 is the hole diameter).

3.3.3 Tensile plane for net tension

The capacity of the tensile plane for net tension $F_{T,net,i}$ is defined as:

$$F_{T,net,i} = A_{T,n} f_{t,0},$$ (12)

where $A_{T,n}$ is the net tensile plane area ($A_{T,n} = b - d_0 n_r t$).

4 Validation of the new design model

An extensive database of tests has been gathered in order to compare the prediction accuracy of the three existing models and the proposal. The validation process has been performed in two stages. The first one considered only the tests that failed in a brittle way in order to check the prediction ability of the studied models. The work of 18 authors, with a total of 236 different configurations and 1193 single test was used (see Table 1). Almost all of the tests considered in this stage were steel-to-timber connections with LVL or glulam.

In the second stage, the discrimination ability between ductile and brittle failure modes for each model was assessed. For this stage, 108 new configurations from 4 test campaigns were added, leading to a total of 22 authors, 344 configurations and 1625 single tests. Most of the new included tests failed in a ductile way, in order to have a representative share of ductile failures.

4.1 Evaluation of the prediction accuracy of brittle load capacity

In order to compare the prediction ability of the calculation models with the test results, the mean level is considered to be more adequate than the characteristic one due to the reduced number of replicates tested per configuration. Therefore, the mean material properties have been obtained from the characteristic ones by means of the model from *Jockwer et al.* (2018). The obtained values were used to calculate the theoretical brittle load capacity of each test configuration according to the four analysed models: Eurocode 5 (2004), *Hanhijärvi and Kevarinmäki* (2008), *Quenneville and Zarnani* (2017) and the proposal.

The prediction ability of all of them is plotted in Fig. 4, where the test results (F_{test}, abscissas axis) are compared to the theoretical predictions ($F_{predicted}$, ordinates axis). A linear fitting passing through the origin of coordinates of the three main types of connection configurations (*sws*, *wsw* and *msp*) and its corresponding slope m and coefficient of correlation R^2 are provided. The perfect correlation 1:1 is given as a reference by means of a dashed line.

It can be seen how the Eurocode 5 (2004) -Fig. 4a- is too conservative, it obtains a very scattered graphic, conservative and quite different slopes among the joint configurations. On the other side, *Hanhijärvi and Kevarinmäki* (2008) -Fig. 4c- tend to overestimate the results, specially for *msp* connections. A better performance is obtained by *Quenneville and Zarnani* (2017) -Fig. 4b-, where the slopes for each configuration type are quite similar among them and close to the ideal slope $m = 1$. However, it is still very scattered, specially for *wsw* connections (lowest R^2 obtained in the whole analysis). Finally, the proposal -Fig. 4d- reaches the best results, with almost the same slopes for every configuration (around 0.99 – 1.00, close to the ideal one) and the least scattered graphic.

Table 1. Summary of the tests used for the validation of the brittle failure models.

Author	Number of		Joint scheme						Fastener Type		Timber product				Failure mode	
	Config.	Tests	sws	ws[a]	ww[a]	wsw	www	msp[b]	Bolt	Dowel	Glulam	LVL	CLT	Solid	Ductile	Brittle
Brittle failure tests																
Massé et al. (1998)[c]	5	15	5	-	-	-	-	-	-	5	5	-	-	-	4	1
Mishler (1998)	73	249	-	-	-	-	-	73	0	73	70	3	-	-	15	58
Quenneville and Mohammad (2000)[c]	37	370	37	-	-	-	-	-	37	-	36	-	-	1	6	31
Mohammad and Quenneville (2001)[c]	13	130	-	1	-	12	-	-	13	-	13	-	-	-	-	13
Anderson (2001)[c]	3	9	-	1	2	-	-	-	3	-	3	-	-	-	-	3
Dodson (2003)	6	27	6	-	-	-	-	-	-	6	6	-	-	-	-	6
Reid (2004)[c]	4	40	4	-	-	-	-	-	-	4	4	-	-	-	-	4
Sjödin and Johansson (2007)	6	30	-	-	-	6	-	-	-	6	6	-	-	-	-	6
Leivo et al. (2000)[d]	4	12	-	-	-	4	-	-	-	4	4	-	-	-	-	4
SP (1992)[d]	2	4	-	-	-	-	-	2	2	-	2	-	-	-	-	2
Kevarinmäki (1997)[d]	1	3	1	-	-	-	-	-	1	-	1	-	-	-	-	1
VTT (2003)[d]	1	3	1	-	-	-	-	-	1	-	1	-	-	-	-	1
VTT2008[e]	39	118	16	-	-	13	-	10	-	39	23	16	-	-	2	37
Hübner (2013)	3	15	3	-	-	-	-	-	3	-	-	-	-	3	-	3
Legras (2009)[f]	3	18	-	-	-	3	-	-	3	-	-	3	-	-	-	3
Misconel et al. (2016)[c]	2	10	-	-	-	2	-	-	1	1	-	2	-	-	-	2
Ottenhaus et al. (2018)	6	30	-	-	-	6	-	-	-	6	-	-	3	3	2	4
Yurrita, J. M. Cabrero, and Quenneville (2019)	28	110	-	-	-	-	-	28	-	28	16	12	-	-	-	28
Total brittle tests	236	1193	72	2	2	46	0	114	64	172	190	36	3	7	29	207
%	-	-	30.5%	0.8%	0.8%	19.5%	0%	48.3%	27.1%	72.9%	80.5%	15.3%	1.3%	3%	12.3%	87.7%
Ductile failure tests																
Ehlbeck and Werner (1989)	45	146	-	-	-	-	45	-	-	45	-	-	-	45	45	-
Ehlbeck, J. and Werner, H. (1992)	47	141	-	-	-	-	47	-	-	47	-	-	-	47	47	-
Jorissen (1998)[c]	8	121	-	-	-	-	8	-	-	8	-	-	-	8	8	-
Ballerini (2012)	8	24	-	-	8	-	-	-	8	-	-	-	-	8	8	-
Total brittle + ductile tests	344	1625	72	2	10	46	100	114	72	272	190	36	3	115	137	207
%	-	-	20.9%	0.6%	2.9%	13.4%	29.1%	33.1%	20.9%	79.1%	55.2%	10.5%	0.9%	33.4%	39.8%	60.2

[a] As there is only two configurations of ww and ws, they have been gathered with the wsw configurations.
[b] All the multiple shear connections have 4 shear planes, except three configurations with 6 and one with 8 shear planes.
[c] Only the test with two or more rows of fastener have been considered.
[d] Results gathered and reported by Kevarinmäki, A. (2009).
[e] One configuration has been discarded as the properties of the timber were not provided.
[f] Only the tests assembled and tested at normal moisture conditions are included.
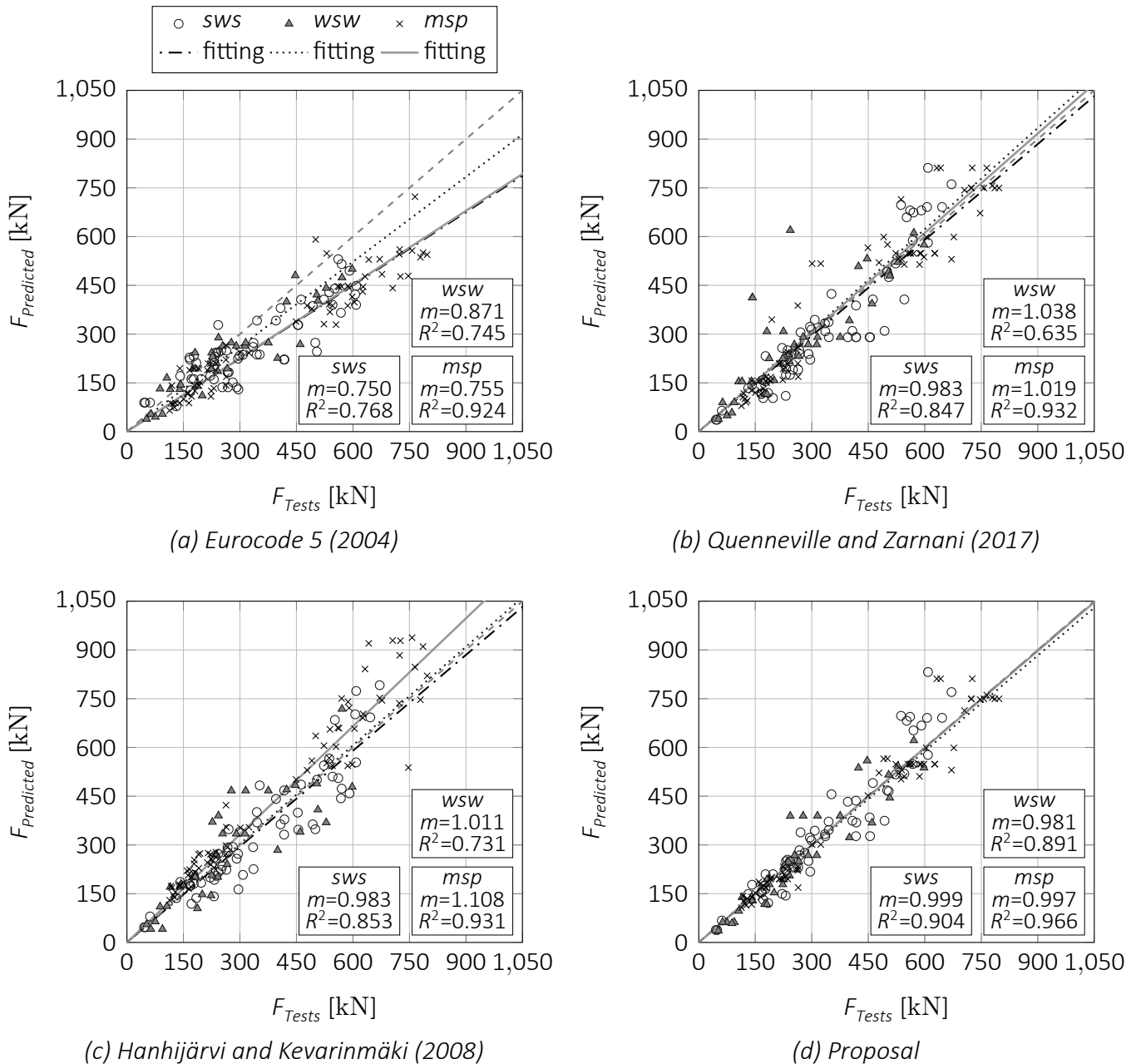
Figure 4. Comparison between the values obtained from the tests F_T and the corresponding theoretical values F_P predicted by the models from Eurocode 5 (2004), Quenneville and Zarnani (2017), Hanhijärvi and Kevarinmäki (2008), and the proposed model. The results are divided by the joint configuration (sws, wsw or msp).

Table 2. Evaluation of the accuracy obtained by the four studied models and the proposal. The used metrics are the coefficient of determination Q^2, the mean root error (MRE) and its standard devition (SD), the slope of the fitting line m, the correlation coefficient c and the concordance correlation coefficient CCC, as described in J. Cabrero and Yurrita (2018).

Model	Q^2	MRE (SD)	m	c	CCC
Eurocode 5 (2004)	0.717	0.253 (0.199)	0.767	0.913	0.832
Quenneville and Zarnani (2017)	0.864	0.154 (0.161)	1.011	0.930	0.938
Hanhijärvi and Kevarinmäki (2007)	0.863	0.172 (0.144)	1.062	0.945	0.938
Proposal	**0.941**	**0.104 (0.103)**	**0.966**	**0.969**	**0.972**

A statistical analysis considering all the results together is given in Table 2. Here, several metrics are used to evaluate the four models: the coefficient of determination Q^2 (best values are those closest to 1), the mean root square error *MRE* and its corresponding standard deviation *SD* (lower values are the best ones), the fitting slope *m*, the correlation coefficient *c* (values closer to 1 are the best) and, finally, the concordance correlation coefficient *CCC* (values close to 1 are the best ones, with a recommended threshold value of 0.85). The reader is referred to *J. Cabrero and Yurrita* (2018) for a detailed description of these metrics.

The statistical analysis confirms the Eurocode 5 (2004) as the worst model, as consistently proved by the least accurate metrics. The models from *Hanhijärvi and Kevarinmäki* (2008) and *Quenneville and Zarnani* (2017) obtain quite even results. The first one reaches a better correlation coefficient and error measurement *MRE*, but a worse slope. In fact, they reach the same value of the *CCC* parameter, which can be considered as a summary of the rest of analysed metrics. Finally, the proposal is consistently rated as the best in all the metrics.

A similar conclusion may be obtained from the boxplot graphic shown in Fig. 5. Here, the ratio between the predicted load F_P of each model and the tested load capacity F_T is used as the main parameter. The Eurocode 5 (2004) is again confirmed as the worst and most conservative model (most of the results, as shown by the box, are below the ratio $F_P/F_T = 1$ and there are several outliers). *Hanhijärvi and Kevarinmäki* (2008) get a low number of outliers, but their model tends to overpredict the connection capacity. The model from *Quenneville and Zarnani* (2017) shows numerous outliers, some of them reaching values of F_P/F_T up to a value of $F_P/F_T = 3$. The proposal presents the most reduced box and whiskers (lowest scatter), with its median value quite close to the ideal ratio $F_P/F_T = 1$ and only a few outliers.

4.2   Discrimination ability between ductile and brittle failure

Moreover, for a comprehensive system such as the ones herein analysed, it is required to additionally verify its ability to correctly discriminate between ductile and brittle failure modes. For such analysis both the ductile (usually the EYM) and brittle models are used. The lower value among them is determined as the predicted failure mode, which should match to the experimental failure mode. Fig. 6 presents in dark gray the positive matches (true ductile and true brittle) and in bright gray the errors (false ductile and false brittle).

The ductile model used for the models by *Quenneville and Zarnani* (2017) and the proposal is the EYM without considering the n_{ef} parameter. *Hanhijärvi and Kevarinmäki* (2008) already include the ductile failure in its model. In the case of the Eurocode 5 (2004), when applying the EYM combined with n_{ef}, it is not possible to determine if a connection fails in a brittle or a ductile way, since the use of the n_{ef} parameter implies
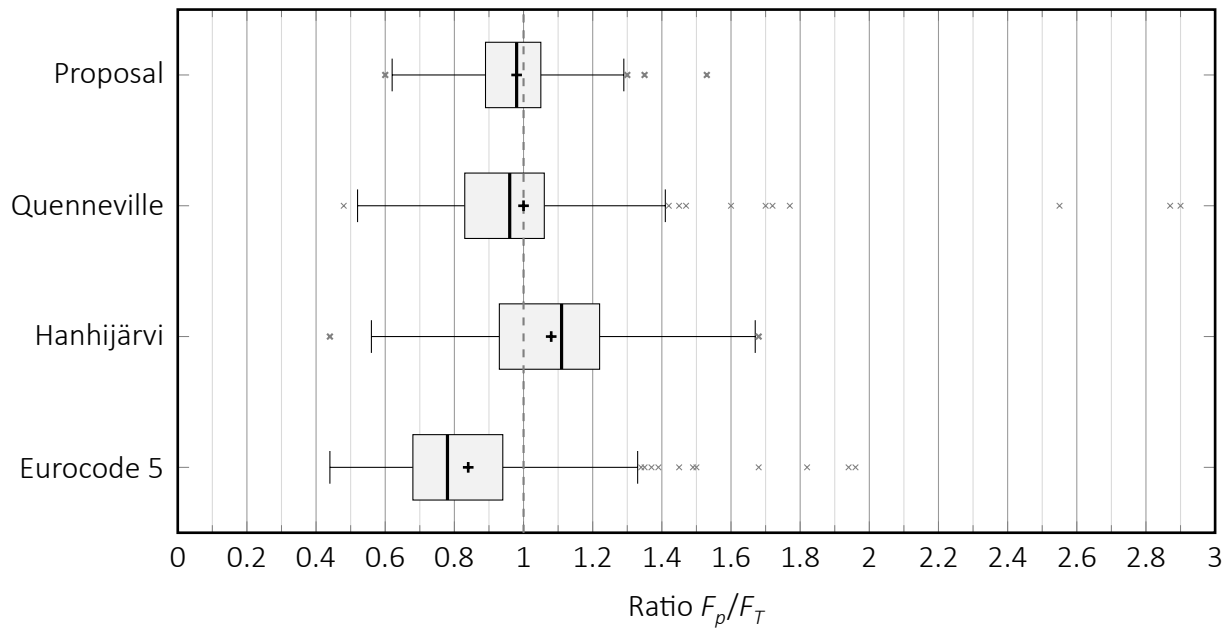
Figure 5. Boxplot considering the accuracy of the predicted ratio between the predicted failure load F_P and the tested failure load F_T. Mean value depicted with a cross.

a brittle failure mode. Therefore, two options are depicted in Fig. 6: one considering all the cases that are expected to fail by the combination of the EYM and n_{ef} as ductile (named as "Eurocode 5 Ductile") and another one considering them as brittle failure ("Eurocode 5 Brittle").

The best discrimination ability is obtained by the proposal (86%). The second position is reached by *Quenneville and Zarnani* (2017) (77%). The results obtained by the model from *Hanhijärvi and Kevarinmäki* (2008), with 64% of positive matches, lie between the two options considered when evaluating the Eurocode 5 (2004) (52% and 68%, respectively).

5 Conclusions and future work

To guarantee a safe design of timber connections, a correct analysis of brittle failure modes is of utmost importance. In this work, a new design model to obtain the brittle capacity of connections loaded parallel to grain with large diameter fasteners (those protruding the whole timber thickness) is proposed. The new model tries to reach a good balance between simplicity and accuracy, and improves those weak points detected in other existing proposals. Finally, an extensive database is used to evaluate and compare the proposal with the previously proposed models. The comparison demonstrates how the new design model reaches the best results regarding both the accuracy and the discrimination ability between ductile and brittle failure modes. Therefore, the proposal can be considered as a good model to be used by designers, as it is at the same time easy to understand and provides a good accuracy.
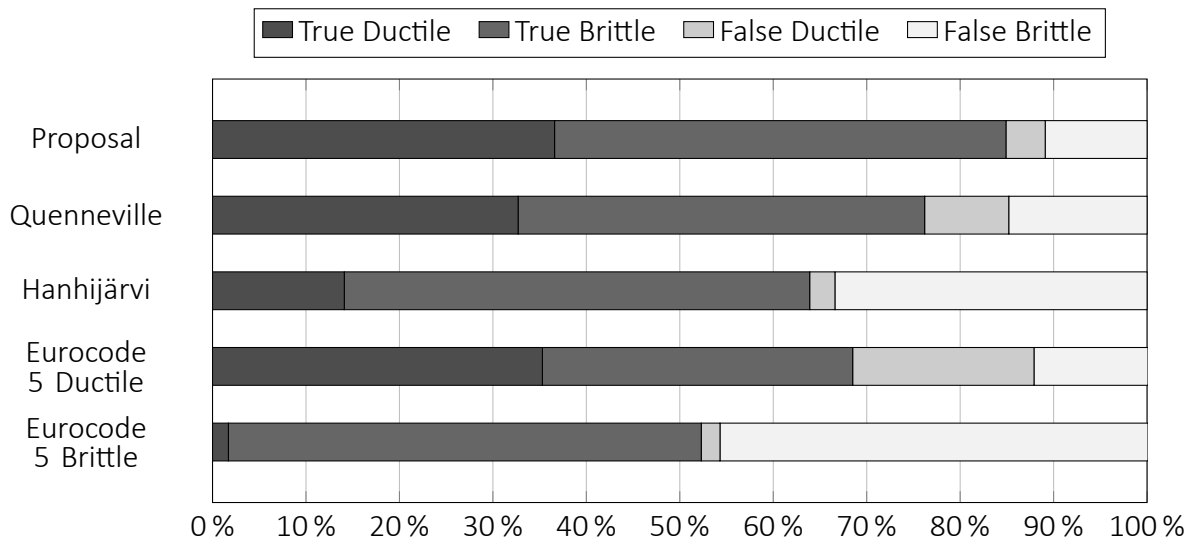
Figure 6. Discrimination ability. Comparison between Eurocode 5 (2004), Hanhijärvi and Kevarinmäki (2007), Quenneville and Zarnani (2017) and the proposal.

As explained , the presented model deals with the brittle failure modes related to large diameter fasteners (those protruding the whole timber thickness). It is still required the development of a similar model dealing with connections with small diameter fasteners.

6   Acknowledgements

7   References

Anderson, G. T. (2001). "Experimental Investigation of Group Action Factor for Bolted Wood Connections". MA thesis. Virginia Polytechnic Institute and State University. ISBN: 9835103658.

Ballerini, M. (2012). "Experimental investigation on parallel-to-grain wood-to-wood joints with self-tapping screws". In: *Proceedings of the Wolrd Conference on Timber Engineering, WCTE*. Auckland New Zealand, pp. 173–182.

Cabrero, J. and M. Yurrita (2018). "Performance assessment of existing models to predict brittle failure modes of steel-to-timber connections loaded parallel-to-grain with dowel-type fasteners." In: *Engineering Struct.* 171. doi:10.1016/j.engstruct.2018.03.037, pp. 895–910.

CSA Standard O86-09 (2009). *Engineering design in wood*. Canadian Standards Association.

Dodson, M. A. (2003). "The Effects of Row Spacing and Bolt Spacing in 6-Bolt and 4-Bolt Wood-to-Steel Connections". MA thesis. Washington State University.

Ehlbeck, J. and Werner, H. (1992). *Tragverhalten von Stabdübeln in Brettschichtholz und Vollholz verschiedener Holzarten bei unterschiedlichen Risslinienanordnungen*. Research report, Versuchsanstalt für Stahl, Holz und Steine, Karlsruhe University.

Ehlbeck, J. and H. Werner (1989). *Tragfähigkeit von Laubholzverbindungen mit stabförmigen Verbindungsmitteln*. Tech. rep. Research report, Versuchsanstalt für Stahl, Holz und Steine, Karlsruhe University.

Eurocode 5 (2004). *Design of timber structures – Part 1-1: General and rules for buildings*. EN 1995-1-1:2004. Brussels, Belgium: Comité Européen de Normalisation (CTN).

Hanhijärvi, A. and A. Kevarinmäki (2008). "VTT PUBLICATIONS 677: Timber Failure Mechanisms in High-Capacity Dowelled Connections of Timber to Steel.ISBN 9789513870904". In:

Hanhijärvi, A. and A. Kevarinmäki (2007). "Design method against timber failure mechanisms of dowelled steel-to-timber connections". In: *CIB-W18 Timber Structures*. Bled, Slovenia, Paper 40-7-3.

Hübner, U. (2013). "Mechanische Kenngrößen von Buchen, Eschen und Robinienholz für lastabtragende Bauteile". PhD thesis. Technische Universität Graz, p. 425.

Jockwer, R., G. Fink, and J. Köhler (2018). "Assessment of the failure behaviour and reliability of timber connections with multiple dowel-type fasteners". In: *Engineering Structures* 172. doi:10.1016/j.engstruct.2018.05.081, pp. 76–84.

Jorissen, A. J. (1998). "Double shear timber connections with dowel type fasteners". PhD thesis. TU Delft, pp. 2–5.

Kevarinmäki, A. (2009). *Design method for timber failure capacity of dowelled and bolted glulam connections. Research report number VTT-S-07046-09*. Helsinki: VTT Technical Research Center of Finland.

Kevarinmäki, A. (1997). *Ristipultilla vahvistetut puurakenteiden liitokset (Cross-bolt Reinforced Joints of Timber Structures). HUT/LSEBP Publication 64*. Tech. rep. Helsinki: Helsinki University of Technology.

Legras, B. D. (2009). "Effet de la teneur en humidité du bois sur la performance des assemblages bois boulonnés de pin gris". MA thesis. Université Laval, Québec, p. 80.

Leivo, M., V. M. Westman, and M. Viinikainen (2000). *Teräslevyinen tappivaarnaliitos - liitoskokeet (Dowelled Steel-to-Timber Connection - Joint Tests)*. Tech. rep. University of Applied Sciences.

Massé, D., J. Salinas, and J. Turnbull (1998). *Lateral strength and stiffness of single and multiple bolts in gluelaminatedtimber loaded parallel to grain*. Tech. rep. Ottawa, Canada: Engineering and Statistical Research Centre, Research Branch, Agriculture.

Misconel, M., M. Ballerini, and V. de Kuilen J W G (2016). "Steel-to-timber joints of beech-lvl with very high strength steel dowels". In: *Proceedings of the Wolrd Conference on Timber Engineering, WCTE*. Vienna, pp. 269–276. ISBN: 978-3-903024-35-9.

Mishler, A. (1998). "Bedeutung der Duktilität für das Tragverhalten von Stahl-Holz-Bolzenverbindungen". PhD thesis. ETH Zürich, p. 76.

Mohammad, M. and P. Quenneville (2001). "Bolted wood-steel and wood-steel-wood connections: verification of a new design approach". In: *Canadian Journal of Civil Engineering* 28.2. doi:10.1139/l00-105, pp. 254–263. ISSN: 0315-1468.

Nozynski, W. (1980). "Investigation of the effect of number of nails in a joint on its load carrying ability". In: *CIB W-18 Timber Structures*. Otaniemi, Finland, Paper 13-7-2.

Ottenhaus, L.-M., M. Li, T. Smith, and P. Quenneville (2018). "Mode cross over and ductility of dowelled LVL and CLT connections under monotonic and cyclic loading". In: *Journal of Structural Engineering* 144.7. doi:10.1061/(ASCE)ST.1943-541X.0002074.

Quenneville, P. and M. Mohammad (2000). "On the Failure Modes and Strength of Steel-Wood-Steel Bolted Timber Connections Loaded Parallel to Grain". In: *Canadian Journal of Civil Engineering* 27.4, pp. 761–773.

Quenneville, P. and P. Zarnani (2017). *Proposal for the Connection Chapter of the New Zealand Design of Timber Structures*. Unpublished.

Reid, M. S. (2004). "Predictions of Two-Row Multi-Bolted Connections Resistance Subjected to Parallel-to-Grain Loading". MA thesis. Royal Military College of Canada.

Sjödin, J. and C.-J. Johansson (2007). "Influence of initial moisture induced stresses in multiple steel-to-timber dowel joints". In: *Holz als Roh- und Werkstoff* 65.1. doi:10.1007/s00107-006-0136-6, pp. 71–77. ISSN: 0018-3768.

SP (1992). *Dragprovning av limträbalkar. Research report number SP 91B1. Ordered by Moelven Limträ A/S*. Tech. rep. Swedish National Testing and Research Intitute.

VTT (2003). *Monileikkeisten tappivaarnaliitosten kuormituskokeet (Loading Tests of Multiple Shear Dowelled Connections). Research report no RTE 1583/03. Ordered by Wood Focus Oy*. Tech. rep. Technical Research Center of Finland.

Yurrita, M. and J. Cabrero (2019). "52 - 7 - 5. Determination of the Effective Thickness of a Dowel-type Fastener of Steel-to-timber Connections under Brittle Failure". In: *6th Meeting of the International Network on Timber Engineering Research (INTER)*. Tacoma, USA.

Yurrita, M. and J. M. Cabrero (2018). "New criteria for the determination of the parallel-to-grain embedment strength of wood". In: *Construction and Building Materials* 173. doi:10.1016/j.conbuildmat.2018.03.127, pp. 238–250.

Yurrita, M., J. M. Cabrero, and P. Quenneville (2019). "Brittle failure in the parallel-to-grain direction of multiple shear softwood timber connections with slotted-in steel plates and dowel-type fasteners". In: *Construction and Building Materials* 216. doi:10.1016/j.conbuildmat.2019.04.100, pp. 296–313.

Discussion

The paper was presented by M Yurrita

M Li and M Yurrita discussed how to interpret the load capacity results where mix failure mode occurred with yielding happening first and then brittle failure.

H Blass asked for explanation of the motivation behind using tension strength parallel to grain in the ratio. M Yurrita responded that this was based on fitting process.

D Dolan stated this paper dealt with nice symmetrical connections and asked what would happen for unsymmetrical cases where for example one side steel plate leading to rolling shear failure being dominate. M Yurrita responded that this was covered in a previous paper but did not have data.

P Dietsch stated that strength values would be needed in the model and asked how they were obtained. M Yurrita stated that they used values in timber design codes and converted characteristic values to mean values. S Winter asked if there was any real tested material properties. M Yurrita responded that yes in some cases there was real test data for material properties in other cases properties were taken from the code.

M Li asked if there was a capacity hierarchy between different timber failure modes in the test data. M Yurrita responded yes with a factor of ~ 0.8 to 0.9.

Embedment test analysis and data in the context of phenomenological modeling for dowelled timber joint design

Michael Schweigler, Depart. of Building Technol., Linnaeus University, Växjö, Sweden

Thomas K. Bader, Depart. of Building Technology, Linnaeus University, Växjö, Sweden

Jean-François Bocquet, ENSTIB/LERMAB, University of Lorraine, Épinal, France

Romain Lemaître, ENSTIB/LERMAB, University of Lorraine, Épinal, France

Carmen Sandhaas, Karlsruhe Institute of Technology, Germany

Keywords: dowelled timber joints, embedment tests, load-displacement curves, numerical analysis, database

1   Introduction

Numerical models, like the phenomenological Beam-On-Foundation (BOF) approach, have proven to be an efficient alternative to the analytical European Yield Model (EYM) for the design of dowelled timber joints according to *EN 1995-1-1* (2004) (EC 5) (see e.g. *Lemaître et al.* (2018), *Bader et al.* (2016)). In contrast to the EYM, BOF-models allow not only for prediction of the load-carrying capacity, but also for prediction of the load-displacement behavior of single-dowel connections, and thus of their stiffness. This makes BOF-models predestined for the design of joints in advanced modern timber structures, which for reason of their complexity rely on a reliable prediction of the joint load-deformation behavior.

BOF-models are used since the early thirties of the last century (*Hager*, 1930). Models of different complexity were used from simplified (i) rigid-ideal plastic models, which allow only for strength prediction (cf. *Johansen* (1949)); to (ii) bi-linear elastic approaches, being able to predict stiffness and strength (*Sawata and Yasumura* (2003), *Cachim and Franssen* (2009)), and (iii) nonlinear elastic models, which are optimized for numerical simulations (*Lemaître et al.*, 2018). BOF-models might be even used for earthquake design by application of plastic, or even hysteresis models (*Izzi et al.* (2018), *Girhammar et al.* (2017)). Developers and users of such phenomenological models face the challenge to find reliable input data on the load-deformation behavior of steel dowels embedded

in wood or wood-based products.

Lack of input data for numerical models, like BOF, is one of the main reasons which hinders application of such models in engineering practice and in research. Since the EYM of EC 5 uses only the embedment strength ($f_{h,EC5}$) but no stiffness, as input, the related European standard for embedment testing, *EN 383* (2007), focuses mainly on the embedment strength determination. However, numerical modeling requires information on the entire load-displacement curve from embedment tests.

The aim of this contribution is to

1. present methods to analyze and parameterize experimental load-displacement curves for BOF-models, with embedment parameters suitable for this purpose;

2. provide a database of embedment parameters for different wood spieces and wood products, and try to find correlations between parameters;

3. give recommendations for embedment testing, with the aim to exploit data in numerical models.

2   Embedment test curve analysis

In embedment tests acc. to *EN 383* (2007), the reaction force, *F*, and two dowel displacements, u_{left} and u_{right}, are measured. Thus, the outcome is a data file with point-wise information on *F* and *u*, giving a nonlinear load-displacement curve. Since documentation, dissemination and standardization of these point-wise load-displacement data is cumbersome, we suggest herein to describe embedment curves by embedment parameters as follows.

Load-displacement curves from embedment tests are analyzed, resulting in strength, stiffness and displacement parameters, similar to what is required acc. to *EN 383* (2007). However, the EN 383-set of parameters needs to be extended. With this extended set of embedment parameters, in combination with parameterized equations (Section 2.2), embedment load-displacement curves can be reconstructed serving as input to numerical simulation methods. The amount of data which needs to be documented and disseminated is much smaller, compared to tabulated data on load-displacement curves. Furthermore, the standardization process can be facilitated by providing regression equations for determination of single embedment parameters, as it is done for the embedment strength $f_{h,EC5}$ in the current version of EC 5.

The required parameters and their determination are discussed in the following.

2.1   Embedment parameters

Depending on the model used to describe the embedment load-displacement behavior (e.g. bilinear or nonlinear curves) and the applied method to reconstruct embedment

curves (*Schweigler et al.*, 2018), a different number of embedment parameters is required. Parameters to describe nonlinear load-displacement curves, including unloading-reloading hysteresis, are illustrated Figure 1, and listed in the following:

- $f_{h,5mm}$: embedment strength at 5 mm

- $f_{h,offset}$: embedment stress in the transition zone

- $k_{f,el}^{load}$: elastic foundation modulus from first-loading sequence

- $k_{f,el}^{unl}$: elastic foundation modulus from unloading sequence

- $k_{f,el}^{rel}$: elastic foundation modulus from reloading sequence

- $k_{f,pl}$: plastic foundation modulus

- u_{max}: maximum displacement

- $f_{h,inter}$: embedment stress at the intersection of $k_{f,pl}$ with the stress axis

- u_0: initial slip
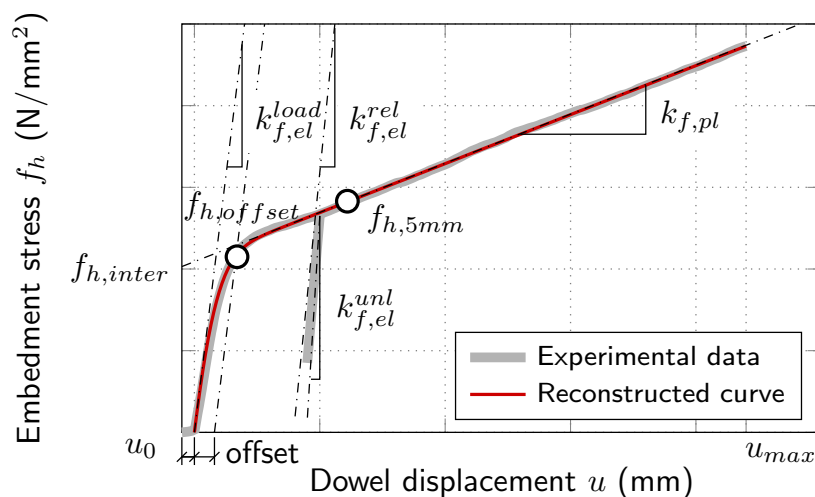
Figure 1. Embedment parameters determined from experiments for curve reconstruction.

Table 1 gives the required parameters for reconstruction of embedment load-displacement curves, to be used in different single-dowel models. Depending on model complexity one to eight parameters are required. For the simplest approach, assuming rigid-ideal plastic embedment behavior, as it is used in the EYM, the only required parameter is the embedment strength, $f_{h,5mm}$. While for plastic and hysteresis models, two strength, four stiffness and one displacement parameters are needed. The parameter $f_{h,inter}$ is set into parentheses, since it is used as substitute for $f_{h,5mm}$ in some cases (see discussion in Section 2.1.5). Initial slip, u_0, is always an optional parameter.

Determination of the above-mentioned embedment parameters, based on experimentally determined load-displacement curves is discussed next.

Table 1. Required embedment parameters for different models to describe the embedment behavior.

Type of model	$f_{h,5mm}$	$f_{h,offset}$	$k_{f,el}^{load}$	$k_{f,el}^{unl}$	$k_{f,el}^{rel}$	$k_{f,pl}$	u_{max}	$f_{h,inter}$	u_0
rigid-ideal plastic	✓	-	-	-	-	-	-	-	-
bi-linear elastic	✓	-	✓	-	-	✓	✓	(✓)	(✓)
nonlinear elastic	✓	✓	✓	-	-	✓	✓	(✓)	(✓)
plastic/hysteresis	✓	✓	✓	✓	✓	✓	✓	(✓)	(✓)

✓…required, (✓)…optional or substitute, -…not required

2.1.1 Embedment strength at 5 mm, $f_{h,5mm}$

The embedment strength, $f_{h,5mm}$, follows the definition of *EN 383* (2007), which is defined as the maximum embedment stress, f_h, up to a dowel displacement u of 5 mm. For the sake of simplicity, it is suggested to include the initial slip, u_0, in the 5 mm displacement definition of the embedment strength, $f_{h,5mm}$. Excluding u_0 would mean an iterative process for determination of $f_{h,5mm}$, since by definition according to Section 2.1.7, u_0, depends indirectly on $f_{h,5mm}$. The embedment strength, $f_{h,5mm}$, is needed for determination of the position of the elasto-plastic curve part. In some cases it is beneficial to substitute $f_{h,5mm}$ by $f_{h,inter}$ (see Section 2.1.5).

2.1.2 Elastic foundation modulus from first-loading sequence, $k_{f,el}^{load}$

The elastic foundation modulus, $k_{f,el}^{load}$, is defined as the inclination of the line connecting stress points on the loading path at 10% and 40% of the embedment strength, $f_{h,5mm}$ (similar to the stress points suggested by *EN 383* (2007)). Alternatively, linear regression could be applied on this curve part.

By the elastic foundation modulus, $k_{f,el}^{load}$, the inclination (i.e. stiffness) of the load-displacement curve at the beginning of the quasi-elastic curve part is defined. Depending on the the applied method and parameterized equation for reconstructing the curve (cf. Table 1), the stiffness reduces from $k_{f,el}^{load}$ at the beginning, to a smaller value at the end of the this curve part, migrating to the transition zone.

2.1.3 Elastic foundation modulus from re- and unloading sequence, $k_{f,el}^{rel}$ and $k_{f,el}^{unl}$

The reloading modulus, $k_{f,el}^{rel}$, is defined in the same way as $k_{f,el}^{load}$. Stress points at 10% and 40% of the reloading path are used. Definition of $k_{f,el}^{unl}$ follows the procedure suggested by *Schweigler et al.* (2017), where $k_{f,el}^{unl}$ is defined as the inclination of the line connecting the stress point on the unloading path at beginning of the unloading sequence and the stress point at 20% load drop. Alternatively, linear regression could be applied on these curve parts.

By $k_{f,el}^{rel}$ and $k_{f,el}^{unl}$ the reloading-unloading path in plastic or hysteresis models can be described.

2.1.4 Embedment stress in the transition zone, $f_{h,offset}$

The parameter $f_{h,offset}$ is defined as intersection of the embedment load-displacement curve with an offset of the $k_{f,el}^{load}$-line (see Figure 1). This method is similar to the offset method for determination of the embedment strength according to *ASTM D5764-97a* (2002). We suggest to use a offset defined relative to the dowel diameter, d. Herein, three different offsets by means of 0.050d, 0.075d and 0.100d were investigated.

The parameter $f_{h,offset}$ allows for calibration of the curvature in the transition zone between the two linear curve parts, i.e., the quasi-elastic and plastic curve part.

2.1.5 Plastic foundation modulus, $k_{f,pl}$

Most parameterized equations used for derivation of nonlinear load-displacement curves allow only for linear description of the loading path in the plastic curve part (see Figure 1, and *Schweigler et al.* (2018)). However, in some experiments a nonlinear behavior after the quasi-elastic limit as e.g. shown in Figure 2 (right) was observed. This makes definition of the plastic foundation modulus, $k_{f,pl}$, challenging. To define $k_{f,pl}$, basically two approaches can be considered. Both were investigated in this study:

- 2-point method: $k_{f,pl}$, is defined as linear path between two stress points on the loading path after the yield limit. From experiments it became obvious, that the stress point at 5 mm displacement is usually located in the plastic curve part. Thus, one suggestion is to define $k_{f,pl}$ between the stress points at 5 mm and at maximum displacement u_{max}, i.e., 15 mm, or the displacement at failure. If failure occurs before a displacement of 5 mm is reached, stress points at u_{max} and 0.75u_{max} are proposed. The advantage of the 2-point approach is its simplicity. However, its main drawback gets obvious from line (2) in Figure 2 (right). The parameter $k_{f,pl}$ might be mispredicted by the 2-point method, since all information between the two defined stress points get lost. To tackle this problem an additional quality condition for the linear approximation could be introduced. If the quality condition is not fulfilled, the maximum displacement has to be reduced until a more-or-less linear part appears between the two stress points (see line (1) in Figure 2 (right)). However, as stated in *Schweigler et al.* (2018) a reliable prediction beyond the displacement at the second stress point is impossible.

- Linear regression: A curve section, covering the plastic part, is isolated from the load-displacement curve and linear regression analysis with optimization by the R^2 is applied. Three different curve sections were investigated, namely 0.1d–u_{max}, 3 mm–u_{max}, and 5 mm–u_{max}. Since linear approximation from regression analysis does not necessarily go through the stress point at 5 mm, i.e. embedment strength $f_{h,5mm}$, an additional stress parameter, $f_{h,inter}$, needs to be defined (see Section 2.1.6). The big advantage compared to the 2-point method is its robust-

ness. Nevertheless, a quality condition should be used here as well, in order to ensure that the plastic curve section can be sufficiently approximated linearly.
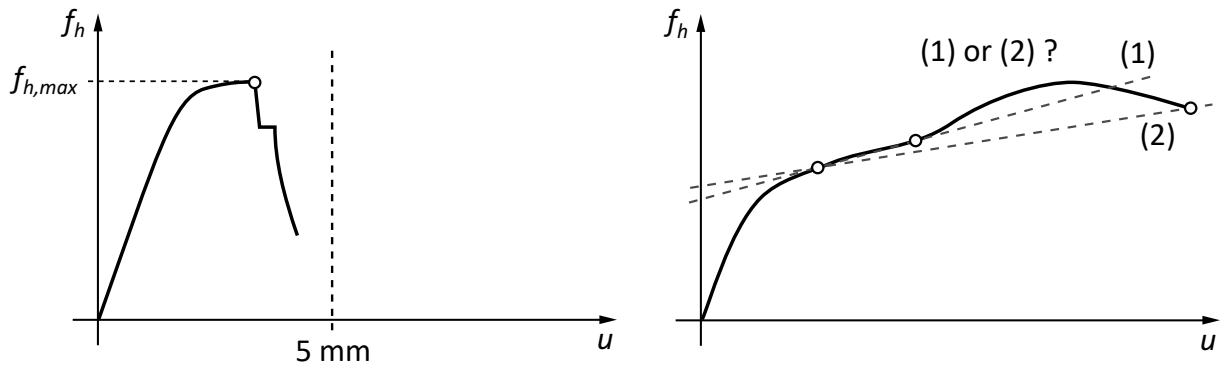
Figure 2. Typical load-displacement curves from embedment tests.

2.1.6 Embedment stress at the intersection of $k_{f,pl}$ with the stress axis, $f_{h,inter}$

The parameter $f_{h,inter}$ is defined as the intersection of the line with an inclination $k_{f,pl}$ (e.g. as outcome from linear regression analysis) with the embedment stress axis. By $f_{h,inter}$, the location of the linear curve part in the plastic region is defined.

2.1.7 Initial slip u_0, and maximum displacement, u_{max}

The initial slip is defined as the displacement, u, at the intersection of the line from determination of $k_{f,el}^{load}$ with the displacement axis, considering that $u = 0$ mm at the beginning of the test. Thus, the size of u_0 depends strongly on test setup related parameters, like the initial position of the loading device, or the assembling of the connection, and the drilling quality of the borehole. In the design of connections, u_0 could be predefined by execution classes, to make it independent from laboratory production and assembling quality. This procedure was suggested in *Schweigler et al.* (2018). The parameter u_0 is an optional parameter for the description of load-displacement curves. As discussed in *Schweigler et al.* (2018), some models allow for direct consideration of u_0 in the definition of nonlinear load-displacement curves, while for others u_0 can simply be added by a corresponding translation of the load-displacement curve.

The maximum displacement, u_{max}, is defined as the displacement at brittle failure, or the displacement when the test is stopped. It gives the displacement limit for reconstruction of the load-displacement curve.

2.2 Analytical equations for load-displacement curves

Mathematical functions allow to define load-displacement curves based on the embedment parameters described in Section 2.1, which then serve as input to numerical models on the single-dowel level. A summary of such methods is given in *Schweigler et al.* (2018). It includes methods, which are based on exponential or power functions (e.g. *Richard and Abbott* (1975)), polynomial functions, or trigonometric functions.

The approach from *Richard and Abbott* (1975) turned out to give good results for description of embedment curves (see *Schweigler et al.* (2018)). The equation reads as

$$f_h(u) = \frac{(k_{f,el}^{load} - k_{f,pl}) \cdot u}{\left[1 + \left[\frac{(k_{f,el}^{load} - k_{f,pl}) \cdot u}{f_{h,inter}}\right]^a\right]^{\frac{1}{a}}} + k_{f,pl} \cdot u, \tag{1}$$

where $k_{f,el}^{load}$ and $k_{f,pl}$ are the gradient of the initial and end tangent of the curve, respectively, while $f_{h,inter}$ describes the intersection between the end tangent and the stress axis. Furthermore, the parameter a controls the transition characteristic between the initial and end tangent of the curve. Parameter a can be defined by $f_{h,offset}$.

3   Embedment parameter database and analysis

The database includes embedment parameters from in total 1565 tests, taken from 7 reports originating from ENSTIB/LERMaB Epinal, Vienna University of Technology (IMWS, TU Wien), Linnaeus University Växjö (LNU), TU Delft and Karlsruhe Institute of Technology (KIT). It includes only test series for which load-displacement data were at disposal. In addition, it was aimed to include data from test series with unloading-reloading hysteresis. References for the specific test series are given in Table 3.

The database comprises parameters from embedment test on 6 soft- and hardwood spieces, 4 wood-based products, 4 dowel diameter, loaded at 7 different load-to-grain angles. The exact number of tests per category is given in Table 2.

Table 2. Number of tests per category included in the embedment parameter database.

	spieces		product		diameter		α
366	spruce	1111	solid	535	12 mm	526	0°
55	pine	196	GLT	654	16 mm	35	15°
28	larch	138	LVL (Kerto-S)	339	20 mm	185	30°
287	poplar	10	LVL (Kerto-Q)	37	24 mm	39	45°
470	beech	110	plywood			286	60°
359	oak					40	75°
						454	90°
			In total: 1565 tests				

Most specimens were reinforced in order to avoid premature splitting before the bearing capacity was reached. More than 80% of setups which tend to split, i.e., $\alpha = 0°$, 15° or 30° were reinforced. Several test specimens were stored at standard climatic conditions of 20 °C and 65% relative humidity prior to testing. The corresponding mean moisture content per test series was between 9.7%.–13.6%. For further details on the single embedment test, the reader is referred to the references given in Table 3.

The database aims to serve as source for engineers and scientists for application in numerical approaches, like BOF-models, and as basis for standardization. It includes

several embedment parameters for parameterized equations for embedment load-displacement curves as discussed in Section 2.1 and 2.2, respectively. Embedment parameters are given as mean values including coefficient of variation and the number of tests. Thus, data can be exploited in stochastic approaches as well.

Embedment parameters were consistently determined as described in Section 2.1 for all tests included in the database. The parameter $f_{h,offest}$ was determined based on an offset of $0.050d$. Over all tests an offset of $0.050d$ turned out to fit the transition zone best, especially for tests with a comparable short transition zone (loading in or close to the grain direction). For loading perpendicular or close to perpendicular to the grain and offset of $0.075d$ or even $0.100d$ would be more suitable, however, an offset of $0.050d$ was used throughout the analysis.

To describe $k_{f,pl}$, the method using linear regression of the experimental data in the curve section between $0.1d$ and u_{max} was applied (see Section 2.1.5). This method was found to be overall most stable for evaluation of $k_{f,pl}$. For tests with larger transition zones, it was seen, that parts of the transition zone were included in the curve section $0.1d$–u_{max}, which should be avoided in order to not falsify the plastic tangent. Nevertheless, it turned out that the parameter $k_{f,pl}$ was hardly influenced therefrom, as long as u_{max} was sufficiently large.

Having at hand embedment parameters from 1445 tests (excluding plywood and LVL/Kerto-Q) it is aimed to find correlations of those embedment parameters with wood density, ρ, and dowel diameter, d. Results from embedment tests loaded in between the principal material directions are not considered for correlation analysis due to its comparable small sample size. The sample size for $\alpha = 0°$ and $\alpha = 90°$ was 460 and 400, respectively.

As it gets obvious from Figures 3–6, a considerable scattering of the embedment parameters was found. In general, scattering of data was found to be stronger for the "stiffnesslike" foundation modulus parameters than for the strength parameters. Interestingly, for most parameters data appeared in two groups, i.e. (I) LERMaB data, and (II) LNU/TU Wien, TU Delft, and KIT data. The LERMaB group, i.e. largest group, showed the tendency to give higher strength values than group (II). For the foundation modulus parameters, diversified results were found. Difference might be explained by different test setups, dowel surface qualities, loading and measurement procedures, etc., used in the individual test series. In general, no obvious influence of wood species, wood product, and dowel diameter on the embedment parameters was found. Correlation plots of the individual embedment parameters are presented and discussed in the following.

3.1 Embedment strength at 5 mm, $f_{h,5mm}$

Embedment strength determination and correlation analysis was the subject of numerous studies. Among others, *Whale and Smith* (1986) and *Ehlbeck and Werner* (1992)

investigated softwood and hardwood subjected to embedment loading, while *Hübner et al.* (2008) focused on European hardwood. Those authors proposed correlation equations of the embedment strength $f_{h,5mm}$ with ρ and d. The proposed design equation for softwood (Eq. (2)) from *Ehlbeck and Werner* (1992) is used in the current version of EC 5 to predict embedment strength for soft- and hardwood, reading as

$$f_{h,EC5} = 0.082 \cdot (1 - 0.010 \cdot d) \cdot \rho. \tag{2}$$

Ehlbeck and Werner (1992) proposed the following equation for hardwood

$$f_{h,Ehlbeck}^{hard} = 0.102 \cdot (1 - 0.010 \cdot d) \cdot \rho. \tag{3}$$

In Eq. (2) and (3) mean mass density, ρ_{mean}, was used as it was done in *Ehlbeck and Werner* (1992). In EC 5, ρ_{mean} was simply replaced by ρ_k to shift from mean to characteristic values of the embemdent strength.
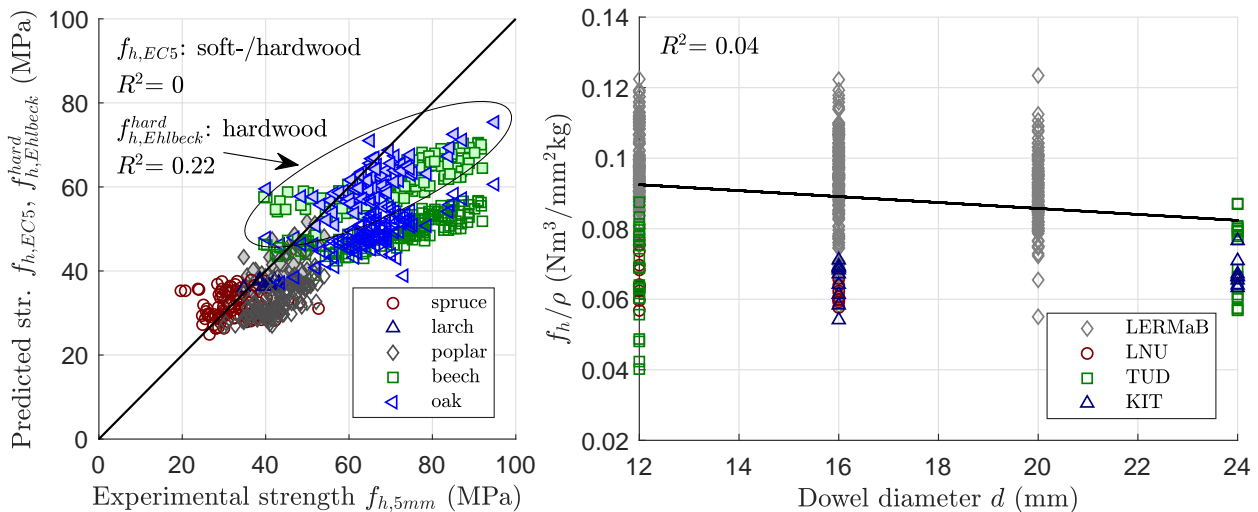
Figure 3. Embedment strength, $f_{h,5mm}$ parallel to the grain (0°); Left: Correlation between experimental $f_{h,5mm}$ and prediction by EC 5, $f_{h,EC5}$ (for soft- and hardwood; empty markers), and by $f_{h,Ehlbeck}^{hard}$ (only for hardwood; filled markers); Right: Ratio $f_{h,5mm}/\rho$ plotted over dowel diameter, d.

In Figure 3 (left) the correlation between predicted embedment strength $f_{h,EC5}$ (Eq. (2)) and $f_{h,Ehlbeck}^{hard}$ (Eq. (3)), and experimentally determined embedment strength, $f_{h,5mm}$ for $\alpha = 0°$ is illustrated. While a sufficient correlation was found for softwood (spruce and larch), hardwood embedment strength was substantially underestimated by EC 5, resulting in a R^2 for the entire sample (soft- and hardwood) of equal to zero, i.e., no correlation. Applying Eq. (3) on the hardwood samples yielded R^2 of 0.22. As illustrated in Figure 3 (right) a small decrease of $f_{h,5mm}$ with increasing d was found for $\alpha = 0°$. Nevertheless, this correlation is very weak as indicated by $R^2 = 0.04$. Stronger correlation was found for $\alpha = 90°$, resulting in $R^2 = 0.20$. Due to the weak correlation of $f_{h,5mm}$ with d, a linear regression analysis for $f_{h,5mm}$, and also the other embedment parameters, was performed with only one dependent parameter, i.e., the density, ρ.
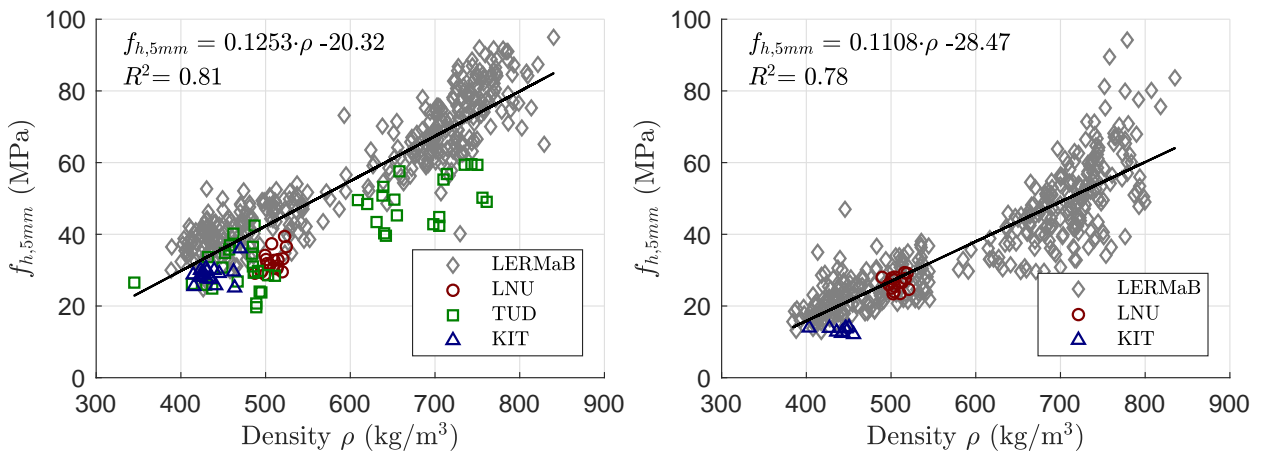
Figure 4. Embedment strength, $f_{h,5mm}$ plotted over density ρ including linear regression equations based on data from (i) LERMaB and (ii) LNU/TU Wien, TU Delft, and KIT; Left: $\alpha = 0°$; Right: $\alpha = 90°$.

In Figure 4 (left), $f_{h,5mm}$ of soft- and hardwood samples is plotted over ρ for $\alpha = 0°$, including the correlation equation and R^2. Higher $f_{h,5mm}$ for LERMaB data, compared to data from other laboratories gets obvious. Interpretation of this finding is difficult, due to the large number of possible influence parameters. One possible explanation could be the use of reinforcement to avoid premature splitting for all LERMaB experiments loaded at $\alpha = 0°$. Experiments from TU Delft and KIT were unreinforced, and thus often failed before the 5 mm limit. Experiments from LNU/TU Wien were reinforced, but LVL (Kerto-S) was used, which might result in lower $f_{h,5mm}$ than solid timber of the same density (cf. *Schweigler et al.* (2016)). For loading perpendicular to the grain, $\alpha = 90°$, a similar trend to $\alpha = 0°$ was found (Figure 4 (right)). Embedment strength showed a quite strong correlation with density, resulting in an $R^2 = 0.78$ for the entire group of tests (soft- and hardwood). The parameter $f_{h,offset}$ showed similar results and trends as $f_{h,5mm}$ (not shown herein).

3.2 Elastic foundation modulus from first-loading sequence, $k_{f,el}^{load}$

Figure 5. Elastic foundation modulus, $k_{f,el}^{load}$ plotted over ρ including linear regression equations based on data from (i) LERMaB and (ii) LNU/TU Wien, TU Delft, and KIT; Left: $\alpha = 0°$; Right: $\alpha = 90°$.

In Figure 5 (left), $k_{f,el}^{load}$ is plotted over the density for loading parallel to the grain ($\alpha = 0°$).

Compared to strength value, $f_{h,5mm}$ the scattering increased substantially. This high-lights the sensitivity of stiffness determination from embedment tests. Similar to the embedment strength parameter, two distinct groups of test results can be found, i.e., group (I) LERMaB, and group (II) incorporating the other sources. Especially for group (I) pronounced scattering of the results was found, which might be partly explained by measuring the dowel displacement, u, only on one side of the test specimen. Thus, due to inhomogeneous stiffness distribution of the wooden material along the dowel axis, the dowel might rotate relative to the midplane of the test specimen, and consequently falsify the measured displacement and the calculated stiffness $k_{f,el}^{load}$. For high density, group (II) showed higher $k_{f,el}^{load}$ than group (I), i.e. LERMaB. This is in contrast to findings for $f_{h,5mm}$. Similar trends were seen for loading at $\alpha = 90°$, shown in Figure 5 (right).

Compared to embedment strength, less literature can be found for embedment modulus. *Hwang and Komatsu* (2002) proposed to estimate the elastic foundation modulus parallel to the grain, $k_{s,0}$, as function of the modulus of elasticity, E_0, and dowel diameter, d. The equation has been adapted to be compatible with SI-units, reading as

$$k_{s,0} = \frac{E_0}{31.6 + 10.9 \cdot d}, \tag{4}$$

with E_0 in (N/mm^2), and d in (mm) to give $k_{s,0}$ in (N/mm^3). For loading perpendicular to the grain, $k_{s,90}$ was estimated by $k_{s,0}/3.4$ according to *Hwang and Komatsu* (2002).

Correlating ρ_{mean} with $E_{0,mean}$ from *EN 338* (2009), and insertion in Eq. (4), gives for $d = 16$ mm, $k_{s,0} = 53.4$ N/mm^3 ($\rho = 420$ kg/m^3) and 68.0 N/mm^3 ($\rho = 750$ kg/m^3), which is 18% higher and 25% lower, respectively, as predicted by the regression equation given in Figure 5 (left) ($R^2 = 0.30$). For $\alpha = 90°$, *Hwang and Komatsu* (2002) underestimates $k_{f,el}^{load}$ predicted by regression equation from Figure 5 (right) ($R^2 = 0.27$) by 23% ($\rho = 420$ kg/m^3) and 61% ($\rho = 750$ kg/m^3), respectively. It should be pointed out, that the validity of this comparison is questionable, for reason of the weak correlation of ρ with $k_{f,el}^{load}$.

For the elastic foundation modulus parameters in the unloading and reloading sequences, i.e., $k_{f,el}^{rel}$ and $k_{f,el}^{unl}$, very similar results to $k_{f,el}^{load}$ were found with even more pronounced scattering and weak correlations with ρ. In general $k_{f,el}^{unl}$ was found to give highest values, followed by $k_{f,el}^{rel}$ and $k_{f,el}^{load}$.

3.3 Plastic foundation modulus, $k_{f,pl}$

The plastic foundation modulus, $k_{f,pl}$, describes the displacement hardening after the elastic limit. Thus, it is not surprising that in Figure 6, higher values can be seen for loading at $\alpha = 90°$ (right) than $\alpha = 0°$ (left). Furthermore, a less pronounced scattering of the data and a stronger correlation with the density (0°: $R^2 = 0.41$; 90°: $R^2 = 0.56$),

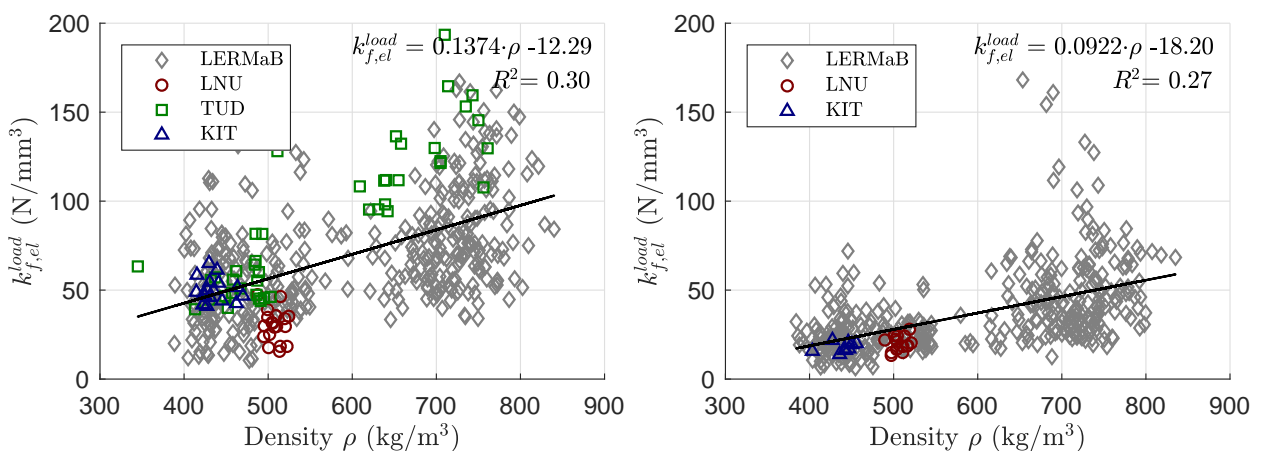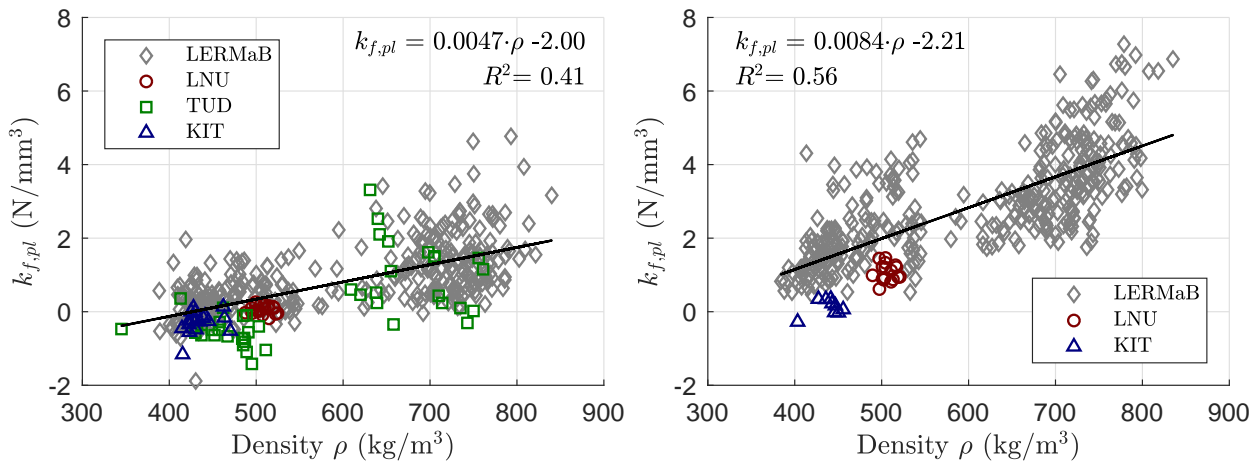Figure 6. Plastic foundation modulus, $k_{f,pl}$ plotted over ρ including linear regression equations based on data from (i) LERMaB and (ii) LNU/TU Wien, TU Delft, and KIT; Left: $\alpha = 0°$; Right: $\alpha = 90°$.

as for $k_{f,el}^{load}$ can be seen. The smaller scattering might be explained by the larger Δu, which is used for calculation of $k_{f,pl}$, compared to $k_{f,el}^{load}$. Thus it reacts less sensitive to inaccuracies in the measured displacements.

4 Prerequisites and recommendations for embedment testing

In order to fully exploit numerical models, like BOF-models, in engineering applications, additional or adjusted parameters from embedment tests are needed as input. For determination of these parameters, adjustments of the (i) displacement range being tested, going hand in hand with necessary (ii) reinforcement measures to avoid premature splitting, and (iii) regulations for testing at an angle to the grain are recommended.

Large scattering of the embedment parameters presented in Section 3 underlines the importance of a precise and complete definition of test setup, as well as test- and evaluation-procedure, in order to ensure reliable results from embedment tests.

Following adjustments are recommended for a revised version of *EN 383* (2007).

4.1 Maximum displacement

Numerical models, like BOF approaches, aim for replacement of time consuming and costly joint tests by simulations. Since the related test standard for joints *EN 26 891* (1991) requires to test up to a displacement of 15 mm, it is necessary to test up to this limit at the embedment level as well. Thus, it is recommended to increase the aimed displacement limit from 5 mm to 15 mm.

4.2 Reinforcement

From multiple studies (e.g. *Sandhaas et al.* (2013)) it was seen, that it can be challenging to reach even the current displacement limit of 5 mm. This is the case for testing

in or close to the grain direction, as well as for some wood species being sensitive to splitting. Premature splitting means, that the plastic limit, $f_{h,5mm}$, cannot be reached, which however, is a prerequisite for the EYM in EC 5. Thus, reinforcement is required in order to ensure ductile behavior for the determination of the plastic limit, $f_{h,5mm}$, as well as the required displacement limit of 15 mm.

For reinforcement of test specimens either glued-on boards, or screws could be considered (*Lathuillière et al.*, 2015). In order to act only as reinforcement to avoid premature brittle failure, screws have to be place at a certain distance from the dowel. In *Lederer et al.* (2016) the influence of different reinforcement measures, and their distance to the loaded dowel was studied. For reinforcement screws, an increase of the embedment force was seen, when the dowel was closer than ca. 5 mm from the screw. Thus, it is recommended to place the reinforcement screw at least at a distance of 15 mm+d from the undeformed, i.e. initial position of the dowel. Furthermore, *Lederer et al.* (2016) highlighted the importance of a sufficient strength of the reinforcement. Following Chapter 8.2.2 of the Austrian National Annex of EC 5, the strength of reinforcement screws can be designed for 30% of the expected embedment force.

4.3 Specimen size

In *EN 383* (2007) no information for testing at an angle to the grain is given. However, since especially in moment loaded connections, arbitrary load-to-grain angles are possible, embedment tests should be conducted for intermediate load-to-grain angles as well. Thus, information on the specimen size for these load-to-grain angles should be included in the test standard. This could be done by interpolation between already existing regulations for 0° and 90°. *Hübner et al.* (2008) proposed linear interpolation of the specimen size between 0° and 90°. Herein we suggest to interpolate dimensions by following an S-shaped curve, which could be done as follows

$$X_\alpha = X_0 \cdot \cos(\alpha)^2 + X_{90} \cdot \sin(\alpha)^2, \tag{5}$$

with X_α as the dimension at a specific load-to-grain angle, and X_0 and X_{90} as the dimensions at 0° and 90°, respectively. This proposal is based on observations from *Schweigler et al.* (2016) and *Schweigler et al.* (2017), which showed that embedment test at 15° and 75° behave very similar to tests at 0° and 90°, respectively.

4.4 Test setups for loading at an angle to the grain

Loading at an angle to the grain causes an unsymmetric stress and stiffness distribution below the loaded dowel. Thus, if the test setup is unconstrained in lateral direction, a lateral displacement is evoked; if the test setup is constrained, a lateral force is evoked, which yields an lower and upper limit for the embedment forces, respectively (cf. *Schweigler et al.* (2017)). This calls for adjusted regulations regarding the test setup

in EN 383. Two possible setups for unconstrained embedment tests are illustrated in Figure 7.
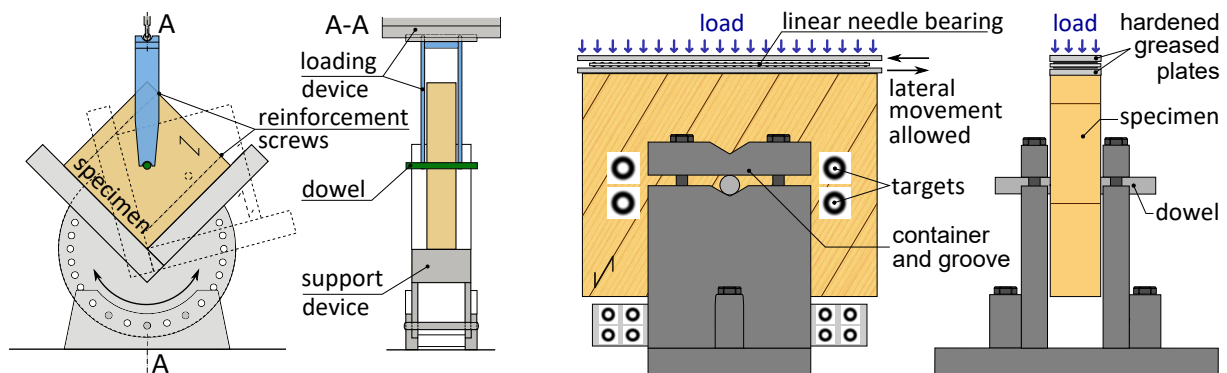
Figure 7. Illustration of embedment test setups for loading at an angle to the grain; Left: Unconstrained loading via pendulum (Schweigler et al., 2016); Right: Unconstrained loading by allowing lateral movement (Lemaître, 2019).

5   Conclusions

A database comprising embedment parameters from 1565 tests, on 6 soft- and hardwood species, 4 wood-based products, 4 dowel diameters, loaded at 7 different load-to-grain angles was presented. Methods for determination of embedment parameters, and methods for derivation of embedment load-displacement curves based on these embedment parameters were discussed.

Based on analysis of the embedment parameters, and observations from embedment tests, it is recommended to adjust the embedment test standard EN 383 by increasing the displacement limit to 15 mm. Embedment tests being sensitive to splitting shall be reinforced. Regulations regarding test setups and specimen size for embedment test at an angle to the grain need to be included. Definitions for execution and evaluation of embedment test shall be extended and more precise, in order to avoid difference in results from embedment tests, carried out at different facilities, as it was observed in this study. Additional embedment parameters, which can serve as input to numerical models, shall be included in EN 383.

The final aim for future versions of EC 5 should be to include regression equations for several embedment parameters, similar to the equation for the embedment strength in the current EC 5. However, the large scattering of embedment parameters, especially for the stiffness parameters, observed in this study, does not allow to give recommendations for regression equations at this time. Additional embedment tests, following regulations of a revised version of EN 383 are required, to allow for determination of reliable regression equations for the proposed parameters.

6 Acknowledgements

7 References

ASTM D5764-97a (2002). "Standard Test Method for Evaluating Dowel-Bearing Strength of Wood and Wood-Based Products". In: *ASTM International*.

Bader, T. K., M. Schweigler, E. Serrano, M. Dorn, B. Enquist, and G. Hochreiner (2016). "Integrative experimental characterization and engineering modeling of single-dowel connections in LVL". In: *Construction and Building Materials* 107, pp. 235–246.

Benistand, T. (2019). "Comportements structurels des Essences de bois feuillus français en vue de leur meilleure intégration aux Eurocodes 5." PhD thesis. University of Lorraine, France (in progress).

Blaß, H. J. and T. Uibel (2007). "Tragfähigkeit von stiftförmigen Verbindungsmitteln in Brettsperrholz (in German)". In: *Karlsruher Berichte zum Ingenieurholzbau Band 8*.

Cachim, P. B. and J.M. Franssen (2009). "Numerical modelling of timber connections under fire loading using a component model". In: *Fire Safety Journal* 44(6), pp. 840–853.

Ehlbeck, J. and H. Werner (1992). "Softwood and hardwood embedding strength for dowel-type fasteners." In: *Proceedings of CIB-W18/25-7-2, Aahus, Sweden*.

EN 1995-1-1 (2004). "Eurocode 5: Design of timber structures – Part 1-1: General – Common rules and rules for buildings". In: *European Committee for Standardization (CEN), Brussels, Belgium*.

EN 26 891 (1991). "Timber structures; Joints made with mechanical fasteners; General principles for the determination of strength and deformation characteristics". In: *European Committee for Standardization (CEN), Brussels, Belgium*.

EN 338 (2009). "Structural timber–Strength classes". In: *European Committee for Standardization (CEN), Brussels, Belgium*.

EN 383 (2007). "Timber structures – Test method – Determination of embedement strength and foundation values for dowel type fasteners." In: *European Committee for Standardization (CEN), Brussels, Belgium*.

Girhammar, U. A., P. J. Gustafsson, and B. Källsner (2017). "Modeling of shear walls using finite shear connector elements based on continuum plasticity". In: *Frontiers of Structural and Civil Engineering* 11(2), pp. 143–157.

Hager, K. (1930). "Der Lochleibungsdruck bei Holzverbindungen (in German)". In: *Der Bauingenieur* 11(50), pp. 865–866.

Hübner, U., T. Bogensberger, and G. Schickhofer (2008). "Embedding strength of European hardwoods". In: *Proceedings of CIB-W18/41-7-5, St.Andrews, Canada*.

Hwang, K. and K. Komatsu (2002). "Bearing properties of engineered wood products I: effects of dowel diameter and loading direction". In: *Journal of Wood Science* 48(4), pp. 295–301.

Izzi, M., G. Rinaldin, A. Polastri, and M. Fragiacomo (2018). "A hysteresis model for timber joints with dowel-type fasteners". In: *Engineering Structures* 157, pp. 170–178.

Johansen, K. W. (1949). "Theory of timber connections." In: *Int Assoc Bridge Struct Eng.* 9, pp. 249–262.

Lathuillière, D., L. Bléron, T. Descamps, and J.F. Bocquet (2015). "Reinforcement of dowel type connections". In: *Construction and Building Materials* 97, pp. 48–54.

Lederer, W., T. K. Bader, G. Unger, and J. Eberhardsteiner (2016). "Influence of different types of reinforcements on the embedment behavior of steel dowels in wood". In: *European Journal of Wood and Wood Products* 74(6), pp. 793–807.

Lemaître, R. (2019). "Développement d'un outil de calcul non linéaire de dimensionnement d'assemblages bois tridimensionnels soumis à des torseurs plans." PhD thesis. University of Lorraine, France (in progress).

Lemaître, R., J.F. Bocquet, M. Schweigler, and T. K. Bader (2018). "Beam-on-foundation modelling as an alternative design method for timber joints with dowel-type fasteners – Part 1: Strength and stiffness per shear plane of single-fastener joints." In: *Proceedings of INTER/51-07-13 , Tallinn, Estonia*.

Richard, R. M. and B. J. Abbott (1975). "Versatile elastic-plastic stress-strain formula". In: *Journal of the Engineering Mechanics Division* 101(4), pp. 511–515.

Sandhaas, C., G.J.P. Ravenshorst, H.J. Blass, and J.W.G. van de Kuilen (2013). "Embedment tests parallel-to-grain and ductility aspects using various wood species". In: *European Journal of Wood and Wood Products* 71(5), pp. 599–608.

Sawata, K. and M. Yasumura (2003). "Estimation of yield and ultimate strengths of bolted timber joints by nonlinear analysis and yield theory". In: *Journal of Wood Science* 49(5), pp. 383–391.

Schweigler, M., T. K. Bader, G. Hochreiner, and R. Lemaître (2018). "Parameterization equations for the nonlinear connection slip applied to the anisotropic embedment behavior of wood". In: *Composites Part B: Engineering* 142, pp. 142–158.

Schweigler, M., T. K. Bader, G. Hochreiner, G. Unger, and J. Eberhardsteiner (2016). "Load-to-grain angle dependence of the embedment behavior of dowel-type fasteners in laminated veneer lumber". In: *Construction and Building Materials* 126, pp. 1020–1033.

Schweigler, M., T. K. Bader, J. Vessby, and J. Eberhardsteiner (2017). "Constrained displacement boundary conditions in embedment testing of dowel-type fasteners in LVL". In: *Strain* 53(6). DOI: 10.1111/str.12238.

Whale, L.R.J. and I. Smith (1986). "The derivation of design clauses for nailed and bolted joints in Eurocode 5." In: *Proceedings of CIB-W18/19-7-6, Florence, Italy*.

Table 3. Embedment parameter database for selected test series, including mean values, coefficient of variation (CV) in %, and number of tests (n).

d (mm)	α (°)	ρ (kg/m³) mean CV n	MC (%) mean CV n	$f_{h,5mm}$ (MPa) mean CV n	$f_{h,offset}$ (MPa) mean CV n	$k^{load}_{f,el}$ (N/mm³) mean CV n	$k^{rel}_{f,el}$ (N/mm³) mean CV n	$k^{unl}_{f,el}$ (N/mm³) mean CV n	$k_{f,pl}$ (N/mm³) mean CV n	$f_{h,inter}$ (MPa) mean CV n	u_0 (mm) mean CV n	u_{max} (mm)
Spruce, solid timber, *Blaß and Uibel* (2007)												
24	0	439 4.0 8	13.6 4.2 8	29.6 8.5 8	29.4 8.5 8	44.4 6.7 8	84.9 6.5 2	116.8 2.1 2	-0.286 69.3 8	30.2 9.5 8	0.14 48.4 8	5.1–5.6
24	90	439 3.4 9	13.4 2.9 9	13.3 5.3 9	12.4 6.3 9	17.9 14.1 9	24.5 6.6 2	32.7 8.2 2	0.129 156 9	12.4 10.3 9	0.05 56.6 9	4.6–6.0
Spruce, LVL (Kerto-S), *Schweigler et al.* (2016)												
12	0	507 1.8 7	11.5 4.8 11	31.8 5.1 7	30.6 7.3 7	29.8 12.8 7	39.7 7.6 7	57.4 16.5 7	0.095 9.3 7	30.6 58.9 7	0.10 132 7	24.0
12	30	515 1.5 6	11.5 4.8 11	27.3 3.2 6	25.1 5.1 6	23.9 8.6 6	32.7 13.9 6	46.9 9.7 6	0.312 35.3 6	25.0 4.7 6	0.15 81.5 5	24.0
12	60	510 0.8 6	11.5 4.8 11	25.1 4.6 6	21.0 4.5 6	20.7 22.1 6	24.5 12.6 6	37.0 12.7 6	0.603 25.4 6	21.8 8.8 6	0.10 68.1 5	24.0
12	90	505 1.9 7	11.5 4.8 11	27.5 4.9 7	20.6 8.1 7	20.3 22.4 7	23.4 13.9 7	34.7 13.6 7	1.17 13.5 7	21.5 8.0 7	0.01 433 7	24.0
Poplar, solid timber, *Benistand* (2019)												
12	0	500 7.2 40	9.7 6.1 40	46.9 8.1 40	40.7 7.4 40	52.4 39.9 40	133.7 22.8 40	135.3 20.8 40	0.730 52.2 40	41.1 11.0 40	0.04 163 40	12.5–14.2
Beech, solid timber, *Benistand* (2019)												
12	0	747 3.6 35	11.6 1.6 35	82.1 8.1 35	72.9 8.4 35	79.8 41.2 35	119.6 28.8 35	121.1 25.9 35	1.60 50.9 35	70.8 10.5 35	0.04 80.0 35	6.9–16.6
12	90	726 6.7 40	11.9 2.9 40	62.3 20.0 40	38.5 18.6 40	48.0 35.7 40	73.8 30.3 40	75.1 28.5 40	5.17 21.7 40	34.4 20.3 40	0.07 47.3 40	11.9–15.3
Oak, solid timber, *Benistand* (2019)												
12	0	710 6.6 30	12.5 6.6 30	68.7 13.6 30	60.1 13.1 30	66.4 34.5 30	106.2 37.1 30	104.3 29.7 30	2.38 41.8 30	56.2 13.9 30	0.02 362 30	1.5–9.2
12	90	707 6.9 30	13.2 5.6 30	52.4 22.2 30	34.9 25.2 30	30.2 30.3 30	40.6 25.5 30	41.6 26.2 30	3.96 24.7 30	30.4 27.4 30	0.04 96.6 30	9.8–17.1

* The complete embedment parameter database can be found at DIVA (http://urn.kb.se/resolve?urn=urn:nbn:se:lnu:diva-87945). In addition to the above mentioned references, the database includes data from: *Sandhaas et al.* (2013), *Schweigler et al.* (2017), and *Lemaître* (2019).

Discussion

The paper was presented by M Schweigler

R Jockwer asked about fitting curves to reflect the high nonlinear behavior. M Schweigler responded that this approach is more practical for use in standards.

S Franke asked about the ½ hole tests with uniformly loaded dowel versus the model and discussed the difference between ½ hole and full hole tests with up to 30% difference. M Schweigler confirmed that all the data considered was based on full hole tests.

YH Chui commented that the poor correlation was surprising and asked whether they looked into the breaking up the data into individual groups for regression analysis. M Schweigler responded that this was done and there was no correlation.

M Li stated the one would expect significant bending in the fastener when loaded up to 15 mm. The ASTM recommended ½ hole test may be more realistic and suggested loading up to 1d rather than 15 mm. M Schweigler agreed.

JM Cabrero discussed where to put the reinforcement. M Schweigler responded that reinforcement was needed to get ductile failure mode. H Blass added that sometimes reinforcement would be needed especially in modified wood.

A Frangi asked whether one could work with this level of high variability. M Schweigler responded that some of this variability came from how the testing was conducted and agreed that one would need to control the influencing parameters better to reduce the variability.

P Palma commented that embedment tests might not be the right way to do this and single fastener tests might be more appropriate.

S Winter asked if there is a proposal for EC test procedure TC 124 WG1. M Schweigler stated they are working on it.

P Quenneville stated if the quality of the dowel cannot be controlled on site, what would be the purpose of tracking this in tests. M Schweigler responded the collected information may lead to more on site quality control.

Beam-on-Foundation Modelling as an Alternative Design Method for Timber Joints with Dowel-Type Fasteners – Part 2: Modelling Techniques for Multiple Fastener Connections

Romain Lemaître, ENSTIB/LERMaB, University of Lorraine, Épinal, France

Jean-François Bocquet, ENSTIB/LERMaB, University of Lorraine, Épinal, France

Michael Schweigler, Department of Building Technology, Linnaeus University, Växjö, Sweden

Thomas K. Bader, Department of Building Technology, Linnaeus University, Växjö, Sweden

Keywords: dowelled timber connections, numerical modelling, beam-on-foundation

1 Introduction

In many design codes for timber structures (e.g. Eurocode 5 and SIA 265), the stiffness of a connection is given by empirical equations for a single dowel-type fastener per shear plane. The global stiffness of the connection is then given by multiplication with the number of dowels and shear planes. In the codes cited above, the empirical equations to estimate stiffness only depend on two parameters, namely the dowel diameter and the wood density. The main difference between different codes and stiffness of different types of fasteners is the choice of the exponent on these two parameters. Development and background of empirical equations for stiffness in different codes were recently reported in Jockwer and Jorissen (2018), who analysed about one thousand double shear timber-to-timber connection tests to evaluate the influence of further parameters on stiffness, such as number of fasteners in a row, number of rows of fasteners and dowel slenderness. From this huge database, they have been able to estimate another empirical stiffness equation, that includes dowel slenderness as an additional parameter. Effects of the latter have even been reported in Lemaître et al. (2018), by using a phenomenological numerical model instead of

experiments. Sandhaas and van de Kuilen (2017) reported that using the slip modulus K_{ser}, calculated according to Eurocode 5 for stiffness prediction of multiple fastener joints, considerably overestimates the experimentally observed stiffness and they proposed to introduce an effective number of dowels in their design, which was also recommended in Jockwer and Jorissen (2018).

This paper continues the work presented in Lemaître et al. (2018) on strength and stiffness estimations of single-fastener connections using a beam-on-foundation (BOF) modelling. In Lemaître et al (2018), the beam-on-foundation model calculations were compared to design equations of Eurocode 5, i.e. the load-carrying capacity and slip modulus. By these comparisons, the validity of the method for the design of single-fastener connections was highlighted. Moreover, effects that are not explicitly covered by the empirical design equations, namely the influence of the dowel slenderness and the nonlinear dowel diameter on the slip modulus were demonstrated.

In the present paper, the same comparisons are made for multiple dowelled connections. Moreover, load distribution between dowels in this type of connection, which was shown to be non-uniform by Blass (1995), is studied by means of the BOF model. Different approaches to estimate the load distribution have been proposed by Cramer (1968), Lantos (1969) and Wilkinson (1986).

2 Methodology

In this section, the beam-on-foundation model, applied for simulation of the mechanical behaviour of timber joints with multiple dowels in a row parallel to the grain is presented. Only joints loaded by a normal force are considered herein. The model is based on an idealisation of the contact between wood and steel dowel by nonlinear springs along the dowel. This modelling enables to predict only the ductile elastoplastic behaviour of a connection. Brittle failure modes are not considered. The phenomenological modelling approach is called beam-on-foundation (BOF) and has among others already been used by Hirai (1983) and Sawata and Yasumura (2003).

The nonlinear springs give only loads parallel to the displacement direction, neglecting friction between shear planes and the wood-steel dowel interface. Thus, no rope effect is considered herein. Moreover, no interaction between adjacent springs is considered in the modelling (Winkler's foundation).

The problem is solved numerically by the finite element method with the French finite element code Cast3M (http://www-cast3m.cea.fr/index.php). The mechanical behaviour of the model components is linearized for each displacement increment (0.02 mm).

2.1 Mesh

A 2-dimensional model with 1-dimensional elements, i.e. beams and springs, is used in order to reduce the problem size. In this model, the contact between wood and steel fastener is idealised by springs along the fastener. The spring behaviour is described in the next Section 2.2. The fastener is modelled by 1-dimensional beam elements with an elastoplastic behaviour. The description of this behaviour is done in the Section 2.3. The number of beam elements to model the fastener is twice the number of springs. Two beam elements are used between adjacent springs and one element at the end of the fastener (Figure 1).

This idealised representation is repeated for each fastener, and the single fasteners are then connected by elastic beams, simulating the elastic deformations of the wood between the fasteners (Figure 1). The latter is a function of the parallel and lateral spacing, the side member thickness and the Young's modulus of wood in the load direction. The distance between each fastener is assumed to be *7d*, where *d* is the dowel diameter.
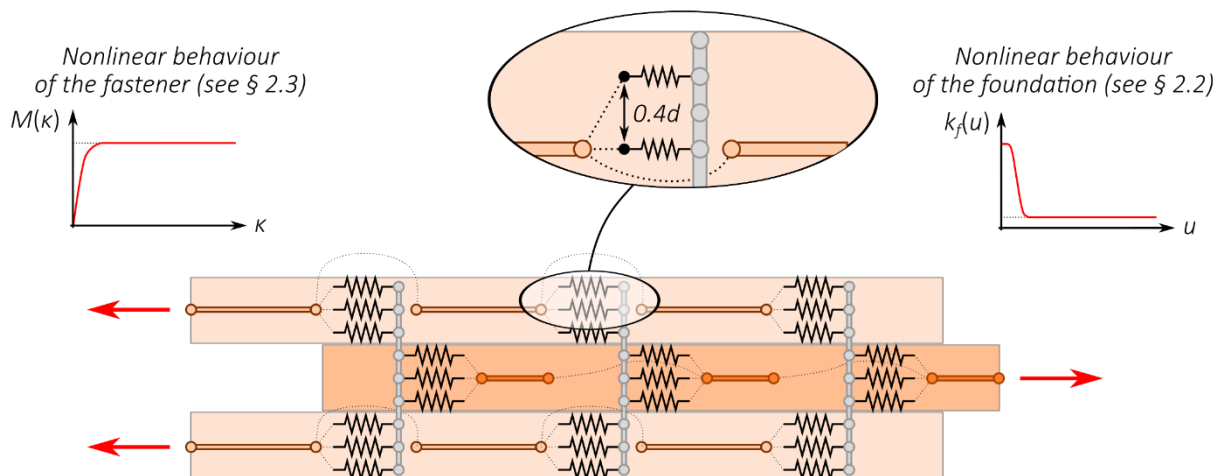
Figure 1. Description of the beam-on-foundation model. Mesh example of a timber-to-timber connection with two shear planes and three dowels in a row.

In order to investigate the influence of the number of springs for each connection member on the numerical results, a sensitivity study was done for one standard configuration: a timber-to-timber connection with two shear planes, five dowels in a row with a dowel diameter equal to 16 mm and thicknesses of outer and inner timber members equal to 48 mm and 96 mm, respectively. Results of this study showed convergence of the numerical results, which are the load-carrying capacity at a connection slip of 5 mm $F_{v,BOF,5mm}$ and the slip modulus $K_{ser,BOF}$ (Figure 2). Based on these results, a minimum spring number of 7 is suggested for this standard configuration. This value is a compromise between a suitable time of calculation and accurate results. For the studied reference configuration, a relative error of about 0.5% between a spring

number equal to 7 and 100 is observed. Since the number of springs depends on the member thickness, a minimum distance between spring elements of *0.4d* is suggested. This value is used for all calculations presented in this paper.
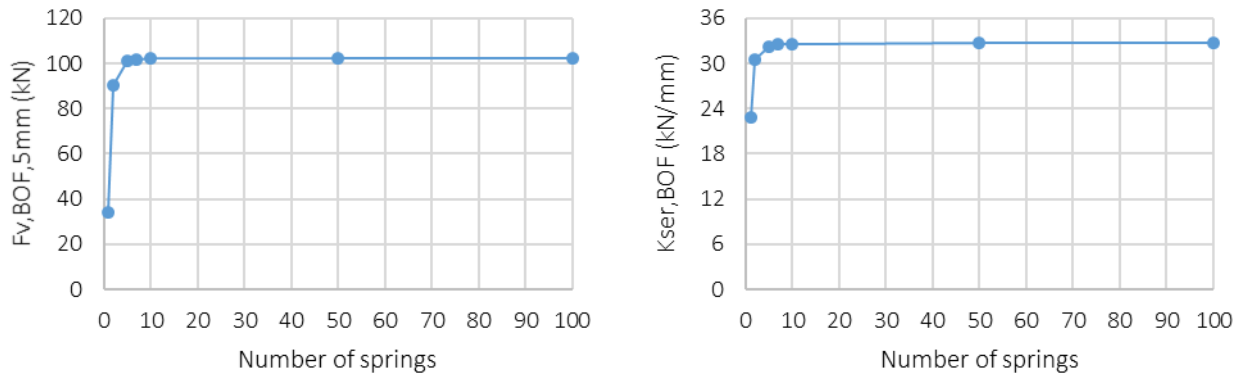
Figure 2. Convergence study as regards number of springs along the fasteners and their influence on the numerical results. $F_{v,BOF,5mm}$ is the load-carrying capacity at a connection slip of 5 mm. $K_{ser,BOF}$ is the slip modulus determined by BOF.

2.2   Foundation behaviour

Several parametrization equations can be found in literature to describe the nonlinear behaviour of embedment; see Schweigler et al (2018) for a review. In this study, the phenomenological function proposed in Sauvat (2001) is used. This equation is based on a trigonometric function,

$$k_f(u) = -a_3 \cdot (\arctan((u \cdot a_6 + a_4)^{a5} + a_1) + a_2). \tag{1}$$

which describes the derivative of the embedment stress with respect to the displacement, i.e., the stiffness of the embedment behaviour, k_f (Figure 3). The parameters a_1 and a_5 can be considered as shape parameters while the parameter a_4 is able to add an initial slip (Figure 3). By physical considerations, parameters a_2 and a_3 can be linked with other mathematical parameters, i.e. a_1 and a_2, and physical parameters, i.e. $k_{f,el}$ and $k_{f,pl}$ which are the elastic and plastic foundation moduli, respectively (Figure 3). Solving Eq. (2) at a dowel displacement of 5 mm allows for determination of a_6, i.e.,

$$\int k_f(u) \, du = f_h, \tag{2}$$

with f_h equal to the embedment stress (in MPa) at a dowel displacement of 5 mm, as defined by the empirical expression (8-16) of EN 1995-1-1,

$$f_h = 0.082 \cdot (1 - 0.01 \cdot d) \cdot \rho, \tag{3}$$

with the dowel diameter d (in mm) and the timber density ρ (in kg/m3).

Compared to the embedment strength, the foundation modulus properties have been less investigated in literature. However, Hwang and Komatsu (2002), proposed an empirical expression for $k_{f,el}$ (in N/mm³) for glulam (the original expression has been adapted herein to be compatible with SI-units),

$k_{f,el} = E_0 / (31.6 + 10.9 \cdot d)$,   (4)

where E_0 is the Young's modulus of wood (in MPa) and d the dowel diameter (in mm). The second foundation modulus $k_{f,pl}$ is assumed to be equal to zero, i.e. the foundation is assumed to be an elastic perfectly plastic material as only parallel to the grain loadings are considered in this paper.

Finally, the following values and analytical expressions of the mathematical parameters in Eq. (1) are suggested:

$a_1 = 2.0$

$a_2 = (k_{f,el} \cdot \pi/2 - k_{f,pl} \cdot \arctan(a_1)) / (k_{f,pl} - k_{f,el})$

$a_3 = - k_{f,el} / (\arctan(a_1) + a_2)$

$a_4 = 0.0$ (no initial slip) or ≤ 0.0 (with initial slip)

$a_5 = 4$

a_6 = set by nonlinear programming
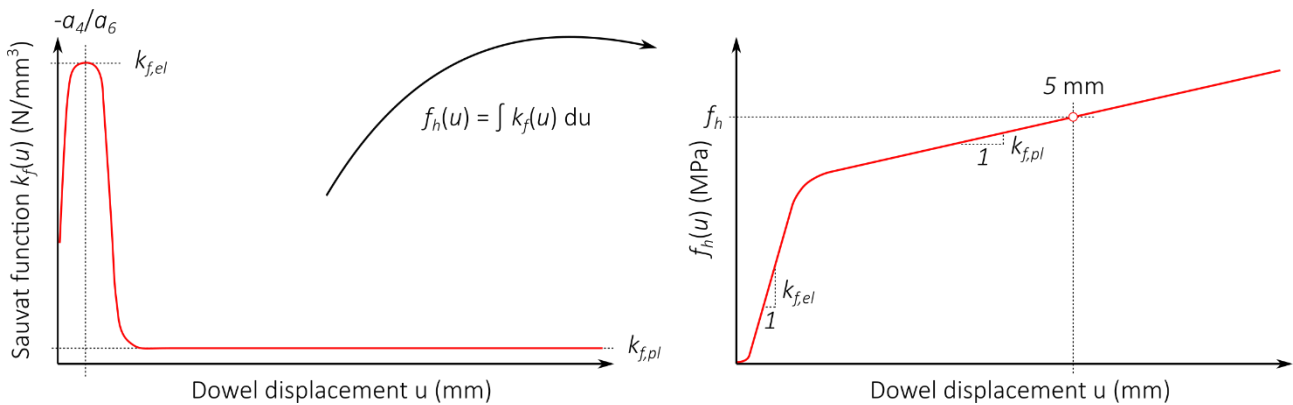
Figure 3. Left: the phenomenological function $k_f(u)$ used in the model (Eq. (1)). Right: the integral of Eq. (1) which is the evolution of the embedment stress $f_h(u)$.

2.3   Fastener behaviour

The elastoplastic behaviour of the steel fastener is modelled by an elastic perfectly plastic material. This nonlinear behaviour is implemented in the model by calculating a new Young's modulus for each beam element constituting the fastener at each displacement increment. For these calculations, the moment-curvature relationship for a circular cross section is defined for $\kappa \geq \kappa_e = 2 \cdot f_y / (d \cdot E)$ by,

$$M(\kappa) = 3/8 \cdot M_y \cdot [2/3 \cdot (1 - (\kappa_e/\kappa)^2)^{3/2} + (1 - (\kappa_e/\kappa)^2)^{1/2} + \kappa/\kappa_e \arcsin(\kappa_e/\kappa)], \quad (5)$$

where, $M_y = f_y \cdot d^3/6$ is the yield moment for a circular cross-section (in MPa), f_y is the yield strength of the dowel (in MPa), d is the dowel diameter (in mm), E is the Young's modulus of the dowel (in MPa).

Through this approach, the model considers the development of plastic hinges along the fastener.

2.4 Material and geometrical properties

Similar to Lemaître et al (2018), a numerical parametric study is carried out. The material and geometrical properties of the connections are chosen to encompass all failure modes defined by Eurocode 5 (see Figures 8-2 and 8-3 in EN 1995-1-1), which led to the following variations:

- dowel diameter d in {8 mm; 12 mm; 16 mm; 24 mm};
- slenderness of the connection t/d in {1; 1.5; 2; 2.5; 3; 3.5; 4; 4.5; 5; 6; 7; 8} where t is the thickness of outer timber members;
- timber density ρ in {420 kg/m^3};
- elastic modulus of timber members E_0 in {11 500 MPa};
- yield strength of the dowel f_y in {240 MPa};
- number of dowels in a row n in {1; 3; 5; 10}.

This study is limited to timber-to-timber joints with double shear planes. The thickness of the inner timber member is twice the thickness of outer timber members.

In Lemaître et al (2018), one assumption was made on the elastic foundation modulus. It was assumed that the elastic behaviour of the foundation remained elastic up to an embedment displacement equal to one millimetre. Thus, the elastic foundation modulus $k_{f,el}$ was equal to the embedment strength f_h according to Eq. (3). Herein, the elastic foundation modulus $k_{f,el}$ is calculated using Eq. (4), and an additional case, assuming an initial slip by using a negative value for the parameter a_5 in Eq. (1). In order to investigate the influence of these assumptions, the following three hypothesis for the foundation moduli are assumed:

- $\mathcal{H}_1$: the elastic foundation modulus $k_{f,el}$ is equal to Eq. (3);
- $\mathcal{H}_2$: the elastic foundation modulus $k_{f,el}$ is equal to Eq. (4);
- $\mathcal{H}_3$: the elastic foundation modulus $k_{f,el}$ is equal to Eq. (4) with an initial slip of 0.5 mm.

576 numerical load-slip curves were computed in this parametric study. All parameters used for the three hypotheses are summarised in Figure 4. The parameters a_5 are defined by intersection of the elastic foundation modulus $k_{f,el}$ with the displacement axis (x-axis) at 0.5 mm (hypothesis $\mathcal{H}_3$). The parameter a_6 is derived through nonlinear solution of Eq. (2).

Hypothesis $\mathcal{H}_1$	D	8	12	16	24
	f_h	31.68	30.31	28.93	26.17
	$k_{f,el}$	31.68	30.31	28.93	26.17
	a_4	0.0	0.0	0.0	0.0
	a_6	1.35	1.35	1.35	1.35
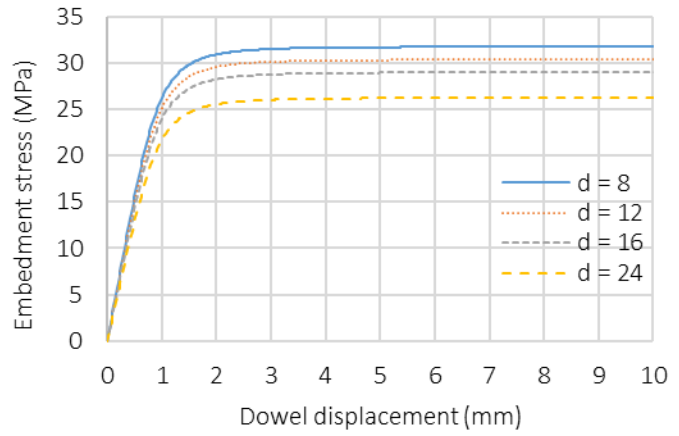
Hypothesis $\mathcal{H}_2$	d	8	12	16	24
	f_h	31.68	30.31	28.93	26.17
	$k_{f,el}$	96.80	70.81	55.83	39.22
	a_4	0.0	0.0	0.0	0.0
	a_6	4.14	3.17	2.61	2.03
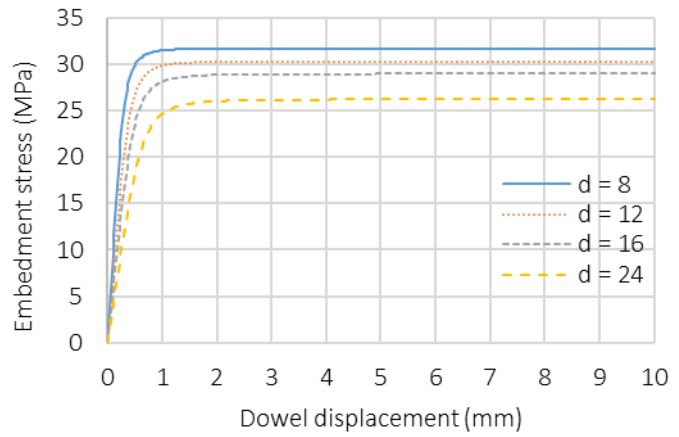
Hypothesis $\mathcal{H}_3$	d	8	12	16	24
	f_h	31.68	30.31	28.93	26.17
	$k_{f,el}$	96.80	70.81	55.83	39.22
	a_4	-5.55	-4.57	-3.98	-3.39
	a_6	8.27	6.32	5.21	4.03
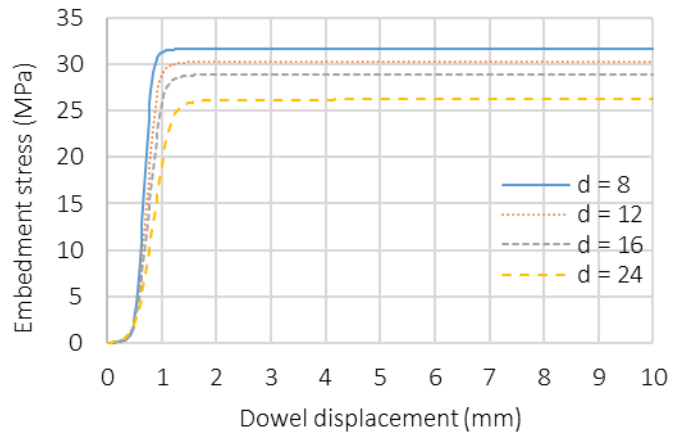
Figure 4. Parameters of the nonlinear embedment foundation and associated embedment curves for the three modelling hypothesis. d is the dowel diameter (in mm), f_h is the embedment strength defined by Eq. (3), $k_{f,el}$ is the elastic foundation modulus (in N/mm^3), a_4 and a_6 are mathematical parameters of the phenomenological function in the Eq. (1). The embedment curves of all charts are approximated using the trapezoidal rule from Eq. (1) between 0 mm and 15 mm discritized into 750 subintervals.

2.5 Evaluation of the slip modulus

The connection slip is measured as the relative displacement between the end nodes of the outer and inner timber members, which were assumed at a distance of 7d from the fasteners (Figure 5).

The slip modulus of the multiple fastener connection, $K_{ser,BOF}$, was then defined as the slope of the line connecting the points on the load-slip curve at 10% and 40% of the load carrying capacity at a connection slip of 5 mm $F_{v,BOF,5mm}$.

Using a beam-on-foundation modelling could help engineers to predict an accurate slip modulus $K_{ser,eng}$. Nevertheless, engineers are used to apply connection stiffness at beam nodes in a structural frame and truss analysis software. In case elastic beam elements are chosen in truss models, the slip modulus estimated by a beam-on-foundation modelling $K_{ser,BOF}$ needs to be corrected by the elastic deformation of the timber or steel over the connection length (Figure 5). It is proposed to calculate $K_{ser,eng}$ by

$$K_{ser,eng} = K_b \cdot K_{ser,BOF} / (K_b - K_{ser,BOF}),$$ (6)

where K_b is the equivalent stiffness of the connection area.
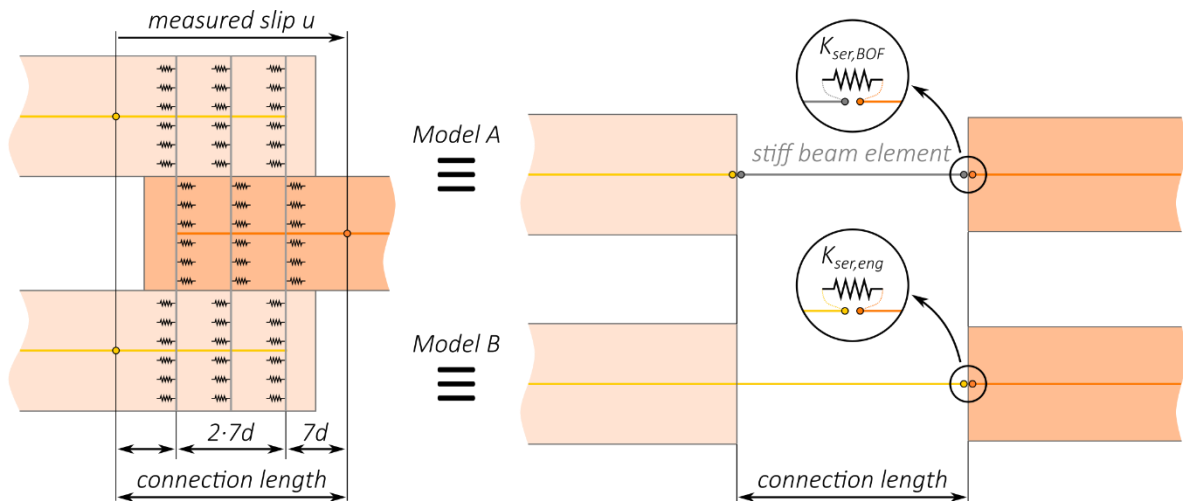
Figure 5. Visualization of the model derived connection slip and the equivalent engineering structural models. Model A should be used with the slip modulus measured by beam-on-foundation modelling $K_{ser,BOF}$. Model B should be used with the slip modulus proposed $K_{ser,eng}$ in Equ. (6).

3   Results

In this section, comparison between numerical results of the beam-on-foundation modelling and predictions from analytical equation of the European Yield Model are made (Section 3.1). This includes a study of the load-carrying capacity as it has been done in Lemaître et al (2018) for one single dowel connection. In Section 3.2, a comparison of the slip modulus is carried out. Finally, a study of the load distribution in multiple fastener timber-to-timber joints is made (Section 3.3).

In order to investigate the sensitivity of geometrical parameters, i.e. the number of dowels in a row n, the dowel diameter d and the dowel slenderness t/d, different series of connections are defined (Table 1).

Moreover, the sensitivity of material parameters is also investigated as regards the three hypotheses of the foundation behaviour defined in Figure 4.

Table 1. Serie definitions used for the comparison.

Series	n	d	t/d
1	1, 3, 5, 10	8, 12, 16, 24	1, 1.5, 2, 2.5, 3, 3.5, 4, 4.5, 5, 6, 7, 8
2	1, 3, 5, 10	12	1, 1.5, 2, 2.5, 3, 3.5, 4, 4.5, 5
3	1, 3, 5, 10	12	3, 6
4	10	16	3

3.1 Load-carrying capacity

In this section, only Serie 1 is considered (Table 1). This includes all parameter varia-tions from Section 2.4. From numerical load-slip curves, the load-carrying capacities at connection slip of 5 mm and 15 mm are analysed. These values are compared with the load-carrying capacity predicted by the European Yield Method of the Eurocode 5 based on the work of Johansen (1949). As in Lemaître et al (2018) for investigation of single dowel connections, the partial safety factors related to the uncertainties of ma-terials and the rope effect are neglected for this comparison.

In order to investigate the influence of the elastic foundation modulus on the load-carrying capacity, the numerical results of hypotheses $\mathcal{H}_1$ and $\mathcal{H}_2$ are illustrated in Fig-ure 6. No considerable difference became obvious between hypotheses $\mathcal{H}_1$ and $\mathcal{H}_2$. For both hypotheses, the numerical results are in very good agreement with the load-carrying capacities predicted by the Johansen's theory according to Eurocode 5.
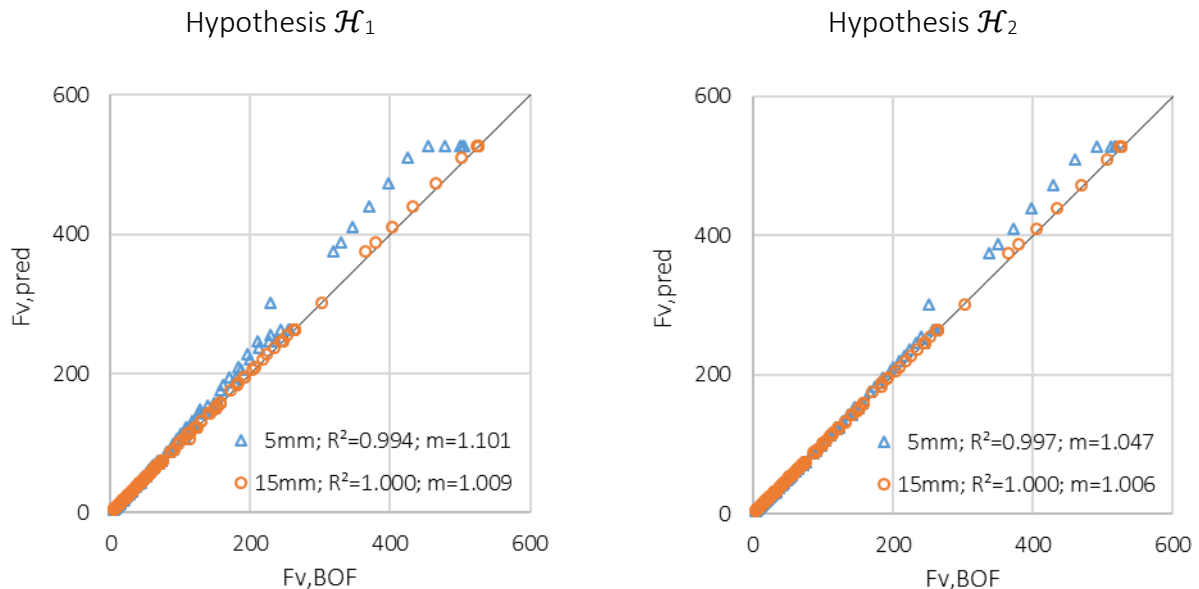
Figure 6. Predicted load-carrying capacity by the Johansen's theory $F_{v,pred}$ versus model-predicted load-carrying capacity by the beam-on-foundation modelling $F_{v,BOF}$ (in kN). R^2 and m are the coefficient of determination and slope of the linear regression, respectively. Left: comparison with $\mathcal{H}_1$. Right: comparison with $\mathcal{H}_2$. $\triangle$ $F_{v,BOF}$ at connection slip of 5 mm. $\circ$ $F_{v,BOF}$ at connection slip of 15 mm.

3.2   Slip modulus

In this section, only Serie 1 and 2 according to Table 1 are considered. Serie 2 includes only one dowel diameter of 12 mm and dowel slenderness ratios between 1 to 5. Serie 2 is representative for the geometry and configurations of the connections used in Jockwer and Jorissen (2018) with the aim to establish an empirical equation for the slip modulus, see Eq. (9).

For both series, BOF-model predicted slip moduli are compared with different empirical equations for the slip modulus of timber-to-timber connections. The latter are given for one shear plane,

Eurocode 5 $\quad\quad\quad\quad\quad\quad\quad\quad K_{ser} = n \cdot \rho_m^{1.5} \cdot d / 23$ $\quad\quad\quad\quad\quad\quad$ (7)

SIA 265 $\quad\quad\quad\quad\quad\quad\quad\quad K_{ser} = 3 \cdot n \cdot \rho_k^{0.5} \cdot d^{1.7}$ $\quad\quad\quad\quad\quad\quad$ (8)

Jockwer and Jorissen (2018) $\quad\quad K_{ser} = 3.5 \cdot n^{1.26} \cdot d^{2.17} \cdot (t / d)^{0.25}$ $\quad\quad$ (9)

where n is the number of dowels in a row, ρ_m (respectively ρ_k) is the mean (respectively characteristic) value of the wood density (in kg/m^3), d is the dowel diameter (in mm) and t is the thickness of outer timber members (in mm).

Figure 7 compares the numerical slip moduli $K_{ser,BOF}$ from the beam-on-foundation modelling with the predicted values according to Eqs. (7-9). Graphs on the left and the right side of Figure 7 are comparison for Serie 1 and 2, respectively.

In general, beam-on-foundation modelling predictions and Eq. (9) are in good agreement. Through the Serie 1 comparison, the significant effect of the dowel slenderness becomes obvious, as the fitting with Eq. (9) is better. However, some differences exist between the hypotheses $\mathcal{H}_1$ and $\mathcal{H}_2$. This indicates that the elastic foundation modulus hypothesis should be reconsidered. However, the drilling tolerance used in the experimental campaign of Jockwer and Jorissen (2018) is unknown. This parameter has an important consequence on a connection stiffness. In practice, higher number of dowels is important and this might reduce drilling tolerance. An investigation on the slip modulus with a combination of hypotheses $\mathcal{H}_2$ and $\mathcal{H}_3$ could be performed and might be more representative for connections with a high number of dowels.

Serie 2 comparisons show that the number of dowels has a nonlinear effect on the slip modulus, as also predicted through an exponent on the number of dowels by Eq. (9).

Based on the numerical results of Serie 1 and hypothesis $\mathcal{H}_1$, a nonlinear regression analysis was applied to derive an empirical equation. This yielded the following equation for the slip modulus of timber-to-timber connections per shear plane (in N/mm),

$K_{ser,prop} = 74.59 \cdot n^{0.78} \cdot d^{1.49} \cdot (t / d)^{0.15}$ $\quad\quad\quad\quad\quad\quad\quad\quad$ (10)
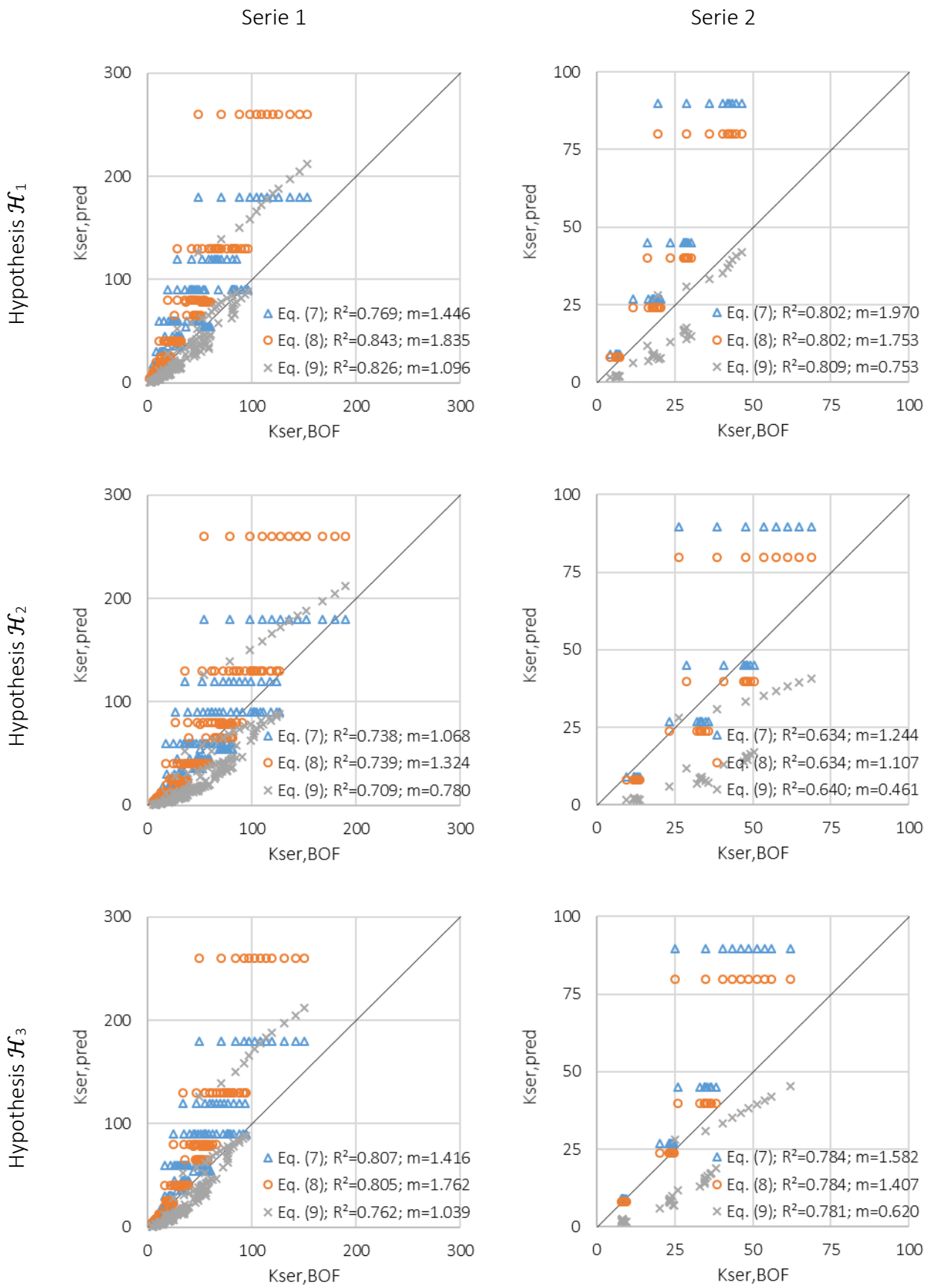
Figure 7. Calculated slip modulus of Eqs. (7-9) $K_{ser,pred}$ versus model-predicted slip modulus from the beam-on-foundation modelling $K_{ser,BOF}$. Values for two shear planes are given (in kN/mm). R^2 and m are the slope and the coefficient of determination of the linear regression, respectively.

3.3   Load distribution

In this section, model predictions from Serie 3 and 4 (Table 1) are exploited for studying load distribution. Figure 8 compares the percentage of effective dowels as compared to the number of dowels in a row, for the different connection configurations of Serie 3 with hypotheses $\mathcal{H}_2$ and $\mathcal{H}_3$. Results with $\mathcal{H}_3$ highlight the influence of the drilling tolerance on the load distribution as an initial slip is considered for the foundation behaviour (Figure 4). Figure 9 compares for one connection configuration (Serie 4) the load distribution at different slip values, i.e. 0.5 mm, 1 mm, 5 mm and 15 mm, with hypotheses $\mathcal{H}_2$ and $\mathcal{H}_3$. Results show that the beam-on-foundation model's efficiency to estimate load distribution and the influence of initial slip on the connection strength at different displacements. For a review of numerical modelling approaches to estimate load distribution, see the paper of Bader et al, in Sandhaas et al (2018), pages 221-239.
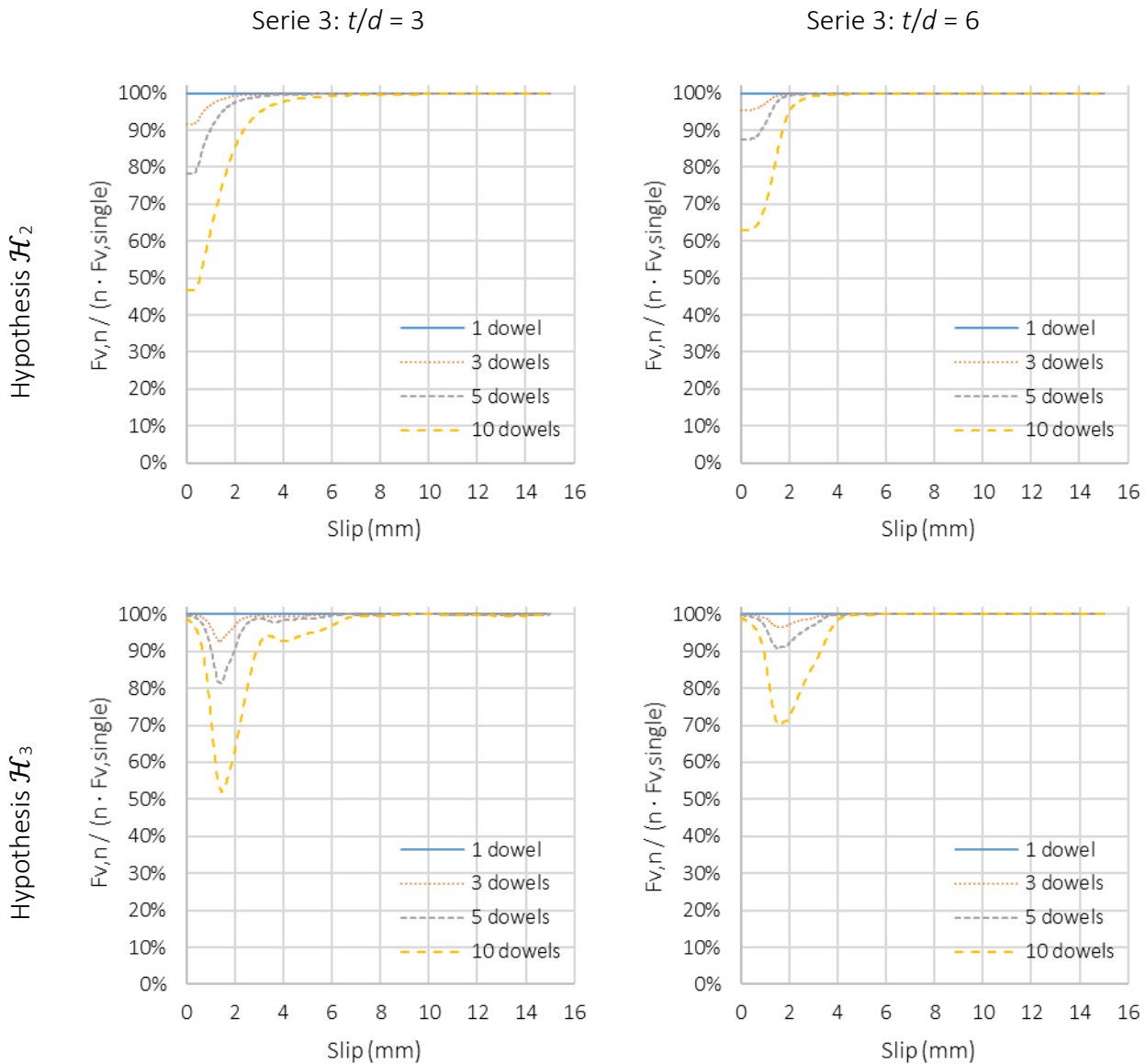
Figure 8. Percentage of effective dowels versus connection slip for Serie 3. $F_{v,n}$ is the load-carrying capacity of a multiple dowel connection with n dowels in a row. $F_{v,single}$ is the load-carrying capacity of a single dowel connection.
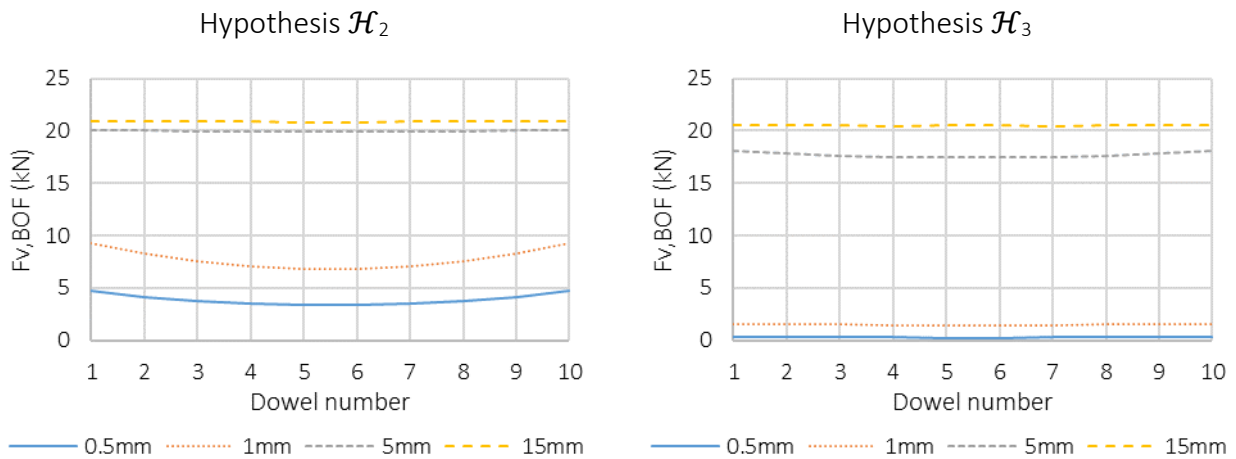
Figure 9. Load distribution in a multiple-dowel connection with 10 dowels in a row, for Serie 4. Left: hypothesis $\mathcal{H}_2$. Right: hypothesis $\mathcal{H}_3$.

4   Conclusion

Beam-on-foundation calculations in Lemaître et al (2018) were limited to single dowel connections loaded parallel to the grain. In this paper, the model was extended to multiple fastener connections loaded by a normal force parallel to the grain. The presented 2-dimensional model is however more general and can be applied to multiple fasteners connections with arbitrary load-to-grain angles.

Beam-on-foundation model calculations and their comparison to the design equations highlights the validity of the method and the advantage of a kinematically compatible model that allows for prediction of the displacement behaviour of multiple dowelled timber connections in addition to their ultimate strength. Compared to Eurocode 5 and SIA 265, Jockwer and Jorissen's proposal considered two major influence factors, namely the number of dowels in a row, and the dowel slenderness. The pronounced influence of these parameters was also revealed by the numerical model. This model could be further exploited by means of the database proposed in the paper IN-TER 2019 -52-07-08.

The elastic foundation modulus for steel fastener to steel plate contact needs further evaluation. This would open possibility for a similar study on steel-to-timber joints. Another important parameter not covered herein is the distance between fasteners in grain direction. Its influence can however easily be assessed with the proposed model.

Beam-on-foundation modelling is more powerful than the approach developed in Wilkinson (1986) for calculation of load distribution. More parameters can be integrated, such as the drilling tolerance, or multi-material and multiple shear planes connections.

This paper is a first step towards a design method, however the methodology needs to be thoroughly validated by experiments, ideally with tests where all parameters are known, i.e. steel quality, steel behaviour (with or without hardening), embedment behaviour, the drilling tolerance, hole positions etc.

5   References

Blass H. J. (1995): Multiple fastener joints. Lecture C15 in Timber Engineering STEP 1, Centrum Hout, The Netherlands.

Cramer C.O. (1968): Load distribution in multiple-bolt tension joints. Journal of the Structural Division, ASCE 94(ST5):1101-1117.

EN 1995-1-1 (2004), Eurocode 5: Design of timber structures: Part 1-1, General common rules and rules for building, Comité Européen de Normalisation (CEN), Brussels, Belgium.

Hirai T. (1983): Nonlinear load-slip relationship of bolted wood-joints with steel side-members II. Application of the generalized theory of a beam on an elastic foundation. Mokuzai Gakkaishi 29(12):839-844.

Hwang K. and Komatsu K. (2002): Bearing properties of engineered wood products I: effects of dowel diameter and loading direction. Journal of Wood Science 48, 295–301.

Jockwer J., Jorissen A. (2018): Load-deformation behaviour and stiffness of lateral connections with multiple dowel type fasteners. INTER meeting 51, paper 51-07-7, Tallinn, Estonia.

Johansen K.W. (1949): Theory of Timber Connections, International Association for Bridge and Structural Engineering (ABSE) Pub. 9, 249-262.

Lantos G. (1969): Load distribution in a row of fasteners subjected to lateral load. Wood Science 1(3):129-136.

Lemaître R., Bocquet J. F., Schweigler M., Bader T. K. (2018): Beam-on-foundation modelling as alternative design method for timber joints with dowel-type fasteners – Part 1: Strength and stiffness per shear plane of single-fastener joints. INTER meeting 51, paper 51-07-13, Tallinn, Estonia.

Sauvat N. (2001): Résistance d'assemblages de type tige en structure bois sous chargements cycliques complexes. PhD thesis. Université Blaise Pascal-Clermont-Ferrand II, France.

Sandhaas, C., Munch-Andersen, J., Dietsch, P. (eds.) (2018): Design of Connections in Timber Structures: A state-of-the-art report by COST Action FP1402 / WG3, Shaker Verlag Aachen.

Sandhaas C. and van de Kuilen J-W G. (2017): Strength and stiffness of timber joints with very high strength steel dowels. Engineering Structures 131:394-404.

Sawata K. and Yasumura M. (2003): Estimation of yield and ultimate strengths of bolted timber joints by nonlinear analysis and yield theory. Journal of Wood Science 49(5), 383-391.

Schweigler M., Bader T.K., Hochreiner G., Lemaître R. (2018): Parameterization equations for the nonlinear connection slip applied to the anisotropic behaviour of wood. Composites Part B: Engineering, 142:142-158.

SIA 265 (2012): Timber structures. SIA Swiss Society of Engineers and Architects, Zurich, Switzerland.

Wilkinson, T. L. (1986): Load Distribution among Bolts Parallel to Load. Journal of Structural Engineering, 112(4):835–852.

Discussion

The paper was presented by M Schweigler

JM Cabreo received confirmation that zero length springs were used and received clarification of the connection analogy.

R Jockwer and M Schweigler discussed the slenderness of the dowel and the stiffness definition of the dowels with different behaviour. They discussed the highly non-linear behaviour of nail connections and the distinction between nail versus large diameter dowels.

P Palma asked how brittle failure modes were accounted for. M Schweigler responded that this is for ductile failure mode. At least this method would allow the load distribution to be estimated which can then be used in the next step for brittle failure prediction.

M Li asked whether this method could capture the uneven distribution of loads between the dowels. M Schweigler stated that this method could do so as non-rigid link elements were used.

S Aicher commented that Figure 7 in the paper indicated EC5 seemed to be 2.5 times larger than the predictions and this is alarming.   M Schweigler responded that EC5 did not consider multiple dowel effects, e.g. n_{ef}. H Blass confirmed this and that EC5 has not been fully tested for such cases as extrapolation was used in EC5.

D Dolan received confirmation that shear lag effect was considered in the model.

Transmission of perpendicular to grain forces using self-tapping screws

Philipp Dietsch, Chair of Timber Structures and Building Construction, Technical University of Munich

Sebastian Rodemeier, Technical University of Munich

Hans Joachim Blaß, Timber Structures and Building Construction, Karlsruhe Institute of Technology

1 Background and Objective

Structural details where timber is loaded in compression perpendicular to the grain are very common, e.g. beam supports or sill/sole plates. The combination of high loads to be transferred over localized areas and low capacities in compression perpendicular to the grain can make it difficult to meet the associated verifications. Fully threaded, self-tapping screws (STS) were identified as an efficient means to improve the stress dispersion into the timber (Bejtka & Blaß, 2006). STS have since then become a common application for the reinforcement of beams at supports.
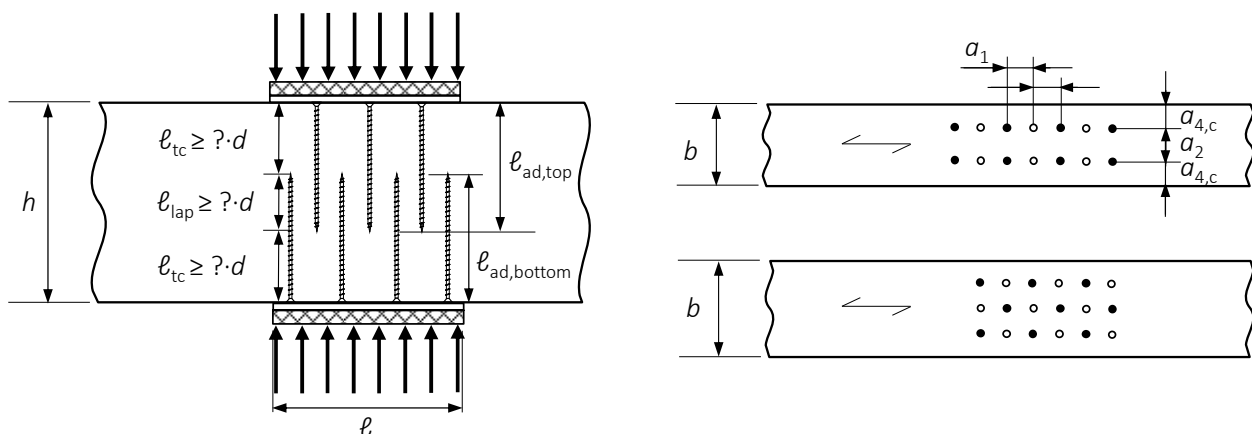
Figure 1. Self-tapping screws applied for transmission of perpendicular to grain forces.

An extended application, enabling the transfer of compression perpendicular to grain stresses through the timber member was first studied by Watson et al. (2013) for post-tensioned frame structures from LVL. Subsequently this application was introduced into one German Technical Approval (Z-9.1-519:2014). The screws are applied with an overlap, see Fig. 1, meant to transfer the compression forces from the screws on one side of the member to the screws on the opposite side. If this load transfer can be achieved, the verification of compression failure of the wood perpendicular to the grain at the screw tips can be neglected. A potential market for this application is seen in multi-story timber buildings.

During the drafting process of the new clauses on reinforcement in a revised Eurocode 5 (Dietsch & Brunauer 2017), a few questions on this application were raised, e.g. minimum overlap length, minimum distance between screw tips and opposite contact plate and arrangement of STS on opposite member edges, see Fig. 1. This paper contributes answers to these questions, based on numerical parameter studies and experiments.

2 Comparison to related structural applications

Due to the few publications dealing with the reinforcement of timber members for compression perpendicular to grain stresses up to date (see Section 1), the literature study was extended to related structural applications.

In the design of overlap joints in reinforced concrete, the type of loading (tension joint or compression joint) is taken into account as well as the effective circumference of the rebars, see Fig. 2. Required overlap lengths in compression joints in normal concrete (C20/25 ÷ C50/60) are in the range of $25 \cdot d \leq \ell_0 \leq 45 \cdot d$ with a minimum length $\ell_{0,min}$ = 200 mm (EN 1992-1-1:2010).
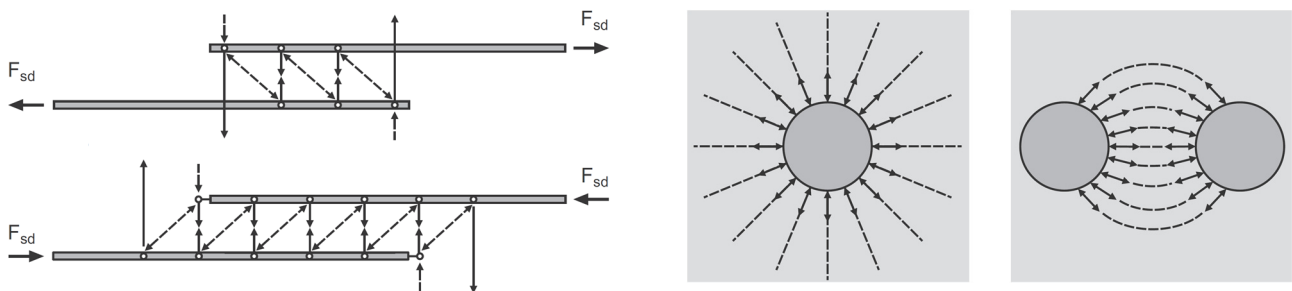
Figure 2. Structural system for the design of overlapping concrete rebars (left) and effective circumference of single rebars and overlapping rebars in concrete (Zilch & Zehetmeier, 2006).

In the design of pile foundations in geotechnical engineering, the different settlement behaviour of single piles in a group of piles (see Fig. 3) is accounted for by verifying the load-carrying capacity of the single piles as well as the load-carrying capacity of the group of piles, schematized as one single substitute pile (EN 1997-1:2013). One main design parameter in both applications is the spacing between rebars or piles.
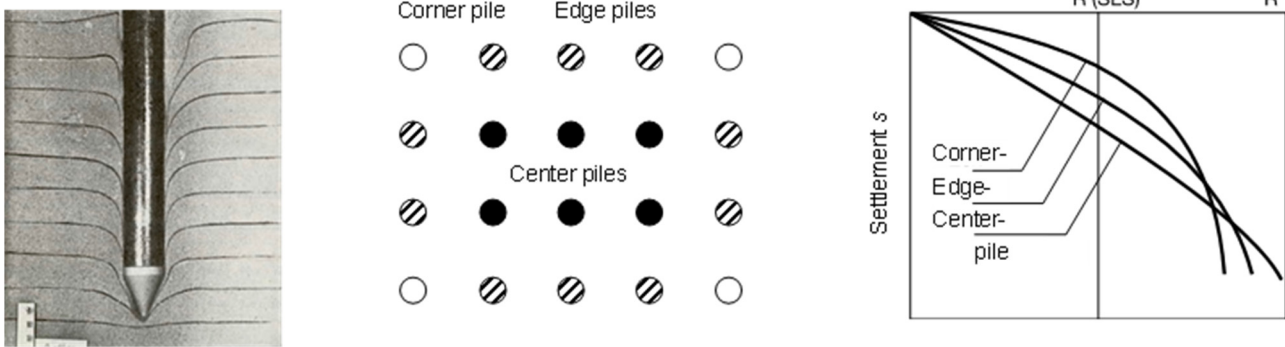
Figure 3. Failure mechanism of pile in dense sand (left; Vesic, 1977); pile categories and settlement behaviour of different pile categories in a group of piles (according to Kempfert, 2001).

3 Configuration for numerical and experimental studies

Both, intermediate supports and end supports should be investigated. The distance between screw tips and opposite contact plate, ℓ_{tc}, should be sufficient to prevent load transfer from the contact plate to the screw tips. The STS should be sufficiently long to investigate load transfer at different overlap lengths ℓ_{lap} between zero and $20 \cdot d$. The following configuration was in best agreement with the above-mentioned boundary conditions. A specimen depth of $40 \cdot d$ enabled overlap lengths ℓ_{lap} between zero ($0 \cdot d$) and half ($20 \cdot d$) of the specimen depth, while the remaining length ℓ_{tc} between the screw tips and the opposite contact plate was at least a quarter of the beam depth ($10 \cdot d \div 20 \cdot d$). Screw spacing in the area of overlap should equal the minimum required spacing ($a_1 \cdot a_2 = 25 \cdot d_1^2$ in most technical approvals) to achieve the optimum reinforcing effect. In order to reach real-size, reasonably to handle specimens, the screw diameter was chosen as $d = 8$ mm. 6 STS from the bottom and 4 STS from the top at minimum spacing were chosen, resulting in dimensions of the contact area of $\ell/b = 200/100$ mm^2 and specimen dimensions $h/b = 320/100$ mm^2.

4 Numerical parameter studies

4.1 Materials and methods

The determined configuration was realized as a parametrized 3-D FE-model (ANSYS Workbench 19.1). Glued-laminated timber GL24h (EN 14080:2013) was taken as basis for the stiffness parameters of the timber specimen. The STS were modelled as cylinders, encircled by a tube representing the transition region containing the screw thread and the wood material. The axial slip modulus of the STS, K_{ax}, is represented by the shear stiffness G of the volume. The axial slip modulus K_{ax} was derived from the modelling of associated experimental investigations (Mestek, 2011), (Danzer, Dietsch & Winter, 2016). The simulation was limited to the linear-elastic state. For verification, support areas with and without reinforcement were modelled and compared to literature (Bejtka, 2005).

4.2 Results – support with single-sided reinforcement

The results for the support area with single-sided reinforcement indicate a concentration of compression perpendicular to grain stresses between the screw tips and the opposite member edge (continuous support) with stress maxima in the plane of the screw tips, see Fig. 4.
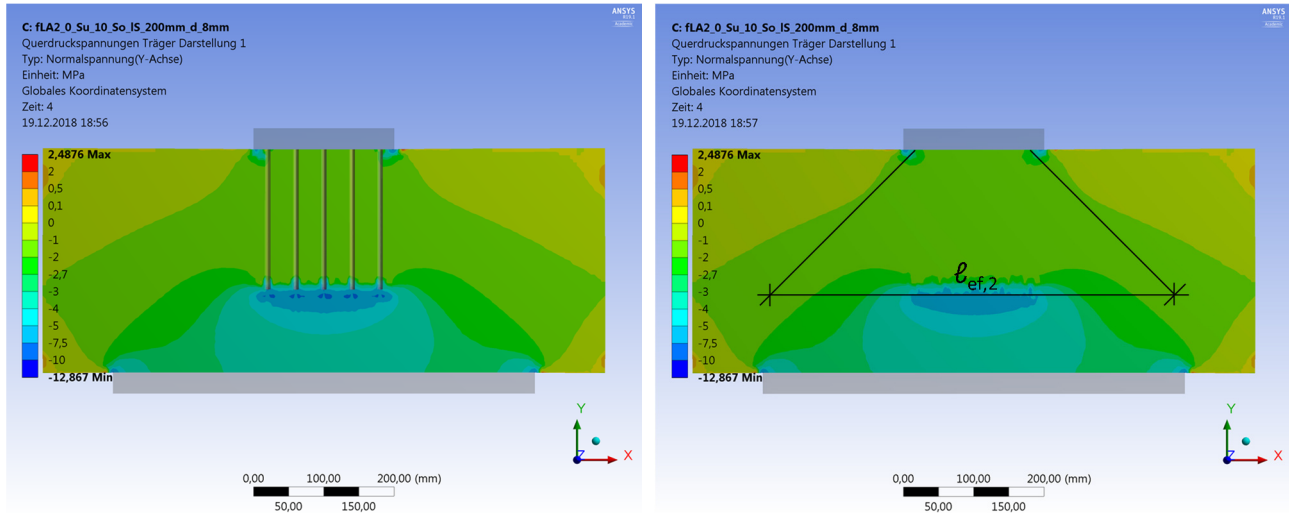
Figure 4. Distribution of compression perp. to grain stresses in reinforced support area.

An evaluation of perpendicular to grain stresses along the length $\ell_{ef,2}$, used for verification of compression capacity perpendicular to grain at the screw tips (e.g. ETA-12/0114:2017), indicates a considerable variation of stresses along this length with stress concentrations in the direct proximity of the screws, see Fig. 5. In the ultimate limit states, this will partly be compensated by stress redistribution due to the elastic-plastic failure mechanism of wood in compression perpendicular to the grain.
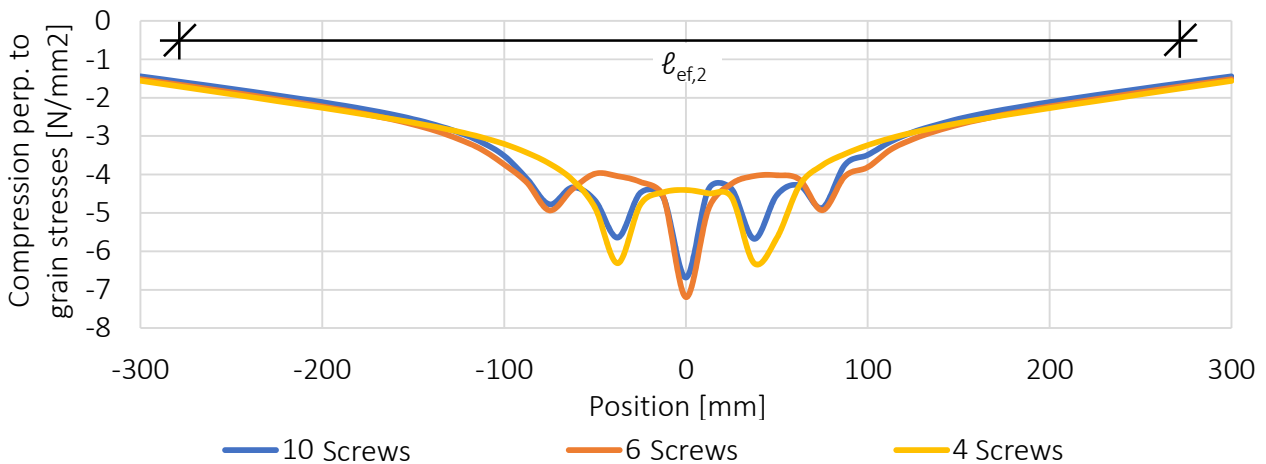
Figure 5. Distribution of compression perp. to grain stresses in horizontal plane at the screw tips.

The axial compression stresses in the screws positioned at the edges/corners of a group of screws are up to one quarter higher than the stresses in the inner screws, see Fig. 6. Reason is a group effect between the screws and the wood material inside the circumference of the group of screws, which leads to a rather homogeneous deformation of both materials. In contrast to that, the wood outside the circumference deforms less than and the group of screws, leading to higher shear between the

194

wood and the outer screws and hence to higher axial compression stresses in these screws. This finding correlates with the load-distribution in a group of piles in a pile foundation, see Fig. 3.
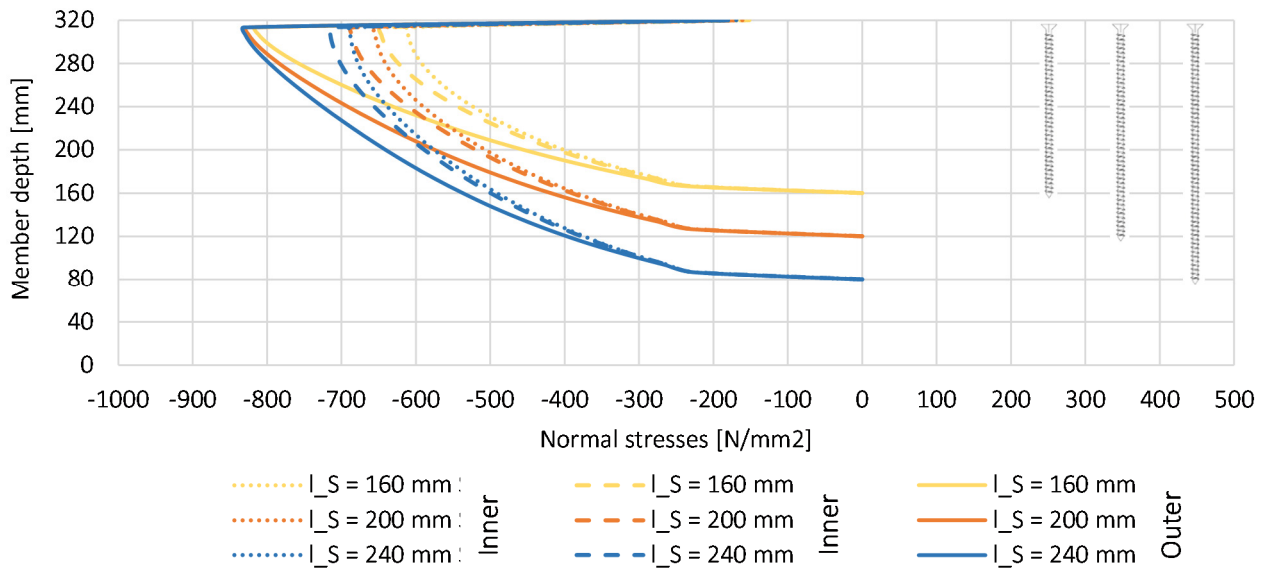
Figure 6. Distribution of axial compression stresses in outer and inner screws in a group of screws.

4.3 Results – double-sided reinforcement

When the configurations are extended to reinforcement by STS applied from opposite edges of the timber member, one additional and potentially governing parameter is given by the overlap length ℓ_{lap}. Configurations in which the screw tips end at one horizontal plane ($\ell_{lap} = 0 \cdot d$) lead to high localized deformations (and hence compression stresses) perpendicular to the grain close to the plane of the screw tips. Increasing the overlap length to $\ell_{lap} = 5 \cdot d$ already leads to a noticeable reduction, however the largest deformations still occur at the screw tips. The lowest values are observed for overlap lengths $\ell_{lap} = 10 \cdot d$, the distribution of deformations is the most homogeneous of all configurations. Overlap lengths $\ell_{lap} > 10 \cdot d$ do not lead to further reduction of deformations, the location of maximum deformations (and hence maximum compression perpendicular to grain stresses) is moved towards the contact areas on the member edges. The maximum axial compression stresses in the screws increase with increasing overlap length, however for overlap lengths $\ell_{lap} > 10 \cdot d$, this increase becomes marginal.
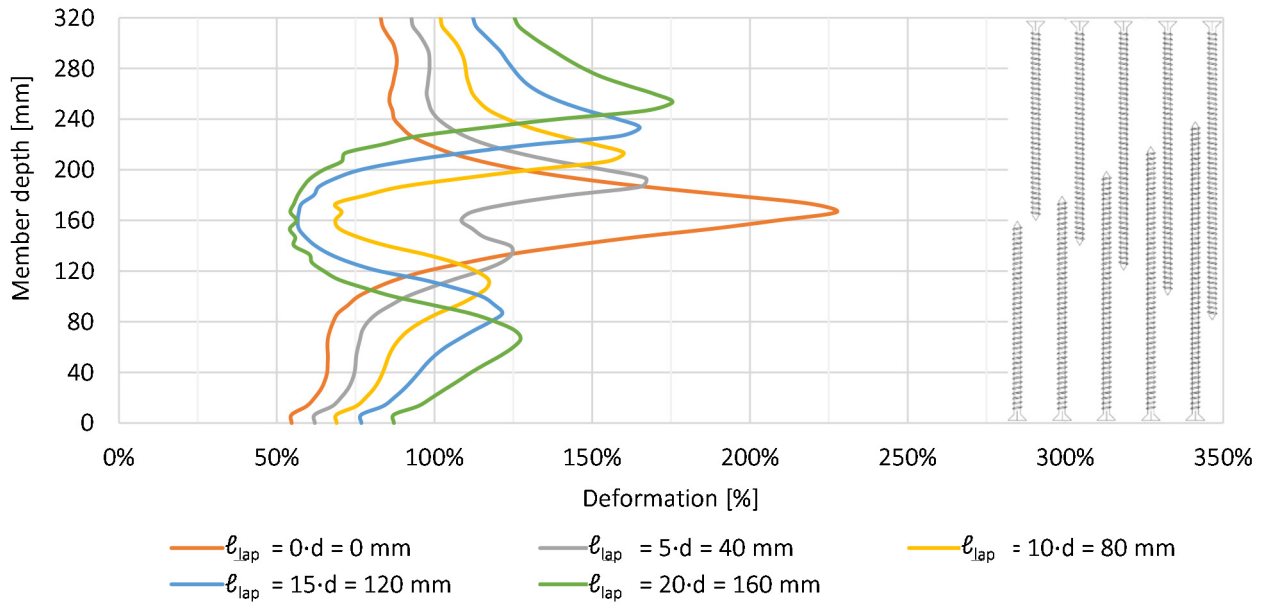
Figure 7. Deformations (percent) perpendicular to the grain over the member depth (vertical path at b/2) at varying overlap length ℓ_{lap}.

Fig. 8 illustrates that increasing overlap lengths also result in a reduced dispersion of compression perp. to grain stresses into the timber member, i.e. a more confined stress bulb. An increase in overlap length ℓ_{lap} leads to a reduction of the distance ℓ_{tc} between the screw tips and the opposite contact plate and to increased concentration of compression perp. to grain stresses in this area. This fact will be further discussed in the evaluation of the experimental campaign. Varying the distance ℓ_{tc} while keeping overlap lengths ℓ_{lap} constant indicates, that the increase in compression perp. to grain stresses in the area between the screw tips and the opposite contact plate becomes substantial for distances $\ell_{tc} < 15 \cdot d$. These stresses can be reduced by an alternating arrangement of the screws (alternative detail in Fig. 1) due to the more direct (i.e. increased) load transfer between two screws arranged at spacing a_2. A variation of screw diameter only showed marginal influence on the described relationships.
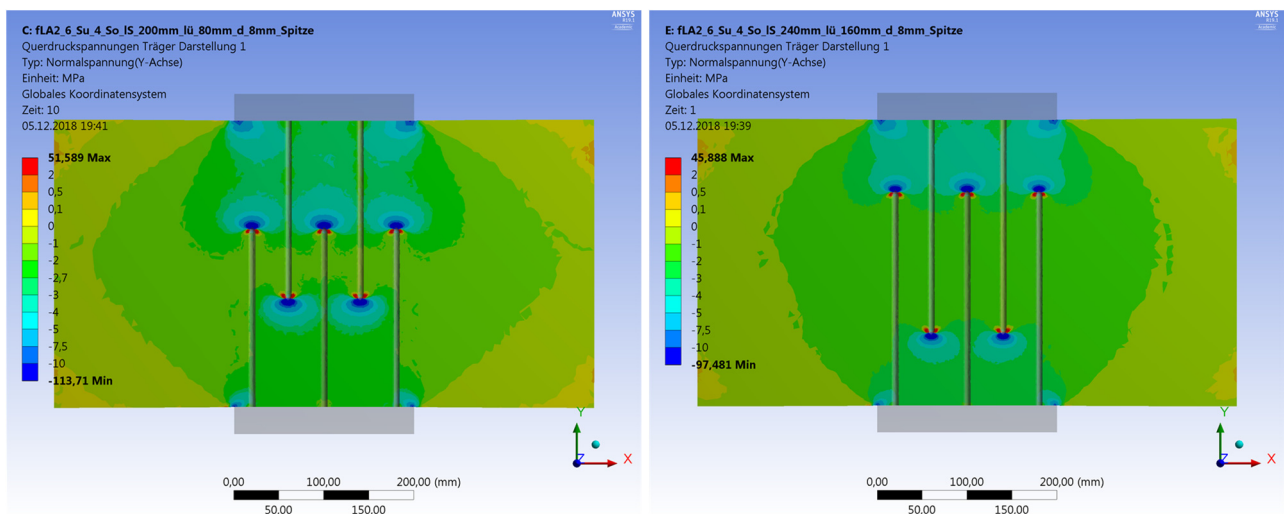
Figure 8. Compression perp. to grain stresses at overlap length $\ell_{lap} = 10 \cdot d$ (left) and $20 \cdot d$ (right).

5 Experimental campaign

5.1 Materials and methods

The experimental campaign consisted of 7 different configurations with in total 32 specimens, see Fig. 9 and Tab. 1. The first configuration, an intermediate support without reinforcement, was tested for comparative reasons. This was followed by tests on four configurations representing intermediate supports (type (a) in Fig. 9) with four STS from the top, six STS from the bottom and overlap lengths ℓ_{lap} = {5·d, 10·d, 15·d, 20·d}. The sixth configuration featured an alternating arrangement of five STS each from top and bottom with ℓ_{lap} = 10·d (type (b) in Fig. 9), while the last configuration represented an end support (type (c) in Fig. 9) with 4 STS x 6 STS and ℓ_{lap} = 10·d.

The self-tapping screws (ETA-12/0114:2017) featured a diameter d = 8 mm and lengths ℓ = {180, 200, 220, 240 mm}. The STS were applied using minimum required spacing, the screw heads flush with the contact surface. The glulam specimens of grade GL 24h (EN 14080:2013) featured dimensions $\ell/h/b$ = 600/320/100 mm and lamella thickness t = 40 mm. The measured timber moisture content was u_{mean} = 10,9 %, the measured density was $\rho_{12\%,mean}$ = 444 kg/m^3, see Tab. 1.
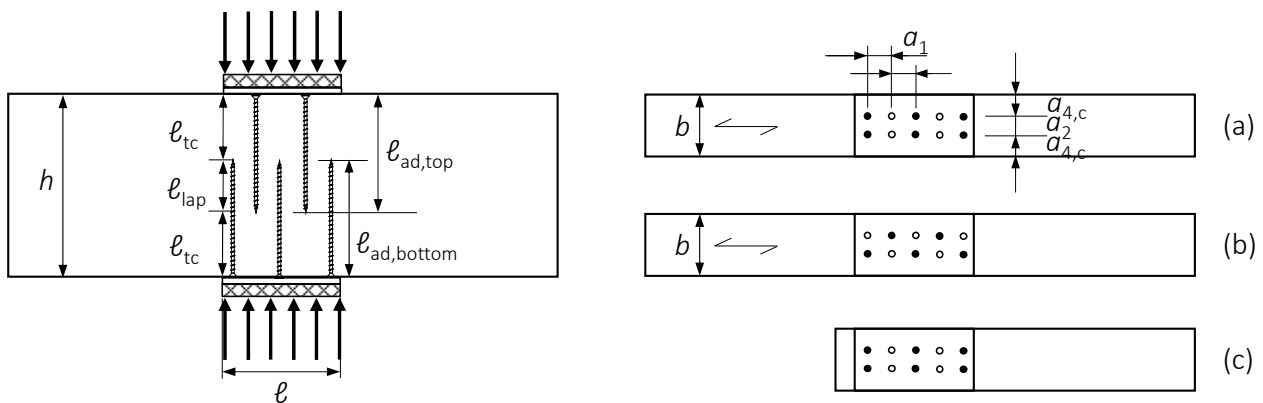
Figure 9. Overview of specimen geometry.

Table 1. Test series and information on specimens and geometry.

Series No.	1	2	3	4	5	6	7
Configuration	-	a	a	a	a	b	c
Arrangement (total-top-bottom)	no screws	10-6-4	10-6-4	10-6-4	10-6-4	10-5-5	10-6-4
Overlap length [mm]	-	5·d = 40	10·d = 80	15·d = 120	20·d = 160	10·d = 80	10·d = 80
Screw length [mm]	-	180	200	220	240	200	200
No. of specimens [-]	3	5	6	5	5	5	3
Density $\rho_{mean,12\%}$ [kg/m^3]	439	449	442	439	439	455	443
COV [%]	3,1	1,1	1,4	2,5	0,6	1,3	0,6
MC u [%]	11,0	11,0	10,9	11,0	10,7	11,0	10,9
COV [%]	1,6	0,8	1,9	2,2	2,1	2,3	2,4

The compression strength perp. to grain of the glulam was determined on five specimens $\ell/h/b$ = 150/200/100 mm^3 according to (EN 408:2012). The resulting compression strength $f_{c,90,mean}$ = 2,9 N/mm^2 and $f_{c,90,k}$ = 2,5 N/mm^2 mirrors the values given in (EN 14080: 2013) for glulam GL24h.

The tests were carried out in a universal testing machine (Zwick600E). The displacement controlled pressure load (1 mm/min) was applied via two steel plates ($\ell/b/t$ = 200/120/30 mm^3), loading the test specimens in compression perpendicular to grain. Three inductive displacement transducers (HBM WA-T) were placed at each side of the specimen to measure deformations over different parts of the specimen depth (e.g. between the two steel contact plates and within the overlap length ℓ_{lap}).

For the reinforced series, the load F_{max} was determined from the load-deformation curve. For the unreinforced series 1, F_{max} was determined according to EN 408. Reason for this choice was that the deformation of the unreinforced series 1 at F_{max}, determined according to (EN 408: 2012), was in the same range as the deformation at F_{max} of the reinforced series. For all test series, the mean modulus of elasticity perpendicular to the grain, $E_{90,tot,mean}$ was determined according to (EN 408:2012).

For a comparison with design approaches, the characteristic values of the individual test configurations, determined according to (EN 14358:2016) are compared to the load-carrying capacities determined with design approaches given in standards (EN 1995-1-1 - pushing-in capacity), Technical Assessment documents (ETA-12/0114:2017 - buckling capacity) or draft standards (PT.1 draft "reinforcement", see Dietsch & Brunauer 2017 - buckling capacity). The load-carrying capacities determined with the latter approach are very close (± 1 %) to the load-carrying capacities determined with the comprehensive approach according to Bejtka (2005). The comprehensive approach (see also Bejtka & Blaß, 2006) was also used to determine the buckling capacity assuming clamped screw head supports. All calculations were based on a characteristic compression strength of the glulam $f_{c,90,k}$ =2,5 N/mm^2 (EN 14080: 2013), the characteristic density determined for the test specimen ρ_k = 428 kg/m^3 and a characteristic yield strength of the STS $f_{y,k}$ = 1000 N/mm^2.

5.2   Results

During the tests, the load in the reinforced test specimens initially increased linearly, see Fig. 10. Then the slope of the load-deformation curve reduced until the maximum load was reached, followed by decreasing load with increasing deformation (load reduction of 12 % - 23 %). This phase was associated with local crushing of the wood fibers below the contact plate and simultaneous failure of the STS in buckling or pushing-in at maximum load. A further increase in deformation led to a slight increase in load-carrying capacity due to the increasing activation of the wood fibers at the edges of the contact plates. Within each test series, the load-deformation curves are comparatively homogeneous in the linear elastic range but exhibit larger scatter in the plastic range. The described behavior was observed for all reinforced configurations representing intermediate supports.
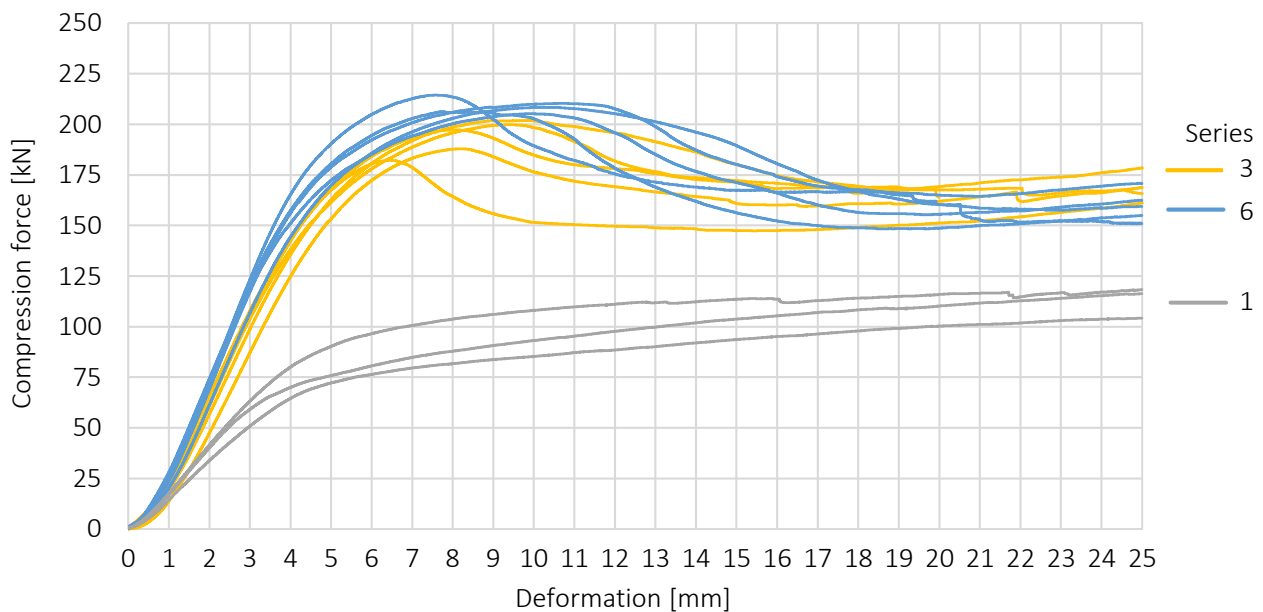
Figure 10. Force-deformation curves for series 1 (not reinforced), 3 (configuration a, $\ell_{lap=10\cdot d}$) and 6 (configuration b, $\ell_{lap=10\cdot d}$).

Four specimens each of series 2 and 3 exhibited pushing-in failure or a combination of pushing-in and buckling failure of the STS. All other specimens of series 2 – 5 exhibited essentially a buckling failure of the STS close to the screw heads (< 60 mm, i.e. < 8·d), perpendicular to grain in direction of the nearest side face. The buckled shape of the STS indicates a clamping effect between the steel plate and the screw heads, see Fig. 12 (right). Screw buckling occurred at the beam edge featuring the smaller number of STS. Specimens of series 6 (alternative arrangement (b)) essentially exhibited a combination of pushing- in and buckling failure in vicinity of either the upper or the lower beam edge. Specimens of series 7 (end support) did not exhibit screw failure but splitting failure of the timber specimens at the end grain due to lateral extension of the wood in direction of the specimen side faces.

Fig. 10 illustrates the considerable increase in stiffness and load-carrying capacity of specimens reinforced with STS applied from both member edges compared to the unreinforced configuration. This is further illustrated in Fig. 11, showing the test data (including mean and characteristic values) compared to load-carrying capacities determined with different design models.

The mean and characteristic values of the test series show a slight increase between overlap lengths ℓ_{lap} = 5·d and 10·d (Series 2+3), followed by a slight decrease for ℓ_{lap} = 15·d and 20·d (Series 4+5) with increasing COV. The best results are determined for an alternating arrangement of the screws. The mean values of series 6 are 7 % higher than the mean values of the corresponding arrangement of series 2, in addition, the COV is considerably reduced. The mean load carrying capacity of reinforced end supports (series 7) is 23 % below the mean load-carrying capacity of the comparable intermediate support (series 2). The mean load-carrying capacities of the reinforced configurations with ℓ_{lap} = 10·d are 119 % resp. 135 % (series 3+6) higher compared to the unreinforced configuration (series 1).

Figure 11. Comparison of test results with design approaches and numerical values from test series.
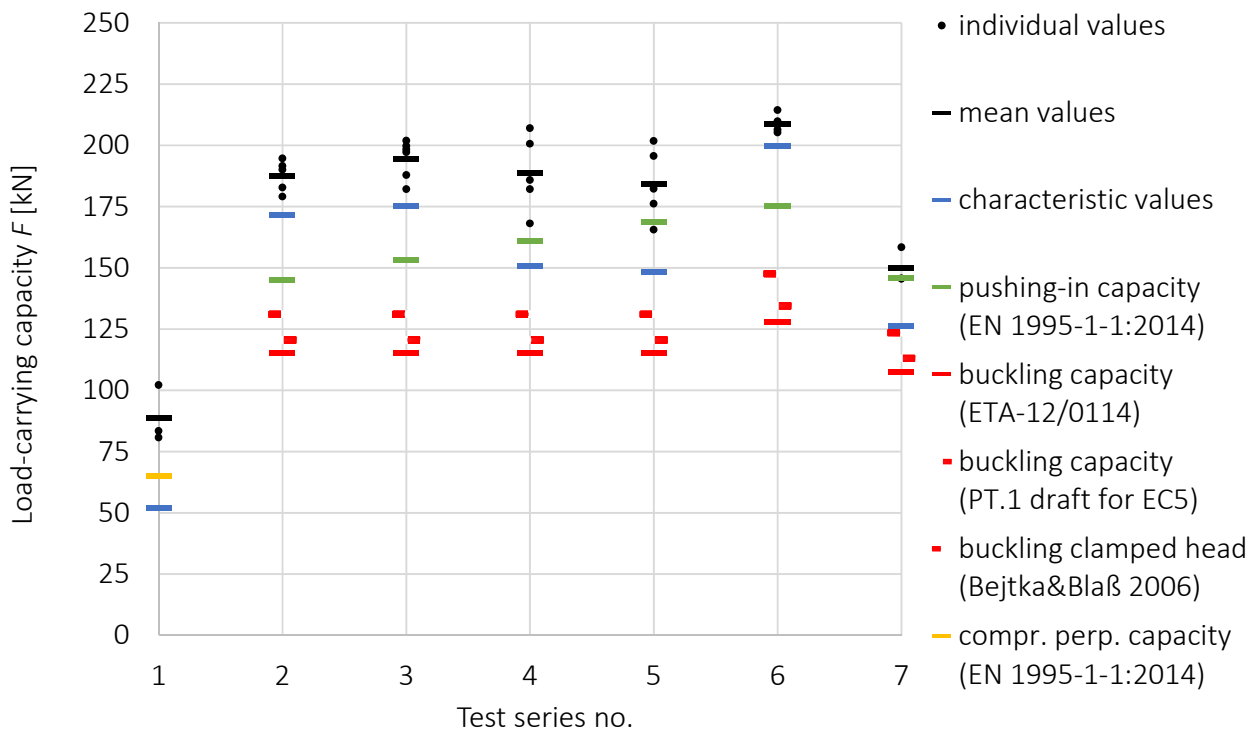
F_{mean} [kN]	88,7	187,6	194,6	188,7	184,3	208,8	149,9
COV [%]	13,2	3,4	4	8,2	8,0	1,7	4,9
F_{char} [kN]	51,9	171,8	175,5	150,7	148,3	200	126,6
$E_{90,tot,mean}$	395	805	839	929	1048	992	813
COV [%]	13,1	10,6	8,2	10,2	1,6	5,6	2,0

A comparison with the available design approaches shows that the characteristic values of test series 2, 3 and 6 are above the values determined with the design approaches. Due to the larger COV determined for series 4 and 5, the characteristic values of the test series are above the calculated buckling capacities but below the calculated pushing-in capacities of the STS.

The majority of the screws failed in buckling perpendicular to the grain in direction of the nearest side face of the specimen. This mirrors the relationships determined with the design approaches. A comparison of test series 3 – 5 shows a decreasing load-carrying capacity with decreasing distance ℓ_{tc} {15·d, 12,5·d, 10·d}. The deformation measurements showed that a reduction of the distance ℓ_{tc} leads to a concentration of deformations in this area and hence increasing strains between the screw tips and the opposite contact plate. The resulting compression perp. to grain stresses lead to lateral extension of the wood. This deformation reduces the horizontal elastic foundation c_h of the screws in this area and hence reduces the buckling load in the zone of highest axial compression stresses in the STS. Fig. 12 illustrates this behaviour. The test results in combination with the numerical results (see Fig. 7) indicate that the distance between screw tips and the opposite contact plate at the beam should be at least ℓ_{tc} = 15·d.

Figure 12. Sketch of deformation behaviour (left), lateral extension of specimen below the contact plate (middle), buckling of STS perpendicular to the grain (right).

The tested end supports did not exhibit failure of the screws but splitting failure of the wood due to lateral extension in direction of the specimen side faces. The mean load-carrying capacities are above the buckling capacities of the STS and the capacities of the timber in compression perp. to grain at the screw tips ($\ell_{ef,2}$ with $F_{c,90,k}$ = 90 kN) but below the pushing-in capacities determined with standardized approaches.

The reinforced configurations exhibit an effective modulus of elasticity $E_{90,tot,ef}$ which is at least doubled compared to series 1 without reinforcement, see Fig. 11. Series 6 featuring the alternative arrangement, exhibits the best relation between stiffness and homogeneous deformation over specimen depth. Stiffness values calculated with the model described in (Bejtka & Blaß 2006) are on average 15 % lower than the determined values $E_{90,tot,mean}$.

6 Conclusions and recommendations for practice

The results presented in this paper show that self-tapping screws applied from opposite member edges and featuring an overlap in the area of half the member depth are an efficient means to transmit concentrated perpendicular to grain forces through timber members. The tested configurations exhibit load-carrying capacities and stiffness which are at least doubled compared to the unreinforced case. To enable good performance of such details, it is recommended to adhere to the following specifications, see also Fig. 13:

• The contact areas should be arranged axially symmetric on opposite sides of the member;

• The screws should be arranged symmetrically to the contact area;

• The overlap length should be at least ℓ_{lap} = 10·d. Larger overlap lengths do not result in higher load-carrying capacities;

• The distance between the screw tips and the opposite contact area should be at least ℓ_{tc} = 15·d. Smaller distances ℓ_{tc} result in lower load-carrying capacities;

• It is recommended to apply minimum spacing in the area of overlapping screws;

• An alternating arrangement of the STS (alternative arrangement in Figs. 9 and 13) with an even number of STS applied from both member sides, leads to the highest improvement in load-carrying capacity and stiffness.

• A variation of screw diameter only showed marginal influence on the described re-lationships. However, in view of missing experimental data for large diameter screws, it is recommended to limit the application of this detail to STS with $d \leq 12$ mm.
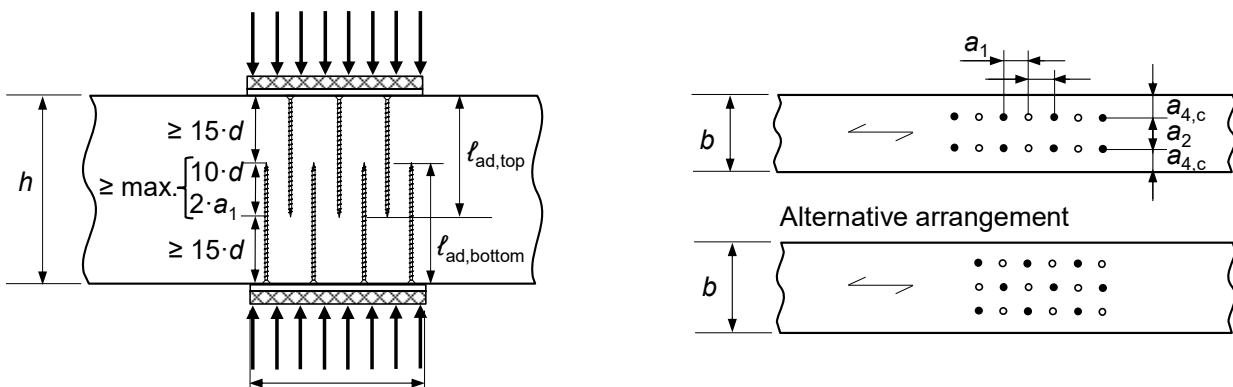
Figure 13. Figure proposed for section "reinforcement" in a revised Eurocode 5.

Compared to the buckling loads derived with current Technical Assessment Docu-ments and draft standards, the results are conservative by considerable margins. In order to enable higher load-carrying capacities for this type of reinforced detail, it is recommended to further study the buckling capacity of STS in the wood. This includes the assumption of hinged or clamped head supports and the horizontal embedment c_h. The influence of concentrated compression perpendicular to grain stresses between the screw tips and the opposite contact plate on the horizontal embedment c_h of the STS in the wood should be investigated as well. Studies on reinforced end supports should include the potential of STS applied from the mem-ber side faces in direction of lateral extension of the wood in order to increase the splitting capacity of the wood at end supports.

Acknowledgement

7 References

Bejtka, I., Blaß, H.J., Self-tapping screws as reinforcements in beam supports, CIB-W18/39-7-2, Proceedings of the international council for research and innovation in building and construction, Working commission W18 – timber structures, Meeting 39, Florence, Italy, 2006.

Bejtka, I., Verstärkung von Bauteilen aus Holz mit Vollgewindeschrauben, Dissertation, Band 2 der Karlsruher Berichte zum Ingenieurholzbau, Lehrstuhl für Ingenieurholzbau und Baukonstruktion, Universitätsverlag Karlsruhe, 2005.

Danzer, M., Dietsch, P., Winter, S., Reinforcement of round holes in glulam beams arranged eccentrically or in groups, Proceedings of the World Conference on Timber Engineering (WCTE 2016), Vienna, 2016.

Dietsch, P., Brunauer, A., Reinforcement of timber structures - a new section for EC5, International Conference on Connections in Timber Engineering, Graz, Austria 2017.

EN 408:2010+A1:2012, Timber structures – Structural timber and glued laminated timber – Determination of some physical and mechanical properties, CEN, Brussels, 2012.

EN 1992-1:2014, Eurocode 2: Design of concrete structures - Part 1-1: General rules and rules for buildings, EN 1992-1-1:2004 + AC:2010, CEN, Brussels, 2014.

EN 1995-1-1:2014, Eurocode 5: Design of timber structures - Part 1-1: General - Common rules and rules for buildings, EN 1995-1-1:2004 + AC:2006 + A1:2008 + A2:2014, CEN, Brussels, 2014.

EN 1997-1:2013, Eurocode 7: Geotechnical design - Part 1: General rules, EN 1997-1:2004 + AC:2009 + A1:2013, CEN, Brussels, 2013.

EN 14080:2013, Timber structures – Glued laminated timber and glued solid timber – Requirements, CEN, Brussels, 2013.

EN 14358:2016, Timber structures – Calculation and verification of characteristic values, CEN, Brussels, 2016.

ETA-12/0114:2017, European Technical Assessment, SPAX self-tapping screws for use in timber constructions, ETA-Denmark, Nordhavn, 2017.

Kempfert, H.-G., Grundbau-Taschenbuch - Teil 3: Gründungen und geotechnische Bauwerke, 6. Auflage, Ernst&Sohn, Berlin, 2001.

Mestek, P., Punktgestützte Flächentragwerke aus Brettsperrholz (BSP) – Schubbemessung unter Berücksichtigung von Schubverstärkungen, Dissertation, Technische Universität München, 2011.

Rodemeier, S., Querdruckverstärkung von Holzbauteilen bei beidseitiger Druckkrafteinleitung, Master's thesis, Lehrstuhl für Holzbau und Baukonstruktion, Technische Universität München, 2019.

Vesic, A.S., Design of pile foundations. National cooperative highway research program, Synthesis of highway practice 42. Transportation research board, National research council, Washington D.C., 1977.

Watson, C.P., van Berschoten, W., Smith, T., Pampanin, S., Buchanan, A.H., Stiffness of screw reinforced LVL in compression perpendicular to the grain, CIB-W18 / 46-12-4, Proceedings of the international council for research and innovation in building and construction, Working commission W18 - timber structures, Meeting 47, Vancouver, 2013.

Zilch, K., Zehetmeier, G., Bemessung im konstruktiven Betonbau, Springer, Berlin, 2010.

Z-9.1-519:2014, Allgemeine bauaufsichtliche Zulassung, SPAX-S Schrauben mit Vollgewinde als Holzverbindungsmittel, Deutsches Institut für Bautechnik, Berlin, 2014.

Discussion

The paper was presented by P Dietsch

A Frangi asked if deformations could be calculated and would this method be recommended for tall buildings. P Dietsch responded that deformation could be calculated with this method of reinforcement and this method could be used multi-storey buildings but should be critically analysed for tall timber buildings. A Frangi commented that 3 to 4 mm of deformation x 10 storeys might be too much.

T Tannert commented that only small number of replicates was used and asked if one would be confident to make code recommendations for only 10d overlap. P Dietsch stated that essentially screw failure was tested one could rely on longer screws which would then fail at the same buckling loads due to their high slenderness.

R Jockwer mentioned that this detail has already been used in practice. He mentioned that load transfer via the overlap zone and screw head load transfer would happen early. P Dietsch agreed and stated that this might be the reason why 10d is sufficient.

B Sullivan and H Blass discussed about using large diameter threaded rod and its practicality.

YH Chui asked for comments about plate size. P Dietsch responded plate size was not varied.

S Breneman asked about the use of this technique in CLT structures with local loads. H Blass stated a PTEC 2019 paper covers this aspect.

Component Method in Timber Construction – Experimental and Numerical Research

Prof. Dr.-Ing. Ulrike Kuhlmann, Head of Institute

Julius Gauß, M.Sc., Scientific Researcher

Institute of Structural Design, University of Stuttgart, Germany

1 Introduction

For complex structural systems such as long span timber constructions moment resisting joints are crucial. In Figure 1.1 an example of such a moment resisting timber column base is shown. The clamping of the column base allows for a reduction of the deflections of the structural system and has a stiffening effect against horizontal loads. In order to take these advantages into account when calculating the occurring deformations and internal forces the component method has proved to be a powerful tool. Such complex moment resisting joints may be reduced to a spring model, which includes all components that contribute to the deformation and the load bearing capacity of the overall joint. Investigations (KUHLMANN & GAUß (2019), POSTUPKA ET AL. (2016)) have

Figure 1.1. Moment resisting timber column base; Source: Schaffitzel Holzindustrie GmbH

shown that the component method as a systematic simplified approach can successfully be applied also for timber joints. For the calculation of the load-deformation behaviour of the joint and the occurring inner forces the single component´s stiffness, in particular for components of low rigidity like dowel type fasteners, has an important influence. Therefore, the good description and appropriate calculation of the load-

displacement behaviour of the various components are of high significance within the component method.

In timber construction, for example for dowel connections under rotational loading, the resulting forces of the single fasteners and the joint stiffness may be calculated considering the stiffness of the single fasteners as given in code rules (see NCI NA.13 in DIN EN 1995-1-1/NA (2013)). However, several investigations (DORN ET AL. (2013), GAUß & KUHLMANN (2018), JOCKWER & JORISSEN (2018), SANDHAAS & VAN DE KUILEN (2017)) showed that the stiffness calculation according to EN 1995-1-1 (2005) is not in all cases satisfying. This is, amongst others, caused by the neglect of important influencing parameters like the load-to-grain angle, the slenderness of the fastener or the type of fastener (rope effect). Furthermore, the reinforcement with fully threaded screws showed a significantly positive influence on the load-displacement behaviour of steel-timber dowel connections which has been described by BEJTKA (2005), but could not yet be fully considered.

Within this paper the results of recently conducted experimental component and joint tests, the recalculation with a component model and theoretical investigations regarding the connection stiffness are presented.

2 Component method

2.1 General

The component method was originally developed for the calculation of steel and composite joints. The characterisation of the response of the joints in terms of stiffness, resistance and ductility was defined by JASPART & WEYNAND (2016) as a key aspect for design, see Figure 2.1. Within the classical component method the characteristic behaviour of a complex joint is assembled from a number of single components, of which mechanical and geometrical properties are known. The characteristic behaviour of the various components can be determined either by experimental or numerical methods. A simplified analytical approach has meanwhile been developed as code rules and in EN 1993-1-8 (2005) and EN 1994-1-1 (2004) more than 20 different basic components for steel and composite joints are listed.
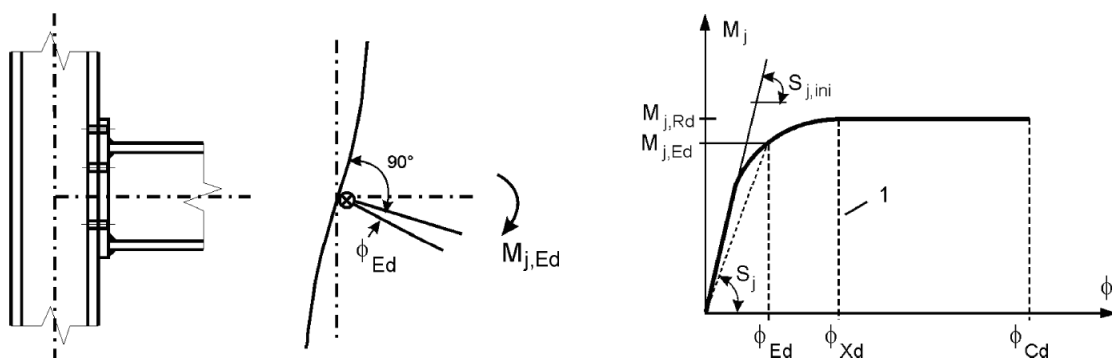
Figure 2.1. Semi-rigid steel joint, model and related M-Φ-curve of a semi-rigid joint according to EN 1993-1-8 (2005)

Using the component method for the design of a moment resisting joint, for every basic component the strength and stiffness either in tension, compression or shear have to be calculated. These calculation results determine the properties of the elastic or plastic springs used to assemble the spring model for the complete joint.

With the initial rotational stiffness $S_{j,ini}$ of the joint, calculated considering the several single components, the moment-rotation behaviour can be approximated as shown in Figure 2.1 (right). There are several possibilities for the approximation of the plastic moment-rotation behaviour of joints. The simplest idealisations are the rigid – plastic and the elastic – perfectly plastic ones. Besides these bi-linear approaches there are also tri-linear or completely non-linear approaches. The tri-linear approach probably is the most preferred way to get a realistic description of the moment-rotation behaviour of the joint at a reasonable expense.

2.2   In timber construction

Several experimental, numerical and analytical investigations have been realised on different aspects of the component method in timber construction. KUHLMANN & BRÜHL (2010) and KUHLMANN & BRÜHL (2013) focused on the ductility of timber connections. Thereby, the scattering of the material properties of timber parts as well as of the connectors and consequently the effects of over-strength of materials played an important role (KUHLMANN ET AL. (2014)). GAUß & KUHLMANN (2018) investigated the initial stiffness of steel-timber dowel connections to predict the occurring deformations and the inner

Components of timber joints
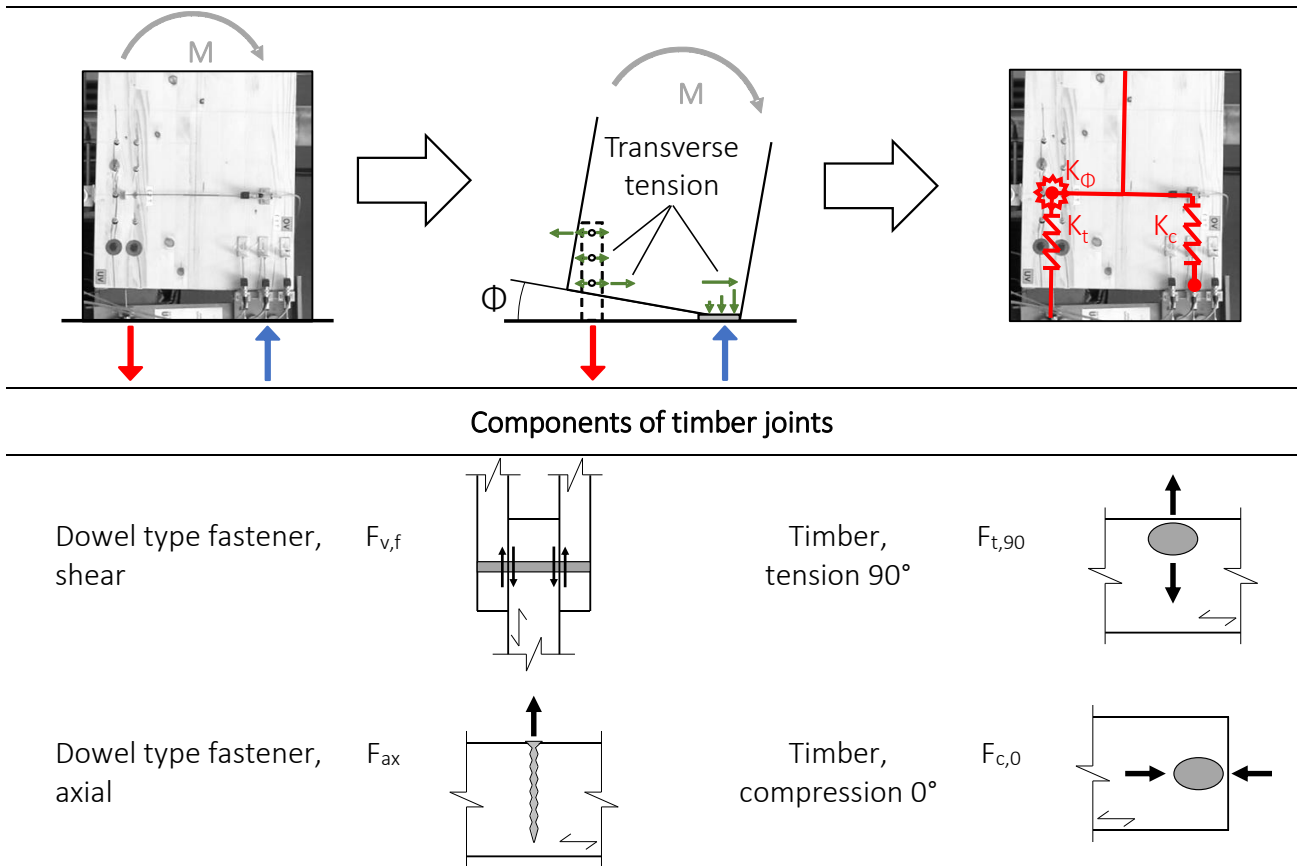
Figure 2.2. Derivation of components of a timber joint (top); extract of component catalogue proposed in KUHLMANN & GAUß (2019) (bottom)

forces of joints more accurate at the quasi-elastic state. The comparison of the analytically predicted and the experimental behaviour of large scale joint tests demonstrated the general applicability of the component method in timber construction (KUHLMANN & GAUß (2019)). In Figure 2.2 (top) the compilation of a spring model is exemplarily shown. In a first step for the real timber joint the distribution of inner forces and deformations under the expected load has to be assessed. Brittle failure modes may either be considered in the spring model or be neutralized by an adequate reinforcement (for example with fully threaded screws). The single components identified in the joint then have to be characterized in view of their load-displacement behaviour, which may be represented by individual springs for each component. These individual springs can then be composed to an overall spring model of the joint considering the respective lever arms (see Figure 2.2 (top)). Finally, with the spring model of the joint an equivalent rotational spring may be determined for further use in the overall calculation of the structural system. Within the research project (KUHLMANN & GAUß (2019)) a proposal for a component catalogue for timber construction considering the basic components of typical timber joints (see Figure 2.2 (bottom)) analogous to EN 1993-1-8 (2005) has been developed. The proposed component catalogue summarizes several approaches from literature for the determination of the load bearing capacity and the stiffness of the individual components, but is also based on new tests. These conducted component and joint tests are presented below.

3 Experimental research

3.1 Component tests

3.1.1 Test programme and setup

Within the scope of a "Zukunft Bau" research project (KUHLMANN & GAUß (2019)) in total 66 component tests on steel-timber dowel connections and 10 large-scale joint tests were conducted by the Institute of Structural Design in 2018.

Table 3.1. Experimental programme of the component tests [short name]

Fastener	$\emptyset$ [mm]	$n_\perp$ x $n_\parallel$	α	Reinforcement	No. of tests
Single (dowel) [SD]	16	1 x 1 [11]	0°	without [1]	8
			0°	centred [2]	6
			0°	close [3]	6
			90°	centred [2]	4
Single (bolt) [B]	16	1 x 1	0°	without [1]	8
			0°	centred [2]	6
			90°	centred [2]	4
Group (bolts + dowels) [SD]	16	1 x 3 [13]	0°	centred [2]	6
		1 x 5 [15]	0°	centred [2]	6
		2 x 5 [25]	0°	centred [2]	6
		2 x 5 [25]	90°	centred [2]	6

Example short name: [SD16 11 0 1] = dowel – Ø = 16 mm – 1x1 – 0° – without reinforcement
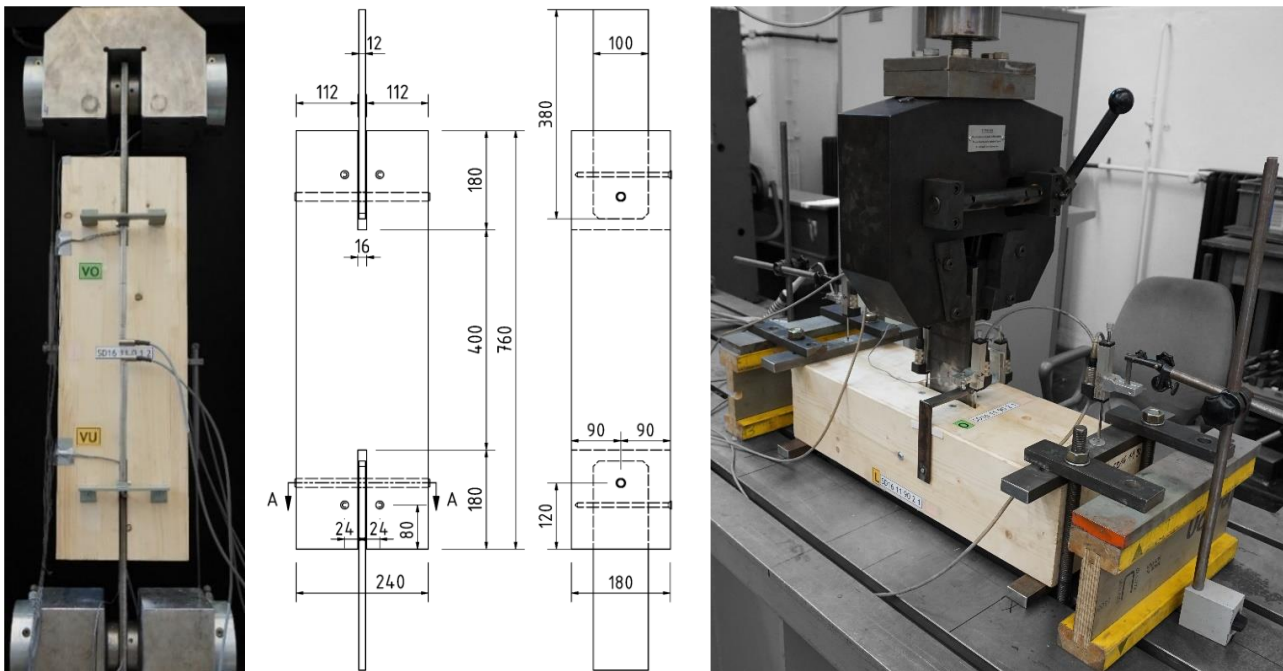
Figure 3.1. Test setup and geometry in [mm] of single fastener tensile tests parallel to the grain (left); test setup of single fastener tensile tests perpendicular to the grain (right)

Table 3.1 shows the experimental programme of the component tests. Besides tensile tests on single fasteners (dowels, bolts) and groups of fasteners (bolts + dowels) as well parallel as perpendicular to the grain, also the rotational behaviour of a 2x5 fastener group was tested. For the single fastener tests also the position of the reinforcement was varied (without, centred, close). The test programme of the component tests aimed to predict the joint behaviour of the tested column footing and to identify relevant parameters on the load-deformation behaviour.

The test setups for the tensile tests parallel and perpendicular to the grain direction are shown in Figure 3.1. For the tests parallel to the grain a symmetrical setup was chosen so that in each case two connections per specimen were tested at the same time. The measurement technology was placed following the specifications of EN 383 (2007). The application of the load followed the procedure according to EN 26891 (1991). Further information on the geometry and the test setup of the component tests are given in KUHLMANN & GAUß (2019) and GAUß & KUHLMANN (2018).

3.1.2 Test results

To illustrate the influence of the position of the reinforcement (without, centred, close) and the type of fastener (dowel, bolt) the mean load-displacement curves of the tensile tests parallel to the grain are summarized in Figure 3.2. In Figure 3.2 (left) for a better comparability the achieved load bearing capacities of the single fasteners are given divided by the characteristic maximum load of a connection with one dowel (Ø 16 mm, f_{uk} = 460 N/mm²) according to EN 1995-1-1 (2005). In Figure 3.2 (right) the curves of the fastener groups are given also divided by the characteristic maximum load according to EN 1995-1-1.
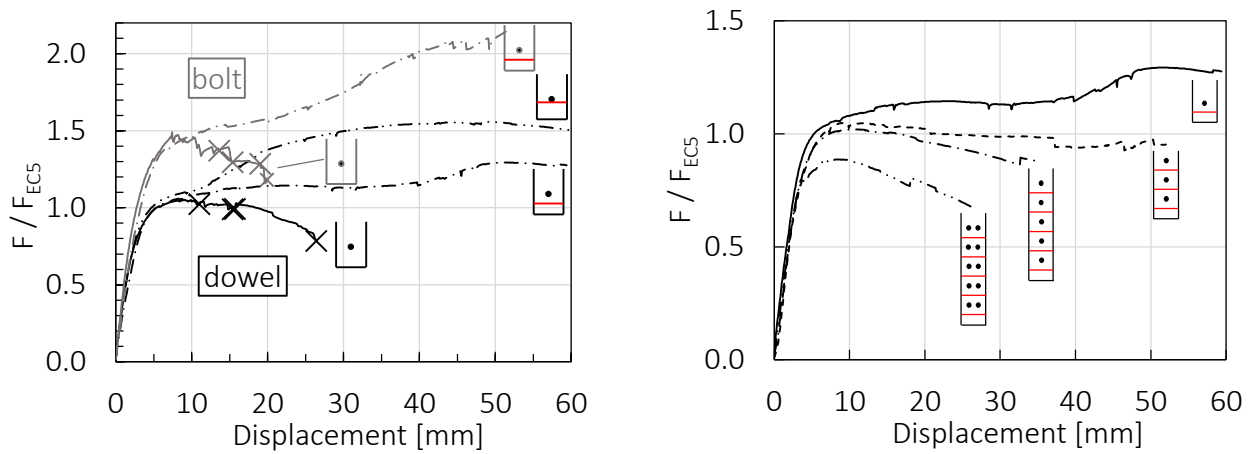
Figure 3.2. Mean load-displacement curves of single fasteners (left) and fastener groups (right) from tensile tests parallel to the grain, different types of reinforcement, connection failure marked by "X"

At a connection displacement between 8 mm to 10 mm all the tested connections reached the beginning of the plastic plateau, which occurred when the fastener itself began to plasticize. At about 12 mm to 16 mm for the unreinforced connections a splitting of the timber member perpendicular to the grain and, consequently, a decrease of load were observed. In contrast, all the reinforced connections (centred + close) showed a ductile behaviour with large plastic deformations on a stable load level or even a further increase of the load. The bolts showed an about 50 % higher load bearing capacity than the dowels. This may be explained by the rope effect and the tensile overstrength of the bolts. The dowels were ordered with a material quality of S235JR, but showed an experimental tensile strength $f_{u,dowels}$ of 458 N/mm². The bolts were ordered as steel 4.6, but actually showed on average a measured tensile strength $f_{u,bolts}$ of 624 N/mm².

For the connections with one single dowel or bolt the determined maximum loads were all higher than the calculated characteristic loads according to EN 1995-1-1. In Table 3.2 the mean values of F_{max} and F_{10mm}, the respective standard deviations (SD) and the coefficients of variation (CV) are given. For the reinforced connections the ultimate experimental loads F_{max} are significantly higher than the loads F_{10mm} observed

Table 3.2. Load-carrying capacities from tensile tests parallel to grain (0°), load at a displacement of 10 mm F_{10mm} and maximum load F_{max}; SD = standard deviation, CV = coefficient of variation

| Series | Mean [kN] (F_{test} / F_{EC5}) | | SD [kN] | | CV [%] | |
	F_{max}	F_{10mm}	F_{max}	F_{10mm}	F_{max}	F_{10mm}
SD16 11 0 1	43.7 (103 %)	43.1 (102 %)	1.3	1.5	3.0	3.4
SD16 11 0 2	52.5 (124 %)	44.3 (105 %)	1.1	3.1	2.1	6.9
SD16 11 0 3	66.1 (156 %)	45.2 (107 %)	3.0	0.9	4.5	1.9
B16 11 0 1	62.4 (119 %)	59.0 (113 %)	4.0	3.7	6.3	6.2
B16 11 0 2	87.1 (167 %)	60.1 (115 %)	8.1	2.4	9.3	2.6
SD16 13 0 2	144.2 (106 %)	141.7 (104 %)	6.7	6.1	4.6	4.3
SD16 15 0 2	221.8 (100 %)	221.4 (100 %)	9.1	6.8	4.1	3.1
SD16 25 0 2	388.9 (88 %)*	383.2 (87 %)	20.7	25.77	5.3	6.7

*massive splitting and failure in tension of effective cross section

at the beginning of the plastic plateau. For the fastener groups (see Figure 3.2 (right)) a group effect has been observed. With an increasing number of fasteners massive splitting and block shear failures of the timber part occurred, which reduced the load bearing capacity and the maximum displacement of the fasteners.

With regard to the reached maximum loads the test results are in a quite good accordance with EN 1995-1-1, if calculated with measured material strength. However, the measured stiffness values differ from the predicted stiffness values K_{ser} of EN 1995-1-1. In Table 3.3 the initial stiffness K_{ser}, the reloading stiffness K_e between 0.1 and $0.4 \cdot F_{ult}$ and the respective standard deviation (SD) and coefficient of variation (CV) values are given for the single fastener tests and for the tests with fastener groups. For the dowels as well as for the bolts the measured initial stiffness K_{ser} according to EN 26891 (1991) is on average about 40 % lower than the value predicted according to EN 1995-1-1. There is a tendency that for the connections with the centred reinforcement for the dowels (SD16 11 0 2) as well as for the bolts (B16 11 0 2) the stiffnesses K_{ser} and K_e are about 20 % lower than for the unreinforced (SD16 11 0 1, B16 11 0 1) and the close reinforced ones (SD16 11 0 3). Because of the large scattering of the measured stiffness values more experimental results are necessary to further investigate this effect. The CV values range from 11 % to 37 %. The reloading stiffness K_e is about three times higher than the initial stiffness K_{ser}, which indicates significant plastic deformations in the contact zone of the dowels at an early loading stage. This is in accordance with findings in DORN (2012).

The tensile tests perpendicular to grain ($\alpha = 90°$) were all reinforced with fully threaded screws (centred) and showed a bi-linear load-displacement behaviour which, however, differed from the load-displacement behaviour of the tests parallel to the grain ($\alpha = 0°$). After a first linear section ($K_{ser,90°}$) at a displacement of about 3 mm ($\sim$22 kN) a loss of stiffness was observed. Then, until the termination of the test, a relatively constant increase of load occurred ($K_{II,90°}$). The definition of the stiffnesses K_{ser}, K_e and K_{II} are displayed in Table 3.4 (right). The reached load bearing capacities were significantly higher than the values according to EN 1995-1-1. However, at a displacement of about

Table 3.3. Stiffness of fasteners from tensile tests parallel (0°) to grain, initial stiffness K_{ser} and reloading stiffness K_e; SD = standard deviation, CV = coefficient of variation

Series	Mean [kN/mm] (K_{test} / K_{EC5})		SD [kN/mm]		CV [%]	
	K_{ser}	K_e	K_{ser}	K_e	K_{ser}	K_e
SD16 11 0 1	15.1 (63 %)	48.4 (202 %)	2.9	12.2	19.4	25.2
SD16 11 0 2	11.6 (49 %)	37.0 (154 %)	2.6	2.8	22.4	7.5
SD16 11 0 3	15.8 (66 %)	45.5 (190 %)	5.9	7.4	37.1	16.3
B16 11 0 1	17.3 (72 %)	54.5 (227 %)	4.2	13.6	24.0	24.9
B16 11 0 2	14.5 (60 %)	50.2 (209 %)	2.7	7.1	18.9	14.1
SD16 13 0 2	41.4 (58 %)	137.9 (192 %)	8.2	16.7	19.8	12.1
SD16 15 0 2	60.9 (51 %)	208.7 (174 %)	6.77	11.9	11.1	5.7
SD16 25 0 2	122.9 (51 %)	373.8 (156 %)	23.2	51.6	18.9	13.8

Table 3.4. Stiffness of single fasteners from tensile tests perpendicular (90°) to grain, initial stiffness K_{ser}, reloading stiffness K_e and stiffness in "section II" K_{II}

	SD16 11 90 2 (K$_{test}$ / K$_{EC5}$)			B16 11 90 2 (K$_{test}$ / K$_{EC5}$)		
	Mean	SD	CV	Mean	SD	CV
	[kN/mm]	[kN/mm]	[%]	[kN/mm]	[kN/mm]	[%]
K_{ser}	10.0 (42 %)	2.58	26.0	15.1 (63 %))	2.88	19.0
K_e	32.53 (136 %)	5.62	17.3	38.29 (160 %)	5.32	13.9
K_{II}	0.7 (3 %)	0.15	20.7	1.4 (6 %)	0.30	21.0
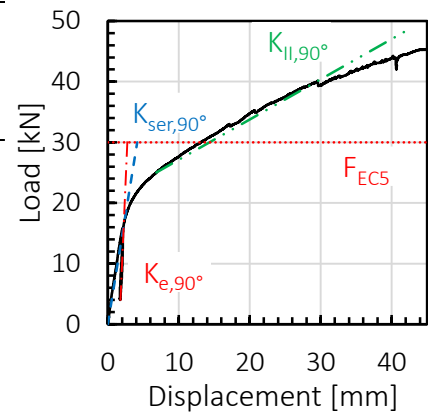
15 mm, which is the stop criterion according to EN 26891 (1991), the calculated values are in good accordance with the experimental ones. For the connections with dowels the initial stiffness $K_{ser,90°}$ perpendicular to the grain was about 33 % lower than the stiffness $K_{ser,0°}$ in grain direction. For the connections with bolts the stiffness $K_{ser,90°}$ was similar to the stiffness $K_{ser,0°}$. The remaining stiffness $K_{II,90°}$ was on average only 3 % of the initial stiffness $K_{ser,90°}$ for the dowels and 6 % for the bolts.

3.2 Joint tests

3.2.1 Test setup

To verify the applicability of the component method in timber construction joint tests on a moment resisting column base were conducted. The joint tests were realized as 4-point-bending tests with a steel beam connected to the timber specimen by a moment resisting joint, see Figure 3.3. The test series T 1.X, T 2.X, T 3.X and T 5.X had a steel plate in the upper third of the timber beam to transfer the compressive force by contact (see Figure 3.3 (left)). In the lower third a steel-timber dowel connection with 2x5 fasteners transferred the tensile force. Test T 4.X had a dowel connection in the tensile as well as in the compressive zone. The reinforcement of the timber members with fully threaded screws was varied within the test series to investigate the influence on the load bearing capacity and the joint stiffness. The load was applied
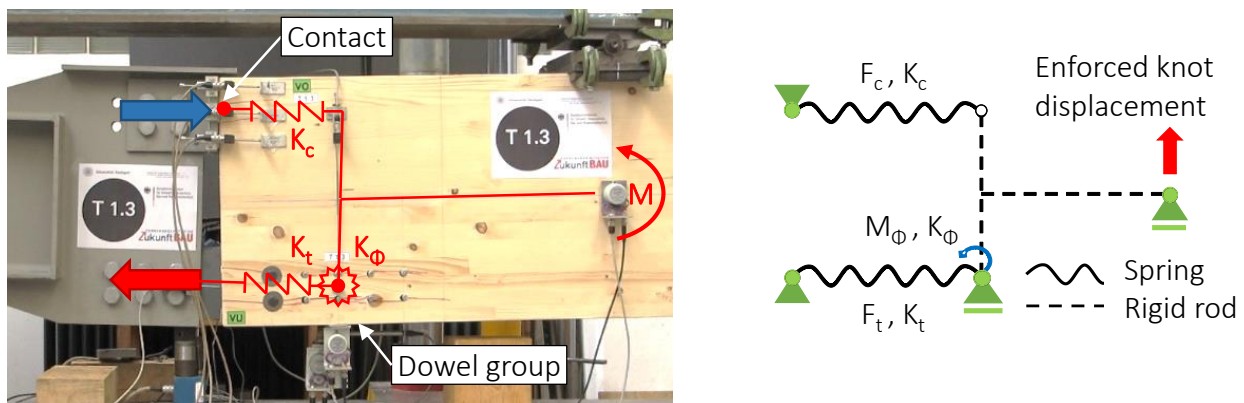
Figure 3.3. Setup of joint test T 1.3 and joint components (left); spring model of the joint (right)

path-controlled at the quarter points by means of a traverse, the points of loading were reinforced with fully threaded screws.

3.2.2   Test results

All the reinforced test specimens (T 1.X, T 2.X, T 3.X, T 4.X) showed a ductile behaviour and large plastic deformations. The unreinforced reference test (T 5.X) failed already on a lower load level without any pre-announcement by brittle splitting and shear failure in the tensile zone. The variation of reinforcement had an influence on the development of the observed cracks in the tensile as well as in the compressive zone. However, no significant influence of the different types of reinforcement on the ultimate load could be observed. The initial stiffness of the joints was higher for the joints with a reinforcement against transverse tension in the compressive zone than for the ones without.

The moment-rotation curves of some of the joints can be found in Figure 4.1 for the comparison of the experimental and the theoretical curves. For detailed test results see KUHLMANN & GAUß (2019).

4   Modelling of the timber joints

4.1   Spring models

Based on the conducted component tests non-linear spring models of the moment resisting joints were derived to predict the moment-rotation behaviour. The basic components are the spring K_c in the compressive zone, the spring K_t in the tensile zone and the rotational spring K_Φ of the fastener group (see Figure 3.3 (right)). The properties of the springs (load-bearing capacity, stiffness, maximum displacement) may be determined in different ways. A most realistic simulation is achieved by conducting component tests for every component, as it was done within the research project. Thereby, group effects, several types of reinforcement and the influence of brittle failure modes on the load-displacement behaviour of the dowel group can be taken into account. The properties of the tensile spring of the 2x5-dowel group could either be determined by tests on 2x5 dowel groups or by assembling an equivalent spring out of test results of single fastener tests considering group effects. The rotational stiffness of the fastener group was determined by component tests, but could also have been calculated with the load-deformation curves of the single fasteners (bolts, dowels) and the polar moment of inertia I_p. However, it is important to consider the significant dependency of the load-displacement behaviour on the grain direction (0° and 90°). The properties of the compressive spring were determined by the experimental results or alternatively by an elastic-plastic equivalent volume based on the properties ($E_{0,g,mean}$, $f_{0,g,k}$) given in the standard.

To calculate the deformations and the force distribution within the spring model, shown in Figure 3.3 (right), the commercial software RSTAB by Dlubal was used. The component model of the joint was validated and calibrated by the experimental joint
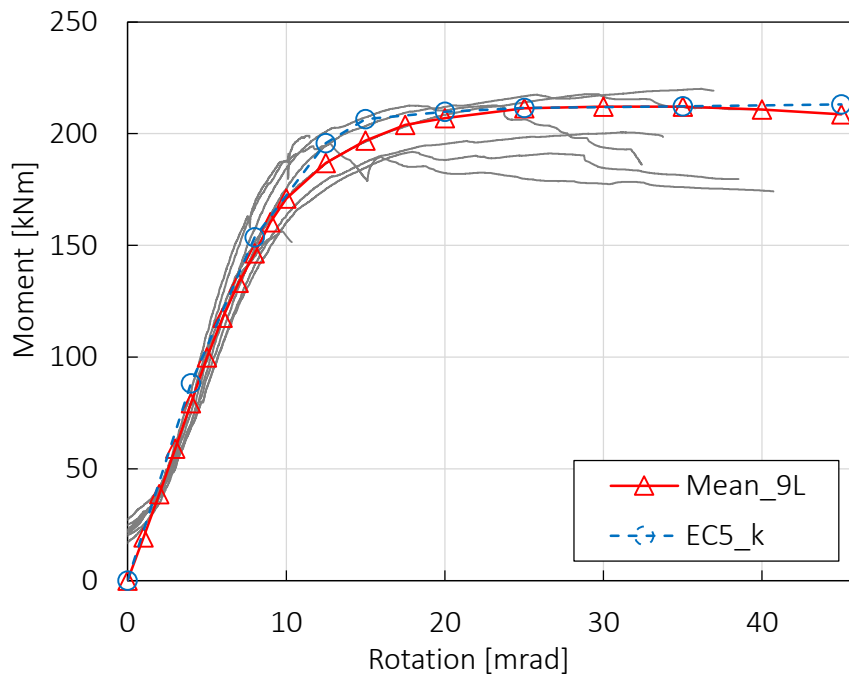
Figure 4.1. Moment-rotation curves of spring models with experimental component properties (Mean_9L) and values according to EN 1995-1-1 (2005) (EC5_K) compared with test results (grey)

tests. Through a parametric study the influence of the single components properties on the maximum load and the occurring deformations were determined. The properties of the compressive zone only showed a small influence on the joint behaviour because the compressive zone was much stiffer than the fastener group and no plastic deformations occurred in the contact zone. However, the properties of the tensile zone are decisive for the joint behaviour and should therefore be calculated as accurately as possible.

In Figure 4.1 the moment-rotation curves of the experimental tests are plotted in grey, the curve with experimental component properties (9-linear approximation) in red and the curve with characteristic component properties according to EN 1995-1-1 (2005) (3-linear approximation) in blue. The "real" material properties of the steel components were used to calculate the load bearing capacity and for the analytical stiffness the values were reduced to 50 % of $K_{ser,EC5}$.

The scattering of the experimental initial stiffness and moment resistance of the joints could be covered well by implementing the range of scattering of the experimental component properties in the RSTAB model. However, the descending part of the test curves within the plastic range could not be modelled in a satisfactory manner for all tested joints. One reason for the overestimation of the moment capacity is probably the neglect of brittle failure modes and the interaction of the different components (tension + rotation) in the plastic range. The state of the art regarding the brittle failure modes is presented in CABRERO & YURRITA (2018) and JOCKWER & DIETSCH (2018). Improved modelling should consider these results. Investigations have also shown that the stiffness (normal and shear) of the timber beam itself has an influence on the joint's moment rotation behaviour. A stiffer timber beam leads to a stiffer joint and also to an earlier beginning of the descending of the moment-rotation curve.

In Figure 4.1 the curve *EC5_k* with characteristic input parameters of EN 1995-1-1 is also in good accordance with the experimental results. The 3-linear approach for the components properties seems to be sufficient to predict the overall moment-rotation behaviour of the joints. However, the stiffness according to EN 1995-1-1 had to be modified to obtain a good accordance between the results of the experiments and the spring models. Therefore, it needs to be dis-

Figure 4.2. Possible definition of the load-displacement behaviour of dowel-type fasteners

cussed which stiffness has to be used for which design situation. One possible solution could be to define different values of stiffness, for example the 5 %-fractile, the mean and the 95%-fractile of the initial stiffness K_{ser}. Furthermore, it is recommended to define a standardized load-displacement curve of dowel type fasteners as it is shown in an extended way in Figure 4.2. More detailed information on the load-deformation behaviour of several types of fasteners would be welcome. Relevant properties are the initial slip (1), the initial stiffness K_{ser} (2), the yield load and the related displacement (3), the remaining stiffness at the plastic plateau (4) and the maximum displacement / stop criterion (5).

4.2   FEM

In HASCHKE (2019) numerical investigations on steel-timber dowel connections (single fasteners and groups) and on the above presented timber joints were conducted. The 3D-FEM model is able to simulate the overall joint behaviour and the most important failure modes. Nevertheless the sophisticated model is highly dependent on a complex calibration with the experimental results. Creating a completely independent universal FE model in order to simulate arbitrary joint geometries seems to be difficult. The overestimation of the connection stiffness (especially for dowel type fasteners) within the FEM remains one of the main deviations, which prevents a realistic prediction of the joint behaviour (see also DORN (2012) and SANDHAAS (2012)). Therefore, simplified solutions like spring models are in many cases currently not only a faster, but also a more accurate method for the prediction of the load-deformation behaviour of timber joints. If for the decisive components realistic properties are assumed, the load distribution within a complex joint and the deformations to be considered in serviceability limit state as well as in ultimate limit state can be predicted in a satisfactory manner. Consequently, the possibilities determining the load-displacement behaviour of connections provided in EN 1995-1-1 should be clarified and extended to achieve improved code rules for practical applications.

5 Conclusions and suggestions for the application of the component method in timber construction

5.1 Conclusions

The tests on moment resisting timber joints and their several components showed the general applicability of the component method in timber construction. Prerequisite is a detailed knowledge of the load-displacement behaviour (including a stop criterion) of the applied components especially for components which are decisively influencing the joint stiffness and the maximum load. The interaction of the various components and the splitting of the timber member, even if it doesn´t lead to a failure of the joint, have an influence on the joint stiffness and therefore have to be considered for large joint deformations.

For the moment, the simulation of complex joints with 3D-FE models seems to be too sophisticated for an application in a standard design process. Spring models based on the component method offer a significantly easier approach to simulate the load-displacement behaviour of timber joints. To enable the use of such spring models, the properties (load bearing capacity, stiffness, maximum deformation) of typical components and the appropriate application of the stiffness value within the design process have to be defined (at best, within Eurocode 5).

5.2 Suggestions for application

Based on the conducted investigations the following suggestions are made:

- The reinforcement of the timber with fully threaded screws is highly recommendable. Unreinforced connections with complex loading (tension parallel and perpendicular to grain) tend to fail suddenly and show much lower ultimate loads and displacements.
- Spring models are suitable for modelling the load-deformation behaviour of timber joints. The models should consider every decisive component influencing the joint deformations and limiting the ultimate load. The single components load-displacement behaviour should be determined as precisely as possible. A uniform definition and a database for the fastener properties (similar to SCHWEIGLER & SANDHAAS (2018) for embedment-slip curves) seems to be advantageous.
- The stiffness K_{ser} of dowel type fasteners according to EN 1995-1-1 is not in all cases sufficiently accurate and therefore should not be used for the determination of inner forces within a joint which is sensitive to changes of the fastener stiffness. Several investigations deliver more precise values for different types of connections, but yet there is a need for a common approach.
- The interaction of the various components and the splitting of the timber, even if it doesn´t lead to a failure of the joint, have an influence on the joint stiffness and therefore have to be considered for large joint deformations. At the quasi-elastic state, the interaction may be neglected.

6   Acknowledgements

7   References

Bader, T. K. et al. (2016): Experimental characterization of the global and local behavior of multi-dowel LVL-connections under complex loading. In: Materials and Structures, 49, 6. pp. 2407–2424.

Bejtka, I. (2005): Verstärkung von Bauteilen aus Holz mit Vollgewindeschrauben (in German). Karlsruhe Institute of Technology, Germany, dissertation.

Bocquet, J.-F. & Lemaître, R. & Bader, T. K. (2018): Design recommendations and example calculations for dowel-type connections with multiple shear forces. In: Design of Connections in Timber Structures – A state-of-the-art report by COST Action FP1402 / WG3.

Cabrero, J. M. & Yurrita, M. (2018): A review of the existing models for brittle failure in connections loaded parallel to the grain. In: Design of Connections in Timber Structures – A state-of-the-art report by COST Action FP1402 / WG3.

DIN EN 1995-1-1/NA (2013): German National Annex - Eurocode 5: Design of timber structures – Part 1-1. DIN, Berlin.

Dorn, M. (2012): Untersuchungen zum Gebrauchstauglichkeitszustand von Dübelverbindungen im Holzbau (in German). TU Vienna, Austria, dissertation.

Dorn, M. & De Borst, K. & Eberhardsteiner, J. (2013): Experiments on dowel-type timber connections. Engineering Structures 47 (2013), pp. 67-80.

EN 383 (2007): Timber Structures – Test methods – Determination of embedment strength and foundation values for dowel type fasteners. CEN, Brussels.

EN 1993-1-8 (2005): Eurocode 3: Design of steel structures - Part-8: Design of joints. European Committee for Standardization (CEN), Brussels, with corrections AC:2009.

EN 1994-1-1 (2004): Eurocode 4: Design of composite steel and concrete structures – Part 1-1: General rules and rules for buildings. European Committee for Standardization (CEN), Brussels, with corrections AC:2009.

EN 1995-1-1 (2004): Eurocode 5: Design of timber structures – Part 1-1: General – Common rules and rules for buildings. European Committee for Standardization (CEN), Brussels, with corrections and amendments + AC:2006 and A1:2008.

EN 26891 (1991): Timber Structures – Joints made with mechanical fasteners – General principles for the determination of strength and deformation characteristics. CEN, Brussels.

Gauß, J. & Kuhlmann, U. (2018): Consideration of the connection stiffness in design process – experimental investigations. WCTE 2018, World Conference on Timber Engineering in Seoul (Republic of Korea), 20.08.-23.08.2018.

Haschke, J. (2019): Numerische Untersuchungen zur Auswertung von Versuchen an Stab-dübelverbindungen (in German). Institute of Structural Design, University of Stuttgart, master thesis.

Jaspart, J.-P. & Weynand, K. (2016): Design of Joints in Steel and Composite Structures. Published by ECCS – European Convention for Constructional Steel – works, Berlin: Wilhelm Ernst & Sohn Verlag.

Jockwer, R. & Dietsch, P. (2018): Brittle failure of connections loaded perpendicular to grain. In: Design of Connections in Timber Structures – A state-of-the-art report, COST Action FP1402 / WG3.

Jockwer, R. & Jorissen, A. (2018): Stiffness and deformation of connections with dowel-type fasteners. In: Design of Connections in Timber Structures – A state-of-the-art report by COST Action FP1402 / WG3.

Kuhlmann, U. & Brühl, F. (2010): Robustheit durch duktile Anschlüsse im Holzbau (in German). Research report, DIBt (German Institute of Building Technology) / University of Stuttgart.

Kuhlmann, U. & Brühl, F. (2013): Vorteilhafte Bemessung von Holztragwerken durch duktile plastische Anschlüsse (in German). Research report, iVTH, AiF IGF 16184N / University of Stuttgart.

Kuhlmann, U. & Brühl, F. & Schänzlin, J. (2014): Ductility in timber structures – investigations on an overstrength factor. RILEM International Symposium on Materials and Joints in Timber Structures, Stuttgart, 8.-10. October 2013, Springer Vieweg, pp. 181-190.

Kuhlmann, U. & Gauß, J.(2019): Optimierung von Anschlüssen im Holzbau zur Verbreitung der ressourcenschonenden Bauweise (in German). Research report, Zukunft Bau (SWD-10.08.18.7-17.12), Institute of Structural Design, University of Stuttgart.

Postupka, J. & Kuhlmann,U. & Brühl, F. (2016): Ductile behaviour of dowel connections – application of the component method in timber construction. WCTE 2016, World Conference of Timber Engineering, Vienna.

Sandhaas, C. (2012): Mechanical behavior of timber joints with slotted-in steel plates, TU Delft, dissertation.

Sandhaas, C. et al. (2018): Design of connections in timber structures – A state-of-the-art report by COST Action FP1402/WG3. Shaker Verlag GmbH, Aachen, Germany.

Sandhaas, C. & Van de Kuilen, J.-W. G. (2017): Strength and stiffness of timber joints with very high strength steel dowels. Engineering Structures 131 (2017), pp. 394-404.

Schweigler, M. & Sandhaas, C. (2018): Database and parameterization of embedment slip curves. In: Design of Connections in Timber Structures – A state-of-the-art report, COST Action FP1402 / WG3.

Discussion

The paper was presented by U Kuhlmann

F Lam asked about the number of replicates. U Kuhlmann said in some cases two replicates were used.

S Winter asked why K_{ser} is so low. U Kuhlmann responded that this could be due to the differences between single fasteners and a group of fasteners S Winter received confirmation that the blue line in slide 23 was based on EC5 with 50% reduction of stiffness and that n_{ef} was not applied because of the reinforcement.

A Frangi commented on the 5d or 7d cases, mentioning that more spacing and less dowels would get better ductility in unreinforced cases. U Kuhlmann will look into this further.

A Frangi asked if both moment and shear were present and if one would consider using a shear key. U Kuhlmann responded that in the design of steel joints one would reserve some of the connections for shear the rest for bending. U Kuhlmann will consider this in future.

JM Cabrero received confirmation that the brittle failures had 2 replicates and one had net section failure and the other case was splitting.

R Jockwer received clarification that the doubling of K_{ser}, allowed by EC5 for steel-timber connections, was not used, i.e. the stiffness from EC5 was actually ¼ not ½.

P Quenneville did not agree that the net tension failure was due to group effect. He agreed that EC5 overestimated the stiffness in multiple dowel case grossly. He asked if higher stiffness could be achieved by using inclined screws rather than dowels. U Kuhlmann agreed.

M Schweigler asked about the rotational springs and received clarification that they were uncoupled.

S Aicher stated that to get the spring stiffness you tested a joint with multiple fasteners and asked how many dowels in a joint to determine the spring stiffness. U Kuhlmann responded that in so called component method one already tested the component of interest. S Aicher questioned how could this method deal with cases with more dowels. U Kuhlmann responded that the number of dowels did not have much influence on stiffness as shown in slide 12 (Figure 3.2). S Aicher stated that size of the connection would have an influence. F Lam and U Kuhlmann further discussed whether slide 12 (Figure 3.2) showed a difference in stiffness between groups.

A Frangi received clarification that the rotational spring properties were determined by tests. He stated that glued in rods may have better stiffness characteristics.

P Quenneville commented that slide 12 (Figure 3.2) is a normalized graph so it did not show the stiffness difference well. He agreed with S Aicher that there would be a test configuration effect.

M Li received confirmation that both sides of the beam had similar bending stiffness.

Duration of Load Effect on Axially-Loaded Self-Tapping Screws Inserted Parallel to Grain in Soft- and Hardwood

Reinhard Brandner [1], Andreas Ringhofer, Raimund Sieder

Institute of Timber Engineering and Wood Technology, Graz University of Technology, Graz, Austria; [1] corresponding author; reinhard.brandner@tugraz.at

1 Abstract

The growing stock of deciduous tree species with high strength capacities predestines their application in plane and spatial frameworks and branched structures. Important prerequisites therefore are economic and high-performing joint solutions. End-grain joints with self-tapping screws can be one efficient solution for such joints as they are highly optimised for axial loads and easy to apply. However, insufficient knowledge, singular test outcomes and fears concerning the duration of load (DoL) behaviour currently prevent economic joint solutions with self-tapping screws inserted parallel to grain. Motivated by this apparent research gap, a project was initiated to investigate the DoL effect on the withdrawal capacity of in tension axially-loaded self-tapping screws inserted parallel to grain in soft- and hardwood species and products. Preliminary results gained after 2.25 years DoL investigations outline the necessity to harmonise test procedures also in respect to the time-to-failure. Considering this, the applicability of current DoL regulations in Eurocode 5 also for axially-loaded self-tapping screws is demonstrated.

2 Introduction

Timber is a visco-elastic, cylindrically anisotropic, natural building material with micro- and macroscopic flaws. It exhibits large variabilities in mechanical properties and shows different failure modes depending on the type and direction of loading. These failure modes may even change with the material quality / grade. Mechanical properties are also influenced by the surrounding climatic conditions, i.e. by the relative humidity and the temperature. In addition, timber features a distinctive long-term behaviour under permanent and variable actions, known as creep and duration of load (DoL) effects.

DoL, frequently named also creep rupture or static fatigue, describes the degradation of strength under stress over time, i.e. failure of timber members after a certain period of time at stress levels below their short-term strength (e.g. Barrett and Foschi 1978). For the description of the DoL phenomena not only the load magnitudes but the whole load history (Foschi and Yao 1986) and because of distinctive mechano-sorptive effects in some loading modes even the whole exposure history, including the climate, needs to be taken into account (e.g. Fridely et al. 1991; Dill-Langer and Aicher 1997; Aicher and Dill-Langer 1997; Ranta-Maunus 1998). Overall, the time-to-failure, T_f, in wood and timber decreases with increasing moisture content and is significantly lower in cyclic varying than in constant climate; see e.g. Schniewind (1967), Hoffmeyer (1990), Fridely et al. (1991), Barrett (1996), Dill-Langer and Aicher (1997) and Ranta-Maunus (1998).

In Eurocode 5 (EN 1995-1-1 2014), effects of DoL and moisture on the resistance are taken into account via the modification factor k_{mod}. This factor depends on (i) the load duration, (ii) the service class (SC), and (iii) the timber product. For structural timber, glulam, LVL and plywood the same k_{mod} factors apply which are also similar for SC 1 and SC 2. There is no differentiation in respect to failure modes nor timber products and joints.

Despite numerous investigations (summaries of these are provided e.g. in Karacabeyli and Soltis 1991, Madsen 1992, Rosowsky and Fridely 1995, Barrett 1996 and Köhler 2007), the DoL effect is not fully understood yet. In 1951 Wood nicely formulated empirical models for the relationship between the stress level (*SL*), defined as ratio between the applied constant long-term stress and the short-term strength, and the logarithm of the time-to-failure ($\log_{10}(T_f)$). Although based on small clear wood bending tests, his models, the linear and the hyperbolic "Madison curve", were adopted for structural timber and timber products, irrespective of species, actions and failure modes, as well as for timber joints. Even nowadays, it is the basis for DoL provisions in a number of international design codes, including the Eurocode 5. Later, Pearson (1972) summarised test data of eight DoL investigations and formulated a new model, close to the linear Madison curve.

Madsen (1973, 1992, a.o.) initiated comprehensive DoL and RoL (rate-of-loading) investigations by directing the focus on structural timber. His main observations were: (i) the functional interrelationship of *SL* vs. $\log_{10}(T_f)$ between structural timber and clear wood is different, (ii) (stepwise) ramp load (RoL) tests can serve as surrogate for DoL tests, (iii) strength / grade and quantile dependent DoL effects, i.e. DoL effects in clear wood, high quality timber and upper quantile levels are higher than for low timber qualities and lower quantile levels, and (iv) failure mode dependent DoL effects, i.e. DoL effects in shear, rolling shear and tension perpendicular to the grain are overall higher than in bending, tension and compression parallel to the grain. However, in literature partly contradicting results are found.

Due to the costly and time-consuming experiments and the necessity to extrapolate test data up to typical service lives of 50 years and beyond, modelling of the DoL effect is of high importance. Available models can be classified in phenomenological (empirical) models (e.g. Wood 1951; Pearson 1972), damage accumulation models (e.g. Barrett and Foschi 1978; Gerhards 1979; Foschi and Yao 1986; Gerhards and Link 1987) and physical / chemical models (models based on fracture mechanics, crack propagation, chemical kinetics, energy or combinations thereof; e.g. Bach 1973; Nielsen 1979; Van der Put 1989; Fridley et al. 1991; Philpot et al. 1994). However, for all these models the parameters need to be calibrated on test data (Hoffmeyer 2003) and the assumptions made for the models might not be adequate for all the different failure modes apparent in timber products and joints (Madsen and Johns 1982b).

Whereas a large number of investigations have substantiated knowledge on the DoL effect on structural timber and thereof made products, this is not so for single fastener and joints in interaction with timber. DoL investigations on laterally-loaded dowel type fasteners are reported in e.g. Kuipers (1977), Wilkinson (1988), van de Kuilen and Blaß (1996), Rosowsky and Reinhold (1999), Rosowsky and Bulleit (2002), Marlor and Bulleit (2005) and Cousin and Salenikovich (2012). Overall, most studies give lower DoL effects in joints than usually observed for timber members, in particular for nail joints; the applicability of similar DoL factors for all failure modes (from embedment up to plastic hinges) is seen to be critical.

With focus on axially-loaded dowel-type fasteners, and here in particular on self-tapping screws, known investigations are limited to Rosowsky and Reinhold (1999), Pirnbacher and Schickhofer (2012), Uibel and Blaß (2013), Koj and Trautz (2016) and Westermayr (2018). Based on RoL tests (target T_f = 0.1 to 10 s) on d = 3.0 mm screws Rosowsky and Reinhold (1999) conclude statistically no significant RoL effect. Uibel and Blaß (2013) did DoL withdrawal tests in SC 2 (sheltered; varying outdoor climate) and state that within five years 19 of 48 screws inserted in the CLT narrow face failed although SL_{mean} was only $\cong$ 28 %; final report is pending. Tests on single screws of Koj and Trautz (2016; α = 0°; Norway spruce) seem to be still running and tests by Westermayr (2018; beech and BauBuche) may have recently or will be started soon.

Pirnbacher and Schickhofer (2012) report on DoL withdrawal tests on d = 8 mm self-tapping screws in Norway spruce inserted at α = 0°, 45° and 90° over a period of two years in an open storage hall (varying climate between SC 1 and SC 2) with specimen individual SL between 0.49 and 1.18. For α ≥ 45° and SL ≤ 0.73 they confirmed the applicability of the k_{mod} factors in Eurocode 5. For α = 0°, however, they report on a tremendous DoL effect as long as the anchored thread was not sufficiently embedded, i.e. featured a clear distance to the timber end-grain of l_{emb} ≥ 2 d. Missing clarity on stress levels, unconsidered moisture effects and uncertainty about a possible influence from slightly oscillating dead loads, as observed during uploading and probably also caused by draught, impedes the overall assessment.

Uncertainty because of limited data and singular experimental observations have led to rather conservative regulations for the withdrawal strength $f_{ax,0}$ of axially-loaded self-tapping screws inserted parallel to grain. For example, for structural timber and glulam ETA-12/0373 (2017) and ETA-11/0190 (2018) state a ratio of $f_{ax,0,k}$ / $f_{ax,90,k}$ = 0.3 although short-term tests give 0.70 to 0.83; see e.g. summaries in Ringhofer (2017) and Brandner et al. (2019). As the k_{mod} factors in Eurocode 5 are similar for all timber and joint properties, given a specific timber product and service class, in fear of a much higher DoL effect for the withdrawal strength at α = 0° this conservative specification was made.

The growing stock of deciduous tree species, which partly feature high strength capacities, predestines their application in plane and spatial frameworks and branched structures. Consequently, end-grain joints gain in importance which necessitates DoL investigations to cover also deciduous timber species and therefore optimised existing and new fastener and joint solutions. Motivated by that and the research gap in respect to DoL and withdrawal, a research project was initiated to investigate the DoL effect on the withdrawal capacity of in tension axially-loaded self-tapping screws inserted parallel to grain, from which preliminary results are presented hereafter.

3   Materials and Methods

3.1   Materials and Test Plan

3.1.1   Timber Species, Products, Specimen Preparation and Climate Conditions

Two timber species, beech (BE; *Fagus sylvatica*) and Norway spruce (NS; *Picea abies*), and one engineered timber product, BauBuche (BB; LVL; ETA-14/0354 2018), are investigated. The beech (grading quality "Superior SUP"; $w \times t$ = 160 × 70 mm²; l = 3.4 m) as well as the BauBuche ($w \times t$ = 160 × 80 mm²; l = 4 m) were delivered by Pollmeier Massivholz GmbH & Co KG, the Norway spruce (visually graded; strength class C24+ acc. to EN 338 (2016); $w \times t$ = 160 × 80 mm²; l = 4 m) by Hasslacher Preding Holzindustrie GmbH. For the reference as well as the DoL tests the beams were split lengthwise in two halves to achieve final cross sections of $w \times t$ = 76 × 70 mm² for beech and 76 × 80mm² for BauBuche and Norway spruce; these cross sections are slightly smaller than ruled in EN 1382 (1999; $w \times t \geq (10 \, d)^2$). All specimens have been free of any local growth characteristics, at least in the central (insertion) zone, following EN ISO 8970 (2010). Irrespective of the thread embedment length, l_{emb}, for the reference withdrawal tests all specimens were crosscut to l = 245 mm. For the DoL tests and to maintain the distance between the screw tips (61 mm) and the chain length in the DoL testing frame, the lengths of the specimens were l = 181, 213 and 245 mm for l_{emb} = 0, 2 and 4 d, respectively. Specimens featuring thread embedment were predrilled with d = 8 mm over l_{emb}.

All specimens were conditioned at 20 °C and 85 % relative humidity to equilibrium moisture contents of 14 to 15 % in beech and BauBuche and 16 to 18 % in Norway spruce. In the same climate chamber and under the same climate conditions later the

DoL tests have been conducted. This climate represents the upper region of SC 2 according to Eurocode 5. It is in-line with the recommendations in EN 1156 (2013) and motivated by similar k_{mod} factors for SC 1 and SC 2 in Eurocode 5. Although literature reports on higher DoL effects at varying climate conditions, in absence of regulations for a representative varying climate in tests here a constant climate has been applied.

3.1.2 Types of Screws

Two types of self-tapping screws, both with a nominal (outer) thread diameter of d = 8 mm, have been tested. Screw type one (ST1; RAPID®, Schmid Schrauben Hainfeld GmbH; ETA-12/0373 2017) represents common self-tapping screws, screw type two (ST2), developed especially for self-tapping application in hardwood products within the research project "hardwood_SCREWS" (Bridge 1; no. 850748; Austrian Funding Agency FFG; Brandner et al. 2019), trades under the name RAPID® Hardwood (Schmid Schrauben Hainfeld GmbH; ETA-12/0373 2017). In contrast to ST1 the thread core diameter in ST2 is thicker ($d_{1,ST1}$ = 5.20 mm; $d_{1,ST2}$ = 6.08 mm).

3.1.3 Test Plan

In the short-term reference as well as the DoL and RoD (rate-of-displacement) tests the following parameters have been investigated:

- timber species / product: NS, BE, BB (in RoD tests only BE);

- type of screw: ST1, ST2;

- thread embedment length: l_{emb} = 0, 2, 4 d (in RoD tests only l_{emb} = 0 d);

- LL in DoL tests: 60, 70, 80 % of $F_{ax,max,mean}$ (mean value of each configuration, determined in short-term tests);

- displacement rates in RoD tests and series names in brackets: 500 (UST), 1.1 (REF), 0.031 (LT), 0.0016 mm / min (ULT).

In all tests the effective thread length (l_{ef} = 60 mm including the screw tip with l_{tip} = 8.8 mm) and the thread-grain angle α = 0° were kept constant. The reason for the relatively short l_{ef} is to avoid steel tensile failures in the reference tests on ST1. Screw insertion over l_{ef} occurred without predrilling. An insertion device was used to insert the screws as accurate as possible. Each test series, defined by a combination of the parameters above, contained ten specimens in the short-term reference tests, six to seven specimens (two screws / specimen resulted in 12 to 14 tests) in the DoL and seven to eleven tests in the RoD series; for further details see Mayr (2018).

To best achieve matched samples, the following sampling procedure was applied: within test series specimens were taken from different planks whereas between test series specimens from the same planks were consecutively taken. This was done to minimise the differences in the specimens of one timber species / product between the short-term reference and the DoL as well as RoD test series, and to maximise the

variability within samples, i.e. focusing on a representative variability of the withdrawal capacity within each test series.

3.2   Methods

3.2.1   Short-Term Reference Withdrawal Tests

To maintain comparability with past investigations, the short-term withdrawal tests were performed according to EN 1382 (1999) and not according to EN 1382 (2016); thus, the ultimate load had to be achieved displacement-controlled within 90 ± 30 s. A "pull-pull" test setup, equally equipped on both specimen's ends similar to the latter DoL test setup, was used.

The chosen "pull-pull" test setup represents a serial system of two elements where only the resistance of the weakest element was observed, i.e. the data is right-censored. To infer the distribution for single screws, knowing that the resistances within specimens are equi-correlated (Brandner et al. 2015), the following maximum likelihood estimation for right-censored, equi-correlated data (MLE_{rceq}) was applied:

$$L\left(\theta|y_1,y_2;\rho_{YY}\right)=\int_{c_2}^{\infty}\mathrm{f}\left(y_1,y_2;\rho_{YY}\right)\mathrm{d}y_2=\mathrm{f}\left(y_1\right)\left[1-\mathrm{F}_{Y_2|Y_1=y_1}\left(c_2\right)\right] \tag{1}$$

with $L\left(\theta|y_1,y_2;\rho_{YY}\right)$ as the likelihood function, y_1 and y_2 as normal variables in the logarithmic domain, representing the observed and right-censored withdrawal resistance, respectively, $\mathrm{f}\left(y_1\right)$ as normal density function of Y_1 and $\mathrm{F}_{Y_2|Y_1=y_1}\left(c_2\right)$ as marginal normal distribution function of Y_2 at c_2 given y_1, with c_2 as censoring load for Y_2; see e.g. Fagbamigbe et al. (2017).

3.2.2   DoL Tests (Constant Load)

For the DoL tests a custom-made steel test frame was constructed which allows to test up to 28 chains, each comprising of three specimens in a "pull-pull" setup, i.e. in each serial chain six screws featuring the same parameter setting are tested (see Figure 3.1 a). After failure of the first, the weakest side of a specimen, the failed screw has been replaced by a d = 12 mm screw (RAPID ®, Schmid Schrauben Hainfeld GmbH; ETA-12/0373 2017). Specimens with failures on both ends have been replaced until the failure of the fifth specimen; afterwards, gaps in the chain are bridged via threaded rods.

The target load level (*LL*) in each chain has been applied via a hydraulic cylinder followed by manual fine-tuning (Figure 3.1 c). To compensate the load reduction due to creep, packages of cup springs (Schnorr 51 CrV 4), in number and arrangement optimised for the target load, have been installed and initially each chain was overloaded by 2 to 4 %. To continuously control the target load in each chain, a custom-made load measurement system based on strain gauges glued on threaded rods has been applied; see Figure 3.1 (b). The load in each chain has been continuously controlled (1 Hz) via the software DAQMaster (Yokogawa). Chains which fall below the target

load due to creep are reloaded at least when the difference exceeds 100 N. Data drifts have been continuously checked and linearly corrected on a regular basis, i.e. every three months, by unloading and reloading each chain.

Figure 3.1. (a) DoL test frame; (b) strain gauges; (c) uploading via hydraulic cylinder and manually.

In evaluating the DoL effects the amount of data from 1 Hz measurement frequency has been significantly reduced and those data points filtered which have ± 10 N difference to the foregoing point in time. By testing chains instead of single specimens it is necessary to assess the whole load vs. time history, including phases of up-, un- and reloading and constant load. The idea is to convert non-constant load phases and / or phases with a load other than the target load to time-equivalent phases of constant target load.

By taking the DoL behaviour of wood / timber and past modelling approaches seriously, because of its simplicity and apparent adequateness (see Section 4.1) the following weighting function, based on the model of Pearson (1972), is introduced (see Mayr 2018):

$$f_{\text{weight},i|j} = \frac{T_{\text{ref},j}}{T_{i|j}} = \frac{10^{(a-LL_{\text{ref},j})/b}}{10^{(a-LL_{i|j})/b}} \tag{2}$$

with regression parameters a, b, gained iteratively by calibration to test data and applying the least squares approach. The load levels for each time step i given a specific screw j are defined as $LL_{\text{ref},j} = F_{\text{ax},LL\_\text{ref},j} / F_{\text{ax,max},j}$ and $LL_{i|j} = F_{\text{ax},i|j} / F_{\text{ax,max},j}$, with $F_{\text{ax,max},j}$ as the short-term resistance allocated to screw j, estimated from the equal-rank assumption approach from Madsen (1992), $F_{\text{ax},LL\_\text{ref},j}$ as target load and $F_{\text{ax},i|j}$ as the observed load on screw j at the i-th time step. Every time step $i|j$ was afterwards multiplied by $f_{\text{weight},i|j}$ and the equivalent time under constant target load determined by summation over all weighted time steps.

The equal-rank assumption according to Madsen (1992) assumes that the order in time-to-failure, T_f, for the DoL specimens is equal to the order in the reference short-term resistance, $F_{\text{ax,max}}$. Hereby it is presumed that the short-term and DoL test series are perfectly matched, i.e. that similar distribution characteristics (location, variability and shape) apply. To be able to fix the rank for screws within a series independent of the latter applied iterative solution procedure and because of the close course at load levels focused here a weighting function based on the hyperbolic model of Wood (1951), following the principles in Eq. (1), was used; see Mayr (2018).

As only three of six to seven specimens per DoL series are tested simultaneously, in a number of series which have not finished yet only a preliminary ranking is possible; these data points are separately marked in Figure 4.2 and not considered in the regression analyses. In these regression analyses reference values are considered by their mean values weighted by the number of observations. Further statistical inference was made for a significance level of 5 %. Confidence intervals for mean values were calculated according to the modified COX-method; see Olsson (2005).

3.2.3   RoD Tests (Ramp Load)

The RoD test setup was again a "pull-pull" configuration but with a d = 12 mm screw at the bottom side forcing withdrawal failure at the upper, target failure side. The maximum withdrawal capacity of all series was adjusted to approx. the average density of the tests of ρ_{12} = 720 kg/m³ via a power model with power coefficient 1.60; see Hübner (2013), and Brandner et al. (2019). Statistical analyses and inference was done in a similar manner as for the DoL tests.

4   Results and Discussion

4.1   Reassessment of the Data Basis for the Hyperbolic Madison Curve

The hyperbolic Madison curve from Wood (1951) is based on three model spots which were deduced from ramp load and constant load tests. Unconsidered differences in load application and uncertainties about the chosen spots motivated the reassessment of this model. This was done by means of the new evaluation procedure which allows to convert non-constant load phases to time-equivalent phases of constant load (see Chapter 3.2.2) and by considering the test data of Wood (1951; DoL tests) and Liska (1950; RoL tests).

For the conversion of the RoL data from Liska (1950) a weighting function based on the DoL model of Pearson (1972) was formulated, which is given as (Mayr 2018)

$$T_{\mathrm{f}} = \int_{T=0}^{T=T_{\mathrm{f}}} f_{\mathrm{weight}}\, \mathrm{d}T = \int_{T=0}^{T=T_{\mathrm{f}}} \frac{10^{(a-SL)/b}}{10^{(a-SL)T/(T_{\mathrm{s}}b)}}\, \mathrm{d}T = \frac{\left(10^{SL/b}-1\right)10^{-SL/b}\, b\, T_{\mathrm{s}}}{SL\ln(10)} \tag{3}$$

with SL as stress level [%], a and b as regression parameters and T_{s} and T_{f} as time-to-failure in ramp and constant load tests, respectively. For example, for T_{s} = 300 s and SL = 100 % the expected equivalent time-to-failure in constant load DoL tests would be T_{f} = 8.2 s. This is well in-line with Aicher and Dill-Langer (1997) who found for the same T_{s} equivalent dead-load times of T_{f} = 7 to 11 s.

This reassessment causes a significant shift of the ramp load tests to the lower end of time-to-failure. Figure 4.1 shows the outcome of this analysis, a new regression model called "Modified Madison curve", from Mayr (2018), in comparison with the models of Wood (1951) and Pearson (1972). The modified Madison curve is given as

$$SL = a - b\log_{10}\left(T_{\mathrm{f}}\right) \rightarrow SL = 91.37 - 5.84\log_{10}\left(T_{\mathrm{f}}\right) \tag{4}$$

It is noticed that these regression parameters are rather close to that of Pearson (1972). Although not statistically significant, the reference point is clearly apart from the regression model. For SL = 100 %, this model gives a time-to-failure, T_f, which is approximately 16-times higher than calculated from T_s = 300 s.
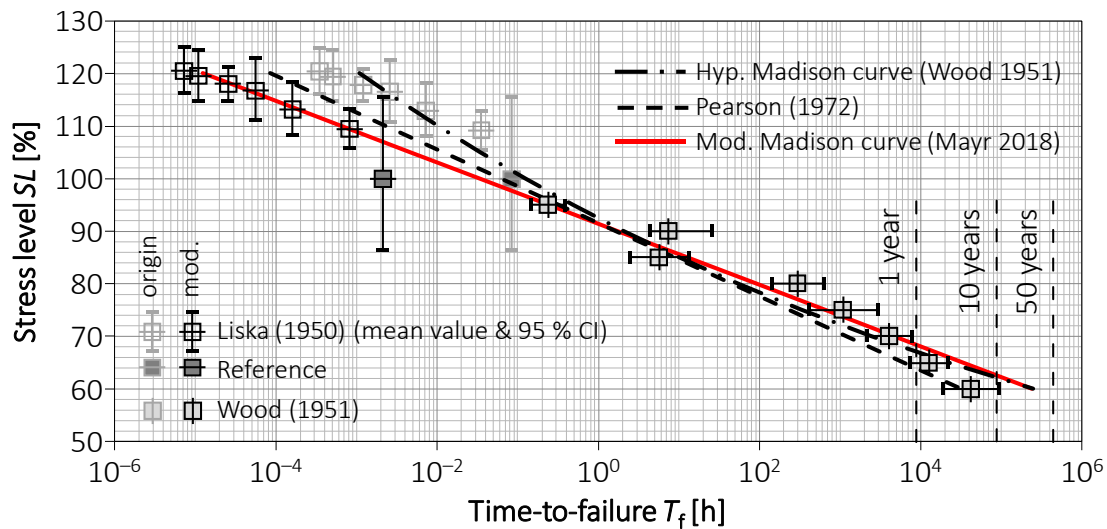
Figure 4.1. Modified Madison curve from Mayr (2018), gained by reassessing the data of Liska (1950) and Wood (1951) in comparison with the hyperbolic Madison curve and the DoL model of Pearson (1972).

4.2 Reference Withdrawal Tests

Table 1 summarises the main statistics from reference "pull-pull" withdrawal tests. In comparison with Norway spruce, in beech and BauBuche the variability in mean values and coefficients of variation (CV) of the moisture content is higher and because of a more distinctive hysteresis effect on average 1 % lower. In respect to the density, series in beech show a larger variation in mean values than series of Norway spruce and BauBuche, with a range of $\rho_{12,mean}$ = 718 to 750 kg/m³. As the relationship between the withdrawal capacity and density in hardwood is much more pronounced than in softwood (e.g. Hübner 2013; Brandner et al. 2019) this variation might also have an influence on the comparability of the overall outcomes. The coefficient of variation for the density in beech is below common values in Norway spruce and overall rather low in BauBuche, which is due to homogenisation effects.

The maximum withdrawal capacity, $F_{ax,max}$, increases with a prolonged thread embedment length, l_{emb}. This can be observed for NS, BE and BB as well as both types of screws, ST1 and ST2. The gain in withdrawal capacity at l_{emb} = 2 d and 4 d is highly variable (between 4 and 22 % at l_{emb} = 2 d and between 7 and 25 % at l_{emb} = 4 d); on average an increase of 13 and 17 % at l_{emb} = 2 d and 4 d, respectively, is found. Pirnbacher et al. (2009) report a 15 % higher resistance for screws in Norway spruce, given l_{emb} = 2 d and α = 90°. For α = 0° Ringhofer (2017) reports no significant influence of l_{emb} on $F_{ax,max}$.

Apart from both series in BB with l_{emb} > 0 d, $F_{ax,max,ST2,mean}$ is on average 10 % below $F_{ax,max,ST1,mean}$; this and the average CV values for NS (15.7 %) and BB (7.9 %) are in-line

with previous investigations, whereas $CV[F_{ax,max}]_{mean}$ = 11.4 % in BE is lower; see Ring-hofer (2017) and Brandner et al. (2019). Mean values $F_{ax,max,mean}$ from NS and BB are well-comparable with past test series, in particular when the influence of moisture on the withdrawal capacity is taken into account. However, the difference between $F_{ax,max,mean}$ for BE in this and previous series, e.g. from Koppauer (2017) and Brandner et al. (2019), cannot be explained by the moisture content alone; the values here are overall approximately 20 % lower.

Table 1. Main statistics from the reference "pull-pull" withdrawal tests.

series [–]	no. [–]	u_{mean} (CV) [%]	$\rho_{12,mean}$ (CV) [kg/m³]	$F_{ax,max,mean,test}$ (CV) [kN]	$F_{ax,mean,MLErc}$ (CV) [kN]
ST1-00-NS	10	16.1 (2.4)	450 (3.3)	5.54 (11.8)	5.76 (12.4)
ST1-16-NS	10	16.1 (1.4)	442 (2.2)	5.70 (15.2)	5.97 (14.6)
ST1-32-NS	10	16.3 (1.7)	451 (4.0)	6.38 (8.6)	6.56 8.8)
ST2-00-NS	10	16.1 (1.8)	447 (3.4)	4.53 (6.5)	4.62 (6.6)
ST2-16-NS	10	16.1 (1.6)	451 (3.5)	5.00 (11.2)	5.17 (11.0)
ST2-32-NS	10	16.2 (1.4)	460 (4.7)	5.52 (15.4)	5.78 (15.2)
ST1-00-BE	10	15.1 (3.3)	708 (5.0)	9.60 (11.1)	9.94 (11.1)
ST1-16-BE	10	15.1 (3.0)	749 (7.3)	11.36 (20.4)	12.07 (19.5)
ST1-32-BE	10	14.6 (4.1)	750 (6.7)	11.51 (23.1)	12.25 (20.5)
ST2-00-BE	10	15.0 (3.1)	715 (6.6)	9.20 (14.7)	9.61 (14.2)
ST2-16-BE	10	15.2 (2.8)	719 (4.8)	10.15 (15.1)	10.62 (14.3)
ST2-32-BE	10	14.8 (3.1)	724 (7.1)	10.44 (15.4)	10.92 (14.5)
ST1-00-BB	10	15.1 (2.3)	810 (1.2)	14.11 (8.8)	14.49 (8.7)
ST1-16-BB	10	15.1 (2.0)	803 (1.0)	15.32 (6.8)	15.66 (7.0)
ST1-32-BB	10	14.5 (3.2)	810 (1.0)	15.19 (5.3)	15.45 (5.3)
ST2-00-BB	10	15.3 (2.1)	800 (1.1)	12.93 (7.8)	13.25 (7.9)
ST2-16-BB	10	14.6 (3.7)	801 (0.9)	15.69 (8.4)	16.11 (8.5)
ST2-32-BB	10	14.3 (2.9)	801 (1.6)	15.42 (9.8)	15.92 (10.2)

4.3   DoL Tests (Constant Load)

The first DoL tests started at the 1st April 2017. The preliminary results presented and discussed hereafter comprise data until the 30th June 2019. The climate during this 2.25 years was kept rather constant, i.e. the average value and daily variations were for the temperature 20 ± 1 °C and for the rel. humidity 85 ± 5 %.

Table 2 summarises the number of failures as well as the average time under constant load according to the DoL test protocol. Apart from one series (ST2 | NS; 0 *d*), for *LL* = 80 % all series have already been completed. At this load level some failures occurred already during the first uploading phase. Considering lognormal variables and $CV[F_{ax,max}]$ between 8 and 15 % the expected probability of failure before reaching *LL* = 80 % is between 0.3 and 7.8 %, respectively. At *LL* = 70 % approximately half

of the series are already completed or only a few failures missing whereas at *LL* = 60 % most of the tests are still running or pending. In most of tested parameter combinations ST2 appears to perform slightly better than ST1, i.e. the number of failures is lower and the time under constant load longer. This outcome was not expected because of the much lower intermeshing of thread in the surrounding timber in case of ST2. Obviously, the number of failures in beech is much lower than in NS and BB. One reason might be too low reference values. However, the chance that this is the case in all six reference series in beech is rather low. Incomparable to the others, in series (ST1 | *LL* = 60 %; NS; 0 *d*) the number of failures is already rather high. The reason therefore is not clear yet but might be due to an uncertain reference.

The statistics of moisture content and density from NS, BE and BB and already failed specimens are well in line with that of the reference tests in Table 1. The influence of non-representative reference values is discussed later.

In analysing the reference short-term tests, it was assumed that the withdrawal capacities of both specimen' ends are highly correlated. Such a high correlation could be also expected from the times-to-failure. A corresponding correlation analysis comprised the time under constant load, $T_{const,prot}$, from the DoL test protocol, and the equivalent time-to-failure under constant load, T_f, according to Eq. (2). For Norway spruce the correlations are ρ_{xx} = 0.60 and 0.48 (75 data pairs), for beech 0.56 and 0.29 (17 pairs), for BauBuche 0.82 and 0.66 (60 pairs), and in total 0.65 and 0.45 (152 pairs), respectively for $T_{const,prot}$ and T_f.

Table 2. Current status on number of failures and average time under constant load (in days) of already failed specimens based on DoL test protocol (not converted; only for series with > 10 failures).

load level *LL*		60 %		70 %		80 %	
material	l_{emb}	ST1	ST2	ST1	ST2	ST1	ST2
NS	0 *d*	13 | 224	1 | −	12 | 52	14 | 123	14 | 3	12 | 47
	2 *d*	5 | −	5 | −	13 | 34	8 | −	12 | 28	12 | 61
	4 *d*	7 | −	3 | −	NA	NA	12 | 59	14 | 5
BE	0 *d*	0 | −	2 | −	9 | −	10 | −	NA	NA
	2 *d*	1 | −	1 | −	12 | 76	6 | −	NA	NA
BB	0 *d*	6 | −	2 | −	14 | 41	9 | −	14 | 6	14 | 23
	2 *d*	5 | −	7 | −	14 | 65	14 | 65	13 | 6	14 | 6

NA … not tested parameter combinations

Figure 4.2 shows the main outcomes and model comparisons in semi-logarithmic scale, *LL* vs. $\log_{10}(T_f)$, for Norway spruce (NS; above) and BauBuche (BB; below). Although the DoL tests run since 2.25 years values up to 10 years are shown. This is because some chains in the testing frame had been inadvertently overloaded, one chain even by 15 % over a period of some months. As the weighting function in Eq. (2) is functionally based on the inverse DoL model of Pearson (1972) the time during over-

loading becomes a relatively high weight which is logical considering the low proba-bility that such highly stressed specimens survive such a long period. The sensitivity of the regression models shown in Figure 4.2 and quantified in Table 3 was checked; omitting of such highly weighted specimens led to similar results.
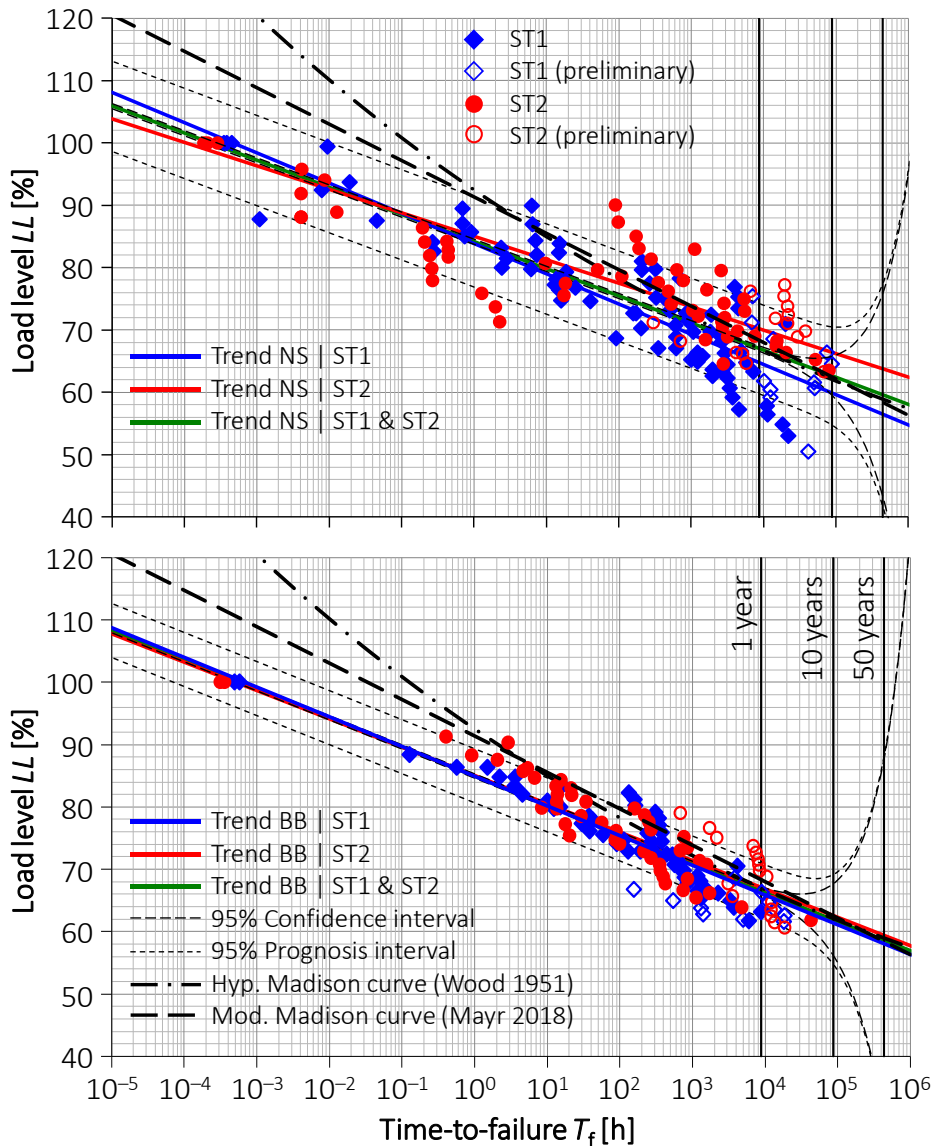
Figure 4.2. Preliminary results of the DoL tests on Norway spruce (NS; above) and BauBuche (BB; below): single data points with fixed and preliminary rank separately for ST1 and ST2.

From Figure 4.2 the following conclusions can be made: (i) differences in the DoL performance between ST1 and ST2 are negligible, (ii) the DoL performance of screws inserted parallel to grain in Norway spruce and BauBuche is similar, (iii) the variation in time-to-failure in BB is much lower than in NS which indicates that $CV[T_f]$ might be a function of $CV[F_{ax,max}]$ (see also Karacabeyli and Soltis 1991), (iv) around one year the DoL effect for self-tapping screws inserted parallel to grain converges to the DoL models of Wood (1951) and Mayr (2018; modified Madison curve) whereas the decrease in resistance is more distinctive at higher load levels, i.e. shorter time-to-failure, and (v) the resistance of screws at T_f corresponding to the reference point common for timber ($LL = 100$ %; $T_s = 300 \pm 120$ s) is 3 % lower than at $T_s = 90 \pm 30$ s,

i.e. differences in T_s from reference short-term ramp-load tests lead to different reference points in the DoL data analysis. The resistance of screws is even 10 % lower at the time-to-failure corresponding to the modified Madison curve at LL = 100 %. In fact, missing an equivalent time-to-failure analysis, at the reference point with LL = 100 % the Madison curve even equate $T_f \equiv T_s$.

Table 3 summarises predictions for the regression parameters a and b, gained by calibration of the DoL model in Eq. (4) to tests data. Apart from beech where the number of observations is too small to further classify, the outcomes for NS and BB differentiated in respect to l_{emb}, type of screw and material substantiate the previously made conclusions of well comparable regression parameters. A common DoL model with regression parameters $a \cong 85.0$ and $b \cong 4.43$ allows to cover all investigated parameters as long as the reference values are determined accordingly.

Table 4 presents average load levels for the load duration classes according to Eurocode 5, representing somehow k_{mod} factors for SC 2. These values were calculated by means of Eq. (4) and the regression parameters in Table 3 and always refer to the longest load duration in each load duration class. It can be concluded that these values are well comparable with preliminary outcomes found after one year testing (Mayr 2018), which somehow supports the adequacy of applied examination procedures and the stability in predictions.

Table 3. Predictions for the regression parameters a, b for each material, type of screw and thread embedment length as well as combinations thereof.

screw type		ST1		ST2		ST1 & ST2	
material	l_{emb}	a	b	a	b	a	b
NS	0 d	83.0	5.15	84.4	3.84	83.5	4.48
	2 d	84.2	4.96	88.5	3.21	85.8	4.15
	4 d	85.2	4.16	79.7	5.51	83.5	4.33
	all	**83.8**	**4.85**	**85.0**	**3.77**	**84.2**	**4.35**
BE	all	87.4	4.16	90.7	3.55	88.6	3.97
BB	0 d	84.2	4.97	87.0	3.83	85.1	4.57
	2 d	85.6	4.61	84.3	4.87	84.9	4.73
	all	**84.9**	**4.76**	**85.1**	**4.55**	**85.0**	**4.66**

The analysis of DoL test data assumes accurate reference values from short-term tests. To gain more confidence on the regression parameters in Table 3 and the predicted load levels in Table 4, the sensitivity of them in respect to changes in the reference values is selectively investigated. For example, unifying CV[$F_{ax,max}$] to 15 % in NS and BE (observed values between 6.6 to 20.5 %) and to 8 % in BB (observed values between 5.3 to 10.2 %) only leads to minor changes in a ($\leq \pm 1$ %), b ($\leq \pm 10$ %) and LL ($\leq \pm 1$ %). Unifying in addition the effect of thread embedment to 1.13 $F_{ax,max,mean}$ (originally 4 to 22 %) and 1.17 $F_{ax,max,mean}$ (originally 7 to 25 %) for l_{emb} = 2 d and 4 d,

respectively, the influence on parameter a is $\leq \pm 6\,\%$, whereas it is $\leq \pm 20\,\%$ on b and $\leq \pm 10\,\%$ (on average $+1\,\%$) on LL. Finally, increasing $F_{ax,max,mean}$ for beech by 20 % (see Section 4.2) in addition to unified $CV[F_{ax,max}] = 15\,\%$ consequences in $\geq -5\,\%$ in a, $\leq +34\,\%$ in b and $\leq -20\,\%$ (on average $-10\,\%$) in LL. Overall, whereas the analysed changes in the reference values can have significant impacts on the regression parameters, only a substantial shift of 20 % in mean values led to a significant influence also on the LL predictions as basis for k_{mod} factors.

Table 4. Predicted average load levels for the different load durations acc. to Eurocode 5.

load duration	ST1			ST2			ST1 & ST2			
	NS	BE [2]	BB	NS	BE [2]	BB	NS	BE [2]	BB	NS & BB
permanent ($10\,a - 50\,a$ [1])	0.56	0.64	0.58	0.64	0.71	0.59	0.60	0.66	0.59	**0.60**
long-term ($6\,m - 10\,a$)	0.60	0.67	0.61	0.66	0.73	0.63	0.63	0.69	0.62	**0.63**
medium-term ($1\,w - 6\,m$)	0.66	0.72	0.68	0.71	0.78	0.69	0.68	0.74	0.68	**0.69**
short-term ($1/10\,s$ [1] $- 1\,w$)	0.73	0.78	0.74	0.77	0.83	0.75	0.74	0.80	0.75	**0.75**
instantaneous ($< 1/10\,s$ [1])	1.06	1.06	1.07	1.02	1.07	1.06	1.04	1.07	1.06	**1.05**

[1] assumed load duration; value not specified in Eurocode 5; [2] values highly uncertain, only few observations

4.4 RoD Tests (Ramp Load)

Table 5 shows the main statistics from RoD tests. Because of significant differences in average densities between some series the withdrawal capacities were corrected to a reference density of 720 kg/m³. The moisture content is well comparable with the reference short-term and DoL tests whereas the average withdrawal capacities here are 12 to 20 % higher than in the reference tests; see Table 1. Overall, the average capacities decrease regressively with increasing time-to-failure, T_s, whereas their variation, $CV[F_{ax,max,cor}]$, appears not to be affected by the time-to-failure. Ringhofer (2017), for example, concluded higher withdrawal resistances at ultra-short-term tests but only insignificant differences at lower displacement rates when compared to reference tests in Norway spruce and $T_{s,mean}$ between 0.5 and 300 s.

Table 5. Main statistics from RoD tests on beech, ST1 and ST2.

series [–]	no. [–]	u_{mean} (CV) [%]	$\rho_{12,mean}$ (CV) [kg/m³]	$T_{s,mean}$ [s; min; h]	$F_{ax,max,mean}$ (CV) [kN]	$F_{ax,mean,cor}$ (CV) [1] [kN]
ST1-UST	10	14.7 (2.3)	744 (8.2)	0.28 s	14.6 (19.4)	13.7 (10.1)
ST1-REF	7	14.8 (2.0)	754 (8.6)	100 s	13.2 (17.8)	12.2 (12.4)
ST1-LT	11	14.8 (2.1)	718 (6.0)	53 min	11.5 (17.6)	11.4 (11.6)
ST1-ULT	8	14.2 (4.4)	729 (7.4)	17.25 h	11.7 (19.8)	11.3 (11.2)
ST2-UST	10	14.6 (2.8)	703 (7.6)	0.28 s	12.0 (12.5)	12.5 (11.0)
ST2-REF	7	15.1 (1.2)	699 (4.8)	100 s	10.3 (10.8)	10.8 (7.1)
ST2-LT	11	14.9 (3.1)	707 (5.0)	53 min	10.3 (15.3)	10.6 (9.4)
ST2-ULT	8	14.0 (4.4)	703 (8.8)	17.25 h	10.0 (18.2)	10.3 (9.3)

[1] withdrawal resistance corrected to a reference density of 720 kg/m³

After converting the times-to-failure, from $T_s \rightarrow T_f$, the linear relationship according to Eq. (4) between LL and $\log_{10}(T_f)$ was calibrated to single and mean values, respectively, and regression parameters a = 76.3 and 72.0 and b = 3.84 and 3.58 found. Overall, although the decrease in resistance is qualitatively comparable with the results from the DoL tests, for the same T_f value the regression parameters calibrated to RoD tests consequence load-levels approximately 10 % below that from the DoL tests.

5 Summary and Conclusions

Preliminary results from meanwhile 2.25 years DoL testing on axially-loaded self-tapping screws inserted parallel to grain in soft- and hardwood and failing in withdrawal were presented. A constant load and climate (SC 2) have been applied. In addition, RoD tests were performed.

For a consistent evaluation of ramp (RoD) and constant load (DoL) test data, a new evaluation procedure was developed. It converts non-constant load phases and / or phases with a load other than the target load to time-equivalent phases of constant target load; see Mayr (2018). DoL graphs on this basis consistently present the load-level (LL) vs. $\log_{10}(T_f)$, as logarithmic time-to-failure at constant load, which is not the case in common DoL graphs found in the literature. These graphs usually mix T_s and T_f on the abscissa, with $T_s \leq T_{ref} < T_f$ and T_{ref} as reference time (typically 300 s), corresponding to LL = 100 %; see also Figure 4.1.

The course of DoL and RoD data from herein presented withdrawal tests can be described by a linear regression model with LL vs. $\log_{10}(T_f)$ which converges rather fast to the clear wood models of Wood (1951) and Pearson (1972). This circumstance should not surprise considering the requirements on withdrawal test specimens according to EN ISO 8970 (2010).

Overall, the DoL behaviour was found to be similar for both tested types of screws, for Norway spruce (NS) as well as BauBuche (BB) and all tested different thread-embedment lengths. The low number of failures in beech prevent conclusions on the same level as for NS and BB; however, current trends indicate similar outcomes.

The time-to-failure, T_s, in standard short-term withdrawal tests on single axially-loaded fasteners like nails, brackets and screws according to EN 1382 (1999, 2016) is much lower than for other timber properties. Although the influence on the short-term strength was found to be small, for a consistent treatment of all timber properties it is proposed to harmonise regulations in respect to T_s and / or to adjust properties determined at T_s others than T_s = 300 ± 120 s accordingly. It is reminded that every characteristic value is linked to a set of reference conditions and corresponding regulations for the adjustment of values determined at non-conform conditions. This set comprises also regulations on the time-to-failure which directly impacts the set of k_{mod} factors in the design procedure.

Table 6 summarises k_{mod} factors for SC 2 as predicted from herein investigations, from Eurocode 5 and the models of Wood (1951) and Pearson (1972). For both models and every load duration k_{mod} predictions for the upper and lower time limits are presented. It appears that in Eurocode 5 current k_{mod} factors base on the lower, non-conservative time limits. Considering this and the circumstance that the k_{mod} factors for the withdrawal tests are calculated for the upper time limit, apart from instantaneous load duration for which the time is not specified in Eurocode 5 an exceptional high level of agreement is observed between the DoL tests on screws and the predictions of Wood (1951) and Pearson (1972).

Table 6. k_{mod} factors based on DoL withdrawal tests, from Eurocode 5 (EC 5), Wood (1951; hyperbolic Madison curve) and Pearson (1972).

load duration	EC 5 SC 1 & 2	Wood (1951) [2]	Pearson (1972) [2]	ST1 & ST2 [3] NS & BB
permanent (10 a – 50 a [1])	0.60	0.62–0.59	0.57–0.52	0.60
long-term (6 m – 10 a)	0.70	0.69–0.62	0.66–0.57	0.63
medium-term (1 w – 6 m)	0.80	0.77–0.69	0.76–0.66	0.69
short-term (1/10 s [1] – 1 w)	0.90	0.92–0.77 (1 h)	0.92–0.76 (1 h)	0.75
instantaneous (< 1/10 s [1])	1.10	1.08 (1 min)	1.04 (1 min)	1.05

[1] assumed load duration; value not specified in Eurocode 5
[2] values for upper and lower time limits; deviating times in brackets;
[3] values for upper time limit calculated acc. to Eq. (4), with a = 85.0 and b = 4.43; see Section 4.3

As a consequence, current regulations in respect to the withdrawal capacity of axially-loaded self-tapping screws inserted parallel to the grain in soft- and hardwood are too conservative. Based on presented DoL outcomes the equivalent treatment of the withdrawal capacity and other timber properties can be widely confirmed although at instantaneous and short-term load durations the DoL effect seems to be slightly higher. This can be, at least in part, explained by differences in T_s.

These conclusions suppose the suitability of current k_{mod} factors in Eurocode 5. However, based on the literature there are some points which motivate a critical view on the current status. This concerns the reference time limit for each load duration but in particular the influence of moisture in static and cyclic climate conditions. Hoffmeyer (1990) and others clearly demonstrated the significant impact of changing climates. Design standards like the SIA 265 (2012) consider differences in the resistances between SC 1 to SC 2 by a 20 % reduction of the reference strength properties, i.e. by η_w = 0.80. DoL investigations on axially-loaded screws in cyclic climates are recommended. Therefore and in general, regulations for reference cyclic climate conditions and corresponding reference short-term properties are prerequisites.

6 Acknowledgements

7 References

Aicher S, Dill-Langer G (1997) DoL effect in tension perpendicular to grain of glulam depending on service classes and volume. CIB-W18:30-9-1, Vancouver, Canada.

Bach L (1973) Reiner-Weisenberg' s theory applied to time-dependent fracture of wood subjected to various modes of mechanical loading. *Wood Science*, 5(3):161–171.

Barrett JD, Foschi RO (1978a) Duration of load and probability of failure in wood. Part I. Modelling creep rupture. *Canadian Journal of Civil Engineering*, 5(4):505–514.

Barrett JD, Foschi RO (1978b) Duration of load and probability of failure in wood. Part II. Constant, ramp and cyclic loading. *Canadian Journal of Civil Engineering*, 5(4):515–532.

Barrett JD (1996) Duration of load – the past, present and future. International COST 508 Wood Mechanics Conference, Stuttgart, Germany.

Brandner R, Bratulic K, Ringhofer A (2015) Serial Correlation of Withdrawal Properties from Axially-Loaded Self-Tapping Screws. ICASP12, Vancouver, Canada.

Brandner R, Ringhofer A, Reichinger T (2019) Performance of Axially-Loaded Self-Tapping Screws in Hardwood: Properties and Design. *Engineering Structures*, 188:677–699.

Cousin A, Salenikovich A (2012) Rate of loading and moisture effects on dowel bearing strength. WCTE, Auckland, New Zealand.

Dill-Langer G, Aicher S (1997) Damage modelling of glulam in tension perpendicular to grain in variable climate. CIB-W18:30-9-2, Vancouver, Canada.

EN 338 (2016) Structural timber – Strength classes. CEN.

EN 383 (2007) Timber Structures – Test methods – Determination of embedment strength and foundation values for dowel type fasteners. CEN.

EN 384 (2016) Structural timber – Determination of characteristic values of mechanical properties and density. CEN.

EN 408 + A1 (2010) Timber structures – Structural timber and glued laminated timber – Determination of some physical and mechanical properties. CEN.

EN ISO 8970 (2010) Timber structures – Testing of joints made with mechanical fasteners – Requirements for wood density. CEN.

EN 1156 (2013) Wood-based-panels – Determination of duration of load and creep factors. CEN.

EN 1382 (1999) Timber structures – Test methods – Withdrawal capacity of timber fasteners. CEN.

EN 1382 (2016) Timber structures – Test methods – Withdrawal capacity of timber fasteners. CEN.

EN 1995-1-1:2004 + AC:2006 + A1:2008 + A2:2014 (2014) Eurocode 5: Design of timber structures – Part 1-1: General – Common rules and rules for buildings. CEN.

EN 13183-1 (2002) Moisture content of a piece of sawn timber – Part 1: Determination by oven dry method (EN 13183-1:2002 + AC:2003). CEN.

ETA-11/0190 (2018) Self-tapping screws for use in timber constructions: DIBt.

ETA-12/0373 (2017) Self-tapping screws for use in timber constructions: Schmid Schrauben RAPID®, STARDRIVE and SP (Schmid Schrauben Hainfeld GmbH). OIB.

ETA-14/0354 (2018) Glued laminated timber made of hardwood – Structural laminated veneer lumber made of beech (Pollmeier BauBuche GL70). OIB.

Fagbamigbe AF, Adebowale AS, Bamgboye EA (2017) A survival analysis model for measuring association between bivariate censored outcomes: validation using mathematical simulation. *Am. J. of Mathematics and Statistics*, 7(1):7-14.

Foschi RO, Barrett JD (1982) Load-duration effects in Western Hemlock lumber. *Journal of the Structural Division*, 108(7):1494–1510.

Foschi RO, Yao ZC (1986) Another look at three duration of load models. CIB-W18/19-9-1, Florence, Italy.

Fridley KJ, Tang RC, Soltis LA (1991) Environmental effects of the load duration behaviour of structural lumber. Int. Timber Eng. Conf., 4:180–187, London, UK.

Gerhards CC (1979) Time-related effects of loads of wood strength. A linear cumulative damage theory. *Wood Science*, 19(2):139–144.

Gerhards CC, Link CL (1987) A cumulative damage model to predict load duration characteristics in lumber. *Wood and Fiber Science*, 19(2):147–164.

Hoffmeyer P (1990) Failure of wood as influenced by moisture and duration of load. Dissertation. State University of New York, USA.

Hoffmeyer P (2003) Strength under long-term loading. In: Thelandersson S, Larsen HJ (eds) Timber engineering. John Wiley & Sons Ltd., New York.

Hoffmeyer P, Sørensen JD (2007) Duration of load revisited. *Wood Science and Technology*, DOI 10.1007/s00226-007-0154-5.

Hübner U (2013) Mechanische Kenngrößen von Buchen-, Eschen- und Robinienholz für lastabtragende Bauteile. Dissertation, Graz University of Technology, Graz, Austria (in German).

ISO 3131 (1996) Wood – Determination of density for physical and mechanical tests.

Karacabeyli E, Soltis LA (1991) State-of-the-art report on duration of load research for lumber in North America. Int. Timber Eng. Conf., London, UK, 4:141–155.

Koj C, Trautz M (2016) Long-term behaviour of timber connections with self-tapping screws in outdoor climate. WCTE, Vienna, Austria.

Köhler J (2007) Reliability of timber structures. Dissertation, Swiss Federal Institute of Technology, Zurich, Switzerland.

Koppauer L (2017) Optimierung von axial beanspruchten Hirnholz-Schraubverbindungen in Hartlaubholz. Master thesis, Graz University of Technology, Graz, Austria (in German).

Kuipers J (1977) Long duration tests on timber joints. CIB-W18:7-7-2. Stockholm, Sweden.

Liska JA (1950) Effect of rapid loading on the compressive and flexural strength of wood. United States Forest Products Laboratory, R1767.

Madsen B (1973) Duration of load tests for dry lumber in bending. *Forest Products Journal*, 23(2):21–28.

Madsen B, Barrett JD (1976) Time-Strength Relationship for Lumber. Structural Research Series, Report No. 13, UBC, Vancouver, BC.

Madsen B, Johns K (1982a) Duration of load effects in lumber. Part II: Experimental data. *Canadian Journal of Civil Engineering*, 9:515–525.

Madsen B, Johns K (1982b) Duration of load effects in lumber. Part III: Code calibrations. *Canadian Journal of Civil Engineering*, 9:526–536.

Madsen B (1992) Structural behaviour of timber. Timber Engineering Ltd., Vancouver, Canada, ISBN 0-9696162-0-1.

Marlor RA, Bulleit WM (2005) Load-Duration Behavior of Wood Connections. *Journal of Structural Engineering*, 131(9):1434–1443.

Mayr P (2018) Einfluss konstanter Langzeitbeanspruchung (DoL) auf die Tragfähigkeit selbstbohrender Holzschrauben appliziert in Faserrichtung in Fichte, Buche und BauBuche. Master Thesis, Graz University of Technology, Graz, Austria (in German).

Nielsen LF (1979) Crack failure of dead-, ramp- and combined loaded viscoelastic materials. Int. Conf. on Wood Fracture, Banff, Alberta, Canada.

Nielsen LF (2004) On the influence of crack closure on strength estimates of wood. *Holz als Roh- und Werkstoff*, 62:81–87.

Nielsen LF (2007) Strength of wood versus rate of testing. *Holz als Roh- und Werkstoff*, 65:223–229.

Olsson U (2005) Confidence intervals for the mean of a log-normal distribution. *J. of Statistical Education*, 13(1), www.amstat.org/publications/jse/v13n1/olsson.html.

Pearson RG (1972) The effect of duration of load on bending strength of wood. *Holzforschung*, 26(4):153–158.

Philpot TA, Fridley KJ, Rosowsky DV (1994) Energy-based failure criterion for wood. *Journal of Materials in Civil Engineering*, 6(4):578–593.

Pirnbacher G, Brandner R, Schickhofer G (2009) Base parameters of self-tapping screws. CIB-W18:42-7-1. Dübendorf, Switzerland.

Pirnbacher G, Schickhofer G (2012) Zeitabhängige Entwicklung der Traglast und des Kriechverhaltens von axial beanspruchten, selbstbohrenden Holzschrauben. Research Report, Competence Centre Holz.Bau Forschungs GmbH, Graz University of Technology, Graz, Austria.

Ranta-Maunus A (1998) Duration of load effect in tension perpendicular to grain in curved glulam. CIB-W18:31-9-1. Savonlinna, Finland.

Ringhofer A (2017) Axially Loaded Self-Tapping Screws in Solid Timber and Laminated Timber Products. In: G Schickhofer, R Brandner (eds.) Timber Engineering & Technology, TET 5, Verlag der Technischen Universität Graz.

Rosowsky DV, Fridley KJ (1995) Directions for duration-of-load research. *Forest Products Journal*, 45(3):85–88.

Rosowsky DV, Reinhold TA (1999) Rate-of-load and duration-of-load effects for wood fasteners. *Journal of Structural Engineering*, 125(7):719–724.

Rosowsky DV, Bulleit WM (2002) Load duration effects in wood members and connections: order statistics and critical loads. *Structural Safety*, 24:347–362.

Schniewind AP (1967) Creep-rupture life of Douglas-fir under cyclic environmental conditions. *Wood Science and Technology*, 1:278–288.

SIA 265 (2012) Timber Structures. Schweizerischer Ingenieur- und Architektenverein.

Spencer RA, Madsen B (1986) Duration of load tests for shear strength. Canadian *Journal of Civil Engineering*, 13:188–195.

Uibel T, Blaß HJ (2013) Joints with Dowel Type Fasteners in CLT Structures. Focus Solid Timber Solutions: European Conference on Cross Laminated Timber (CLT): The State-of-the-Art in CLT Research. COST Action FP1004, Graz, Austria.

van de Kuilen JWG, Blaß HJ (1996) Does Damage Accumulate in Timber Joints Loaded at Load Levels Below 50% of the Average Short Term Strength? Int. Wood Engineering Conference, 4:46–53, Omnipress, Madison, WI.

van der Put TACM (1989) Deformation and damage processes in wood. Dissertation, Delft University press, Netherlands.

Westermayr M (2018) Beech connect: Optimierte Materialnutzung von Laubholz unter Verwendung moderner Verbindungskonzepte. Presentation, Technischer Ausschuss Brettschichtholz, 2018-10-24 (in German).

Wilkinson TL (1988) Duration of load on bolted joints – A pilot study. United States Department of Agriculture, Forest Service, Forest Products Laboratory, FPL-RP-488, Madison, Wisconsin.

Wood LW (1951) Relation of strength of wood to duration of load. United States Department of Agriculture, Forest Service, Forest Products Laboratory, Madison, Wisconsin, Report No. 1916.

Discussion

The paper was presented by R Brandner

A Frangi commented that parallel to end grain application is allowed in Swiss code with strength adjustment factor since 30 years. R Brandner confirmed that groups of fasteners will be studied.

R Jockwer commented that moisture content might have an effect. R Brandner agreed and responded that DOL effect will be much higher with cyclical conditions.

H Blass stated that variable climate would lead to more severe load duration effects. He also questioned the influence on withdrawal capacity when fasteners were loaded in shear for rope effect.   R Brandner responded that this cannot be answered now. A Ringhofer stated that some of the results (Pirnbacher) had open climate conditions and moisture content did not seem to play a significant role. It would be useful to examine the open climate condition by itself.

T Tannert questioned if there would be more effect for groups of fasteners. R Brandner discussed that block shear failure would be expected in short term and change of failure mode might be experienced in long term.

S Winter questioned the starting point of the moisture in the specimens. R Brandner stated that the moisture did not change and provided clarification of DOL factors in EC5. S Winter and R Brandner discussed brittle failure would occur for variable climate and group of fasteners.

F Lam received clarification that the specimens were not predrilled.

YH Chui received clarification that there were 3 specimens loaded in series and when a failure occurred the failed specimen was replaced and the series was reloaded.

R Jockwer received clarification that perpendicular to grain results were only available in Pirnbacher's study.

S Aicher questioned the use of linear interpolation of data in slide 19 compared to the nonlinear case. One would get more significant load duration effect at longer time to failure and Foschi model might be more appropriate.   R Brandner explained the linearity of data around the regression line and large uncertainties existed at longer time to failure.

Compressive strength and buckling resistance of GLT columns made of European beech (*Fagus sylvatica* L.)

Thomas Ehrhart [1)2)], René Steiger [2)], Pedro Palma [2)], Ernst Gehri [3)], Andrea Frangi [1)]

[1)] ETH Zürich, Swiss Federal Institute of Technology, Institute of Structural Engineering (IBK), CH-8093 Zürich, Switzerland

[2)] Empa, Swiss Federal Laboratories for Materials Science and Technology, Structural Engineering Research Laboratory, CH-8600 Dübendorf, Switzerland

[3)] Prof. emeritus ETH Zürich, Rüschlikon, Switzerland

Keywords: Compressive strength parallel to the grain, buckling resistance, glued-laminated timber GLT, European beech, Eurocode 5, effective-length method

1 Introduction

In Eurocode 5 (EN 1995-1-1:2010) and SIA 265:2012, the design method for columns prone to buckling is based on the effective-length method and the design verification (Equation 10) assumes that the compressive strength is reduced due to the effect of instability-related factors (Equations 10-13). This procedure is identical to the design of steel columns (EN 1993-1-1:2010). Two important parameters in this design method are the straightness factor β_c (= 0.10 for glued laminated timber, GLT) and the critical relative slenderness $\lambda_{rel,0}$ (= 0.30), which were selected based on investigations on softwood GLT by Blaß (1987a, 1987b). For European beech (*Fagus sylvatica* L.) GLT, the ratio between compressive strength and modulus of elasticity (MOE) is about 1/250 (Ehrhart et al. 2018, Westermayr et al. 2018), whereas for softwood GLT, ratios between 1/370 and 1/420 have been reported (Blaß, 1987a). It was therefore deemed necessary to assess the applicability of the current design methods to beech GLT columns. In this paper, experimental and numerical investigations on the compressive strength parallel to the grain and buckling resistance of beech GLT columns are presented and adapted buckling curves are proposed.

2 Material and Methods

2.1 Material

Swiss-grown European beech boards were used for the production of the GLT columns. The boards were strength graded into strength classes T33 (to produce GL 40h), T42 ($\rightarrow$ GL 48h), and T50 ($\rightarrow$ GL 55h), in accordance with the strength grading rules described in Ehrhart et al. (2015). The laminations were surface bonded using a one-component polyurethane adhesive and a primer, following the findings of investigations on appropriate bonding procedures conducted by the project partners Henkel Engineered Wood Adhesives and BFH/AHB Biel (Lehmann et al., 2018). The final lamination thickness was chosen 25 mm and the wood moisture content was $\omega = 8 \pm 2\%$, which represents the climatic conditions of the primary indoor application of beech GLT.

2.2 Compression tests on stocky columns

Stocky columns, i.e., columns not prone to buckling failures, were tested in compression according to EN 408:2012 (Figure 1a), to determine the compressive strength ($f_{c,0}$) and the MOE in compression ($E_{c,0}$) parallel to the grain. The investigated GLT strength classes were GL 40h, GL 48h and GL 55h. The widths of the specimens with square cross-sections were b = 150, 200 and 280 mm, the length of the columns was $L = 6 \times b$ and thus L = 900, 1'200 and 1'680 mm (Table 1). Due to the support conditions prescribed by EN 408:2012 (loading-heads locked against rotation or angular movement during the test), a buckling length of $L_c = 0.6 \times L$ was assumed (Tetmajer, 1888), resulting in a slenderness ratio of $\lambda = 12.5$. The force was applied displacement controlled, at a constant displacement rate of 0.025 mm/s.

2.3 Buckling tests on slender columns

2.3.1 Experiments

Slender columns of strength classes GL 40h and GL 48h were tested in axial compression (Figure 1b). The width of the specimens with square cross-sections was b = 200 mm. The buckling lengths of the columns, including the specimen's length and the height of the pinned supports at both ends (Figure 1d), were $L_c = 12 \times b$ (2'400 mm) and $L_c = 18 \times b$ (3'600 mm), resulting in slenderness ratios of $\lambda = 41.5$ and $\lambda = 62.3$, respectively (Table 1). Axial displacements were measured over a length of $3 \times b = 600$ mm on all four sides of the columns. Horizontal deflections were measured by means of three displacement transducers mounted on an aluminium bar (Figure 1c). Loading was displacement controlled, at a constant displacement rate of 0.025 mm/s. The force was applied with an initial eccentricity of 6.3 ± 0.3 mm to the longitudinal axis of the columns, which corresponds to relative eccentricities of $e = 1/380$ (for $L_c = 2'400$ mm) and $e = 1/570$ (for $L_c = 3'600$ mm). For GLT columns prone to lateral instability, Eurocode 5 and SIA 265 recommend that the deviation from straightness measured midway between the supports should be limited to 1/500 times the column's length.
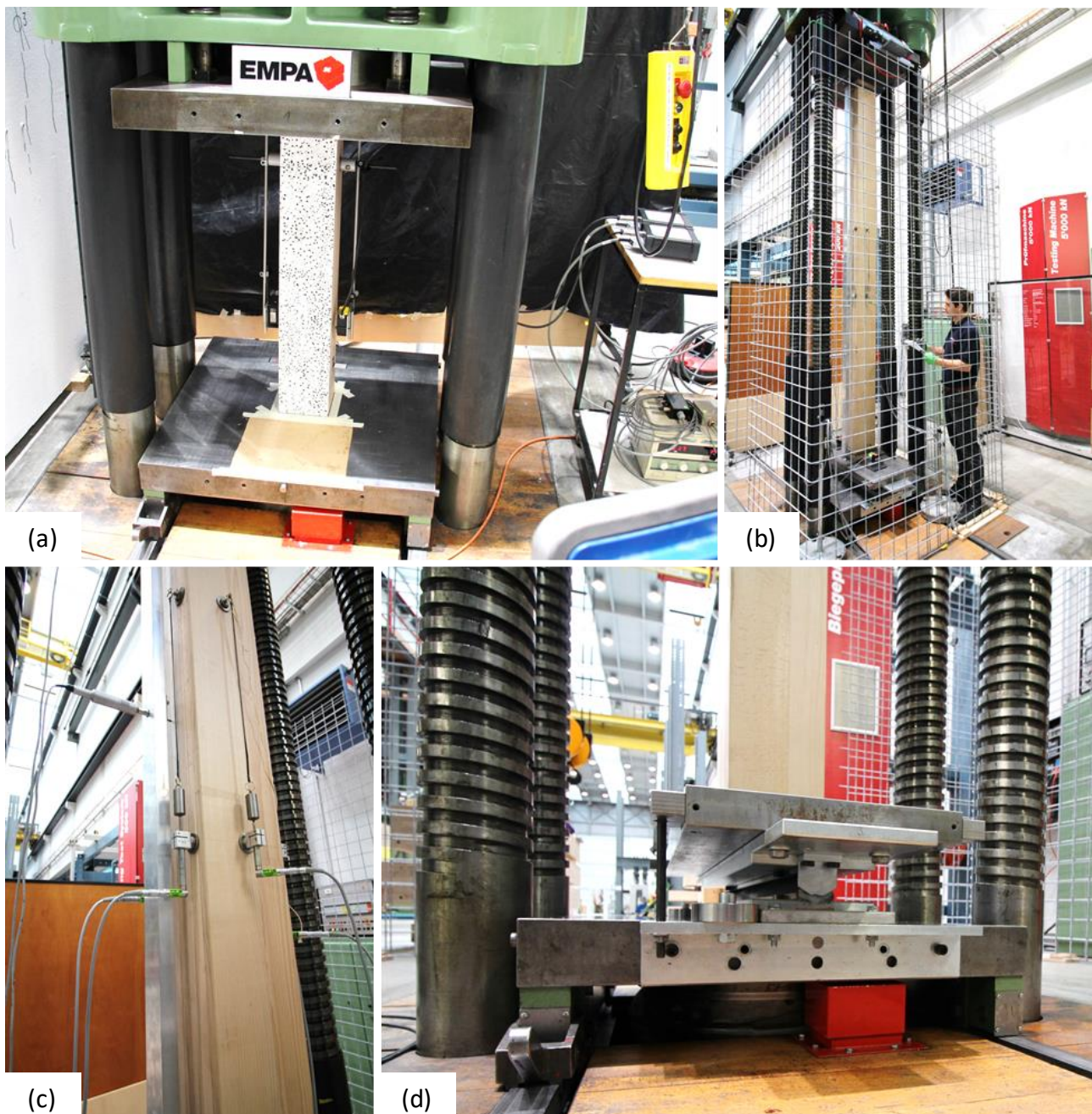
Figure 1 Compression test on a stocky column (a), buckling test on a column with a buckling length of 3'600 mm (λ = 62.3) (b), displacement sensors to measure vertical deformations in the columns (c) and uniaxial pinned support (d).

The eccentricity of the applied force was directed parallel to the glue lines, so that buckling occurs with the laminations in edgewise bending, involving a homogenisation effect and reducing the influence of weak sections in the outermost laminations.

2.3.2   Numerical simulations

Additionally to the experimental investigations, numerical simulations of the buckling resistance of beech GLT columns were conducted. Investigations by Blaß (1987a, 1987b), Theiler et al. (2012, 2014) and Frangi et al. (2015) have shown that appropriate numerical models can complement experimental tests and contribute to a better understanding of the buckling behaviour. Mentioned authors used a strain-based

model, which takes into account the constitutive model proposed by Glos (1978) for the plastic behaviour of wood in compression parallel to the grain. For the numerical simulations presented in this paper, the code developed by Theiler (2014) was adapted to consider a length-dependent eccentricity of $e = L/500$ and to use the constitutive model proposed by Glos et al. (2004) for beech wood (Equations 1-5). As mentioned before, $L/500$ corresponds to the maximum allowed deviation from straightness for GLT according to Eurocode 5. According to Glos et al. (2004), the stress-strain curve may be described by means of Equation 1.

$$\sigma = \frac{\varepsilon + k_1 \cdot \varepsilon^4}{k_2 + k_3 \cdot \varepsilon + k_4 \cdot \varepsilon^4} \tag{1}$$

The coefficients k_i are calculated using Equations 2-5, taking into account the compressive strength ($f_{c,m,0}$) and the strain at failure ($\varepsilon_{c,0}$), the asymptotic residual compressive strength ($f_{c,m,u,0}$) and the MOE in compression ($E_{c,0}$) parallel to the grain.

$$k_1 = \frac{f_{c,m,u,0}}{3 \cdot E_{c,0} \cdot \varepsilon_{c,0}{}^4 \cdot \left(1 - \frac{f_{c,m,u,0}}{f_{c,m,0}}\right)} \tag{2} \qquad k_2 = \frac{1}{E_{c,0}} \tag{3}$$

$$k_3 = \frac{1}{f_{c,m,0}} - \frac{4}{3 \cdot E_{c,0} \cdot \varepsilon_{c,0}} \tag{4} \qquad k_4 = \frac{1}{3 \cdot E_{c,0} \cdot \varepsilon_{c,0}{}^4 \cdot \left(1 - \frac{f_{c,m,u,0}}{f_{c,m,0}}\right)} \tag{5}$$

Following O'Halloran (1973), the parameter β_ε, which describes the ratio between the total strain when reaching the compression strength and the elastic strain (Equation 6), is assumed to be 1.25. The parameter β_f for the calculation of $f_{c,m,u,0}$ (Equation 7) was set to 0.85, according to Hartnack (2004).

$$\varepsilon_{c,0} = \beta_\varepsilon \cdot \frac{f_{c,m,0}}{E_{c,0}} = 1.25 \cdot \frac{f_{c,m,0}}{E_{c,0}} \tag{6} \qquad f_{c,m,u,0} = \beta_f \cdot f_{c,m,0} = 0.85 \cdot f_{c,m,0} \tag{7}$$

Beech GLT columns of strength class GL 48h, with square cross-sections ($w = 200$ mm), lamination thickness of 25 mm (i.e., 8 laminations per column), and buckling lengths of 720, 1'200, 1'800, 2'400, ..., 7'200 mm were numerically investigated. A stochastic model for the board parameters density and dynamic MOE, previously developed by the authors (Ehrhart 2019), was used to generate physically plausible laminations. The parallel to the grain compressive strength and MOE of the generated boards were estimated using Equations 8 and 9 (Ehrhart 2019). The generated boards were then combined into GLT columns (8 boards per column) with different lengths between 720 and 7'200 mm. For each column length, 100 GLT columns were generated and the same number of simulations was performed.

In the simulations presented in this paper, the strain-based model ("model 1") presented by Theiler et al. (2012, 2014) was used. In this model, the buckling mode shape of the columns is predefined and averaged material parameters of the eight laminations are used. Given that in the tests buckling occurred with the laminations in edgewise bending, this simplification is deemed to be appropriate, since there is a

homogenisation effect. The stress-strain relationship is determined based on these averaged material properties. The force-deformation behaviour of each column can be estimated using the strain-based model and the predefined buckling mode shape. The force is continuously increased and, for each load step, the equilibrium stresses in the cross-section at mid-height are computed based on the deformed shape of the column. The maximum load carrying capacity is reached when these cross-sectional stresses are no longer able to balance the internal forces induced by the applied force (Theiler, 2014). Similar approaches, where strain-based models were applied to solve the equilibrium problem in the deformed state, were used by Roš & Brunner (1931), Buchanan (1984), Blaß (1987a, 1987b) and Hörsting (2008).

3 Results and discussion

Table 1 summarises the results of the experimental compression and buckling tests. The cross-section widths (b), the specimen and buckling lengths (L, L_c), the slenderness ratios (λ) and the numbers of tests per series (n) are listed. The mean and 5%-fractile values were calculated assuming a lognormal distribution of the compressive strength and MOE, and a normal distribution of density (JCSS Probabilistic Model Code 2006).

The mean compressive strengths of the stocky columns were similar for all tested configurations, i.e., no significant influence of the strength class, the cross-sectional width, or the column length was found. The observed mean values of compressive strengths were between 58.2 MPa (GL 48h, b = 280 mm) and 65.8 MPa (GL 55h).

Table 1 Compressive strength ($f_{c,0,g}$), MOE ($E_{c,0,g}$) and density ($\rho_{\omega=8\%}$) of stocky (λ = 12.5) and slender columns (λ = 41.5 / 62.3). Information on the cross-section width (b), specimen and buckling lengths (L and L_c) and the number of tests (n) is provided (moisture content for all specimens ω = 8 ± 2%).

		Stocky columns					Slender columns			
	GL	40h	48h	48h	48h	55h	40h	48h	40h	48h
	b [mm]	200	150	200	280	200	200	200	200	200
	L [mm]	1'200	900	1'200	1'680	1'200	2'400	2'400	3'600	3'600
	L_c [mm]	720	540	720	1'008	720	2'400	2'400	3'600	3'600
	λ [-]	12.5	12.5	12.5	12.5	12.5	41.5	41.5	62.3	62.3
	n [-]	7	7	7	7	7	3	5	3	5
$f_{c,0,g}$ [MPa]	mean	60.4	59.9	63.8	58.2	65.8	43.2	45.3	28.8	30.5
	5%-fractile	59.7	56.4	62.5	55.9	63.7	-	44.2	-	29.7
	cov	0.01	0.04	0.01	0.02	0.02	-	0.01	-	0.02
$E_{c,0,g}$ [MPa]	mean	15'100	15'600	16'000	15'500	17'000	15'000	16'500	14'800	16'300
	5%-fractile	14'400	14'600	15'400	14'800	16'700	-	16'200	-	15'800
	cov	0.03	0.04	0.02	0.03	0.01	-	0.01	-	0.02
$\rho_{\omega=8\%}$ [kg/m³]	mean	693	690	712	690	708	689	728	686	722
	5%-fractile	682	664	706	674	697	-	721	-	710
	cov	0.01	0.02	0.00	0.01	0.01	-	0.01	-	0.01

Within each tested configuration, the variation of the strength values was very low, with coefficients of variation (cov) below 0.04. Taking all series into account, a marked relationship between compressive strength parallel to the grain and density was observed (Figure 2a). A respective linear regression model has a coefficient of determination $r^2 = 0.51$, which corresponds to a medium correlation (JCSS Probabilistic Model Code 2006).

The mean MOE in compression ($E_{c,0,mean}$) parallel to the grain was 15'100 MPa for strength class GL 40h, 16'000 MPa for GL 48h, and 17'000 MPa for GL 55h. These differences are attributed to the strength-grading procedure where the dynamic MOE being a very good indicator of the static MOE is a key grading parameter. As with the compressive strength, no influence of specimen length or cross-sectional area was observed in the MOE in compression. Taking all test series into account, a significant relationship between compressive strength and density was observed (Figure 2b). A respective linear regression model has a coefficient of determination $r^2 = 0.43$, which corresponds to a medium/low correlation (JCSS Probabilistic Model Code 2006).

Two linear regression models were fitted to results of tests on the stocky columns, namely compressive strength and MOE in compression, as a function of the basic parameters density (in kg/m³) and dynamic MOE (in MPa) of the boards. By including normal distributed error terms in the regression models to account for model uncertainty, Equations 8 and 9 allow obtaining estimates of the compressive strength and MOE parallel to the grain based on density and dynamic MOE ($\varepsilon_{fc,0}$: $\mu = 0$, $\sigma = 0.03$; $\varepsilon_{Ec,0}$: $\mu = 0$, $\sigma = 0.04$).

$$\ln(f_{c,0}) = 2.61 + 1.45 \cdot 10^{-3} \cdot \rho + 2.90 \cdot 10^{-5} \cdot E_{dyn} + \varepsilon_{f_{c,0}} \tag{8}$$

$$\ln(E_{c,0}) = \ln(E_{t,0}) = \ln(E_m) = 8.67 + 5.80 \cdot 10^{-5} \cdot E_{dyn} + \varepsilon_{E_{c,0}} \tag{9}$$
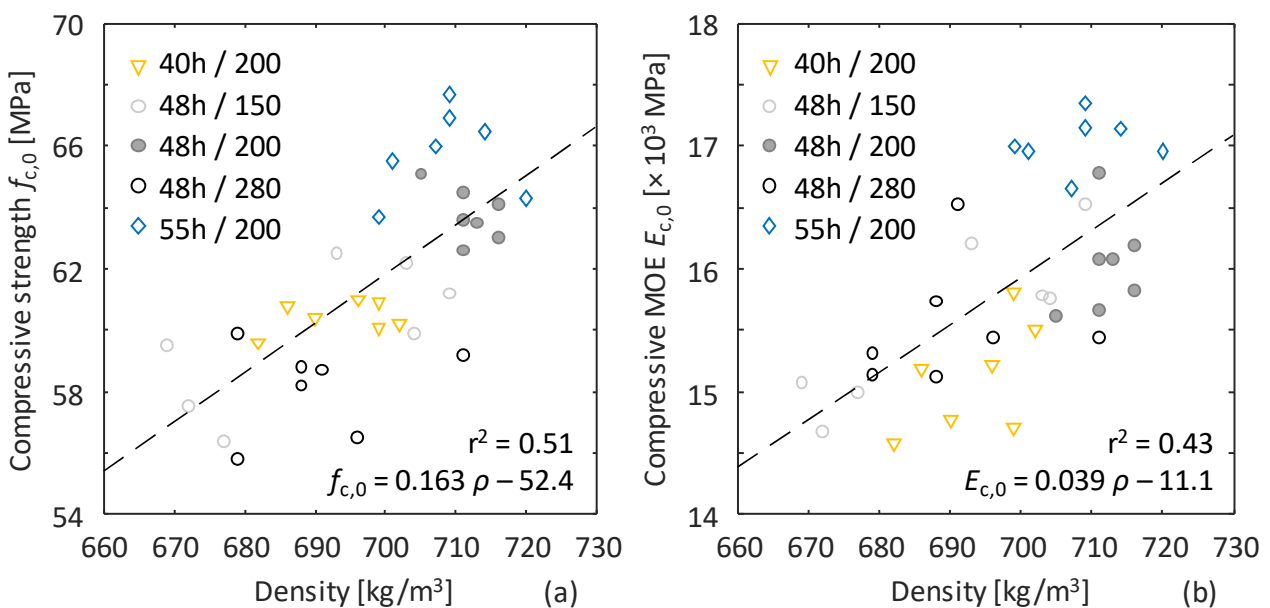
Figure 2 Compressive strength $f_{c,0}$ (a) and MOE $E_{c,0}$ versus density (b). Markers indicate the strengh class and the cross-section width. ($\omega = 8 \pm 2\%$).
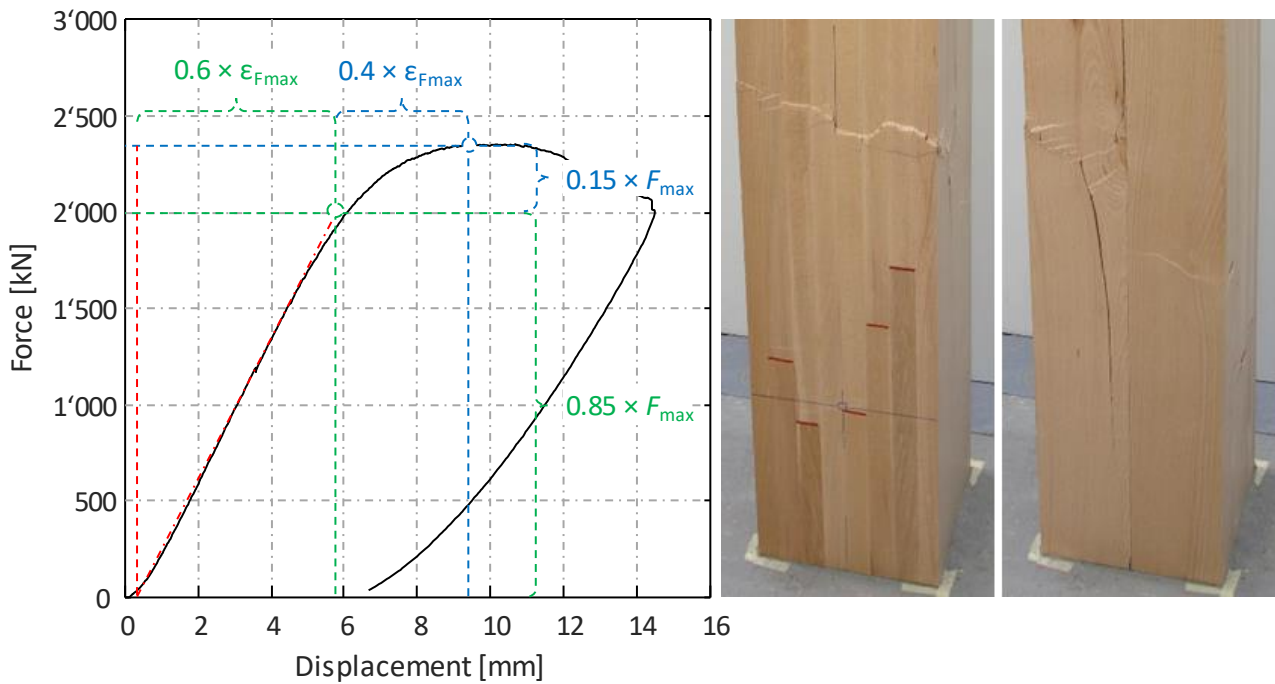
Figure 3 Force-displacement behaviour of a stocky column (GL 40h, b =200 mm, L = 1'200 mm, no. 3). After a phase of linear-elastic behaviour, local crushing of wood fibres causes plastic deformations and leads to a ductile failure behaviour.

Ductile failure behaviour was observed in the compression tests on stocky columns. The force-displacement curve was almost linear until a level of approximately 85% of the maximum force F_{max} (Figure 3). The remaining 15% of the load-carrying capacity corresponded to about 30 to 40% of the total displacement at maximum force F_{max}. Local crushing of wood fibres, frequently developing near finger joints, knots or obvious fibre deviations, contributed to this ductile failure mechanism (Figure 3).

The columns with higher slenderness ratios of $\lambda = 41.5$ ($L_c = 2'400$ mm) and $\lambda = 62.3$ ($L_c = 3'600$ mm) exhibited a significant decrease in load-carrying capacity. Compared to the overall mean compressive strength of the stocky columns of strength class GL 48h (60.1 MPa = 100%), the nominal compressive strength reached in the slender columns was only 45.3 MPa ($\lambda = 41.5$, 75.4%) and 30.5 MPa ($\lambda = 62.3$, 50.7%). For strength class GL 40h, the reduction was similar.

Figure 4 shows the longitudinal deformations measured at the centre of the "compression" (v_1 & v_2), "tension" (v_3 & v_4) and "bending" (v_5 & v_6) faces, as function of the applied force, for buckling lengths of 2'400 mm (a) and 3'600 mm (b). These longitudinal deformations were measured at mid-height of the columns over lengths of 600 mm. The initial behaviour is linear elastic. When the applied force was approaching the buckling force, the less slender columns (buckling length of 2'400 mm) did not exhibit elongations on the tension side (Figure 4a), which shows that the entire cross-section was subjected to compression stresses (Figure 5a). With the more slender columns (buckling length of 3'600 mm), elongations did appear on the tension side shortly before the buckling force was reached (Figure 4b), letting conclude that tensile stresses were present in parts of the column's cross-section (Figure 5b).
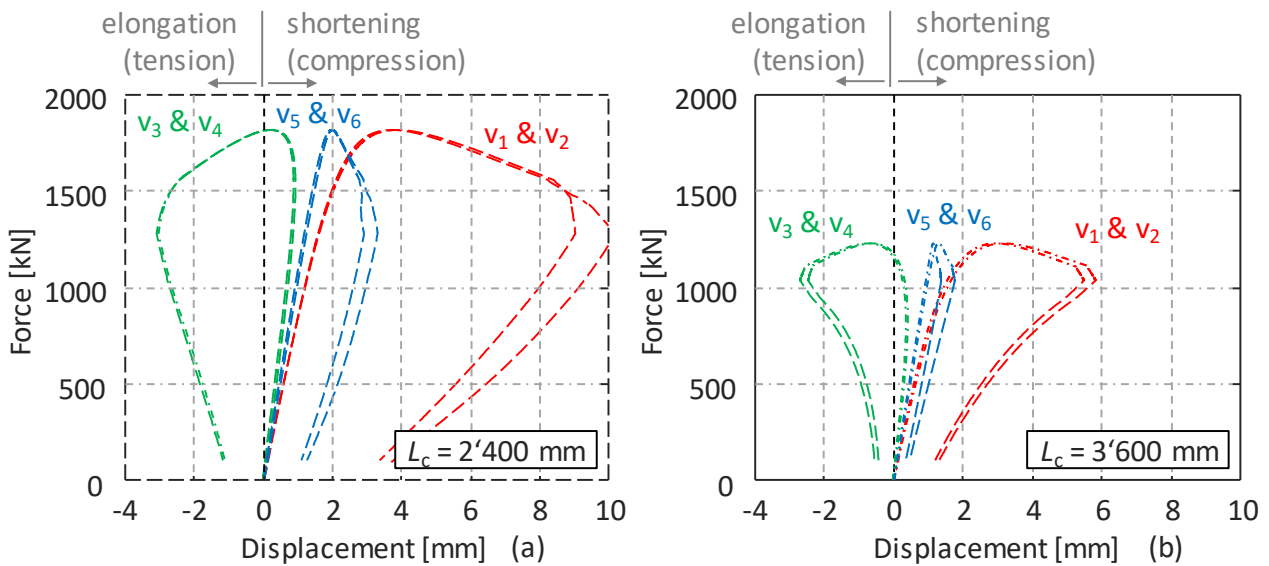
Figure 4 Typical force-displacement curves for buckling tests on columns with buckling lengths of 2'400 mm (a) and 3'600 mm (b). The displacements were measured over a length of 600 mm at mid-height of the column on the compression (v_1 & v_2), tension (v_3 & v_4) and bending sides (v_5 & v_6).

The average strain recorded on the compression side at the level of maximum (buckling) force was 6.21 ‰ for buckling length 2'400 mm (Figure 5a) and 5.16 ‰ for buckling length 3'600 mm (Figure 5b).
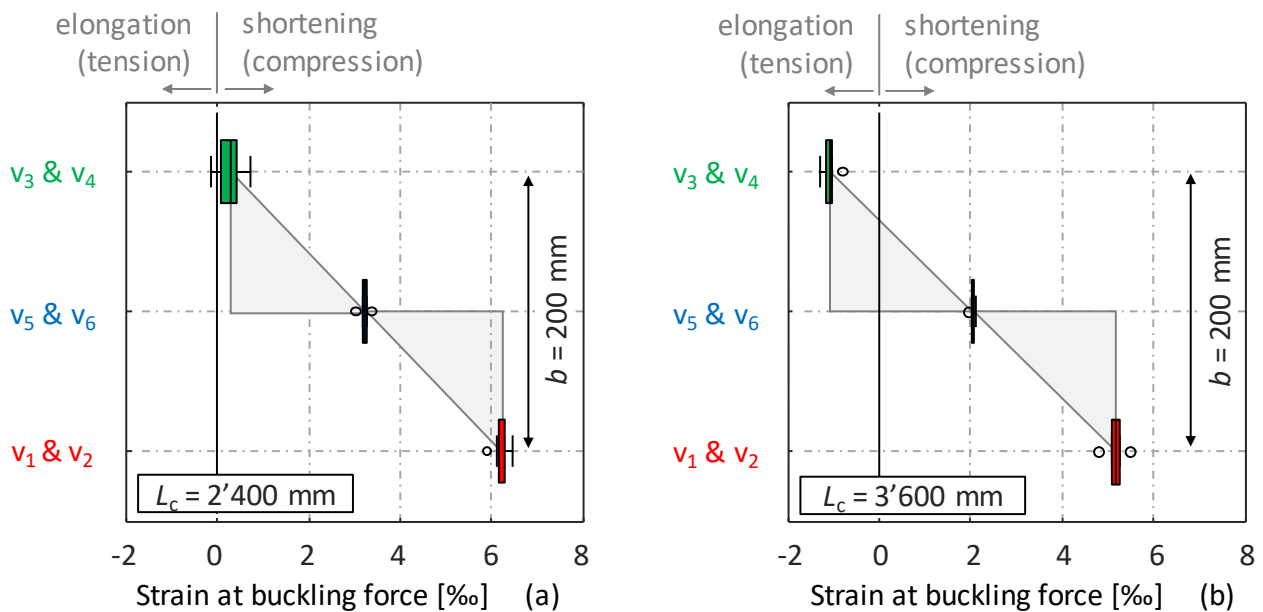
Figure 5 Boxplots of strains (in ‰) on the compression (v_1, v_2), tension (v_3, v_4) and bending surfaces (v_5, v_6) at the buckling force. In the columns with a buckling length of 2'400 mm (a), shortening was observed in the whole cross-section ($\varepsilon_i \geq 0$) at the buckling force, showing that only compressive stresses are present. In the columns with a buckling length of 3'600 mm (b), elongation was observed on the tensile side, showing that tensile stresses occured in parts of the cross-section.

The compressive strengths of the stocky columns ($\lambda = 12.5$) and the nominal compressive strengths of the slender columns ($\lambda = 41.5$ and 62.3) are depicted in Figure 6 (black triangles). The results of the simulations on the generated columns (see Section 2.3.2) are also graphed in Figure 6 (grey crosses).

254
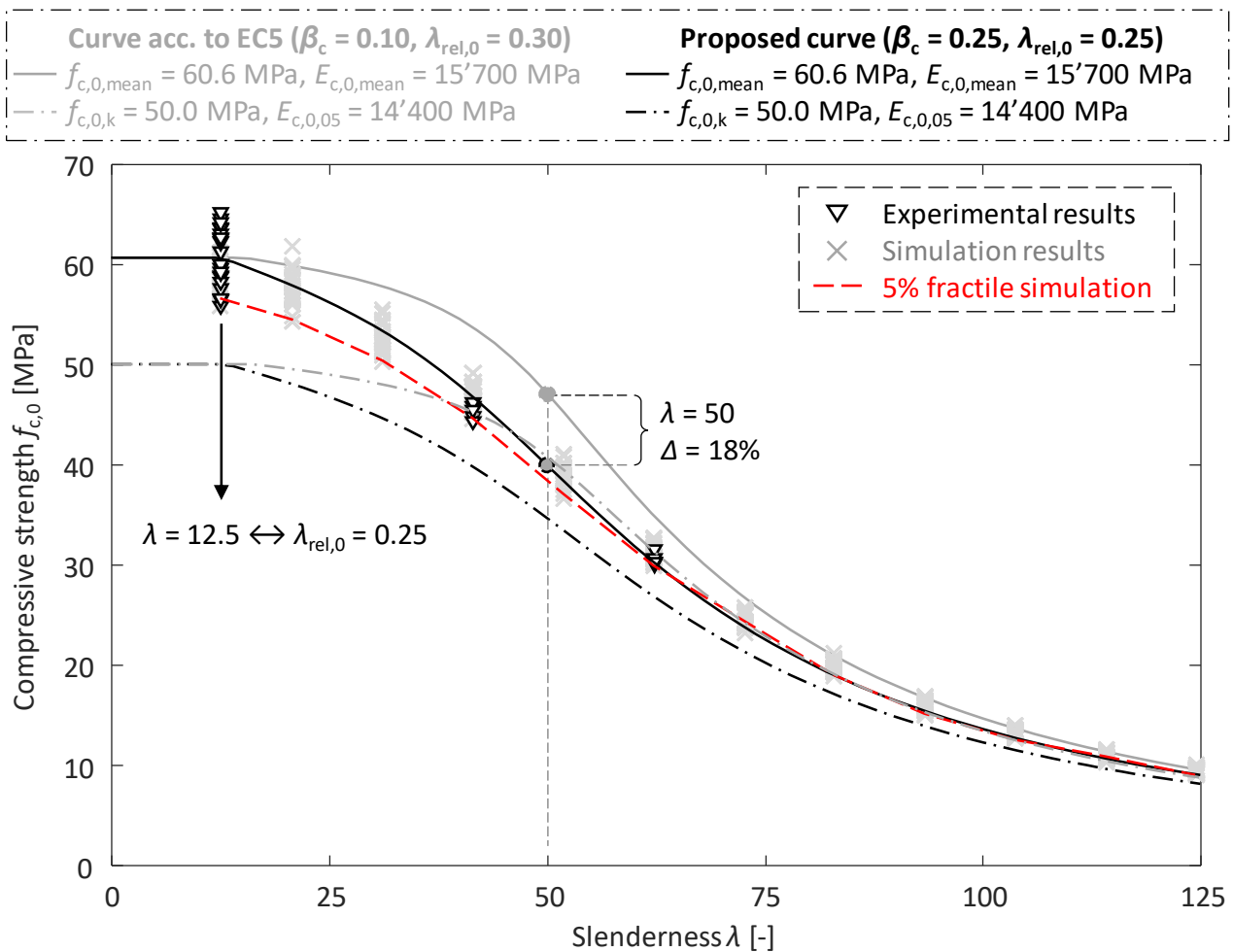
Figure 6 Experimental and simulated compressive strengths for columns of strength class GL 48h and different slenderness ratios λ. Designing according to Eurocode 5 (β_c = 0.10, $\lambda_{rel,0}$ = 0.30) leads to an overestimation of the compressive strength by up to 18%. A better fit with the experimental and simulation results can be reached by changing the parameters to β_c = 0.25 and $\lambda_{rel,0}$ = 0.25.

The compressive strengths obtained from the simulations agree well with the experimental data. For λ = 12.5, the simulation results lead to values 2% lower than the experimental results on average. For the slenderness ratios λ = 41.5 and λ = 62.3, the simulation results are 3% and 2% higher than the experimental results on average. The differences for λ = 41.5 can partly be attributed to the larger eccentricity in the experimental tests (e = L/380) compared to the simulations (e = L/500).

The Eurocode 5 design approach used for the verification of the stability of columns under compression is described by the Equations 10-13. The instability factor (or buckling coefficient) k_c is calculated based on the relative slenderness ratio λ_{rel} and the factor k, which is a function of the critical relative slenderness ratio $\lambda_{rel,0}$ and the straightness factor β_c. The critical relative slenderness represents the slenderness level above which buckling has to be considered in design. The straightness factor describes the slope of the buckling curve after that point. The values $\lambda_{rel,0}$ = 0.3 and β_c =0.1 (for GLT) adopted in Eurocode 5 are based on investigations on softwood GLT by Blaß (1987a, 1987b). However, in the case of beech GLT, these values lead to unsafe estimates of the buckling resistance of columns (Figure 6). If the mean values for

compressive strength and MOE parallel to the grain experimentally determined for GL 48h ($f_{c,0,mean}$ = 60.6 MPa, $E_{c,0,mean}$ = 15'700 MPa) are used in Equation 13, which is appropriate for comparison with test results, the curve according to Eurocode 5 overestimates the (mean) experimental and simulation results by up to 18% (Figure 6). Even when using the 5%-fractile value for the MOE $E_{c,0,05}$ = 14'400 MPa and the rather conservative 5%-fractile value for compressive strength $f_{c,0,k}$ = 50.0 MPa, determined by Ehrhart (2019) (Table 2), the curve according to Eurocode 5 overestimates the mean experimental and simulation results for slenderness ratios $\lambda \geq 45$ (Figure 6).

$$\sigma_{c,0,d} \leq k_c \cdot f_{c,0,d} \qquad (10)$$

$$k_c = \frac{1}{k + \sqrt{k^2 - \lambda_{rel}^2}} \qquad (11)$$

$$k = 0.5 \cdot \left[1 + \beta_c \cdot \left(\lambda_{rel} - \lambda_{rel,0}\right) + \lambda_{rel}^2\right] \qquad (12)$$

$$\lambda_{rel} = \frac{\lambda}{\pi} \cdot \sqrt{\frac{f_{c,0,k}}{E_{0,05}}} \qquad (13)$$

As mentioned before, the parameters β_c and $\lambda_{rel,0}$ were calibrated based on investigations on softwood and, thus, to strength/stiffness ratios between 1/370 and 1/420 (Blaß, 1987a). In our experiments, however, a strength/stiffness ratio of about 1/250 was found for beech GLT, which agrees well with the ratios calculated from the results presented by Westermayr et al. (2018). Therefore, the parameters β_c and $\lambda_{rel,0}$ must be adapted when applying the Eurocode 5 design rules to beech GLT columns.

Taking into account that the test specimen for determining the compressive strength in accordance with EN 408:2012 has a slenderness of $\lambda = (0.6 \times 6 \times b) / (0.289 \times b)$ and that $f_{c,0} / E_{c,0} = 1/250$ for beech GLT, a critical relative slenderness ratio $\lambda_{rel,0} = 0.25$ is obtained (Equation 13). Buckling phenomena below this threshold are therefore included in the compressive strength determined in accordance with the standard EN 408:2012, which justifies a sharp bend in the buckling curve.

The imperfection coefficient β_c, which describes the slope of the buckling curve, was calibrated based on the experimental and simulation results. Assuming $\beta_c = 0.25$ leads to a buckling curve that fits well to the mean values of the experimental and simulation results (Figure 6).

If the 5%-fractile values of $f_{c,0}$ and E_0 determined by Ehrhart (2019) (Table 2) are used with the proposed $\lambda_{rel,0}$ and β_c parameters, the effective-length method of Eurocode 5 can be safely used to verify the stability of beech GLT columns of strength classes GL 40h, GL 48h and GL 55h subjected to axial compression.

Table 2 Compressive strength and MOE in compression parallel to the grain of beech GLT determined by Ehrhart (2019) for strength classes GL 40h, GL 48h and GL 55h.

Property	Symbol	Unit	GL 40h	GL 48h	GL 55h
Compression strength	$f_{c,0,g,k}$	MPa	45.0	50.0	55.0
Modulus of elasticity	$E_{c,0,g,mean}$	MPa	14'200	15'400	16'600
	$E_{c,0,g,05}$	MPa	13'200	14'400	15'600

4   Conclusions

The current Eurocode 5 design rules for verifying the stability of columns subjected to axial compression, based on the effective-length method, do not allow to accurately predict the buckling resistance of GLT columns made of European beech (*Fagus sylvatica* L.) wood. Full scale experiments on columns with lengths of 2'400 mm ($\lambda = 41.5$) and 3'600 mm ($\lambda = 62.3$) accompanied by numerical investigations have shown that the parameters $\lambda_{rel,0} = 0.30$ and $\beta_c = 0.10$ currently specified in Eurocode 5 for GLT lead to an overestimation of the compressive strength of up to 18% in case of beech GLT columns.

On the one hand, these differences are due to the different ratios between compressive strength and MOE parallel to the grain between softwood GLT and beech GLT. While ratios of $f_{c,0} / E_{c,0}$ between 1/370 and 1/420 are reported for softwood GLT (Blaß 1987a), ratios of about $f_{c,0} / E_{c,0} = 1/250$ have been found for beech GLT (Ehrhart et al. 2018, Westermayr et al. 2018). Since the values of $\lambda_{rel,0}$ and β_c adopted in Eurocode 5 are based on research on softwood, disparities between the Eurocode 5 predictions and the experimental results for beech GLT had to be expected. For the verification of beech GLT columns subjected to axial compression, a critical relative slenderness ratio $\lambda_{rel,0} = 0.25$ and a straightness factor $\beta_c = 0.25$ are proposed, instead of the current values in Eurocode 5 ($\lambda_{rel,0} = 0.30$; $\beta_c = 0.10$). The parameter $\lambda_{rel,0}$ defines the level of relative slenderness above which buckling has to be considered in the design and the proposed value results from the geometrical requirements in the test standard EN 408:2012. The proposed imperfection coefficient $\beta_c = 0.25$ was chosen with this particular value because it leads to the best fit with the experimental and numerical results.

On the other hand, the more conservative values proposed in this paper for European beech GLT are due to the differences regarding the assumptions related to relevant material properties and imperfections. The buckling resistance of columns is predominantly influenced by (i) the compressive strength, (ii) the MOE parallel to the grain, and (iii) the structural and geometrical imperfections. The design buckling curves proposed in this paper for European beech GLT columns represent the buckling behaviour of columns with (i) 5%-fractile values of compressive strength, (ii) 5%-fractile values of MOE (both determined according to EN 408), and (iii) a geometrical imperfection of $e = L/500$ as specified in Eurocode 5 and the Swiss standard SIA 265 to be the maximum geometrical imperfection permitted. In contrast, the buckling curves in Eurocode 5 represent the 5%-fractile value of the buckling resistance, i.e., the columns either have a low compressive strength, a low MOE parallel to the grain, or an imperfection close to the maximum limit $e = L/500$. The eccentricities used in the simulations by Blaß (1987a) were predominantly markedly below the maximum limit of $L/500$ defined in Eurocode 5 and SIA 265 (approximately 66% of the simulated columns had eccentricities of $e \leq L/2000$ and approximately 95% had eccentricities of

$e \leq L/1000$). When developing the buckling curves, the imperfections used as input data for the numerical simulations by Blaß (1987a) had been assessed by measuring eccentricities of columns in building practice. In any case, the determination of buckling design curves for softwood and beech GLT should be based on the same assumptions, especially regarding the imperfections considered.

5 Acknowledgements

6 References

Blaß, HJ (1987a): Tragfähigkeit von Druckstäben aus Brettschichtholz unter Berücksichtigung streuender Einflussgrössen. Dissertation, Universität Fridericiana Karlsruhe, Karlsruhe, Germany.

Blaß, HJ (1987b): Design of Timber Columns. Paper 20-2-2. CIB - Meeting Twenty. Dublin, Ireland.

Buchanan, A (1984): Strength model and design methods for bending and axial load interaction in timber members. Dissertation, University of British Columbia, Vancouver, Canada.

Ehrhart, T; Fink, G; Steiger, R; Frangi, A (2015): Strength grading of European beech lamellas for the production of GLT and CLT. Paper 49-5-1. INTER − Meeting Forty-Nine. Graz, Austria, pp. 29-43.

Ehrhart, T; Steiger, R; Palma, P; Frangi, A (2018): Mechanical properties of European beech (*Fagus sylvatica* L.) glued laminated timber. Paper 51-12-4. INTER − Meeting Fifty-One. Tallinn, Estonia, pp. 343–360.

Ehrhart, T (2019): European beech glued laminated timber. Dissertation, ETH Zurich, Zurich, Switzerland.

EN 408:2012. Timber structures - Structural timber and glued laminated timber - Determination of some physical and mechanical properties. CEN European Committee for Standardization.

EN 1993-1-1:2010: Design of steel structures - Part 1-1: General rules and rules for buildings. CEN European Committee for Standardization.

EN 1995-1-1:2010: Design of timber structures - Part 1-1: General - Common rules and rules for buildings. CEN European Committee for Standardization.

Frühwald, K; Schickhofer, G (2004): Strength grading of hardwoods; World Conference on Timber Engineering 2004. Lahti, Finland.

Glos, P (1978): Zur Bestimmung des Festigkeitsverhaltens von Brettschichtholz bei Druckbeanspruchung aus Werkstoff- und Einwirkungsgrössen. Dissertation, TU Munich, Munich, Germany.

Glos, P; Denzler, JK; Linsenmann, P (2004): Strength and stiffness behaviour of beech laminations for high strength glulam. Paper 37-6-3. CIB - Meeting Thirty-Seven. Edinburgh, Scotland.

Hartnack, R (2004): Langzeitverhalten von druckbeanspruchten Bauteilen aus Holz. Dissertation, Bauhaus-Universität Weimar, Weimar, Germany.

Hörsting, OP (2008): Zum Tragverhalten druck- und biegebeanspruchter Holzbauteile. Dissertation, TU Braunschweig, Braunschweig, Germany.

JCSS Probabilistic Model Code (2006): Part 3 – Resistance Models. ISBN 978-3-909386-79-6.

Lehmann, M; Clerc, G; Lehringer, C; Strahm, T; Volkmer, T (2018): Investigation of the bond quality and the finger joint strength of beech glulam. World Conference on Timber Engineering 2018. Seoul, Republic of Korea.

O'Halloran, MR (1973): Curvilinear stress-strain relationship for wood in compression. Dissertation, Colorado State University, Fort Collins, US.

Roš, M; Brunner, J (1931): Die Knickfestigkeit der Bauhölzer. Kongress des internationalen Verbandes für Materialprüfung. Zürich, Switzerland.

SIA 265:2012: Timber Structures. Schweizerischer Ingenieur- und Architektenverein.

Tetmajer, L von (1888): Zur Frage der Knickfestigkeit der Bauhölzer. Schweizerische Bauzeitung, Vol. 17(11/12), pp. 110–113.

Theiler, M; Frangi, A; Steiger, R (2012): Design of timber columns based on 2nd order structural analysis. Paper 45-2-1. CIB – Meeting Forty Five. Växjö, Sweden, pp. 81–96.

Theiler, M (2014): Stabilität von axial auf Druck beanspruchten Bauteilen aus Vollholz und Brettschichtholz. Dissertation, ETH Zurich, Zurich, Switzerland.

Frangi, A; Theiler, M; Steiger, R (2015): Design of timber members subjected to axial compression or combined axial compression and bending based on 2nd order theory. Paper 48-2-2. CIB – Meeting Forty Eight. Šibenik, Croatia, pp. 45–60.

Westermayr, M; Stapel, P; Van de Kuilen, JWG (2018): Tensile and compression strength of small cross-section beech glulam members. Paper 51-12-2. INTER – Meeting Fifty-One. Tallinn, Estonia, pp. 307–322.

Discussion

The paper was presented by T Ehrhart

H Blass stated that he has no preference of including eccentricity explicitly in buckling curves or just giving guidance that designers should consider eccentricity in design. T Ehrhart responded since we never have zero eccentricity, we should include some considerations in standard.

S Winter discussed second order analysis and mentioned that eccentricity of L/400 included geometric and structural imperfection. Also production process can lead to geometric imperfection. How to distinguish and include both is difficult. Furthermore EC5 is only an execution rule. In tests you need to measure the real deviations and then add the additional eccentricities. T Ehrhart responded that curvatures were measured and load application was the only way. 2/3 of the members had L/2000 deviation.

H Blass commented that in his work he did not have any structural eccentricity but the code considered eccentricity via simulations.

S Winter commented that proposal for a code would need buckling results from other buckling directions also. T Ehrhart said that this was done via simulations. S Winter said you would not be able to consider structural imperfections in simulations. A Frangi said that the code is allowing this level of eccentricity in production. H Blass said that this is only a limit but this limit is not observed in production. A Frangi felt that one should still consider this eccentricity level in simulations. P Dietsch said that changes of moisture content could also lead to additional eccentricity.

H Blass commented that in real structures you never have hinged supports; hence, there would be inherent safety.

M Westermayr added beech column tests were also conducted at TUM with consideration of both buckling directions and that they did not see an influence of buckling direction.

H Daneshvar commented that in practice we do not have columns but beam-columns. He questioned what type of failure modes were observed. T Ehrhart responded that at ultimate load compression failure were observed first.

Cross laminated timber at in-plane shear loading – Comparison of model predictions

Henrik Danielsson, Division of Structural Mechanics, Lund University, Sweden

Erik Serrano, Division of Structural Mechanics, Lund University, Sweden

Keywords: Cross laminated timber, CLT, in-plane shear, FM III, models, FE-analysis

1 Background, aim and objectives

The mechanical behaviour and the stress distribution between layers and laminations of cross laminated timber (CLT) at in-plane shear loading is complex, due to the composition of orthogonally oriented layers of laminations. The load-bearing capacity is governed not only by the gross cross section dimensions, the strength of the laminations and the strength of the glue-lines, but also by the element lay-up and the dimensions of the individual laminations as discussed by e.g. Flaig & Blass (2013), Brandner et al. (2017) and Danielsson et al. (2017).

Three failure modes (FM) are in general considered in design for CLT at in-plane shear loading (see Figure 1.1): gross shear failure (FM I), net shear failure (FM II) and shear failure in the crossing areas (FM III).
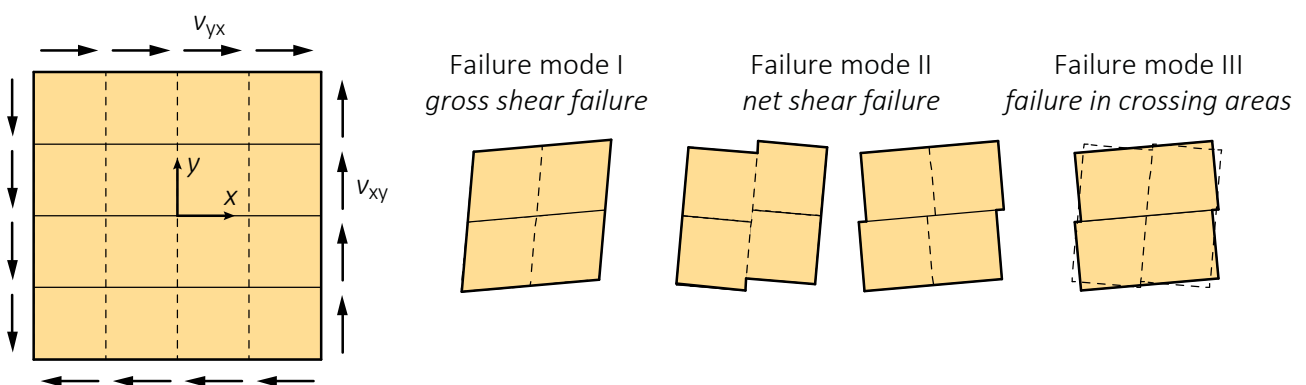
Figure 1.1. Illustration of CLT at in-plane shear loading and failure modes I, II and III.

FM I relates to full interaction between the laminations, commonly relevant only for edge-bonded CLT. FM II relates to failure in either the longitudinal or the transversal layers, along a failure plane at a gap between un-bonded laminations oriented in the orthogonal direction. FM III relates to the torsional moments and shear stresses acting in the crossing areas between orthogonally bonded laminations of adjacent layers, involving shear stress components τ_{zx} and τ_{zy}.

Models for stress and strength analysis found in the research literature and in contemporary design codes and handbooks differ in several aspects regarding FM II and III. The differences relate for example to assumptions regarding distributions of lamination cross sectional forces and stresses in the element thickness (z) direction, yielding significantly differing predictions of design-relevant maximum stresses.

The aim of the paper is to compare and discuss models for stress analysis and for calculation of load-bearing capacity for in-plane shear loading of CLT. Stress and force distributions according to analytical models found in the literature and according to 3D finite element (FE) models are compared. The comparison is focused on the influence of the element lay-up and the individual layer thicknesses on the stress and force distributions relevant for design with respect to FM III – shear failure in the crossing areas.

2   Analytical models for in-plane shear FM III

The models considered for comparison include the so-called Representative Volume Sub-Element (RVSE) approach according to Bogensperger et al. (2010), the approach stated by Wallner-Novak et al. (2013) and the approach stated in ÖNORM B 1995-1-1/ A:2018-11 (2018). The latter approach is also included in the working draft of design of cross laminated timber for Eurocode 5 (2018). The model proposed by Danielsson & Serrano (2018), Jeleč et al. (2018) and Danielsson et al. (2019), originally derived for CLT at in-plane beam loading conditions, is also considered for comparison purposes.

The comparison considers CLT elements composed of three layers (CLT 3s) and five layers (CLT 5s), with geometry and load parameters according to Figure 2.1. The elements are loaded in pure shear, by in-plane shear flows $v_{xy} = v_{yx}$ [N/m]. CLT elements without edge-bonding and with symmetric lay-up in the element thickness (z) direction are considered. Since elements without edge-bonding are considered, all narrow faces of the laminations are traction-free. The elements are composed of longitudinal laminations of width b_x and transversal laminations of width b_y. The individual layer thicknesses are denoted $t_{x,k}$ and $t_{y,k}$, where index k refers to the position of the longitudinal and transversal layers in the element thickness (z) direction. The total number of crossing areas in the element width direction is denoted n_{CA}, i.e. $n_{CA} = 2$ for CLT 3s and $n_{CA} = 4$ for CLT 5s. The number of crossing areas that a longitudinal lamination k shares with adjacent transversal laminations is denoted $n_{CA,k}$, i.e. $n_{CA,k} = 1$ for external layers and $n_{CA,k} = 2$ for internal layers.
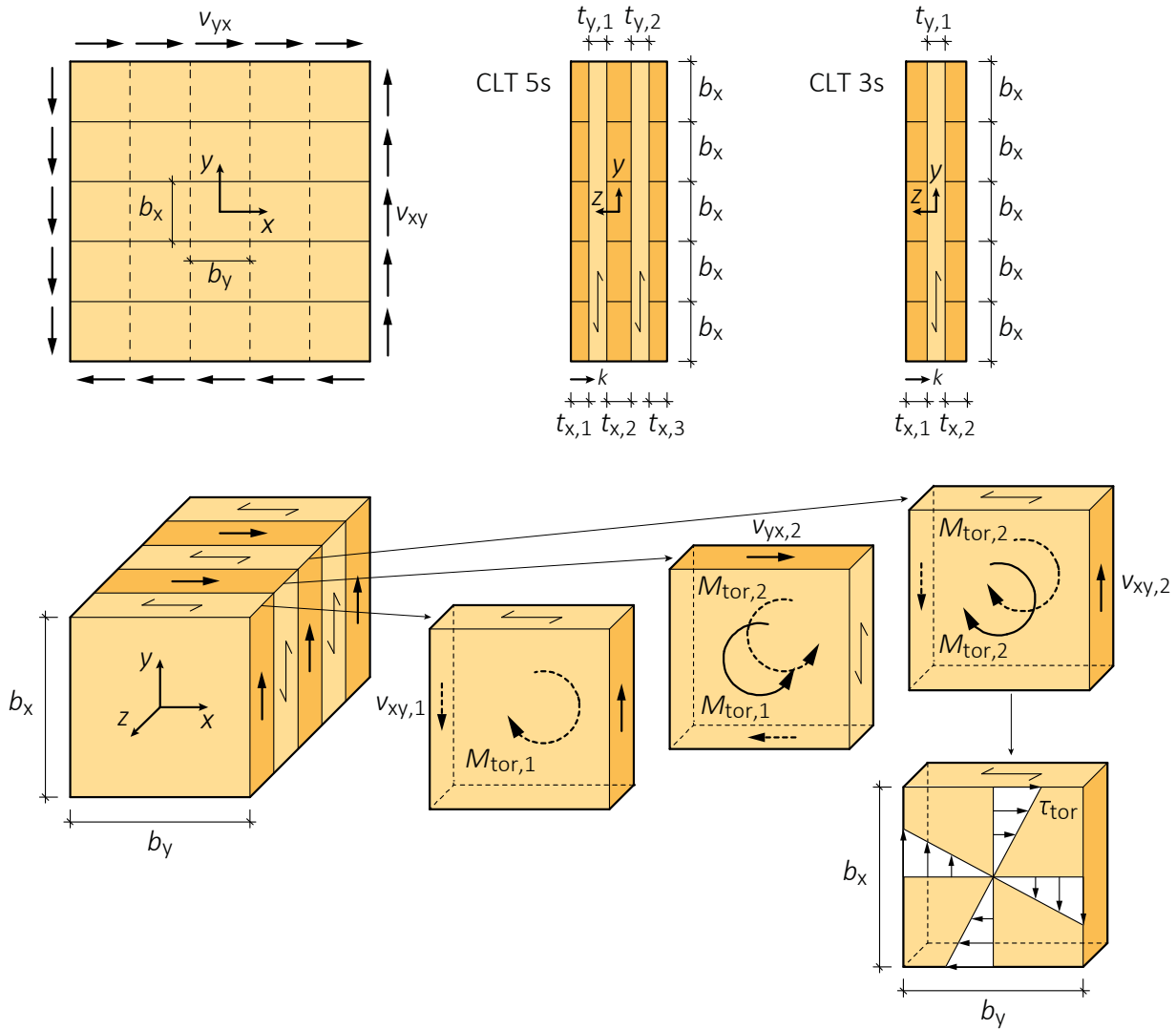
Figure 2.1. Definitions of geometry and load parameters.

For CLT without edge-bonding, the shear flows $v_{xy,k}$ and $v_{yx,k}$ acting in the individual longitudinal and transversal laminations, respectively, must be balanced by torsional moments M_{tor} acting in the crossing areas between adjacent and orthogonally bonded laminations. In the models for stress analysis considered here, these torsional moments are assumed to give rise to torsional shear stresses τ_{tor} in the crossing areas with a stress distribution according to that due to rigid body rotation over a shear compliant medium and considering the polar moment of inertia, see Figure 2.1. The maximum shear stress at the midpoints of the four sides of the crossing area is then given by

$$\tau_{tor} = \frac{M_{tor}}{I_{P,CA}} \frac{b_{max}}{2} \tag{1}$$

where

$$I_{P,CA} = \frac{b_x b_y}{12}\left(b_x^2 + b_y^2\right) \tag{2}$$

and where $b_{max} = \max(b_x, b_y)$. For equal longitudinal and transversal lamination widths, i.e. $b_x = b_y = b$, Equation (1) can be expressed as

$$\tau_{tor} = \frac{3\,M_{tor}}{b^3} \tag{3}$$

For verification of load-bearing capacity, the torsional shear stress should fulfil the criterion $\tau_{tor} < f_{tor,node}$, where $f_{tor,node}$ is a torsional shear strength parameter determined from tests of single crossing areas and making use of Equation (1). For further discussions about the failure criterion and compilation of test results, see e.g. Brandner et al. (2017), Danielsson et al. (2017), Serrano (2018) and Jeleč et al. (2019). Tests results for single crossing areas and failure criteria for shear failure mode III for CLT at in-plane beam loading conditions are further discussed by e.g. Flaig & Blass (2013).

The equations for calculation of design-relevant torsional shear stresses τ_{tor} according to the four different models mentioned above are reviewed in Sections 2.1 – 2.4. Note that slight reformulations of the original equations are introduced to increase consistency in the notation and to facilitate the comparison of the models.

2.1 Model A

The Representative Volume Sub-Element (RVSE) approach, as presented by Bogensperger et al. (2010), is based on consideration of a theoretically infinitely thick CLT element with layers of equal thickness. Subsequent adjustments are then introduced to account for the lay-up of real CLT elements with an odd number of layers and different layer thicknesses. The approach considers a series of so called ideal RVSEs with thicknesses according to Table 2.1.

The maximum torsional shear stress at in-plane shear loading is according to the RVSE-approach given by

$$\tau_{tor} = \frac{3 \, v_{xy}}{b} \frac{\max(t_j^*)}{\Sigma t_j^*} \tag{4}$$

where $\max(t_j^*)$ represents the maximum RVSE thickness and $\sum t_j^*$ represents the sum of the RVSE thicknesses according to Table 2.1.

Table 2.1. Thicknesses t_j^* of ideal RVSEs.

# RVSE	CLT 3s	CLT 5s	CLT 7s
1	$\min(2t_{x,1}, t_{y,1})$	$\min(2t_{x,1}, t_{y,1})$	$\min(2t_{x,1}, t_{y,1})$
2	$\min(t_{y,1}, 2t_{x,2})$	$\min(t_{y,1}, t_{x,2})$	$\min(t_{y,1}, t_{x,2})$
3	-	$\min(t_{x,2}, t_{y,2})$	$\min(t_{x,2}, t_{y,2})$
4	-	$\min(t_{y,2}, 2t_{x,3})$	$\min(t_{y,2}, t_{x,3})$
5	-	-	$\min(t_{x,3}, t_{y,3})$
6	-	-	$\min(t_{y,3}, 2t_{x,4})$

2.2 Model B

According to the Austrian design handbook by Wallner-Novak et al. (2013), the maximum torsional shear stress at in-plane shear loading can be calculated as

$$\tau_{tor} = \frac{3 \, v_{xy}}{b} \frac{1}{n_{CA}} \tag{5}$$

where n_{CA} is the total number of crossing areas in the element width (z) direction.

2.3 Model C

The design-relevant torsional shear stress at in-plane shear loading should according to ÖNORM B 1995-1-1/A:2018-11 be determined according to

$$\tau_{tor} = \frac{3}{2} \frac{v_{xy}}{b} \frac{t_{max}}{\min(t_x, t_y)} \tag{6}$$

where t_{max} refers to the maximum individual layer thickness and where $t_x = \sum t_{x,k}$ and $t_y = \sum t_{y,k}$ are the total longitudinal layer thickness and the total transversal layer thickness (the net cross section thicknesses), respectively. The lamination width b should be taken as the mean lamination width and may be assigned the value 80 mm if no further information is available.

Design with respect to in-plane shear is included in the draft version of design of cross laminated timber for a revised version of Eurocode 5 (CEN/TC 250/SC5, 2018). The text and the equations regarding the design-relevant torsional shear stress in that draft version is by the authors of this paper interpreted as being identical to Equation (6).

2.4 Model D

Derivation of crossing area torsional moments and torsional shear stresses can be made by equilibrium considerations of short parts of individual laminations, see e.g. Danielsson & Serrano (2018), Danielsson et al. (2019) and Andreolli et al. (2012). At sections corresponding to gaps between laminations (considering CLT without edge-bonding), the shear flow must be carried by the layers oriented in the direction perpendicular to these sections, see Figure 2.1. At these sections, the distribution of the total shear flow $v_{xy} = v_{yx}$ between the individual longitudinal and transversal layers may be assumed according to

$$v_{xy,k} = \beta_{x,k} v_{xy} \tag{7}$$

$$v_{yx,k} = \beta_{y,k} v_{yx} \tag{8}$$

where $\beta_{x,k}$ and $\beta_{y,k}$ are dimensionless weighting factors for the longitudinal and transversal layers, respectively. The weighting factors may be chosen based on the individual layer thicknesses according to

$$\beta_{x,k} = \frac{t_{x,k}}{t_x} \tag{9}$$

$$\beta_{y,k} = \frac{t_{y,k}}{t_y} \tag{10}$$

where index k refers to the position of the individual longitudinal and transversal layers in the element width (z) direction and where $t_x = \sum t_{x,k}$ and $t_y = \sum t_{y,k}$.

Weighting factors for the transversal layers of symmetric CLT 5s should (due to symmetry) be $\beta_{y,1} = \beta_{y,2} = 0.5$. Weighting factors for symmetric CLT 3s should also (due to symmetry) be $\beta_{x,1} = \beta_{x,2} = 0.5$ and $\beta_{y,1} = 1.0$. For comparison of model predictions in Section 4, weighting factors according to Equations (9) and (10) are referred to as Model D1.

Based on adjustment to results from FE-analyses of CLT 5s exposed to in-plane beam loading conditions, weighting factors according to

$$
\beta_{x,k} = \begin{cases} \dfrac{1}{8}\left(1+4\dfrac{t_{x,k}}{t_x}\right) & \text{for } k = 1, 3 \\[2ex] \dfrac{1}{4}\left(1+2\dfrac{t_{x,k}}{t_x}\right) & \text{for } k = 2 \end{cases}
\tag{11}
$$

are presented by Jeleč et al. (2018) and Danielsson et al. (2019). For comparison of model predictions in Section 4, weighting factors $\beta_{x,k}$ according to Equation (11) are referred to as Model D2.

Using Equation (7) for the shear flow in the individual longitudinal layers, $v_{xy,k}$, the torsional moments $M_{tor,k}$ for CLT 3s and 5s can be determined from equilibrium considerations as

$$
M_{tor,k} = v_{xy}\, b^2\, \frac{1}{n_{CA,k}}\, \beta_{x,k}
\tag{12}
$$

and the torsional shear stress is then according to Equation (3) found as

$$
\tau_{tor,k} = \frac{3\, v_{xy}}{b}\, \frac{1}{n_{CA,k}}\, \beta_{x,k}
\tag{13}
$$

where index k refers to the position of the longitudinal layers in the element width (z) direction, see Figure 2.1. The maximum torsional shear stress according to Equation (13) is found for the crossing area/areas of the longitudinal lamination/laminations having the highest ratio $\beta_{x,k}/n_{CA,k}$.

For CLT 3s with $\beta_{x,1} = \beta_{x,2} = 0.5$ and $n_{CA,1} = n_{CA,2} = 1$, both crossing areas in the element width direction are equally stressed and the maximum torsional shear stress may be expressed as

$$
\tau_{tor} = \frac{3}{2}\frac{v_{xy}}{b}
\tag{14}
$$

since the ratio $\beta_{x,k}/n_{CA,k}$ is constant ($\beta_{x,k}/n_{CA,k} = 0.5$).

For CLT 5s, the maximum ratio $\beta_{x,k}/n_{CA,k}$ and hence the maximum torsional shear stress depend on the relative width of the individual longitudinal layers $t_{x,k}$. For elements having a ratio between longitudinal layers $t_{x,2}/t_{x,1} = t_{x,2}/t_{x,3} < 2.0$, the maximum torsional shear stress is found for the crossing areas of the external longitudinal layers ($k = 1$ and 3). The ratio $t_{x,2}/t_{x,1} = t_{x,2}/t_{x,3} = 2.0$ gives equal torsional shear stress for all crossing areas in the element width direction, while $t_{x,2}/t_{x,1} = t_{x,2}/t_{x,3} > 2.0$ yields maximum torsional shear stress in the two crossing areas of the internal longitudinal layer ($k = 2$).

3   Finite element model

3D finite element (FE) analyses of CLT at in-plane shear loading conditions were carried out to study the distribution of internal forces and how they are influenced by various parameters. The study concerns elements consisting of three layers (CLT 3s) and five layers (CLT 5s). The basic CLT element geometries illustrated in Figure 2.1 were considered for all analyses, with gross cross section thickness t_{CL} = 100 mm for CLT 3s and t_{CL} = 200 mm for CLT 5s. Longitudinal and transversal laminations of equal lamination width, $b_x = b_y = b$ = 150 mm, were furthermore considered for all analyses and adjacent laminations within the same layer were modelled with a 0.2 mm gap. The parametric study presented in Section 4 considers various lay-ups in terms of the ratio between the total longitudinal and transversal layer thicknesses, t_x/t_y, and for CLT 5s also the relative thicknesses of the individual longitudinal layers, $t_{x,2}/t_{x,1} = t_{x,2}/t_{x,3}$.

The FE-analyses were performed using Abaqus/CAE 2019. The laminations were modelled as 3D solids with a linear elastic and orthotropic behaviour according to the stiffness parameters stated in Table 3.1. Rectilinear orientation of the material principal directions was assumed with the longitudinal (L) direction oriented in the length direction of the laminations, the tangential (T) direction oriented in the lamination width direction and the radial (R) direction oriented in the lamination thickness direction (which is the same as the CLT element thickness direction).

The bonding between the laminations over the crossing areas was modelled using a surface-to-surface contact formulation. The formulation uses a combination of hard contact in compression and linear elastic response in tension perpendicular to the crossing area and in the two in-plane shear directions. The linear elastic traction-separation responses in the three directions were modelled using a single value of the stiffness parameters, according to $K_{nn} = K_{ss} = K_{tt} = 10^3$ N/mm³.

The loading was introduced by application of loads at the end-faces of the laminations. The load distribution between the different layers of the longitudinal and transversal laminations was chosen according to Equations (7) and (8), using the weighting factors according to Equations (9) and (10). The total applied external loading corresponds to shear flows $v_{xy} = v_{yx}$ = 100 N/mm for CLT 3s and $v_{xy} = v_{yx}$ = 200 N/mm for CLT 5s.

Linear 8-node brick elements with full integration (denoted C3D8 in Abaqus) were used to model the laminations. The FE-mesh consisted mostly of cubically, or close to cubically, shaped elements with an element side length s of approximately 6 mm. Symmetry in the z-direction was considered for all FE-models.

Table 3.1 Lamination stiffness parameters used for FE-analyses.

E_L [MPa]	E_T [MPa]	E_R [MPa]	G_{LT} [MPa]	G_{LR} [MPa]	G_{TR} [MPa]	v_{LT} [-]	v_{LR} [-]	v_{TR} [-]
12 000	400	600	750	600	75	0.50	0.50	0.33

The torsional moments were evaluated at the crossing areas located at the centre of the element with respect to the x- and y-directions, see Figure 2.1. Due to the uneven stress distribution over the crossing areas found from the FE-analyses, the results presented below are based on resulting torsional moments which are determined by integration of the shear stress acting in the respective crossing areas. From these torsional moments, corresponding torsional shear stresses according to Equation (3) were calculated and used for comparison to the torsional shear stresses as calculated according to Models A – D. Results of shear flows $v_{xy,k}$ and $v_{yx,k}$ in the individual laminations likewise represent nominal values based on the shear forces in the laminations, $F_{xy,k}$ and $F_{yx,k}$, found from the FE-analyses and the lamination width b = 150 mm.

Preliminary analysis of the influence of some modelling parameters were carried out, relating to the elastic stiffness of the crossing area contact formulation, the load application and the FE-mesh density. For these analyses, CLT 5s with lay-up 40-40-40-40-40 and hence with t_x/t_y = 120/80 = 1.5 and $t_{x,2}/t_{x,1}$ = $t_{x,2}/t_{x,3}$ = 1.0 was considered. Results are presented in Tables 3.2 – 3.4, showing only very minor influence of these modelling parameters on the results in terms of the torsional moments $M_{tor,1}$ = $M_{tor,3}$ and $M_{tor,2}$. As an example, load application in either only the internal longitudinal lamination or only in the external longitudinal laminations gives no more than a 3.6% difference for the torsional moments, compared to the reference case with load application according to Equations (7) – (10).

Table 3.2 FE-results of torsional moments $M_{tor,1}$ and $M_{tor,2}$ for different distributions of $v_{xy,k}$.

	$v_{xy,1}$ = $v_{xy,3}$ = 0 N/mm $v_{xy,2}$ = 200 N/mm	$v_{xy,1}$ = $v_{xy,3}$ = 66.7 N/mm $v_{xy,2}$ = 66.7 N/mm	$v_{xy,1}$ = $v_{xy,3}$ = 100 N/mm $v_{xy,2}$ = 0 N/mm
$M_{tor,1}$ [Nmm]	1 184 000	1 228 000	1 250 000
$M_{tor,2}$ [Nmm]	1 016 000	1 008 000	1 004 000

Table 3.3 FE-results of torsional moments $M_{tor,1}$ and $M_{tor,2}$ for different contact stiffnesses K.

	K_{nn} = K_{ss} = K_{tt} = 10^2 N/mm³	K_{nn} = K_{ss} = K_{tt} = 10^3 N/mm³	K_{nn} = K_{ss} = K_{tt} = 10^4 N/mm³
$M_{tor,1}$ [Nmm]	1 228 000	1 228 000	1 217 000
$M_{tor,2}$ [Nmm]	1 025 000	1 008 000	977 300

Table 3.4 FE-results of torsional moments $M_{tor,1}$ and $M_{tor,2}$ for different finite element side lengths s.

	s = 8 mm	s = 6 mm	s = 5 mm
$M_{tor,1}$ [Nmm]	1 234 000	1 228 000	1 231 000
$M_{tor,2}$ [Nmm]	998 000	1 008 000	1 006 000

4 FE-results and model comparisons

Results from FE-analyses according to the model description in Section 3 are presented in this section. The results relate to analyses of CLT 3s and CLT 5s and numerical results are compared to model predictions according to Models A – D as reviewed in Section 2.

Results regarding maximum torsional shear stress τ_{tor} for CLT 3s are presented in Figure 4.1, for element lay-ups within the range from $t_x/t_y = 0.67$ (lay-up 20-60-20) to $t_x/t_y = 4.0$ (lay-up 40-20-40). Models A, B and D are in full agreement with the numerical results, while Model C predicts maximum torsional shear stresses in agreement with the numerical results only within the range $1.0 \leq t_x/t_y \leq 2.0$.

Results regarding CLT 5s are presented in Figures 4.2 and 4.3, for different lay-ups in terms of the individual layer thicknesses. Ratios between the total longitudinal and transversal layer thicknesses within the range $0.56 \leq t_x/t_y \leq 2.57$ and ratios between the individual longitudinal layer thicknesses within the range $0.50 \leq t_{x,2}/t_{x,1} = t_{x,2}/t_{x,3} \leq 2.62$ are considered.

The results in Figure 4.2 relate to distributions of shear flows $v_{xy,k}$ and $v_{yx,k}$ in the longitudinal and transversal layers, respectively, for different element lay-ups. The distributions of the total shear flow $v_{xy} = v_{yx}$ between the individual longitudinal layers according to Model D1 and Model D2 agree very well for lay-ups with $t_{x,2}/t_{x,1} = t_{x,2}/t_{x,3} = 2.0$, i.e. for an internal longitudinal layer thickness twice the external longitudinal layer thicknesses. For other lay-ups, some discrepancies between the numerical results and Models D1 and D2 are found. Model D1 assumes that the shear flow v_{xy} is distributed over the longitudinal layers according to their respective relative width according to Equations (7) – (10). According to the FE-results, the internal longitudinal layer does however carry a greater part of the total shear flow than predicted by Models D1 and D2 for $t_{x,2}/t_{x,1} = t_{x,2}/t_{x,3} < 2.0$ (and vice versa for $t_{x,2}/t_{x,1} = t_{x,2}/t_{x,3} > 2.0$).

$b = 150$ mm
$t_x = t_{x,1} + t_{x,2}$
$t_y = t_{y,1}$
$t_{CL} = t_x + t_y = 100$ mm
$v_{xy} = v_{yx} = 100$ N/mm

Figure 4.1. Maximum torsional shear stress for CLT 3s according to FE-analyses and models A − D, as influenced by the ratio of the longitudinal and transversal layer net cross section thicknesses t_x/t_y.

Figure 4.2. Normalised shear flows $v_{xy,k}$ (longitudinal layers) and $v_{yx,k}$ (transversal layers) for CLT 5s according to FE-analyses and Models D1 and D2, as influenced by the ratio of the longitudinal and transversal layer thicknesses t_x/t_y and the relative thicknesses of the individual longitudinal layers $t_{x,2}/t_{x,1} = t_{x,2}/t_{x,3}$.
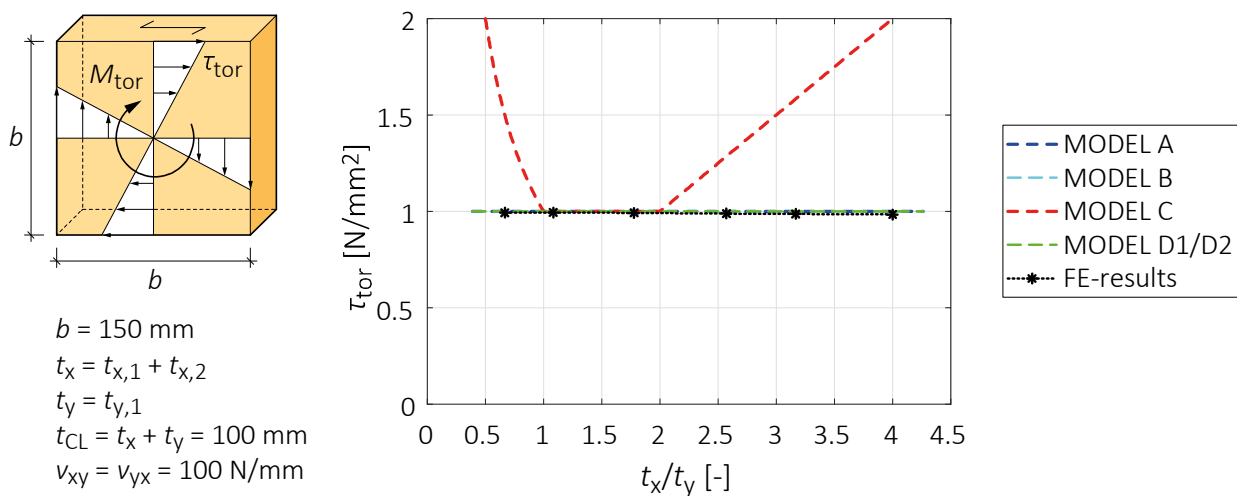
Figure 4.3. Maximum torsional shear stress τ_tor for CLT 5s according to FE-analyses and Models A – D, as influenced by the ratio of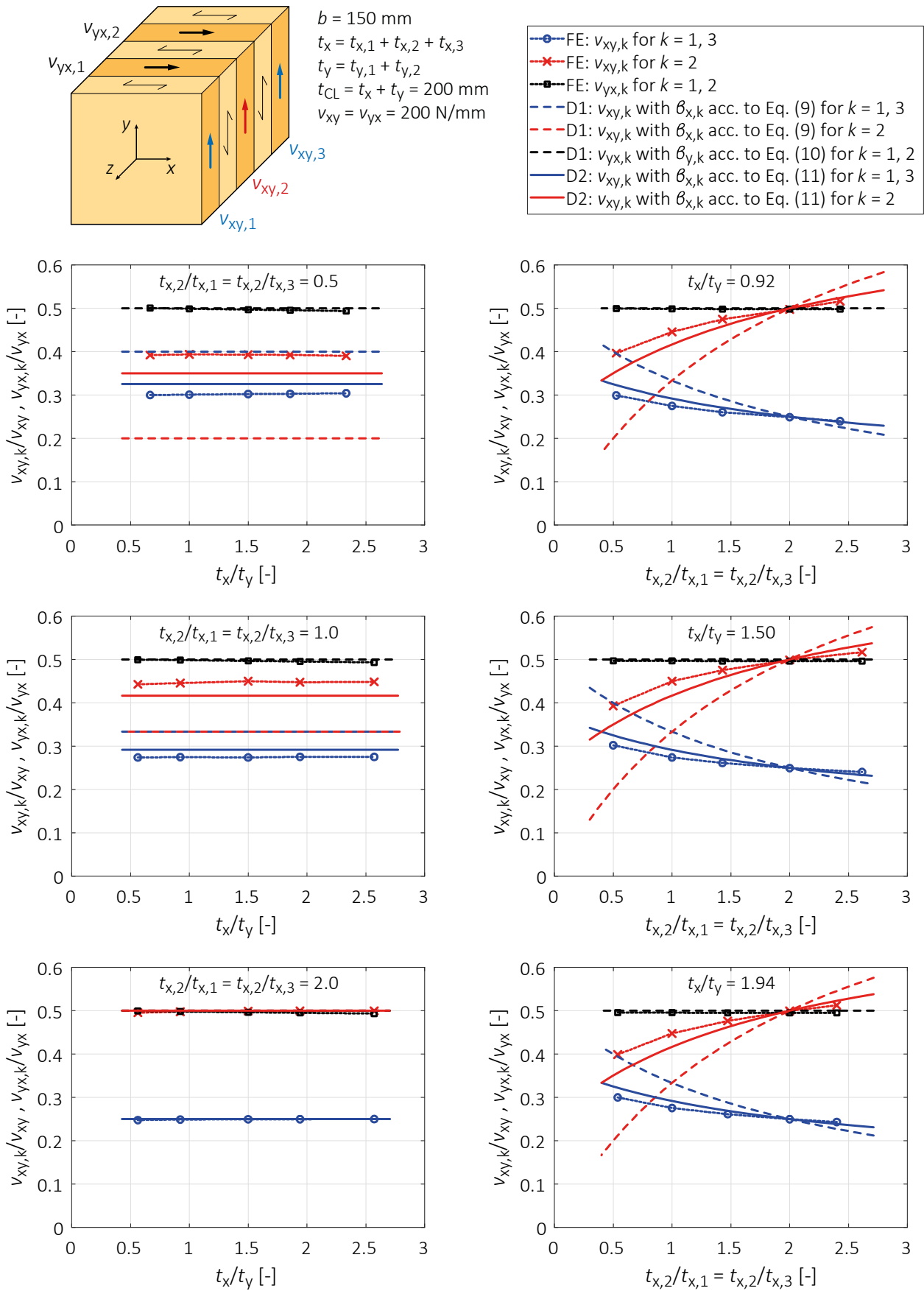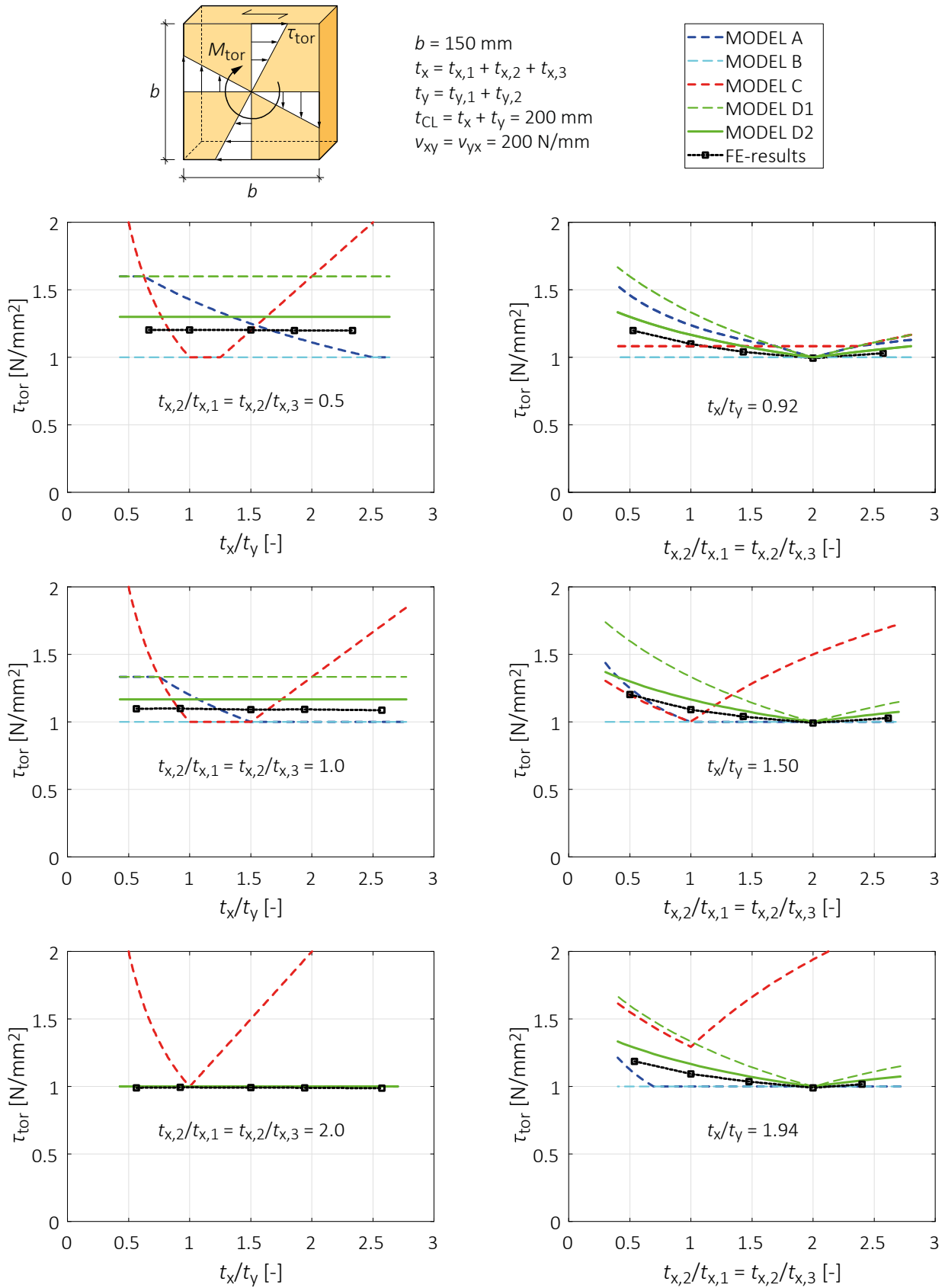 the longitudinal and transversal layer thicknesses t_x/t_y and the relative thicknesses of the individual longitudinal layers, $t_{x,2}/t_{x,1} = t_{x,2}/t_{x,3}$.

Maximum torsional shear stresses as influenced by the element lay-up for CLT 5s are presented in Figure 4.3. The maximum torsional moments, max($M_{tor,k}$), are according to the FE-analyses found for the crossing areas at the external longitudinal laminations (k = 1 and 3) for $t_{x,2}/t_{x,1} = t_{x,2}/t_{x,3} < 2.0$ and at the internal longitudinal laminations (k = 2) for $t_{x,2}/t_{x,1} = t_{x,2}/t_{x,3} > 2.0$. For a specific value of the ratios $t_{x,2}/t_{x,1} = t_{x,2}/t_{x,3}$ the maximum torsional shear stresses found from the FE-analyses are unaffected by the ratio between the total longitudinal and transversal layer thicknesses t_x/t_y.

Models A − D show significant differences concerning the predicted influence of the CLT element lay-up and predicted maximum torsional stresses. An important difference between the model predictions is that of the most favourable lay-up, i.e. the lay-up giving rise to the smallest torsional shear stresses. From Figure 4.3 it is evident that $t_{x,2}/t_{x,1} = t_{x,2}/t_{x,3}$ = 2.0, meaning an internal longitudinal layer of twice the thickness as the external longitudinal layers, is predicted as the most favourable lay-up by the FE-analyses. This is also predicted as the most favourable lay-up by models D1 and D2. In contrast, Model C predicts the ratio $t_{x,2}/t_{x,1} = t_{x,2}/t_{x,3}$ = 1.0 to be the most favourable lay-up for ratios between the total longitudinal and transversal layer thicknesses as t_x/t_y = 1.50 and 1.94 and predict no influence of the relative longitudinal layer thicknesses for t_x/t_y = 0.92. Model C further predicts a significant influence of the ratio between the total longitudinal and transversal layer thicknesses t_x/t_y, for different (fixed) ratios of the relative longitudinal layer thicknesses $t_{x,2}/t_{x,1} = t_{x,2}/t_{x,3}$.

Models D1 and D2 predict the same basic behaviour as found from FE-analyses regarding the influence of the ratios $t_{x,2}/t_{x,1} = t_{x,2}/t_{x,3}$ and t_x/t_y. Models D1 and D2 however predict a slightly stronger influence of the relative longitudinal layer thicknesses, $t_{x,2}/t_{x,1} = t_{x,2}/t_{x,3}$, than found from the FE-analyses. The ratios between the maximum torsional shear stress predicted by Models D1 and D2, and the maximum torsional shear stress according to the FE-analysis are 1.01–1.33 and 1.01–1.08, respectively.

5 Discussion

The results presented here are focused on model predictions for torsional stresses, relevant for design with respect to FM III. Within the on-going work of establishing guidelines for design of CLT in Eurocode 5, the question of models for predicting design-relevant stresses for in-plane shear loading is very important. This question is also closely related to the question of the corresponding shear strength parameters ($f_{v,xy,k}$, $f_{v,yx,k}$, $f_{tor,node,k}$, $f_{r,k}$) and standardisation of test procedures. It is of utmost importance to establish a consistent approach for the complete chain from test setups and procedures, evaluation of test results and determination of characteristic strength properties to models for stress analysis and verification of load-bearing capacity. The issue of FM III is also relevant for CLT elements at in-plane beam loading conditions. The results presented in Figure 4.2 may furthermore be of interest also in relation to models for design with respect to FM II (net shear failure).

6   Conclusions

Analytical models for stress analysis with respect to CLT shear failure mode III have been reviewed and compared to 3D FE-models. The following conclusions can be drawn from the FE-analysis, considering various element lay-ups for constant gross cross section widths and constant lamination widths:

1. The maximum torsional shear stress for CLT 3s is unaffected by the maximum layer thickness $t_{max} = \max(t_{x,k}, t_{y,k})$.

2. The maximum torsional shear stress for CLT 3s is unaffected by the lay-up in terms of the ratio between the total longitudinal and transversal layer thicknesses t_x/t_y.

3. The maximum torsional shear stress for CLT 5s is affected by the ratio between the longitudinal layer thicknesses $t_{x,2}/t_{x,1} = t_{x,2}/t_{x,3}$.

4. The maximum torsional shear stress for CLT 5s is, for a fixed ratio $t_{x,2}/t_{x,1} = t_{x,2}/t_{x,3}$, unaffected by the ratio between the total longitudinal and transversal layer thicknesses t_x/t_y.

Design-relevant torsional shear stresses are according to ÖNORM B 1995-1-1/A:2018-11 and the draft version of design of cross laminated timber for Eurocode 5 (2018), above referred to as Model C, governed by:

- The maximum individual layer thickness $t_{max} = \max(t_{x,k}, t_{y,k})$.

- The minimum of the total longitudinal and transversal layer thicknesses, $\min(t_x, t_y)$.

Model C is hence in agreement with the FE-results for CLT 3s only within the range of lay-ups with $1.0 \leq t_x/t_y \leq 2.0$, see Figure 4.1 and conclusions (1) and (2) above. Outside this range, significant discrepancies are found between Model C and the FE-results. Discrepancies are also found for CLT 5s regarding predicted influence of the element lay-up in terms of the ratios t_x/t_y and $t_{x,2}/t_{x,1} = t_{x,2}/t_{x,3}$, see Figure 4.3 and conclusions (3) and (4) above.

Models D1 and D2 are, among the models considered here, the only ones which have the same basic behaviour as that predicted by the FE-analyses *both* as regards the influence of the ratio between the longitudinal layer thicknesses, $t_{x,2}/t_{x,1} = t_{x,2}/t_{x,3}$, and as regards the influence of the ratio of the two net cross sections thicknesses, t_x/t_y.

7   Acknowledgments

8   References

Abaqus/CAE 2019 (2018), Dassault Systèmes.

Andreolli M, Tomasi R, Polastri A (2012): Experimental investigation of in-plane behaviour of cross-laminated timber elements. In: Proc. CIB-W18, CIB-W18/45-12-4, Växjö, Sweden.

Bogensperger T, Moosbrugger T, Silly G (2010): Verification of CLT-plates under loads in plane. In: Proc. World Conference on Timber Engineering (WCTE), Riva del Garda, Italy.

Brandner R, Dietsch P, Dröscher J, Schulte-Wrede M, Kreuzinger H, Sieder M (2017): Cross laminated timber (CLT) diaphragms under shear: Test configuration, properties and design. Construction and Building Materials 147:312–347.

CEN/TC 250/SC5 (2018): Working draft of design of cross laminated timber in a revised Eurocode 5-1-1, Version 2018-04-13, part of N892.

Danielsson H, Serrano E (2017): In-plane loaded CLT beams – Tests and analysis of element lay-up. In: Proc. INTER, INTER/50-12-2, Kyoto, Japan.

Danielsson H, Serrano E (2018): Cross laminated timber at in-plane beam loading – Prediction of shear stresses in crossing areas. Engineering Structures 171:921–927.

Danielsson H, Jeleč M, Serrano E, Rajčić V (2019): Cross laminated timber at in-plane beam loading – Comparison of model predictions and FE-analyses. Engineering Structures 179:246–254.

Flaig M, Blass HJ (2013): Shear strength and shear stiffness of CLT-beams loaded in plane. In: Proc. CIB-W18, CIB-W18/46-12-3, Vancouver, Canada.

Jeleč M, Danielsson H, Serrano E, Rajčić V (2018): Cross laminated timber at in-plane beam loading – New analytical model predictions and relation to EC5. In: Proc. INTER, INTER/51-12-5, Tallinn, Estonia.

Jeleč M, Danielsson H, Rajčić V, Serrano E (2019): Experimental and numerical investigations of cross-laminated timber elements at in-plane beam loading conditions. Construction and Building Materials 206:329–346.

ÖNORM B 1995-1-1 /A:2018-11 (2018): Eurocode 5: Design of timber structures – Part 1-1: General – Common rules and rules for buildings – National specifications for the implementation of ÖNORM EN 1995-1-1, national comments and national supplements (Amendment), Austrian Standards International.

Serrano E (2018): Test methods for in-plane shear tests of cross laminated timber. In: Brandner R, Tomasi R et al (eds): Properties, Testing and Design of Cross Laminated Timber: A state-of-the-art-report by COST Action FP1402, Shaker Verlag Aachen.

Wallner-Novak M, Koppelhuber J, Pock K (2013): Brettsperrholz Bemessung – Grundlagen für Statik und Konstruktion nach Eurocode. ProHolz Austria, Druck Eberl Print, Immenstadt, Austria.

Discussion

The paper was presented by H Danielsson

R Brandner commented that the Austrian code model is not the same as that considered in EC5 as there was an error in transfer of the model from Bogenspergers work.

A Frangi commented that this is important to EC5. One should be looking into the lastest draft of the Austrian code and the EC5 draft and check if the assumptions were correct.

P Dietsch asked if torsional strength can be included based on laminate thickness. H Danielsson responded that may be this is possible.

Net-section tension and shear strength of in-plane loaded CLT panels

Thomas Tannert, Associate Professor, Wood Engineering, University of Northern British Columbia, Prince-George, Canada; thomas.tannert@unbc.ca

Cristiano Loss, Assistant Professor, Wood Science, The University of British Columbia, Vancouver, Canada; cristiano.loss@ubc.ca

Marjan Popovski, Principal Scientist, Building Systems, FPInnovations, Vancouver, Canada, marjan.popovski@fpinnovations.ca

Hercend Mpidi Bita, Structural Engineer, Mass-timber Component Design, Equilibrium-Katerra, Vancouver, Canada; hercend.mpidibita@katerra.com

1 Introduction

1.1 Cross-laminated Timber

Cross-laminated Timber (CLT) is a plate-like engineered wood product, mostly made of an odd number of lumber board layers arranged orthogonally to each other (Brandner et al. 2016). The light weight relative to steel and concrete, high dimensional stability, as well as ease of erection make CLT a promising option for mid- and high-rise structures. Research on determining the strength on bending, shear parallel and compression perpendicular to grain in out-of-plane loading supported CLT floor applications, (e.g. Bogensperger et al. 2011; Brandner and Schickhofer 2014). Compression perpendicular to the grain also occurs in platform-type construction at the location where the floors are sandwiched by the walls of upper and lower stories. When CLT panels are used as wall element to carry gravity loads, compression strength parallel to the grain of the outside layers is of interest (Pang and Jeong 2018; Oh et al. 2015). Rolling shear is also relevant in out-of-plane loading and is affected by the single lamination aspect ratio, sawing pattern and species (Ehrhart and Brandner 2018).

CLT in-plane bending and shear stiffness were studied by Blass and Fellmoser (2004), Mossbrugger et al. (2006) and others. Shear strength is essential for in-plane loading of walls and floors (Fink et al. 2018). Three failure mechanisms in shear have been defined: gross shear, net shear, and torsion (Brandner et al. 2017). Gross shear failure

occurs due to the longitudinal shear in elements with narrow face bonded layers. The exceedance of the cross layer shear strength without narrow face bonding causes net shear failure. Torsion failure happens at the location of orthogonally glued lamella.

Tension stress is induced in CLT walls subjected to lateral loads, e.g., earthquake or wind load, at the bottom corners of the wall where the- are installed (Izzi et al. 2018). Yet, little experimental and theoretical research on the tension strength of CLT exists. Brander et al. (2016) proposed a formula to predict the resistance based on the tensile strength of layers in longitudinal direction. Ido et al. (2016) investigated the effect of layups and width on tensile strength of Sugi CLT. They observed that in the major strength axis, failure mostly happened at the finger joints or knots in outermost layers and close to the edge of perpendicular to grain plies for inner layers.

Although developed in Europe, CLT is yet to be included in the Eurocode 5 (EN 1995, 2004). The lack of a standardized test methods for characterization of CLT panels, the variability of regulations used by CLT producers, as well as significant differences between the material properties, were mentioned as challenges (Fink et al. 2018). The North American ANSI/APA PRG320 (ANSI 2018) standard for performance-rated CLT was instrumental for the recognition of CLT in the 2016 update to the 2014 Canadian Standard for Engineering Design in Wood CSA O86 (CSA 2016), the National Design Specification for Wood Construction (NDS 2015), and the International Building Code (IBC 2015). As an example, CSA O86 provides the elastic properties for different CLT grades as well as the strength properties for tension (f_t), shear (f_s), and compression (f_c) strengths, for both longitudinal and transverse layers.

1.2   Brittle failure modes of connections in CLT

Failure modes of timber connections vary depending on member and connection geometry as well as material type. In tension and shear, timber essentially exhibits a linear elastic behavior, and failure is marked by a brittle fracture. The orthogonal layup, in contrast to glued laminated timber, requires additional attention when designing connection in CLT such as fastener positioning (in the CLT side face or narrow face) and the influence of gaps as placing fasteners in gaps may seriously weaken the connection (Ringhofer et al. 2018). In general, connections with dowel-type fastener inserted into the CLT side face and loaded laterally behave in a quite ductile manner. However, depending on connection configurations, tension failures in layers close to the shear plane, successive shear & rolling shear failures and some block shear failures have also been observed (Blass and Uibel 2007). Particularly for multi-fastener and very large diameter fastener connections, these brittle failures could be the governing failure mode. Nevertheless, CSA O86 explicitly states that 'for CLT, the row shear failure and group tear-out failure need not be considered'. Zarnani and Quenneville (2015) adapted a design approach to determine the block-tear out resistance of connections in CLT by considering the effect of perpendicular layers. The

method was validated against test results on riveted connections and provided reasonable predictive accuracy and could be used to control brittle failure of wood in CLT connections.

As an alternative, failure criteria based on either continuum mechanics that consider the nature and magnitude of stresses can be applied to predict the brittle failure of CLT connections. Major issues for the application of any suitable criterion is the inherent large variability of mechanical parameters of timber and the associated size effect, especially if considering strength data. Material strength will exhibit a scale sensitivity or size effect when the strength decreases with increasing specimen size under the same test conditions. For brittle materials, statistically based size effects on strength are adequately explained by probabilistic theories such as the Weibull strength theory. The Weibull statistical distribution (Weibull 1939), has been extensively used in the characterization of mechanical properties of brittle materials and has been successfully applied to characterize the magnitude of size effects of timber (Tannert et al. 2010). A particular case of the Weibull distribution is called a 2-parameter distribution, which allows a direct implementation of size effects in numerical procedures by relating two volumes V_1 and V_2 submitted to constant stresses σ_1 and σ_2:

$$\frac{\sigma_1}{\sigma_2} = \left(\frac{V_2}{V_1}\right)^{1/k} \tag{1}$$

Barrett and Lau (1994) demonstrated that the scale factor, k, is correlated to the coefficient of variation (CoV):

$$k = CoV^{-1.085} \tag{2}$$

1.3 Application of CLT as Seismic Load Resisting System

CLT panels have been used for the lateral load resisting system (LLRS) of multi storey buildings around the world, e.g. as shearwalls; and 'designing and building CLT structures in earthquake-prone regions is no longer a domain for early adopters, but is becoming a part of regular timber engineering practice' (Tannert et al. 2018).

The 2016 update to CSA O86 (CSA 2016) includes provisions for the design of CLT elements and connections, as well as CLT shearwalls and diaphragms of platform-type buildings. The consensus from tests that investigated the seismic behaviour of CLT buildings (Ceccotti and Follesa 2006, Ceccotti et al. 2013) was that the structural performance is governed by the energy dissipative connections, while CLT panels behave as almost rigid bodies. In this assumption, also adopted in the CSA O86 standard provisions, the resistance of LLRS is governed by the hold-downs and the connections between the wall panels. Using the capacity -based design principle, the non-dissipative connections have to remain elastic when the energy-dissipative connec-

tions reach their 95th percentile of the ultimate resistance or the target displacement. The CLT panels also have to be capacity-protected to ensure they remain elastic.

The weight of timber structures makes them prone to overturning under lateral loads. This must be mitigated by installing hold-downs of adequate strength and stiffness at the bottom corners of shear walls, to anchor the walls to their foundation or floors below. Traditional commercially available hold-downs, such as straps emerging from the foundation and nailed to the shear walls, can provide the required strength, stiffness, and ductility for low-rise timber buildings. These connectors, although often applied in low-rise CLT buildings given their capacity of up to 100kN (Simpson Strong-Tie 2017), are not suited for taller structures where lateral loads become significantly larger. For mid and high-rise buildings, slip-friction connectors as an energy dissipative device can be used as hold-down as shearwalls given its strength and stiffness (Loo et al. 2014). This detailing was further improved to the resilient slip friction (RSF) connector to improve resilience through self-centring (Hashemi et al 2016). To obtain nonlinear behaviour in pre-defined ductile zones, Zhang et al. (2018) investigated the HSK™ system, based on glued-in perforated steel plates, as a hold-down for CLT shearwalls. With capacity-based design procedure, the capacity is governed by the strength of the steel plate, while the adhesive bond and CLT panel remain undamaged.

As another alternative, a steel tube connector (Schneider et al. 2018) can overcome some of the limitations of traditional hold-downs for CLT shearwalls in terms of capacity and ductility. The detailing is simple; the tube is placed inside the CLT panel into a predrilled hole of the same diameter (Figure 1). The round shape allows for a uniform stress distribution along its circumference. In the vertical direction, the hold-down forces cause compression but might lead to net section tension and shear failures. Schneider et al. (2018) tested the connector in a 3-ply CLT and showed that when installed at a distance of 100mm away from the edge of the panel, brittle wood failure was avoided and all deformations were supplied by the steel tube. Subsequently, Mpidi Bita and Tannert (2019) optimised the connection for a target strength, stiffness and ductility, and investigated the robustness in presence of uncertainties in material properties, as well as geometry.
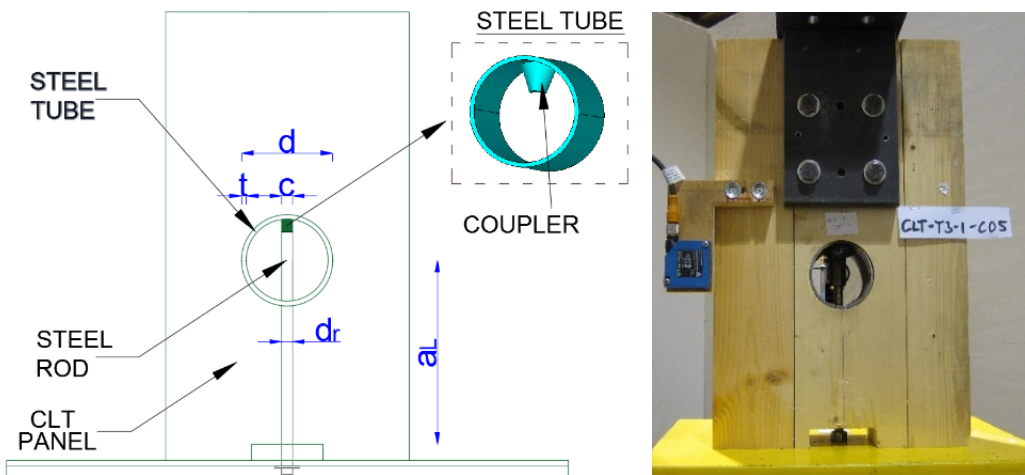
Figure 1: Schematic representation of tube hold-down (left) and photo (right)

2 Experimental Investigation

2.1 Objectives

Providing gravity and seismic design provisions for CLT elements and structures in CSA O86 presented a significant accomplishment. Nevertheless, the standard does not (yet) provides any specific procedures to estimate the resistance of CLT shearwalls based on capacity-design-based principles. In addition, no specific guidance with respect to the net section tension and shear strengths of CLT panels at connections, including hold-downs, is provided. The standard explicitly states that 'for CLT, the row shear failure and group tear-out failure need not be considered' and the guidance with respect to loaded-end distance are specific to bolts and not large diameter steel tubes.

The primary objective of the research presented herein was to determine the net section tension and shear strengths of CLT panels loaded in plane and to provide guidance for the end distances during the design of internal-bearing hold-downs. Secondary objectives consisted of determining the mechanical characterisation of the involved wood and the stress state inside the tested specimens. To achieve these objectives, small-scale tension perpendicular to grain and shear parallel to grain tests as well as full-scale uniaxial tension tests on CLT specimens were conducted.

2.2 Materials

The CLT panels were 3-ply or 5-ply with equal layer thickness of 33mm for a panel thickness of 99mm and 165mm, respectively. The panels were rated according to ANSI/APA PRG 320 (2018) as stress E1 grade; the longitudinal layers were machine stress-rated 2100 1.8E Spruce-Pine-Fir (S-P-F) lumber, whereas the transverse layers were No. 2 S-P-F grade lumber. The different layers were glued together crosswise on their wide faces only using Polyurethane adhesive. Prior to manufacturing and testing, the CLT was stored in an indoor climate (temperature around 20°C and relative humidity around 50%). The apparent wood density based on volume and weight was

determined from all selected samples; the average was 470 kg/m^3. The average MC of the specimens determined before testing was 11%.

CSA O86 (2016) does provide specified strength values for tension parallel to grain ($f_{t,\text{II}}$) for longitudinal and transverse layers and rolling shear ($f_{s,R}$); however it does not provide any shear parallel to grain ($f_{s,\text{II}}$) or tension perpendicular to the grain strength ($f_{t,T}$) values for CLT as these properties are usually not used in the design. Neither are these values provided for machine stress rated lumber when used in CLT. Therefore, it was deemed necessary to determine $f_{s,\text{II}}$, $f_{s,R}$ and $f_{t,T}$ according to ASTM D143-09. These tests involve samples exhibiting different shapes and volumes, for a more in-depth discussion on this topic, the reader is kindly referred to Tannert et al. (2012).

A total of 15 tension and 60 shear specimens each were cut from the (tested) CLT panels. Failure in all tests was brittle, characterized by complete specimen separation as shown in Figure 2.The average $f_{t,T}$ was determined as 1.96N/mm^2 (on a failure plane with an average area of 842mm^2) with a coefficient of variation (CoV) of 38%. The average $f_{s,\text{II}}$ and $f_{s,\text{II}}$ were determined as 7.95N/mm^2 and 1.85N/mm^2, respectively, (on failure planes with an average area of 1,421mm^2) with CoVs of 42% and 41%. The experimentally determined values are comparable in magnitude with those reported in Wood Handbook (2015), which validates the approach for their determination.
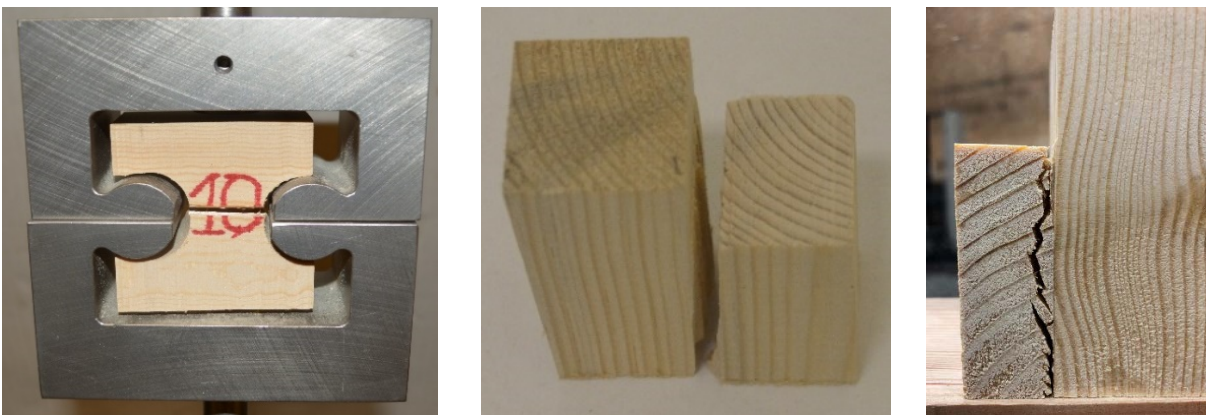
Figure 2: Failed small-scale specimens: tension (left) and shear (middle) and rolling shear (right)

2.3 CLT Specimen Description

The test specimens were cut from the CLT panels to an average width (w) of 200mm. The panel average thickness was 104mm and 173mm for the 3-ply and 5-ply panels, respectively, whereas the length was 800mm. At both ends of the specimens, 76.2mm (3") diameter (d) holes were drilled to insert a solid circular steel section of the same diameter, defining the loaded end-distance (a_L), measured from the centre of the hole to the edge of the specimen. Three parameters were varied: i) the CLT layup (3-ply and 5-ply), ii) the orientation of the outer CLT layers (parallel or perpendicular to the loading), and iii) the loaded end-distance (a_L: 150mm (2d) and 300mm

(4*d*)). In each of the eight test series, as summarized in Table 1, six replicates were manufactured and subsequently tested for a total of 48 specimens. The areas of the possible failure planes are included for the subsequent strength prediction.

Table 1: Test series overview (all areas in mm^2)

Series ID	CLT	Outer layer	a_L	$A_{t,T}$	$A_{s,\parallel}$	$A_{S,R}$
3-par-2d	3-ply 105mm	Parallel	2*d*	4,375	21,000	37,500
3-par-4d	3-ply 105mm	Parallel	4*d*	4,375	42,000	75,000
5-par-2d	5-ply 175mm	Parallel	2*d*	8,750	31,500	75,000
5-par-4d	5-ply 175mm	Parallel	4*d*	8,750	63,000	150,000
3-perp-2d	3-ply 105mm	Perpendicular	2*d*	8,750	10,500	37,500
3-perp-4d	3-ply 105mm	Perpendicular	4*d*	8,750	21,000	75,000
5-perp-2d	5-ply 175mm	Perpendicular	2*d*	13,125	21,000	75,000
5-perp-4d	5-ply 175mm	Perpendicular	4*d*	13,125	42,000	150,000

2.4   Methods

All experiments were performed in a universal testing machine. The quasi-static tensile loads were displacement-controlled at a rate of 1.0 mm/min up to failure, so that the total test duration was approx. six minutes, which is in accordance with EN-26891 (1991). The study was conducted within controlled laboratory conditions at the Laboratory of FPInnovations in Vancouver, Canada. Figure 3 shows the test set-up. For all tests, the load was recorded using a calibrated load cell up to the maximum load (F_{ult}). The test was stopped when the corresponding force applied on the specimens dropped below 80% of the recorded ultimate load. Since, only the material strength was of interest and not the stiffness, the displacement was only recoded as the movement of the actuator loading head. To obtain more data, the specimens with 2*d* end distance were re-tested after cutting off the broken end from the first tests, approximately 50mm away from the fixture hole, and installing a new 76.2mm diameter hole with the same 2*d* end distance.
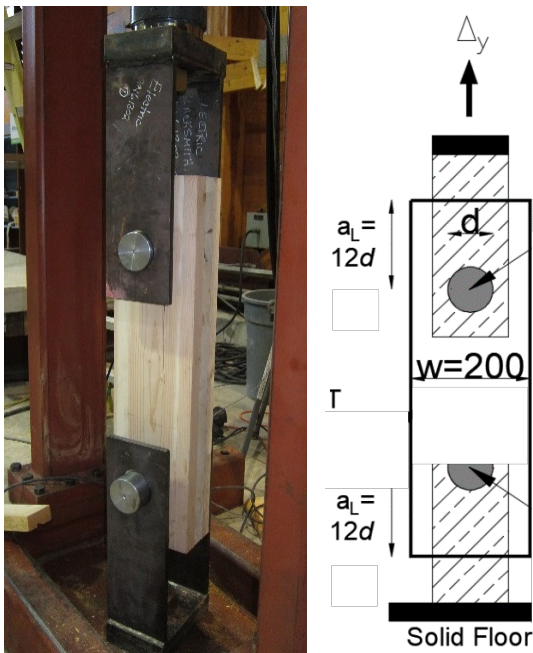
Figure 3: Test set-up: Photo (left) and schematic representation (right)

2.5 Results

The load-deformation curves for all tested specimens are presented in Figure 4. In all cases, the load-displacement behaviour was linear up to failure, with little displacement capability beyond, due to the brittle failure of the CLT panels. The observed initial alignment behaviour was not caused by any material property, but by the slip in the test fixture. The load-displacement curves for the re-tested specimens were almost identical for the respective test series and are not presented here for brevity.
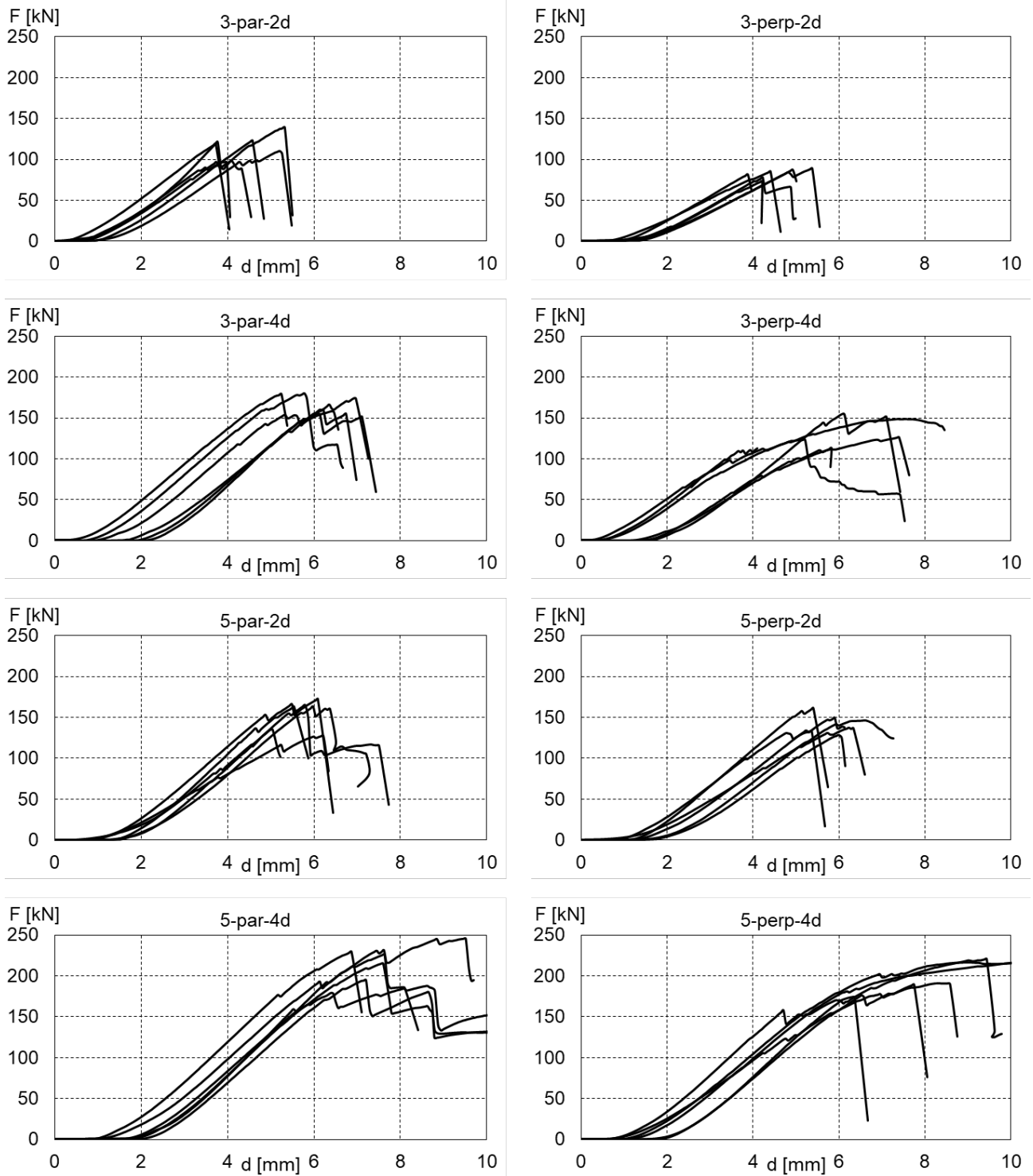
Figure 4: Load-displacement curves for individual test specimens

The average capacities and respective CoVs for all test series are shown in Table 2. As expected, the 5-ply panels were consistently stronger than the 3-ply panels: 37% in case of specimens with 2d end distance, and 29% for specimens with 4d end distance for loading parallel to the longitudinal layer. A rational explanation lies in the fact that 3 layers instead of 2 are loaded in parallel direction in case of 5-ply panels. In contrast, the specimens loaded perpendicular to the longitudinal layers were 70% and 67% stronger for 2d and 4d end distance, respectively.

With respect to a_L, the increase from 2d to 4d led to an average increase in capacity of 47% (40% for 5-ply-par, 50% for 5-ply-perp). Less intuitively was the change in capacity as a function of outer layer orientation, while the increase for the 3-ply panels was 38% for both end distances, it was only 12% and 5% for 5-ply panels for 2d and 4d end distance, respectively. The re-tested specimens exhibited almost the same average capacities demonstrating that the first test only failed the weaker end and did not have any impact on the unbroken end of the specimen.

Table 2: Test results summary

Series ID	F_{ult} [kN] (CoV)
3-par-2d	114.3 (14%)
3-par-2d-rt	110.7 (12%)
3-par-4d	167.7 (7%)
5-par-2d	154.3 (12%)
5-par-2d-rt	155.3 (8%)
5-par-4d	122.4 (12%)
3-perp-2d	82.3 (7%)
3-perp-2d-rt	81.0 (8%)
3-perp-4d	216.6 (10%)
5-perp-2d	142.7 (8%)
5-perp-2d-rt	133.5 (8%)
5-perp-4d	204.5 (11%)

Typical failed specimens from each test series are depicted in Figure 5. Independently from loaded-end distance a_L and outer layer orientation, failure always occurred as a combination of shear parallel to the grain failure for the layers in parallel to the load and tension perpendicular to the grain failure in those layers perpendicular to the load. In addition, rolling shear failure close to the interface between layers was observed, regardless of a_L. Based on the visual observations during the tests, it was not possible to determine any specific failure sequence and it is postulated that all failure modes occurred concurrently. As an exception, some specimens of series '5-par-4d' failed in tension parallel to the grain in the net areas of the longitudinal layers, see Figure 5 (d). The failure modes for repeated tests were identical and the failure occurred seemingly random at either the re-tested or the new hole.

(a) 3-par-2d
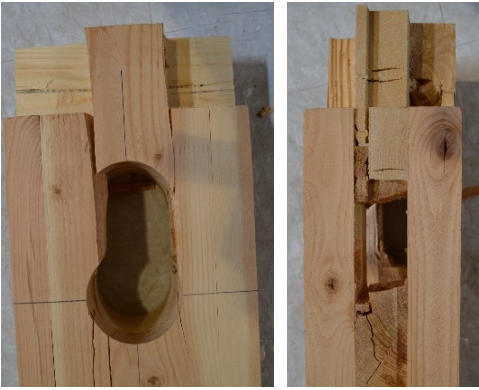
(b) 3-par-4d

(c) 5-par-2d

(d) 5-par-4d

(e) 3-perp-2d

(f) 3-perp-4d

(g) 5-perp-2d

(h) 5-perp-4d

Figure 5: Typical failed specimens

2.6   Simplified stress-based strength prediction of brittle CLT failure

The dominant failure mode observed were net section tension perpendicular to the grain failure in the layers perpendicular to the load combined with shear parallel to the grain failure for the layers in parallel to the load and rolling shear failure close to the layer interface. As a simplified approach to predict strength based on stresses, it is postulated that the individual resistances of each failure plane can be summed up. To predict tension perpendicular to grain and shear parallel to grain resistance, the experimentally determined material strength are converted into size specific values using equations 1 and 2.

Table 3 lists the size-corrected strength properties and the individual resistances (considering the areas listed in Table 1) for each failure mode and each test series. Finally, the total predicted resistance R and the ratio between R and F_{ult} is included. The proposed simplified approach provided on average excellent prediction for the brittle failure strength. Strength of panels loaded in parallel to their longitudinal layers is under-predicted by on average 5% while strength of panels loaded perpendicular to these layers is over-predicted by on average 8%.

The contribution of the tension perpendicular to grain resistance to overall connection resistance is on average only 5% and can potentially be neglected. The shear parallel to the grain and the rolling shear strength contributions to the total resistance are on average 47% and 48%, respectively. Furthermore, the net section parallel to grain tension resistance of the side section has to be checked.

The simplified approach to predict strength based on stresses acting on an area will be extended towards integrating these stresses over the volume in which the act. Further experimental testing on a wider range of geometric parameters will provide data for validating the proposal.

Table 3: Test results summary

Series ID	$f_{t,T}$ [N/mm^2]	$f_{s,II}$ [N/mm^2]	$f_{s,R}$ [N/mm^2]	$R_{t,T}$ [kN]	$R_{s,II}$ [kN]	$R_{s,R}$ [kN]	R [kN]	R/F_{ult}
3-par-2d	1.10	2.78	0.53	4.8	39.1	20.0	83.2	0.74
3-par-4d	1.10	2.12	0.98	4.8	59.6	73.2	167.1	1.00
5-par-2d	0.86	2.37	0.98	7.6	50.0	73.2	155.5	1.00
5-par-4d	0.86	1.81	0.75	7.6	76.3	112.0	233.7	1.08
3-perp-2d	0.86	3.64	1.27	7.6	25.6	47.8	93.6	1.15
3-perp-4d	0.86	2.78	0.98	7.6	39.1	73.2	139.1	1.14
5-perp-2d	0.75	2.78	0.98	9.8	39.1	73.2	141.4	1.02
5-perp-4d	0.75	2.12	0.75	9.8	59.6	112.0	211.0	1.03

3   Conclusions

The results of experimental tests on 3-ply and 5-ply CLT specimens loaded at a single large diameter (76mm) fastener that forced the connection to fail in a brittle failure mode are presented. Subsequently, a simplified stress-based strength prediction method is presented. The following conclusions can be drawn:

1) Depending on connection layout, in particular the loaded end distance a_L in relation to the connector stiffness, brittle failure in tension and shear of the CLT net net-section can occur and has to be accounted for in design.

2) Provision to account for the brittle strength of CLT connections, while currently explicitly excluded for dowel-type fasteners in CSA-O86 are required in the context of capacity-based design of seismic load resisting systems.

3) Within the range of the tested geometric and material parameters, failure always occurred as a combination of shear parallel to the grain for the layers in parallel to the load and tension perpendicular to the grain failure in layers perpendicular to the load in addition to rolling shear failure close to the interface between layers.

4) As a simplified approach to predict strength based on stresses, it is postulated that the individual resistances of the individual failure planes can be summed up. Using experimentally determine small clear specimens strength values provided good predictions for the net section strength of CLT panels.

5) While the results can provide some design guidance to practicing engineers, more work is required before these findings and the proposed strength prediction methods can be presented to the Technical Committee of CSA O86 for potential inclusion into the next edition of the Canadian Standard for Engineering Design in Wood.

Acknowledgements

References

ANSI/APA (2018) PRG 320, Standards for performance-rated cross-laminated timber, American National Standard, APA, Tacoma, USA.

Barrett J D, Lau W (1994) "Canadian lumber properties." Canadian Wood Council, Ottawa, Canada. 346 pp.

Blass HJ, Fellmoser P (2004). "Design of solid wood panels with cross layers." In proc. WCTE, Lahti, Finnland.

Blass HJ, Uibel T (2007) Tragfähigkeit von stiftförmigen Verbindungsmitteln in Brett-sperrholz. Karlsruher Berichte zum Ingenieurholzbau, Band 8, Karlsruhe, Germany.

Bogensperger T, Augustin M, Schikhofer G (2011). Properties of CLT-panels exposed to compression perpendicular to their plane. In proc. CIB W18.

Brandner R, Schickhofer G (2014) Properties of cross laminated timber (CLT) in compression perpendicular to grain. In proc. INTER, Bath, UK.

Brandner R, Dietsch P, Dröscher J, Schulte-Wrede M, Kreuzinger H, Sieder M (2017). Cross laminated timber (CLT) diaphragms under shear: Test configuration, properties and design. Construction and Building Materials, 147:312-327.

Brandner R, Flatscher G, Ringhofer A, Schickhofer G, Thiel A (2016). Cross laminated timber (CLT): overview and development. European Journal of Wood and Wood Products, 74(3):331-351.

Ceccotti A, Follesa M (2006) Seismic behaviour of multi-storey X-Lam buildings. In proc. COST Action E29, Coimbra, Portugal.

Ceccotti A, Sandhaas C, Okabe M, Yasumura M, Minowa C, Kawai N (2013) SOFIE project–3D shaking table test on a seven-storey full-scale cross-laminated timber building. Earthquake Engineering Structures, 42(13): 2003-2021.

CSA O86 (2016). Engineering Design in Wood 2014 with Update 1, Canadian Standards Association, Canada.

Ehrhart T, Brandner R (2018). Rolling shear: Test configurations and properties of some European soft-and hardwood species. Engineering Structures, 172:554-572.

EN 1995 (2004) Eurocode 5. Design of timber structures. Part 1-1: General- Common rules and rules for buildings. European Committee for Standardization (CEN), Brussels, Belgium

EN-26891 (1991) Timber structures, Joints made with mechanical fasteners, General principles for the determination of strength and deformation characteristics, European Committee for Standardization (CEN), Brussels, Belgium

Fink G, Kohler J, Brandner R (2018). Application of European design principles to cross laminated timber. Engineering Structures, 171:934-943.

Hashemi A, Masoudnia R, Quenneville P. (2016) A numerical study of coupled timber walls with slip friction damping devices. Construction and Building Materials; 121: 373–385.

Ido H, Nagao H, Harada M, Kato H, Ogiso J, Miyatake A (2016). Effects of the width and lay-up of sugi cross-laminated timber (CLT) on its dynamic and static elastic moduli, and tensile strength. Journal of wood science, 62(1), 101-108.

Izzi M, Casagrande D, Bezzi S, Pasca D, Follesa M, Tomasi R (2018). Seismic behaviour of Cross-Laminated Timber structures: A state-of-the-art review. Engineering Structures, 170:42-52.

Loo WY, Quenneville P, Chouw N. A new type of symmetric slip-friction connector. Journal of Constructional Steel Research 2014; 94: 11–22.

Moosbrugger T, Guggenberger W, Bogensperger T (2006). Cross-Laminated Timber Wall Segments under Homogenous Shear - with and without Openings. In proc. WCTE, Portland, USA.

Mpidi Bita H, Tannert T (2018) Numerical Optimisation of Novel Connection for Cross-Laminated Timber Buildings, Engineering Structures 175: 273-283

Oh JK, Lee JJ, Hong JP (2015) Prediction of compressive strength of cross-laminated timber panel. Journal of Wood Science, 61(1):28-34.

Pang SJ, Jeong GY (2018) Load sharing and weakest lamina effects on the compressive resistance of cross-laminated timber under in-plane loading. Journal of Wood Science, 64(5):538–550.

Ringhofer R, Brandner B, Blaß HJ (2018) Cross laminated timber (CLT): Design approaches for dowel-type fasteners and connections. Engineering Structures 171:849–861

Schneider J, Tannert T, Tesfamariam S, Stiemer SF (2018) Experimental Assessment of a Novel Steel Tube Connector for Cross-Laminated Timber; Engineering Structures 177: 283–290

Simpson Strong-Tie Company Inc. Strong-Rod^{TM} systems. https://www.strongtie.com [accessed 20 July 2017].

Tannert T, Lam F, Vallée T (2010) Strength prediction for rounded dovetail connections considering size effects, ASCE Journal of Engineering Mechanics, 136:358-366.

Tannert T, Vallée T, Franke S, Quenneville P (2012) Comparison of test methods to determine Weibull parameters for wood. In proc. WCTE Auckland, New Zealand.

Tannert T, Follesa M, Fragiacomo M, González P, Isoda H, Moroder D, Xiong H, van de Lindt J. (2018) Seismic Design of Cross-laminated Timber Buildings, Wood and Fiber Science, 50:3–26.

Weibull, W. (1939). A statistical theory of strength of materials. Proceedings of the Royal Swedish Institute, Research No.151, Stockholm, Sweden.

Wood handbook (2010) Wood as an engineering material. General Technical Report FPL-GTR-190. Forest Products Laboratory, Madison, USA.

Zarnani P, Quenneville P (2015) New design approach for controlling brittle failure modes of small-dowel-type connections in Cross-laminated Timber (CLT), Construction and Building Materials 100 172–182

Zhang X, Tannert T, Popovski M. High-capacity hold-down for tall timber buildings, Construction and Building Materials 2018; 164: 688-703.

Discussion

The paper was presented by T Tannert

F Lam stated that one should not add the capacity of individual failure mode together to estimate the total capacity of the connection. Although it seemed to work here, it is only fortuitous and cannot be generalized.   F Lam further commented that Weibull approach should be based on stressed volume integral and simple area ratio approach would only be valid for uniform stress cases. Also using Weibull approach with combinations of failure is tricky. T Tannert agreed.

BJ Yeh commented that fasteners have concentrated stress condition and volume effect may not be appropriate.

YH Chui agreed with F Lam's comments. Results of small scale test and large specimen test will be different.

H Blass commented that EC5 split ring design includes size effect considerations.

M Li asked about size effect for longitudinal shear and received confirmation that similar shape factors were used for all three strengths. Also f[MPa] are average values.

P Quenneville stated that the testing matrix is not large enough to have a reliable model and in reality there would be more complication with sharing of loads between loaded surfaces. T Tannert said that there were more data available and will try to include them in the revised paper. Also there is interest from designers to look at this type of hold-downs.

R Brandner stated that block shear tests do not represent real shear strengths. T Tannert said that based on past results there was agreements between ASTM block shear tests and EC5 approach. R Brandner said that this type of hold down is not new and there are existing information.

E Serrano agreed that Weibull theory would not work without considering stress distribution. K= Cov-1.085 is from statistics.

Prediction of Load-bearing Capacity of Notched Cross Laminated Timber Plates

Erik Serrano, Division of Structural Mechanics, Lund University, Sweden

Per Johan Gustafsson, Division of Structural Mechanics, Lund University, Sweden

Henrik Danielsson, Division of Structural Mechanics, Lund University, Sweden

1 Background and aim

Notches in cross laminated timber (CLT) can be used at supports or to realise connections between elements. At a notch, concentrated perpendicular to grain tension and shear stress appear and the load bearing capacity can be governed by cracking. The aim of this paper is to discuss the design of notched CLT-plates in relation to the current design approach of Eurocode 5 (2004) (EC5) for solid timber beams and suggested design approaches for notched CLT members and to compare these with analytical and numerical calculations and experimental evidence. Of special concern is whether the current approach for solid timber beams can be adapted to CLT plates with notches. The numerical work presented is in part based on Serrano (2018).

2 Current design rules and experimental results

2.1 Theoretical basis of design approach in EC5

Design equations for end-notch timber beams found in codes and design recommendations are typically either empirical or with a rational theoretical basis from fracture mechanics. The most frequently used fracture mechanics approach for end-notched beam design equations is based on energy balance considerations (Griffith, 1921) by means of linear elastic beam theory (Gustafsson, 1988). Here assumptions, derivation and result will be summarized for an end-notched timber beam, see Figure 1a. This end-notched beam has from the beam theory analysis point of view the same strength and stiffness as the slit cut beam shown in Figure 1b.

a)

b)
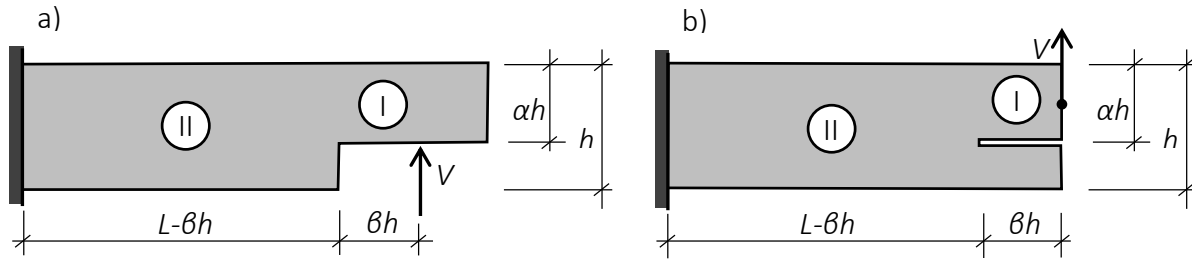
Figure 1. a) Notched beam with notation defining geometry. b) Equivalent slit cut beam.

The material is assumed to be homogeneous and orthotropic and fracture is assumed to be due to crack propagation along the beam, starting at the tip of the notch. The propagation starts when the release of potential energy W during increase of crack length from βh to $\beta h + d(\beta h)$ equals the dissipation of energy at the crack tip during the same crack length increase. The potential energy is the sum the potential energy of the force V and the elastic strain energy in the structure:

$$W = -V\delta + \frac{V\delta}{2} = -\frac{V^2(\delta/V)}{2} = -\frac{V^2C}{2} \tag{1}$$

where δ is the displacement of the point of loading in the direction of the load and $C = \delta/V$ is the compliance of the structure. The decrease of potential energy $-dW$ during the crack extension $d(\beta h)$ can then be calculated as:

$$-dW = -d(\beta h)\frac{\partial W}{\partial(\beta h)} = d(\beta h)\frac{V^2}{2}\frac{\partial C}{\partial(\beta h)}. \tag{2}$$

The dissipation of energy is in linear elastic fracture mechanics (LEFM) assumed to be proportional to the crack opening area, *i.e.* $G_c b d(\beta h)$, where G_c is the critical energy release rate of the material and b is the width of the beam at the tip of the notch. Energy balance between the decrease of potential energy dW and the dissipated energy $G_c b d(\beta h)$ gives the magnitude of the load V_f that starts crack propagation:

$$V_f = \sqrt{\frac{2bG_c}{\partial C/\partial(\beta h)}}. \tag{3}$$

The material parameter G_C is affected by the ratio between normal and shear stress at the crack tip. In applied analyses of end-notched beams G_C is, however, commonly assigned the value for pure normal stress, *i.e.* the value found from Mode I loading fracture tests. This is an approximation on the safe side, although commonly of insignificant magnitude.

The compliance C has three components:

$$C = \delta/V = (\delta/V)_{bending} + (\delta/V)_{clamping} + (\delta/V)_{shear}. \tag{4}$$

These three deflection parts are illustrated in Figure 2 for a cantilever attached to an elastic half-space. The bending part and the shear part are calculated according to conventional Bernoulli/Euler and Timoshenko theory, respectively, for the two beam

parts, I and II. Deformation due to the compliant attachment of beam part I to beam part II is constituted by development of non-plane cross-sections in the vicinity of the notch tip even in case of pure bending. The corresponding deflection is represented by a rotational spring with stiffness set to:

$$k_\theta = 1 / \sqrt{(1/(KGA)_I - 1/(KGA)_{II})(1/(EI)_I - 1/(EI)_{II})} \qquad (5)$$

where $(KGA)_i$ and $(EI)_i$ are the Timoshenko shear stiffness and the bending stiffness, respectively, of beam cross sections I and II. This particular spring stiffness was derived from results of finite element analysis of beams as shown in Figure 2 suggesting as a reasonable approximation that the compliance of such beams may be expressed as (Petersson, 1974):

$$\delta / V = D(E + L)^3 \qquad (6)$$

where L is the length of the cantilever beam and D and E are constants.

Bending
$\delta/V \sim L^3$

Compliant clamping
$\delta/V \sim L^2$

Shear
$\delta/V \sim L$
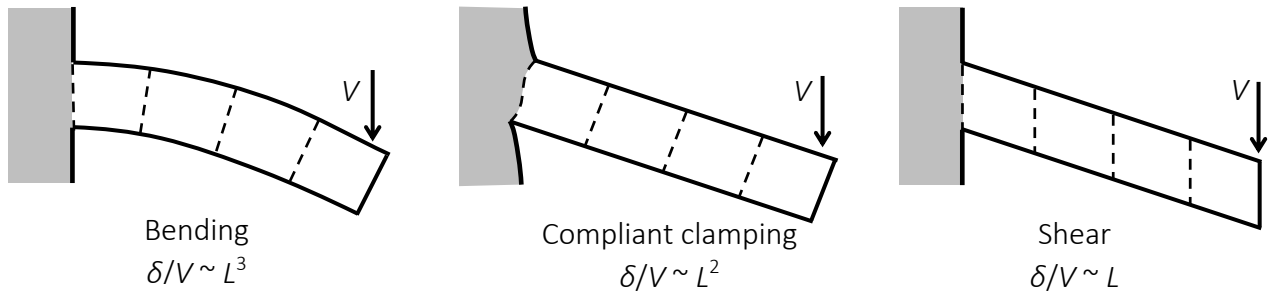
Figure 2. A cantilever beam with length L attached to an elastic half-space.

With C determined as outlined above, Equation (3) can be reformulated as:

$$V_f = \frac{\sqrt{2bG_c}}{\sqrt{1/(KGA)_I - 1/(KGA)_{II} + \beta h \sqrt{1/(EI)_I - 1/(EI)_{II}}}} . \qquad (7)$$

If the compliant clamping is disregarded, *i.e.* if $k_\theta \rightarrow \infty$, then the result would become:

$$V_f = \frac{\sqrt{2bG_c}}{\sqrt{1/(KGA)_I - 1/(KGA)_{II} + \beta h(1/(EI)_I - 1/(EI)_{II})}} . \qquad (8)$$

Equation (7) has been found to be in better agreement with test results than Equation (8). Note that the length βh may be replaced by the bending moment to shear force ratio (M/V) at the tip of the notch.

For a beam with a homogeneous rectangular cross section bh, the cross section quantities are $K=5/6$, $A_I=b\alpha h$, $A_{II}=bh$, $I_I=b(\alpha h)^3/12$ and $I_{II}=bh^3/12$, and Equation (7) can be written as:

$$\frac{3}{2}\frac{V_f}{b\alpha h}=1.5\,\frac{\sqrt{\dfrac{G_c G}{0.6}}}{\sqrt{h}\left(\sqrt{\alpha-\alpha^2}+\beta\sqrt{10(G/E)}\sqrt{1/\alpha-\alpha^2}\right)} \tag{9}$$

where the left hand side of the equation is the formal maximum shear stress in beam part I at the instant of fracture at the notch.

2.2 Current EC5 design approach for solid beams

The current version of EC5 (Eurocode 5, 2004) includes provisions for strength design of end-notched structural members made of timber, laminated veneer lumber (LVL) and glulam. The provisions are based on Equation (9) and assuming that

$$E/G=15.6 \quad\Rightarrow\quad \sqrt{10G/E}=0.8 \tag{10}$$

and assuming that

$$1.5\sqrt{\frac{G_c G}{0.6}}\,/\,f_v=k_n[\mathrm{mm}^{1/2}]=\begin{cases}4.5 \text{ for LVL}\\5.0 \text{ for solid timber}\\6.5 \text{ for glulam}\end{cases}. \tag{11}$$

The EC5 design approach for (90°) end-notched members is formulated in terms of the shear stress capacity of beam part I:

$$\tau_d=\frac{1.5V}{b\alpha h}\leq k_v f_{v,d} \tag{12}$$

where k_v is a strength reduction factor given by

$$k_v=\min\begin{cases}1\\k_n\,/\left(\sqrt{h}\left(\sqrt{\alpha-\alpha^2}+0.8\beta\sqrt{1/\alpha-\alpha^2}\right)\right)\end{cases}, \tag{13}$$

with k_n being defined by Equation (11) and the factor 0.8 by Equation (10).

2.3 Current design approach for notched CLT plates

Since EC5 (Eurocode, 2004) does not include structural design of CLT, such design is instead done by following the European Technical Assessment (ETA) documents of the respective CLT-producers. Other sources of technical information, such as technical guidelines (handbooks) are also used in cases when the ETA does not cover a specific design situation. An example of an ETA giving design provisions for notched CLT member is OIB (2017) while Wallner-Novak *et al.* (2013) is an example of a handbook giving such provisions. Both these technical documents recommend the use of the EC5-approach as formulated in Equations (11) – (13).

Depending on the placement of the notch corner in relation to longitudinal and transverse layers, see Figure 3, the shear acting at the corner may give rise to either

longitudinal shear or rolling shear in any case, however, always in combination with perpendicular to grain tensile stresses. The *rolling shear* strength $f_{v,r}$ is suggested to be used in both the above-mentioned technical documents, OIB (2017) and Wallner-Novak *et al.* (2013), thus assuming that an appropriate design criterion would be:

$$\tau_d = \frac{1.5V}{b\alpha h} \leq k_v f_{v,r,d} \, . \tag{14}$$

The effective depth, $h_{ef} = \alpha h$, is in the case of the ETA (OIB, 2017) interpreted according to Figure 3, disregarding the thickness of the lower-most layer at the notched support if that layer is a transverse layer. In Wallner-Novak *et al.* (2013) it is instead assumed that h_{ef} equals the physical depth of the notched part, *i.e.* including all layers of that part, irrespective of their orientation.
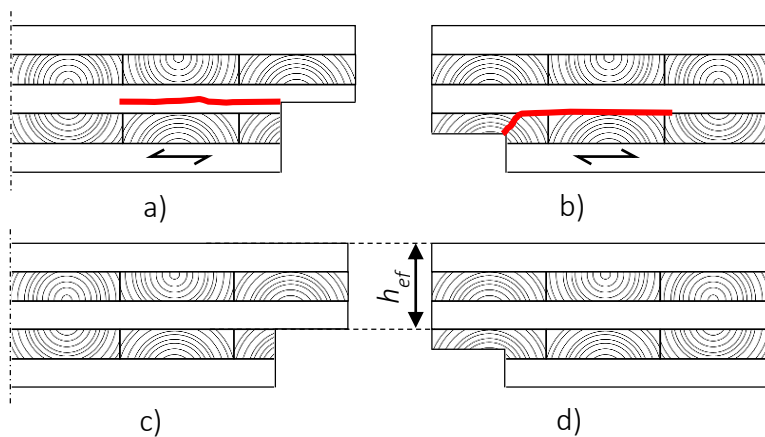
Figure 3. a) and b): Different locations of the notch corner in CLT, and probable crack paths. c) and d): Definition of h_{ef}, i.e. the effective depth of the notched part of the member.

The choice of definition of the effective depth h_{ef} may influence the predicted load bearing capacity to a significant extent. In addition, CLT plates behave differently from solid timber beams in several aspects. Different values of material strength, stiffness and fracture energy might be relevant to consider depending on the position of the notch in relation to the CLT layers. Furthermore, the ratio of bending stiffness to shear stiffness of the cross section can be very different in a CLT plate compared to a solid timber beam. Equations (11) – (13) are based on the compliance method, for which it is necessary to express the change of the compliance, C, of the structural member as a function of crack length during crack propagation. It is by no means self-evident that the use of Equations (11) – (13), which are based on simplifications reasonable for solid timber beams, give accurate results even if fitted to (a limited amount of) CLT test data. These simplifications, expressed in Equations (10) – (11), are not valid for a layered element, and it seems unlikely that a fit of the equations using only the parameter k_n would be valid for more than a very limited number of sizes, material qualities and CLT lay-ups.

2.4 Experimental evidence of behaviour of notched CLT plates

In Friberg (2017) a 5-layer CLT plate notched at the end and loaded in three-point bending was investigated using the set-up shown in Figure 4, showing also the notch depths tested. The lay-up of the 160 mm thick CLT was (40-20-40-20-40), without structural edge bonding, quality C24. The specimens had a notch at both ends and thus a larger amount of tests could be performed on a relatively limited amount of material. The notch locations tested were for all cases but one at the interface between a transverse and a longitudinal layer. In addition, a notch depth of 80 mm was also tested, in order to verify the case of crack propagation along grain, within a longitudinal layer. Crack propagation typically took place as indicated in Figure 3 a) and b) and the tests were in general stopped before the crack reached half the length of the span. For each notch depth, 6–8 nominally equal specimens were tested.
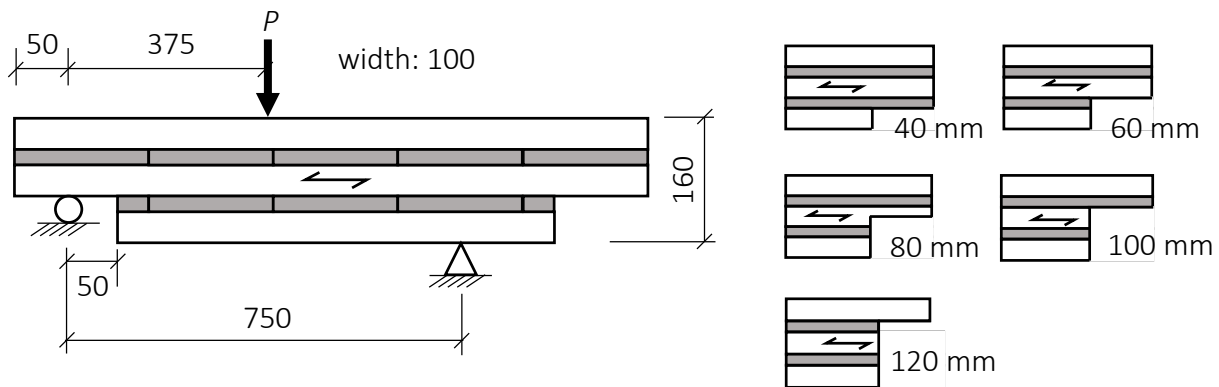
Figure 4. Test-setup used for notched CLT plates. Dimensions in mm. Steel plates were used at the load introduction and at the supports to avoid indentation. Five different notch depths were tested.

The outcome of the tests was that there was no significant difference in load bearing capacity between notch depths 40 and 60 mm nor between notch depths 100 and 120 mm. The test results are summarized in Table 1.

Table 1. Ultimate shear force capacity from tests (Friberg, 2017).

Notch (mm)	Shear force (kN)	Standard dev. (kN)	Num. of tests
40	15.0	1.6	6
60	14.4	1.7	7
80	8.9	1.3	6
100	5.5	0.80	8
120	5.3	0.65	8

It was noted during the tests that cracking always started from the re-entrant corner of the notch. For notch depths of 40 and 100 mm the crack propagated at an approximately 45° angle through the transverse layer. For the cases were the notch corner was at the lower edge of a longitudinal layer (notch depths 60 and 120 mm) or in the

middle of the longitudinal layer (notch depth 80 mm), the crack propagated along the grain direction of the longitudinal layer. It was not always possible to identify, from the force-displacement curves, at which load level the crack propagation started.

3 Design of notched CLT plates: rational methods

3.1 Overview of methods and input parameters

In the following, four different methods are presented: a) analytical beam theory by consistent use of the EC5-aproach, b) structural element approach (FE-based), c) 2D-continuum element approach based on LEFM and d) 2D-continuum element approach based on cohesive zone modelling, including softening. The material parameters used in these analyses are given in Table 2.

Table 2. Material properties assumed in the analyses.

Parameters	Values	Description
E_0 ; E_{90}	12 000 ; 500	MOE along grain; perp. grain [MPa]
$G_{0,90}$; $G_{90,90}$	600 ; 75	Shear modulus, longitudinal; rolling shear [MPa]
$v_{0,90}$; $v_{90,90}$	0.3 ; 0.3	Poisson's ratios [-]
$G_{C,I}$; $G_{C,II}$	400 ; 1500	Critical energy release rate, Mode I; Mode II [J/m^2]
f_t ; $f_{v,r}$	5; 2	Material strength, tension perp; rolling shear [MPa]

3.2 Consistent use of design equation based on compliance method

A consistent derivation of an analytical compliance method approach should use Equation (7) as a starting point, instead of applying directly Equations (11) – (13). The calculation of the shear stiffness KGA_i and the bending stiffness EI_i is for the non-homogeneous case of CLT-plates very involved, and closed-form solutions are not practical. An algorithm for calculation of the shear stiffness is given in *e.g.* Wallner-Novak *et al.* (2013), and that algorithm was applied here. In the calculation of the load level at which crack propagation occurs, it was assumed that $G_C = G_{C, I}$. This gives a lower-bound LEFM-solution to the problem, noting that LEFM-solutions, in general, overestimate the capacity (since they assume infinite material strength).

3.3 Structural element model

The second approach adopted included modelling with structural beam elements in a configuration according to Figure 5 and making use of the above described compliance method. In the model, the notched part has length $L_1 + a$ and the un-notched part has length $L_2 - a$, where a is the current crack length. A rigid link element connects the two shear flexible beam elements via a rotational spring. The link element is used in order to account for the possible effect of eccentricity between parts I and II. This type of beam model can be made to coincide with the analytical expressions of Equa-

tions (7) – (8), if Timoshenko beam type elements are used and, of course, if the rotational spring stiffness is set to the same value, *e.g.* according to Equation (5).

Another way of introducing a compliant coupling in the beam model is to assume an additional (fictitious) length of the crack, which indeed is also a way to interpret Equation (6). In that case the crack length *a*, mentioned above, would be different from the length of the physical crack. A similar approach to account for the compliant coupling was used in Danielsson & Gustafsson (2015).

In the analyses presented in this paper the shear flexible beams were of Timoshenko type, as for the method in section 3.2. Furthermore it was assumed that $G_C=G_{C,\,I}$, $k_\theta=\infty$ and that the crack extended an additional length equal to the notch depth, *i.e.* $(1-\alpha)h$. This choice of additional crack length was made to obtain a reasonable fit to test results and 2D-continuum model results. The choice can also be motivated by the fact that for a larger notch depth, the activation of the full cross section will take place at a larger distance from the notch. According to Danielsson & Gustafsson (2015) another choice could be to extend the crack length with the amount of $\alpha h/2$.
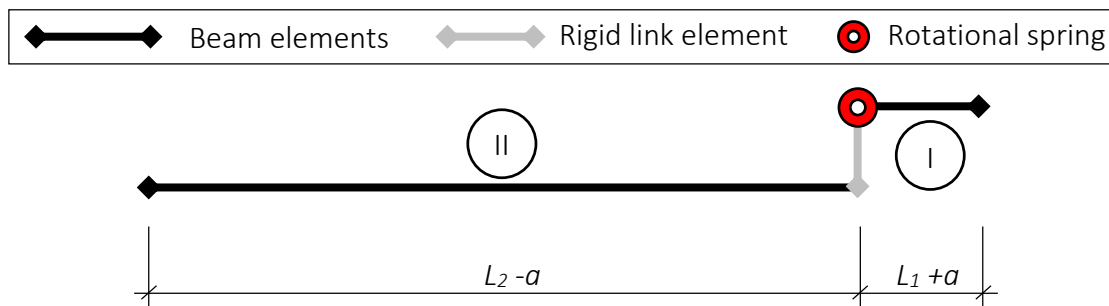
Figure 5. Beam model for analysis of notched members according to LEFM (compliance method).

3.4   2D Linear elastic fracture mechanics model

A convenient compliance method approach is to use 2D-plane stress elements to model the geometry of the CLT plate, including a crack. With such a model, a number of linear elastic analyses are performed, each analysis for a different crack length along a pre-defined crack path. Thus, the compliance of the structure as a function of crack length can be calculated by pure post-processing, *i.e.* the critical load for crack propagation, as a function of crack length, can be determined by use of Equation (3).

An example of a FE-mesh used is shown in Figure 6. The model relates to analyses for a notch depth of 40 mm, *i.e.* equalling the thickness of the outermost longitudinal layer. For cracking within a longitudinal layer, the crack path followed the grain direction. The crack path within the transverse layers was set to be 45° to the longitudinal layers. When the crack reached the border to the next longitudinal layer, the path was assumed to be oriented along the longitudinal layer. These assumptions of the crack paths are in accordance with the experimental observations in Friberg (2017). The bond lines between the laminations were not specifically modelled. The supports and the loading point were modelled with linear constraints.
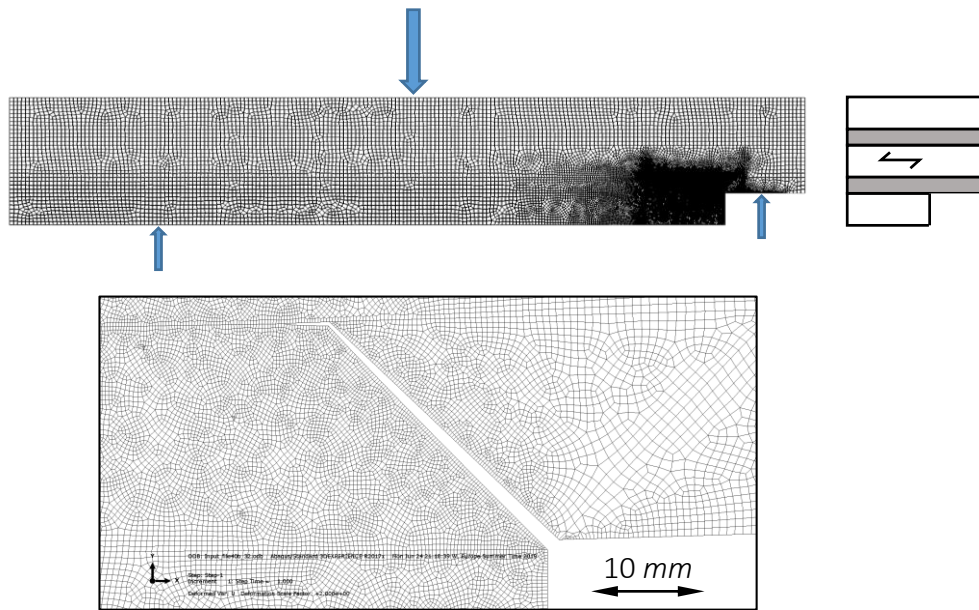
Figure 6. Example of FE-mesh. The crack length is 32 mm and the part with a 45° orientation has reached the 2nd longitudinal layer from below and has, after that, propagated horizontally.

3.5   2D Nonlinear cohesive zone model

Cohesive zone models have been used in many different applications related to timber engineering, see *e.g.* Serrano & Gustafsson (2006). The main advantage with such models is that they are relevant to use for a wide range of material parameters and absolute sizes of members, *i.e.* for a wide range of brittleness. In the present study, the built-in feature known as cohesive contact in the software (Dassault, 2017) was used to model the cohesive softening behaviour along pre-defined crack paths. The same crack paths as those used for the 2D LEFM model described above were adopted. An example of a FE-mesh used in the analyses is shown in Figure 7. In these analyses, both the supports and the loading point were modelled by the use of rigid surfaces interacting with the CLT-member (coefficient of friction was set to 0.3).
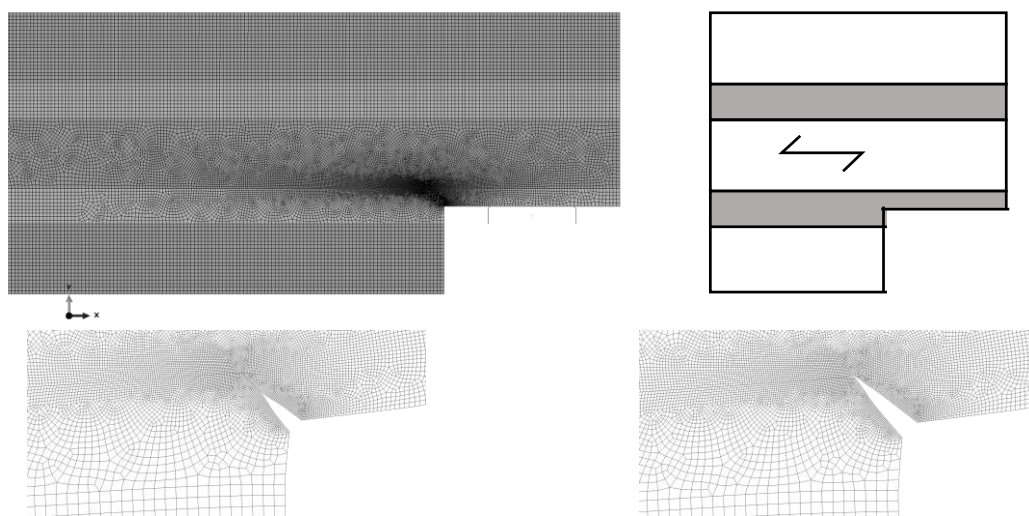
Figure 7. Top: FE-mesh used in nonlinear analyses. Bottom: Deformed mesh during crack propagation. The notch depth is 50 mm, i.e. with the corner of the notch in the centre of a transverse layer.

4 Results and discussion

4.1 Comparison of theoretical results and test results

Table 3 gives an overview of the results from the tests and from the predictions using the four approaches discussed above.

The consistent application of the EC5-approach gives reasonable results in relation to test results for notches less than 50% of the plate thickness. For larger notches it turns out that the equations produce unphysical results. The assumptions of shear flexible beam theory based on the use of the Timoshenko definition of shear stiffness, *KGA,* produce non-compatible strain distributions for the notched and un-notched parts of the beam. As a consequence, and depending on the value of the rolling shear modulus, even complex values can be the outcome (*i.e.* the value of KGA_I is larger than the value of KGA_{II}), *cf.* Equation (7). As an example, if the rolling shear modulus is set to 60 MPa (instead of the assumed 75 MPa), complex values are obtained from Equation (7) for a notch depth of 100 mm.

Table 3. Tested and predicted ultimate shear force capacity (kN). For the results in boldface, the EC5 approach gives unrealistic results, and results highly dependent on the value of the rolling shear modulus. Values in parenthesis refer to evaluating the ultimate load at a crack length of 12 mm.

Notch	Test	Consistent EC5	Structural elements	2D LEFM		2D non-linear
40	15.0	13.9	15.9	13.8		13.6
50	N/A	13.6	15.2	14.4		14.2
60	14.4	13.5	14.7	14.1		14.0
80	8.9	9.7	9.9	12.1	(10.4)	10.3
100	5.5	**11.1**	5.1	5.2		5.4
120	5.3	**9.8**	4.2	6.0	(5.1)	5.6

As compared to the test results, it seems like the other three methods give reasonable predictions. Note that the approach using structural elements, *cf.* Figure 5, involves calibration to test results in terms of choice of crack length, as mentioned previously.

The two methods based on 2D FE-analyses give credible predictions, and the relative influence of the notch depth is indeed in accordance with the test results. It should be underlined that no detailed calibration of material parameters such as fracture energies was done.

An important outcome is also that the assumption of $G_C = G_{C, I}$ during crack propagation, assumed in the LEFM analyses, seems accurate. Even when mixed mode behaviour is accounted for, in the 2D non-linear analyses, that mixed mode behaviour

seems to have a very limited influence on the predicted load bearing capacity. Another observation is that, since LEFM and non-linear fracture theory give similar results, the influence of local material strength is very limited. Thus, failure is instead (in terms of material properties) governed by fracture energy and material stiffness.

As mentioned previously, the result from the compliance method approach is in terms of crack propagation load as a function of crack length. Thus, it is in general not possible to give a specific crack propagation load without also including some other criterion, *e.g.* choice of critical crack length. The results from all 2D continuum element analyses are shown in Figure 8. There, the compliance method analyses are represented by curves and the non-linear analyses based on a cohesive zone approach and the test results are represented by markers. It is seen that for all cases except 80 and 120 mm notch depths, a local maximum of the ultimate load versus crack length curve can be seen. For these cases, this local maximum is used as the ultimate load level in Table 3, whereas for the 80 and 120 mm notch depths, the initial failure load is used. As an alternative (Serrano & Gustafsson, 2006), the critical load can be defined for a crack length which depends on the material properties and the current state of mixed mode. A rough estimate of such a length, taking into account the current material properties and assuming a pure Mode I state, would be 5-12 mm depending on if a transverse layer or a longitudinal layer is considered. Thus, it is possible to define the ultimate capacity from the 2D-LEFM analyses by choosing the crack propagation load corresponding to such a crack length. The difference in results can be seen in Table 3, where the values in parenthesis are based on a 12 mm crack length estimation. For the case of a notch depth of 80 mm, using the estimate based on 12 mm crack length, an improved prediction of the failure load is obtained, from 24.2 kN to 20.8 kN, *i.e.* from 12.1 kN to 10.4 kN shear force (the results in Figure 8 relate to the ultimate load applied, in this case twice the shear force, *cf.* Figure 4).
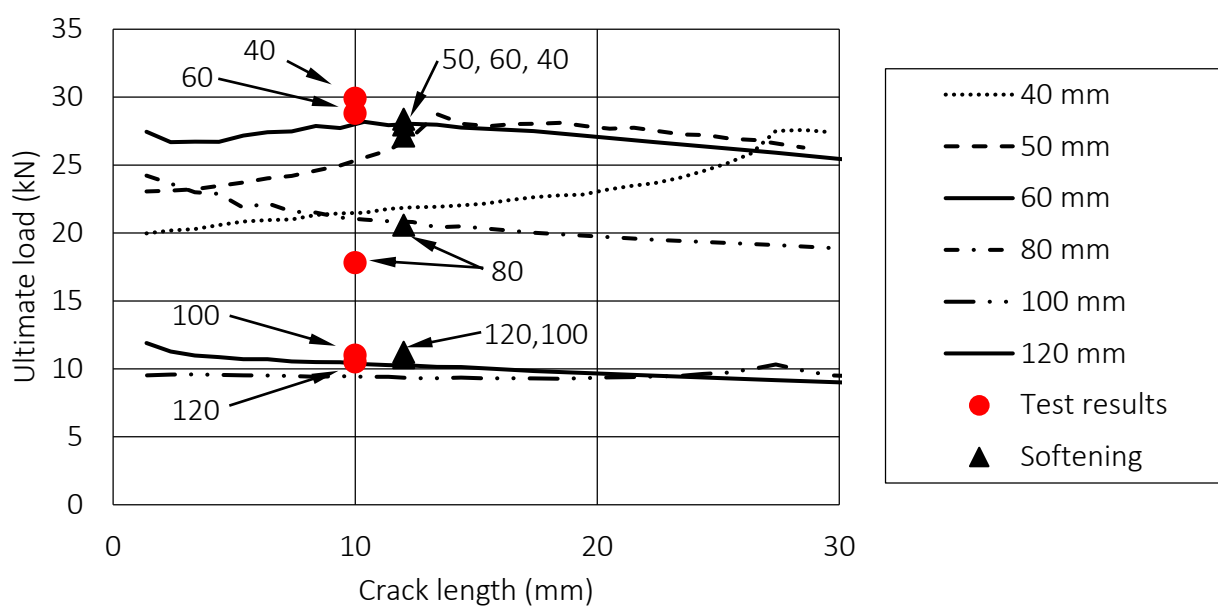
Figure 8. Results from FE-analyses using compliance method (curves), from analyses using a softening cohesive model and from tests (shown with markers and indicating notch depths with numbers).

4.2   Comparison with current ETA-approach

A comparison with the design approach of (OIB, 2017), is done in the following. First of all, it would be of interest to compare the relative influence of the notch sizes (length and depth), but limited test data is available in open sources. Therefore, the current comparison is restricted to the cases already presented here and where test results are available in Friberg (2017). Since design is done based on characteristic, 5% values, it is difficult to compare with results from a limited test series. Therefore, the comparison is made with the relative influence of notch depth on the predicted shear force capacity. For the different approaches and for the test results, the shear force capacity is normalised such that it is set to 1.0 for α = 0.5. Doing so also eliminates the influence of the choice of the factor k_n, *cf.* Equation (11). The results from this comparison are shown in Figure 9. Note that the results from the compliance-based 2D continuum approach, for notch depths of 80 and 120 mm (=relative notch depth of 0.5 and 0.75, respectively), relate to a critical crack length of 12 mm.
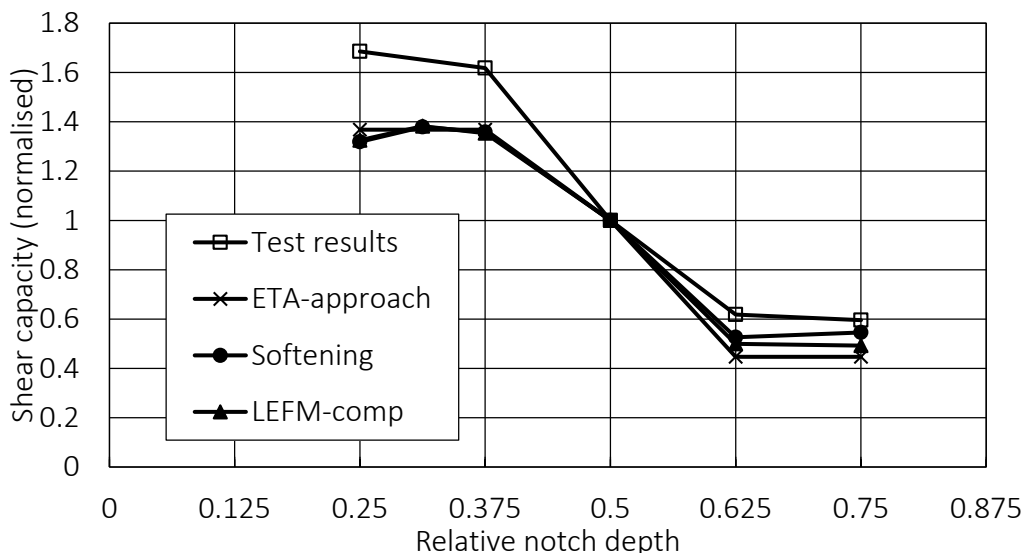
Figure 9. Comparison of test results, theoretical models and design approach.

The ETA (OIB, 2017) mentions that characteristic values of rolling shear strength (0.8–1.2 MPa) should be used as a basis for design. Applying the ETA approach assuming a shear strength value of 1.2 MPa and k_n=4.7, results in a characteristic shear force capacity of the CLT-plate with a 50% notch of 2.86 kN. The tests, see Table 1, gave an *average* of 8.9 kN, based on 6 tests. An estimate of the corresponding *characteristic* capacity, using the procedure of EN 14358 (CEN, 2016), assuming 15% COV and 6 nominally equal test specimens, *cf.* Table 1, gives $8.9(1-2.3\times0.15) \approx 5.8$ kN. Thus, it seems like the ETA approach is very much on the safe side.

At first glance, it seems like all the applied approaches predict accurately the influence of the notch depth. It must be emphasized, however, that the current investigation only has considered one lay-up, one notch length and, above all, only one orientation of the notch in relation to the main directions of the CLT. The notch orientation considered in the present work is probably relevant for supports. Another im-

portant application of notched members would be for joining CLT plates using a half-in-half type of joint, with the joining line being *parallel* to the main load bearing direction of the plate(s). This case has not been considered here, and it is not evident that the influence suggested by the ETA-approach is correct also for that case. It should be noted that the ETA-approach only mentions an orientation of the notch according to Figure 3, and also limits the application of the design equation to $\alpha \leq 0.5$.

4.3 Conclusions, recommendations for design and further work

The following conclusions, including recommendations for design, are the results from the work presented in this paper:

- A consistent application of the EC5-approach for notched solid timber beams is not useful in general, due to incompatibilities with the underlying beam theory when applied to CLT.

- Both LEFM and non-linear softening theory seem appropriate approaches in determining the load bearing capacity of notched CLT plates.

- The use of LEFM involves the non-trivial choice of critical crack length.

- It has been shown that the definition of effective member depth, h_{ef}, should *not* include outer transverse layers at the notch.

- As regards recommendations for design, the approach of OIB (2017) can be used. However, it must be emphasised that this EC5-based method should be treated as an empirical approach, valid only for CLT lay-ups and orientations for which the expression has been calibrated.

For future work it is essential that test data be made public, such that the applicability of design formulae can be verified for more load cases and CLT lay-ups. Furthermore, it would be of great interest to extend the current study to also include notch orientations relevant for CLT-plate joints. In terms of further development of the theoretical basis, it would be of interest to apply fracture mechanics based methods using higher order beam theories, see *e.g.* Tessler *et al.* (2009). Possibly also methods developed for other layered products, such as plywood, see *e.g.* Nairn (2006), could be useful in order to find analytical formulations.

5 Acknowledgments

6   References

CEN (2016): EN 14358:2016. Timber structures. Calculation and verification of characteristic values.

Danielsson, H. & Gustafsson, P. J. (2015): A beam theory fracture mechanics approach for strength analysis of beams with a hole. In: International Network on Timber Engineering Research – Proceedings Meeting 48, Paper INTER/48-19-1, Sibenik, Croatia.

Dassault (2017): Dassault Systemes Simulia Corp. ABAQUS, User Documentation, Version 2017.

Eurocode 5 (2004): EN 1995-1-1:2004, Eurocode 5: Design of timber structures – Part 1-1: General – Common rules and rules for buildings.

Friberg, A. (2017): Bärförmåga för KL-trä med urtag – Provning och beräkningsmetoder (in Swedish). (*Load-bearing capacity of CLT with notches – Testing and calculation methods*). Bachelor thesis, Report THID-5526, Division of Structural Mechanics, Lund University.

Griffith, A. A. (1921): The phenomena of rupture and flow in solids. *Philosophical Transactions of the Royal Society of London, A.* 221 (582–593): 163–198.

Gustafsson, P. J. (1988): A study of strength of notched beams. In: Proceedings CIB-W18 Meeting 21, Paper CIB-W18/21-10-1, Parksville, Canada.

Nairn, J. A. (2006): On the calculation of energy release rates for cracked laminates with residual stresses, International Journal of Fracture, 139, 267–293.

OIB (2017): European Technical Assessment, ETA-06/0138 of 20.2.2017.

Petersson, H. (1974): Analysis of loadbearing walls in multistorey buildings. Stresses and displacements calculated by a continuum method. Thesis, Chalmers University of Technology, Sweden.

Serrano, E. (2018): Cross Laminated Timber Plates with Notches – Analyses based on fracture mechanics. In: Timber – Bonds, Connections and Structures. G. Dill-Langer (Ed.), ISBN 978-3-946789-01-7, MPA University of Stuttgart, Stuttgart.

Serrano, E. & Gustafsson, P. J. (2006): Fracture mechanics in timber engineering – Strength analyses of components and joints. *Materials and Structures*, 40:87–96.

Tessler, A., Di Sciuva, M., Gherlone, M. (2009): Refined zigzag theory for laminated composite and sandwich plates. NASA/TP-2009-215561.

Wallner-Novak, M., Koppelhuber, J. & Pock, K. (2013): Brettsperrholz Bemessung – Grundlagen für Statik und Konstruktion nach Eurocode. ProHolz Austria, Immenstadt, Austria.

Discussion

The paper was presented by E Serrano

R Jockwer asked if clamping effect was included, would the capacity decrease. E Serrano responded that it could play a big role and should be considered in future.

M Li commented that FEM used cohesive element and crack propagation was considered at inclined angle. Would the model consider the crack propagation later along the glue line. E Serrano responded that this is done.

J Chen asked about the E/G ratio of 15.6 and Rs value of 2 MPa. E Serrano responded that the E/G ratio was referenced to a 1988 CIB W18 paper and it is an assumption with strength class data indicating a value of 16. E Serrano also said that Rs value was not important for fracture energy in tension perpendicular to grain.

S Winter said in EC5 the limit of Alpha is to 0.5 as larger notches are not right because it could lead to vibration and other issues; therefore, higher values for Alpha are not meaningful. S Winter suggests to limit at 0.5, setting a range for which the formula was applicable. E Serrano confirmed that the beam width is 100mm.

Compressive strength and stiffness of end grain contact joints in glulam and CLT

Marcus Flaig[1], Tobias Schmidt[2] and Hans Joachim Blass[1,3]

[1]Blass und Eberhart GmbH, Karlsruhe
[2]Timber Engineering and Structural Analysis, University of Applied Sciences, Augsburg
[3]Timber Structures and Building Construction, Karlsruhe Institute of Technology

1   Introduction

The design of timber members loaded in compression parallel to grain, e.g. columns, walls and bracing elements, is usually governed by buckling, lateral torsional buckling or a combination of both. However, in members with small slenderness ratio or with local reduction of the cross-sectional area, strength may govern the design. Current design codes therefore require the verification of both, stability and strength, the latter usually in consideration of cross-sectional reductions.
If load is transferred via contact between two end grain surfaces, e.g. in stacked columns of multi-storey buildings or pre-stressed CLT bracing walls, yet another kind of failure may occur, which is not covered by design codes so far.

In compressive tests with continuous timber members, failure is usually observed around defects, e.g. knots or fibre deviations, or in areas with reduced cross section. In tests with end contact joints, in contrast, failure is observed almost exclusively directly in or close to the joint. Compressive failure in timber members is usually characterised by compressive wrinkles and local buckling of split-off fibre bundles. In members with end grain contact joints a similar failure can be observed, but here, in addition, deep imprints of the latewood parts of the annual rings of the counterpart occur in the contact surfaces of the jointed members (Fig 1).

Figure 1:   Typical compression failure at end grain contact joint in CLT: joint after failure (left), contact surfaces with mutual imprints of annual rings (right)

2   Experimental work

2.1   Test series

Four different test series were performed to determine the strength and the stiffness of end grain contact joints in glulam and CLT, the latter also with different moisture contents and with steel plates in the contact joints. In addition, to determine the decrease of the mechanical properties resulting from the joints, two reference test series (REF), with CLT and glulam specimens without contact joint, were performed. The strength class of all CLT specimens was C24, the glulam specimens complied with strength class GL24h. Table 1 gives an overview of the test series.

Table 1:   Overview of test series

material	contact joint	steel plate	service class	number of specimens	layup/layer thickness in mm (cross layers underlined)	length in mm	width in mm	depth in mm
CLT (REF)	no	no	1	15	40-20-40-40-20-40	1200	600	200
CLT	yes	no	1	15	40-20-40-40-20-40	2 x 600	600	200
CLT	yes	no	1[a)]	13	40-20-40-40-20-40	2 x 600	600	200
CLT	yes	yes	1[a)]	15	40-20-40-40-20-40	2 x 600	600	200
GL (REF)	no	no	1	16	20-40-20	480	100	80
GL	yes	no	1	16	20-40-20	2 x 240	100	80

a)   The moisture content of the test specimens corresponded to service class 1. In addition, the contact surfaces were wetted for 30 minutes before the tests to simulate possible rainfall or other precipitation during transport and erection.

2.2   Test setups

For all test series with CLT specimens a test setup according to EN 408 was chosen, i.e. the length of specimens was 6-times the depth and the deformation u_{glob} was measured within a length of 4-times the depth. In test series with end grain contact joint, in addition, the local deformation u_{loc} near the joint was measured within a length of 60 mm. Figure 2 shows the principle test setup used in test series with CLT specimens.
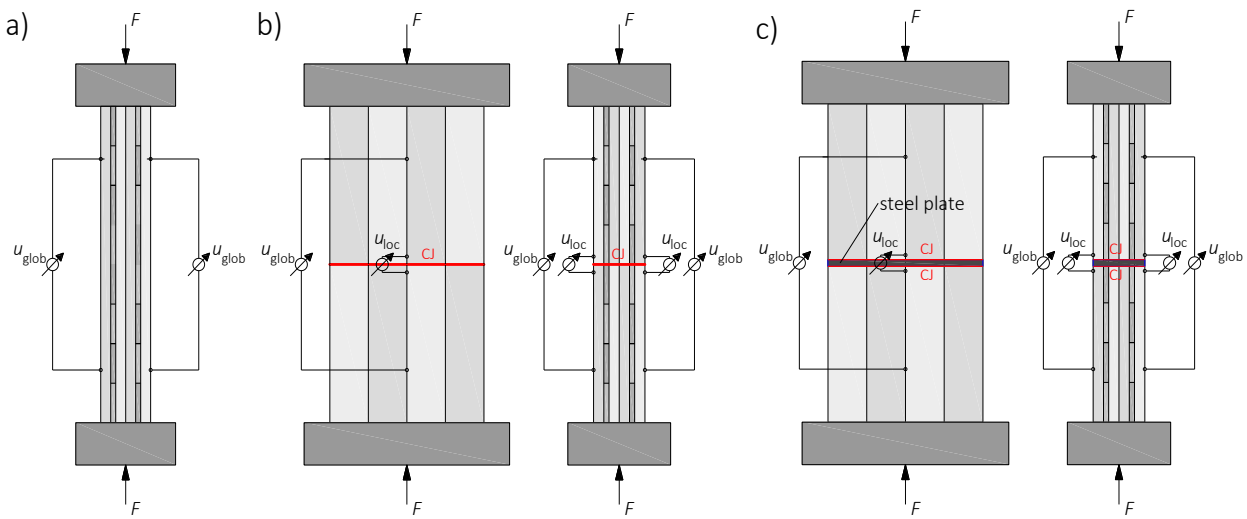
Figure 2: Test setup used for CLT specimens without contact joint (a), with contact joint (b) and with steel plate in the contact joint (c)

For the test series with glulam specimens the principle test setup also was chosen according to EN 408. However, the deformation was not measured as required in the standard within a length of 4-times the depth but within a length of 100 mm. Figure 3 shows the test setup used in glulam test series.
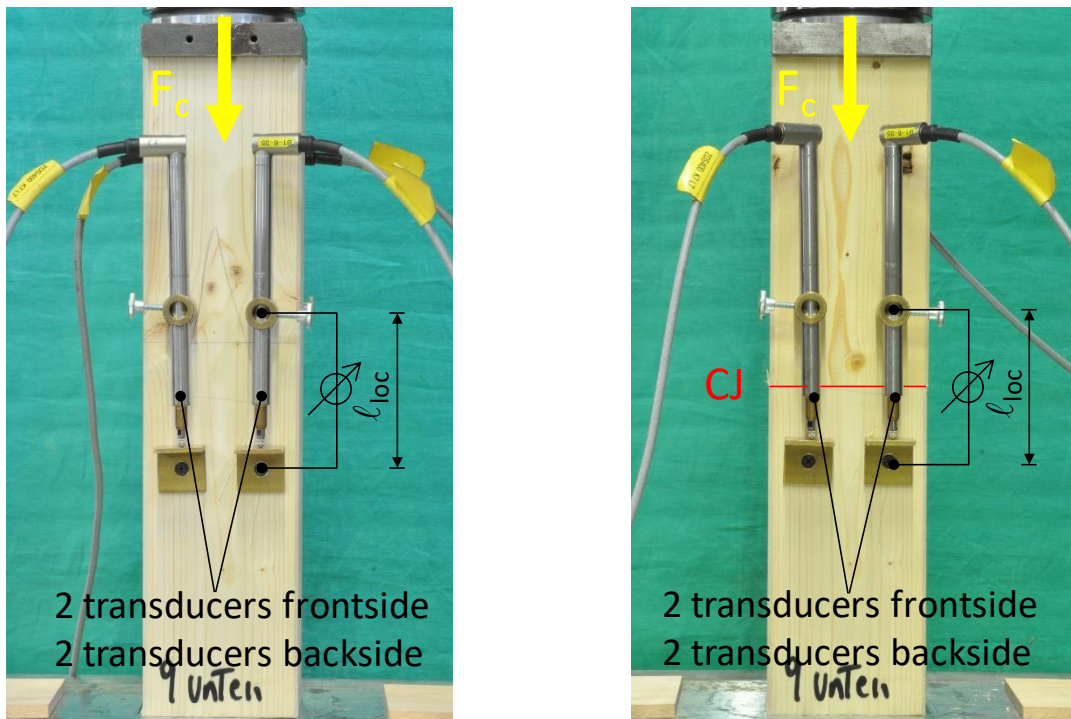
Figure 3: Test setup used for glulam specimens to determine the MOE in the joint (left) and to determine the strength and stiffness of the end grain contact joint (right) by Schmidt and Blass. The tests were carried out at KIT and partially by A. Berti / Italy.

3 Test results

3.1 Test data and evaluation

For every specimen the applied load F, the global deformation u_{glob}, and in test series with contact joint also the local deformation u_{loc} were measured with a frequency of 1 Hz. The load deformation curves generated from the test data are shown in the following sections. The moisture content and the density were also determined for each specimen or for each part of specimen in test series with contact joint. From the test data the compressive strength, the modulus of elasticity and the slip modulus of the joint were calculated and compared to determine the impact of the joints on the load bearing capacity and the stiffness of the tested members.

The compressive strength was calculated as the ratio between the ultimate load and the cross-sectional area of lamellae with grain direction parallel to the applied load, i.e. for glulam the full cross section and for CLT the net cross section of longitudinal layers.

$$f_{c,0,GL} = \frac{F_{max}}{A} \qquad \text{and} \qquad f_{c,0CLT} = \frac{F_{max}}{A_{net,long}} \qquad (1)$$

For the reference series without end grain contact joint the MOE was determined according EN 408 from the load-deformation curves of the global deformation u_{glob} between 10% and 40% of the ultimate load using a linear regression.

$$E_{c,0,eff,GL} = \frac{\Delta F}{\Delta u} \cdot \frac{\ell_{glob}}{A} \qquad \text{and} \qquad E_{c,0,eff,CLT} = \frac{\Delta F}{\Delta u} \cdot \frac{\ell_{glob}}{A_{net,long}} \qquad (2)$$

In test series with contact joint two different methods were used to determine MOE and slip modulus of the joint:

i)   In test series with <u>CLT</u> the MOE and the slip modulus were evaluated from the deformation measured during main compressive tests

ii)   In test series with <u>glulam</u> the MOE of each (part of a) specimen was determined separately in a pre-test

3.1.1 Evaluation of test series with CLT

For the evaluation the MOE and the slip modulus of the mechanical model shown in Figure 4 was used. It was further assumed, that each of the measured deformations, u_{glob} and u_{loc}, consists of two parts, one resulting from strain in the timber and the other from local indentations in the vicinity of the joint. With the axial stiffness of the timber parts EA and the stiffness of the end grain contact joint K_{CJ}, the measured deformations u_{glob} and u_{loc} can be described by the expressions given in eq. (3).

$$\begin{bmatrix} \Delta u_{glob} = \dfrac{\Delta F \cdot \ell_{glob}}{EA} + \dfrac{\Delta F}{K_{CJ}} \\[2mm] \Delta u_{loc} = \dfrac{\Delta F \cdot \ell_{loc}}{EA} + \dfrac{\Delta F}{K_{CJ}} \end{bmatrix} \tag{3}$$

Using the substitution $m = \dfrac{\Delta F}{\Delta u}$ and solving eq. (3) for the MOE of the members E and the slip modulus of the end grain contact joint K_{CJ} the expressions given in eq. (4) is obtained:

$$\begin{bmatrix} E_{c,0} = \dfrac{\ell_{glob} - \ell_{loc}}{A_{net,long} \cdot \left(1/m_{glob} - 1/m_{loc}\right)} \\[3mm] K_{CJ} = \dfrac{\ell_{glob} - \ell_{loc}}{\ell_{glob} \cdot 1/m_{loc} - \ell_{loc} \cdot 1/m_{glob}} \end{bmatrix} \tag{4}$$

To determine slip moduli independently of the member size the values calculated from eq. (4) were divided by the cross sectional area of the test specimens, i.e. for CLT the net cross section of longitudinal layers.

$$k_{CJ} = K_{CJ} / A_{net,long} \tag{5}$$
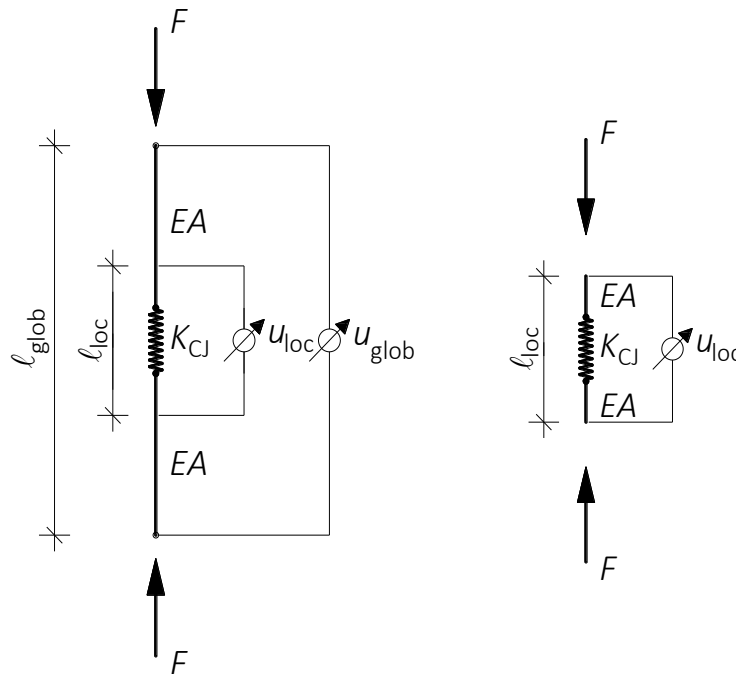
Figure 4:   Mechanical model used for the evaluation of CLT tests (left) and glulam test (right)

3.1.2   Evaluation of test series with glulam

A slightly different method was used to determine the stiffness of the contact joints in glulam, see Figure 5. At first, all specimens were loaded up to 40 % of the esti-mated failure load in a pre-test series and the modulus of elasticity within the length ℓ_{loc} was evaluated from the obtained data according to eq. (6).

$$E_{0,c} = m \cdot \frac{\ell_{loc}}{A} \qquad \text{with } m = \frac{\Delta F}{\Delta u} \qquad (6)$$

In a second step, half of the specimens were loaded until failure without implement-ing end grain contact joints (REF series). The second half of the specimens were cut in the middle, and one part was turned by 180° around its longitudinal axis to ensure different orientations of the annual rings in opposite contact surfaces. Then, the two parts were put on top of each other and loaded until failure.
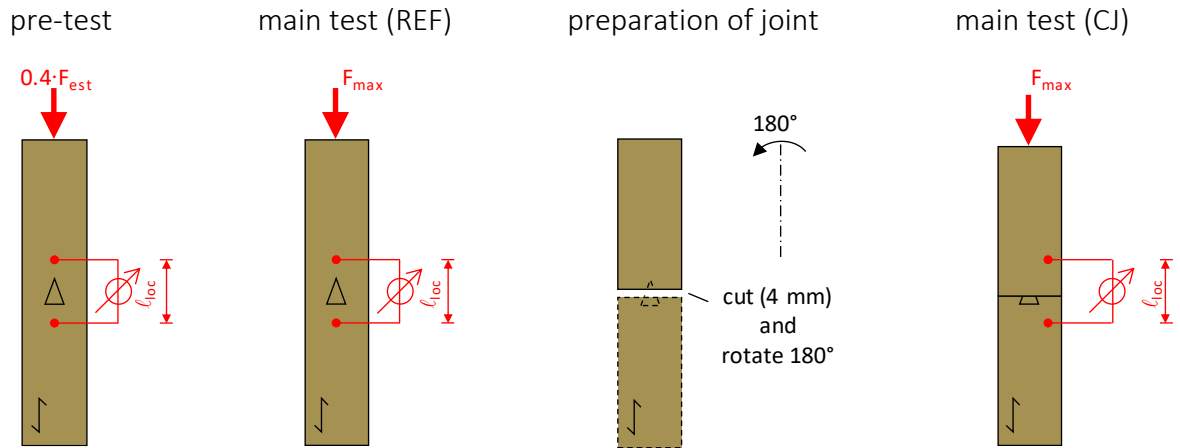
Figure 5: Test setup used for glulam specimens by Schmidt and Blass

For specimens with end grain contact joint the MOE determined in advance was used to calculate the joint stiffness K_{CJ} from the local deformation u_{loc} measured in the main tests. The expression given in eq. (7) for the local deformation can be derived from the model shown in figure 4 (right). After few transformations and simplifica-tions, the expression in eq. (8) is obtained for the stiffness of the end grain contact joint K_{CJ}.

$$\Delta u_{loc} = \frac{\Delta F \cdot \ell_{loc}}{EA} + \frac{\Delta F}{K_{CJ}} \qquad (7)$$

$$K_{CJ} = \left(\frac{\Delta u}{\Delta F} - \frac{\ell_{loc}}{EA} \right)^{-1} \qquad (8)$$

As for CLT, the slip moduli calculated from eq. (8) were divided by the cross sectional area of the test specimens to obtain values independent of the member size.

$$k_{CJ} = K_{CJ} / A \qquad (9)$$

In the following sections the load deformation curves, the density, the moisture content and the stiffness parameters $E_{0,c}$ and k_{CJ} for all test series are given in detail.

3.1.3 Test results for CLT

Table 2: Test results for CLT specimens without contact joint

specimen No.	ρ_1 in kg/m³	ρ_2 in kg/m³	MC_1 in %	MC_2 in %	$f_{c,0,net}$ in N/mm²	$E_{c,0,eff}$ in N/mm²
1	454	-	10.9	-	38.2	12387
2	467	-	10.7	-	36.5	12328
3	438	-	11.0	-	38.3	12377
4	451	-	10.9	-	36.8	11519
5	446	-	10.9	-	36.4	11713
6	442	-	10.0	-	41.0	13064
7	429	-	10.0	-	38.0	11371
8	427	-	10.0	-	37.6	12116
9	465	-	10.5	-	38.0	11917
10	442	-	10.7	-	37.9	11566
11	432	-	10.4	-	36.3	11403
12	449	-	10.7	-	38.5	11820
13	444	-	10.2	-	38.0	11530
14	480	-	10.1	-	39.6	12561
15	436	-	10.3	-	36.0	12564
MIN	427		10.0		36.0	11371
MEAN	447		10.5		37.8	12016
MAX	480		11.0		41.0	13064
5th percentile					35.2	

Table 3: Test results for CLT specimens with contact joint

specimen No.	ρ_1 in kg/m³	ρ_2 in kg/m³	MC_1 in %	MC_2 in %	$f_{c,0}$ in N/mm²	$E_{c,0}$ in N/mm²	$E_{c,0,eff}$ in N/mm²	k_{CJ} in N/mm³
1	430	447	10.1	10.7	35.5	11262	8126	139
2	443	442	10.8	10.4	34.7	10135	7583	198
3	418	444	10.9	10.7	34.1	11193	8003	123
4	432	428	10.9	10.2	32.8	11273	7923	106
5	419	438	10.9	10.8	33.9	10644	7636	121
6	436	455	10.8	10.4	33.6	11035	8257	216
7	434	444	10.9	11.1	33.6	10816	8017	183
8	456	458	11.2	10.7	36.3	12234	8671	126
9	448	462	11.2	10.9	37.0	12014	8911	205
10	457	462	11.2	11.0	35.5	11604	8374	141
11	458	457	11.2	10.8	36.2	12424	8968	151
12	459	447	11.2	11.0	36.4	11260	8268	167
13	435	464	10.2	11.0	33.8	11185	7978	120
14	439	461	10.5	11.0	34.6	11222	8256	171
15	420	454	10.5	11.1	32.6	10027	7292	133
MIN	418	428	10.1	10.2	32.6	10027	7292	106
MEAN	439	451	10.8	10.8	34.7	11222	8151	153
MAX	459	464	11.2	11.1	37.0	12424	8968	216
5th percentile					32.0			

Figure 3: Load-deformation curves for CLT specimens
left: reference series without contact joint
middle and right: series with contact joint
red curves represent mean values

3.1.4   Test results for glulam

Table 4:   Test results for glulam specimens with and without contact joint

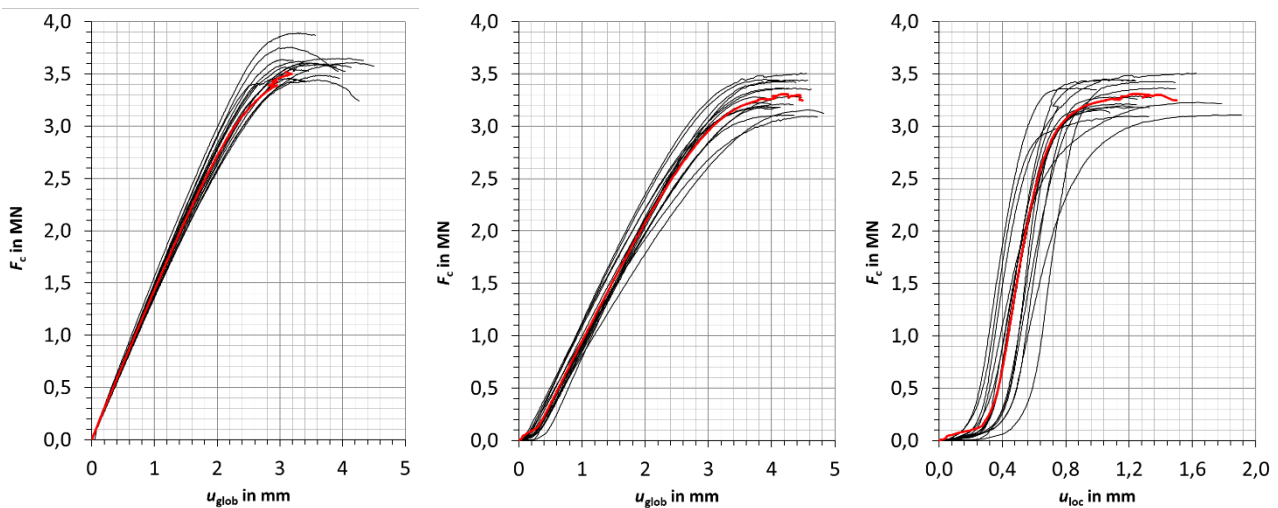| Reference series without contact joint				Test series with contact joint				
specimen no.	ρ in kg/m³	$f_{c,0}$ in N/mm²	$E_{c,0}$ in N/mm²	specimen no.	ρ in kg/m³	$f_{c,0}$ in N/mm²	$E_{c,0}$ in N/mm²	k_{CJ} in N/mm³
1	489	38.5	14520	1	482	32.0	14120	363
2	488	40.8	13490	2	484	33.2	11350	261
3	439	34.5	12050	3	488	33.8	16660	362
4	451	31.1	11580	4	456	33.2	9220	275
5	502	39.2	11140	5	494	34.4	9850	266
6	494	40.1	14300	6	425	32.2	10340	252
7	443	36.5	10670	7	499	29.6	13170	330
8	507	37.3	13980	8	506	31.1	13520	307
9	483	35.5	13990	9	443	32.6	10260	259
10	429	34.7	11900	10	449	33.9	11270	274
11	504	35.6	11830	11	432	35.6	10900	370
12	419	35.5	11290	12	503	41.2	16130	365
13	459	37.0	14240	13	496	40.8	13300	283
14	497	38.3	14330	14	412	32.8	11310	263
15	517	35.9	12110	15	508	40.2	14330	482
16	470	37.0	14330	16	459	36.2	12110	375
MIN	419	31.1	10670	MIN	412	29.6	9220	252
MEAN	474	36.7	12859	MEAN	471	34.5	12365	318
MAX	517	40.8	15200	MAX	508	41.2	16660	482
5th percentile		32.2		5th percentile		28.5		

The mean moisture content was 11.8 % (COV 9.2 %).
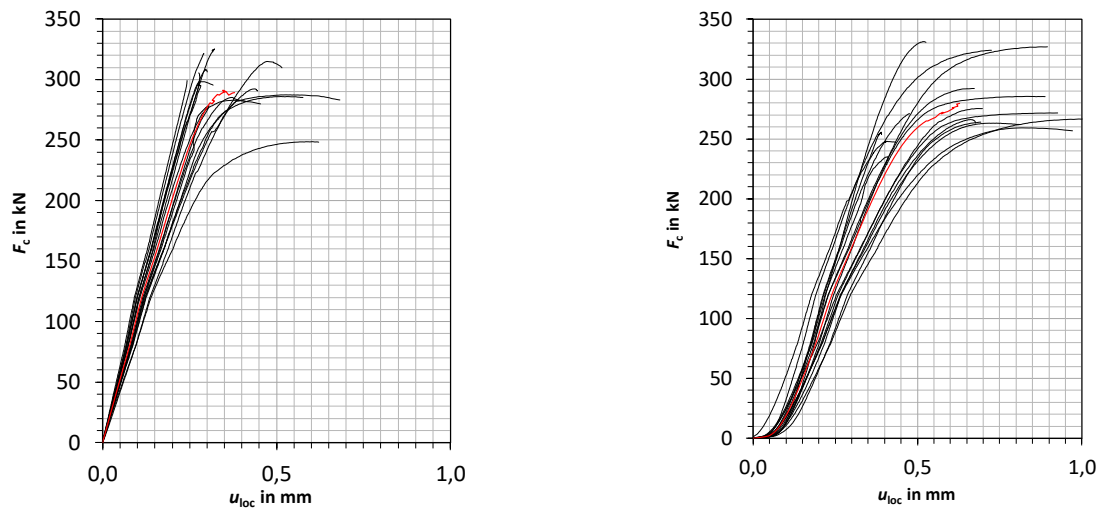
Figure 7: Load-deformation curves for glulam specimens
left: reference series without contact joint
right: series with contact joint
red curves represent mean values
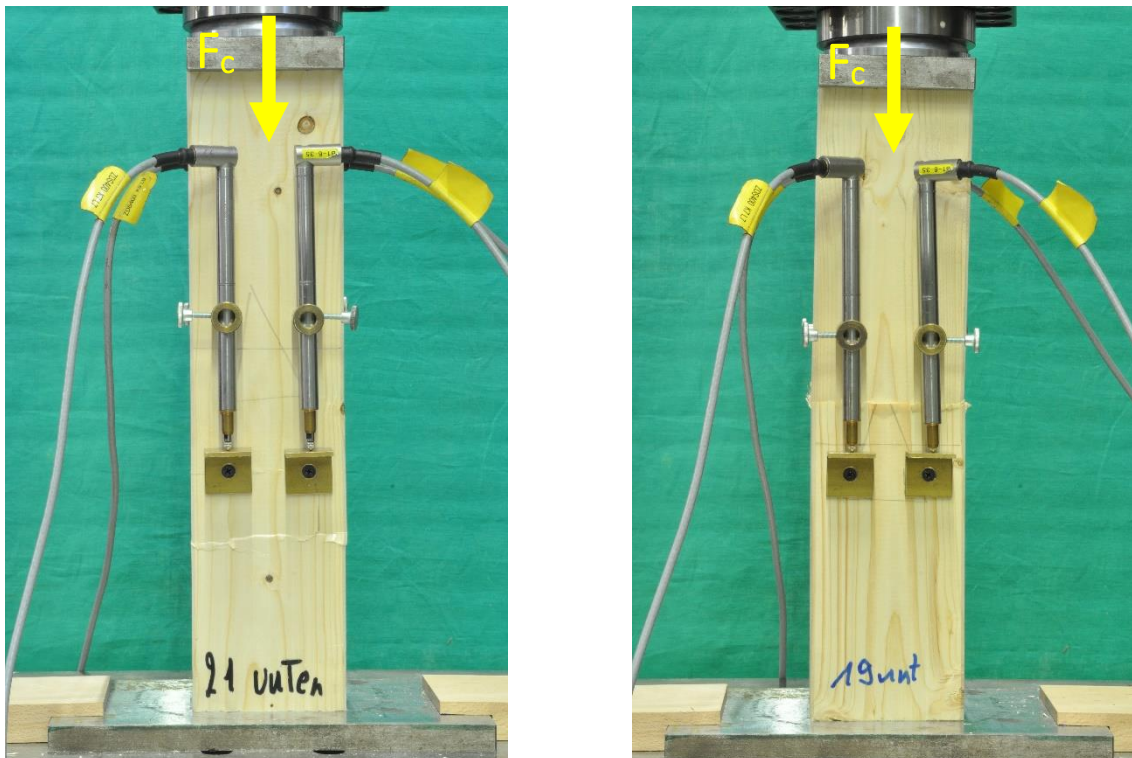
Figure 8: Glulam specimen after failure
left: without contact joint
right: with contact joint

3.1.5 Test results for CLT and wetted contact surfaces

Table 5: Test results for CLT specimens with contact joint tested with wetted contact surfaces

specimen no.	ρ in kg/m³	MC in %	$f_{c,0}$ in N/mm²	$E_{c,0}$ in N/mm²	k_{CJ} in N/mm³
1	446	12.4	24.8	12300	31.3
2	434	12.7	26.0	9000	38.0
3	467	12.5	26.3	11900	9.26
5	473	12.6	27.8	12900	33.4
6	452	12.8	27.2	11700	37.7
7	460	12.7	25.7	12200	42.9
8	456	12.7	26.3	11500	24.2
9	465	11.7	26.5	13300	30.3
10	447	11.7	26.9	10000	44.4
11	435	7.9	27.5	12000	23.9
12	439	11.1	27.8	11500	41.5
14	441	12.7	27.7	11500	26.5
15	432	12.3	27.3	8850	51.7
MIN	432	7.90	24.8	8850	9.26
MEAN	449	12.0	26.8	11435	33.5
MAX	473	12.8	27.8	13300	51.7
5th percentile			24.9		

Figure 9: Load-deformation curves for CLT specimens with contact joints tested with wetted contact surfaces; red curves represent mean values

Figure 10: Typical compression failure at contact joint in CLT specimen: joint after failure (left), contact surfaces with mutual imprints of annual rings (right)

Table 6: Test results for CLT specimens with contact joint and steel plate tested with wetted contact surfaces

specimen No.	ρ in kg/m³	MC in %	$f_{c,0}$ in N/mm²	$E_{c,0}$ in N/mm²	k_{CJ} in N/mm³
1	433	11.2	29.9	12300	34.1
2	433	12.2	29.0	10900	17.9
3	456	11.5	29.5	11300	32.8
4	463	11.6	28.2	12600	33.0
5	467	12.5	30.9	14600	28.2
6	453	12.8	28.9	12000	33.6
7	456	12.9	30.4	11500	30.8
8	442	12.6	29.5	11400	35.6
9	450	12.8	31.6	12500	39.8
10	453	11.1	30.5	12900	41.4
11	440	11.6	30.4	13300	27.7
12	458	12.4	30.2	17100	29.2
13	458	12.7	32.5	12600	31.2
14	451	12.2	31.8	12300	40.3
15	450	12.8	31.3	10800	37.7
MIN	433	11.1	28.2	10900	17.9
MEAN	451	12.1	30.1	12692	32.0
MAX	467	12.9	32.5	17100	41.4
5th percentile			28.0		

Figure 11: Load-deformation curves for CLT specimens with steel plate in the contact joint tested with wetted contact surfaces; red curves represent mean values
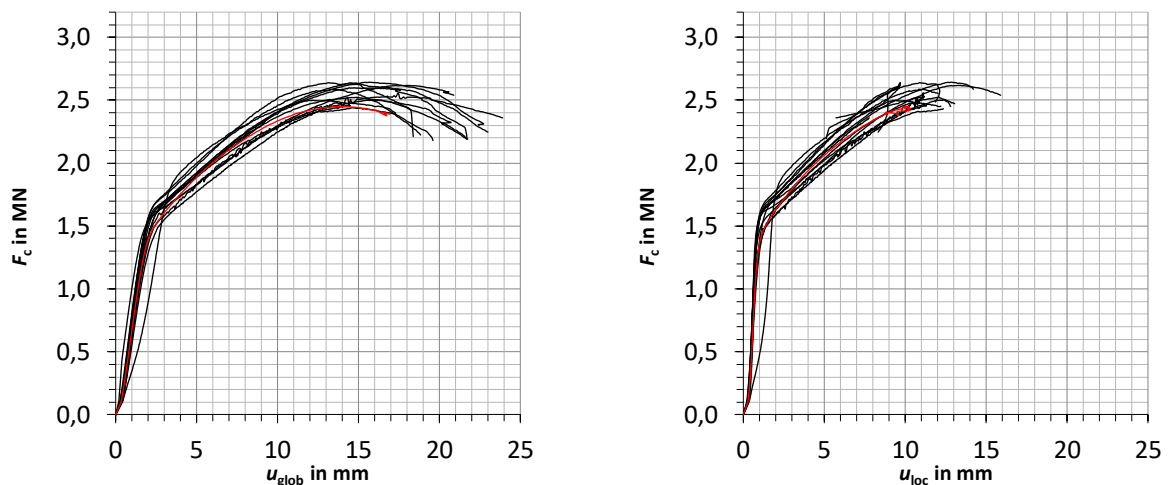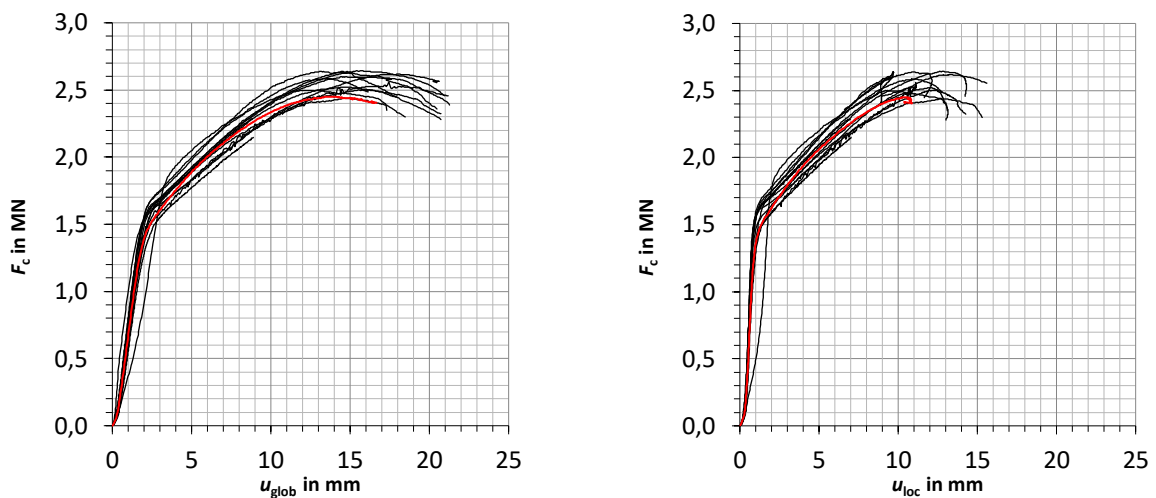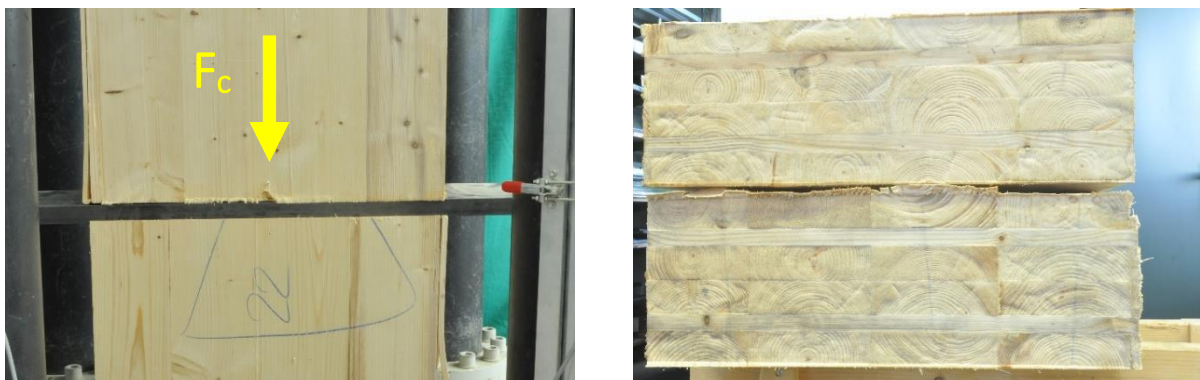

Figure 12: Typical failure of CLT specimens with steel plate in the contact joint CLT joint after failure

4 Discussion and conclusions

In all of the tested specimens, in CLT and glulam and without as well as with wetted surfaces, compressive failure and large deformation were observed close to the contact joint. In a few cases, also locally limited failure was observed at defects apart from the contact joints, e.g. knots or finger joints, but no significant impact on the overall deformation could be observed.

CLT and glulam | (values for glulam in brackets)

For CLT and glulam reductions of the compressive strength resulting from the end grain contact joints of 8.2 % (6.0 %) for the mean values and 9.1 % (11.5 %) for the characteristic values were found. Although, the strength reduction is significant, the reduced values of characteristic strength of 32.0 N/mm² (28.5 N/mm²) is still by far higher than the nominal values of the tested strength classes.

For CLT and glulam the additional deformation resulting from the end grain contact joints is about 1 mm (0.5 mm) under ultimate load and about 0.5 mm (0.2 mm) under the design compressive stress at ultimate limit state which equals approximately 40 % of the ultimate load measured in the tests.

CLT with wetted surfaces | (values for steel plate joints in brackets)

For CLT tested with wetted surfaces reductions of the compressive strength resulting from the end grain contact joints of 29.1 % (20.3 %) for the mean values and 29.3 % (20.5 %) for the characteristic values were found. Although the strength reduction is very significant, the reduced values of characteristic strength of 24.9 N/mm² (28.0 N/mm²) are still higher than the nominal value of the tested strength classes.

However, for CLT with wetted surfaces (simulation of a possible rainfall or other precipitation during transport and erection) the additional deformation resulting from the end grain contact joints is more than 10 mm under ultimate load for both, contact joints without and with steel plate in the contact joint. Under the design compressive stress at ultimate limit state which equals approximately to 40 % of the ultimate load measured in the tests the deformation is still about 1.0 mm.

The test results show, that the deformation resulting from end grain contact joints, including a relatively large joint slip, can reach values that are incompatible with serviceability requirements. This is particularly the case in constructions with several end grain contact joints arranged in a row, e.g. multi-storey buildings where the deformation of the contact joints and elastic and creep deformation of the members can

add up to critical values. Moreover, the long-term behaviour of loaded end grain contact joints is currently unknown, and additional creep deformation of end grain contact joints cannot be excluded.

In fact, the influence of moisture content on the compressive strength and the stiffness of end grain contact joints is enormous and by far higher than in continuous members. Therefore, it is crucial to plan and implement appropriate measures to prevent the absorption of moisture during transport and erection especially wetting of end grain surfaces must be avoided by any means.

5   References

Blass, HJ, Flaig, M. (2014) Keilgezinkte Rahmenecken und Satteldachträger aus Brettsperrholz. Karlsruher Berichte zum Ingenieurholzbau, Bd. 29, KIT Scientific Publishing, Karlsruhe, Germany.

EN 408 - Timber structures - Structural timber and glued laminated timber - Determination of some physical and mechanical properties; German version EN 408:2010+A1:2012

Frese M, Enders-Comberg M, Blass HJ, Glos P (2011) Strength of spruce glulam subjected to longitudinal compression. Alghero, Italy. (CIB-W18/44-12-2)

Schneider P (2015) Brettsperrholzbauteile mit stirnseitigem Druckkontakt. KIT, Timber Engineering and Buildings Construction. Bachelor-Thesis (in German, unpublished)

Discussion

The paper was presented by H Blass

P Quenneville received confirmation that the 20% reduction was due to wetting effects.   He wondered what would happen if further cuts were made. H Blass responded that the weak link is not location dependent.

S Winter received confirmation that the reduction values were provided for both the mean and characteristic values. Also recovery from drying was not considered as this deals with structural safety during construction.

R Brandner asked whether a flexible layer rather than a rigid steel plate was tried. H Blass said no this was not done.

A Frangi said he would expect even more damage in practice and that we are lucky that at even 40% reduction is no major issue since we do not have full design load during construction. H Blass said design for construction phase may be one consideration in design for Service Class 3.

R Jockwer said in Swiss standard there is a 20% reduction factor considered for timber to timber contact joint without steel plate.   A Frangi stated that this reduction in Switzerland is not for moisture content but for uneven contact surfaces.

YH Chui received confirmation that the specimens were tested wet without drying. H Blass also clarified that the specimens were rotated 180 degrees after cutting to make sure their end grains were different.

From Testing to Codification: Post-tensioned Cross Laminated Timber Rocking Walls

Shiling Pei, Colorado School of Mines

James Dolan, Washington State University

Reid B. Zimmerman, KPFF Consulting Engineers

Eric McDonnell, Holmes Structures

Aleesha Busch, Colorado School of Mines

Philip Line, American Wood Council

Marjan Popovski, FP Innovations

Keywords: Seismic design, Cross laminated timber, Rocking wall, Shake table test

1 Introduction

Wood buildings in North America have been predominantly constructed using light-framed wood systems since the mid 1900's, with the exception of heavy timber construction in some non-residential applications. This situation is likely to change in the future with the growing acceptance of mass timber construction in the region. In fact, a number of mass timber buildings have been constructed in recent years in the U.S. and Canada, including low- to mid-rise mixed-use buildings (e.g. University of Massachusetts Amherst Student Center, T3 building in Minneapolis, MN) and tall towers (e.g. Brocks Commons at University of British Columbia). Most of these buildings utilized cross laminated timber (CLT) or nail laminated timber (NLT) floors and heavy timber framing systems to support gravity loads, and a non-wood lateral system such as concrete shear walls or steel braced frames to resist wind and seismic loads. Although CLT material and glulam products have been recognized in the U.S. and Canada (IBC (2018) and NBCC (2015)), there is currently no mass timber lateral system in the U.S. that is recognized by the building codes. As a result, special design procedures and review/approval processes must be followed for any building intended to use a mass timber lateral system. At the time of this paper, there has been only limited on-going effort to codify mass timber lateral systems in the U.S., including one project to develop seismic design parameters for panelized CLT shear walls (Amini et

al., 2014) following the FEMA P695 procedure. Another lateral system that has attracted significant attention in research is the post-tensioned mass timber rocking wall system, which has potential applicable to balloon framed low- to high-rise wood buildings. This paper will focus on recent research development on mass timber rocking wall system in the U.S., especially with the use of CLT wall panels, and the effort to develop a seismic design procedure for this system for inclusion in the Special Design Provisions for Wind and Seismic (SPDWS)(2015).

2 Post-tensioned Rocking Wall System

The post-tensioned rocking wall concept was first formalized in concrete rocking walls. By applying a post-tensioning force at the center of a precast concrete panel, the panel was able to alternatively rock about each end under lateral loads but would always re-center as long as the post-tensioning strand or rod did not yield. The concrete rocking wall system has been extensively tested (e.g., Lu, et al. 2018 and Marriott, et al., 2008) and applied in real building projects (Suncoast Post-Tension, 2017; SEAOC, 2016). A design procedure for precast rocking walls already exists in the building code in the U.S. (ACI, 2007). However, no such similar design procedure has been codified for mass timber rocking walls. Mechanistically though, the rocking wall concept is applicable to panels made of any solid material, thus giving rise to the idea of a wood-based rocking wall system.

Combining large engineered wood members with post-tensioning techniques, researchers in New Zealand pioneered the development of low-damage and self-centering wood lateral force resisting systems and studied a variation of this concept starting in the early 2000's (Buchanan et al. 2008, Palermo et al. 2005, 2006). These earlier studies experimented with post-tensioning techniques on wood-frame moment connections and LVL walls (Buchanan et al. 2008, Iqbal et al. 2015, Iqbal et al. 2016a, Iqbal et al. 2016b). Some of these systems were used in real building projects in New Zealand (Palermo et al. 2012, Holden et al. 2012). In the U.S., reversed cyclic load tests of a number of full-scale post-tensioned CLT rocking walls was conducted by Ganey et al. (2017). Calibrated modelling parameters for CLT rocking walls were derived from the test data by Akbas et al. (2017). The understanding of rocking timber lateral system from these earlier efforts was applied to the design of a full-scale, two-story building that the authors tested on the UCSD shake table in 2017 as part of the NHERI TallWood Project (Pei et al. 2019). During this test program, the full-scale building with CLT rocking wall system survived 14 seismic excitations with only minimal damage. In fact, the structural system remained damage-free during all design-basis earthquake (DBE) events. Damage was only observed during the maximum considered earthquake (MCE) events. Following this two-story building test, two parallel efforts are currently on-going to further the design of post-tensioned rocking mass timber wall system in the U.S. The first effort is to develop a design methodology for mass timber rocking walls for consideration in SDPWS adoption (funded by U.S. Forest Services). The second effort is the planning (also by the NHERI TallWood Project

team) of a full-scale 10-story wood building shake table test with non-structural components in 2021. This large test is aimed at validating the resilience-based design methodology proposed, thus referred to as the NHERI TallWood Validation Test in this paper. It is envisioned that through these research and development efforts, post-tensioned mass timber rocking walls will become a well-validated and accepted lateral option for multi-story mass timber buildings.

3 NHERI TallWood Project: Vision and Current Results

NHERI TallWood Project is a six-university collaborative research project funded by the National Science Foundation (NSF) spanning a period of 5 years from 2016 to 2021. Its ultimate goal is to develop and validate a seismic design methodology for tall wood buildings that incorporates high-performance structural and non-structural systems to achieve a resilience objective following major earthquakes. The project mainly includes four research components, namely the tall wood archetype development, a holistic modelling approach, a resilience-based seismic design methodology, and a final validation test.

3.1 Tall Building Archetypes:

During the first year of the project, the research team collaborated with Lever Architecture and KPFF Consulting Engineers and developed a group of tall wood building archetypes intended for mixed-use applications (residential and commercial). These archetypes are all based on a 100 x 200 ft lot size which is typical for urban areas in the U.S. with population density suitable for this type of buildings. Three building heights, namely 6, 12, and 18 story-buildings, were considered (see Figure 1). All of the archetypes utilized a glulam beam and column gravity system to enable an open floor plan that can be reconfigured to different uses (see Figure 1). Different internal floor plans (including non-structural partition and typical contents arrangement) were also developed for residential, office, and commercial usage. These non-structural components will play a major role in building resilience assessment and be tested in the final full-scale validation test.

3.2 Investigative testing of a two-story mass timber building

In order to generate building system level dynamic response data for model calibration, a 2-story mass timber building was built and tested as an investigative test in 2017. The concept for the 2-story test building specimen is shown in Figure 2, with an open floor plan. The building had a relatively high aspect ratio diaphragm via diaphragm cantilevering to specifically study the lateral responses of the CLT diaphragm. Two sets of coupled CLT rocking walls were inserted into the diaphragm and connected using shear-transfer-only slotted connections (see Figure 3). In order to accommodate the expected large inter-story drift, the gravity framing connections
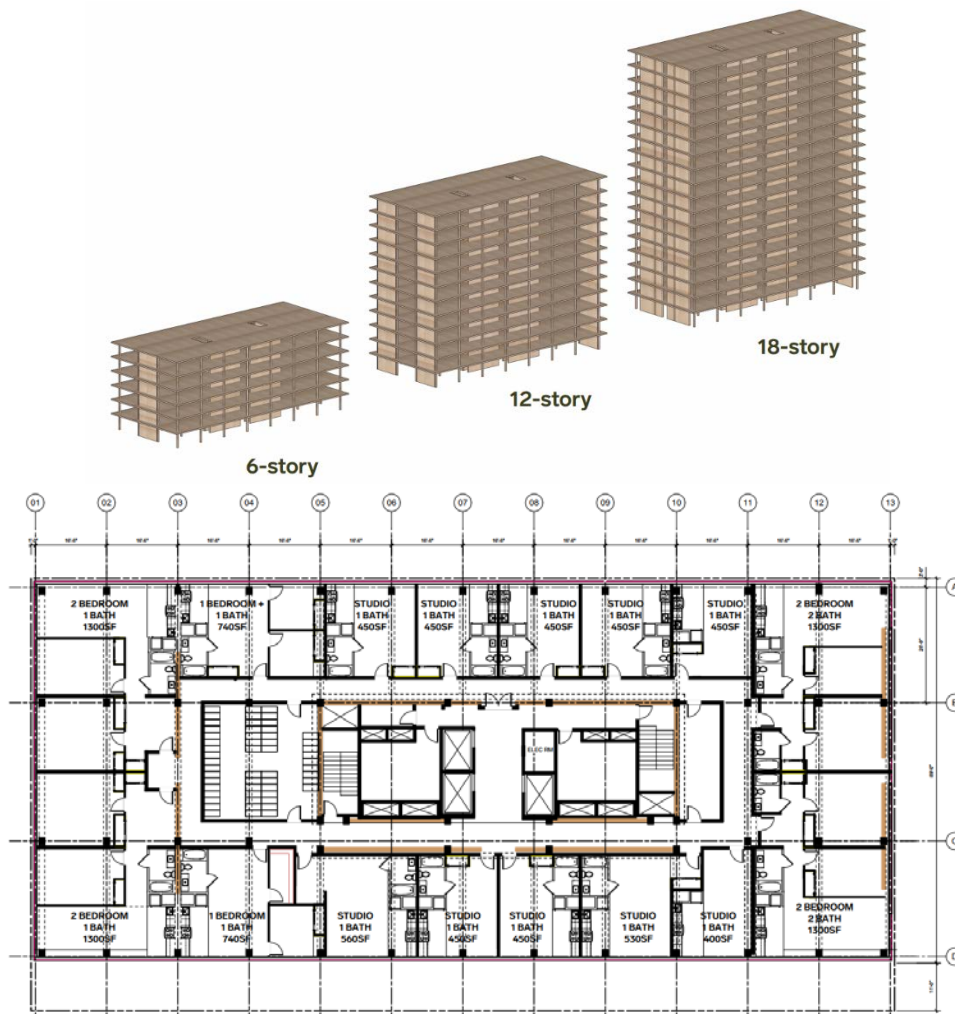
Figure 1: Archetypes and example floor plan for NHERI Tallwood Project

were designed to rock at the beam-to-column interface (i.e. the gravity frame was not part of lateral force-resisting system). The overall seismic mass of the frame and CLT floor/roof was approximately 321 kg/m^2 (64 psf) for the floor and 386kg/m^2 (79 psf) for the roof. The CLT panel joints were constructed following typical CLT top spline floor splice details with pre-routed panel edges covered with plywood strips. The floor and roof diaphragms were designed to remain elastic under the planned seismic excitations. A shear demand calculation was conducted to determine the number of structural screws (Simpson Strong-Tie SDS screws) needed for shear transfer across the panel splices. The chord tensile forces in the diaphragm were carried over panel joints using custom sized metal plates installed with screws.

The CLT rocking walls were coupled using steel U-shaped flexural plate (UFP) energy dissipaters. Similar energy dissipaters have been used in concrete rocking wall systems (Priestley et al. 1999, Johnston et al. 2014), as well as the CLT rocking walls tested by Ganey et al. (2017). The walls and UFPs were initially sized using approximate demands calculated using ASCE 7-10 (ASCE 2010) for a Class B soil site in San Francisco with an assumed seismic force reduction factor, R, of 6. Detailed description of the design configuration of the test building can be found in Pei et al. (2019).

The installation of the test building was completed in two weeks, and the major construction stages illustrated in Figure 4.
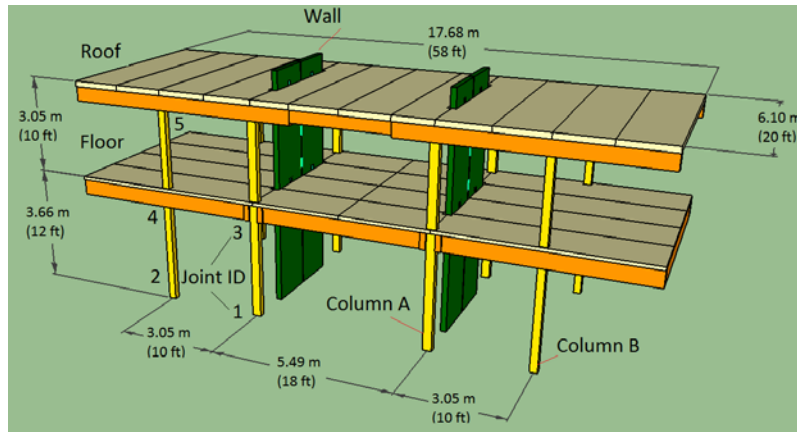
(a)

(b)

Figure 2: Investigative testing of a full-scale two-story mass timber building with rocking walls. (a) schematic drawing showing dimensions, (b) specimen completed and ready for testing.

Figure 3: Post-tensioned CLT rocking walls coupled with UFP connectors and attached to the CLT diaphragm with shear-transfer-only connectors (viewed from the 2nd floor)
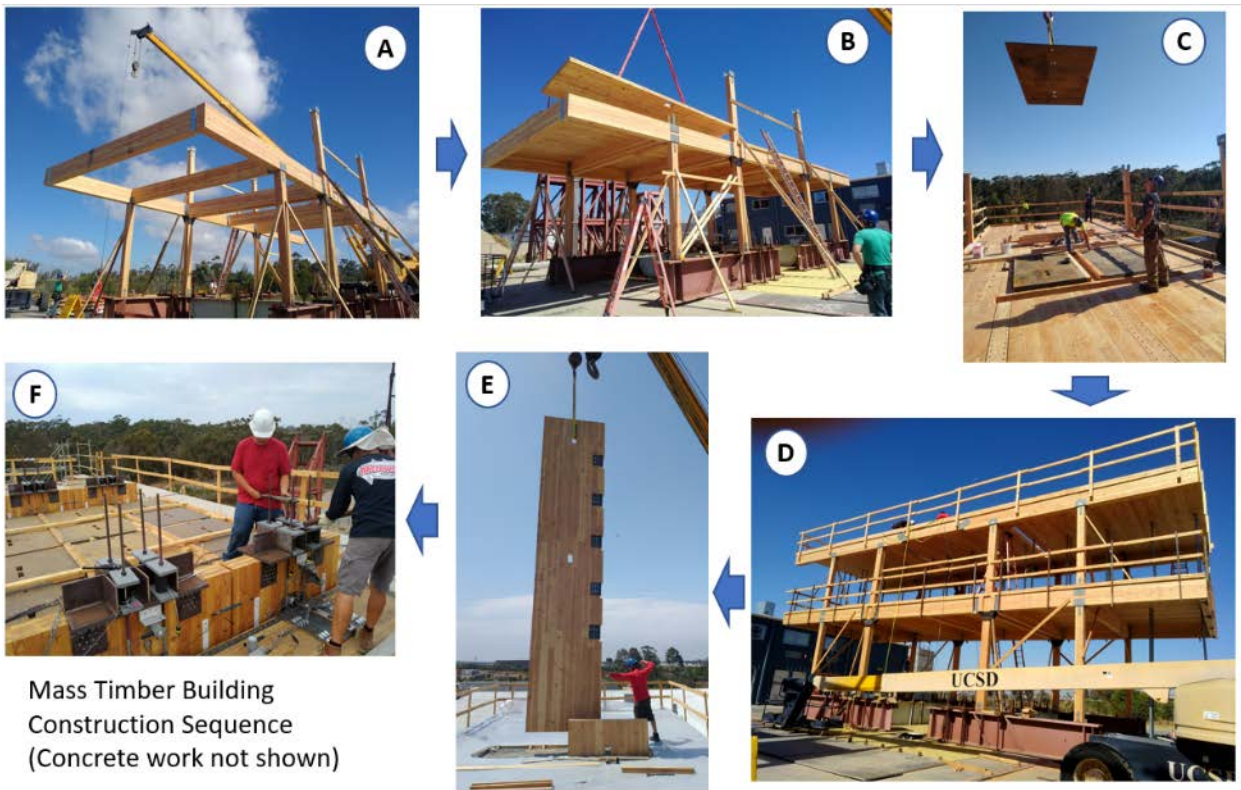
Figure 4: Construction process of the two-story test building. (A) installation of the gravity force resisting system, (B) instalation of the CLT diaphragms, (C) Installation of Intertial mass, (D) Completed gravity system with floors, (E) Installation of Rocking Shear Walls, (F) Post-tensioning of rocking wall.

A total of fourteen (14) seismic tests with different historical records and various intensity levels were conducted with over 350 channels of data measurement installed on the building. A variety of sensors were installed on the test building, providing measurement of force, displacement, strain, and acceleration. The 14 earthquake excitations were selected to represent three hazard levels: (1) Service Level Earthquake (SLE) (i.e., 50% probability of exceedance in 50 years), (2) Design Basis Earthquake (DBE) (i.e., 10% probability of exceedance in 50 years), and (3) Maximum Considered Earthquake (MCE) (i.e., 2% probability of exceedance in 50 years) for the San Francisco site considered in the design. Ground motion records from historic California earthquakes were used with different scaling factors. During the public tests (Tests 6 and 8) which themselves occurred on different days, the unscaled ground motion from the Northridge earthquake (Canoga Park Station record) was run twice without stopping in between. The objective of such particular tests was to illustrate the ability of the building to withstand multiple consecutive strong earthquakes without the need for repair in between. All ground motions were applied uni-axially in the short direction of the building (i.e., along the direction of the CLT rocking walls). The response spectrum of the measured table ground motions are plotted in Figure 5, which represents the actual seismic excitation experienced by the test building.
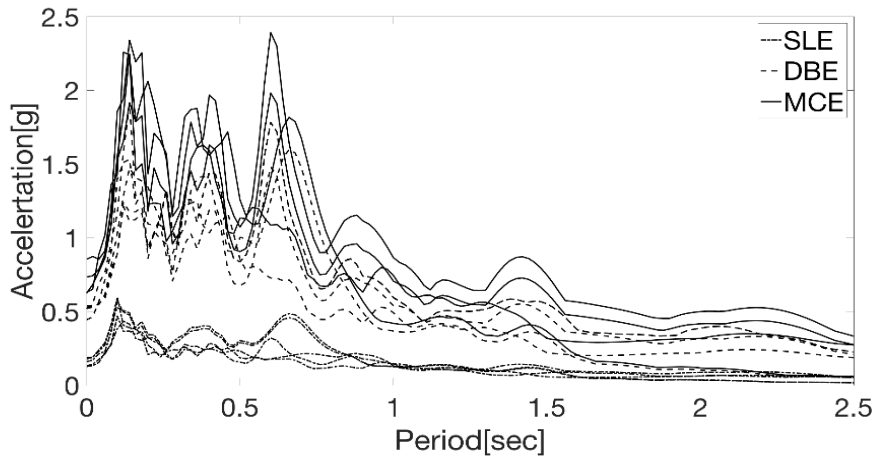
Figure 5: Response spectra of all 14 shake table test inputs

The peak building displacements at the roof and floor levels (relative to the shake table) were presented in Figure 6. One can see that the maximum roof response among all seismic tests was about 350 mm (14 in), which corresponds to approximately 5% overall building drift ratio. Throughout these tests, the building had negligible residual deformations at all levels of shaking. Test 14 was conducted using a ground motion scaled beyond the MCE level intensity with the intent to induce yielding in the PT bars.
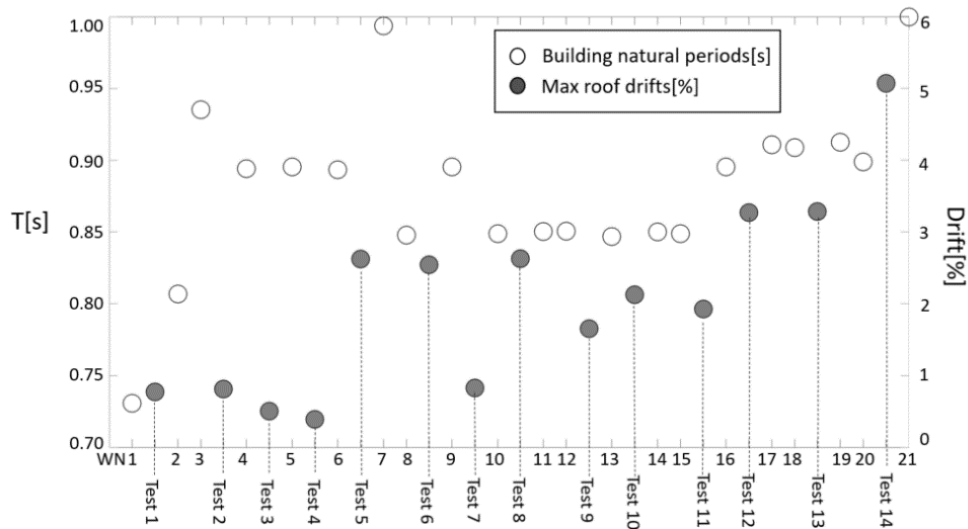
Figure 6: Maximum building responses and natural periods

The PT forces where monitored during all tests using load cells. The maximum, minimum, and residual (RES) PT forces during each test are plotted in the upper left plot in Figure 7. As examples for different intensity levels, time-history plots of selected PT bars are also shown. For some PT bars, the post-tension loss was significant during large earthquakes. The MCE-plus test (Test 14) resulted in tension force loss of about 37 kN (8.4 kips), so the residual force was approximately 16 kN (3.6 kips) measured following the test, (the initial PT force was 53.4 kN (12 kips)) This was mainly caused by the yielding of the bar itself (i.e. the maximum PT force recorded by the load cell was about 150 kN (33.7 kips), while the theoretical yielding force of the PT bar is only

134 kN(30.1 kips)). Tension force loss was found for only a few PT bars, while most did not experience significant loss. Thus, the building was able to re-center with negligible residual drift even for these large events (with partial PT yielding).
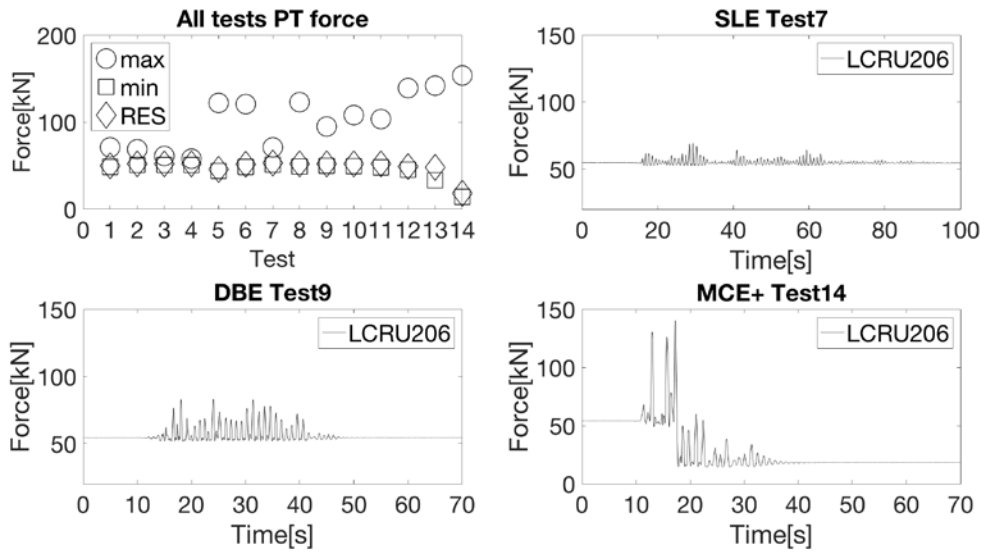
Figure 7: Peak PT forces and example PT time history during tests

The diaphragms were designed to remain elastic during most of the ground motions and very limited deformation (maximum measured deflection, at roof diaphragm in Test 14, was only 24 mm (0.94 inch) over a 17.7m (58 ft) diaphragm span) occurred during the tests.

The specimen was inspected for damage after each test at DBE or MCE level. The structural system was designed to achieve a resilient performance objective, and there was no significant damage to the building at any time during the entire testing program. The only visible damage was found at the bottom corners of the rocking wall panels after large DBE and MCE ground motions. The damage was relatively minor (e.g., splitting of the outside wood fiber and slight deformation of the toe, see

Slight compression deformation at the rocking wall corner

Chipping of wood at the rocking wall corner

Figure 8: Minimal structural member damage observed after 14 earthquake tests

Figure 8) and did not warrant structural repair. It should also be noted that the building was intentionally pushed to very large drift levels, beyond what is required by current building codes. At the code-specified drift levels, the structural system was essentially damage-free.

3.3 Holistic performance modelling and RBSD:

A number of numerical models have been developed in order to simulate seismic response of wood buildings with a CLT rocking wall system. These models include linear finite element models constructed using commercial software packages such as ETABS (CSI, 2018) for preliminary design and demand calculations, detailed nonlinear dynamic models built in OpenSees that utilized fiber elements, nonlinear spring elements, and contact elements, and simplified nonlinear mechanistic models with limited degrees of freedom that are designed for reliability simulations. Some of these models are currently still under development, but many have already been validated using full-scale test data. An example is the simple lumped mass rocking wall model which simulates the rocking wall as an elastic beam with a nonlinear rotational spring foundation and which was shown to accurately estimate the response of the 2-story test (see Figure 9).
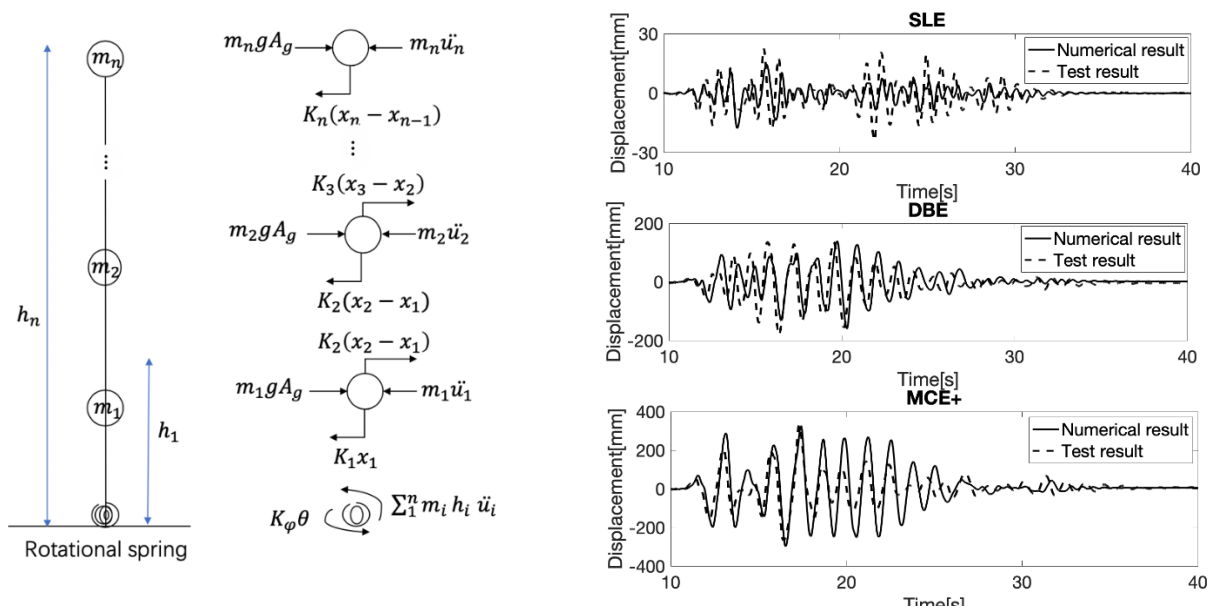
Figure 9: One of the numerical prediction models used by the project team

Once a set of satisfactory simulation models for mechanical responses of the building are obtained, a fragility-based approach will be used to produce building damage and recovery status using engineering demand parameters such as inter-story drift and floor acceleration. These metrics will further be integrated into the down-time of the building after an earthquake. An iterative process will then be followed to design a tall wood building given a target resilience level. Finally, this procedure will be formalized into a resilience-based seismic design approach for tall wood buildings. These research tasks are currently on-going and expected to be used for the design of the 10-story validation test structure.

3.4   Ten-story Validation Test

While tests result from the two-story building validated the structural robustness of the proposed mass timber system, the resilience of tall wood buildings is closely tied with the damage to non-structural components within the building. Additionally, the dynamic responses of a tall rocking wall may include significant higher-mode interactions that could increase structural demands (mostly force demands on wood components and connections). In order to truly validate the numerical model and design methodology developed in this study, a full-scale, 10-story building will be tested at the end of the project in 2021. The test will, similar to the 2-story, be conducted at UCSD's large outdoor shake table. Currently, the gravity design and floor plan layout for the 10-story test building is completed considering the geometric limitations of the shake table. The gravity design considered a Dead Load of 3.3 kN/m^2 (70 lb/sq.ft.) for all floors and roof, plus a Live Load of 3.1 kN/m^2 (65 lb/sq.ft.) for all floors. All columns and beams were designed with sacrificial layers ensuring 2-hour fire rating (@ 4 cm/hr (1.6 inch/hr) char rate on all exposed surfaces) in order to truly represent the practical condition (i.e., exposed) where those members would be used in an actual building. A 4.0 m (13 ft) floor height was assigned to the bottom floor while other floors use a 3.4 m (11 ft) height. Allowable Stress Design provision from NDS 2015 were used to consider the member residual strengths after fire. The resulting test building configuration is shown in Figure 10 on the shake table. A more detailed floor plan for beam-column grid on the shake table is shown in Figure 11.

Full-scale 10-story test building
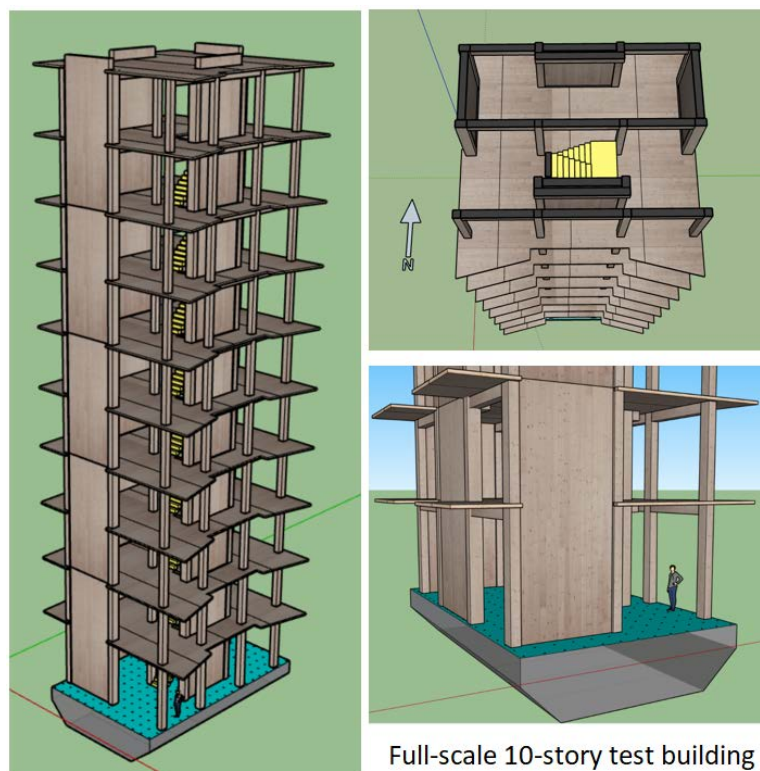
Figure 10: 3D model of the planned 10-story test building on the UCSD shake table
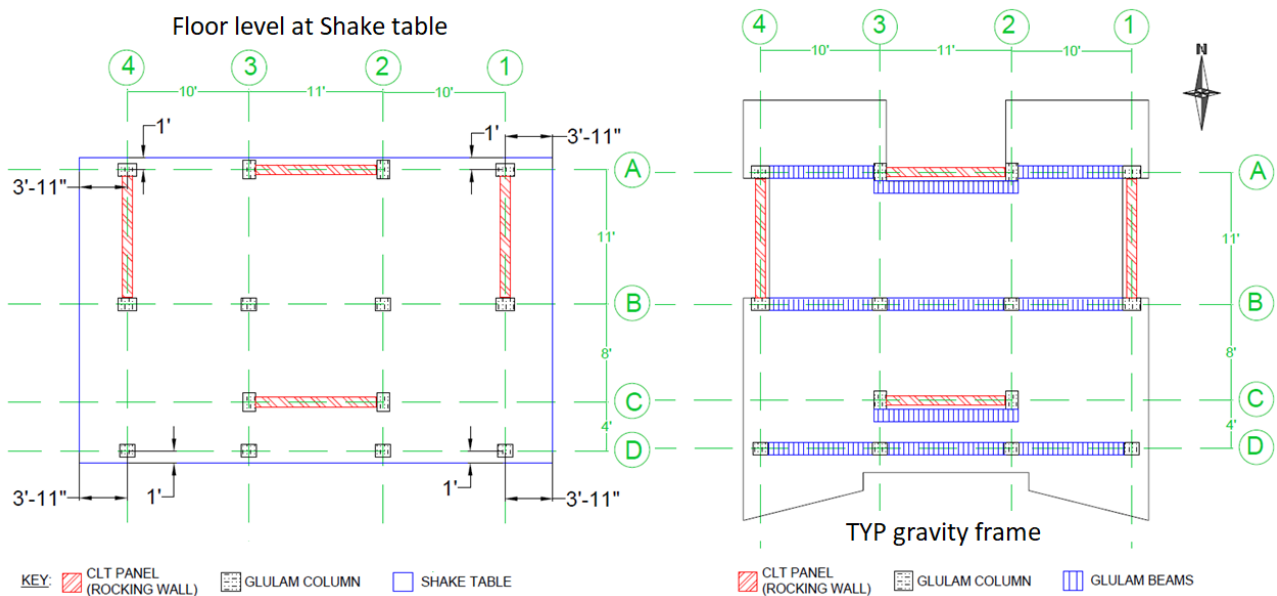
Figure 11: Floor plan of the gravity framing relative to the shake table.

The lateral design of the test building is currently being completed, together with the design of building envelop and interior non-structural configurations. The research team is working to secure material and funding support for the test through industry and academic partners. The building floor plan and dimensions are published on the project website: http://nheritallwood.mines.edu/ to serve as an informational basis for potential donors (of building products) and collaborators (for pay-load testing ideas). The project team is scheduled to complete the building design by early 2020, finalize construction documents by mid-2020, and start construction early 2021. The UCSD shake table is also being upgraded to enable 3D seismic excitation capacity. The upgrade is scheduled to be completed by March 2021. The test building will be constructed on the shake table afterwards. This validation test program is scheduled to be completed by the end of 2021.

4 Design Guide and Provisions for Post-Tensioned CLT Rocking Walls

As the NHERI TallWood Project focuses on developing "above-code" resilience design methodology, another on-going project was funded by the U.S. Forest Services to develop a design guide for post-tensioned mass timber rocking walls within the ASCE 7 and SDPWS framework. This project is led by a research team at Colorado School of Mines and KPFF Consulting Engineers. Through collaboration with AWC and FPInnovations, the ultimate deliverables from the project include a design code provision package (including commentary and examples) that can potentially be considered for adoption into the SPDWS.

The proposed design procedure for post-tensioned mass timber rocking walls follows closely the design provisions already codified for post-tensioned rocking concrete walls (ACI, 2007). For demand calculations, the design procedure does not require

nonlinear response history analysis but rather is suitable with either the equivalent lateral force or modal response spectrum procedures of ASCE 7 (ASCE, 2016). Where nonlinear response history analysis is pursued, however, the design procedure also permits its use. The equivalent lateral force and modal response spectrum procedures in ASCE 7 rely on what is known as the response modification coefficient, R (i.e., a ratio of inelastic to elastic force demands). Since a response modification coefficient for mass timber rocking walls has not yet been established through a formal FEMA P695 (FEMA, 2009) study, which would be necessary for final code adoption in the U.S., the design procedure provides commentary suggesting that a R equal to 6 is likely appropriate. This stems from consideration of the similarity in behaviour between a rocking concrete and a rocking mass timber wall. In other words, a rocking mass timber wall can be seen as an emulative system to a rocking concrete wall to support the use of the same response modification coefficient. Rocking concrete walls are given a R equal to 6 in ASCE 7 as special reinforced concrete walls.

For capacity calculations, the design procedure outlines a set of provisions which establish the capacity of the rocking mechanism for each wall or, where coupling of walls is used such as in the 2-story NHERI test specimen, line of coupled walls. Once the capacity of the rocking mechanism has been established and shown to exceed the flexural rocking demand, all remaining components of the lateral force-resisting system are force-protected using capacity design principles. For example, the shear strength of a mass timber wall is compared to the shear corresponding to the probable flexural rocking capacity of that wall, considering both material overstrength and higher mode amplification of shear.

Additional provisions require checking that stresses and strains in the post-tensioning and energy dissipation elements are within those specified by other material standards (e.g., the American Institute of Steel Construction for steel elements). A chapter in the provisions also provides criteria to ensure sufficient initial post-tensioning force to achieve re-centering, sufficient energy dissipation capacity for energy absorption, and that wall configurations meet prescriptive limits.

The project was initiated at the end of 2018 and t a first draft of the design guide for the rocking wall system has been written. The research team is currently working through design examples and the final design provisions, commentary, and examples will be complete by the end of 2020.

5 What the future holds

In summary, a combination of experimental, analytical, and developmental work has been conducted to date in the U.S. to better understand the dynamic behaviour of post-tensioned CLT rocking walls and their potential incorporation into the design code. This body of work was built upon earlier pioneering studies of post-tensioned low-damage concrete and wood systems originating in New Zealand. Although most of the work discussed in this article is still on-going, intermediate results and valida-

tions have shown great promises. With the scheduled completion of the mass timber rocking wall design guidelines and the validation of the resilience-based seismic design methodology through full-scale testing, it is envisioned that post-tensioned rocking mass timber walls will play an important role in the expansion of mass timber construction in regions with high seismicity around the world. Once the technical know-how and public perception gaps are filled through research and demonstration, this easy-to-design/install and highly resilient lateral system will provide cost competitive solutions for both new construction and structural retrofit. Tall wood buildings will become one of the integrated components of future earthquake resilient cities world-wide in the next a few decades.

6 Acknowledgements

7 References

ACI (2007). *Acceptance Criteria for Special Unbonded Post-Tensioned Precast Structural Walls Based on Validation Testing and Commentary, ACI ITG-5.1-07*. American Concrete Institute. Farmington Hills, MI.

Amini, M. O., van de Lindt, J. W., Pei, S., Rammer, D., Line, P., & Popovski, M. (2014). Overview of a Project to Quantify Seismic Performance Factors for Cross Laminated Timber Structures in the United States. In Materials and Joints in Timber Structures (pp. 531-541). Springer Netherlands.

ASCE (2016). *Minimum Design Loads and Associated Criteria for Buildings and Other Structures, ASCE/SEI 7-16*. American Society of Civil Engineers, Reston, VA.

AWC (2015). Special Design Provisions for Wind and Seismic, AWC SDPWS 2015. American Wood Council, Leesburg, VA.

Buchanan, Andy, Bruce Deam, Massimo Fragiacomo, Stefano Pampanin, and Alessandro Palermo. (2008) "Multi-storey prestressed timber buildings in New Zealand." *Structural Engineering International* Vol. 18, No. 2: 166-173.

Ceccotti, Ario, Carmen Sandhaas, Minoru Okabe, Motoi Yasumura, Chikahiro Minowa, and Naohito Kawai. (2013) "SOFIE project–3D shaking table test on a seven-storey full-scale cross-laminated timber building." *Earthquake Engineering & Structural Dynamics* 42, no. 13: 2003-2021.

CSI (2018). *ETABS Integrated Building Design Software, User's Guide.* Computers and Structures Incorporated. Berkeley, CA.

Federal Emergency Management Agency, FEMA (2009) "Quantification of building seismic performance factors: FEMA P695" Federal Emergency Management Agency, Washington DC.

Ganey, R.S. (2015) *M.Sc. Thesis: Seismic Design and Testing of Rocking CLT Walls*, University of Washington, Seattle, WA USA.

International Code Council (2018). *International Building Code* (IBC). International Code Council, Washington, D.C.

Iqbal, A., Pampanin, S., Palermo, A., & Buchanan, A. H. (2010). Seismic Performance of Full-scale Posttensioned Timber Beam-column Joints. *11th World Conference on Timber Engineering*, Riva del Garda, Trentino, Italy (Vol. 10).

Lu, X., B. Yang, and B. Zhao (2018). "Shake-table testing of a self-centering precast reinforced concrete frame with shear walls." *Earthquake Engineering and Engineering Vibration*, Vol. 17, Issue 2, pp 221-233.

Marriott, D., S. Pampanin, D. Bull, and A. Palermo, 2008. "Dynamic Testing of Precast, Post-Tensioned Rocking Wall Systems with Alternative Dissipating Solutions." *Bulletin of the New Zealand Society for Earthquake Engineering*. Vol. 41, No. 2, pp. 90-103.

National Research Council of Canada. (2015). *National Building Code of Canada* (NBCC). National Research Council Canada, Ottawa, Ontario, Canada

Pei, S., van de Lindt, J.W., Popovski, M., Berman, J.W., Dolan, J.D., Ricles, J., Sause, R., Blomgren, H., and D.R. Rammer, (2015) "Cross Laminated Timber for Seismic Regions: Progress and Challenges for Research and Implementation," *Journal of Structural Engineering*, ASCE, (doi: 10.1061/(ASCE)ST.1943-541X.0001192).

Pei, S., van de Lindt, J.W., Barbosa, A., Berman, J.W., McDonnell, E., Dolan, J.D., Blomgren, H., Zimmerman, R.B., Huang, D., and Wichman, S. (2019) "Experimental Seismic Response of a Resilient Two-Story Mass Timber Building with Post-Tensioned Rocking Walls" ASCE Journal of Structural Engineering. Accepted In Press.

Popovski, M., Schneider, J., & Schweinsteiger, M. (2010). Lateral load resistance of cross-laminated wood panels. *World Conference on Timber Engineering* (pp. 20-24).

SEAOC Excellence in Structural Engineering Awards (2016). Stanford University, Comstock Graduate Student Housing, Poster by KPFF Consulting Engineers.

Suncoast Post-Tension (20170. 84-story *Panorama Tower*. https://suncoast-pt.com/projects/panorama-tower/

van de Lindt, J. W., Pei, S., Pryor, S. E., Shimizu, H., & Isoda, H. (2010). Experimental seismic response of a full-scale six-story light-frame wood building. *Journal of Structural Engineering*, 136(10), 1262-1272.

Discussion

The paper was presented by A Busch

A Frangi asked about design considerations for diaphragm and wall connection. D Dolan responded that special details were made to transfer only lateral forces and shear key was also made available to ensure compatibility.

F Lam received confirmation that 3 D shaking will be available.

M Li stated that 10 storey structures will be wind governed and asked how to achieve both the stiffness demand from wind and rocking motions in earthquake. R Zimmerman said that in a 6 storey situation seismic drift demand would govern. In US there is no code requirement for wind design for serviceability at this building height.

M Li asked about the connectivity between multiple panels along the building height. A Busch responded that rigid splines that are stronger than the wood would be used.

L Epp asked under 12 storeys there is no code requirements for wind loads in US but will the design guide consider wind design. R Zimmerman said that the design guide will only reference other standard.

J Brown asked about aspect ratio for walls and coupled walls.   R Zimmerman responded that there will be some limitations in the design guide for coupled walls, for example, modeling box types are not included. D Dolan said that the aspect ratio of walls will be governed by transportation.

P Quenneville asked what level of acceleration would be expected at the top level. R Zimmerman said no information yet.

T Tannert asked if only one rocking plane will be expected. A Busch responded yes. T Tannert asked if this design method goes into NDS only how would designers design this type of systems without ASCE7. A Busch responded that this is just the starting point and will aim to go into ASCE 7 down the road and it will be a long road.

A Ceccotti asked about the floor plan. D Dolan commented that there could be torsional issues. S Aicher agreed that torsional response might result as wall elements may have different stiffness. D Dolan agreed as ongoing 2 D testing will help guide this aspect of the program.

Seismic Performance of End Brace Connections in Ductile Braced Timber Frame

Hossein DANESHVAR, Post-Doctoral Fellow, University of Alberta, Edmonton, Alberta, Canada, hossein.daneshvar@ualberta.ca (Corresponding Author)

Jan NIEDERWESTBERG, Research Associate, University of Alberta, Edmonton, Alberta, Canada

Carla DICKOF, Senior Technical Specialist, Fast+Epp, Vancouver, Canada

John Spencer, MSc Student, University of Alberta, Edmonton, Alberta, Canada

Jean-Philippe LETARTE, Mass Timber Connections Specialist, MyTiCon Timber Connectors, Canada

Ying Hei CHUI, Professor, University of Alberta, Edmonton, Alberta, Canada

Keywords: Timber Braced Frame, Lateral Load Resisting System (LLRS); Seismic Design; End Brace Connections, Ductile Connection; Perforated steel plate; Ductility

1   Introduction

In the recent years, tall timber buildings have become more popular for several reasons including ease and pace of construction, competitive cost and low carbon foot prints. Most of these high-rise buildings are hybrid structures e.g. using concrete cores as their main lateral load resisting system (LLRS). There are some opportunities to use timber solutions for the LLRS in order to approach more sustainable structural systems. Cross-laminated timber panels (CLT) shear wall elements and timber braced frames are two feasible sustainable options that can be employed as LLRS to stabilise buildings against wind and earthquake loads. The former system has gained special interests in the last few years; however the latter system, has not been paid enough attention despite its more efficient material usage and architectural openness compared to CLT shear walls. Braced frame systems can also be used as effective retrofit option to sub-

stantially increase stiffness, the ease of erection within limited room in existing struc-tures, and aesthetic appearance. As shown schematically in Figure 1, the timber braced frame consists of an assembly of vertical columns, horizontal beams and diagonal members with pinned connections at both ends (shown in grey). Under lateral loads, the diagonals act as tension or compression members, depending on its orientation and the loading direction. Different configurations for braced frame can be achieved as shown in Figure 1. Structurally, the braces shown in Figures 1(a) to 1(c), whether single or double, are the most efficient solutions in terms of lateral stiffness due to vertical triangular truss configurations. It is noted that the middle brace connection requirements for the Figure 1(b) is very difficult to achieve with minor added benefit compared to 1(a) or 1(c); so not recommended for timber braced frames. Also, config-urations shown in Figure 1(a) to 1(c) might be obstructive from an architectural point of view. In order to overcome the potential architectural hardship, K-type bracings (V-Bracing and Inverted V-Bracing), shown in Figures 1(d) and 1(e) can be used to provide openings for doors and windows, if needed. In these configurations, the horizontal beams are subjected to bending moments in addition to axial forces which must be accounted for in design. Additionally, there is another type of brace, so called eccentric bracing, which provides more architectural freedom in terms of openings, demon-strated in Figure 1(f). Unlike the other types of braced frames, this type moves the fuses from the end brace connections, to the beam segment between the two braces, called "link". Usually, links are designed as reinforced steel section; allowing it to with-stand the flexural demand imposed during seismic motions. This type is considered out of the scope of this project.
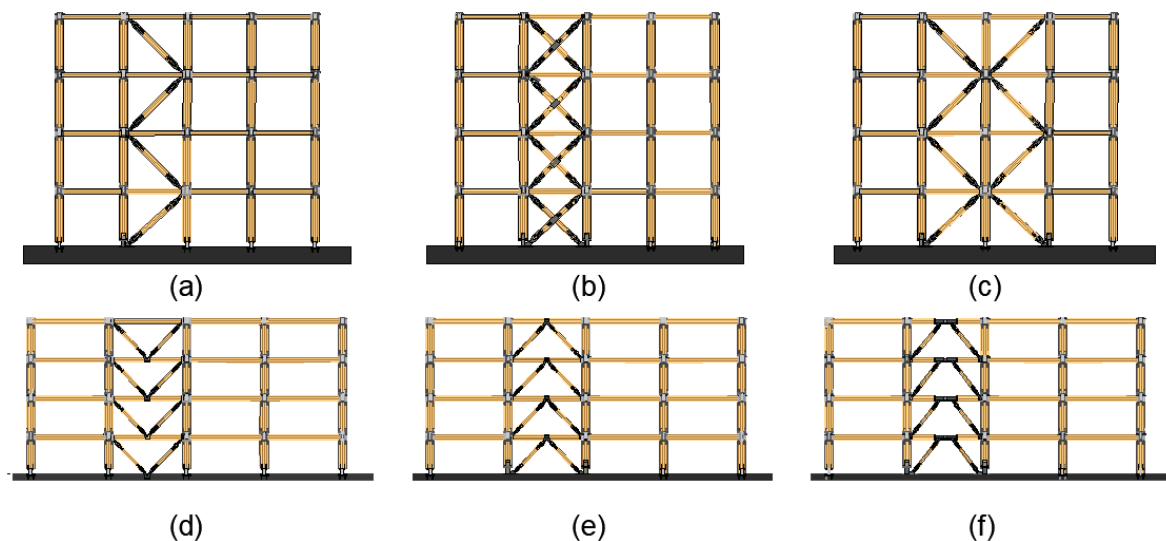

Figure 1: (a) Diagonal bracing (b) Cross bracing (c) Multi –storey cross bracing (d) V-Bracing (e) Inverted V-bracing (Chevron) (f) Eccentric

The focus of this research is on end braced connections applicable to concentrically braced frames in which the centreline of the members aligns concentrically at the locations of the joints. This application is limited to vertical braced frames resisting major lateral loads, mainly earthquake, not in other components such as horizontal diaphragms. Additionally, buckling-restrained braces, self-centering braced frames, multitier braced frames, and zipper configuration are out of the scope of this study.

This paper presents a solution where braces dissipate energy during major earthquake events. The energy would be dissipated within the end brace connections which are designed to experience ductile behaviour in anticipated locations, thereby acting as "fuses". The inherent characteristics of typical timber braced frames may result in a less desirable seismic performance such as low drift capacity. In order to overcome this obstacle, the fuses should be capable of going through large ductile deformation while the neighbouring components are protected based on the principles of capacity design procedure. For the timber braced frames, the primary source of kinematic motion is due to yielding of the steel connections. Unlike counterpart steel braced frames, buckling of the brace itself may not be considered as a potential source of ductility due to potential brittle failure of the timber members. Similar to steel braced frames, the end brace locations should be treated as "protected zones" —regions that attachments are restricted to allow the fuse to be formed without disruption— particularly in unexposed frames.

In terms of system behaviour, the braces should be well proportioned; so that in the event of a major earthquake, the anticipated ductile behaviour is occurring in all storeys. Special attention should be paid to relative stiffness of adjacent floors, to have control over the demand imposed on the braced bays during major events. Accurate application of principles of capacity design at the system level is of significance to avoid undesirable behaviour. It is good practice to use the braced frames at the building perimeter to increase torsional resistance of the building against lateral loads, if architectural demands permit. In this study, the focus will be on the end brace connections, designed as a fuse or protected zone and how to achieve a ductile behaviour at the component level. The results presented in this study are at a preliminary stage as part of an ongoing extensive research program on tall mass timber balloon structural systems.

2   Selected Literature Review

In this section, a literature survey of past studies on timber braced frames and their pertinent connections are discussed. The review is not intended to be comprehensive; just some sample research projects to demonstrate the gist of attempts in this area. Nevertheless, the fact that there is limited data available on the braced timber frames is evident; necessitating more research studies.

Dowel-type connections are the most common type of connectors in braced timber frames due to the availability of the fasteners as well as ease of construction. Designers can use the European Yield Model —adopted by the many building codes including CSA O86 (2014) — to predict the capacity and failure mechanism of dowel connections (Johansen, 1949). One type of dowel-type connection, traditionally deemed appropriate for mass timber braced frames, is the end brace bolted connections. Yasumura (1990) is considered as one of earlier researcher who studied timber braced frames with bolted connections. He investigated the effects of steel plate arrangement at the connection location (whether the steel plates are being on the sides or internal) as well as the effect of the bolt diameter. Based on the test results of 2 storey frames, he suggested that timber braced frames with bolted connections could be categorized into three different classes of semi-ductile frames, non-ductile frames and others.

Popovski (2000) tested timber braced frames with bolted connectors as well as timber rivets. He found that the slenderness ratio of bolts is the most important contributor to ductile behaviour of bolted connections in timber braces. The rivets showed good ductile behaviour as well as pinching commonly observed in cyclic behaviour of timber connections. Most of the ductile behaviour of the rivet connection is due to the deformation of the rivets themselves, while the pinching is due to the irrecoverable crushing of the fibres around the rivets. He concluded that the braced frames with bolted end brace connections performed worse than the timber rivets which consistently failed in a ductile manner and had a higher energy dissipation level. He proposed different ductility factors for the timber braced frames using different types of EBC. In order to improve the dowel type EBC performance, Popovski reinforced the bolted connection with a threaded rod which exhibited a less brittle failure mechanism with significantly higher nonlinear deformation.

There are new products that have the potential for utilization in timber braced frame connection systems such as tube dowel connections (Schneider et al., 2017) and perforated plate connections. The performance of latter system which is the modified version of Holz-Stahl-Komposit (HSK)^{TM} are well-established in works done by Bathon et al. (2014a and 2014b). A timber hold-down connection with a glued-in perforated steel plate as designated yield area was investigated by Zhang et al. (2018). Their tests showed that perforated steel plates can be reliably designed to fail in a ductile manner with a desired yield force, capacity and stiffness. The rigid adhesive connection in combination with the perforated steel plate resulted in a steel like behaviour during cyclic tests. Unlike the rivet connection, the hysteresis curve of the glued-in perforated plate connection showed no pinching and therefore a higher energy dissipation potential.
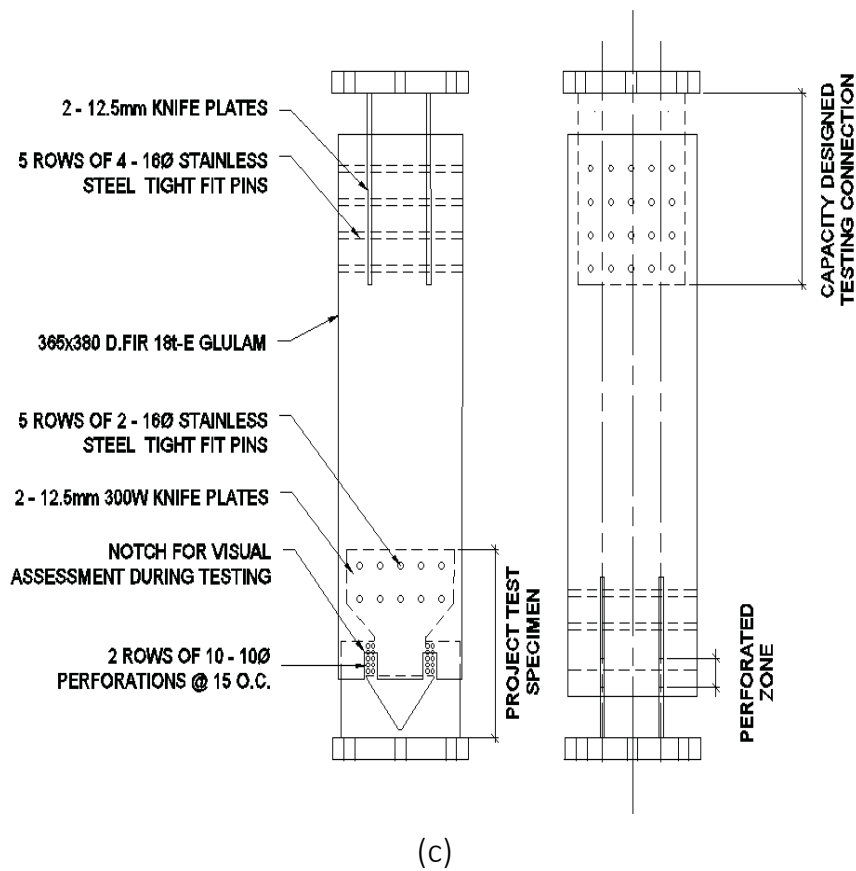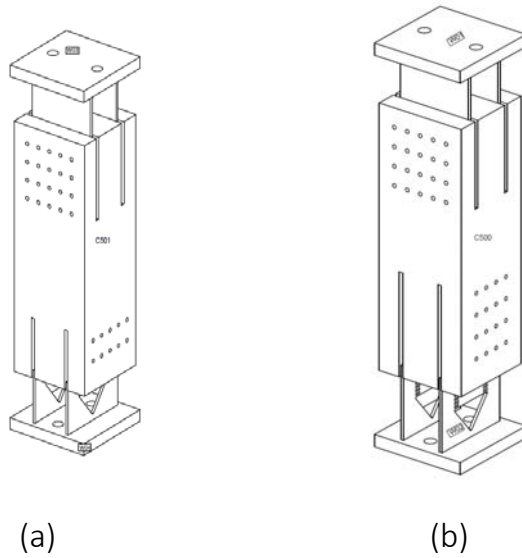
The National Building Code of Canada (NBCC, 2015) specifies the minimum vertical and lateral loads that shall be considered for building design including the seismic loads, similar to its equivalent American code, ASCE7-16 (2017). NBCC considers ductility-re-

lated force modification factors (R_d) and overstrength-related force modification factors (R_o) for different LLRSs in order to account for a structures ability to dissipate energy and therefore reduce the equivalent static design load, while ASCE7-16 (2017) adopts the response modification coefficient (R) serving the same purpose. The $R_d R_o$ (NBCC, 2015) or R (ASCE7-16, 2017) factors directly influence the lateral earthquake loads that are used for the seismic design in the respective procedures. Two different timber brace frames are considered in NBCC (2015), brace frames with moderate and limited ductility. Moderately ductile timber brace frames are assigned R_d and R_o values of 2.0 and 1.5 respectively, while limited ductile frames have a value of 1.5 for both R_d and R_o (NBCC, 2015). ASCE 7-16 (2017) acknowledges one type of timber frame with a R value of 1.5. In general, these factors are largely based on engineering judgment, qualitative comparisons (FEMA P965, 2009) and experience. As a result, more research is required to establish reliable R factors. It is believed that end brace connections are the main source of ductile behaviour in mass timber braced frames, this will be discussed in the subsequent sections. This study seeks to initiate the process of behaviour evaluation of timber braced frames, first at the component level and then for the entire system behaviour, in future studies.

3   Perforated Plate Connection Design

In this research, the connection design concept allocates all yielding to the steel plate elements of the brace connection, and form a rather rigid connection between the steel element and the timber brace. Such rigid connection could be achieved using an adhesive, but these glued solutions are costly and time-consuming on construction and are not yet regulated or codified in North America. Alternatively, the rigid behaviour proposed here is achieved by capacity protecting a doweled connection using stainless steel tight fit pins (SSTFP) or self-drilling dowels (SDD). The latter has a diameter of 6.35mm (1/4"), a dowel shear strength of 17.6kN and a yield strength of 870MPa (MyTiCon, 2019) and can penetrate plate thickness up to 7.9mm (5/16"). The dowels are self-drilling through steel plates, forming a tight fitting stiff connection between the steel elements and the timber member. Pre-drilling is recommended for knife plates thicker than 3.2mm (1/8"). For thicker knife plates, the SSTFP are considered to be a practical option, as implemented in the current research. In order to ensure steel yielding, perforated steel plates were chosen to obtain a designated dissipative zone with specific yielding characteristics; the concept of the perforated plates with SSTFP are shown in Figure 2. Although, some post-yielding behaviour due to deformation of the dowels or pins is expected, it is assumed to be negligible; assuming the stiff connection ensures that the majority of the deformation occurs in the designated dissipative zone within the perforated area of the steel knife plates. It should be noted that the connection under investigation is the connection located at one end of the specimen (the bottom); the connections at the other end are capacity protected. In order to validate the accuracy of the assumptions, two phases of connection tests are designed. Phase

one includes two connection configurations with different small scale loads as shown in the Figure 2; the main difference between specimens 1-A and 1-B is the number of perforations and the associated number of pins in the capacity protected steel to timber connection. The purpose of this phase is to investigate the predictability of the design concept of the perforated plates for this application and scalability of the system. Phase 2 contains the full-scale brace member intended to be implemented in a tall timber building, demonstrated in Figure 3, and is designed to verify the perforated plate fuse concept as well as overall behaviour of the brace at a much larger scale.

(a)   (b)

2 - 12.5mm KNIFE PLATES

5 ROWS OF 4 - 16Ø STAINLESS STEEL TIGHT FIT PINS

365x380 D.FIR 18t-E GLULAM

5 ROWS OF 2 - 16Ø STAINLESS STEEL TIGHT FIT PINS

2 - 12.5mm 300W KNIFE PLATES

NOTCH FOR VISUAL ASSESSMENT DURING TESTING

2 ROWS OF 10 - 10Ø PERFORATIONS @ 15 O.C.

CAPACITY DESIGNED TESTING CONNECTION

PROJECT TEST SPECIMEN

PERFORATED ZONE

(c)

(d)
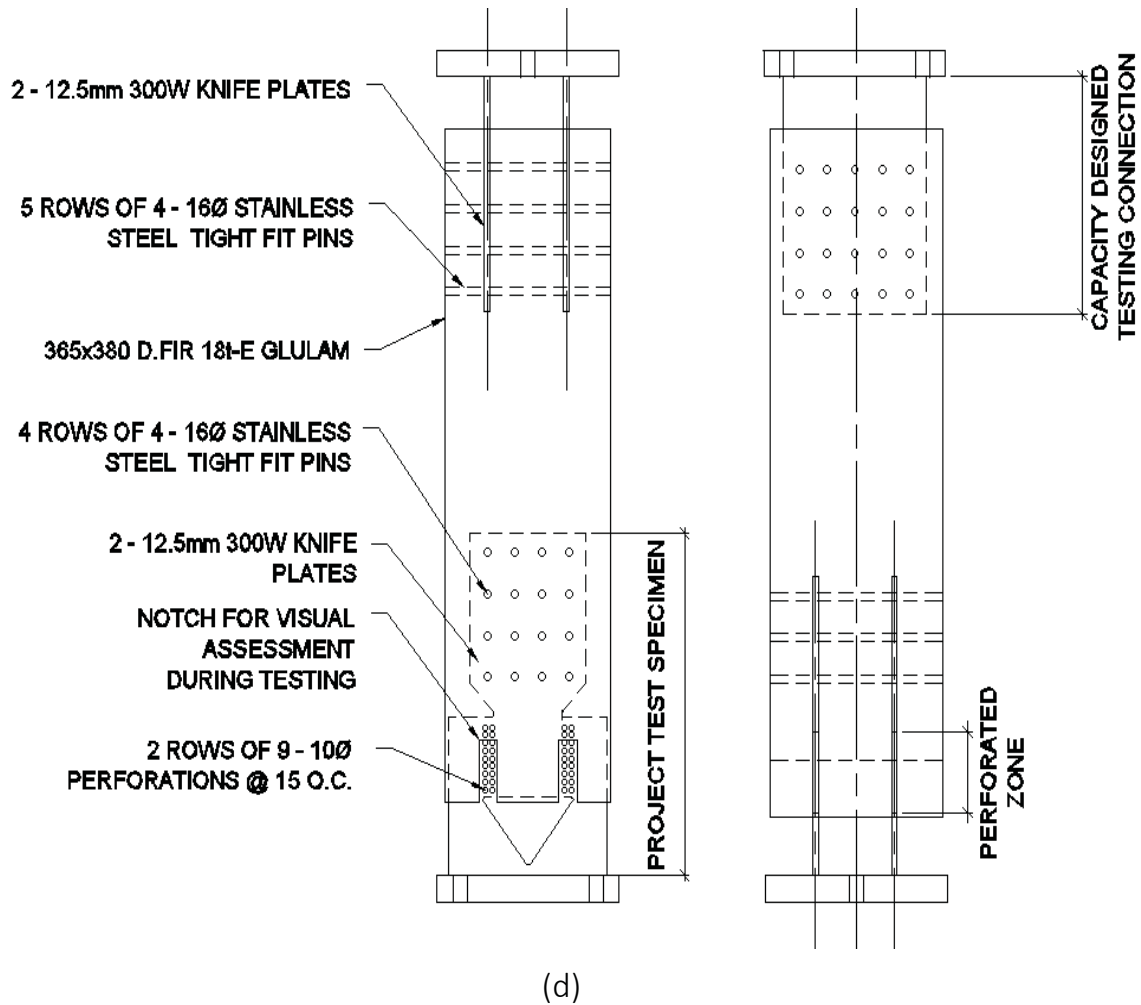
Figure 2: End brace connection experiment Phase 1 (a) Specimen 1-A: 3D view,(b) Specimen 1-B: 3D view, (c) Specimen 1-A: sections in both directions,(d) Specimen 1-B: sections in both directions

Table 1 summarizes the geometric and mechanical properties of specimens 1-A, 1-B and 2, which are required to calculate the expected capacities. It is noted that the links in the perforated zones, defined as clear steel plate between two adjacent holes, are the critical segments for the connection behaviour Table 2 summarizes the calculation regarding the expected deformations. As discussed in Section 2, the performance of the perforated plates, which are a modified version of Holz-Stahl-Komposit (HSK)[TM] and well-established in work done by Bathon et al. (2014a and 2014b), as well as recently by Zhang et al. (2018). The latter reference provides a design approach which is used for the calculations in this study. The method assumes the capacity of connection is governed by link capacities. Their cumulative strength governs the connection total response. The links fail in shear providing ductile performance, necessary for seismic fuse. The use of a fuse in timber brace connections is novel and yet not well-researched.

5 ROWS OF 5 - 16Ø STAINLESS STEEL
TIGHT FIT PINS IN 40mm HORIZONTALLY
SLOTTED HOLES

2 - 16mm 300W
KNIFE

380x365 SPF
14c GLULAM

5 ROWS OF 5 - 16Ø STAINLESS STEEL
TIGHT FIT PINS IN 40mm HORIZONTALLY
SLOTTED HOLES

2 - 16mm 300W KNIFE PLATES

NOTCH IN STEEL PLATE

GLULAM NOTCH FOR VISUAL
ASSESSMENT DURING TESTING

3 ROWS OF 16 - 10Ø PERFORATIONS
@ 16 O.C. AS SHOWN

TRIANGULAR OPENING

PERFORATED ZONE

(a)   (b)

Figure 3: Brace connection - Specimen 2 (a) 3D view, (b) sections in both directions

Tensile monotonic tests accompanied by reversed cyclic load tests will be conducted to obtain the load-slip hysteresis response, from which the connection capacity, stiffness and ductility can be determined. These results will be compared to the design calculated values. The load-slip response will be used in non-linear analyses of braced timber frame systems in order to investigate the response of the frame system under seismic loads. Based on the test results the connection will be classified into a ductility class and an appropriate failure criterion for the connection will be determined. Meanwhile, detailed finite element (FE) analyses of the specimens, 1-A and 1-B, are performed to get more insight about the prospect behaviour, discussed in Section 4.

Table 1. Expected capacities calculated for specimens 1-A, 1-B and 2.

	Description	Specimen 1-A	Specimen 1-B	Specimen 2
Perforated Plate Geometry	Plate Thickness (mm)	12.5	12.5	16
	Hole Diameter (mm)	10	10	10
	Link Size (mm)	5	5	5
	No. Hole in Each Zone	5	9	16
	Perforated Zone Length (mm)	80	140	245
	Yield Length (mm)	30	50	85
	Number of Zones per Plate	2	2	2
	Number of Plates	2	2	2
	Moment of Inertia of Link (mm^4)	130.2	130.2	166.7
	Link Length (mm/hole)	24.0	24.0	24.0
Expected Capacities (Calculation) [Note4]	Minimum Yielding Capacity (kN)	261.0	435.0	946.6
	Probable Yielding Capacity (kN)	335.0	558.3	1214.8
	Probable Ultimate Capacity (kN)	430.7	717.8	1561.8

Notes

1: Steel properties: Minimum yield = 300MPa; Probable yield=385MPa; Probable ultimate=495MPa; Modulus of elasticity= 200000MPa

2: Timber mechanical property: Modulus of elasticity= 12500MPa

3: Timber geometry: Width=365mm; Height = 380mm

4: Material resistance factor (Φ=0.9) has been excluded in order to make the table comparable with finite element and prospect test results.

Table 2. Expected deformation calculated for specimens 1-A, 1-B and 2.

	Description	Specimen 1-A	Specimen 1-B	Specimen 2
Stiffness Calculations	Link Equivalent Spring Stiffness (kN/mm/hole)	22.6	22.6	28.9
	Stiffness of each perforated plate (kN/mm)	226.1	406.9	925.9
	Total Stiffness of perforated plates (kN/mm)	452.1	813.8	1851.9
	Glulam Equivalent Spring Stiffness (kN/mm)	1803.1	1803.1	601.0
	Connector Equivalent Spring Stiffness (kN/mm)	2128.4	2135.1	2741.6
Expected Deformations (Calculation)	Elastic - Glulam (mm)	0.14	0.24	1.57
	Elastic - Connector - Perforation Excluded (mm)	0.12	0.20	0.35
	Elastic - Connector - Perforation (mm)	0.74	0.69	0.66
	Elastic -Total (mm)	1.0	1.1	2.6
	Plastic - Assumed (mm)[Note 2]	5.0	5.0	8.0
	Total - Elastic and Plastic (mm)	6.0	6.1	10.6

Notes

1: Different parts locations: Glulam lengths = 1000mm (1-A, 1-B), 3000mm (2) ; Steel connector length= 370mm; Steel connector average width = 315mm

2: Tests done by Zhang et al. (2018) on perforated plate (different plate thickness and material type compare to this research) showed higher plastic deformation than what is assumed here. Assumptions herein, is based on engineering judgement; will be verified once the material and component tests are done.

4 Finite Element Analysis (FEA)

4.1 Model Description:

The commercial finite element (FE) analysis software, Abaqus (Dassault Systèmes, 2009) has been utilized to simulate highly non-linear complex behaviours. The created FE models consist of the timber section, the connection of timber to steel, as well as the steel plates including the perforated zones with its complete detailing as shown in Figures 4. Since the perforated zones are the main point of interest, all the characteristic features necessary are included in the model. For the connections of timber to steel plates, connector elements are implemented, assuming rigid behaviour in the longitudinal direction. The model is restrained fully at the bottom while a displacement in the main axis is imposed on the top surface of the timber element, depicted in Figures 4(b). Both steel and timber parts are made of three-dimensional solid elements, 8-node linear brick, reduced integration and hourglass control elements. A refined mesh is implemented at the perforated zones, also within the thickness. More information regarding the material properties as well as failure criteria are summarized in the following sections. Deflected shapes of the specimens are shown in Figures 4(c).

4.2 Material Properties:

It is assumed that wood behaves elastically while having different properties in different directions. The steel behaves elasto-plastic assuming isotropic hardening. The steel utilized is CSA G40.21 300W with the properties shown in Table 3. In order to transform the nominal minimum strengths (MINS) to the expected values (EP), appropriate values based on standard industry practice have been selected, called transformation factors (TF). Additionally, the engineering stress and strain values are converted to true strain and stress in order to be applicable as an Abaqus input, the conversions are undertaken using Equations 1 and 2. Table 4 summarizes the assumed post-yielding behaviour of the steel.

$$6_{true} = 6_{nom} (1 + \varepsilon_{nom})$$
(1)

$$\varepsilon_{true} = ln(1 + \varepsilon_{nom})$$
(2)

It is noted that Equations (1) and (2) are valid before the occurrence of localized necking.

Table 3. CSA 300W - Engineering strain–stress properties.

ε_{eng}	6_{eng}(MPa) - MINS	TF
0.000	300	1.28
0.013	300	1.28
0.228	450	1.1

Table 4. CSA 300W - True strain–stress properties.

ε_{true}	σ_{true}(MPa) - MINS	σ_{true} (MPa) - EP
0.000	300.0	385.0
0.013	303.9	390.0
0.205	552.6	607.9

4.3 Failure Criteria:

Preliminary investigations reveal that stress-based criteria do not establish an accurate failure capacities for the numerical models. As a result, a strain-based failure criteria has been implemented based on equivalent plastic strain, PEEQ in Abaqus, defined below:

$$\text{PEEQ} = \left.\overline{\varepsilon_p}\right|_0 + \int_0^t \dot{\overline{\varepsilon_p}}\ dt \tag{3}$$

where $\left.\overline{\varepsilon_p}\right|_0$ is the initial equivalent plastic strain. For classical (Mises) plasticity $\dot{\overline{\varepsilon_p}}$ is defined in Equation (4)

$$\dot{\overline{\varepsilon_p}} = \sqrt{\frac{2}{3}\dot{\varepsilon}_p : \dot{\varepsilon}_p} \tag{4}$$

At this stage, PEEQ of 0.1 and 0.3 are assumed to be the threshold of yielding and ultimate capacity of the steel material. This assumption will be verified later against the test results with more mesh studies.

4.4 Preliminary Results:

Table 5 shows the results of the FE models in comparison with the values calculated in Section 3 for specimens 1-A and 1-B. As can be seen, the results of FEA look promising regarding the prediction of the capacities, both in yielding (initiation and progression) as well as ultimate states. The difference between calculated results and FEA results are mostly less than 10% which are deemed to be acceptable.

Table 5. Abaqus input for CSA 300W steel.

Description	Specimen 1-A	Specimen 1-B
Probable Yielding Capacity - FEA - (Initiation : PEEQ = 0.05) (kN)	301.2	502.7
Deviation from Calculated Probable Yielding Capacity (%)	-10.1	-10.0
Probable Yielding Capacity - FEA - (Progression : PEEQ = 0.1)	339.4	575.3
Deviation from Calculated Probable Yielding Capacity (%)	1.3	3.1
Probable Ultimate Capacity - FEA - (PEEQ = 0.3)	438.4	749.3
Deviation from Calculated Ultimate Capacity (%)	1.8	4.4

The distribution of PEEQ for the two specimens 1-A and 1-B are shown in Figures 5 and Figure 6, respectively.

(a)   (b)   (c)
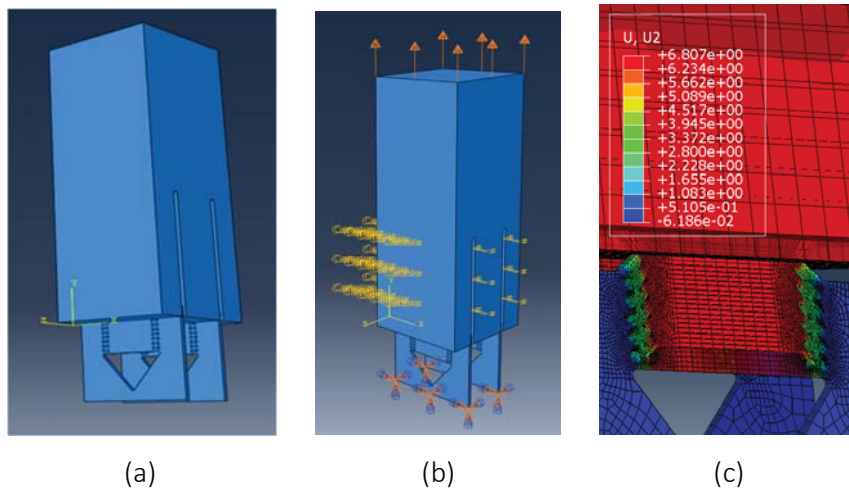
Figure 4: FE model of brace connection with perforation plates - Specimen 1-B (a) 3D view, (b) boundary conditions, constrains and applied displacement (c), sample deformed shape

(a)   (b)   (c)
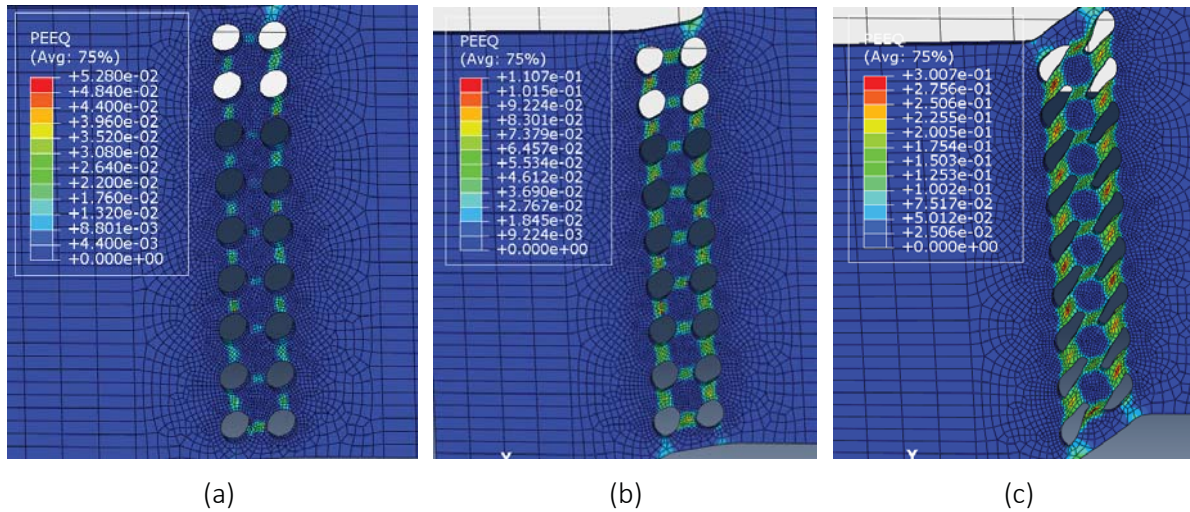
Figure 5: Specimen 1-B (a) yielding initiation (PEEQ=0.05), (b) Yielding progression (PEEQ=0.1), (c) Ultimate state (PEEQ=0.3)

(a)   (b)   (c)
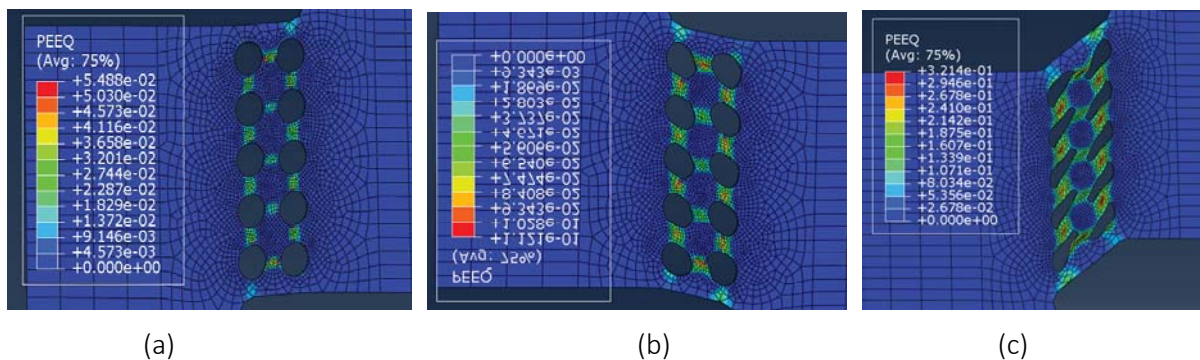
Figure 6: Specimen 1-A (a) Yielding initiation (PEEQ=0.05), (b) Yielding progression (PEEQ=0.1)< (c) Ultimate state (PEEQ=0.3)

Figure 7 illustrates the force-deformation curves of the specimens 1-A and 1-B. As can be seen, there is an acceptable agreement between the FEA results and the calculated values in Section 3. The difference at the beginning is due to bilinear assumption for the calculated design curve. Defining a tri-linear curve will improve the agreement of the two approaches at early stages. These curves will be verified against experimental data once the tests are done.
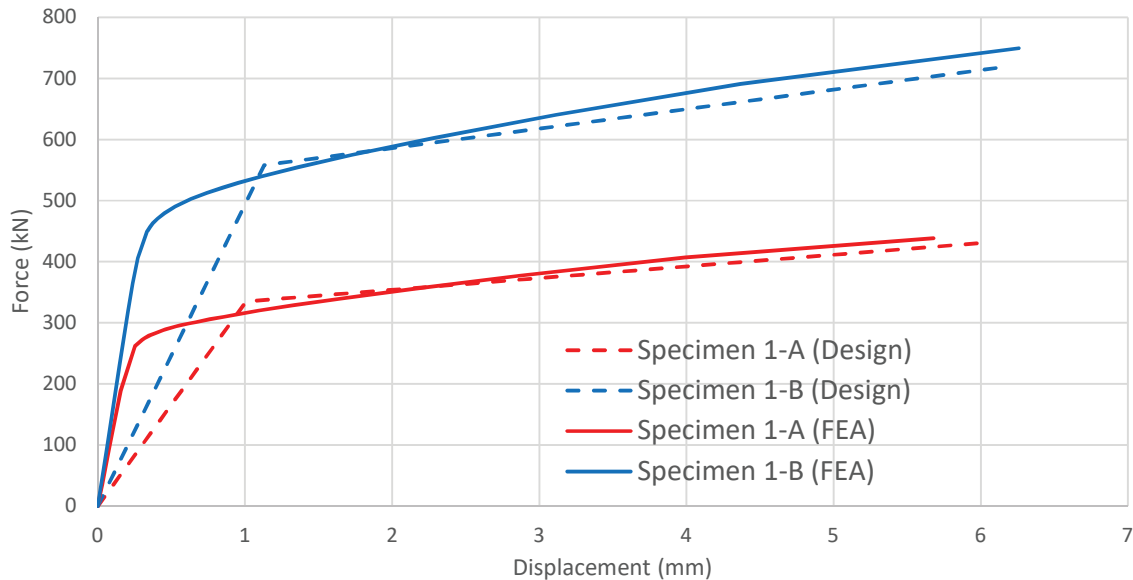
Figure 7: Comparison of FEA results versus design calculations: Expected response of connection specimens for phase 1

5 Conclusions

The current study introduces the application of perforated plate concept to the connection of diagonal braces in the braced frames. The design calculations as well as preliminary results of finite element models are in acceptable agreements; confirming promising results and desired behaviour expected from connections under consideration. As a result, it is concluded that perforated plate, with the detailing discussed, can potentially act as a fuse for timber braced frames during major events such as earthquake. The results of experiments are pending to verify the design calculation as well as finite element analyses results. These outcomes will be the basis for the evaluation of an appropriate R_d (or R) value for the system using the appropriate methodologies such as in FEMA P965 (2009). The outcome of this research will shed some lights on seismic behaviour of the timber end brace connections that are designed as seismic fuses to dissipate energy. The results may pave the way for the eventual assignment of ductility class and R_d factor for timber frame systems with perforated steel plates in NBCC (2015) and ASCE 7-16 (2017).

6 References

American Society of Cilvil Engineers (ASCE) (2017): Minimum Design Loads and Associated Criteria for Buildings and Other Structures. ASCE/SEI 7-16. Reston, VA, USA.

Bathon, L.; Bletz-Mühldorfer, O.; Schmidt, J. & Diehl, F. (2014a): Fatigue performance of adhesive connections for wooden wind towers. Materials and Joints in Timber Structures: 375-380. Dordrecht.

Bathon, L.; Bletz-Mühldorfer, O.; Schmidt, J. & Diehl, F. (2014b): Fatigue design of adhesive connections using perforated steel plates. Proceedings of the World Conference on Timber Engineering 2014: 996-1001. Quebec City, Canada.

Canadian Standards Association (CSA) (2014): Engineering design in wood. CSA Standard 086-14. Toronto, ON, Canada.

Dassault Systèmes (2009): Abaqus Analysis User's Manual. Dassault Systèmes Simulia Corp. Providence, RI, USA.

Federal Emergency Management Agency (FEMA) (2009): Quantification of Building Seismic Performance Factors. FEMA P695. Washington, D.C., USA.

Johansen, K. W. (1949): Theory of timber connectors. Publication of the International Association of Bridges and Structural Engineering. No.9: 249–262. Bern, Switzerland.

MyTiCon (2019): Self-Drilling Dowel Desing Guide. Retrieved 02 27, 2019, from http://www.my-ti-con.com/products/self-drilling-dowel

National Research Council of Canada (NRC) (2015): National Building Code. NRC Ottawa, ON, Canada.

Popovski, M. (2000). Seismic performance of braced timber frames. PhD Thesis, University of British Columbia, Vancouver, British Columbia.

Schneider, J.; Zhang, X.; Tannert, T.; Popovski, M.; Karacabeyli, E.; Stiemer, S. & Tesfamariam, S. (2014): Novel steel tube connection for hybrid systems. Proceedings of the World Conference on Timber Engineering 2014. Quebec City, Quebec.

Yasumura, M. (1990): Seismic behaviour of braced frames in timber construction. Proceedings of Meeting 23 of the International Council for Building Research Studies and Documentation, Working Commission W18 - Timber Structures. Vol. 23-15-4. Lisbon, Portugal.

Zhang, X.; Popovski, M.; & Tannert, T. (2018): High-capacity hold-down for mass-timber buildings. Construction and Building Materials. 164: 688-703.

Discussion

The paper was presented by H Daneshvar

F Lam questioned whether shaping of the steel plate is a better option compared to a perforated plate. H Daneshvar agreed that it is possible. F Lam commented that this paper described only a proposed test program of a new connection system aiming to quantify Rd Ro factors for seismic design; the work is incomplete and not suitable for INTER. H Daneshvar responded that the experimental work was delayed. F Lam said that the FEM work is also incomplete as it deals with monotonic loading only and shows large difference to codes.

P Quenneville asked about the amount of deformation for these types of plates and how many cycles can the plates sustain. H Daneshavr responded 10 mm for 3 rows and will look into the number of cycles. P Quenneville asked about capacity design factor for these connectors. H Daneshavr responded this is not clear yet as there is no guideline. P Quenneville said it would depend on variability and should be >1.5.

A Frangi asked whether ductile timber frame can be combined with shear walls. H Daneshvar responded this is common in concrete systems. D Dolan disagreed and said that ASCE does not allow combining concrete shearwalls with ductile frames.

M Li asked why there is such a big difference in initial stiffness between model and code. H Daneshvar said that the design case is based on two points and the FEM should be more accurate. As material was assumed to be linear and perfectly plastic, real material properties input should be used.

T Tannert said that your work seems to aim to combine two lateral load resistance systems which necessitates to achieve the same ductility. H Daneshvar said that the work aims to study how these two systems can act together. T Tannert and H Daneshvar discussed the difference between mean fy values and the expect fy.

A Ceccotti received confirmation that the dowel diameter was 16 mm.

Lateral Resistance and Deflection of Cross-laminated Timber Shear Walls

Md Shahnewaz, Postdoctoral Research Fellow, Wood Engineering, University of Northern British Columbia, Prince George, Canada; md.shahnewaz@alumni.ubc.ca

Marjan Popovski, Principal Scientist, Building Systems, FPInnovations, Vancouver, Canada, marjan.popovski@fpinnovations.ca

Thomas Tannert, Associate Professor, Wood Engineering, University of Northern British Columbia, Prince-George, Canada; thomas.tannert@unbc.ca

1 Introduction

1.1 Cross-laminated timber shear walls

CLT panels can be used for wall, floor and roof assemblies, as a part of the lateral load resisting system of the building. The CLT panel in-plane bending and shear stiffness was investigated by Blass and Fellmoser (2004), Mossbrugger et al. (2006) and Brandner et al. (2017). CLT panels are also commonly used in shear walls in multi storey buildings around the world for resisting seismic loads (Izzi et al. 2018). Designing and building CLT structures in earthquake-prone regions is no longer a domain for early adopters, but is becoming a part of regular timber engineering practice (Tannert et al. 2018).

The SOFIE project was the most comprehensive endeavour to quantify the seismic behaviour of CLT structures (Ceccotti and Follesa 2006, Ceccotti et al. 2013). Reversed cyclic tests on CLT shear walls, dynamic tests on one-story building, and shaking table tests on 3-story and 7-story buildings were conducted. These tests allowed for evaluation of the behavior of CLT panels and their connections, and were used to validate the design assumptions for CLT structure regarding strength and ductility. The consensus from these tests was that the structural performance of CLT buildings is governed by the connections that dissipate the seismic energy, while CLT panels behave as almost rigid bodies (Figure 2). Finite element models and non-linear time history analyses led to the proposal of a behavior "q factor" of 3.0 for CLT buildings, where shear walls composed of multiple CLT panels connected to each other by vertical joints with dowel-type fasteners such as self-tapping screws (STS).
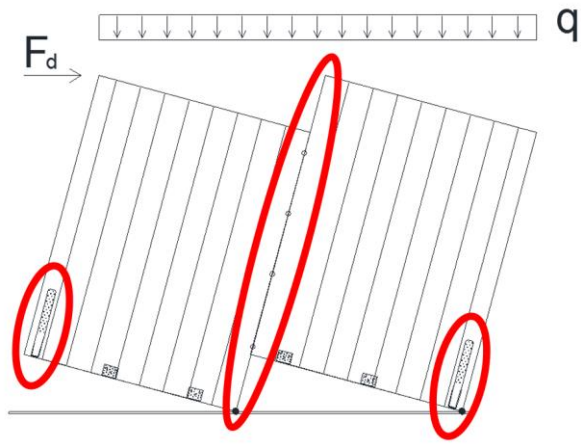
Figure 1: CLT shear-wall system under rocking motion

1.2 North American research on performance and design of CLT shearwalls

The bi-national Canada and USA ANSI/APA PRG320 (ANSI 2018) standard for performance-rated CLT was instrumental for the recognition of CLT in the 2016 supplement to the 2014 Canadian Standard for Engineering Design in Wood CSA O86 (CSA 2016), the National Design Specification for Wood Construction (NDS 2015) and the International Building Code (IBC 2015).

In Canada, FPInnovations conducted comprehensive research on performance of CLT walls and a two-storey CLT house subjected to reversed quasi-static loads (Popovski et al. 2010; Gavric et al. 2015; Popovski and Gavric 2015). Different hold-downs, brackets and shear connections were tested and it was observed that brackets have similar capacity and stiffness under tension and shear loading. A two-storey structure was designed using the Equivalent Static Force Procedure (ESFP) (R_d = 2.0, R_0 = 1.5). Failure was observed under combined sliding and rocking. Subsequently, these force reduction factors were proposed for CLT structures in the Canadian version of the CLT handbook (Gagnon and Pirvu 2012). Schneider et al. 2015, studied the performance of bracket connections with three types of fasteners, confirmed the findings found from the FPInnovations' studies.

Shahnewaz et al. (2017 and 2018) developed finite element analyses (FEA) models of CLT panels with openings and proposed analytical expression to estimate the in-plane stiffness of CLT walls with the consideration of size, shape and location of openings. They also investigated the stiffness, strength and resistance of CLT walls with various connections and found that walls with brackets and hold-downs (HDs) exhibited better strength and stiffness performance compared to walls without HDs.

A comprehensive numerical work was conducted to determine the ductility-based force modification factor (Rd-Factor) for platform-type CLT structures for the National Building Code of Canada (NBCC 2015). Results from these analyses (Pei et al. 2013; Popovski et al. 2014; Koliou et al. 2019) conducted using a modified FEMA P-695 method, were used to propose Rd-factor of 2.0 and Ro=1.5 for implementation of CLT as SFRS in 2020 NBCC.

In the USA, seismic design is performed using one of the methods outlined in ASCE 7 (ASCE 7-16 2016). Research by Amini et al. (2016, 2018), van de Lindt et al. 2019 and Pei et al. (2013, 2017) was aimed on determining the R-factor for CLT buildings up to 6-storeys for implementation in ASCE-7. Based on the findings from this research that followed the FEMA P-695 method (FEMA 2009), CLT as a Seismic Force Resisting System is in process of introduction in the next edition of ASCE-7.

1.3   Seismic design of CLT buildings in Canada

Building design in Canada is regulated by the National Building Code of Canada (NBCC 2015) where performance requirements are tied to objectives. Code compliance is achieved through prescriptive 'acceptable solutions' and innovative 'alternative solutions'. An 'alternative solution' must achieve at least the minimum level of performance that is attributed to an 'acceptable solution'. Seismic design in Canada is mostly carried out in accordance with the ESFP where elastic design force levels are decreased by reduction factors R_d and R_o for ductility and over-strength, respectively.

The 2016 update to CSA O86 (CSA 2016) includes provisions for CLT elements manufactured in accordance with ANSI/APA PRG320, design of connections, as well as a new clause "Design of CLT shearwalls and diaphragms" that deals with design of CLT as platform-type LLRS of platform-type buildings not exceeding 30m in height for medium seismic zones, and 20m for high seismic zones. The CSA O86 provisions are based on the assumption that CLT panels act as rigid bodies and the resistance of LLRS is governed by the hold-downs and the connections between the wall panels. The energy dissipative connections need to be designed so that the yielding mode governs their failure, have at least moderate ductility, and sufficient deformation capacity to allow the CLT panels can develop their assumed kinematic motion. Using capacity-based principles, all non-dissipative connections have to remain elastic (under their force and displacement demands) when the energy-dissipative connections reach their 95th percentile of the ultimate resistance or the target displacement.

The kinematic motion of the CLT panels should be rocking or combination of rocking and minimal sliding. To promote this motion, CLT wall segments must have an aspect ratio (height-to-length) 1:1 and 4:1. Wall segments with smaller aspect ratio need to be divided and joined with energy dissipative connections, or the LLRS needs to be designed according to the alternative solution procedure. The 2019 edition of CSA O86 which has recently undergone public review, proposes changes related to acceptable kinematic motions (no longer allowing combined rocking and sliding, but rocking only) and the acceptable CLT panel aspect ratio (limited to between 2:1 and 4:1). Within these design consideration in mind, CLT structures can be designed using seismic modification factors R_d =2.0 and R_d = 1.5. Other CLT LLRS have to be treated as alternative solution in accordance with NBCC (2015) and have to be designed for a seismic force determined using $R_d \cdot R_o$ = 1.3.

2   Objectives

Providing seismic design provisions for CLT structures in CSA O86 presented a significant accomplishment. Nevertheless, the standard does not (yet) provides any specific procedures to estimate the resistance of CLT shear walls or how to facilitate the targeted kinematic mode in the presence of vertical loads, especially for multi-panel CLT walls. Further, CSA-O86 states that "deflections shall be determined using established methods of mechanics" but no specific guidance is provided other than that calculations shall account for deformations of shearwall and connections while CLT panels can be assumed to act as rigid bodies.

This paper provides a simplified method for seismic design of CLT shear walls, based on some assumptions mentioned below in the text. As the new 2019 provisions of CSAO86 limit the permitted kinematic motion to rocking only, only the rocking motion is taken into account.

3   Resistance of CLT Shear Walls

3.1   Monolithic CLT shear wall with brackets only

The rocking behaviour of CLT shear wall is shown in Figure 1. It has been assumed that under lateral loading the CLT wall rotates about the right corner point without formation of a compression zone. Therefore, the reactions of the connectors follow a triangular distribution. The rocking resistance of the CLT shear wall can be calculated by taking summation of the moment at the lower right corner of the wall:

$$F_r\,h = N_{1y}x_1 + N_{2y}x_2 + N_{3y}x_3 + N_{4y}x_4 + q\frac{b^2}{2} \tag{1}$$

where N_{iy} is the rocking reaction of each connection, x_i is the distance of each connector from the right corner, b is the width of the CLT panel, q is the vertical load on top of the panel. The rocking resistance of the CLT shear wall is reached when the first bracket (left corner) has reached its ultimate resistance, i.e. $N_{1y} = N_B$. As seen in Eq. (1), the first bracket carries the maximum moment due to the rocking of the wall since it has the highest lever arm, i.e. it locates at a maximum distance from the right side of the wall, x_1. Therefore, when it reaches its ultimate resistance (i.e. fails) the rocking resistance of the wall will reduce immediately with the subsequent failure of the rest of the brackets. Therefore, using the triangular distribution of the bracket's forces in Figure 2a, the reaction forces of the brackets can be written as:

$$N_{1y} = N_B;\; N_{2y} = (x_2/x_1)N_B;\; N_{3y} = (x_3/x_1)N_B;\; N_{4y} = (x_4/x_1)N_B \tag{2}$$

Substituting Eq. (2) into Eq. (1), the rocking resistance can be estimated as:

$$F_r = \frac{N_B}{h\,x_1}\left(\sum_1^{n_B} x_i^2\right) + q\frac{b^2}{2h} \tag{3}$$
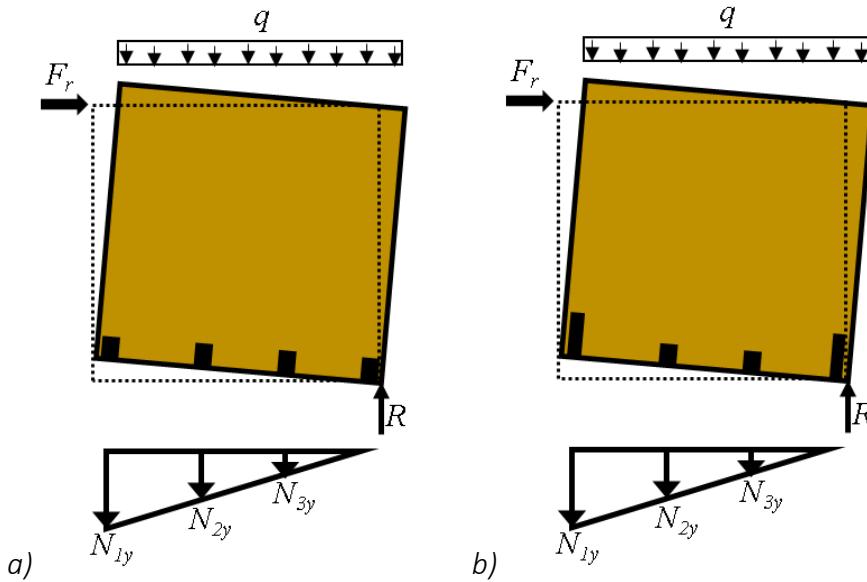
Figure 2: Rocking of single CLT walls: (a) with brackets only and (b) with brackets and HDs

3.2 Monolithic CLT shear wall with brackets and HDs

The rocking resistance of the CLT shear wall's hold-down and bracket connections can be calculated by taking a summation of the moment at the lower right corner of the CLT shear wall (Figure 1b):

$$F_r h = N_{1y} x_1 + N_{2y} x_2 + N_{3y} x_3 + N_{4y} x_4 + q \frac{b^2}{2} \tag{4}$$

The rocking resistance of the CLT shear wall will be reached when the left hold-down has reached its ultimate resistance -i.e. $N_{1y} = N_{HD}$. The rocking reaction for the remainder of the brackets will follow the triangular load distribution as shown in Figure 1b. The resistance of the two intermediate brackets can be calculated following the triangular distribution as:

$$N_{1y} = N_{HD}; N_{2y} = (x_2 / x_1) N_B; N_{3y} = (x_3 / x_1) N_B; N_{4y} = (x_4 / x_1) N_{HD} \tag{5}$$

Substituting Eq. (5) into Eq. (4), the resistance of the wall under rocking is:

$$F_r = \frac{N_{HD} x_1}{h} + \frac{N_B}{x_1 h} \left(\sum^{n_B} x_i^2 \right) + q \frac{b^2}{2h} \tag{6}$$

3.3 Coupled CLT shear wall with brackets only

The kinematic behaviour of coupled CLT shear walls with brackets only is illustrated in Figure 2. The rocking resistance of the CLT shear wall's bracket connections can be calculated by taking the moment at the lower right corner of the CLT shear wall:

$$F_r h + R_1 b_2 = N_{1y} (x_1 + b_2) + N_{2y} (x_2 + b_2) + N_{3y} (x_3 + b_2) + N_{5y} x_5 + N_{6y} x_6 + N_{7y} x_7 + q \frac{b^2}{2} \tag{7}$$

where N_{iy} is the rocking reaction of each of the connections, x_i is the distance of each connector from the right corner of the panel, b_1 and b_2 *are* the widths of the left and

right panels, b is the total width of the CLT shear wall ($b= b_1+b_2$), and q is the vertical load on top of the wall.

The rocking resistance of the CLT shear wall will be reached when the left corner bracket has reached its factored resistance, i.e. $N_{1y} = N_B$. The rocking reaction for the remainder of the brackets will follow a triangular load distribution as shown in Figure 2a. Therefore, the reaction forces of the brackets can be written as:

$$N_{1y} = N_B; N_{2y} = (x_2/b_1)N_B; N_{3y} = (x_3/b_1)N_B;$$
$$N_{5y} = (x_5/b_2)N_B; N_{6y} = (x_6/b_2)N_B; N_{7y} = (x_7/b_2)N_B \tag{8}$$

where N_{iy} is the vertical reaction of the ith bracket located at a distance x_i from the right side of each segment of the wall, and b_1 and b_2 are the widths of the left and right panels of the coupled wall, respectively. The reaction force R_1 can be calculated from the equilibrium of the forces in the y-direction for the left panel only:

$$N_{1y} + N_{2y} + N_{3y} + qb_1 = N_s + R_1 \tag{9}$$

The screws in the vertical joints will yield first and will reach their shear resistance, N_S, which can be calculated using Eq. (9). Substituting the vertical reaction forces from Eq. (8) with Eq. (9), the equation can be rewritten as:

$$R_1 = N_B + N_B\left(\frac{x_2}{b_1}\right) + N_B\left(\frac{x_3}{b_1}\right) + qb_1 - N_s \tag{10}$$

By substituting Eq. (10) and Eq. (8) into the moment Equation (7), the rocking resistance for a CLT coupled shear wall can be estimated as:

$$F_r = \frac{1}{h}\left[N_B x_1 + \frac{N_B}{b_1}(x_2^2 + x_3^2) + \frac{N_B}{b_2}(x_5^2 + x_6^2 + x_7^2) + q\frac{b^2}{2} - qb_1b_2 + N_s b_2\right] \tag{11}$$

Eq. (11) can be simplified as Eq. (12) if we consider equal panel length:

$$F_r = \frac{1}{h}\left[\frac{2N_B}{b}\left(\sum_{n=1}^{n_B} x_i^2\right) + q\frac{b^2}{4} + \frac{N_s b}{2}\right] \tag{12}$$

3.4   Coupled CLT shear wall with brackets and HDs

The rocking resistance of the CLT shear wall's hold-down and bracket connections can be calculated by taking the moment at the lower right corner of the CLT shear wall (Figure 2b):

$$F_r h + R_1 b_2 = N_{1y}(x_1 + b_2) + N_{2y}(x_2 + b_2) + N_{3y}(x_3 + b_2) + N_{5y}x_5 + N_{6y}x_6 + N_{7y}x_7 + q\frac{b^2}{2} \tag{13}$$

where N_{iy} is the rocking reaction of each of the connections, x_i is the distance of each connector from the right corner of the panel, b_1 and b_2 are the respective widths of the left and right panels, b is the total width of the CLT shear wall ($b= b_1+b_2$), and q is the vertical load on top of the panel. The rocking resistance of the CLT coupled wall is reached when the hold-down in the left panel reaches its factored resistance, i.e. N_{1y}

= N_{HD}. The rocking reaction for the remainder of the brackets will follow the triangular load distribution as shown in Figure 2b:

$$N_{1y} = N_{HD};\ N_{2y} = (x_2/b_1)N_B;\ N_{3y} = (x_3/b_1)N_B;$$
$$N_{5y} = (x_5/b_2)N_B;\ N_{6y} = (x_6/b_2)N_B;\ N_{7y} = (x_7/b_2)N_B \tag{14}$$

where N_{iy} is the vertical reaction of the ith brackets located at a distance x_i from the right side of each segment of the wall and b_1 and b_2 are the widths of the coupled wall's left and right panels, respectively. The reaction force R_1 can be calculated by taking a summation of forces in the y-direction for the left panel only:

$$N_{1y} + N_{2y} + N_{3y} + qb_1 = N_s + R_1 \tag{15}$$

By substituting Eqs. (14) and (15) with Eq. (13), the rocking resistance for a CLT coupled shear wall with brackets and four hold-downs can be determined as:

$$F_r = \frac{1}{h}\left[N_{HD}(x_1 + x_5) + \frac{N_B}{b_1}(x_2^2 + x_3^2) + \frac{N_B}{b_2}(x_6^2 + x_7^2) + q\frac{b^2}{2} - qb_1b_2 + N_s b_2 \right] \tag{16}$$

Eq. (16) can be simplified considering equal panel length -i.e. $b_1 = b_2 = b/2$:

$$F_r = \frac{1}{h}\left[N_{HD}b + \frac{2N_B}{b}\left(\sum^{n_B} x_i^2\right) + q\frac{b^2}{4} + \frac{N_s b}{2} \right] \tag{17}$$
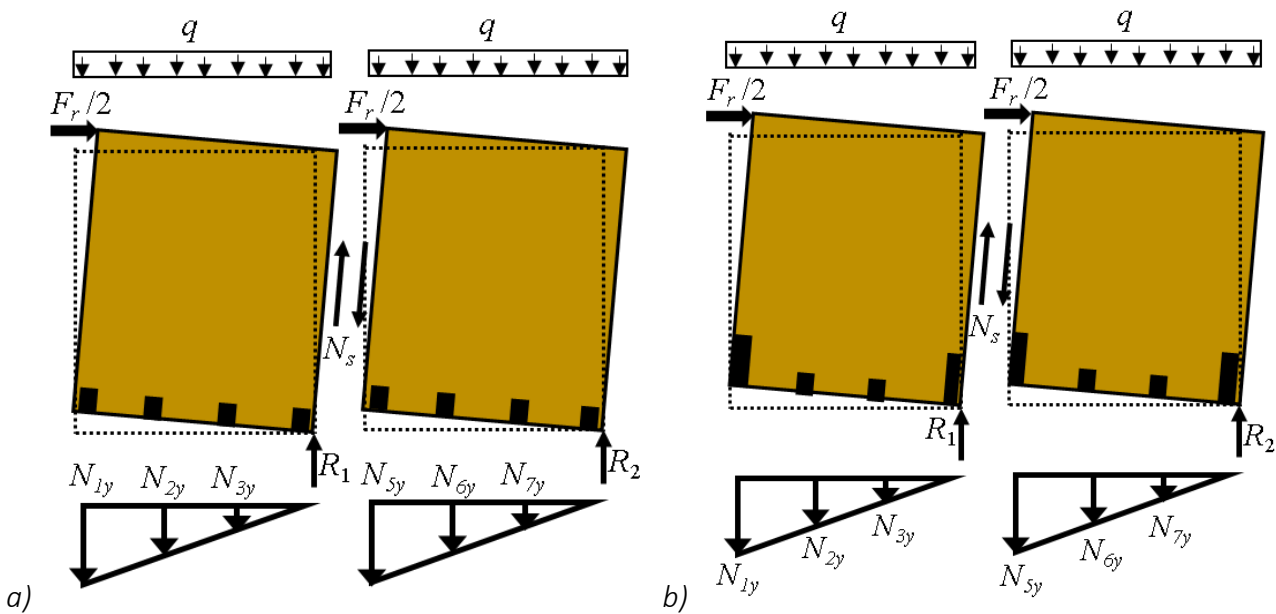
Figure 3: Rocking of coupled CLT walls: (a) with brackets only and (b) with brackets and HDs

3.5 Comparison of the equations to test results

The proposed equations to estimate the resistance of CLT shear walls were compared against test results from Gavric and Schneider. The rocking ($F_{d,r}$) resistance of the tested single and coupled walls configurations were estimated using the proposed equations and compared to the peak loads obtained from the hysteresis envelops of

the load-deflection curves, see Figure 4. This comparison illustrated that the rocking resistance formulas produced resistance results, with and average ratio of $P/F_{d,r}$ = 2.0.
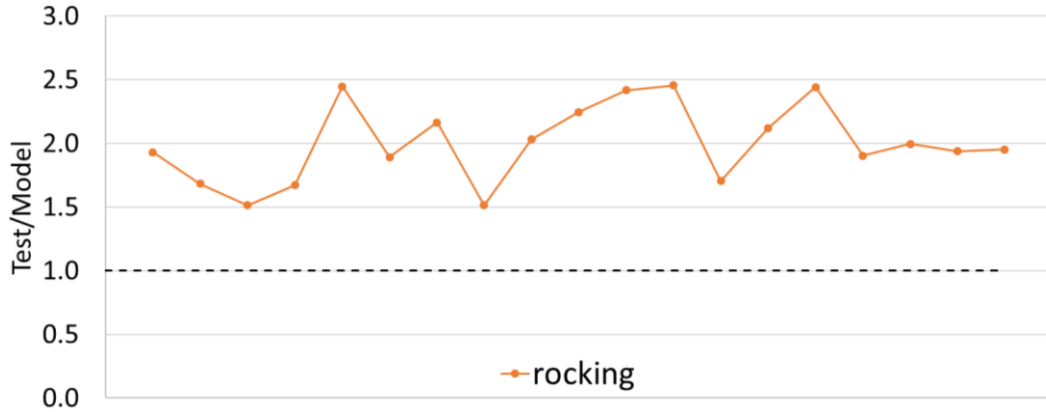
Figure 4: Resistance models comparison test vs model

4 Deflection of CLT Shear Walls

4.1 Monolithic CLT shear wall

Total deflection of a single shear wall δ can be calculated as the summation of deflection due to panel bending (δ_b) and shear (δ_s) and wall sliding (δ_{sl}) and rocking (δ_r):

$$\delta = \delta_b + \delta_s + \delta_{sl} + \delta_r \tag{18}$$

Figure 5 illustrates these four components. The procedure to estimate each part of the deflection components are discussed in the following sections.
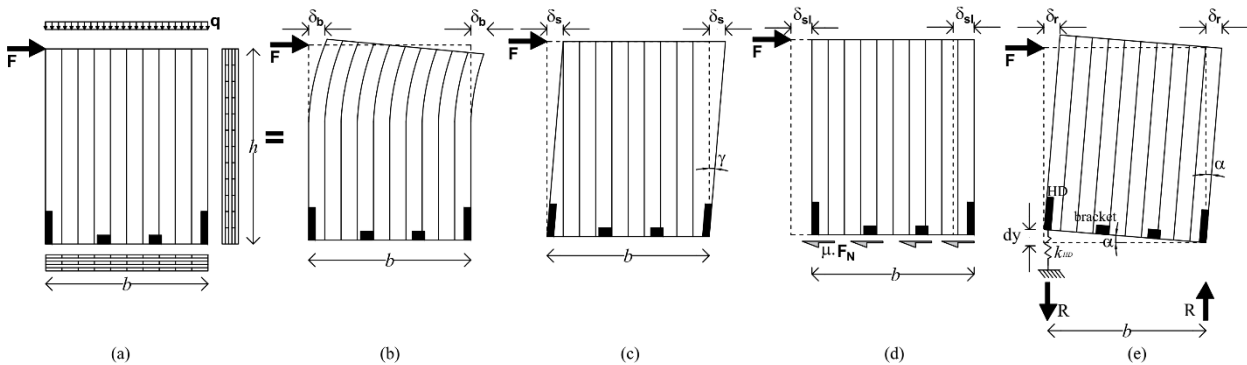
Figure 5: (a) CLT shear wall; Deflection of single shear wall due to: b) bending of CLT panel; c) shear deformation of CLT panel d) sliding of CLT shear wall and e) rocking of CLT shear wall

Therefore, under lateral loading the elastic bending deflection, δ_b is:

$$\delta_b = \frac{Fh^3}{3EI_{eff}} \tag{19}$$

where F is the lateral force on the wall, h is the height of the wall, and EI_{eff} is the effective bending stiffness of the CLT panel.

The shear deflection of the CLT panels can be evaluated as:

$$\delta_s = \frac{Fh}{G_{CLT} t_{CLT}\, b} \tag{20}$$

where F is the lateral force, h is the height of the wall, b is the width of the wall, G_{CLT} is the shear modulus of CLT panel and t_{CLT} is the total thickness of CLT panel.

Hold-downs and angle brackets provide sliding resistance to CLT shear walls. Gravity loading also contributes to the sliding resistance through friction. The sliding deflection of the CLT shear wall can be estimated as:

$$\delta_{sl} = \frac{F'}{n_B k_B} = \frac{F - \mu F_N}{n_B k_B} = \frac{F - \mu(qb)}{n_B k_B} \tag{21}$$

where F' is the resultant force on shear walls, i.e. the difference between the lateral force F and the frictional force (μF_N) between CLT panel and floor or foundation, q is the vertical load (herein assumed as a uniformly distributed load) on the shear wall, b is the width of the wall, n_B is the number of brackets and k_B is the stiffness of the bracket connections. Under certain loading conditions, there is no guarantee that the friction will act; ttherefore, it should be ignored and Eq. (21) can be simplified to:

$$\delta_{sl} = \frac{F}{n_B k_B} \tag{22}$$

The rocking or overturning of the CLT shear wall is resisted by the corner connectors, i.e. hold-downs, as shown in Figure 5e. The reaction force of the corner connectors, R, can be calculated from the equilibrium of the forces:

$$R = \frac{1}{b}\left(F\,h - \frac{qb^2}{2} \right) \tag{23}$$

where q is the vertical force on shear walls, b is the length of the wall.

The rotation of the shear wall due to lateral force can be calculated as:

$$\tan \alpha \approx \alpha = \frac{dy}{b} = \frac{\delta_r}{h} \tag{24}$$

where α is the rotation of the CLT shear wall and dy is the vertical deformation of the corner connection which can be calculated as the ratio of reaction force and connection stiffness as:

$$dy = \frac{R}{k_{HD}} \tag{25}$$

where k_{HD} is the stiffness of the hold-down.

Replacing Equations (23) and (24) into Eq. (25), the deflection due to rocking is:

$$\delta_r = \left(\frac{F\,h^2}{b^2} - \frac{qh}{2} \right) \frac{1}{k_{HD}} \tag{26}$$

By replacing Equations (19), (20), (21) and (26) into Eq. (18), the total deflection of the single CLT shear wall can be estimated as:

$$\delta = \frac{Fh^3}{3EI_{eff}} + \frac{F.h}{G_{CLT}.t_{CLT}.b} + \frac{F}{n_B k_B} + \left(\frac{F.h^2}{b^2} - \frac{qh}{2} \right) \frac{1}{k_{HD}} \tag{27}$$

4.2 Coupled CLT shear wall

Coupled CLT shear walls that are formed by connecting two or more panels vertically are common in a CLT platform building. In Canada, CSA O86 imposes a restriction on the minimum aspect ratio of shear walls (height-to-length) of 1.0 (2.0 in its 2019 version). Therefore, in case of walls with aspect ratio less than 1.0, commonly two or more panels are connected vertically to form a coupled wall. Typical vertical joints in coupled walls are half-lap and spline joints connected by STS. The deflection of a typical coupled shear wall under lateral loading is shown in Figure 6.
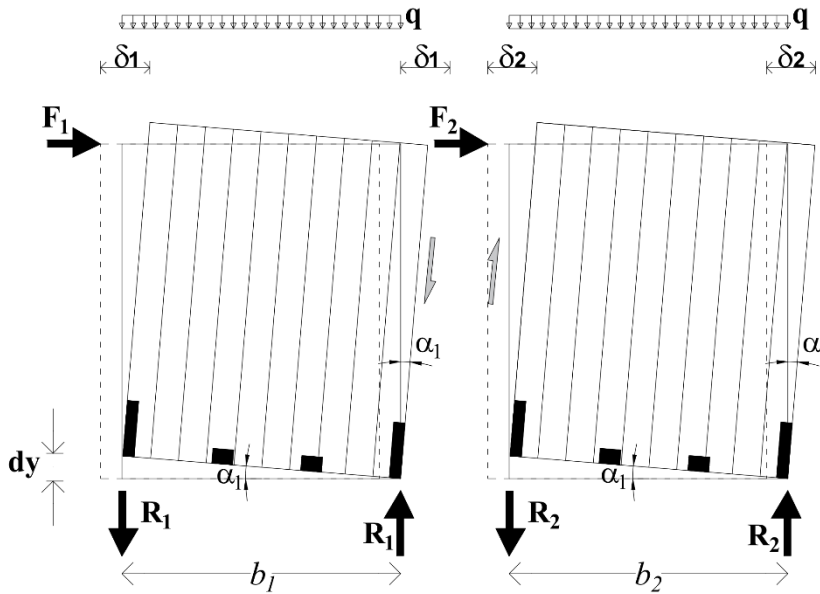
Figure 6: Deflection of coupled CLT shear wall with 4-HDs

Since each panel rocks individually, the deflection equation of single CLT shear walls can be utilized to estimate the deflection of each panel in a coupled wall. After rearranging Eq. (27), the deflection of each panel in a coupled wall with 4-HDs can be estimated as:

$$\delta_i = \frac{F_i}{\left(\frac{3EI_{eff}}{h^3} \right)} + \frac{F_i}{\left(\frac{G_{CLT}.t_{CLT}.b_i}{h} \right)} + \frac{F_i}{\left(n_B k_B \right)} + \frac{F_i}{\left(\frac{b_i^2 k_{HD}}{h^2} \right)} - \left(\frac{qh}{k_{HD}} \right) \tag{28}$$

where F_i is the lateral force on each panel, EI_{eff} is the effective bending stiffness of the CLT shear walls, b_i is the width of each panel in the coupled wall, h is the height of the wall, G_{CLT} is the shear modulus of the panel, t_{CLT} is the thickness of the panel, q is the vertical force on shear walls, n_B is the number of brackets, k_B is the stiffness of the bracket, and k_{HD} is the stiffness of the hold-down.

Eq. (28) can be rewritten in terms of the bending K_b, shear K_s, sliding K_{sl} and rocking K_r stiffness of each panel in the coupled wall:

$$\delta_i = F_i \left(\frac{1}{K_{b,i}} + \frac{1}{K_{s,i}} + \frac{1}{K_{sl,i}} + \frac{1}{K_{r,i}} \right) - \frac{qh}{k_{HD}} \tag{29}$$

where the bending $K_{b,i}$, shear $K_{s,i}$, sliding $K_{sl,i}$ and rocking $K_{r,i}$ stiffness of each wall segment can be calculated as:

$$K_{b,i} = \frac{3\left(EI_{eff}\right)_i}{h^3} \tag{30}$$

$$K_{s,i} = \frac{G_{CLT}.t_{CLT}.b_i}{h} \tag{31}$$

$$K_{sl,i} = n_{B,i} k_{B,i} \tag{32}$$

$$K_{r,i} = \frac{b^2 k_{HD,i}}{h^2} \tag{33}$$

The total stiffness of each panel in the CLT coupled wall, K_i can be expressed as the summation of the reciprocal stiffness of each panel in the coupled wall:

$$\frac{1}{K_i} = \frac{1}{K_{b,i}} + \frac{1}{K_{s,i}} + \frac{1}{K_{sl,i}} + \frac{1}{K_{r,i}} \tag{34}$$

Eq. (29) can be simplified by replacing Eq. (34):

$$\delta_i = \frac{F_i}{K_i} - \frac{qh}{2k_{HD}} \tag{35}$$

where the deflection of each panel can be written as:

$$\delta_1 = \frac{F_1}{K_1} - \frac{qh}{2k_{HD}} \tag{36}$$

$$\delta_2 = \frac{F_2}{K_2} - \frac{qh}{2k_{HD}} \tag{37}$$

where F_1, F_2, δ_1, δ_2 and K_1, K_2 are the lateral force, the deflection and stiffness on the left and right panels of the coupled wall, respectively. The summation of the forces F_1 and F_2 shall be equal to the total lateral force, F:

$$F = F_1 + F_2 \tag{38}$$

where the forces F_1 and F_2 are proportional to the stiffness of each segment of the coupled wall:

$$F_i \approx K_i \tag{39}$$

Since it is assumed that the deflection at the top of each coupled wall's segment are equal ($\delta_1 = \delta_2 = \delta$), substituting Eqs. (36) and (37) into Eq. (38), the deflection of a coupled CLT shear wall with two or more panels can be calculated as:

$$\delta = \frac{F}{\sum K_i} - \frac{qh}{k_{HD}} \tag{40}$$

5   Conclusions

CLT shear walls under lateral loading can experience three types of kinematic motions i.e., sliding, rocking and a combination of sliding and rocking. The new 2019 provisions of CSA O86 limit the permitted kinematic motion to rocking only, therefore only the rocking motion is discussed in detail in this paper. The CSA provisions do not include any guidance how to estimate the resistance and deformation of single and coupled CLT shear walls for platform-type construction.

A simplified methodology and formulae to calculate the resistance and deflection of CLT shear walls under lateral loading considering the rocking kinematic behaviour are presented. Both single and coupled CLT shear walls with connectors such as brackets, hold-downs and vertical joints are considered. When the proposed equations were compared against experimental results of CLT shear walls, they have produced average force ratio $P/F_{d,r}$ of 2.0. Depending of the desired over-strength in the design, this comparison illustrates that the proposed method may be over or under estimating the design resistance of the CLT shearwalls.

Although further experimental validation is required, the findings and proposed formulae can be useful tool for initial design of CLT platform-type buildings. As such they will be presented to the CSA O86 Technical Committee of for potential inclusion into the next edition of the standard's commentary.

Acknowledgements

References

Amini M.O., JW van de Lindt J. W., D Rammer D., S Pei S., P Line P., M Popovski M. (2016). Determination of Seismic Performance Factors for CLT Building Systems. WCTE 2016, Vienna, Austria.

Amini M.O.van de Lindt. J., Line, P., Rammer, D., Pei, S., Popovski, M. 2018. Systematic experimental investigation to support the development of seismic performance factors for CLT shear wall systems. Engineering Structures, 172 (2018) 392-404.

ANSI/APA (20178) PRG 320, Standards for performance-rated cross-laminated timber, American National Standard, APA, Tacoma, WA.

ASCE. Minimum Design Loads for Building and Other Structures. ASCE Standard ASC/SEI 7-16, American Society of Civil Engineers, Reston, Virginia; 2016.

Blass, H.J. & Fellmoser P. (2004). Design of solid wood panels with cross layers. In Proceedings of 8th World Conference on Timber Engineering, Lahti, Finland.

Brandner, R., Flatscher, G., Ringhofer, A., Schickhofer, G., Thiel, A. (2016). Cross laminated timber: overview and development. Eur. J. Wood. Prod. 74(3):331–351.

Ceccotti A., Follesa M. (2006) Seismic behaviour of multi-storey X-Lam buildings. Proceedings COST Action E29, International Workshop - Earthquake Engineering on Timber Structures, pp: 81-95, Coimbra, Portugal.

Ceccotti A., Sandhaas C., Okabe M., Yasumura M., Minowa C., Kawai N. (2013) SOFIE project–3D shaking table test on a seven-storey full-scale cross-laminated timber building. Earthquake Eng Structures, 42(13): 2003-2021.

CSA O86 (2016). Engineering Design in Wood 2014 with with Update 1. , Canadian Standards Association, Canada.

FEMA P-695 (2009). Quantification of building seismic performance factors: FEMA P695. Federal Emergency Management Agency, Washington, D.C.

Gagnon S., Pirvu C. (2012) Cross-laminated timber (CLT) Handbook, Canadian Edition. FPInnovations Special Publication SP-528E, Vancouver, Quebec, Canada. 594 pp.

Gavric I., Fragiacomo M., Ceccotti A. (2015) Cyclic behavior of CLT wall systems: Experimental tests and analytical prediction models. Journal of Structural Engineering, 141(11), 04015034.

IBC. (2015). International Building Code.

Izzi, M., Polastri, A., Fragiacomo, M. (2018). Investigating the hysteretic behaviour of Cross-Laminated Timber wall systems due to connections. Journal of Structural Engineering 2018;144(4).

Koliou Maria, John W. van de Lindt, Popovski Marjan. (2019). Development of Ductility-related Force Modification Factors for CLT Structures. 12th Canadian Conference on Earthquake Engineering, Quebec, Canada.

Moosbrugger, T., Guggenberger, W., & Bogensperger, T. (2006). Cross-Laminated Timber Wall Segments under Homogenous Shear - with and without Openings. In Proceedings of World Conference on Timber Engineering, Portland, USA.

NBCC (2015). National Building Code of Canada 2015., Canadian Commission on Building and Fire Codes. National Research Council, Ottawa, Canada.

NDS. (2015). National Design Specification for Wood Construction.

Pei S., van de Lindt J.W., Popovski M. (2013). Approximate R-factor for cross-laminated timber walls in multistory buildings. J. of Arch. Eng., 19(4): 245-255.

Pei S., van de Lindt J.W., Popovski M., Berman J.W, Dolan J.D., Ricles J.M., Sause R., Blomgren H-E.; Rammer D.R. (2015). Cross Laminated Timber for Seismic Regions: Progress and Challenges for Research and Implementation. Journal of Structural Engineering, 10.1061/(ASCE)ST.1943-541X.0001192 , E2514001.

Popovski M., Gavric I. (2015). Performance of a 2-story CLT house subjected to lateral loads. Journal of Structural Engineering, 142(4), E4015006.

Popovski M., Schneider J., Schweinsteiger M. (2010). Lateral load resistance of cross laminated wood panels Pages 20-21, Curran Associates, Proc of 11th World Conference on Timber Engineering, 20- 24 June 2010, Riva del Garda, Italy.

Popovski, M., Pei, S., van de Lindt, J. W. Karacabeyli, E. (2014). Ductility Based Force Reduction Factors for Symmetrical Cross-Laminated Timber Structures. Proceedings of the 2nd European Conference on Earthquake Engineering, Istanbul, Turkey.

Schneider, J., Shen. Y., Stiemer, S.F., Tesfamariam, S. (2015). Assessment and comparison of experimental and numerical model studies of cross-laminated timber mechanical connections under cyclic loading. Construction and Building Materials, 77, 197-212.

Shahnewaz M, Tannert T, Alam MS, Popovski M (2017) In-Plane Stiffness of Cross-Laminated Timber Panels with Openings. Structural Engineering International, 27(2): 217-223.

Shahnewaz, M., Alam, M.S., and Tannert, T. (2018). In-Plane Strength and Stiffness of Cross-Laminated Timber Shear Walls. Buildings; 8(8), 100.

Shahnewaz, M., Tannert, T. & Popovski, M. (2019). Resistance of Cross Laminated Timber Shear Walls for Platform-Type Construction. Journal of Structural Engineering, ASCE, DOI: 10.1061/(ASCE)ST.1943-541X.0002413.

Tannert, T., Follesa, M., Fragiacomo, M., González, P., Isoda, H., Moroder, D., Xiong, H., van de Lindt, J. (2018). Seismic Design of Cross-laminated Timber Buildings, Wood and Fiber Science 50: 3-26.

van de Lindt J.W., Line P., Barbosa A., Furley J., Amini M. O., Pei S., Rammer D., Tamagnone G., Popovski, M., Fragiacomo, M. (2019). Experimental Seismic Behavior of a two-Story CLT Platform Building. Eng. Str., 183 (2019) 408-422.

Discussion

The paper was presented by Md Shahnewaz

H Blass commented that if acoustic insulation layer was not considered in the research, there would be large difference in deformation with acoustic insulation layer considered. M Shahnewaz said the work was based on modeling and may be able to add this as part of the model in future.

BJ Yeh received confirmation that there were 19 wall tests results presented with a test result/equation prediction factor of 2. M Li asked if this information included corner walls. MD Shahnewaz said no and that in the model the corner wall was assumed rigid but this is not reality. T Tannert said there is no data with perpendicular walls and that they need data for confirmation.

M Li said that there is good agreement between model and test results for ultimate capacity of wall. He questioned if a wrong guess was made for the ultimate capacity of the hold-down component of the model. MD Shahnewaz responded that how you calculate ultimate capacity of the connection made the difference. Even if we had test data, they are not the same connections used.

D Dolan and MD Shahnewaz discussed the FBD of the connection in relation to the boundary conditions including the gravity load and the connectivity of the components. T Tannert said gravity load was ignored.

H Mpidi Bita asked about the combination of shear and rotation in the connection. MD Shahnewaz said interaction was ignored in model.

Development of timber buckling-restrained braces for mass timber braced frames

Colton Murphy, University of Utah

Chris Pantelides. University of Utah

Hans-Erik Blomgren, Katerra

Douglas Rammer, Forest Products Laboratory

1   Abstract

Buckling Restrained Brace Frames (BRBF) are a proven and reliable method to provide an efficient lateral force resisting system for new and existing structures in earthquake prone regions. The fuse-type elements in this system facilitate stable energy dissipation at large load deformation levels. Currently, the new trend towards mass timber vertical structures creates a need for a lightweight compatible lateral force resisting system. A Buckling Restrained Brace (BRB) component is possible to construct and feasible to implement when combining a steel core with a mass timber casing herein named the Timber-Buckling Restrained Brace (T-BRB). T-BRBs when combined with mass timber beam and column elements can create a system that will have advantages over the current steel framed BRBF system when considering recyclability, sustainability, framing compatibility, and performance. This paper presents findings on small scale testing of candidate engineered wood products for the T-BRB casing and testing of six full scale 12 ft long 60 kip braces according to code prescribed loading protocols and acceptance criteria.

2 Introduction & Motivation

Research has proven that Buckling Restrained Braces provide satisfactory stiffness, strength and stable energy dissipation (Black et al. 2004). These braces also provide adequate rigidity necessary to satisfy building interstory drift limits. The manufacturing of lightweight and economical fuse-type BRBs are important for ease of handling during construction. Recent advancements in timber technology is making multi-story mass

timber buildings an attractive option to replace traditional steel and concrete systems. Mass timber buildings attract less seismic inertial forces, however, they lack code defined lateral force resisting systems (Blomgren et al. 2016); the authors proved that a buckling restrained brace with a Glulam casing can be built which exhibits superior qualities when compared to conventional dowel end timber braces. The T-BRB exhibited higher axial load, higher stiffness, more stable axial deformation capacity, and significantly greater energy dissipation characteristics when compared to conventional timber braces. Ductility and seismic damping of conventional timber braces is a concern in high seismic regions and extra care should be taken in the design of the connections to reach high ductility demands during an earthquake (Popovski 2000). Issues with conventional timber brace connections include ductility and consistency of performance regarding strength and stiffness.

3 T-BRB Design Methodology

Design of the casing dimensions used Euler buckling principles to avoid global brace buckling (Watanabe et al. 1988). Research aimed at exploring the high-mode buckling responses of the BRB core plates by Wu et al. (2013) was used for the design of the core and understanding of the internal modal responses of the T-BRB. Methods to design the casing bolts were developed which resist both the weak and strong axis core buckling forces. The bulging force from the weak axis core buckling can be predicted and prevented using adequate casing design (Lin et al. 2011). Gaps present between the core and casing can diminish the ability of the BRB to dissipate energy in compression (Genna and Gelfi 2012) by exacerbating lateral casing thrusts and making internal forces difficult to predict.

To inform the design, various types of small-scale timber block specimens were tested to determine mechanical properties that would be beneficial for a T-BRB casing. Wood type, screw reinforcement and direction of load, parallel or perpendicular to lamination, were considered as variables. Screw reinforcement in timber can promote load transfer and can compensate for wood with low compressive strength when loaded perpendicular to grain (Blass and Bejtka 2003). The anisotropic nature of engineered timber and wood in general leads to non-uniform load distribution. Experimentation into dowel connections showed both underestimation and overestimation in strength and stiffness when using a simplified calculation approach (Bader et al. 2016).

4   Small Scale Block Tests

The strength and stiffness of various mass timber engineered wood products under certain loading conditions is not well known. In addition, the influence of compression screw perpendicular to grain reinforcement on the mechanical behavior is also not well known. The localized compressive strength and stiffness under concentrated loads of Laminated Veneer Lumber (LVL), Parallel Strand Lumber (PSL), Glued laminated timber (Glulam), and Mass Plywood Panel (MPP) are investigated.

4.1 Block Test Program

The compressive tests conducted included both monotonic and cyclic tests. All mass timber specimens were 6in.x6in.x12in. Select specimens were loaded both perpendicular and parallel to the wood grain of their laminations. Additional specimens were tested with perpendicular to grain compression screws used for reinforcement. The reinforced specimens included four 3/8in. diameter x 4 in. screws spaced in a 2in.x2in. square pattern. A 3in.x3in. steel fixed head platen was used to apply the vertical compressive load to the face of the specimen. Two replicates of each type of test were carried out. Alternative tests focusing on glulam were carried out; this included adjusting the screw pattern to 2in.x3in., and 2in.x4in. along with adjusting the platen dimensions to 3in.x4in., and 3in.x5in., respectively. These four additional trials used the quasi-static cyclic load protocol shown in Fig. 1, which was continued until critical failure. The cyclic load protocol used a loading rate of 1 cycle per second. The monotonic loading protocol, also shown in Fig. 1, is a quasi-static, linear compressive load; this load was also continued until failure. Fig. 2 shows the typical 2in.x2in. screw reinforcement after being loaded to failure from the 3in.x3in. platen. Figure 2 also shows an unreinforced glulam specimen loaded to failure in the parallel to lamination direction.

4.2 Block Test Results

Figures 3 and 4 represent a sample of the load versus displacement plots from the monotonic tests conducted. These figures display data from the monotonic tests perpendicular to the laminations and parallel to the laminations both with and without reinforcement. The nomenclature is as follows: M=MPP, G=Glulam, P=PSL, L=LVL, A=parallel to lamination, B=perpendicular to lamination, U= unreinforced. These figures clearly show the improved stiffness and maximum load when compressing MPP parallel to the laminations. These figures also show an increased stiffness when applying load parallel to the laminations. Figure 5 provides cyclic test samples for each wood type and

configuration. These cyclic tests show MPP loaded perpendicular to lamination has a lower yield force when compared to parallel to lamination, however it has a hardening characteristic and exhibits more ductility. Unreinforced Glulam underperforms when compared to other engineered wood products tested; this wood type consistently fails before reaching 0.1in. MPP loaded perpendicular to laminations and without screw reinforcement also underperforms compared to MPP loaded parallel to laminations.

Research in T-BRBs identified that a high elastic stiffness with a high maximum compressive load capacity is desirable for a T-BRB casing (Blomgren et al 2016). If the modulus of elasticity of the casing is too low, localized weak axis buckling occurs which leads to premature failure. Higher elastic stiffness of the casing suppresses high mode weak axis buckling throughout the length of the core, which is desirable. Unreinforced MPP loaded parallel to the laminations outperformed LVL, PSL, and Glulam. The fact that screw reinforcement is not necessary to maintain good results, brings economy in materials and labor to the manufacturing process of the braces.
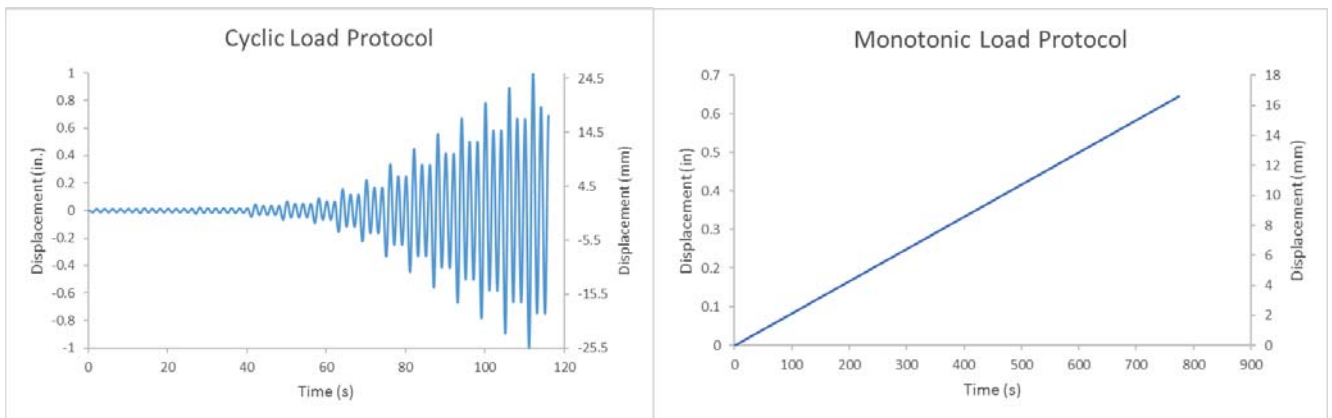
Figure 1. Block Specimen Load protocols.

| (a) | (b) |

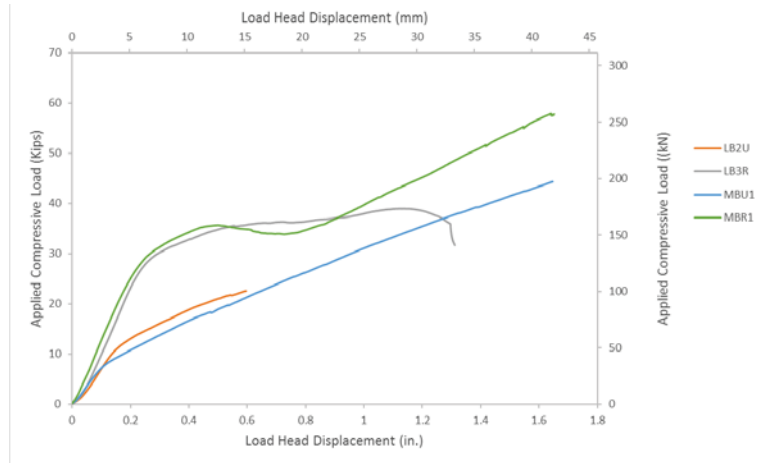Figure 2. Glulam specimens post-test: (a) no screw reinforcement; (b) 2 in. x 2 in. reinforcement.

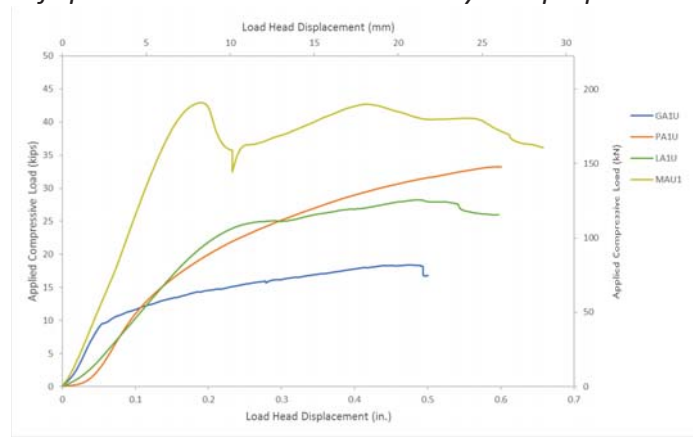*Figure 3. Sample of specimens loaded monotonically and perpendicular to lamination.*

Figure 4. Sample of specimens loaded monotonically and parallel to lamination without reinforcement.
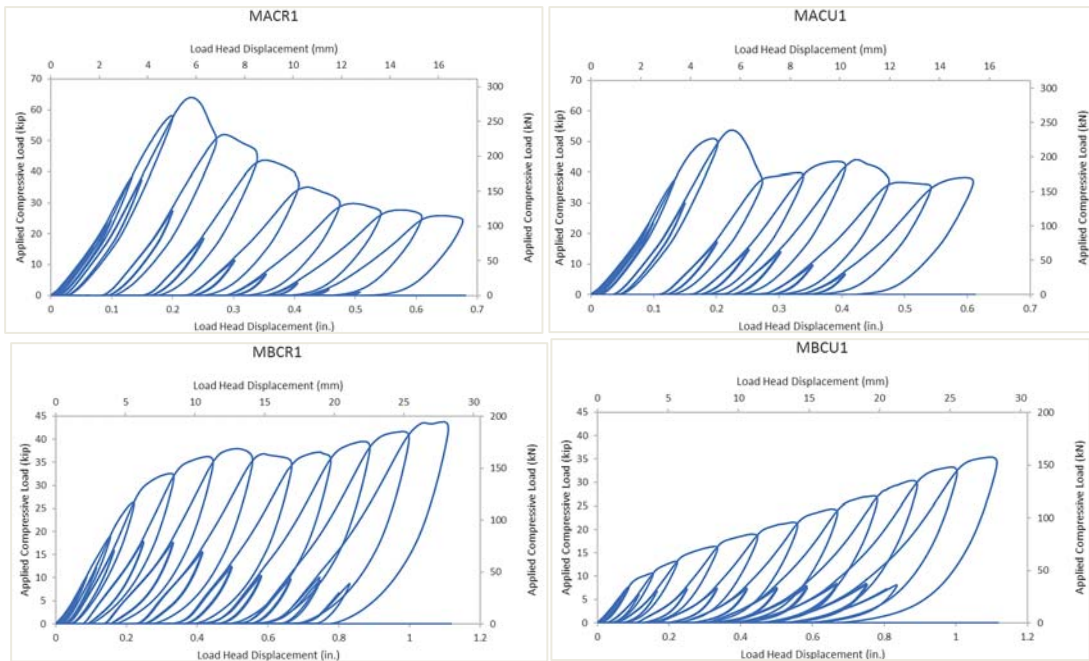

Figure 5. Individual cyclic test sample hysteresis curves.

5 T-BRB Full Scale Element Tests

T-BRBs act as a structural fuse dissipating energy by yielding the steel core and thus protecting the beam and column elements of the braced frame system during a seismic event. Six full scale, 12-ft long, T-BRBs were constructed and tested under cyclic axial load in this research. The first three T-BRBs were loaded using a fatigue-based load protocol in which a high number of cycles was applied at significant steel core strain. The final three T-BRBs were loaded using a drift-based load protocol in which higher steel core strain cycles were applied until failure.

5.1 T-BRB Specimens

The six T-BRBs were constructed using 41ksi yield strength steel cores and mechanically fastened Mass Plywood Panel (MPP) casings as shown in Fig. 6. Figure 7 (left) shows an exploded view of the T-BRB components. In order to increase ductility and improve overall performance a low yielding steel core was chosen. The stiffener plates at each end of the core plate are fabricated with the same steel. The design value for yield strength was taken as 41ksi and tensile ultimate strength was taken as 62.5ksi. The core cross-sectional dimensions along the yield zone are 3in.x0.5in. to form a 1.5in.^{2} yield area. The stiffener plates were welded to the core to prevent localized buckling outside of the timber casing. Two cheek plates were also welded to the ends of the T-BRBs around the pin connection to prevent a tear out failure. A steel dowel was welded to the core at mid-length to encourage an even distribution of core buckling forces.

Hardwood spacers were used to restrain strong axis buckling of the core plate. A laminated German beech wood material was used for the spacer. The material was cut to the exact dimensions necessary to fill the void made by the steel core between the timber casing material. Several ½in. diameter, A449 thru bolts were used to connect the two MPP casing elements; these bolts are also used to secure the hardwood spacers. A 7in. spacing of the bolts was used throughout the yielding length of the T-BRB; however, this spacing was reduced near the ends of the T-BRB to account for an increase in bending forces that were predicted. The 7in. bolt spacing throughout the yielding zone is a conservative estimate based on the calculations in Eqs. (1) and (2) and using the Fig. 7 (right) free body diagram of the buckled core inside of the casing.

$$\Delta_{gap} = v\varepsilon_{max}t_f \qquad\qquad (1)$$
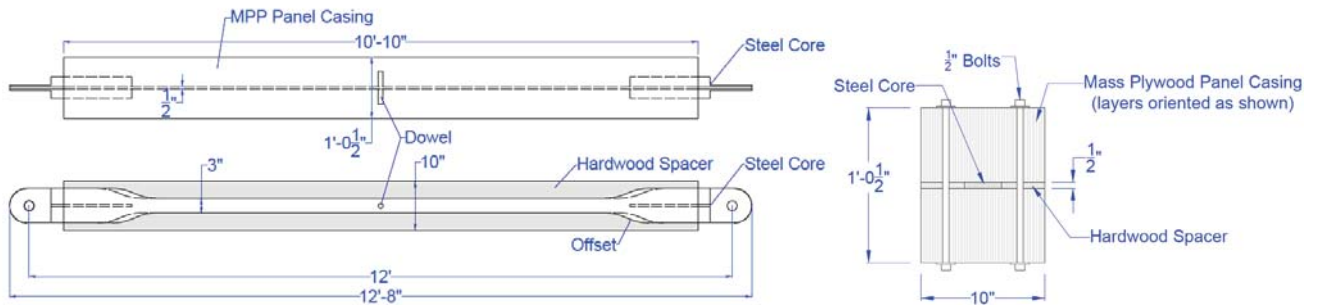
Figure 6. T-BRB Layout (bolts not shown).
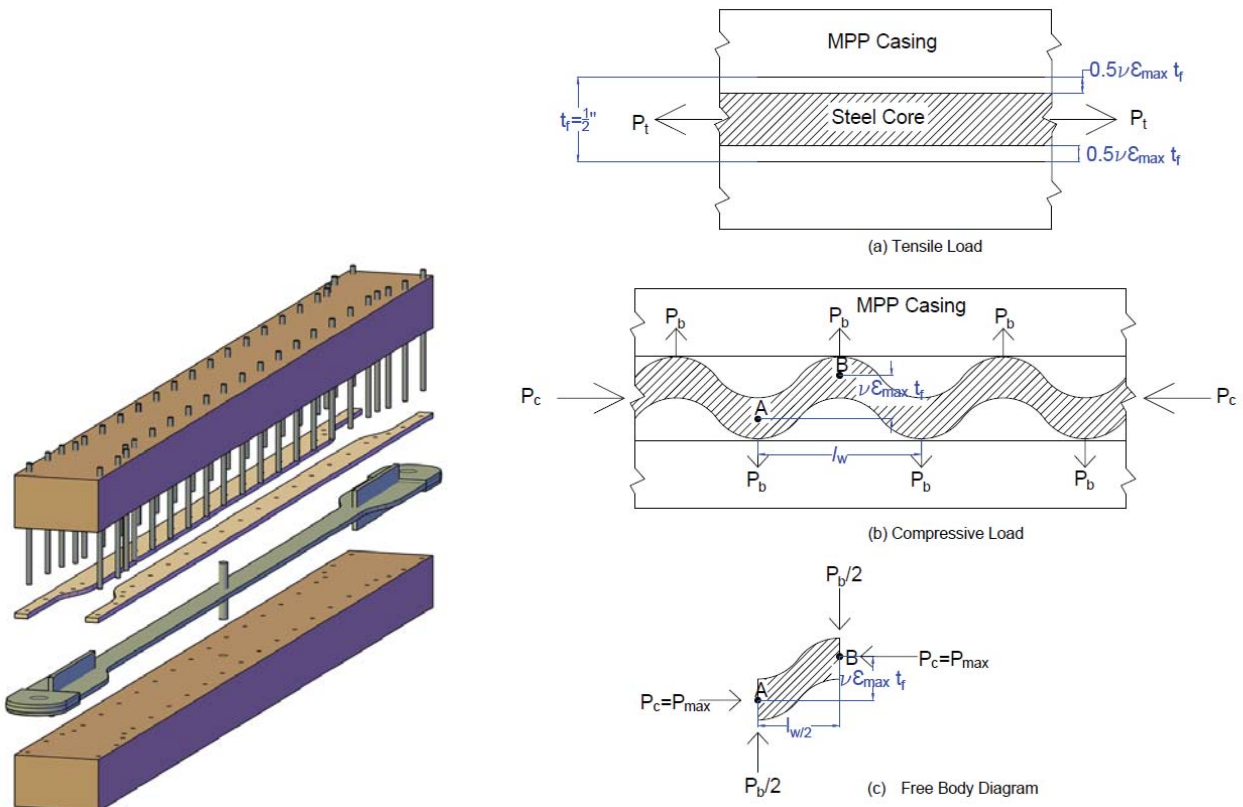
Figure 7. Exploded view visualization of the T-BRB design (left) and internal mechanics of buckling T-BRB (right).

The original steel core thickness, t_f, is ½in. Once the steel core goes into tension, a gap forms between the steel and the timber casing of increasing magnitude throughout the cyclic test due to Poisson effect. A Poisson's ratio, ν, of 0.5 was used for the steel core, which would be subject to high strains and would be in the plastic region. This gap is equal to Δ_{gap} in Eq. (1); ε_{max} is the maximum tensile strain in the steel during the test and is assumed to be 0.04. The wavelength of the buckled steel core, l_w, is assumed to be 11 times the thickness of the steel core (Wu et al. 2013) or 5.5in. P_{max} is the estimated maximum compressive force developed by the T-BRB; this value was estimated as 1.6 times the yield strength of the steel core to account for hardening and friction. A value

of 100kips was used for P_{max}. By summing the moments in the free body diagram of Fig. 7 (right) and solving for P_b, the buckling force of the steel core, Eq. (2) is formed:

$$P_b = \frac{4P_{max}\nu\varepsilon_{max}t_f}{l_w} \tag{2}$$

By solving Eq. (2), P_b is 727lbs. This value was rounded up to 1000lbs to apply a safety factor of 1.4. This force is exerted onto the core throughout the yield length a total of 36 times due to the 5.5 in. wavelength spacing. This results in a total casing outward force of 36 kips. By allocating 1.5 kips of allowable force per bolt, which factors in bolt prestressing strength loss during the pneumatic torque tightening process, 24 A449 bolts with ½in. diameter are needed throughout the yield length of the core. The 7in. bolt spacing provides 28 bolts throughout the 98in. yield zone. The design also satisfies the T-BRB global buckling capacity based on the National Design Specification for wood construction section for built up mechanically laminated timber columns (ANSI/AWC 2018). This spacing is conservative; failure involving bolt fracture was avoided during design so the failure modes of interest could be observed during testing.

Three layup grades of MPP panels were used in the six T-BRB tests. Each 10in. thick MPP plywood layup utilized a varying elastic modulus of 1.0×10^6psi or 2.2×10^6psi layers. The three MPP casing types are denoted as soft (s), medium (m), and hard (h). Figure 8 represents the lamination layup for the three MPP specimen types. The soft specimens consisted of four center 1in. thick laminations of 1.0×10^6psi plywood with three outer laminations on each side of 2.2×10^6psi plywood as shown in Fig. 8(a). The medium specimens contained only two 1in. laminations of 1.0×10^6psi with the remaining laminations made of 2.2×10^6psi plywood as shown in Fig. 8(b). The hard specimens were made entirely of 2.2×10^6psi laminations as shown in Fig. 8(c). Specimens 1-3 were soft, medium, and hard, respectively; specimens 4-6 were hard, medium, and soft respectively.

5.2 T-BRB Loading Program

Two loading protocols were used for the six T-BRB experiments: fatigue-based and drift-based. The fatigue-based cyclic loading protocol was developed using AISC 341 (AISC 2016) Chapter F4 and Appendix K3. Since the experiment is uniaxial with pin end connections, a subassemblage test was not performed. Cyclic drift was increased by 0.5% until a 2% drift ratio was reached; subsequently the drift ratio was reduced to 1.5%. Finally, the 1.5% drift ratio was cycled until failure. In the drift-based loading protocol, the T-BRB drift was increased by 0.5% until failure with these steps: 0.5%, 1.0%, 1.5%, 2.0%, 2.5%, and 3.0%. A 98in. yield zone was used to calculate strain and axial displacement.
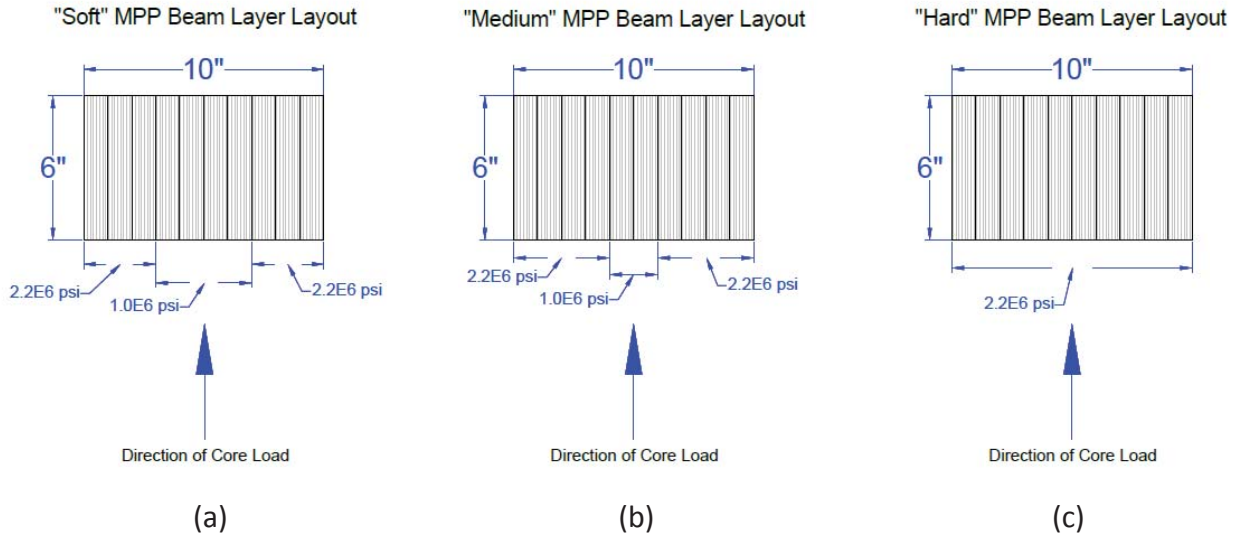
Figure 8. MPP layup detail for the three specimen casing types.

AISC 341-16 requires the brace to be tested to the design story drift and to achieve a Cumulative Inelastic Deformation (CID) of 200 times the yield deformation. The design story drift, Δ_{bm}, and the brace yield deformation, Δ_{by}, were determined as follows. The value of Δ_{bm} was calculated as 1.00% which is 1.28 in. The value of Δ_{by} was calculated using the following equations:

$$\Delta_{b-ysc} = \frac{F_{ysc}L_{ysc}}{E} \tag{3}$$

$$\Delta_{b-ends} = 2\frac{A_{sc}}{A_{end}}\left(\frac{F_{ysc}L_{end}}{E}\right) \tag{4}$$

$$\Delta_{by} = \Delta_{b-ysc} + \Delta_{b-end} + \Delta_{apparatus} \tag{5}$$

The value of $\Delta_{apparatus}$ was taken as zero due to the details of the instrumentation; F_{ysc} is the yield strength of the steel; L_{ysc} is the length of the yield zone; A_{sc} is the area of the yield zone; A_{end} is the area of the end of the T-BRB core which includes the stiffeners and cheek plates; L_{end} is the length of the ends of the core excluded by the yield zone. The brace yield deformation Δ_{by} was determined to be equal to 0.16 in. CID was calculated per AISC 341-16 table C-K3.1. CID is the accumulation of deformation, both positive and negative, beyond yield which is then converted multiples of brace yield deformation, Δ_{by}. The adjustment factors were determined using the hysteresis curves shown in Figs. 12-17. The compressive adjustment factor β was calculated using:

$$1.00 < \beta = \frac{P_{max}}{T_{max}} < 1.50 \tag{6}$$

β is the ratio between the maximum measured compressive load and the maximum measured tensile load per loading cycle, which should remain below 1.5 per AISC 341-16. The strain hardening adjustment factor was calculated using the following equation:

$$\omega = \frac{T_{max}}{R_y P_{ysc}} \geq 1.00 \qquad\qquad (7)$$

ω is the ratio between the maximum measured tensile load and the yield force per cycle. Because coupon tests were conducted to determine yield stress, R_y is equal to 1.0.

5.3 T-BRB Test Results

Table 1 represents a summary of results from the six T-BRB tests. Hysteresis curves along with time-displacement figures for the six specimens are provided in Figs. 9-12. All hysteresis curves remained stable throughout each test. Figures 13-15 show images of the failure in each test.

Specimen 1 failed in tension at 39 cycles; the steel core fractured due to low cycle fatigue and the compressive adjustment factor, β, ranged from 1.05 to 1.20; the strain hardening adjustment factor ω ranged from 1.00 to 1.40. Specimen 2 failed in compression at 35 cycles; the MPP layers ruptured due to high compression transferred from the steel core, which buckled about the weak axis; β, ranged from 1.05 to 1.15; ω ranged from 1.00 to 1.32. Specimen 3 failed in compression at 28 cycles; failure was similar to specimen 2 because the MPP layers ruptured due to the load demand from the weak axis buckling of the steel core; β, ranged from 1.03 to 1.20; ω ranged from 1.00 to 1.35.

Specimen 4 failed in compression on the 13th cycle at 3.92% strain; slight strong axis buckling of the steel core was visible after inspection, but weak axis buckling was dominant and the ultimate failure mode was a ruptured casing; β, ranged from 1.04 to 1.23 and ω ranged from 1.00 to 1.43. Specimen 5 failed in compression on the 12th cycle at 3.92% strain; both weak- and strong-axis buckling of the steel core were present and the ultimate failure mode was a ruptured and split casing; β, ranged from 1.10 to 1.20 and ω ranged from 1.00 to 1.38. Specimen 6 failed on the 13th cycle at 3.92% strain;

Table 1. Results summary for T-BRB tests cycled to failure.

Protocol Type	Specimen Order #	MPP Layout Stiffness	Max % Strain	Max % Drift	Cycles to Failure	CID	Total Hysteretic Energy Dissipation (kip*in.)
	1	soft	2.61%	2.00%	39	1571	19422
Fatigue	2	medium	2.61%	2.00%	35.5	1416	16840
	3	hard	2.61%	2.00%	28.5	1107	13161
	4	hard	3.92%	3.00%	13.5	580	7140
Drift	5	medium	3.92%	3.00%	12.5	488	6379
	6	soft	3.92%	3.00%	13.5	580	7188

weak- and strong-axis buckling of the steel core were present, however strong-axis buckling of the steel core was severe and dominant. The casing layers split and opened due to the strong axis buckling force; β, ranged from 1.11 to 1.25 and ω ranged from 1.00 to 1.41. The load transferred to the MPP from strong axis steel core buckling in specimens 4-6 worked to pull apart plywood laminations. This cross-lamination force exacerbated compression failures under high drift loading once laminations split apart. Figure 16 shows the split resulting from this type of failure mode.
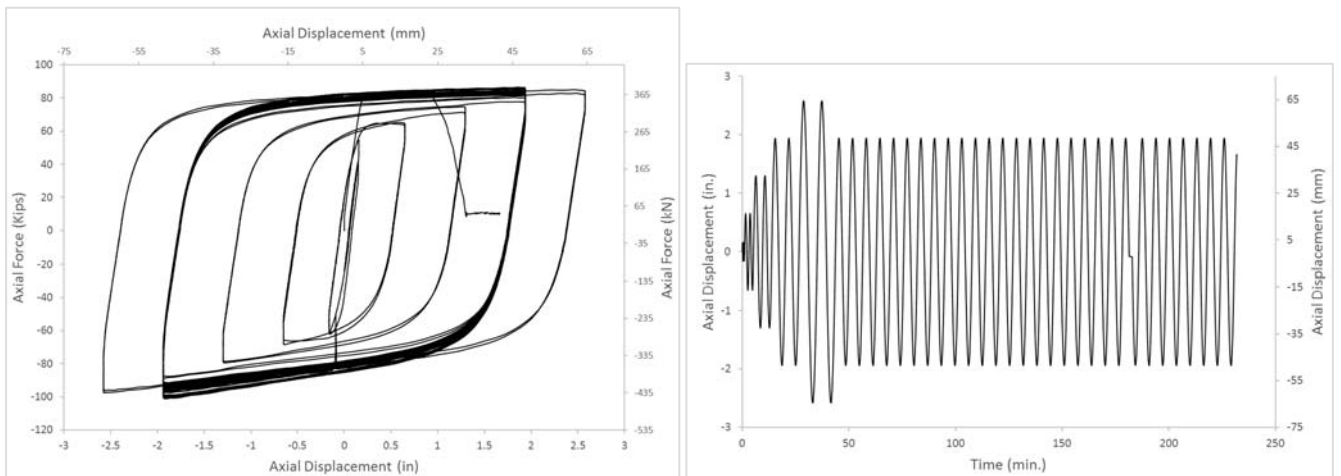
Figure 9. Specimen 1: hysteresis (left) and displacement vs time (right).
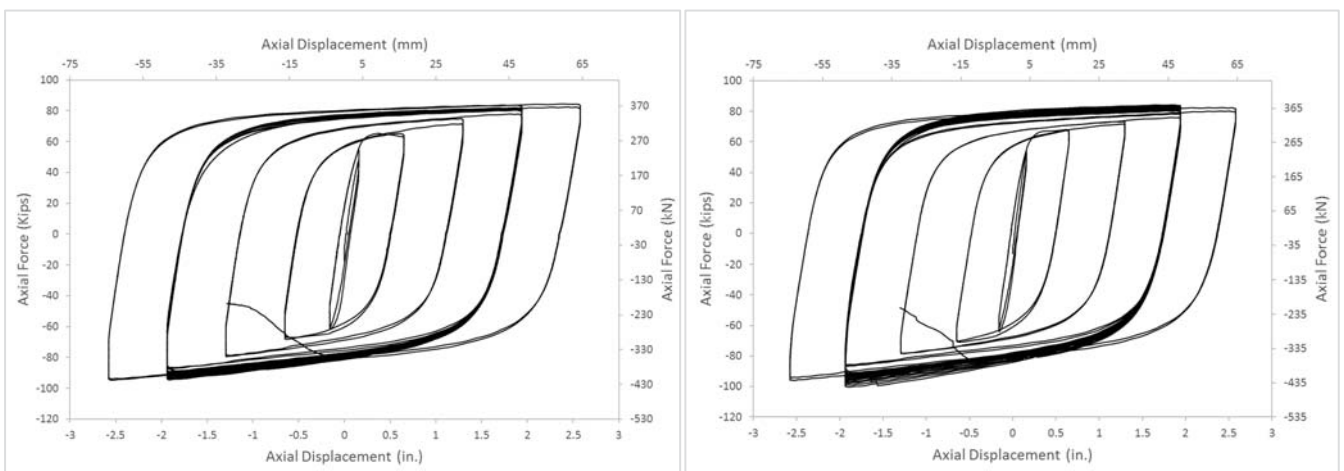
Figure 10. Specimen 2 (left) and Specimen 3 (right) hysteresis.
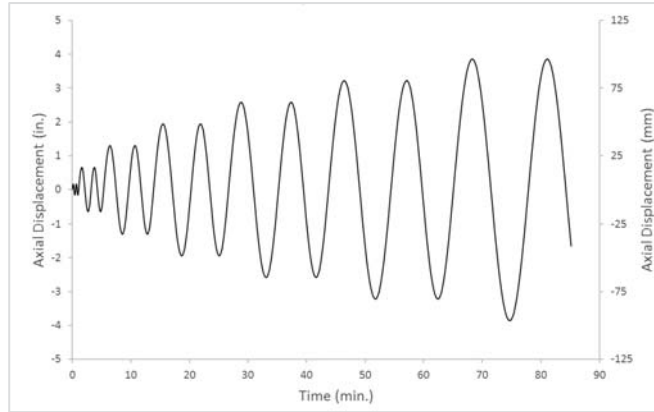
Figure 11: Specimen 4: hysteresis (left) and displacement vs time (right).
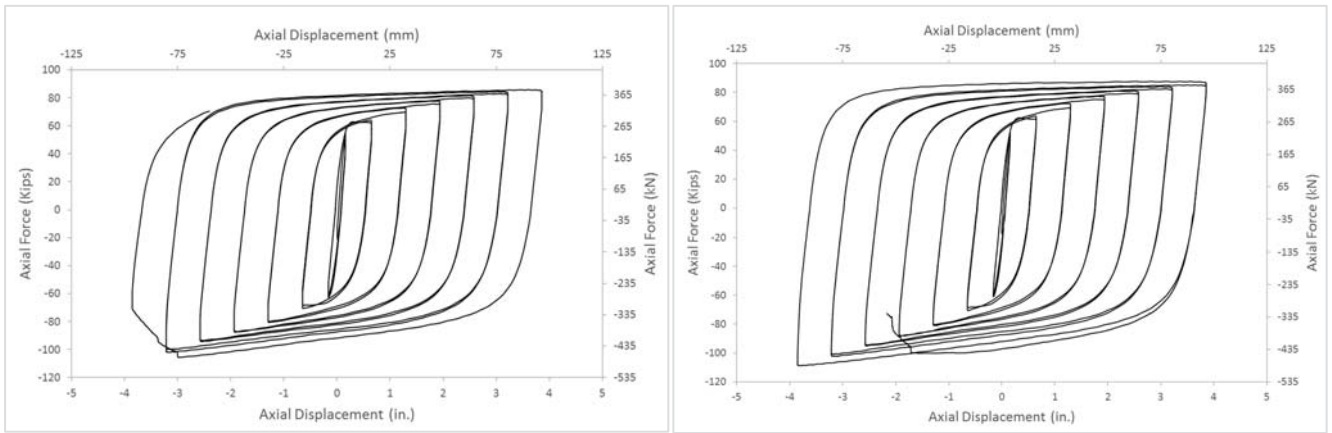
Figure 12: Specimen 5 (left) and Specimen 6 (right) hysteresis.
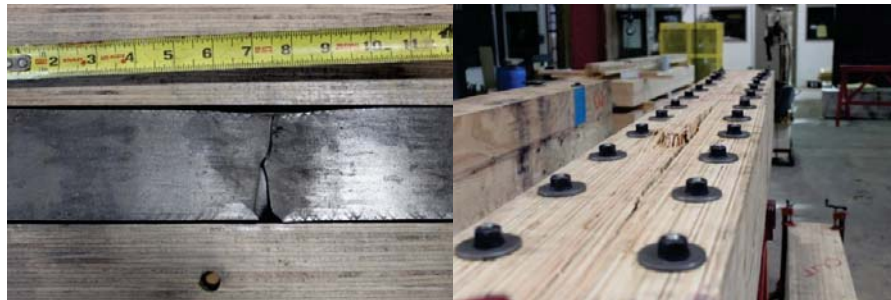
Figure 13. Failure mode of Specimen 1 (left) and Specimen 2 (right).

Figure 14. Failure mode of Specimen 3 (left) and Specimen 4 (right).

Figure 15. Failure mode of Specimen 5 (left) and Specimen 6 (right).

Figure 16. MPP casing split resulting from strong axis steel core buckling.

6 Conclusions

This research demonstrated that a reliable and efficient T-BRB is possible to construct and feasible to implement when combining a steel core with an engineered timber casing. The following conclusions can be drawn:

1. Unreinforced Glulam underperforms when compared to other engineered wood products; this wood type consistently fails before reaching 0.1in. of displacement when loaded in the parallel to lamination direction.
2. MPP loaded perpendicular to laminations without screw reinforcement also underperforms compared to MPP loaded parallel to laminations when considering elastic stiffness. Average elastic stiffness of perpendicular loaded samples resulted in 77 kip/in. while parallel loaded samples resulted in 257 kip/in.
3. The T-BRBs tested in this research using MPP loaded parallel to grain meet the requirements of ASCE-341-16. The hysteresis curves from these specimens prove that sufficient energy dissipation is readily achievable with a T-BRB.
4. Specimens 1-6 reached cumulative inelastic deformations of 1571, 1416, 1107, 580, 488, and 580 times the yield deformation, respectively which exeeds ASCE 341-16 requirements for ductility corresponding to 2.0 times the design story drift and a cumulative inelastic axial ductility of 200 times the yield displacement.
5. The hysteretic curves prove stable damping is possible with T-BRBs.

6. A 3.9% strain was sustained under the drift-based loading protocol. The T-BRB has a long fatigue life at 1.5% strain, as shown for the fatigue tested T-BRB specimens.

7. The compressive adjustment factor, β, remained below 1.5 per AISC 341-16 for all specimens; this factor ranged from between 1.05 to 1.25. The strain hardening adjustment factor, ω exceeded 1.0 per AISC 341-16 for all specimens and ranged from 1.00 to 1.43.

7   References

American Institute of Steel Construction - AISC 341 (2016): *Seismic provisions for Structural Steel Buildings*, Chicago, Illinois.

Bader, T, Schweigler, M, Hochreiner, G, and Eberhardsteiner, J (2016): Load Distribution in Multi-dowel Timber Connections under Moment Loading-Integrative Evaluation of Multiscale Experiments. *World Conference on Timber Engineering,* 2016. Vienna, Austria.

Black, CJ, Makris, N, and Aiken, ID (2004): Component Testing, Seismic Evaluation and Characterization of Buckling-Restrained Braces. *Journal of Structural Engineering*, 130(6), 880–894.

Blass HJ, and Bejtka I (2003): Reinforcements Perpendicular to Grain Using Self-Tapping Screws. University of Karlsruhe, Karlsruhe, Germany.

Blomgren, H, Koppitz, J, Valdes, A and Ko, E (2016): The Heavy Timber Buckling-Restrained Braced Frame as a Solution for Commercial Buildings in Regions of High Seismicity. Vienna, Austria: WCTE.

Genna, F, and Gelfi, P (2012): Analysis of the Lateral Thrust in Bolted Steel Buckling-Restrained Braces. II: Engineering Analytical Estimates." *Journal of Structural Engineering*, 138(10), 1244–1254.

Lin, P-C, et al. (2011): Seismic design and hybrid tests of a full-scale three-story buckling-restrained braced frame using welded end connections and thin profile. *Earthquake Engineering & Structural Dynamics*, 41(5), 1001–1020.

Popovski, M (2000): Seismic Performance of Braced Timber Frames. Ph. D. thesis, Department of Civil Engineering, the University of British Columbia, Vancouver, B.C.

Watanabe, A, Hitomoi Y, Saeki E, Wada A, and Fujimoto M (1988): Properties of Brace Encased in Buckling-Restraining Concrete and Steel Tube. *Proceedings of the 9th World Conference on Earthquake Engineering, Tokyo-Kyoto, Japan,* 719-724.

Wu, A-C, Lin, P-C, and Tsai, K-C (2013): High-mode buckling responses of buckling-restrained brace core plates. *Earthquake Engineering & Structural Dynamics*, 43(3), 375–393.

Discussion

The paper was presented by H-E Blomgren

D Dolan asked at this level of drift what would be the rotation requirement of the beam column. HE Blomgren agreed that there would be a need to get commercially available systems and joints and detailing to handle this as needed. More work is being done.

K Voulpiotis asked about the performance of the brace after effect of long term loading. HE Blomgren said this is an interesting question but do not have an answer. He added that there would not be gravity load for this brace.

H Daneshvar received clarification that the load protocol followed ASCE chapter K load protocol. He asked if the use of this brace open to public. HE Blomgren said there is a provisional patent filed.

M Li commented that there are lots of interest in New Zealand to use this type of system and asked what would be overstrength factor on the components of BRB for capacity design. HE Blomgren said factors would be defined by practitioners.

M Li commented that NZ tested glulam frames with steel BRB. They performed well but how to connect the BRB to the frame was critical. He said the overstrength factor used was 1.5.

H Blass asked regarding the bolted connections, if self-tapping screws would be an alternative. HE Blomgren said this would be possible but have not done this.

Preliminary design model for wooden I-joists in fire

Katrin Nele Mäger, Tallinn University of Technology

Alar Just, Tallinn University of Technology

Keywords: fire design, charring, load-bearing capacity, wooden I-joists

1 Introduction

There is a great demand for environmentally conscious building materials, products and practices. Wooden I-joists, being factory-made ultra-light and highly optimised products for load-bearing frame structures, provide an extended use for light timber frame assemblies. The joists consist of flanges (made of sawn wood, LVL or glulam) and a web (made of a wood-based board). Fire resistance of such wooden structural products is a complex matter. However, the current European design standard for timber structures in fire – Eurocode 5 Part 1-2 (2004) provides no guidance for I-joists.

The fire resistance of wooden I-joists has been previously investigated by König (2006) and Schmid et al. (2011) who developed calculation models to analyse the load-bearing capacity of wooden I-joists exposed to fire for floors and walls, respectively. There have been significant changes in the variety and types of materials used in conjunction with I-joists. Therefore, the application of these models is nowadays limited. Additionally, they focus on the reduced properties method. In the revised Eurocode 5 Part 1-2 only the effective cross-section method will be included.

A few full-scale furnace fire tests have shown that the predictions of the load-bearing capacity made with the existing calculation models are inaccurate. In some cases the prediction was unconservative due to many assumptions needed for the model to be used for the tested configuration.

The aim of this ongoing research project is to develop a unified model for wooden I-joists in both wall and floor assemblies which follows the philosophy of the effective cross-section method. Additionally, it should be able to be used with all types of cavi-

ty insulation and fire protection systems. The unified model for I-joists is aimed to be introduced to the new revised Eurocode 5 Part 1-2.

The load-bearing capacity of wooden I-joists exposed to fire is influenced by charring and the loss of strength and stiffness at elevated temperatures. Within this research project, a large amount of thermal simulations has been made to investigate the influence of various factors (e.g. flange size, cavity insulation material, protective boards) on the charring behaviour of the fire exposed flange and the web. The combination of different materials and the slender nature of I-joists makes their fire resistance a complicated issue. The thin web is very sensitive to elevated temperatures and charring. Additionally, adhesives used in finger joints in the flanges and the joint between the flanges and the web influences the load-bearing capacity.

This paper describes the charring calculations and the development of the necessary coefficients. The principles of the new model are also introduced.

2 Current models

The fire resistance of I-joists has been investigated previously by König (2006) and Schmid et al. (2011) who developed calculation models for floors and walls. These models have been thoroughly investigated and multiple limitations were identified. The detailed description of the current models and the necessary improvements have been presented by Mäger & Just (2019).

A comparison of available full-scale furnace test data and the calculation methods was made. The results show that the available methods do not adequately predict the fire resistance. The graphical comparison of test results and calculations is shown in Figure 1. Table 1 provides more details regarding the test setups.
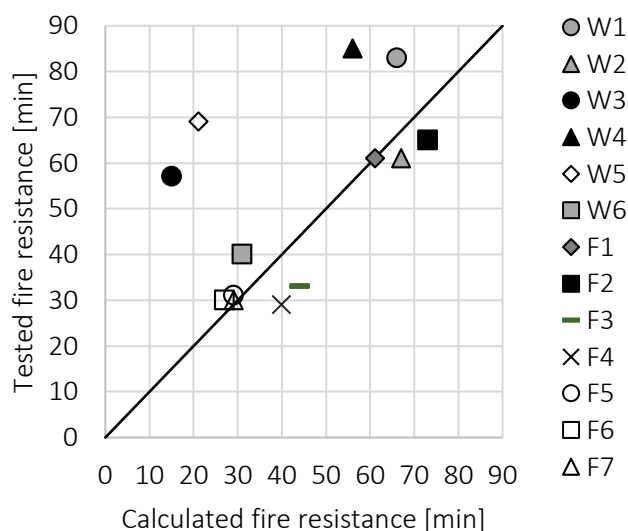
Figure 1. Comparison of tested and calculated fire resistance times

The main restrictions of the current models are:

- The prevalent use of the reduced properties method which gives modification factors for strength and stiffness
- Severely limited number of cavity insulation materials – stone wool and glass wool (which is allowed only in protection phase)
- Limited research into the effect of adhesives
- A large variety of charring coefficients which differ between the models for I-joists and are also named differently from rectangular sections
- Lack of verification by full-scale tests

Table 1. Overview of full-scale test configurations (TTF=time to failure)

Wall/ Floor	Test	Load, kN or kN/m²	Fire protection system	Fall-off time of fire protection system	TTF of the assembly (tested)	TTF of the assembly (calculated)	I-joist, height in mm
W	1	54	2GF15+battens	66	**82,9**	**66**	250
W	2	17	GF 15+GtA12,5	61	**61**	**67**	250
W	3	22	GtA 12,5	21	**57**	**15**	200
W	4	22	GF15+GtA12,5	77	**85**	**56**	200
W	5	24	GtF 12,5+laths 34x70	47	**69**	**21**	200
W	6	17	GtA12,5	27	**40**	**31**	200
F	1	1,35	2GF15	44	**61**	**61**	250
F	2	1,35	GF15+GF12,5	59	**65**	**73**	200
F	3	1,35	GtA12,5+resilient channel	22,5	**33**	**44**	200
F	4	2,7	GtA 12,5	15	**29**	**40**	300
F	5	1,5	GtA15	27	**31**	**29**	220
F	6	0,7	GtA15	25	**30**	**27**	220
F	7	1	GtA15	27	**30**	**29**	220

3   New design model

The load-bearing capacity of a timber member in a timber frame assembly is influenced by charring and the loss of strength and stiffness properties at elevated temperatures. Charring of wood and wood-based materials is considered to occur at a temperature of 300°C. Timber frame assemblies usually consist of small timber ele-

ments, boards and insulation in the cavities. The charring of the load-bearing timber members is influenced mostly by the protection offered by the boards, but also the cavity insulation material.

The charring model for wooden I-joists is based on the model for timber frame assemblies with rectangular cross-sections by Tiso (2018). As I-joists are more sensitive to elevated temperatures due to the small cross-section area of the flanges, thin web and the presence of adhesives, the charring calculations proposed by Tiso have been modified to consider I-joists more accurately. The naming of the parts of an I-joist are shown in Figure 2a.

(a)   (b)
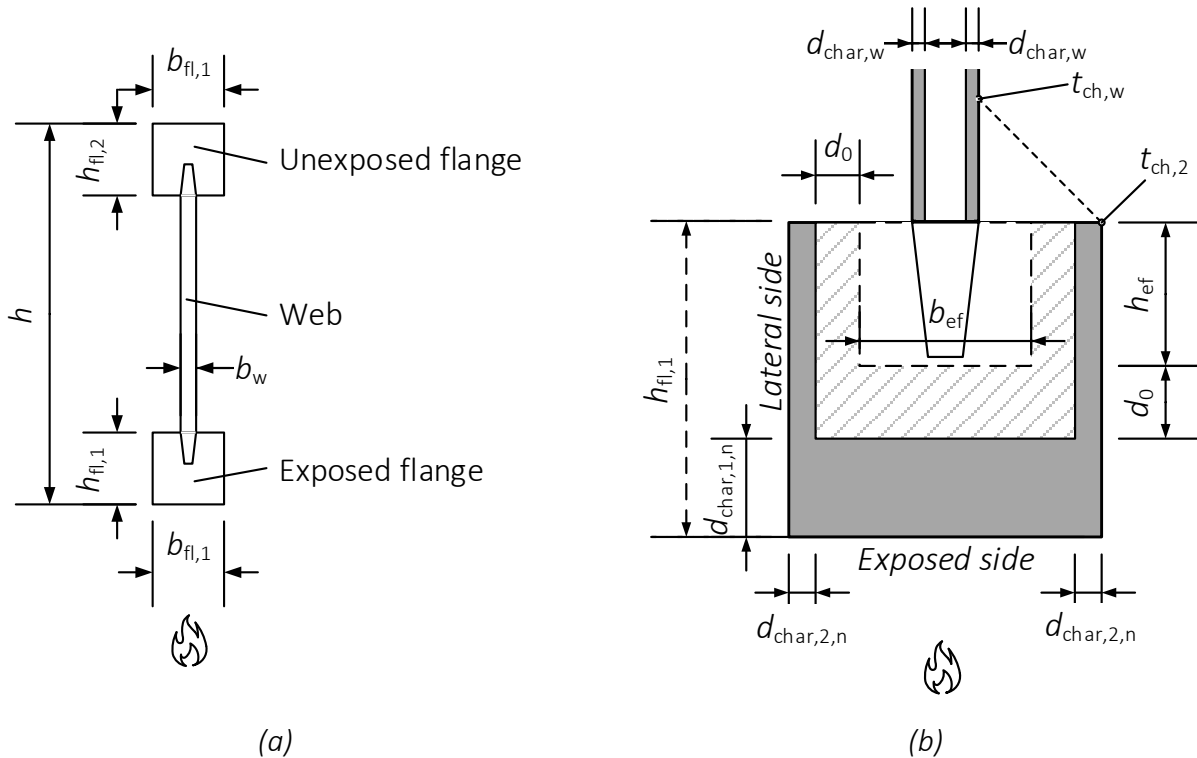
Figure 2. I-joist. (a) Naming of the parts of an I-joist; (b) Principles of the new design model

The design model takes into account different charring phases. See Figure 3.

Charring on the fire side of the cross-section can consist of 4 phases. In Phase 1 no charring occurs behind the protection until time t_{ch}. The start time of charring t_{ch} is dependent on the cladding thickness, material and the substrate. Phase 2 considers charring behind the cladding (from time t_{ch} until time t_f). The fall-off time of the cladding t_f is dependent on the cladding material, orientation and fixation. After the failure of the claddings the structural member and cavity insulation will be directly exposed to fire and the charring rate of the wooden flange will be much higher compared to the charring rate behind the cladding.

Fast charring can occur for a short time and will consolidate at time t_a. After the consolidation time t_a the charring Phase 4 is considered.

Depending on the fire protection properties of the cladding materials and their fixation the Phase 2 or Phase 3 can be neglected in some cases. Charring on the lateral sides of flanges is dependent on the cavity insulation materials.

The start time of charring on the lateral side $t_{ch,2}$ can occur in Phase 2, Phase 3 or Phase 4 depending on the cladding and the cavity insulation. After time $t_{ch,2}$ the flange width will be reduced.

The general expressions to calculate the notional charring depth of the flanges of an I-joist are shown in equations (1) to (3). The coefficients presented in this paper are shown in bold.
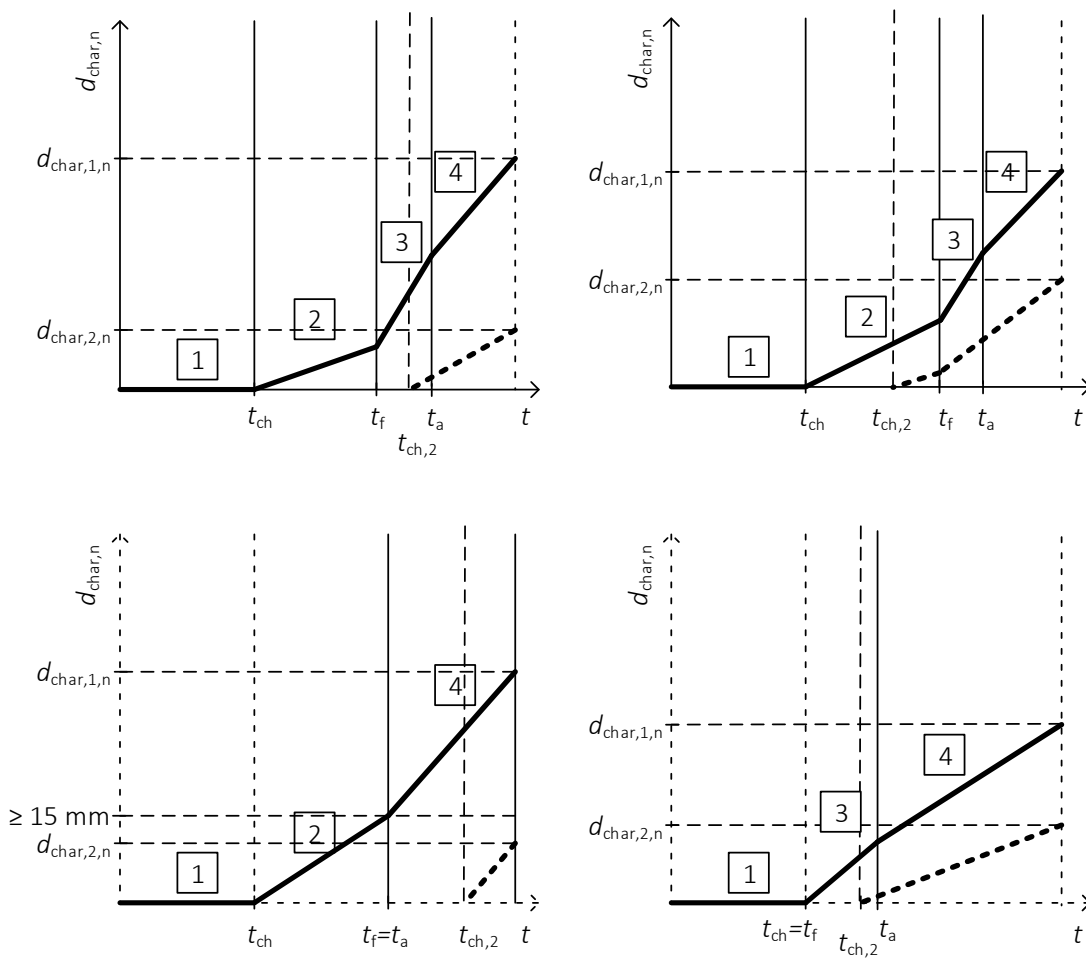
Figure 3. Charring scenarios

The notional charring depth on the fire-exposed side of the flange may be calculated as:

$$d_{char,1,n} = \beta_0 \cdot \mathbf{k_{s,n}} \cdot k_2 \cdot (t_f - t_{ch}) + \beta_0 \cdot \mathbf{k_{s,n}} \cdot \mathbf{k_3} \cdot (\mathbf{t_a} - t_f) + \beta_0 \cdot \mathbf{k_{s,n}} \cdot \mathbf{k_4} \cdot (t - \mathbf{t_a}) \qquad (1)$$

where

β_0 is the basic design charring rate of the flange material [mm/min];

k_2 is the protection factor of the fire protection system [-];

$k_{s,n}$ is the combined section and conversion factor [-];

t_{ch} is the start time of charring behind the fire protection system [min];

t_f is the fall-off time of the fire protection system [min];

t_a is the consolidation time [min];

k_3 is the post-protection factor for the fire-exposed side [-];

k_4 is the consolidation factor [-];

t is the fire resistance time [min].

The actual charring scenario may include one or more charring phases (see Figure 3) and the equation (1) shall be modified for each case accordingly.

If the charring on the lateral sides of the flange starts before the fall-off of the fire protection system, then the charring on the lateral sides occurs in two phases, see equation (2).

$$d_{char,2,n}=\beta_0 \cdot k_{s,n} \cdot k_2 \cdot (t_f - t_{ch,2}) + \beta_0 \cdot k_{s,n} \cdot k_{3,2} \cdot (t - t_f) \tag{2}$$

where

$k_{s,n}$ is the cross-section factor for the lateral side [-];

$k_{3,2}$ is the post-protection factor for the lateral side [-];

$t_{ch,2}$ is the start time of lateral charring [min].

If charring on the lateral sides occurs only in post-protection phase, then notional charring depth on the lateral sides of the flange may be calculated as:

$$d_{char,2,n}=\beta_0 \cdot k_{s,n} \cdot k_{3,2} \cdot (t - t_f) \tag{3}$$

The charring depth of the web is considered from time $t_{ch,w}$ and calculated according to (4).

$$d_{char,w}=\beta_{0,w} \cdot k_3 \cdot (t - t_{ch,w}) \tag{4}$$

where

$\beta_{0,w}$ is the basic design charring rate of the web material [mm/min];

k_3 is the post-protection factor for the web (equal to 2) [-];

$t_{ch,w}$ is the start time of charring of the web [min].

4   Thermal simulations

The charring of I-joists was investigated using finite element (FE) thermal simulations. Within this simulation programme, the effect of cross-section dimensions, applied fire protection system and cavity insulation on the charring behaviour of the fire exposed flange was investigated.

The simulations were conducted in 2D using the SAFIR v2014a1 software. The thermal properties were taken from Eurocode 5 Part 1-2 (2004) and Schleifer (2009). All structures were exposed to the ISO 834 standard temperature-time curve with the

coefficient of convection taken as 25 W/m²K on heated surfaces and 4 W/m²K on un-heated surfaces and emissivity as 0,8.

The simulated sections were discretised into rectangular elements. The sizes of the elements were varied between 1x1 mm and 5x5 mm. The time steps were kept at maximum 5 seconds. Half of a frame assembly (see Figure 4a) with the stud distance of 600 mm centre-to-centre was simulated. The sides of the structure were adiabatic surfaces.

The unexposed side was covered by a 20-mm thick wooden fibreboard. The height of the I-joist was 200 mm in all cases. The cavities were completely filled with stone wool insulation with a density of 26 kg/m³.

The factors which were varied with each thermal simulation were the size of the flanges (both width and height), the length of the fire exposure (up to 120 minutes) and the thickness and fall-off time of the fire protection system (gypsum board), see Table 2 and Table 3.

(a)   *(b)*
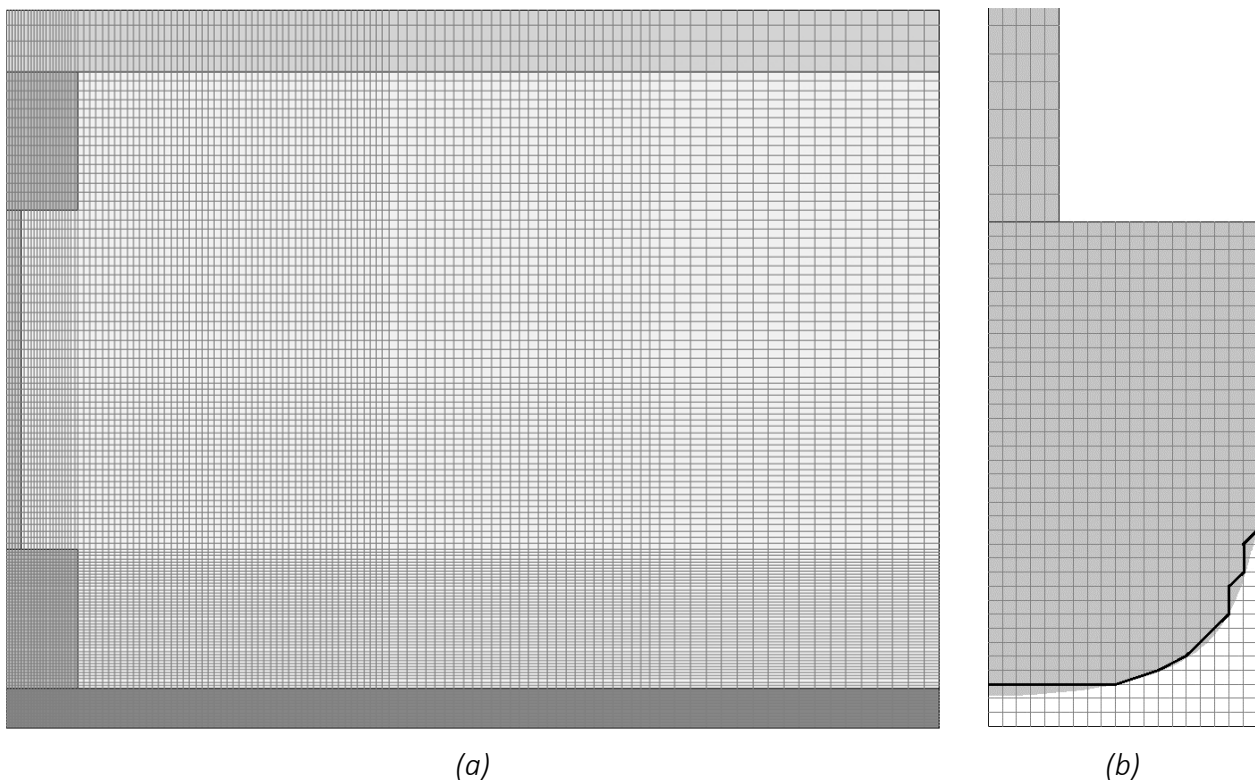
Figure 4. FE simulation. Fire exposure from below. (a) the simulated structure; (b) residual cross-section in grey.

The 10 flange sizes used for all cases are given in Table 2. The various thicknesses and fall-off times of the gypsum boards are given in Table 3. The simulated combinations of flange heights and widths and board thicknesses and fall-off times are marked with a "V". All flange sizes were simulated without protection in the first set of simulations and then, all cases shown in Table 3 were simulated for each flange size. Fall-off of the fire protection system was imposed at various times by removing the material

from the simulation and continuing the calculation until the full charring of the exposed flange.

Table 2. Flange sizes (in mm)

Flange heights (mm)	Flange widths (mm)				
	38	46	70	96	140
36	V	V	V		
45		V	V	V	V
69		V	V	V	

Table 3. Fire protection systems

Board thickness (mm)	Fall-off times (min)		
	30	45	60
13	V	V	
15	V	V	V
20	V	V	V

In order to analyse the data created from the thermal simulations, a MATLAB script was developed, which would read all the temperatures at all nodes and all times of the FE simulation results. Then, the materials outside the I-joist were removed. The charring depth in the middle of the flange, on the lateral side of the flange and the web was plotted against time.

The residual area of the fire exposed flange was calculated for each time step based on summarising the areas of the trapezoidal slices. Figure 4b shows half of an exposed flange discretised into 1x1 mm elements. The number of nodes in each row where the temperature was less than 300°C were counted and trapezoids created (see thicker black line).

5   Analysis

The load-bearing capacity of I-joists is strongly dependent on the area of the flanges. Therefore, the charring coefficients were developed based on the change of area of the fire exposed flange. For each case shown in Table 3 (and initially unprotected) the reductions in the area of the exposed flange were plotted against time. The reduction of area was determined by dividing the residual area by the initial area of the flange.

The various phases and the times separating them present for each flange size were determined. Then, using the SLOPE function in Excel, the gradient of the reduction of the area was determined assuming a linear regression. The various gradients represent the charring coefficients for each phase. For example:

$$\frac{A_{fi}(t)}{A_{in}} = k \cdot t + b$$

where

A_{fi}/A_{in} is the reduction of the area [-];

k is the gradient [min^{-1}];

b is the intercept [-].

5.1   Combined section and conversion factor $k_{s,n}$

In the following section, the determination of the expressions for the combined section and conversion factors for the exposed and the lateral sides of the exposed flange is described.

Figure 5 presents two examples of the reduction in area and charring depth in the middle of the width of the flange plotted against time. In both cases the fall-off time of the fire protection system was 45 minutes and the flange width was 46 mm. the grey lines are for a case with lateral charring behind protection and the black lines when lateral charring started after the fall-off. The denser dashed lines are linear approximations of the simulation results for the reduction in area.
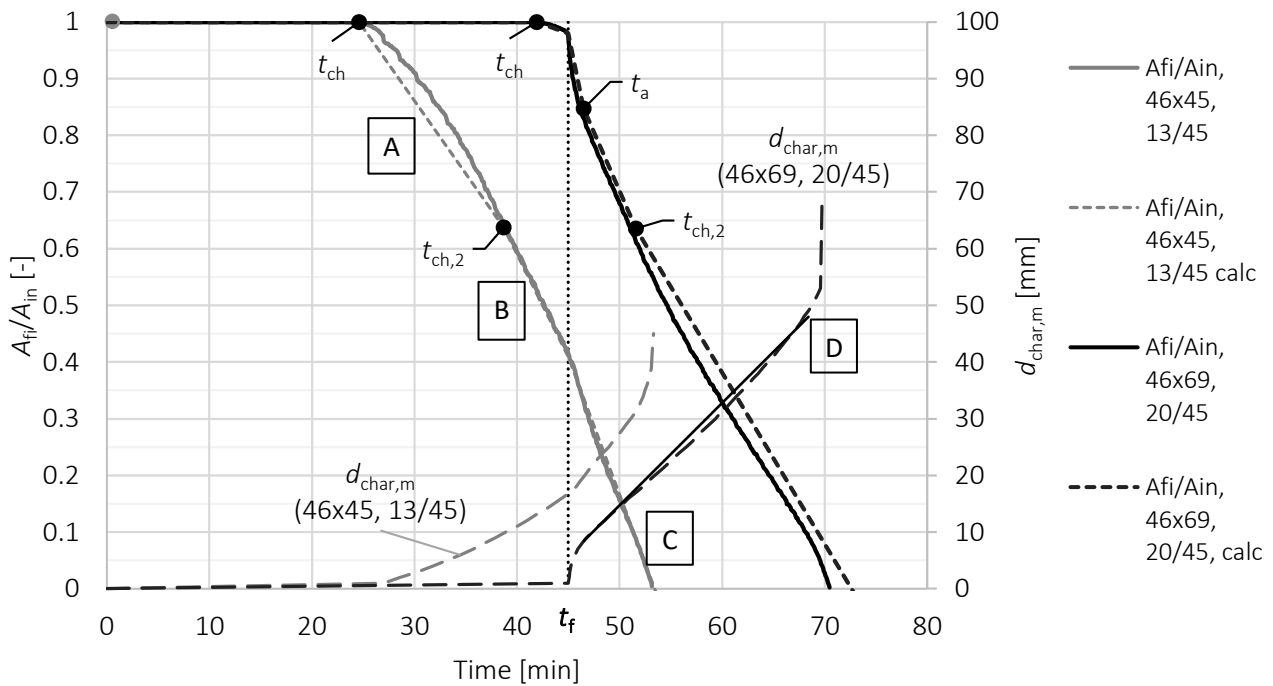
Figure 5. Simulated reductions in area with linear simplifications and charring depths in the middle of the flange width

First, the coefficients $k_{s,n}$ for the exposed side were determined for all flange sizes with every protection system. The reduction of area before the start of lateral charring is shown in Figure 5 as line A:

$$\frac{A_{fi}\left(t_{ch,2} - t_{ch}\right)}{A_{in}} = 1 - k_A \cdot \left(t_{ch,2} - t_{ch}\right)$$

Since only the height of the flange changes, the reduction of the height of the flange is the same as the reduction of the area:

$$\frac{h_{fi}\left(t_{ch,2} - t_{ch}\right)}{h_{in}} = 1 - k_A \cdot \left(t_{ch,2} - t_{ch}\right) = \frac{h_{in} - d_{char,1,n}}{h_{in}} \rightarrow$$

$$\rightarrow d_{char,1,n} = \beta_0 \cdot k_{s,n} \cdot k_2 \cdot \left(t_{ch,2} - t_{ch}\right) = k_A \cdot h_{in} \cdot \left(t_{ch,2} - t_{ch}\right)$$

Therefore, the coefficient $k_{s,n}$ for the exposed side is:

$$k_{s,n} = \frac{k_A \cdot h_{in}}{\beta_0 \cdot k_2}$$

The protection coefficient k_2 is taken according to Eurocode 5 Part 1-2 (2004).

The results of the coefficients $k_{s,n}$ are summarised in Figure 6 which presents the different values of $k_{s,n}$ depending on the flange width and the properties of the fire protection material (thickness/failure time). The variation of the values is due to the difference of the length of protection times. Equation (6) was derived based on the maximum values of each flange width (shown as the solid line in Figure 6).
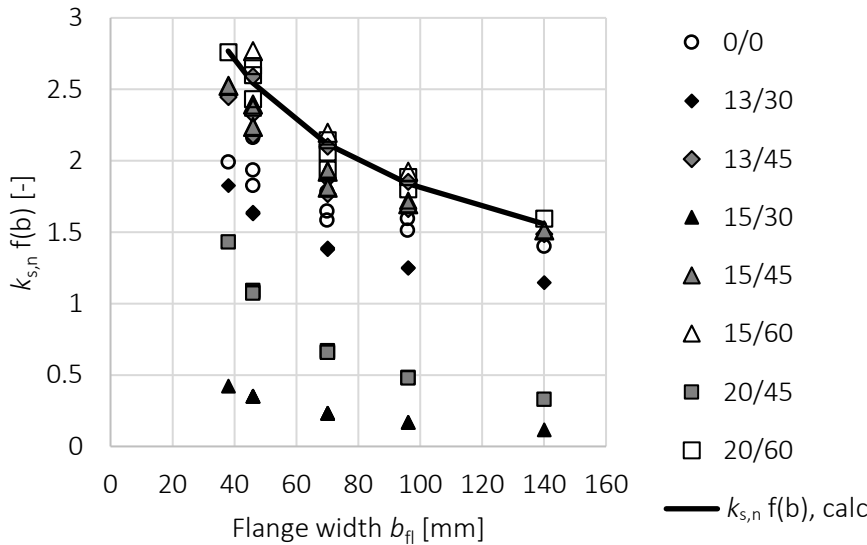
Figure 6. Values of coefficient $k_{s,n}$ depending on the flange width

The expression for $k_{s,n}$ for the fire exposed side is:

$$k_{s,n} = 14 \cdot b_{fl}^{-0,44} \tag{6}$$

where

b_{fl} is the width of the fire exposed flange [mm].

The coefficient $k_{s,n}$ for the lateral sides was developed based on the increased reduction of the flange area after the start of lateral charring (see 5.3). In Figure 5 it is shown as line B. The steps taken are similar to the development of coefficient $k_{s,n}$ for the exposed side. It may be calculated as:

$$k_{s,n} = 2 - 0,013 \cdot h_{fl} \tag{7}$$

where

h_{fl} is the height of the fire exposed flange [mm].

5.2   Post-protection factor k_3 and consolidation factor k_4 for the exposed side

The coefficients k_3 and k_4 consider the protection offered by the cavity insulation after the fall-off of the fire protection system has occurred. The expressions were developed based on the evolution of the char depth in the middle of the flange ($d_{char,m}$). Figure 5 presents two examples of the char depth in the middle of the width of the

flange plotted against time (long dashed lines labelled with $d_{char,m}$ and the flange size and protection thickness/fall-off time).

Firstly, the cross-section factor k_s was developed based on the gradients of the $d_{char,m}$ graphs without initial protection using a linear approximation.

$$k_s = \frac{\beta_m}{\beta_0}$$

Then, the length of time between the fall-off time and the consolidation time was investigated. In Figure 5 the long dashed line marked as "$d_{char,m}$ (46x69, 20/45)" shows that there is a short time of accelerated charring after the fall-off time. If the charring depth is more than 15 mm at the fall-off time, the faster charring can be neglected (see "$d_{char,m}$ (46x45, 13/45)" in Figure 5).

The time t_a was assumed to occur when the gradient of the $d_{char,m}$ became relatively constant. The time t_a can be calculated according to (8) and it depends on the fall-off time t_f and the protection factor k_2 of the fire protection system.

$$t_a = t_f + 3{,}8 \cdot k_2 - 0{,}03 \cdot k_2 \cdot t_f \tag{8}$$

The post-protection coefficient k_3 for the exposed side (9) was developed based on the gradient of $d_{char,m}$ between the fall-off time and the consolidation time.

$$k_3 = 0{,}07 \cdot t_f + 1 \tag{9}$$

The fast charring which occurs at the end of the simulations was also disregarded and the coefficient k_4 was derived based on dividing the gradient β_m (of line D in Figure 5) by the basic design charring rate and k_s:

$$k_4 = \frac{\beta_m}{\beta_0 \cdot k_s}$$

The consolidation factor for the fire exposed side is:

$$k_4 = 0{,}017 \cdot t_f + 1 \tag{10}$$

Similarly to the development of the expression for $k_{s,n}$ for the lateral side, the post-protection coefficient $k_{3,2}$ for the lateral sides was derived as a compensating factor to correctly fit the reduction in area in the final phases. The post-protection coefficient for charring on the lateral side of the flange $k_{3,2}$ is:

$$k_{3,2} = 1 - 0{,}0081 \cdot t_{ch,2} \tag{11}$$

where

$t_{ch,2}$ is the start time of lateral charring [min].

5.3 Start time of lateral charring $t_{ch,2}$ and web $t_{ch,w}$

The start of lateral charring $t_{ch,2}$ is the time it takes for the 300°C isotherm to reach the full height of the exposed flange. It may be calculated using the Component Additive Method (CAM) (Schleifer, 2009) or according to (12).

$$t_{ch,2} = t_{ch} + \frac{h_{fl}}{v_{rec} \cdot k_2} \qquad \text{If } t_{ch,2} < t_f$$

$$t_{ch,2} = t_f + \frac{h_{fl} - v_{rec} \cdot k_2 \cdot (t_f - t_{ch})}{v_{rec}} \qquad \text{If } t_{ch,2} > t_f$$

$$(12)$$

where

t_{ch} is the start time of charring, according to the CAM [min];

v_{rec} is the recession speed of the insulation [mm/min].

For stone wool the recession speed is 4 mm/min.

The charring of the web has a significant influence on the load-bearing capacity of the I-joist exposed to fire. Therefore, it is important to consider it in the calculations. If the web chars fully, the load-bearing capacity of the joist can be considered as exhausted.

The start of charring of the web is the time when the 300°C isotherm reaches the point marked with $t_{ch,w}$ in Figure 2b calculated according to the CAM or (13).

$$t_{ch,w} = t_{ch,2} + \frac{(b_{fl} - b_w) \cdot \sqrt{2}}{2 \cdot v_{rec}} \qquad (13)$$

where

$t_{ch,2}$ is the start time of lateral charring [min].

6   Verification

The model scale furnace fire test results obtained within the research of Schmid (Oct 2010-Apr 2011) were used as the basis for the verification of the previously developed coefficients. The residual cross-sections in the centre of the beams had been photographed after the test. Then, the area was measured using AutoCAD.

All available test results with information about the residual area were conducted with cavities completely filled with stone wool insulation (density 30 kg/m^3) and beams with a height of 200 mm. The initial dimensions of the flanges were 47x47 mm. An overview of the test setups is given in Table 4.

The test results consider different charring scenarios with different lengths of protected and unprotected charring phases. A comparison (see Figure 7) of test results and results calculated according to the proposed design method shows that the design model gives safe results.

The calculated residual cross-section of the test number 9 is slightly unconservative but remains within the 10% deviation. However, the relevant residual cross-section areas in fire design remain within 20 to 40% of the original cross-section areas.

Table 4. Overview of model-scale verification tests (TTF=time to failure, A_{fi}=residual area)

Test	Beam	Cladding	Start time of charring t_{ch}	Fall-off time t_f	TTF of the assembly (tested)	A_{fi} of the exposed flange [mm²]
Test 2	beam 26	GtF15	25,7	-	27	1981
Test 3	beam 1	GtF15	23,9	-	42,2	1157
Test 4	beam 22	GtF15	26,5	-	48,2	824
Test 5	beam 37	GtF15	26,1	50,3	53,2	528
Test 6	beam 19	GtA12,5	20,7	20,7	35,7	618
Test 7	beam 34	GtA12,5	16,6	16,6	26,6	1008
Test 8	beam 24	GtF+GtA	58,5	71,7	71,7	1017
Test 9	beam 36	GtA12,5	19,8	19,8	30,2	1081
Test 10	beam 8	GtF15	25,5	40,4	40,4	1208

A graphic comparison between the tested and calculated residual areas is shown in Figure 7.
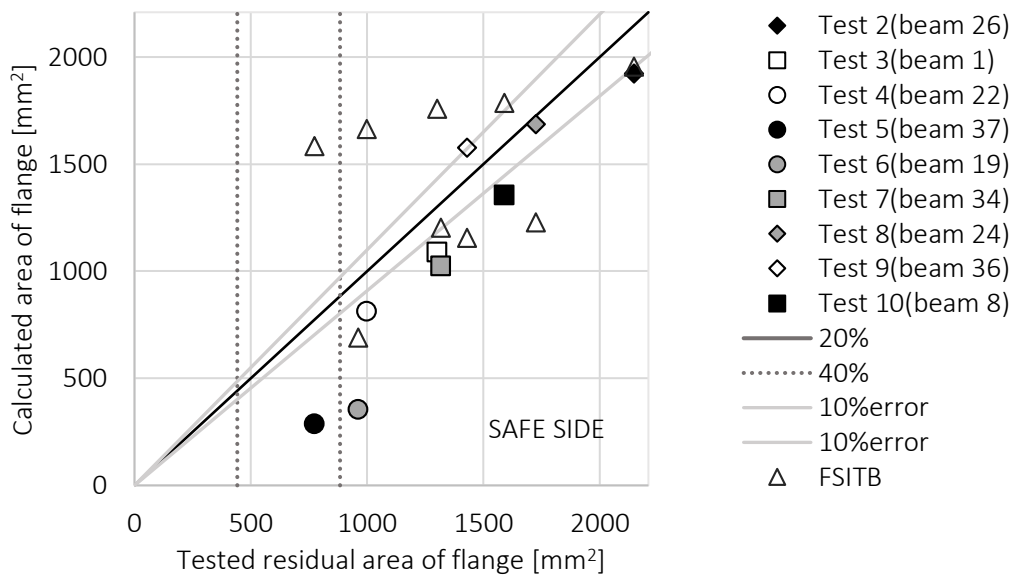
Figure 7. Comparison of calculated and tested residual areas

Figure 7 presents also a comparison of the proposed design method and previous design method. The triangular markers show the design results with the same tested configurations according to the available design methods by König (2006) and Schmid et al. (2011). It can be shown that the currently presented design method gives safe and more optimized results compared to the current design models.

7   Summary and outlook

The improved universal design method for charring of wooden I-joists is proposed in this paper. The method is able to consider different charring phases using various coefficients developed within this work.

In an ongoing research project, the fire resistance of wooden I-joists is investigated. The next step is to consider the contribution of different cavity insulation materials and the loss of strength and stiffness at elevated temperatures. In the unified model, the zero-strength layer will be used to take into account the effect of the loading conditions.

The zero-strength layer will be used to take into account the reduction of strength due to elevated temperatures. The research is ongoing by the authors to determine the values of zero-strength layers.

Additionally, adhesives used in finger joints in the flanges and the joint between the flanges and the web may influence the load-bearing capacity. The flanges of I-joists loaded in tension are sensitive to the behaviour of adhesives at elevated temperatures. The load-bearing capacity of compression members might be influenced by the location of knots. The influence of these phenomena is under investigation.

8   References

Eurocode 5 (2004): Design of timber structures - Part 1-1: General and rules for buildings. CEN. (EN 1995-1-1).

König, J (2006): Fire exposed simply supported wooden I-joists in floor assemblies. Stockholm: SP Swedish National Testing and Research Institute. (SP Report 2006:44).

Schmid, J, Just, A, König, J (2011): Fire exposed wooden I-joists for wall assemblies. Stockholm: SP Technical Research Institute of Sweden. (SP Report 2011:27).

Mäger, K, Just, A (2019): Design methods for wood-based I-joists exposed to fire – State-of-the-art and improvements. Interflam 2019

Tiso, M (2018): The Contribution of Cavity Insulations to the Load-Bearing Capacity of Timber Frame Assemblies Exposed to Fire. TTÜ Press, Tallinn. (PhD Thesis).

Schleifer, V (2009): Zum Verhalten von raumabschliessenden mehrschichtigen Holzbauteilen im Brandfall. Thesis (PhD). ETH Zürich.

Discussion

The paper was presented by K N Mäger

A Frangi commented that the flange size of the I joist was small and asked if one should consider the full cross section rather than symmetry as there would be heat accumulation from both sides. KN Mäger agreed and will check later.

A Frangi commented that at temperature of 300C how would it be possible for the profile to exist. KN Mäger responded that the image was just an illustration.

H Blass and KN Mäger discussion the possibility of insulation falling off the protection layer. H Blass mentioned that the possibility of the insulation layer falling off would necessitate prescriptive rules.

P Palma commented that the results would depend on workmanship. KN Mäger agreed that this was possible.

BJ Yeh asked if the model would always assume the failure occur in the flange. KN Mager responded that if charring occurred in the web, the failure would be governed by the web. BJ Yeh responded that based on N.A. fire test experience web would govern and the profile shown has not been seen in N.A. fire tests. S Winter said that this was because glass wool was used and not rock wool.

S Winter asked about the cases of having another layer for acoustic profile and partially insulated cavity. This situation would be helpful. KN Mäger responded that acoustic profile case would need to be tested. Also having a cavity should equalize the temperature a little bit. Partially insulated cases would need further investigation and the web should be fully insulated as a minimum.

A Frangi commented that one should limit the contribution to 15 minutes after the gypsum layer was compromised regardless of the fact that modelling results are conservative.

Code calibration for timber in fire – On the use of 20 % fractiles for the strength

Reto Fahrni, ETH Zurich

Gianluca De Sanctis, EBP Schweiz AG

Andrea Frangi, ETH Zurich

Keywords: timber, fire, code calibration, reliability analysis, code-format, EN 1995-1-2, Eurocode 5

1   Introduction

In the history of design codes, the format shifted from 'experience based' to more statistically informed approaches, such as the nowadays used semi-probabilistic approach of the load and resistance factor design (LRFD). The same transition should be observable for the code calibration process as well. However, new design codes were often only "soft conversions", meaning they were calibrated to deliver similar designs as the previous codes. A proper code calibration would be based on the underlying (statistical) concepts.

Such a soft conversion was done for timber in fire when the current version of Eurocode 5 (2004) was introduced (König, 2005). However, as the partial safety factor (psf) for the material strength in fire $\gamma_{M,fi}$ was fixed to unity for all materials, there was actually no psf to be calibrated in fire. Though, with $\gamma_{M,fi} = 1$ and the usual 5 % fractiles for the strength ($f_{0.05}$), the resulting design values were larger compared to the previous national codes. Thus, the fractile was chosen as 20 % ($f_{0.2}$), having the same result as if the psf was smaller than unity. This was recently questioned by TC250 HGF, as (1) 20 % fractiles imply a reduced reliability (compared to 5 % fractiles) and (2) timber is treated differently in comparison to other building materials.

This paper analyzes the current version of the code with a reliability-based code calibration. The aim is to provide a sound foundation for the LRFD-code-format and to provide scientific evidence for the use of 20 % fractile value. The following chapter gives a short introduction to reliability-based code calibration. The actual calibration procedure is addressed in the following chapters.

2 Reliability-based code calibration

A reliability analysis investigates the probability of failure P_f of a given structure, or, as often simplified, only of a structural element such as a beam or column. The reliability is usually expressed in terms of the reliability index β, which is the negative of the inverse standard normal cumulative distribution function of the probability of failure ($\beta = -\Phi^{-1}(P_f)$). In order to deliver unbiased probabilities of failure that are comparable with actual failure rates, a reliability analysis is required that covers all appearing uncertainties by appropriately chosen probability distributions.

The reliability of an arbitrary structure that is designed by the code, will not meet exactly the target reliability β_t. It is the aim of a calibration to minimize this deviation to the target reliability for a given set of structures by optimizing the psfs. A usual optimization target is to minimize the error according to equation 1, where $\beta_i(\gamma_j)$ is the reliability of structure i, designed according to the code with the given psfs γ_j.

$$Error = \sum_i \left(\beta_i(\gamma_j) - \beta_t\right)^2 \tag{1}$$

It is important that the structures taken into account cover the whole range of structures that are and could be designed according to the code now and in the future. This difficulty is often faced by using generalized structures (e.g. Köhler + Fink 2012), which are able to represent any kind of structures (beam, columns, etc.) and any live to dead load ratio.

3 Uncertainties of structures in fire

3.1 Fire exposure

Failure in fire can be defined in many ways, for example in terms of unsafe egress routes. This paper treats only structural failures due to fire.

As a structural failure could happen at any time in a fire, the reliability must be calculated for the most critical point in time, respectively for the whole duration of a fire. In order that the reliability analysis can return an unbiased probability of failure, all uncertainties must be considered. However, there are many uncertain variables (e.g. fire loads, their arrangement and their burn rates, ventilation conditions, sprinklers, …) which influence the fire. Models exist to describe the fire and its impact on the structure. Such natural fire models were successfully used for reliability analysis for non-combustible materials (e.g. De Sanctis, 2015). They often rely on (1) a probabilistic heat release rate model and (2) a simulation of an enclosure fire resulting in a time-temperature curve and then (3) a calculation of the reliability of a structure given this exposure considering resistance and load uncertainties. However, as the uncertainties cannot be introduced on their physical source but rather on model parameters, the reliability analysis is prone to not return the unbiased probability of

failure anymore, which makes a comparison to cost-optimized reliability targets difficult. Chapter 4 introduces an approach to overcome this problem.

3.2   Timber in fire

Natural fire models and its effects on structural elements vary in terms of the accuracy of the representation of a real fire. Unfortunately, the models are not yet applicable to timber, for multiple reasons:

- In order to calculate the resistance of a timber structural element in a real fire (step 3), the fire impact on timber is not sufficiently described by the time-temperature curve. The behavior of timber in a fire significantly depends on the available oxygen content and the gas flow (i.e. speed and turbulence) (Schmid et al, 2018, Richter, 2019). Both have an important impact especially in the fully developed fire phase of a fuel-controlled fire and in the cooling phase. Thus, the definition of the fire exposure for timber would require these two factors as well.
- Models that can predict the behavior of timber for an exposure as described above are still in development (Richter, 2019) and do not yet show the accuracy needed for reliability analysis.
- Moreover, for timber, the above procedure is not sequential anymore, since the exposure of the timber is also dependent on its reaction: Timber does not only heat up, but thereby also produces combustible gases that react exothermally with the oxygen, which is an additional heat release. In other words, the structure itself is an additional fire load whereby the above procedure is not sequential anymore but rather an iterative loop. This fact is especially important for the end of a fire: While fires in non-combustible structures will extinguish as soon as the available fire load is completely burned, the timber structure itself might produce sufficient heat that the fire will not extinguish and may finally fail due to a progressive charring. This process is not yet understood to a degree that would allow a reliability analysis.

It is concluded that for timber in fire the available knowledge is not sufficient for a performance based reliability analysis without significant simplifications and assumptions.

Timber design in fire is predominately based on prescriptive fire regulations: Structural elements are required to resist a certain duration (e.g. 30, 60, 90, 120 minutes) under standard fire exposure (EN 1363-1, 2012). The oxygen content during testing is thereby specified as well. The behavior of timber in standard fire is well understood and moreover simple and accurately describable.

A reliability analysis on the basis of a required fire resistance (i.e. the duration of exposure to standard fire) calculates the probability of failure at the required time, which is equal to the probability that the structure fails before the required time. As

the exposure is deterministically fixed, it must be assumed that many of the basic physical uncertainties (e.g. fire loads) are covered in the deterministic requirement and that the differentiation in the requirements finally leads to comparable levels of reliability. The rough classification in usually 30 minutes steps shows that this condition cannot be fulfilled. Moreover, the requirements of some countries nowadays are set on the basis of factors that do not affect the structural failure probability at all. For example, the required fire resistance for hospitals is often elevated, because the evacuation takes longer, but the actual fire exposure of the structure is short since the fire load is usually low.

Additionally, as the prescriptive design is independent of the behavior and response of the structure in the fire (i.e. not iterative), it cannot reproduce the mentioned loop dependency of exposure and reaction to it. As stated above, this is especially important in fires where the structure keeps burning after the available fire load is consumed. In that case the difference between a reliability analysis based on a standard fire and a reliability analysis based on a natural fire will be enormous: A reliability analysis that is based on natural fire models will correctly state a probability of failure of near 100 %, since the progressive burning of the timber structure is modelled. Contrary, a standard fire based reliability analysis will return a small probability of failure related to the required fire resistance (time), but does not take into account that the fire is not stopped by then and that the probability failure would further increase. This effect can be considered by introducing additional provisions to the fire resistance requirement that ensure the structural timber to stop burning. This for example can be achieved by limiting the exposed surface of timber elements and is implemented in such a way in several prescriptive regulations already.

Despite the fact that standard fire is state of the art for timber, all the downsides of using it for a reliability analysis reduce the value of the statement made, i.e. the calculated probability of failure is not comparable to the one of a real fire anymore. Nevertheless, when used in a relative code calibration, as explained in the next chapter, this approach can be applied to get an estimate of calibrated design parameters for timber in fire.

4 Relative reliability targets β_t

In a code calibration, the probability of failure respectively the reliability index β is compared to the target reliability β_t, for which values are found in the relevant codes (Eurocode 0, 2002, JCSS model code, 2001). The target reliabilities are founded by a cost minimization (e.g. Rackwitz, 2000), taking into account the rising construction cost and sinking risk of failure with increasing safety factor respectively increasing target reliability.

The application of reliability targets derived in such a way is correct only when the used reliability models are able to represent the empirical failure rates. However, the

statistics about structural element failures show (1) significantly less failures than would correspond to the target reliability and (2) by far most of these failures are due to human errors during design and execution. Certainly, real structures often have more structural capacity than the codes would require, e.g. due to overdesign, plasticity and load redistribution. Nevertheless, inter alia for lack of consideration of the latter two effects and for conservative tail-modeling of the uncertainty distributions (Massini, 2019), the probabilities of failure received in a reliability analysis are in general (very) conservative and thus can (strictly seen) not be compared to the absolute reliability targets derived with cost minimization. Though, presuming that the reliability level of existing structures is accepted and deemed to be sufficient, even biased reliability models can be used together with so-called relative reliability targets to perform a code calibration and thereby decrease the inhomogeneity of reliability levels reached with the code.

The relative reliability target β_t thereby is the mean reliability level over a given set of structures designed to meet exactly the current codes. The relative reliability target is then used for the code calibration, which ideally relies on the same reliability models as were used to calculate the target. Thereby, biases in the reliability models only have a small effect on the calibration result, as they appear in the derivation of the target as well as in the calibration. However, the uncertainties on the different parameters are very important, especially relative to each other.

Such a relative code calibration was chosen for example by Baravalle et al. (2017) and provided the basis for the calibration of the load psfs in the Eurocodes. The use of relative reliability targets has proven to be effective, since a calibration to the target reliability of 4.7 given in Eurocode 0 (2002) would have required a significant increase of the partial safety factors (i.e. the mean of the current Eurocodes was found to be 4.08) and would also not be appropriate for all materials since the reliability level differences among material were found to be high already.

For the case of fire there are two additional good reasons to use relative reliability targets:

- The derivation of target reliabilities in Eurocode 0 (2002) was done for structures in persistent and transient design situations. The founding cost minimization would be different for the accidental design situation of fire and thus also different absolute target probabilities would have to be used in fire. Moreover, a cost minimization would be difficult or even impossible, as the cost minimum changes over the time in fire, with progressing smoke and fire damage and decreasing humans exposed to a possible sudden collapse.
- As the fire accidental situation is a rare and not a persistent design situation, the probability of the situation must be accounted to be in line with the return period of the probability of failure, usually one or 50 years. The following section elaborates on this.

The probability of a fully developed fire p_{fi}, as standard fire is, can be calculated as the product of the following (conditional) probabilities (e.g. Schleich et al 2002):

$$p_{fi} = p_{ig} * p_{f,occ} * p_{f,sp} * p_{f,brig} \tag{2}$$

- p_{ig} probability of ignition
- $p_{f,occ}$ probability of occupants failing to extinguish the fire
- $p_{f.sp}$ probability of sprinklers failing to control or extinguish the fire
- $p_{f,brig}$ probability of the fire brigade failing to extinguish the fire

The conditional target reliability given fire $\beta_{t,fi}$ is then calculated as follows:

$$\beta_{t,fi} = -\Phi^{-1}(p_{f|fi}) \tag{3}$$

$$p_{f|fi} = \frac{p_f}{p_{fi}} = \frac{\Phi(-\beta_t)}{p_{fi}} \tag{4}$$

In a relative code calibration, the same probability p_{fi} is applied during the calculation of the relative reliability target as well as in the calibration, which makes the calibration result insensitive to the value chosen for p_{fi}. An error definition according to equation 1 on the level of the conditional target reliability $\beta_{t,fi}$ would even make the calibration completely independent of p_{fi}. However, the error definition (equation 1) would lead to slightly different weighting of the target deviations since the reliabilities are not linearly transformed and the smaller reliabilities would be unfamiliar. Therefore, the calibration presented here is done in the usual way.

The fact that above (conditional) probabilities are of minor significance for the calibration result is important for multiple reasons:

- All four probabilities are hard to be determined[1]. The probability of ignition is dependent on the use of the building and the compartment size. The sprinkler reliability varies significantly from country to country, e.g. in the US sprinklers are operating and effective in 88 % ($p_{f,sp} = 12\ \%$) of cases[2] (Ahrens 2017), whereas for Europe Schleich et al 2002 combined statistics from multiple countries and determined a reliability of around 98 % ($p_{f,sp} = 2\ \%$). In terms of probability of failure the difference of factor six shows how uncertain the parameter is and as the parameter deterministically enters the total probability of failure, also the latter would be uncertain by a factor of six.
- The derivation of the probabilities must be coordinated, which can be difficult as different sources must be combined: For example, in some statistics the probability of ignition might already contain the probability of occupants extinguishing the fire since only fires where the fire brigade is alarmed are counted. In

---

[1] The uncertainties cannot be taken into account in the reliability analysis as they are applied on the probability target and not in the reliability analysis.

[2] where the fire was large enough to activate the sprinklers

contrast, insurance statistics usually also cover fires extinguished by occupants (see De Sanctis 2015 for extended discussion). If both statistics were available for the same region, the probability of occupants extinguishing the fire could be derived from the difference, given the sprinkler influence is appropriately covered.

- In some countries it is not accepted that sprinklers and/or the fire brigade are part of the reliability analysis. It is often justified either by the over proportional consequences when these active measures fail or by stating that the fire brigade cannot take the responsibility to be successful. Nevertheless, from a probabilistic point of view, considering these two probabilities is valid and from a financial point of view not considering these active measures is a waste of costs to society.

The basic requirement for a code calibration with relative reliability targets is that the current reliability level is acceptable. Since fire and especially fire in timber structures are rare events, a conclusion based on yearly statistics on the acceptability of its occurrence rate is difficult. Therefore Östman (2017) analyzed the Swedish statistics for a period of 20 years and could conclude that fires with fire brigade intervention occur less often in timber buildings than on average over all buildings, mainly because they are more modern and new. At the same time the appearing fires in timber did not give reason to assume that timber fires are unusually severe. However, concluding about the correctness of the current reliability level based on statistics is delicate since it is heavily linked to the fire regulations that were applicable during the statistics report time respectively the time the structures were built and finally also on the kind of buildings (e.g. single family houses or high-risers) present in the report time.

Nevertheless, the code calibrations presented here rely on the relative reliability analysis as (1) the assumption of a currently acceptable reliability level could not be disproven and (2) an absolute reliability analysis would suffer under the needed absolute definition of p_{fi}.

5   Defining structural elements for calibration

The considered structures in most code calibrations are chosen in a generic way (e.g. Köhler & Fink, 2012, Baravalle et al, 2017), which allows to cover any structure with just one or a few parameters. Unfortunately, this approach is not possible for timber structures in fire, since the charring process introduces uncertainty on the dimensions of the structural elements (e.g. beams), preventing the simplifications that normally allow a generic representation of the structure. Therefore, a set of explicit structures must be defined for the code calibration.

The benefit of an explicit set of structures is that structures with larger reliability deviations can be clearly identified. The downside is that not explicitly covered structures might have a higher deviation in their reliability level.

The probability of a fully developed fire p_{fi} was fixed to 3.2*10[-4] (per year), which is a realistic value for open-plan offices without considering sprinklers (Fischer et al, 2012, Schleich et al, 2002). For dwellings p_{fi} would be lower, however, as stated in chapter 4, the relative code calibration is insensitive to this choice. The only place where p_{fi} has a key effect is in the determination for which structures the fire design is decisive. The differentiation is made based on reliability analyses for the persistent and for the fire design and compares the dimensions needed to reach a target reliability of 4.2 for both design situations. In structures that require larger dimensions to fulfill the reliability in the persistent situation (e.g. for long spanning beams and with high loads), the fire situation is less often decisive than for smaller structures.

5.1 Beams

Totally 960 simple beams were considered, of which only 280 were decisive and taken into account. The beams were weighted with 2.46 in order to have in total the same weight as the columns, which were weighted with unity. The following properties were varied: dead load (1/2/3/4 kN/m^2), live load (dwelling/office/store), height to width ratio (2/3), time in fire (30/60/90/120 min), length of beam (3/5/8/12/20 m), exposition (narrow side/narrow side + both long sides). The interval of the beams was fixed to one fifth of the length.

5.2 Columns

The columns were modeled as stocky (i.e. no stability problem), rectangular and on all sides exposed to the fire. The loads were modeled as acting on a given area in every story above the column. The dead load of the columns was neglected. The following properties were varied: dead load (1/2/3/4 kN/m^2), live load (dwelling/office/store), height to width ratio (1/1.5), time in fire (30/60/90/120 min), area per floor (16/25/36 m^2), number of stories (2/3/5/8). For 690 out of 1152 structures the fire design was decisive.

6 Reliability model for timber in fire

6.1 Code format

The code format defines the calculation rules for the design, especially on which parameters psfs are applied. In general, psfs should be applied on uncertain parameters that have a high importance on the result.
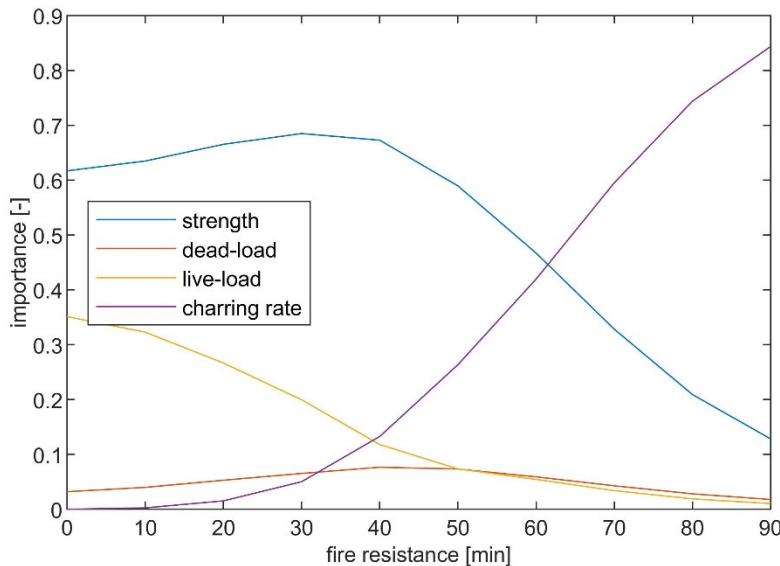
Figure 1: importance factors of a FORM analysis of a simple beam for different fire resistance times. For fire resistance times <50 min, the persistent deisgn situation was decisive for the dimensions of the beam.

Figure 1 shows the importance factors returned from a preliminary analysis with the first order reliability method (FORM) of an exemplary simple beam for different fire resistance times. The strength, dead and live loads and the charring rate where modeled probabilistically. The figure shows that with increasing fire resistance the charring rate gains on importance. After approximately 60 min the charring rate is even more important than the strength. The reason is that the charring rate is multiplied with the time and leads to a higher variability of the residual cross section when time is increasing. This means that a better calibration would be reached, in terms of reducing the error as stated in equation 1, when a calibratable psf on the charring rate ($\gamma_{d_{char}}$) was considered. This is not the case in the current code format (Eurocode 5, 2004).

For timber in fire the design is usually performed with the reduced cross section method (e.g. Schmid et al, 2015, Eurocode 5, 2004). The idea is that the exposure to the standard fire curve is modeled as a reduction of the remaining cross section by an effective depth d_{ef}, more precisely every fire exposed side is reduced by the notional charring rate[3] β_n multiplied by the fire resistance time t and the time invariant[4] zero strength layer d_0.

$$d_{ef} = d_{char,n} * \gamma_{d_{char}} + d_0 = \beta_n * t * \gamma_{d_{char}} + d_0 \tag{5}$$

For a rectangular cross section of a simple beam with a constant loading, the code format, including the usual safety factor on the strength in fire $\gamma_{m,fi}$ ($\gamma_{m,fi} = 1$ in the

---

[3] Attention: In literature, the charring rate and the reliability unfortunately share the same Greek letter. The authors nevertheless assume that the context is always clear and so the usual notation is used anyway.

[4] In the current EN 1995-1-2 (2002); will probably be changed in the next version.

current Eurocodes) and the partial safety factor for the charring $\gamma_{d_{char}}$ (within d_{ef}) looks as follows:

$$0 = \frac{(b-n_w d_{ef})(h-n_h d_{ef})^2}{6} \frac{f_{0.2}}{\gamma_{m,fi}} - \frac{(g_k+q_k\psi_2)l^2}{8} \tag{6}$$

where b and h are the dimensions, n_w and n_h are the number of fire exposed sides in width and height, l is the length of the beam, g_k, q_k and ψ_2 are the characteristic dead and live loads and the combination factor. Apart of $\gamma_{d_{char}}$ the code format is equivalent to the current Eurocode 5 (2004).

6.2 Limit state function

The limit state function $g(x)$ (lsf) is central to the reliability analysis and must be able to distinctively predict the binary (resist/fail) behavior of a structure for deterministic inputs, i.e. known strength and loads. For the prediction to be accurate, the underlying reliability model must be accurate as well. For example for timber in fire it would have to account for effects that are neglected or simplified in the code format such as a time dependency of the charring rate, the effect of corner rounding and the true zero strength layer, which is dependent on the geometry and is correlated to the charring rate.

However, as the calibration is done relatively, these effects are assumed to have a negligible effect on the calibration result and are neglected here. Thus, the lsf was chosen analogous to the code format. The charring rate X_{d_r}, the strength X_f and both loads (X_g and X_q) are introduced as random variables. Additionally, the strength and the live load have a model uncertainty ($X_{m,f}$ and $X_{m,q}$) which is introduced as random variable as well. The limit state function can be formulated by:

$$g(x) = 0 = \frac{\left(b-n_w(X_{d_r}*t+d_0)\right)\left(h-(X_{d_r}*t+d_0)\right)^2}{6} X_f X_{m,f} - \frac{(X_g+X_q X_{m,q})l^2}{8} \tag{7}$$

6.3 Error definition

The error function defined in equation 1 has to be adjusted for the relative code calibration, as the resulting mean reliability level β_{mean} would generally not meet exactly the target reliability β_t. Thus, equation 1 is extended with a weighted penalty term that vanishes for $\beta_{mean} - \beta_t$ (equation 8). The weight (10^5) is chosen such that the deviations get insignificant. Higher weights could lead to problems with the optimization for the first term.

$$error = \left(\sum_i \frac{(\beta_i-\beta_t)^2}{\beta_t^2}\right) * (1 + 10^5 * (\beta_{mean} - \beta_t)^2) \tag{8}$$

6.4   Probabilistic models

6.4.1   Dead load

The dead load is modeled with a normal distribution. The mean is chosen as defined in the structure and the coefficient of variation is 10 % (as in Baravalle et al 2017). The fractile value used is the mean value.

6.4.2   Live load

The fractile values for the three different live loads are chosen as given (recommended values) in the Eurocode 1 (2002). For the reliability analysis, the live loads are modeled according to the JCSS model code (2001). As fire is an accidental design situation, the point-in-time models from the JCSS model code (2001) are used directly, whereby only the gamma-distributed sustained load part is applied.

For the reliability analysis for the persistent conditions (used to check for which structures the fire situation is decisive), Monte Carlo (MC) simulations were used to derive the probabilistic representations for the one-year maximum live load by combining the sustained and the intermittent live load. 100'000 years of load history were simulated. A Gumbel distribution was then fitted to the tail ($0.7 < p < 0.9995$) of the yearly maxima by the least-square method. The area dependency of the live load was considered according to the JCSSS model code (2001).

6.4.3   Strength and resistance uncertainty

GL24h (EN 14080) is the material considered in the code calibration. The strength was not varied, as its effect would be similar to the varied beam length respectively the varied total load area acting on a column. The strength was defined from the fractile value according to the JCSS model code (2001). The following properties for bending and compression resulted: $f_{m,mean} = 31\ \text{MPa}, f_{m,std} = 4.65\ \text{MPa}, f_{c,mean} = 29.4\ \text{MPa}, f_{c,std} = 3.53\ \text{MPa}$.

The model uncertainty was modeled with a lognormal distribution with mean equal to unity and a coefficient of variation of 10 %, as used in the calibration for the next Eurocode 0 by Baravalle et al (2017).

6.4.4   Charring rate

The charring rate is modeled with a lognormal distribution with a mean of 0.67 mm/min and a coefficient of variation of 10 % (Frangi & Fontana, 2003). In the code format the charring rate for glulam is fixed at 0.7 mm/min as it is in the current Eurocode 5 (2004).

It could be assumed that the uncertainty on the charring *rate* reduces with increasing fire resistance time, respectively that the uncertainty on the charring *depth* increases under-linearly with the time. To proof this assumption, four solid timber panels (960x760 mm) made of vertical oriented timber boards with graded density from 390-490 kg/m3 from side to side in each specimen were tested in standard fire for 30/60/90/120 min respectively. The charcoal on the specimen was then removed and a 3D model of the remaining solid created. Analyzing the surface of the 3D model showed that the uncertainty on the charring rate is time independent and was between 9 % and 10 % in all specimens.

6.5   Implementation of the code calibration

The code calibration is performed in Matlab. For the reliability analysis the UQLab Framework (Marelli and Sudret 2014) was used. The first order reliability method (FORM) was used for the reliability calculations.

7   Results and discussions

All calculations were conducted with the lsf described above (equation 7). Setting both calibratable psfs to unity thereby corresponds to the current code. Three different code 'calibrations' for timber in fire are compared. Table 1 shows the results of the calibrations.

First the current Eurocode 5 (2004) was evaluated for the totally 970 structures, which returned a mean reliability of 3.937. This reliability then served as calibration target for two following calibrations.

Table 1: Overview of different calibrations. Partial safety factors in brackets were fixed and not calibrated. All calibrations lead to the same mean reliability level of 3.937.

	fractile	$\gamma_{m,fi}$	$\gamma_{d_{char}}$	error
Eurocode 5 (2004)	20 %	(1)	(1)	60.40
5 % fractile	5 %	(1)	0.96	140.2
calibrated	20 %	0.94	1.02	47.25

The first code calibration was done for the claimed 5 % fractile for the strength and with $\gamma_{m,fi} = 1$. This means, that only the psf on the charring rate $\gamma_{d_{char}}$ could be calibrated. As the mean reliability must stay the same, the calibrated $\gamma_{d_{char}} = 0.96$ was below unity. Only in the second calibration both psfs were calibrated and thus also a homogenization of the reached reliability levels was possible.

Despite the fact that the difference from 20 % to 5 % fractiles is equivalent to an increase of $\gamma_{m,fi}$ of around 11 %, $\gamma_{d_{char}}$ only reduces to 0.96 (from 1) when the reliability level is kept constant. This can be explained with the fact that a small change in the charring rate has a significant influence on the final geometry since the charring rate is multiplied with the fire resistance time.

Conversely, when the code format is calibrated for both psf, $\gamma_{m,fi}$ reduces to 0.94 while $\gamma_{d_{char}}$ increases relatively little to 1.02. As a psf below unity is generally not accepted, the same workaround as was done for Eurocode 5 (2004) by changing the fractile value could be applied here too. Keeping $\gamma_{m,fi} = 1$ would be equivalent to change the fractile from 20 % to 33.5 %.

The total calibration error is the best indicator for the homogeneity of the reliability level among the structures. The calibrated code format shows a lower error (47.25) than the current code format (60.40) and thus is slightly better. The use of the 5 % fractile however would result in a significantly worse calibrated code with a less homogenous reliability level and an error of 140.24. The same result is observed when comparing the reliability span (maximum difference in the reliability levels of the different structures). It is comparable for the current code and the calibrated code (0.42 respectively 0.39), but it is significantly higher with the 5 % fractile value (0.53).

Analyzing the structures separately it is observed that beams have a slightly lower mean reliability (3.920) than columns (3.953). This probably follows from the section modulus' quadratic dependency from the height, while the cross section only linearly depends on it. Nevertheless, the difference is small enough that the effect does not need to be covered in the code format.

Overall, the results for the current Eurocode 5 (2004) show that safety margin on the strength is slightly too high compared to the safety margin on the charring rate. . Albeit that the importance factors (section 6.1) clearly indicate the use of a psf on the charring rate, the calibrated $\gamma_{d_{char}} = 1.02$ is still close to unity. This is mainly because the charring rate in the code (currently) is 0.7 mm/min, while in the reliability analysis a mean of 0.67 mm/min with 10 % coefficient of variation is applied, which is equivalent to the 69 % fractile[5]. The claimed use of the 5 % fractile value for the strength in fire would result in a significantly less homogenously calibrated code than what we have currently. This prevents the harmonization with other material's codes.

8   Conclusion and outlook

The relative code calibration for timber in standard fire presented in this paper shows that using 20 % fractile values for the strength in fire is justifiable. However, the research indicates that it would be more appropriate to apply additional safety on the

---

[5] Note that a higher charring rate is conservative.

charring rate, i.e. by applying a safety factor or increasing the fractile value taken, and to slightly reduce the safety on the strength in fire. Using 5 % fractile values for the strength is not reasonable, as it reduces the homogeneity of the reached reliability levels of arbitrary structures significantly. As it is a relative code calibration, a statement whether the current code is safe enough cannot be made from this calibration, but it is rather presumed that the current reliability level is safe enough. Real world experience with modern timber buildings at least does not indicate a lack of safety.

In order to be able to perform a reliability analysis for a structure outside today's experience domain (i.e. outside the domain for which the current models lead to sufficient safety), the same knowledge gaps that also prevent an absolute code calibration must be faced. The most important one is a deep understanding of the mutual influence of fire and timber.

9 Acknowledgement

10 References

Ahrens, M. (2017) US Experience with Sprinklers. NFPA Research.

Baravalle, M. et al (2017) Reliability-Based Calibration of Partial Safety Factors in the Eurocodes. Appendix B in: Baravalle, M. (2017): "Risk and Reliability Based Calibration of Structural Design Codes. Dissertation. NTNU 2017:342.

De Sanctis, G. (2015) Generic risk assessment for fire safety. Dissertation. ETH Zurich

EN 1363-1 (2012) Fire resistance tests – Part 1: General requirements. CEN.

Eurocode 0 (2002) Basis of structural design. CEN. (EN 1990).

Eurocode 1 (2002) Actions on structures – Part 1-1 : General actions – Densities, self-weight, imposed loads for buildings. CEN. (EN 1991-1-1).

Eurocode 5 (2004) Design of timber structures - Part 1-1: General and rules for buildings. CEN. (EN 1995-1-1).

Eurocode 5 (2004) Design of timber structures - Part 1-2: General – Structural fire design. CEN. (EN 1995-1-2).

Fischer, K. et al (2012) Wirtschaftliche Optimierung im vorbeugenden Brandschutz. IBK Report. ETH Zurich.

Frangi, A., Fontana, M. (2003) Charring rates and temperature profiles of wood sections. Fire Mater. 2003; 27: 91–102 (DOI: 10.1002/fam.819)

JCSS model code (2001) Parts 1, 2.00, 2.01, 2.02, 3.00, 3.05.

Köhler, J., Fink, G. (2012) Reliability based code calibration of typical Eurocode 5 design equations. Proc. World. Conf. on Timber Engineering (WCTE2012), Auckland.

König, J. (2005) Structural fire design according to Eurocode 5--design rules and their background. Fire Mater. 2005; 29: 147–163.

Marelli, S., Sudret, B. (2014) UQLab: A framework for uncertainty quantification in Matlab. Proc. 2nd Int. Conf. on Vulnerability, Risk Analysis and Management (ICVRAM2014), 2554-2563, Liverpool (United Kingdom).

Massini, G. (2019) Safety concept of codes: why do fewer structures collapse than codes expect?. Master project thesis. ETH Zurich.

Östman, B. (2017) Fire safety in modern wooden houses – mapping of fire incidents in Sweden. International Fire protection. 9.2017.

Rackwitz, R. (2000) Optimization — the basis of code-making and reliability verification. Structural Safety. 22-1.

Richter, F. (2019) Heterogeneous kinetics of timber charring at the microscale. Journal of Analytical and Applied Pyrolysis. 2019; 138(3): 1–9. Schleich, J.-B. et al. (2002) Competitive steel buildings through natural fire safety concepts.

Schmid, J. et al. (2015) The Reduced Cross-Section Method for Evaluation of the Fire Resistance of Timber Members: Discussion and Determination of the Zero-Strength Layer. Fire Technol 201551: 1285–1309.

Schmid, J. et al. (2018) Timber under real fire conditions – the influence of oxygen content and gas velocity on the charring behavior. Journal of Structural Fire Engineering 2018; 9: 222–236.

Discussion

The paper was presented by R Fahrni

F Lam commented that the errors were based on sum of squares and it would be interesting to separate the errors into conservative versus non-conservative cases. R Fahrni agreed and said it would be interesting to study the cases where large errors occurred.

P Palma commented the structures did not take into consideration the behaviour of connections. R Fahrni said that a method to calculate the reliability of connections in fires would be needed.

U Kuhlmann appreciated the basic assumptions leading to the bias solution. It would be important to hold up the calibration process with relative code calibration to avoid making gross errors. R Fahrni agreed and said that there are always bias in models and true reliability would not be possible.

BJ Yeh was amazed by the difference between N. American and European approaches, especially in terms of reliabilities in fire. In N. America codes are calibrated to mean values rather than 20th percentile. R Fahrni responded that in N America the full load would be used but in Europe a reduced live load would be used. It seemed that making a reduction to live load would make more sense as the full design live load would be unlikely to occur in fire.

Investigations concerning screw-press gluing of assemblies with CLT

K. Bratulic, holz.bau forschungs gmbh, Competence Centre for Timber Engineering and Wood Technology, Graz, Austria

M. Augustin, holz.bau forschungs gmbh, Competence Centre for Timber Engineering and Wood Technology, Graz, Austria

G. Schickhofer, Institute of Timber Engineering and Wood Technology, Faculty of Civil Engineering, Graz University of Technology and holz.bau forschungs gmbh, Competence Centre for Timber Engineering and Wood Technology, Graz, Austria

1   Introduction

As an alternative to hydraulic presses, timber components can be joined by applying the so-called "screw-press gluing" (SPG). Thereby, the clamping capacity of screws is used to induce the needed contact pressure between timber members during the curing time of adhesive. The distribution and level of the realised contact pressure can be controlled by choosing an adequate screw-grid in accordance with the properties of the glued timber parts and clamping capacity of the used screws.

Beside reinforcing and repairing purposes (e.g. gluing plywood panels to reinforce openings), SPG is also convenient for the assembly of glued structural components (ribbed plates or boxed cross sections), non-standard cross-sections as well as moment resisting joints between elements (Figure 1.1).
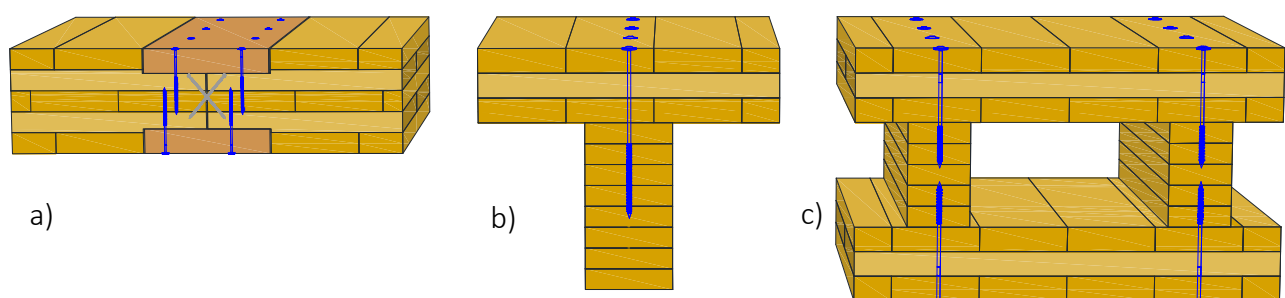

Figure 1.1. Application of SPG: a) moment resisting joint, b) CLT/GLT ribbed plate and c) CLT/GLT boxed cross-section.

Recommendations in the national annex to EN 1995-1-1 for Austria, ÖNORM B 1995-1-1 (2015) (rules regarding SPG adapted from DIN 1052:2004) are given for the general utilisation of screw spacings, regardless of the orientation of layers or the screw clamping capacities. The rules are restricted to element thicknesses between 20 and 45 mm for engineered wood products and 10 and 50 mm for solid wood boards. As known from the literature (e.g. Kairi et. al (1999)) the contact pressure realised with SPG is unevenly distributed and relatively low. If designed and implemented properly, SPG can indeed provide reliable bond lines. However, parameters investigated in all known studies so far are restricted to the mentioned element thicknesses.

The present contribution proposes a simplified analytical approach based on a beam on elastic foundation model which can be applied to optimize the screw-grid. Parameters include the type of the applied timber components, its thicknesses and the layup orientation, clamping capacities of screws as well as the minimum / basic bond line pressure. The focus in this paper is set on assemblies with cross-laminated timber (CLT) which exceed the thicknesses restricted in ÖNORM B 1995-1-1 (2015). Due to high stiffnesses of the examined system, if timber components are even slightly deformed, a high load is needed to compensate these deformations and thereby provide full surface contact between the elements. To quantify the necessary input parameters experimental investigations of the elements' planeness and the clamping capacity of screws were carried out. Finally, a calculation example is given followed by related experimental verifications.

1.1 General aspects regarding gluing with SPG

According to Kairi et. al (1999) SPG enables relatively low bond line pressures of 0.05 to 0.20 N/mm^2 (in comparison, common hydraulic presses provide pressures $\geq$ 1.0 N/mm^2). Therefore, to efficiently implement SPG, one needs to consider several parameters influencing the pressure distribution.

As stated in Baumann und Marian (1961) a standardized, optimum level of pressure cannot be defined for all combinations of adhesive types and gluing conditions. In their discussion they distinguished between two types of pressures: (a) an <u>outer, operating pressure</u>, which is mechanically applied onto timber components and (b) <u>the resulting, inner pressure</u> in the bond line. In practise they are never the same.

The outer pressure is inevitably higher since it is needed to compensate the local surface irregularities, to close all gaps and to squeeze out the exceeding amount of adhesive and/or captured air out of the bond line. Thereby a uniform and sufficiently thin bond line needs to be provided. In dependence on the curing behaviour of the adhesive, additional stresses can occur due to its shrinking or swelling behaviour, therefore it is important to maintain the pressure during the entire curing time. In any case, the requirements on the maximum allowed bond line thickness and the gluing conditions given by the adhesive producers must be respected. However, it is often not indicated what is the minimum / basic required pressure for the purpose of SPG, thus in this paper a value is adopted from literature.

1.2   Influencing components of SPG

The pressure in the bond line provided with SPG is a function of the following inter-connected components:

- screws

The level of the applied local force is directly related to the clamping capacity of screws, i.e. the pressed area under the screw head and the timber resistance perpendicular to grain (stiffness $E_{c,90}$ and strength $f_{c,90}$). The resulting pressure distribution is controlled by screw spacings and edge distances. The influence of parameters such as the thread length, the length of embedded shank and sequence of tightening remains to be analysed. Another point to be considered is the relaxation in timber and the related reduction of the screw force which is in reciprocal relation with the adhesive curing time.

- timber components

Certain wood properties, such as the timber density, the moisture content and the surface properties (surface treatment, cell structure and orientation of annual rings) affect the bonding quality by influencing the wettability and adhesive penetration. The pressure distribution is influenced by the bending properties of the covering and the response of the counterpart, which depend on the width and thickness (w and t) of the elements, Young's modulus parallel- and perpendicular to grain ($E_{c,0}$ and $E_{c,90}$) as well as the type of the applied load (screws and their spacings). Another important point for SPG are the possible distortions of timber elements to be glued such as twist, bow or cup. These discontinuities lead to the irregular occurrence of gaps and local contacts that make the formation of a uniform distribution of pressure even more difficult.

- adhesive system

Several adhesive types are available on the market and can be used for SPG. In many cases gap-filling adhesive types (e. g. phenolic and aminoplastic adhesives acc. to ÖNORM EN 301 (2015)) enabling bond line thicknesses up to 1.5 mm are the means of choice. If a bond line thickness of 0.3 mm can be guaranteed also polyurethane adhesives (acc. to ÖNORM EN 15425 (2017)) may be applied. Since SPG can be also applied on-site the attention has to be given to the environment conditions as well as the moisture content of the components at the time of gluing. Applying pressure with screws is not instantaneous for the entire surface as it is the case with hydraulic presses, so if larger areas need to be glued by SPG, the open time of adhesive should be kept in mind as well.

- production quality

A really important aspect of SPG is the quality of production. Beside the requirements for the standard gluing conditions (open time, curing time, etc.) an advisable distinctions for SPG include additional parameters related to production, such as the limitations on dimensional distortions of timber elements, a systematic sequence of tightening of screws, the usage of torque wrench (to reduce the unequal application of

screw forces), a larger amount of applied adhesive and the even spreading of the adhesive over the entire gluing surface. Since occasional human errors are unavoidable, it is essential to regularly inspect the production and the quality of the finalized bonds in the frame of a production control.

Gluing elements of larger dimensions, such as CLT/GLT ribbed plates, provides more uniform pressure distribution. Its production nevertheless requires special attention due to their higher stiffness and therefore higher necessary compensation load to even out inaccuracies. In order to use the most of what SPG components provide one should consider the interaction of several parameters and therefore, the standardized effective area per screw currently recommended for all SPG combinations needs a revision, for thin as well as for thicker timber components.

2 State-of-the-art

2.1 Standards and guidelines

The recommendations regarding SPG given in ÖNORM B 1995-1-1 (2015) are derived in its main parts from DIN 1052:2004. A brief overview of rules is given on an example of a moment resisting joint of CLT-elements (Figure 2.1.).

- design of SPG

The maximum allowed area per screw amounts to 15,000 mm^2 combined with a maximum screw spacing of 150 mm. Additional requirements given in ÖNORM B 1995-1-1 (2015) are depicted in Figure 2.1. Generally, the gluing process has to be carried out by manufacturers with an adequate certificate.
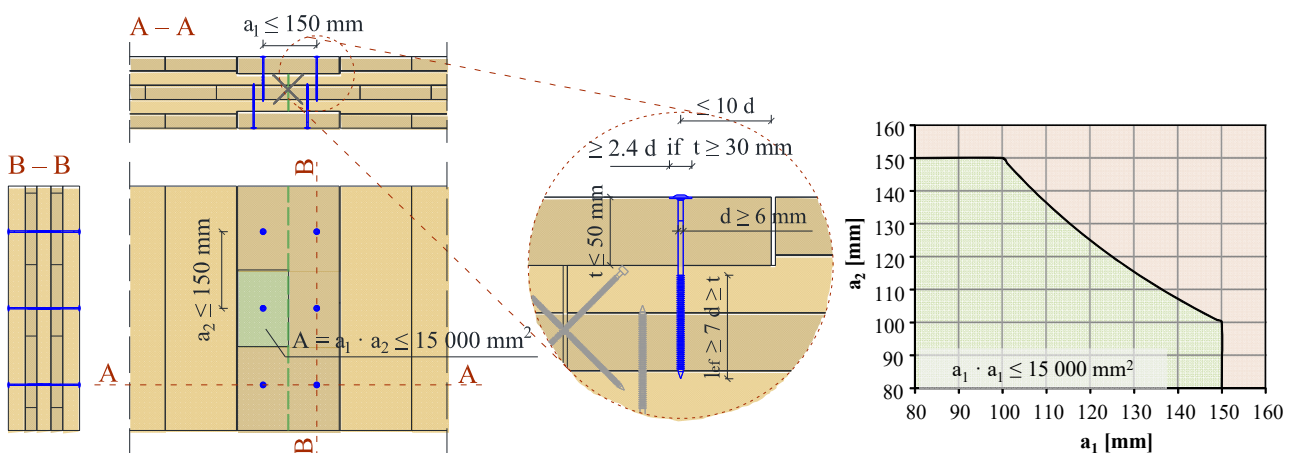
Figure 2.1. Overview: rules regarding SPG in ÖNORM B 1995-1-1 (2015)

- requirements on SPG components

For SPG partially or fully threaded screws with a diameter $d \geq 6$ mm has to be used, providing that no screw thread is present within the covering element. The thickness of the material to be glued is limited to 45 mm for solid timber and 50 mm for engineered wood products. If fully threaded screws will be applied, the covering needs to

be pre-drilled. Regarding the adhesive types, gap-filling adhesives should be used, but if a bond line thickness of 0.3 mm can be ensured, also adhesive acc. to ÖNORM EN 15425 (type I) and ÖNORM EN 301 may be applied.

- requirements on SPG conditions at the gluing stage

The conditions during the gluing process should meet the requirements given by the adhesive producer. The moisture content of the glued elements should not exceed 15 % and the difference in moisture between glued components should be less than Δu = 4 %. Timber surfaces should be planed or sanded at a maximum of 24 hours prior to gluing.

- verification of the bond line quality

ÖNORM B 1995-1-1 (2015) states that the bond line quality should be verified either by delamination or shear tests according to ÖNORM EN 14080 (2013). The shear strength of each specimen is limited to a minimum of 3 N/mm^2.

2.2   Published research

Despite the available research on either nail or screw press gluing stretches back to the 1970s, it is not easy to draw a comparison due to a broad variety of both, the applied materials as well as the research/test methods. Since the quality of adhesive bonds in SPG significantly depends on the interaction of all aforementioned components some of the authors tested additionally the same configuration but glued with a uniform and constant pressure which then represented the reference bond line quality. Most authors used shear tests to compare both gluing methods, SPG and the "ideal one". As representatives, the results of two research projects involving polyurethane adhesive are shortly described in the following.

Kairi et. al (1999) investigated SPG of ribbed panels assembled with the laminated veneer product Kerto-S using polyurethane adhesive and screws with a diameter d = 6 mm. He varied screw spacings, the amount of applied adhesive and moisture content of the material. The small specimens were cut out of the ribbed plates and tested in shear. Additional series were glued with a uniform pressure from 0.01 to 0.80 N/mm^2. When tested in shear the specimens with pressures between 0.03 and 0.10 N/mm^2 showed no considerable difference. Relating to SPG, the bond line quality of assemblies with a screw spacings of 400 mm and an amount of adhesive of 250 g/m^2 were evaluated as adequate. As an important fact Kairi et. al (1999) emphasized the importance of flat and smooth surfaces for SPG.

In a most recent study Schiere et. al (2018) investigated the quality of press gluing methods using polyurethane adhesives which require curing pressures starting from 0.1 up to 1.0 N/mm^2 (acc. to the technical data sheet as indicated by the authors). In their study three different pressure levels of 0.02 N/mm^2, 0.13 N/mm^2 and 0.20 N/mm^2 were compared when assembled in ideal conditions (by maintaining a constant level

of pressure by using a testing machine) and production conditions (by applying fasteners in a 150 mm spacing: scrails, screws with d = 5.0 mm and d = 6.0 mm respective to aforementioned pressure levels). For the former case, two boards with dimensions $t \cdot b \cdot l$ = 30·100·600 mm³ were glued together and for the latter a solid wood panel $t \cdot b \cdot l$ = 27·100·700 mm³ was jointed to a solid wood rib $t \cdot b \cdot l$ = 100·100·700 mm³. By analyzing the results of shear tests (acc. to EN 14080 (2013)) cut out of the glued samples only the specimen assembled with pressures of 0.13 N/mm² and 0.20 N/mm² passed the requirement in EN 14080 (2013). Additional series were glued applying a pressure of 0.13 N/mm² and simulating other conditions that can occur when gluing with fasteners: a) an uneven application of adhesive, b) constant gap of 0.3 mm, c) a wedge gap from 0 to 0.6 mm and d) maintaining a constant gap distance after applying the pressure on two adhesive types differing in their viscosity. For the cases involving intentionally produced gaps and the series with a low viscosity adhesive failed to fulfill the requirement in EN 14080 (2013).

In relation to the used materials, both studies report good bond line quality of SPG, even at low pressures, if straight and smooth elements are glued with an appropriate adhesive and its amount.

3 Methodology

The focus of the present contribution is set on two types of composites with CLT where SPG was applied: a) *plate-formed* as shown in Figure 1.1a, as well as b) *stripe-formed* (Figure 1.1b and c) – particularly on CLT/GLT ribbed plates.

In the first part of the study separate investigations of relevant influencing parameters of SPG-components were carried out (screw clamping capacity, minimum ("basic") bond line pressure, dimensional accuracy).

The results were used to define two main criteria: on one hand to determine the level of applicable pressure $p_{appl.}$ in the bond line and on the other to define the minimum pressure $p_{req.}$ required to ensure an adequate bond line quality. The latter one consists as a sum of two conditions: a) p_{IC} a state of "ideal gluing conditions (IC)" implies perfectly straight and even timber elements and b) p_{RC} the "real gluing conditions (RC)", which implies certain dimensional deviations of the timber members from the ideal planeness. To satisfy the requirements p_{appl} needs to top p_{req}.

$$p_{appl.} = \frac{F_{clamp}}{a_1 \cdot a_2} \quad > \quad p_{req.} = p_{IC} + p_{RC} \tag{1}$$

$p_{appl.}$	pressure in the bond line applicable with screws [N/mm²]
F_{clamp}	clamp force of a screw [N]
a_1, a_2	screw spacings parallel and perpendicular to the orientation of top layers [mm]
$p_{req.}$	required pressure in the bond line [N/mm²]

p_{IC} minimum "basic" bond line pressure for ideal gluing conditions [N/mm^2]

p_{RC} bond line pressure necessary to compensate dimensional irregularities of the timber members [N/mm^2]

4   Applicable clamping pressure

A distinctive feature of SPG is a high concentration of the bond line pressure underneath the screw head, that rapidly decreases with the growing distance from the screw. The rate of that decrease depends on timber properties: the same clamping force will enable a lower but wider and more uniform pressure when using thicker / stiffer components in contrast to high, but severely concentrated pressures in the case of thin components (Figure 4.1). It is important to emphasise that the screw-grid should be chosen in such a manner that no uplift between the screws appears.
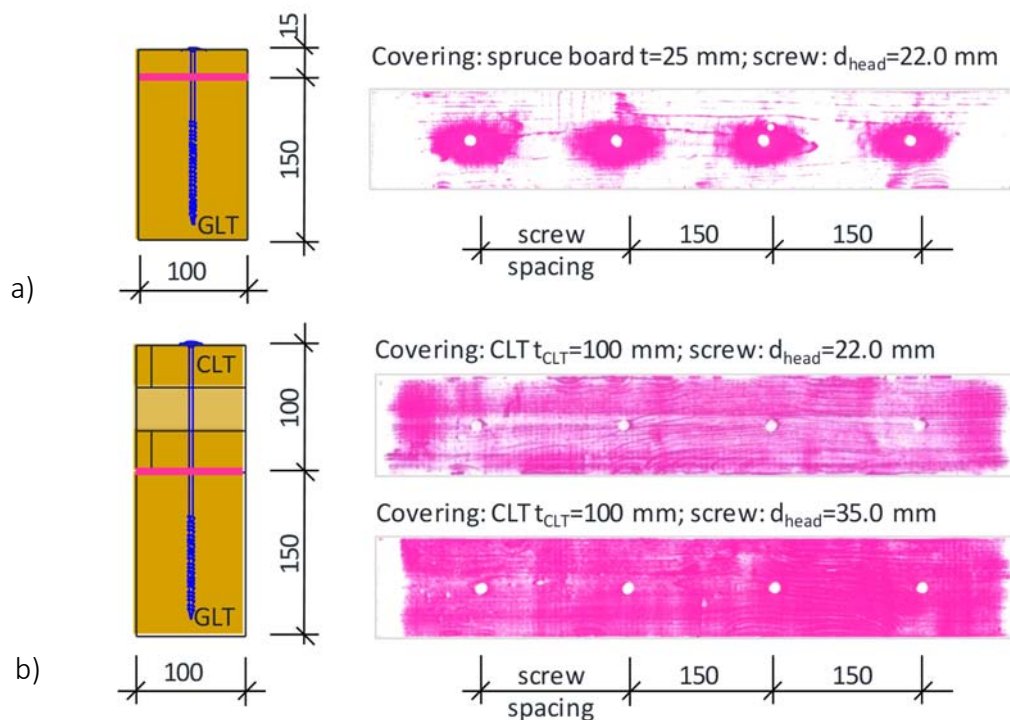
dimensions in mm

Figure 4.1. Qualitative representation of pressure distribution measured by placing a FUJI pressure measurement film (sensibility from 0.05 to 0.20 N/mm^2) between a GLT element and a) a covering made of solid spruce board with 15 mm thickness and b) a covering made of CLT with 100 mm thickness | screws spacings amounted to 150 mm (Bratulic, K. and Augustin, M. (2016))

4.1   Model for the determination of screw spacings

For plate-formed composites the pressure distribution in the bond line can be analysed as an orthotropic plate on elastic foundations loaded by concentrated loads (= screw loads). Their partial differential equation (neglecting the torsional stiffness of the plate) can be formulated as

$$B_x \cdot \frac{\partial^4 w(x,y)}{\partial x^4} + B_y \cdot \frac{\partial^4 w(x,y)}{\partial x^4} + k_0 \cdot w(x,y) = q_z(x,y). \tag{2}$$

To overcome the complexity of this formulation the simplification of the load sharing method proposed by Marcus (1929) can be applied. This approach follows the idea of a grid consisting of two beams (in x- and y-direction) orthogonally hinged on all four supporting lines. The single load (= screw load) acts in the crossing points of the beams and causes there the same deflection (w_x and w_y) (Figure 4.2a). If the loading at all supports should be the same, an equation interconnecting the stiffnesses (($E·I$)$_x$ and ($E·I$)$_y$) and the spans (l_x and l_y) in both directions can be formulated. With this equation, the plate equation degenerates into a grid of two beams that can be solved separately with common methods. The mathematical formulation can be written as

$$w_x = w_y = \frac{5 \cdot q_x \cdot l_x^4}{384 \cdot (E \cdot I)_x} = \frac{5 \cdot q_y \cdot l_y^4}{384 \cdot (E \cdot I)_y} \quad \rightarrow \quad l_y = l_x \cdot \sqrt[4]{\frac{(E \cdot I)_y}{(E \cdot I)_x}}. \tag{3}$$

This model can also be applied as an analogy to the more complex plate on elastic foundation. Since the stiffness of the beam is known from the pre-assumptions of the design, the "span" of the screw-grid can be chosen in a manner to assure a continuous contact pressure (no uplift) of the beam (Figure 4.2b)). The base component in this case is modelled as a set of closely aligned springs not mutually connected to each other, i.e. the vertical deformation of the spring is proportional to the amount of pressure acting on it (Winkler foundation).
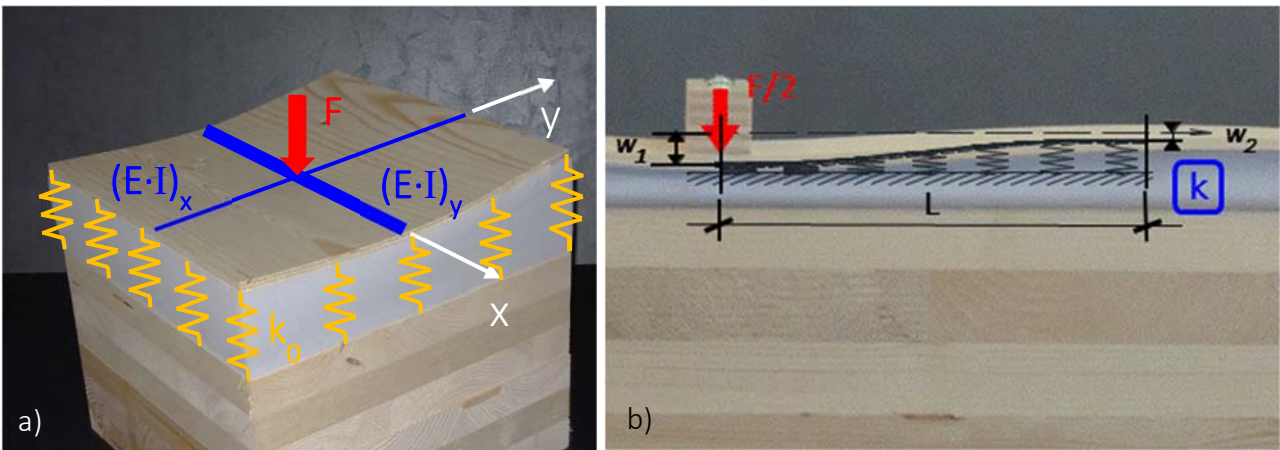

Figure 4.2. Model of the pressure distribution for SPG: visualisation of an elastically bedded a) plate and b) beam

This model can be expressed with the well-known ordinary fourth order differential equation of the beam on elastic foundation given by

$$w^{IV}(x) + 4 \cdot \beta^4 \cdot w(x) = -\frac{q}{E \cdot I} \quad \text{where} \quad \beta = \sqrt[4]{\frac{k}{4 \cdot E \cdot I}}. \tag{4}$$

E	modulus of elasticity (of the covering) [N/mm²]
I	second moment of inertia (of the covering) [mm⁴]

Solutions for this equation can be found in mechanical textbooks and/or papers (e.g. Eisenberger (1985)). By applying the boundary conditions given below, one can retrieve the deflection curve of the beam. Relating to Fig. 4.2 b) in particular the deflection "w_2" is of interest: an ultimate limiting condition is $w_2 = 0$. Since the pressure of the beam on elastic foundation can be calculated by $p = w \cdot k$, this is equivalent to the occurrence of no uplift stresses.

With the boundary conditions at the ends of the beam

$$w'(0) = 0, \ V(0) = F/2, \ w'(L) = 0, \ V(L) = 0 \tag{5}$$

an equation for the deflection "w_2" follows as

$$w_2 = y_2 = \frac{F \cdot \beta}{k} \cdot \frac{\left[\cosh(\beta \cdot L) \cdot \sin(\beta \cdot L) + \sinh(\beta \cdot L) \cdot \cos(\beta \cdot L)\right]}{\cos(2 \cdot \beta \cdot L) - \cosh(2 \cdot \beta \cdot L)}. \tag{6}$$

Finally, the distance until losing the contact can be calculated by the determination of the roots (width b of the beam taken as 1) as

$$a_1 = 2 \cdot L = 2 \cdot \frac{3 \cdot \pi}{4 \cdot \beta} = \frac{3}{2} \cdot \pi \cdot \sqrt[4]{\frac{4 \cdot E \cdot I}{k}}. \tag{7}$$

The only remaining unknown, the foundation modulus k, can be estimated as

$$k = \frac{E_{c,90,mean}{}^*}{t}. \tag{8}$$

$\quad E_{c,90,mean}$ mean MoE of wood in compression perpendicular to grain [N/mm²]

$\quad E_{c,90,mean}{}^*$ equivalent value of MoE of wood in compression perp. to grain [N/mm²]

$\quad t$ foundation depth; for SPG (as an engineering estimation) proposed as a 1/3 of the threaded screw length [mm]

The equivalent MoE value $E_{c,90,mean}{}^*$ follows from the strain stress state of the related volume loaded in compression perp. to grain. This value can be estimated from the stiffness matrix by setting the strains ε_L and ε_T to zero and calculating the equivalent MoE in radial direction. The following elastic parameters were used for the determination:

$$\begin{aligned} \nu_{LT} &= 0.01750 & \nu_{TL} &= 0.52500 & \nu_{LR} &= 0.02875 \\ \nu_{RL} &= 0.46000 & \nu_{TR} &= 0.71250 & \nu_{RT} &= 0.38000 \end{aligned}. \tag{9}$$

With these parameters the equivalent MoE follows as

$$E_{c,90,mean}{}^* \approx 1.42 \cdot E_{c,90,mean}. \tag{10}$$

For strip-shaped assemblies $a_2 = b_{rib}$. A proposal to restrict the maximum rib width $b_{rib,max}$ is given by the equation

$$b_{\text{rib,max}} \leq d_{\text{head}} + 2 \cdot t_{\text{CLT}} \ , \tag{11}$$

assuming a load distribution angle of $\alpha = 45°$ under the screw head over the CLT thickness t_{CLT}.

4.2 Experimental investigations on the clamping capacity of screws

The clamping of the components to be glued starts as the screw head comes into contact with the surface of the covering. The withdrawal along the screw thread in the counterpart is opposing to the compression under the screw head and further drilling-in the screw causes its elastic head embedment. The timber directly under the screw head undergoes plastic deformations and the process continues, until one of the following failure modes occurs: (i) head-pull through, (ii) withdrawal failure or (iii) screw (tensile) failure. To realize the required clamping pressure the system needs to withstand the embedment of the screw head just beneath the surface of the covering.

However, the head-pull through capacity f_{head} as defined in ÖNORM EN 1383 (2016) is going to be distinguished from the clamping parameter f_{clamp}. This is the fact since the application of screws for the purposes of SPG requires only minor embedment depth of screw head and does not nearly reach a failure as defined in ÖNORM EN 1383 (2016), namely by pulling the screw through entire specimen thickness. f_{clamp} was investigated in detail by Fürst (2019) who carried out a test program with approx. 700 tests. The following parameters were varied: (a) screw types (countersunk and washer head screw) and (b) diameters (from 9 to 22 mm) in combination with different (c) timber products (1- and 3-layered solid wood panels, OSB, solid timber boards and plywood (spruce and beech)) and (d) thicknesses of timber specimens. Thereby the thicknesses of the tested products were respected, so not every series satisfied the condition on minimum specimen thickness as given in ÖNORM EN 1383 (2016). As noted in Schiere et. al (2018) a deeper embedment of the screw head results in higher compression and higher pull-through resistance resp. In Fürst (2019) the clamping capacity f_{clamp} was evaluated at a point when the top of the screw head was embedded 2 mm below the timber surface, so the embedment depth was adopted individually for each screw type as a sum of the screw head thickness plus additional 2 mm. In Figure 4.3. results obtained in such manner are compared with the ones acc. to ÖNORM EN 1383 (2016) (based on the complete head-pull through failure). As expected, the evaluation approach adopted in Fürst (2019) resulted in lower clamp capacities and a smaller spread of the data. Further evaluation with the "absolute embedded depth" shows a considerably lower influence of the screw head diameter on the characteristic clamping capacities while a decreasing trend was found for evaluation acc. to ÖNORM EN 1383 (2016).
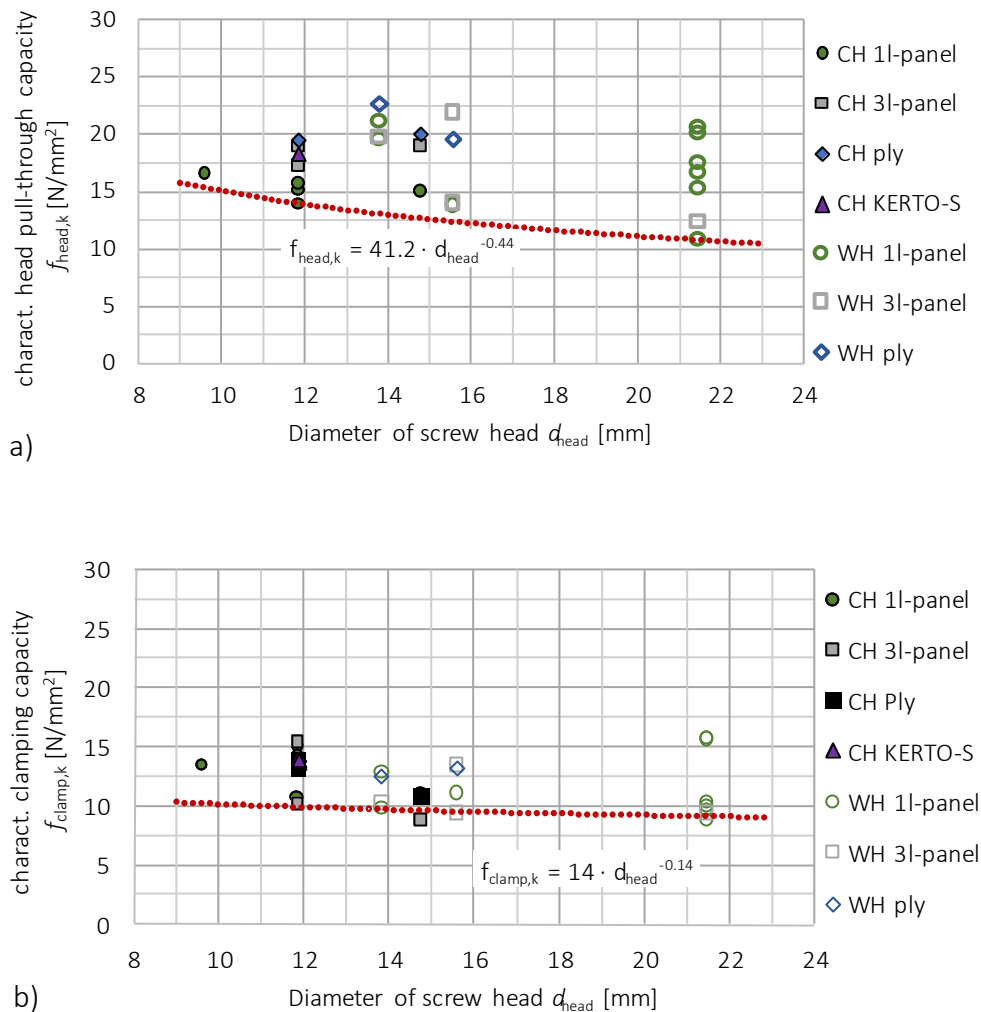
Figure 4.3. Results of the test campaign of Fürst (2019) on applicable clamping capacities of screws in products of spruce; tested acc. to ÖNORM EN 1383 (2016) – charact. values are given for 10 specimen per series: a) head-pull through capacity evaluated acc. to ÖNORM EN 1383 (2016) and b) evaluation acc. to the absolute embedment depth of the screw head + 2 mm

* Denotations: (CH) … countersunk screw, (WH) … washer head screw, (1l- panel) … 1-layer solid wood panels, (3l- panel) … 3-layer solid wood panels, (ply) … plywood
** Values calculated regarding a reference density of $\rho_{mean} = 350 kg/m^3$ with $(\rho_i / \rho_{mean})^{0.8}$

For the clamping capacity of spruce timber products a characteristic clamping capacity $f_{clamp,k} = 14.0 \cdot d_{head}^{-0.14}$ N/mm² is proposed as a result of the tests. Due to the higher density, a much higher level could be found for beech plywood ($f_{clamp,k} \geq 25.0$ N/mm²). Although the behavior of countersunk and washer head was different in the tests (for spruce products) no significant influence could be found on the related charact. value of the clamping capacity.

Higher clamping forces can be applied by placing larger washers under the screw head with consideration of sufficient thread length in the counterpart. A further possibility is offered by the application of double threaded screws with a different thread pitch enabling clamping in the threadless spacing between the two threaded parts.

4.3 Relaxation of the clamping force

Due to the rheological behaviour of timber under the screw head loaded in compression perp. to grain the clamping force is not constant but time dependent. For SPG this effect can be considered by a relaxation factor k_{relax} defined as

$$k_{relax} = \frac{F_{t=t1}}{F_{t=t0}} .$$

(12)

$F_{t=t1}$ force at a certain time t_1 (proposal: t_1 = 3 h) [kN]

F_{t0} initial force (in Schiere et. al (2018) denoted as a peak of load) [kN]

In the present study the relaxation factor k_{relax} (valid for spruce) was estimated based on the results of a small test series (n = 6) following ÖNORM EN 1383 (2016) but contrary to continuously increasing load, a defined deformation of 7 mm was applied and the accompanying force was measured for a duration of three hours. The tests were conducted on CLT-specimens (t_{CLT} = 100 mm) using single screws Ø 8 mm and two different head diameters: first applied directly with screw head (d_{head} = 22.0 mm) and the second one using a washer (d_{head} = 35.0 mm). In these tests a reduced force after three hours of about 30 % could be recognized (Fig. 4.5.). Thus, the relaxation factor could be estimated as $k_{relax} \approx 0.30$. It should be mentioned that this factor will be influenced by the tightening sequence of SPG, in general decreasing this factor.
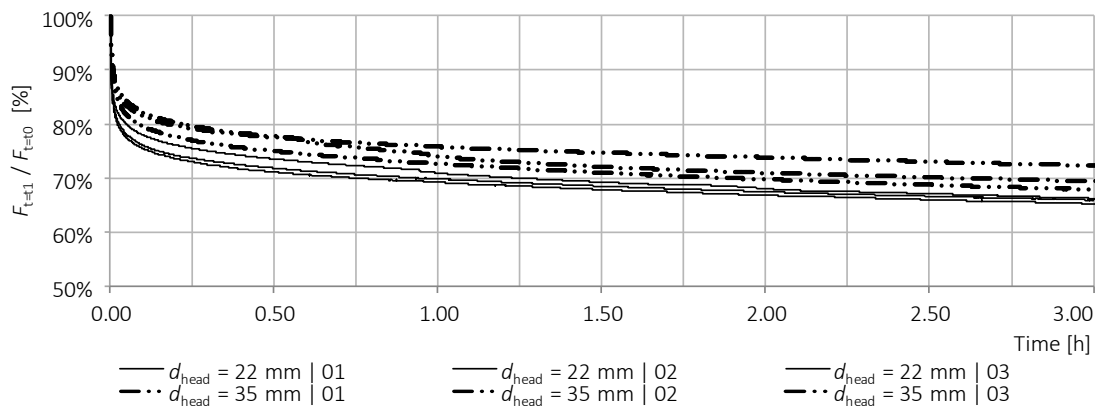

Figure 4.5. Test series for determination of relaxation of timber under screw head: test setup acc. to ÖNORM EN 1383 (2016) with modification of load application (constant deformation 7 mm)

5 Required clamping pressure

5.1 SPG in ideal conditions

If ideal conditions are assumed the applied screw-grid needs to provide a minimum ("basic") curing pressure p_{min} which depends on the interaction of the adhesive and the timber members. p_{min} is necessary to: a) spread the adhesive evenly over the entire bonding surface, b) to enable a sufficient penetration of adhesive in pores, c) apply

additional stresses which are specific to the curing type of adhesive (shrinking or swelling) and d) to force out the excess of adhesive and air, so that the uniform bond line can be formed within the restricted thickness prescribed by the adhesive manufacturer. It also includes the compensation of timber surface irregularities (e.g. mentioned in Grüll et.al (2014): surface roughness of 140 µm) caused by the surface treatment methods (e.g. planing or sanding).

For the purpose of the present study the necessary pressure p_{min} was estimated by tests as 0.10 N/mm^2 (compare also with Stapf (2014)).

5.2   SPG in real conditions

The term "real conditions" as used in the given context implies dimensional deformations of timber elements, such as warps, cups and/or twists of timber members. For example, such deviations are the longitudinal curvature of glulam ribs in ÖNORM EN 14080 limited to 4 mm on a 2 m distance. Despite the common application of automated and highly sophisticated inspection systems in industry, no specific measurement data on geometric irregularities could be provided by several producers. Therefore an experimental campaign was carried out to estimate the irregularities occurring in practice and implement them in the analytical approximation of the compensating pressure.

5.2.1   In-situ measurements of production accuracy

The production accuracy of CLT and GLT elements was measured at four different production plants in Austria. The development of the applied test procedure and the measurements were carried out in cooperation with the Institute of Engineering Geodesy and Measurement Systems at Graz University of Technology. A detailed description of the equipment and procedure is provided in Bauer (2017). The applied method is a kind of "surface scan", where the surface is measured by moving a round prism (Taylor-Hobson prism MS 60) over the specimens' surface as shown in Figure 5.1., while the laser beam from the total station (AT 402, Leica Geosystems) continuously tracked and recorded the change in position of the prism.
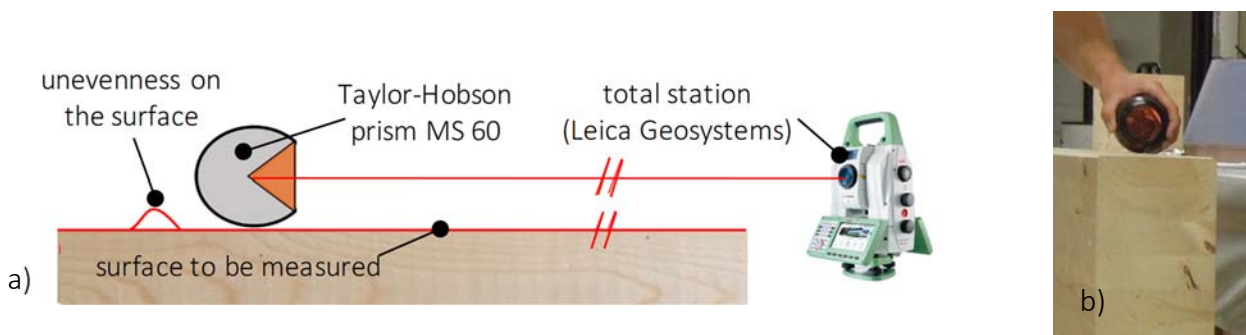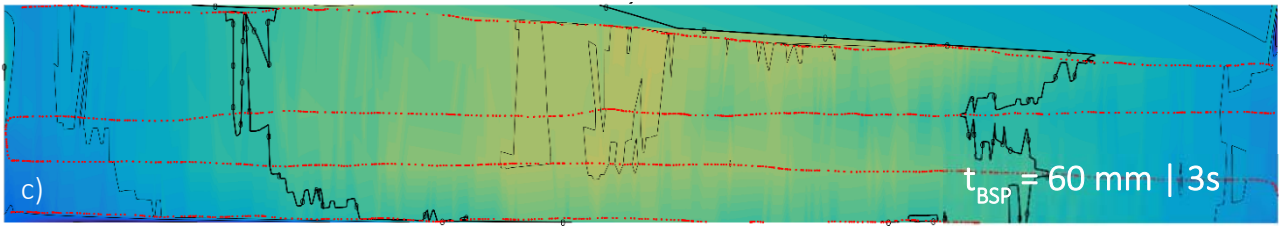
Figure 5.1. In-situ measurements of the dimensional accuracy of CLT: a) test-setup, b) surface measurement and c) data processing of measured surface.

For the evaluation the recorded measurement data were merged in the software package Matlab R2016a and surface profiles were generated (see Fig. 5.1.c)). A section through this surface allows the evaluation of the dimensional accuracy over the entire length of a specimen. Deformations f were evaluated as a height difference in the centre of the lag distance that was set to 2 m (Figure 5.2.). The lag distances were shifted in steps of 5.0 cm over the entire profile length in x and y-direction.
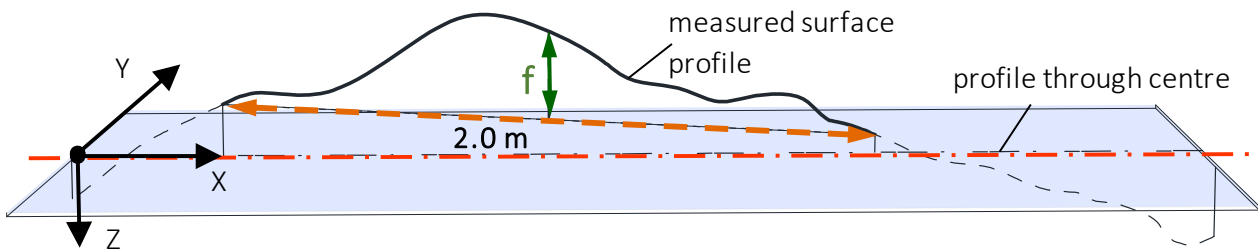

Figure 5.2. Shematic example of the evaluation of dimensional irregularities

Test results are summarized in Table 1., where measurements are divided according to producers (A to D) and the type of the product (CLT or GLT). The width of the CLT elements is not specified since most of the tested plates did not have a rectangular shape and had openings. The denotation $\Delta (M_1 - M_2)_{max}$ represents the maximum differences between two measurements M_1 and M_2, which were carried out on a same test sample but from different positions of the total station. While an excellent accuracy of ± 0.1 mm was reached under laboratory conditions, the "real" conditions proved to be more challenging. In a couple of cases the measurements in the plants were excluded since they showed deviations between two measurements of the same surface larger than 1.0 mm. The maximum differences between two measurements $\Delta (M_1 - M_2)_{max}$ were added to the maximum measured deformation of test sample f_{max} to take the worst case scenario into account. As a result the measure of geometrical irregularities for SPG of CLT/GLT ribbed plats is set to 2.5 mm / 2 m.
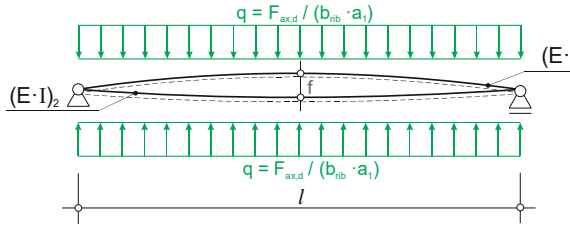
Table 1. Evaluation of dimensional irregularities of CLT and GLT.

Producer	Product	Thickness [mm]	Width [mm]	$\Delta (M_1 - M_2)_{max}$ [mm]	f_{max} [mm]	$f_{max + \Delta M}$ [mm]
		60	-	0.276	0.469	0.764
A	CLT*	60	-	0.330	0.879	1.209
		120	-	0.299	0.272	0.570

		120	-	0.486	0.220	0.706
		95	-	0.960	1.136	**2.100**
B		140	-	0.616	0.636	1.252
		140	-	0.663	0.727	1.390
		120	160	0.708	1.036	1.744
C		120	160	0.563	0.930	1.495
		160	200	0.709	1.719	**2.493**
		160	200	0.653	0.990	1.643
	GLT	100	160	0.955	0.843	1.798
		120	160	0.767	0.995	1.762
D		160	160	0.832	0.924	1.756
		200	440	0.823	0.814	1.643
		200	440	0.502	0.859	1.361

5.2.2 Analytical approximation for the geometrical irregularities

As a simplified approach two curved beams were considered in the further calculations as a type of geometrical irregularity. To estimate the compensating pressure necessary to level out the curved form of the elements, the expressions for deflection of simply supported beams with continuous load (for both CLT and GLT) were coupled $f = f_{CLT} + f_{GLT}$ as given by

$$f = f_1 + f_2 = \frac{5}{384} \cdot q \cdot l^4 \cdot \left[\frac{1}{(E \cdot I)_1} + \frac{1}{(E \cdot I)_2} \right]$$

$$p_{RC} = \frac{q}{b_{rib}} = \frac{1}{b_{rib}} \cdot \frac{384}{5} \cdot \frac{f}{l^4} \cdot \left[\frac{(E \cdot I)_1 \cdot (E \cdot I)_2}{(E \cdot I)_1 + (E \cdot I)_2} \right] \quad (13)$$

Figure 5.1. Shematic representation of the deflected beams (left) and the expressions for the estimation of the compensating load (right)

6 Calculation example and experimental investigation

To illustrate the proposed design procedure, a calculation example of a CLT/GLT ribbed plate is shown below. The example refers to the assembly of a single GLT rib to CLT plate (Figure 6.1.) by means of screws arranged in one row using polyurethane adhesive.

Input parameters:

$CLT: \underline{40} + 20 + \underline{20} + 20 + \underline{40}$ mm $\quad$ GL24h acc. EN 14080 $\quad$ Screw

$b_{CLT} = 600$ mm $\qquad\qquad\qquad b_{GLT} = 140$ mm $\qquad\qquad d = 8.0$ mm

$t_{CLT} = 140$ mm $\qquad\qquad\qquad t_{GLT} = 240$ mm $\qquad\qquad d_{head} = 22.0$ mm

$E_{0,mean} = 11\,600$ N/mm^2 $\qquad\quad E_{0,mean} = 11\,600$ N/mm^2 $\;\, l_{screw} = 260.0$ mm

$I_{Y,CLT} = 1.27 \cdot 10^8$ mm^4 $\qquad\quad E_{c,90,mean} = 300$ N/mm^2 $\;\, l_{thread} = 100.0$ mm

$I_{Y,CLT}* = I_{Y,CLT}/b_{GLT} = 2.11 \cdot 10^5$ mm^3 $\;\, E*_{90,mean} = 426$ N/mm^2 Assumption for p_{RC}

$\qquad\qquad\qquad\qquad\qquad\quad I_{Y,GLT} = 1.61 \cdot 10^8$ mm^4 $\qquad f = f_{CLT} + f_{GLT} = 2 + 2 = 4$ mm

$\qquad\qquad\qquad\qquad\qquad\qquad\qquad\qquad\qquad\qquad\quad l = 2,000$ mm

Calculation:

APPLICABLE PRESSURE p_{appl} $\qquad\qquad$ REQUIRED PRESSURE $\;\; p_{req}$

Foundation modulus k (rough estimation) $\qquad p_{IC} = 0.10$ N/mm^2

$$k \approx \frac{E*_{c,90,mean,GLT}}{l_{thread}/3} \approx 12.8\,\text{N/mm}^2 \qquad p_{RC} = \frac{1}{b_{GLT}} \cdot \frac{384}{5} \cdot \frac{f}{l^4} \cdot$$

Screw spacing

$$\qquad\qquad\qquad\qquad\qquad\qquad\qquad\qquad \cdot \left[\frac{\left(E_{0,mean} \cdot I\right)_{CLT} \cdot \left(E_{0,mean} \cdot I\right)_{GLT}}{\left(E_{0,mean} \cdot I\right)_{CLT} + \left(E_{0,mean} \cdot I\right)_{GLT}} \right]$$

$$a_1 = \frac{3}{2} \cdot \pi \cdot \sqrt[4]{\frac{4 \cdot E_{0,mean,CLT} \cdot I_y*}{k}} = 784\,\text{mm} \qquad\quad = 0.11 \text{ N/mm}^2$$

Screw force $\qquad\qquad\qquad\qquad\qquad\qquad p_{req} = p_{IC} + p_{RC} = 0.21$ N/mm^2

$$F_{clamp} = \frac{14 \cdot d_{head}^{-0.14} \cdot d_{head}^2}{1 + k_{relax}} = 3.38\,\text{kN}$$

$k_{relax} = 0.3$ ...relaxation factor of the applicable screw force

Applicable pressure $\quad p_{appl} = \dfrac{F_{clamp}}{a_1 \cdot b_{GLT}} = 0.03\,\text{N/mm}^2$

Adopted screw spacing / applicable pressure:

case I: $\;\; a_1 = 100$ mm $\;\to\; p_{appl} = \dfrac{F_{clamp}}{a_1 \cdot b_{GLT}} = 0.24$ N/mm^2 $> p_{req} = 0.21$ N/mm^2

case II: $\;\; a_1 = 450$ mm $\;\to\; p_{appl} = \dfrac{F_{clamp}}{a_1 \cdot b_{GLT}} = 0.05$ N/mm^2 $< p_{req} = 0.21$ N/mm^2

6.1 Experimental investigation on the bond line quality

The two calculated cases were assembled by means of SPG in an Austrian CLT production plant using a polyurethane adhesive (Henkel HBS 709; applied amount: ≈200 g/m²) and partially threaded washer head screws Ø 8 mm with l / l_{thread} = 260 / 100 mm. The first case approximated the requirement on the maximum effective area per screw given in the standard with 14,000 mm², while the second one was over three times larger, amounting to 63,000 mm². Figure 6.1. shows a cross section of the assembled ribbed plate as well as the ground plan including the arrangement of small test specimens. These were cut out after curing of the adhesive and tested acc. to ÖNORM B

1995-1-1 (2015). This code states that one can choose to test the SPG bond line quality by <u>either</u> shear or delamination tests. In order to investigate the efficacy of both validation types, the presented test program included in total 60 shear tests (shear area = 50x50 mm^2) and 40 delamination tests (core diameter d = 100 mm and height h = 260 mm). The position of the specimens in the ribbed plates was varied in relation to the screws (each 10 samples per series): (i) under the screw, (ii) between the screws in the middle of the rib and (iii) between the screws at the edge of the rib (shear tests only). Delamination tests acc. to ÖNORM 14080 (2013), procedure B were carried out at the production plant where the components were assembled. Only delamination of the bond line between the plate and rib was evaluated (Delam$_{TOT}$). The shear tests were tested with a universal testing machine. The bond line thickness was measured prior to each test with a digital microscope camera with a magnification of 55.8. After the tests the sheared area was examined with an UV light to check the percentage of failed adhesive.
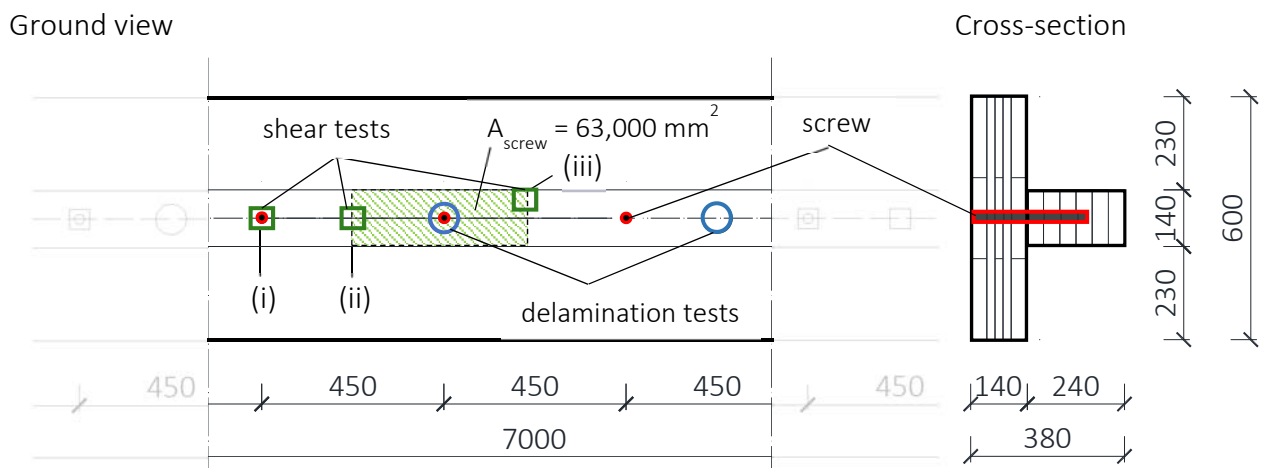

Figure 6.1. Test plan for the bond line quality tests of CLT/GLT ribbed plates glued with SPG (depicted here for CASE II of the calculation example)

Figure 6.2. shows the results of the shear tests. The crossed values represent specimens which did not satisfy the condition acc. to ÖNORM 14080 (2013). Two specimens had to be disregarded due to the presence of finger joints and knots. The mean value of density amounted to 464 kg/m^3 (CoV: 23 %) and a mean value of the moisture content u = 11.8 % (CoV: 4.95 %).
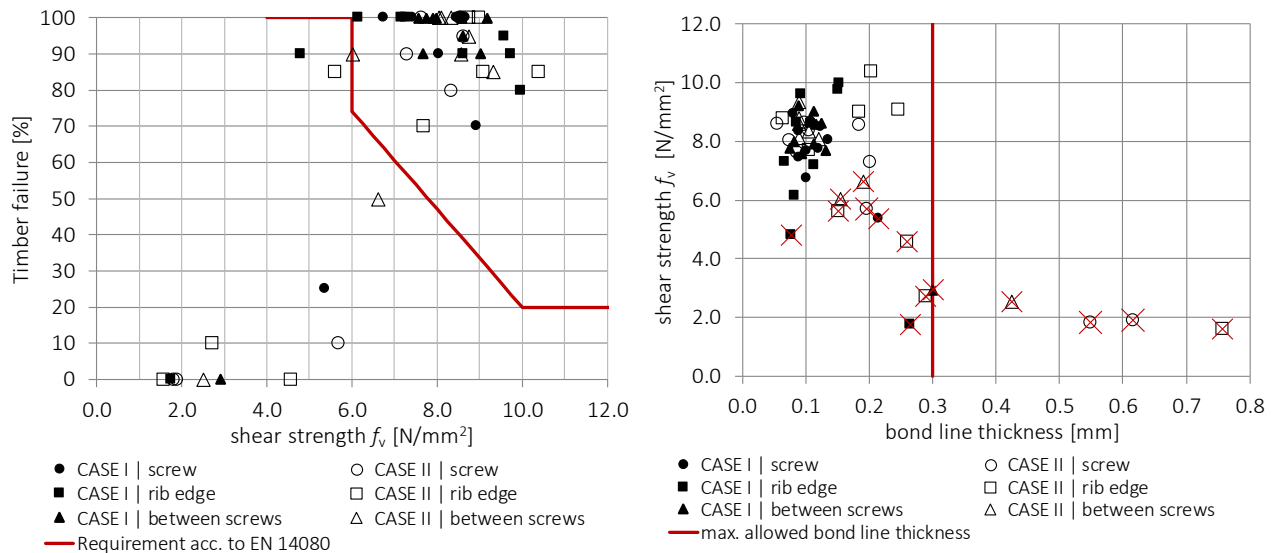
Figure 6.2. Results of shear tests acc. to ÖNORM EN 14080 (2013): a) relation of shear strength to percentage of timber failure and b) relation of shear strength to bond line thickness

The spread of the bond line thicknesses and the amount of timber failure in the shear tests were in general larger in CASE II (screw distance 450 mm). Eight of 28 specimen with a lower shear strength had an adhesive failure. The same type of failure was also evident in four (of 30) samples in CASE I (screw distance 100 mm). No specific trend could be noticed when comparing the position of the test specimen in relation to the position of the screws in the composite member.

Regarding delamination tests, seven of 14 specimens (50 %) in CASE II did not satisfy the condition acc. to ÖNORM 14080 (2013). Additional six delaminated pieces were disregarded since they showed knots or pith at the adherend surfaces after separation. Only two samples of 20 (10 %) in CASE I failed in delamination.

The delamination procedure does expose the specimen to severe conditions reflecting the aging process during the service time of a product and, at least from the small test campaign presented, it shows more sensitivity to deficient bond lines. It is therefore recommended to include it as a compulsory test procedure when it comes to the evaluation of the bond line quality of SPG.

7 Conclusion and recommendations

The present contribution investigated the correlation between the main influencing factors on SPG and proposed a simplified analytical approach for an optimised design of the screw-grid. The following conclusions can be drawn:

- General requirement for the SPG: $\quad p_{appl} = \dfrac{F_{ax}}{a_1 \cdot a_2} \quad > \quad p_{req} = p_{IC} + p_{RC}$

- Proposal for the determination of maximum screw spacings a_1 and a_2 based on a beam on elastic foundation model: $a_i = \dfrac{3}{2} \cdot \pi \cdot \sqrt[4]{\dfrac{4 \cdot E \cdot I}{k}}$

- Determination of max. allowed rib width in CLT/GLT ribbed plates is proposed as:
$$b_{rib,max} \leq d_{head} + 2 \cdot t_{CLT}$$

- Clamping parameter of screws for SPG was determined based on tests acc. to ÖNORM EN 1383 (2016) at the point of head-pull through deformation which was adopted as the screw head thickness + 2 mm

- Adopted charact. value of the clamping parameter for screws (for SPG) valid for wood and engineered wood products from spruce: $f_{clamp,k} = 14 \cdot d_{head}^{-0.14} \left[N / mm^2 \right]$

- By carrying out an experimental investigation on dimensional irregularities focused on CLT and GLT elements, production inaccuracies f_{CLT} and f_{GLT} were estimated to about 2.5 mm / 2 m

The proposed simple model is given in a general form, so that new, improved values can be easily implemented. For example, this could be the consideration of other screw types with higher clamping capacities (e.g. double threaded screws), adhesive systems which need a lower minimum pressure during the curing time, or even timber components with higher production accuracies than the ones suggested in the present contribution (if a producer can ensure them).

Furthermore, it is essential to regularly verify the quality of SPG bonds since it is very sensitive to production boundary conditions as well. However, current standards (ÖNORM B 1995-1-1 (2015) and ÖNORM EN 14080 (2013)) do not offer a uniform set of rules. This leaves place for the producers to choose between two types of tests (shear or delamination tests), specimen geometry (drill core or rectangular shape) or/andits dimensions, which may influence the results. Therefore, there is a necessity for further review on the impact that those variables have on the results.

The present contribution shows that the high potential provided by CLT in terms of a more uniform distribution of pressure in the bond line is restricted by the high forces necessary to compensate production inaccuracies. Instead of maintaining the current dense screw spacings, it should be elevated if higher applicable clamping forces or a smaller inaccuracies of the gluing surface can be ensured. Of course, under the assumption that an adequate production quality of SPG is provided as well.

8   References

ÖNORM B 1995-1-1 (2015): Eurocode 5: Design of timber structures – Part 1-1: General – Common rules and rules for buildings – National specifications for the implementation of ÖNORM EN 1995-1-1.

ÖNORM EN 14080 (2013): Glued laminated timber and solid timber – Requirements.

ÖNORM EN 301 (2015): Adhesives, phenolic and aminoplastic, for load-bearing timber structures — Classification and performance requirements.

ÖNORM EN 15425 (2017): Adhesives - One component polyurethane (PUR) for load-bearing timber structures -Classification and performance requirements.

ÖNORM EN 1383 (2016): Timber structures – Test methods – Pull through resistance of timber fasteners.

Bratulic. K. and Augustin, M. (2016): Screw Gluing - Theoretical and Experimental Study on Screw Pressure Distribution and Glue Line Strength, WCTE 2016.

Bauer, P. (2017): Formbestimmung von Holzelementen mittels Oberflächenmessung Master Thesis, Graz University of Technology, Institute of Engineering Geodesy and Measurement Systems (in German).

Baumann, H. and Marian, J.E. (1961): Der Verleimungs-Preßdruck als Funktion physikalischer Faktoren, Holz als Roh- und Werkstoff, 19/(11), p. 441-446. (in German)

Eisenberger, M. and Yankelevsky, D. (1985): Exact stiffness matrix for beams on elastic foundation, Computers & Structures, Vol. 21, No. 6, pp. 1355-1359.

Fürst, H. (2019): Überprüfung und Optimierung der Regelungen für streifen- und plattenförmige Schraubpressverklebungen in ÖNORM B 1995-1-1, Master Thesis, Graz University of Technology, Institute of Timber Engineering and Wood Technology (in German).

Grüll, G., Wegschneider, A., Neumüller, A. (2014): Hobelqualität von Brettschichtholzlamellen, Holzforschung Austria, Vienna (in German).

Kairi, M., et. al (1999): Screw gluing Kerto-LVL structures with Polyurethane, OTA-WOOD publication, Helsinki University of Technology, Laboratory of Wood Technology, VTT Building Technology.

Marcus, H. (1929): Die vereinfachte Berechnung biegsamer Platten, Springer, Berlin, 1929 (in German).

Schiere, M., Franke, S., Franke, B. (2018): Investigation and analysis of press glued connections for timber structures, Research report, Bern University of Applied Sciences, Institute for Timber Constructions, Structures and Architecture.

Stapf, G., Aicher, S. (2014): Einfluss des Pressdrucks – Möglichkeiten und Grenzen der Niedrigdruck-Vakuumverpressung bei der Herstellung von geklebten Holzbauteilen (in German).

Z-9.1-765: 1K-PUR-Klebstoffe LOCTITE HB S109 bis S709 PURBOND für die Verklebung tragender Holzbauteile, 28th September 2021 (in German).

Discussion

The paper was presented by K Bratulic

M Li received confirmation that the screws were for pressure and most manufacturers would not take them out after. He commented that as clamping forces were important how were they measured. K Bratulic responded that the pull through test method for flat head screws were conducted and from the results one could establish the clamping forces based on the deformation of the press-in depth. M Augustin added that the clamping force could be measured with strain gauges in screws and also under the screw head; this was done.

S Franke asked would one get 5 mm insertion in timber in press screwing. K Bratulic responded that the 5 mm was used as an example only. The absolute deformation value was defined as screw head height + 2 mm as press in depth.

S Franke and K Bratulic discussed the dependence of clamping force on bond quality.

S Franke asked why only small specimens and not full width specimens were extracted. K Bratulic responded that this was done to check local effects.

T Lim commented about the pressure film technique and received confirmation on where they were applied.

H Blass asked whether the self weight of the beam was considered. K Bratulic said no.

H Blass commented that if the webs do not have the same depth one would need to pull up the web which would further reduce the pressure.

S Aicher agreed that the pull through strength of individual screws would be important in screw press application. He commented about the dense spacing of screws and the graph of shear strength. He asked what was the explanation for the low values of shear strength. He also stated that the German code was amended to take care of the influence of thicker plates.

K Bratulic responded on the relationship between bond line thickness versus shear strength, mentioning that in some cases even though bond line thickness was small, failure was observed. S Aicher said may be one should not allow screws with countersunk head as it would provide localized deformation. M Augustin commented that they were not happy with the shear tests for CLT and there were issues with the delamination tests.

S Aicher commented that the normalized pull through capacity should be equal for all types of screws but washer head screws seemed to be better.

S Franke asked if the mean values were checked. K Bratulic said no. S. Franke received clarification of the amount of PU glue applied and that it was not dependent on glueline thickness at this range.

Catenary Action for Cross-laminated Timber Floor Systems

Hercend, Mpidi Bita, Structural Engineer, Mass-timber Component Design, Equilibrium-Katerra, Vancouver, Canada; hercend.mpidibita@katerra.com

Thomas Tannert, Associate Professor, Wood Engineering, University of Northern British Columbia, Prince-George, Canada; thomas.tannert@unbc.ca

Keywords: Mass-timber buildings; Disproportionate Collapse Prevention; Robustness

1 Introduction

1.1 Robustness of CLT Platform-type Construction

In recent years, the design of mid-rise cross-laminated timber (CLT) platform-type buildings has become a part of regular structural engineering practice (Tannert et al. 2018). Platform-type construction is characterized by CLT floors supported on top of CLT walls to form the platform for the next level, see Figure 1. In this configuration, all walls are loadbearing and are used as part of the lateral and/or gravity lateral load-resisting systems. Figure 1 also shows conventional connections for this structural system: off-the-shelf angle brackets fastened with screws or nails for the joints between floor and wall above, and self-tapping screws (STSs) inserted at 90 degrees for the joints floor-to-floor as well as floor-to-wall below.

Although platform-type CLT buildings demonstrated good performance (Brandner et al. 2016; Izzi et al. 2018), studies on structural robustness and disproportionate collapse prevention for this construction type are scare (Huber et al. 2018) and are often left solely to the designer's engineering judgment. With an increase in building height and occupancy level, considerations for structural safety after extreme events become more relevant. As an indirect approach for achieving robustness, ensuring minimum tie-forces at the joint levels, with adequate strength and stiffness for structural integrity, allows the load distribution to the undamaged parts of the building in case of initial damage, e.g. the loss of a single vertical supporting element. Further, ductility is required to trigger collapse-resistance mechanisms that allow the building to maintain its load-carrying capacity while supplying the deflections required after initial damage.

To ensure robustness, catenary action is preferred as a floor system collapse-resistance mechanism to prevent debris loading on the floor below (Mpidi Bita et al. 2018) However, conventional connection detailing for CLT platform-type buildings are primarily designed for regular gravity and lateral loads. Consequently, generic tie-force

requirements approach found in the EN1991-1-7 (CEN 2006) and the Timber-Frame (TF 2000) guideline (Milner et al. 2003) are neither practical nor economic. Available technical guidance (STA 2017) is essentially conceptual and limited to general recommendations and no design guidelines on catenary action for floor systems in CLT platform-type construction exist. This brings concerns over the structural performance for this systems, hence the need for further research.
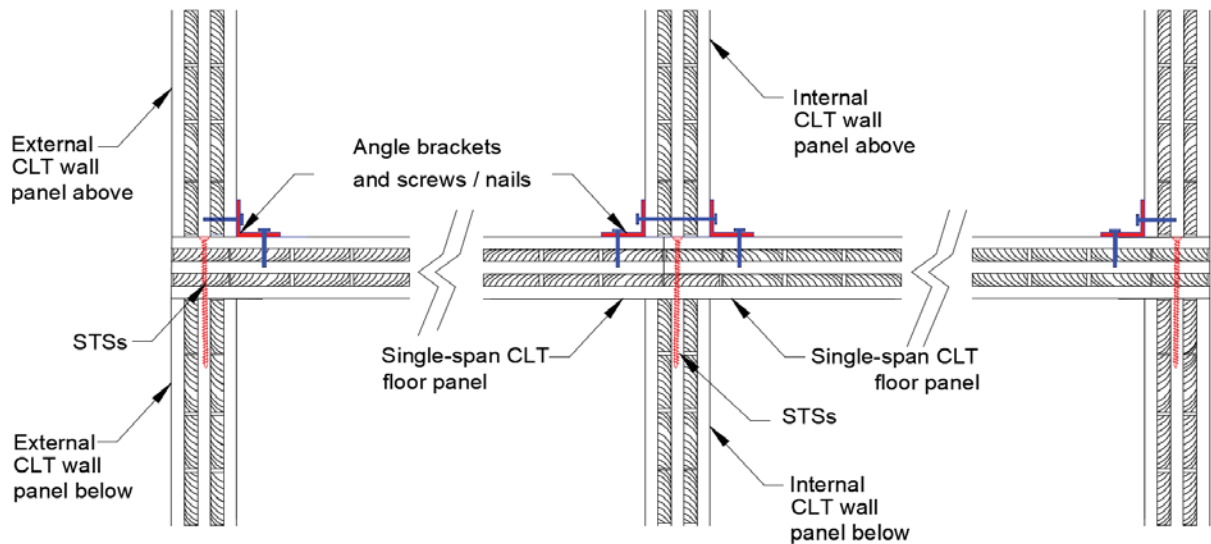

Figure 1: CLT Platform-type Construction

1.2 Catenary Action and Novel Connection Detailing

After internal wall removal, there are two main collapse-resistance mechanisms that allow the floor system carry the applied loads, preventing debris loading on the level, below which can trigger further collapse (Stevens 2008; Stylianidis et al. 2016). The first, compressive arching, develops at deflections $d < \Delta < 2{\times}d$, where d is the floor depth, with its maximum force (F_c) at $\Delta{=}d$. The second, catenary action, develops at $\Delta > 2{\times}d$ when the floor system is laterally restrained. Typically, its maximum force (F_t) occurs at $\Delta \geq 8\%$ and 10% of the floor span (L) for laterally restrained steel and concrete floors, respectively. Here, any increase in floor deflection is associated with a linear increase in load-carrying capacity demands. Therefore, catenary action is often seen as the ideal floor system collapse-resistance mechanism to prevent disproportionate collapse (Stevens 2008; Stylianidis et al. 2016).

The aforementioned deflections usually represent limits, defined as acceptance criterion, beyond which the building exhibits high probability for disproportionate collapse. Previous studies (Mpidi Bita et al. 2018; Mpidi Bita & Tannert 2019) demonstrated that available guidance for catenary action (CEN 2006; DoD 2013) are neither practical nor economic for CLT platform-type construction, as they are mainly based on steel, concrete and light-frame timber structures. In addition, given the limited capacity and deformation-supply of conventional connections used for CLT

platform-type constructions when loaded in shear (Hossain et al. 2018), the feasibility to trigger catenary action has to be questioned. Therefore, there is a need to investigate novel connection detailing to propose improved tie-force procedures for structural robustness for this type of construction.

Previous studies (Schneider et al. 2018, Mpidi Bita & Tannert 2018) demonstrated that steel tubes shown in Figure 2a have the axial strength, stiffness and ductility to be used as hold-down connection that carry large uplift forces. It is anticipated that if implemented as floor-to-floor connection in addition to conventional connections, this novel detailing can allow CLT floor systems to meet the axial resistance and ductility required to trigger catenary action. Figure 2b illustrates the installation process: i) the tubes are installed to both sides of the rods, ii) the connectors are first placed on top of the CLT floor panels with predrilled holes and slots, and iii) then they are pushed into their final position as illustrated in Figure 2c.
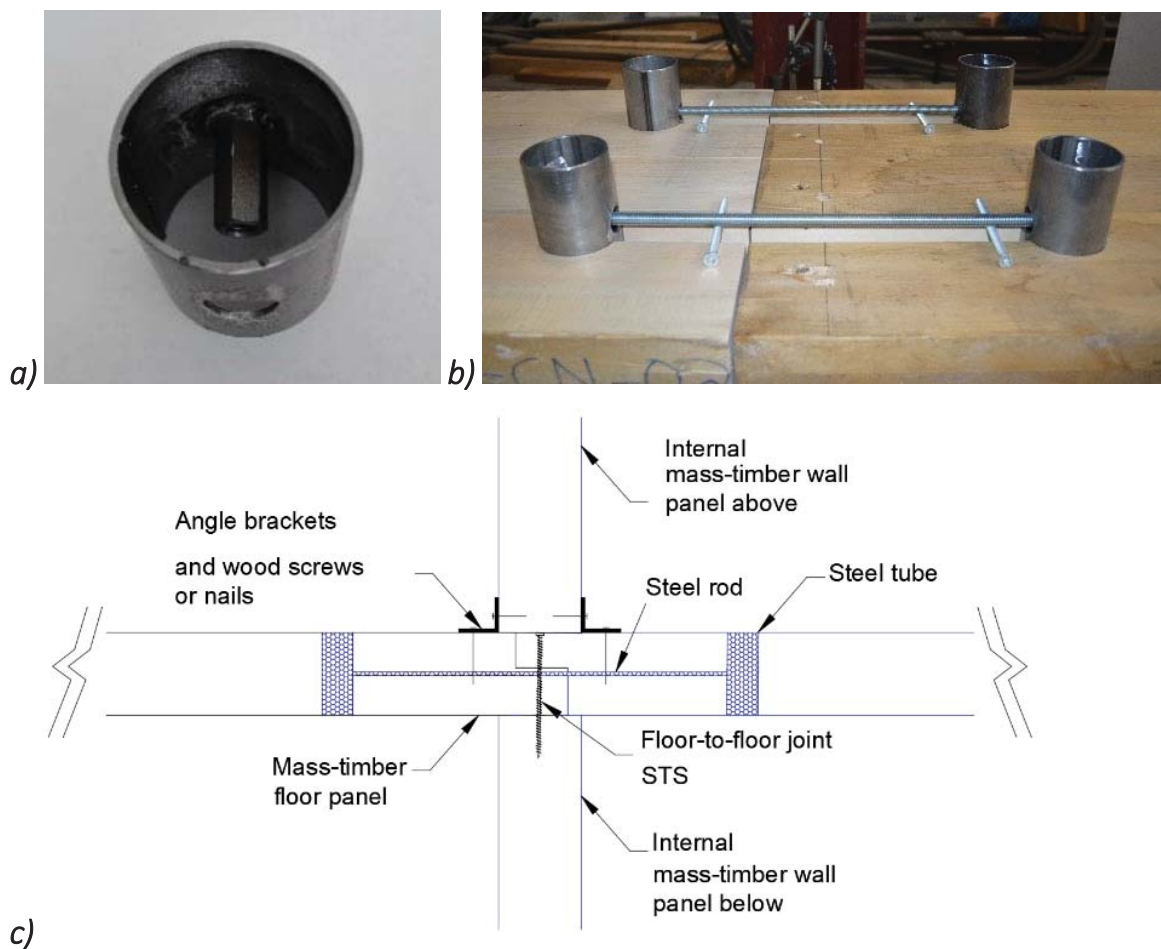

a)   b)

c)

Figure 2: Novel steel tube connection detailing: a) tube, b) tubes before installation sequence, and c) schematic representation of the joint

2   Objectives

Experimental studies that demonstrate the ability CLT floor systems to develop catenary action following the loss of internal loadbearing walls enable to quantify their performance in terms of strength and stiffness, as well as the maximum deflections that the floor can sustain before collapse, setting acceptance criterion for disproportionate collapse prevention. The first objective of the research presented herein is to propose deflection acceptance criteria, based on testing CLT platform-type floor systems with both conventional and novel connection detailing. The second objective is to analytically evaluate the required tie-force and deformation demands necessary to trigger catenary action of CLT platform-type construction.

3   Experimental and Analytical Investigation

3.1   Materials

The tested CLT floor panels were 5ply, 139mm (35-17-35-17-35) thick and 580mm wide. The floor system was platform-type construction, as shown in Figure 1, composed of two segments spanning 1,980mm (*L*), connected at mid-span, and simply supported over the external walls. The walls were 5ply CLT and 425mm high. The CLT panels were *E1* stress grade, as per CSA-O86 (2016).

To investigate the influence of the mid-span connections for possible catenary action, two different floor configurations were considered for testing: i) with conventional floor-to-floor connection detailing, noted as *CLT-Trad*, and ii) with novel floor-to-floor detailing, noted as *CLT-Novel*. Two specimens were used for each configurations. The considered detailing emphasised on the axial performance of the floor-to-floor joint, with the floor-to-wall connections designed for overstrength with negligible contributions on the axial deformation-supply of the system.

Conventional floor-to-floor connection was composed of lap-joint with four fully threaded STS, 8mm diameter and 120mm long, spaced at 150mm on centre. With the same spacing, four partially threaded STS, 8mm and 300mm long were connected the floor to the external walls. The angle brackets were spaced at 300mm, fastened with 18 4mm diameter ring-shank nails on the wall and floor panels. The novel tube connection detailing, spaced at 300mm on centre, was installed for the floor-to-floor joint over the internal wall. The steel tubes had 76.2mm diameter and 3mm thickness, while the steel rods had a diameter of 12.7mm.

3.2   Methods

To study catenary action, a displacement was applied at the location of the removed wall, as shown in Figure 3a. The anticipated collapse mechanism was one-way bending along the span with negligible contribution in the transverse direction. The rate of loading was 25mm/min; the test stopped when the 250mm maximum actuator stroke

was attained. The 250mm deflection represented 12% of *L*, which is within the deflection acceptance criterion for catenary action. The vertical load-carrying capacity (*F*), corresponding to the applied deflection (*Δ*), can be estimated for residential and office buildings of 5m × 5m typical gridlines, up to ten storeys, with 2.4kPa and 1.0kPa as floor live and dead loads, respectively.

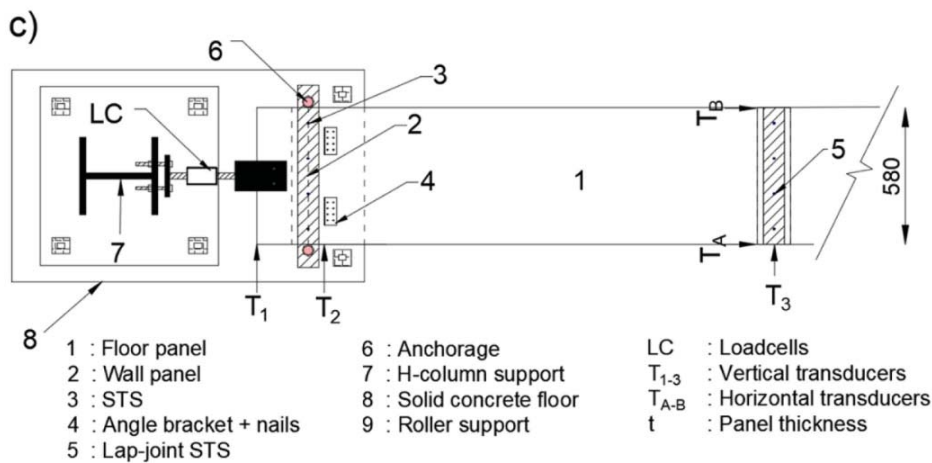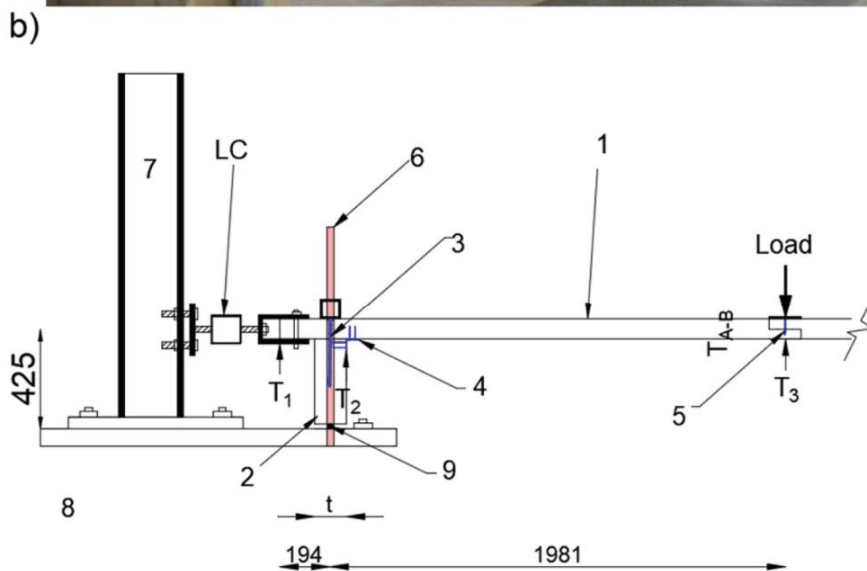|				
1 : Floor panel	6 : Anchorage	LC	: Loadcells
2 : Wall panel	7 : H-column support	T_{1-3}	: Vertical transducers
3 : STS	8 : Solid concrete floor	T_{A-B}	: Horizontal transducers
4 : Angle bracket + nails	9 : Roller support	t	: Panel thickness
5 : Lap-joint STS			

Figure 3: Test setup: (a) Photo, (b) Elevation view schematic, and (c) Plan view schematic

The floor specimens rested on the laboratory floor on one side and on roller support on the other side to minimise shear effects and friction on the base. In a platform-construction, the weight of the floor above the damaged level provide additional stability. To represent this scenario, anchorage was used to clamp the floor panels on the walls. These restraints, maintained during the entire test, also ensured that all axial deformations (δ) were exclusively provided by the floor-to-floor connections. Furthermore, to mimic the bays adjacent to the damaged area, axial restraints were considered at both ends of the floor panels using the loadcells (LC) after the external walls. These lateral horizontal supports, installed at the neutral axis of the floor system, were important for possible catenary actions, transferring the tie forces. At the floor-to-floor connection, the tests recorded the applied deflections and the axial deformations to quantify the deformation compatibility. At the floor-to-wall connections, measurements were done for the axial forces using the LC.

3.3   Analytical Tie-force Procedure

To estimate the required tie-force (F_t) for catenary action, linear elastic procedures based on engineering mechanics could be utilised. Here, F_t is derived through equilibrium of moments: the applied moments for a simply supported system, point-loaded at mid-span ($M_z = F_t{\times}2L/4$) equal the resisting moment ($M_r = F_t{\times}\Delta$). Furthermore, given that catenary action is only mobilised at large deformation, the analytical procedure considered a nonlinear factor (NF) to reduce the elastic F_t and obtain realistic behaviour. To develop catenary action, compatibility between the vertical deflection (Δ) and horizontal deformations (δ) should be ensured. Assuming that the CLT panels were rigid in-plane and all axial deformations were supplied by the floor-to-floor connections alone, the provided connection detailing should meet the δ demands, which can be estimated from trigonometry of the deformed shape of the floor system under the applied Δ.

4   Results and Discussion

4.1   Load-carrying Capacity

Figure 4 shows deformed shape of the tested specimens. This confirmed that the CLT panels remained rigid while all δ were supplied by the connectors alone for compatibility between δ and Δ. Figure 5 shows the forces (F) plotted against the applied mid-span deflection (Δ). Consistency in the load-deformation response was observed for all CLT floor panels, for both traditional (*CLT-Trad*) and novel (*CLT-Novel*) connection detailing: an initial elastic condition (Stage 1), then compressive action (Stage 2), followed by possible catenary action (Stage 3). The elastic condition was observed up to Δ<20mm, representing 1% of the floor span (L=1,981mm).

Figure 4: Specimen deformed shape of the floor system

Stage 1 was controlled by the connection stiffness in the longitudinal direction; and *CLT-Novel* was found to be stiffer than *CLT-Trad*. The average maximum compressive arching (F_{com} =9kN) in Stage 2 occurred at Δ=70mm, corresponding to the floor effective depth (d) for all floor assemblies. At Stage 2, the behaviour was ductile; supplied by the axial stiffness and shear deformation of the STS.

At the end of Stage 2 (Δ>2×d or 8% of L), when F_{com} dropped to zero, *CLT-Trad* assemblies were not able to trigger catenary action given the limited shear strength and deformation capabilities of STS. The load-deformation curves showed a ductile behaviour until the maximum deflection (Δ=250mm) was attained. After failure of STSs, for *CLT-Trad*, resistance against collapse was supplied by axial restraints at the floor-to-walls, in addition to the bearing between the two floor segments at the lap joint as shown in Figure 7a. The observed average maximum load-carrying capacity (F_{max}) of this system with conventional floor-to-floor detailing was 15kN.

Given the high axial strength and large axial deformation capabilities of the steel tube and rod detailing, *CLT-Novel* assemblies were able to reach Stage 3 and develop catenary action. When triggered, catenary action allowed the *CLT-Novel* floor system to carry more load while undergoing large deformations, observed at Δ>2×d. In this study, after the maximum Δ=250mm or 12% of L, no failure was observed, and F_{max}=30kN. This finding highlights the advantage of *CLT-Novel* over *CLT-Trad* systems, in terms structural safety and disproportionate collapse prevention.
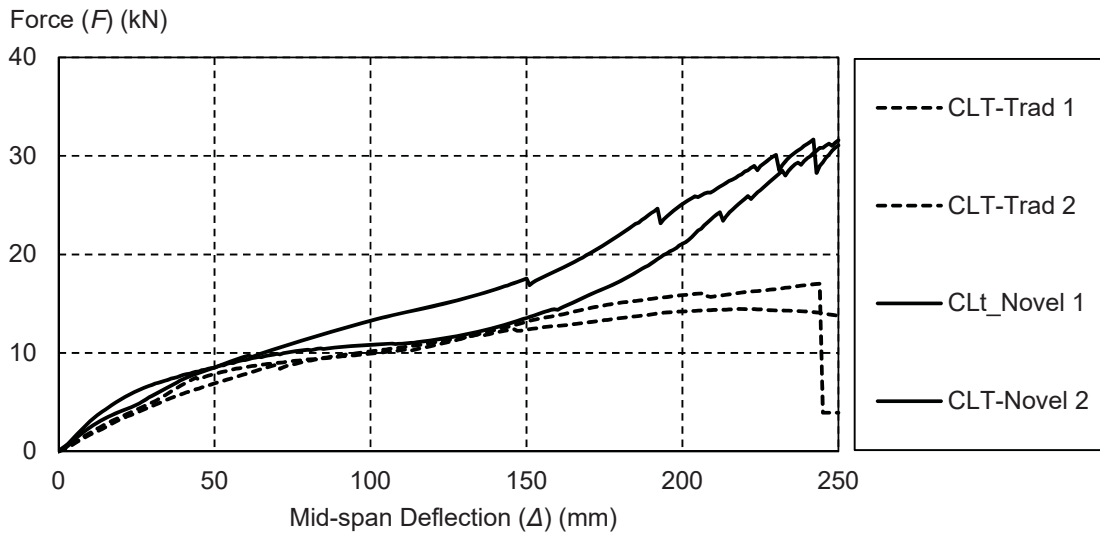
Figure 5: Vertical forces against applied deflection curves

4.2   Tie Forces

Figure 6 shows the curves of the axial (tie) forces (F_t) plotted against the applied Δ, for the tested assemblies. Given that F_t was recorded at the neutral axis of the floor assemblies, its value was negligible at Stage 1 when the behaviour is elastic. Stage 2, where the compressive arching was formed, was noted by wood crushing at the top fibre of the section (see Figure 7a). The aforementioned ductile behaviour at Stage 2 was confirmed in Figure 6 with the tie forces increasing with the increase in the applied Δ. For CLT floor assemblies with lap joint STSs (*CLT-Trad*), the collapse acceptance criterion could therefore be taken as 8% of *L*, with a maximum tie-force F_t=20kN. For CLT floor systems with adequate axial strength and ductility, e.g. *CLT-Novel*, 15% of *L* could be considered as the acceptance criterion as the floor assemblies were able to carry F_t=65kN without failure.
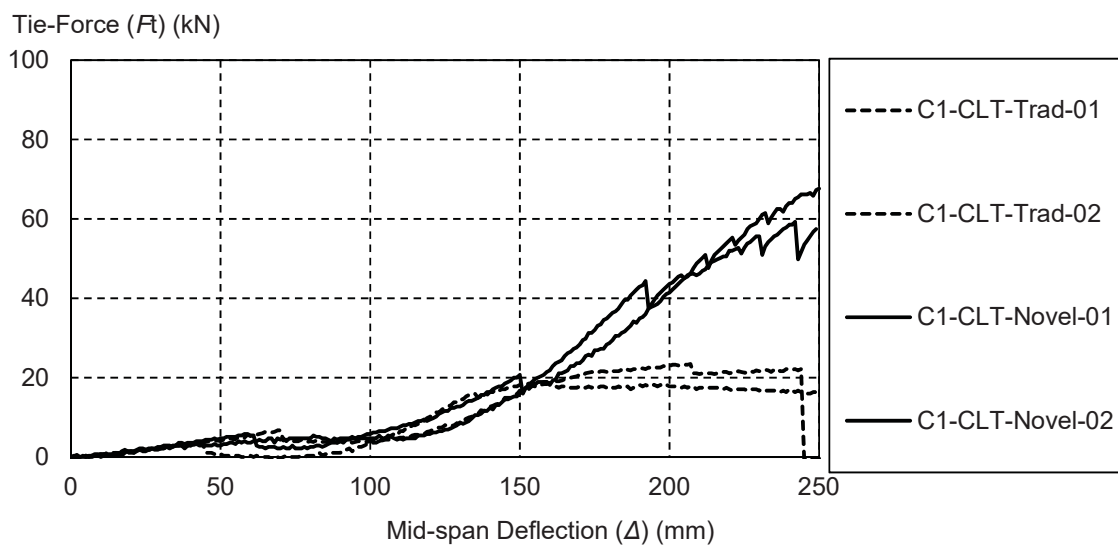

Figure 6: Tie-force against applied deflection curves

During catenary action, the axial deformations at the floor-to-wall connections were negligible. The novel detailing held the floor segments together until the maximum deflection, see Figure 7a. At Δ=150mm, the average δ was measured to 11mm for *CLT-Trad*. After failure of STSs in shear due to the applied tie-force, the axial deformations of the entire floor assembly were supplied by the steel tubes alone. The axial forces pulling the steel rods caused buckling of the tubes at the area connecting to the steel rods, as shown in Figure 7b. The axial deformations were measured to 7mm on tubes on either sides of the detailing. The additional deformations resulted to δ=25mm for *CLT-Novel* floor assemblies. To ensure robustness, this detailing localised all failure at the tubes while the wood member remained undamaged. The robustness of the novel detailing would also be relevant for building rehabilitation, where the system could be re-used after replacing the damaged components.
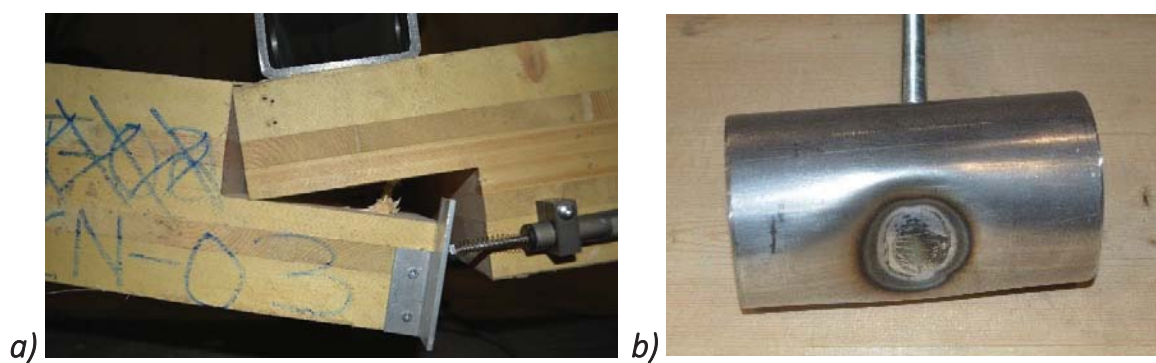

Figure 7: Connection deformation: (a) lap joint with STSs, and (b) steel tube buckling

4.3   Tie-Force Procedure

For disproportionate collapse prevention, for the considered maximum floor loads of 3.4kPa and 5m span, the floor system should be able to carry 34kN per meter width at the location of the removed wall. This load demand could only be met by *CLT-Novel* assembly given that failure was not observed after F_{max} =30kN, corresponding to Δ=250mm. These results also confirmed that the floor system cannot rely on compressive arching alone for disproportionate collapse prevention given the small d; CLT floor systems with conventional connection detailing were not robust. For catenary action of CLT floor assemblies, a nonlinear factor (NF= 0.55) should be applied to F_t calculated from linear elastic equilibrium ($F_t = F_{max} \times L / 2\Delta$) to account for the nonlinearity associated to the required large deformations. This value was obtained by comparing the tie-force (F_t=118kN), at Δ=250mm with average F_{max}=30kN, calculated analytically against the average values observed during the tests (F_t=65kN). This study also demonstrated the importance of connection ductility; to meet the large deflection, large axial deformations capabilities of the connections is prerequisite. Here, a minimum axial deformation of δ=25mm, supplied by the tubes (2×7mm) and the STSs (11mm), was required at the floor-to-floor connections in order to achieve a deflection Δ=250mm for catenary action.

5 Conclusions

In this paper, the results of experimental studies for possible catenary action for CLT floor systems with either conventional or novel floor-to-floor joint detailing are presented. The conventional joint consisted of STS inserted at 90 degrees whereas the novel joint additionally included steel tubes tied together with rods. The following conclusions can be drawn:

(1) CLT floor systems can develop both compressive arching and catenary actions as floor system collapse-resistance mechanisms against disproportionate collapse. Given their small effective depths, CLT floor systems cannot rely on compressive arching alone to ensure structural robustness.

(2) For Catenary action, in addition to the required tie-forces, compatibility between the applied deflection and the axial deformation is important. Conventional connections are not adequate; novel connection detailing , e.g. steel tubes and rods, are required in order to meet the axial forces and deformation demands.

(3) The deflection acceptance criterion for disproportionate collapse prevention of CLT floor system in platform-type construction is 8% and 15% of the single span for conventional and novel connection, respectively.

Acknowledgements

References

Brandner, R., Flatscher, G., Ringhofer, A., Schickhofer, G., Thiel, A. (2016). Cross laminated timber (CLT): overview and development. Eur. J. Wood. Prod. 74(3):331–351

CSA (2016) CSA-O86-14. "Engineering design in wood" 2016 supplement to the 2014 edition, Canadian Standards Association Mississauga, Ontario, Canada.

CEN (2006). EN 1991-1-7 Actions on structures – Part 1-7: Accidental actions. Brussels, Belgium: CEN European Committee for Standardisation.

DoD. (2013). Unified Facility Criteria - Design of buildings to resist progressive collapse. Department of Defence, Washington DC.

Hossain, A., Popovski, M., & Tannert, T. (2018). Cross-laminated timber connections assembled with a combination of screws in withdrawal and screws in shear. Engineering Structures; 168:1-11.

Huber, J., Ekevad, M., Girhammar, A., Berg, S., Girhammar, U. A. (2018). Structural robustness and timber buildings – a review. Wood Materials Science and Engineering 14(2):107-128.

Izzi M, Casagrande D, Bezzi S, Pasca D, Follesa M, Tomasi R. (2018) Seismic behaviour of Cross-Laminated Timber structures: A state-of-the-art review. Engineering Structures, 170:42-52

Milner, M., Bullock, M., Pitts, G. (2003). Multi-Storey Timber Frame Building: A Design Guide. (BRE, Ed.) (1st ed). London.

Mpidi Bita, H., Currie, N., Tannert, T. (2018). Disproportionate Collapse analysis of mid-rise cross-laminated timber buildings. Structure and Infrastructure Engineering. 14(11):1547-1560.

Mpidi Bita H, Tannert T (2018) Numerical Optimisation of Novel Connection for Cross-Laminated Timber Buildings, Engineering Structures ,175:273-283.

Mpidi Bita, H., Tannert, T. (2019). Disproportionate Collapse Prevention Analysis for a Mid-rise Flat-plate Cross-laminated Timber Building. Engineering Structures, 178:460–471.

Schneider, J., Tannert, T., Tesfamariam, S., Stiemer, S.F. (2018). Experimental assessment of a novel steel tube connection in cross-laminated timber. Engineering Structures, 177: 283–290.

STA. (2017). STA Advice Note 14 - Robustness of CLT structures. London, UK: Structural Timber Association. Retrieved from www.structuraltimber.co.uk.

Stevens, D. J. (2008). Assessment and Proposed Approach for Tie Forces in Frames and Load-bearing Wall Structures. Texas, USA: Protection Engineering Consultants.

Stylianidis, P. M., Nethercot, D. A., Izzuddin, B. A., Elghazouli, A. Y. (2016). Study of the mechanics of progressive collapse with simplified beam models. Engineering Structures, 117:287–304.

Tannert, T., Follesa, M., Fragiacomo, M., Gonzalez, P., Isoda, H., & Moroder, D. (2018). Seismic design of cross-laminated timber buildings. Wood Fiber Science. 50:3-26.

Discussion

The paper was presented by H Mpidi Bita

P Dietsch asked why the screws were not applied at inclined angle and how would this system be adapted for outer walls. H Mpdi Bita responded that given the limitation of the number of specimens available for the project, self tapping screws could not be used, also the lap joint considered would be commonly used in Canada. Also the case of outer wall would be a good topic for a future project.

S Winter commented that such connection would create channels in crossing walls which would create issues for fire and acoustic performance.

H Daneshvan and H Mpdi Bita discussed the relationship between the catenary and shear forces and that the boundary condition in the test might not be realistic as it would be driven by the anchorage forces allowed. The clamping force would depend on the surrounding structure which would also influence the end wall stiffness.

D Dolan commented on robustness in terms of earthquake safety.

E Toumpanaki received clarification of the boundary conditions that would represent the bracket connection. E Toumpanaki stated as the bracket was installed below, this would act differently compared to reality. H Mpdi Bita mentioned that testing slabs supported on three edges was not possible. T Tannert responded that FEM will be developed to address boundary conditions issues. He commented that concrete and steel industry developing similar guidelines would give little details.

S Aicher asked do you really intend to use platform type construction for 15 storeys buildings. H Mpdi Bita mentioned that compression perpendicular to grain issues would be problematic. S Aicher said such systems could be use with modifications.

P Quenneville asked how would this system act compared to a continuous CLT panel and would such large catenary forces be needed if similar actions could be developed via some continuous structural system. H Mpdi Bita responded LVL floor plates could offer continuity and develop high forces; however, their behaviour would be brittle. He added the focus of the work was to study how catenary action could be developed. Such forces would not be available in a system that was not continuous and also not available in continuous systems that were brittle.

U Kuhlmann commented that she was not too convinced that the joint could take rotational demand at centre point and ends of member. She agreed that continuous plates could help with catenary action at high deformations also joints would need to take moments. H Mpdi Bita agreed but stated that availability of moment resisting joints would be critical.

M Li commented on dynamic effects, e.g. from removal of columns. H Mpdi Bita said that the current study only dealt with the linear static case. In design, factors would be applied to amplify forces to account for nonlinear dynamic effects. F Lam commented that this work represented a good starting point but many issues still exit as indicated by the questions raised by the delegates. The issue of dynamics would be critical as it would deal not only with amplified loads but also dynamic effects on capacity including rate of loading effect on strengths and low cycle fatigue behaviour.

Addressing design for robustness in the 2nd-generation EN 1995 *Eurocode 5*

Pedro Palma   Empa – Swiss Federal Laboratories for Materials Science and Technology,

Structural Engineering Research Laboratory, Dübendorf, Switzerland,

pedro.palma@empa.ch

René Steiger   Empa – Swiss Federal Laboratories for Materials Science and Technology,

Structural Engineering Research Laboratory; Dübendorf, Switzerland

Robert Jockwer   Chalmers University of Technology, Division of Structural Engineering,

Gothenburg, Sweden

Keywords: *disproportionate collapse*; *robustness*; conceptual *design*; *Eurocode 5*

1   Introduction

1.1   Background

In the 1st generation of the Eurocodes, structural robustness was only addressed in EN 1991-1-7:2006 *Eurocode 1 − Part 1-7: Accidental actions*. However, new robustness-related provisions have recently been introduced in the latest drafts of the 2nd−generation European Standard prEN 1990:2019 *Eurocode − Basis of structural and geotechnical design*. These new provisions include a short Subsection with only two clauses (Section 4 *General rules* / 4.4 *Robustness*) and a longer Informative Annex on *Additional robustness provisions for buildings*. Therefore, Working Group (WG) 10 *Basis of design and materials*, of the European Standardisation Committee TC 250/SC 5 *Eurocode 5: Design of timber structures*, started a discussion on developing provisions related to resistance to disproportionate collapse and design for robustness for the 2nd−generation Eurocode 5 (EN 1995-1-1:2004 *Eurocode 5: Design of timber structures*), which is currently being drafted.

1.2   Scope

This paper presents and discusses previous and ongoing work on resistance to disproportionate collapse in general, giving examples related to timber structures. Different design strategies are also presented and possibilities of *codification* within the

framework of the Eurocodes are discussed. Finally, an initial working draft proposal on how to address resistance to disproportionate collapse in EN 1995-1-1 *Eurocode 5* is presented and its main assumptions and limitations are discussed. The objective of presenting this draft is mainly to promote a discussion on what should be included in Eurocode 5, how it could be included, and to try to make sure that ongoing research can also address standardisation-related issues regarding robustness of timber structures.

1.3 Disclaimer

The opinions expressed in this paper are those of the authors and do not represent the official opinion of the Technical Committee CEN/TC 250/SC 5/WG 10 or of its other members.

2 Definitions

The latest draft of prEN 1990:2019 defines *robustness* as the "ability of a structure to withstand adverse and unforeseen events without being damaged to an extent disproportionate to the original cause". The Swiss standard SIA 260:2013 *Basis of Structural Design* uses a slightly different formulation and defines robustness as the "ability of a structure and its members to keep the amount of deterioration or failure within reasonable limits in relation to the cause". These broad definitions of *robustness* coincides with what has also been defined as *resistance to disproportionate collapse* or *collapse resistance* (Ellingwood et al. 2007; Starossek and Haberland 2010; Huber et al. 2018). Therefore, the definition of *robustness* adopted in this paper is insensitivity to initial damage, which is one of the aspects of *collapse resistance* (Figure 1), alongside with *vulnerability* (susceptibility of structural component to be damaged by an abnormal event) and *exposure* (abnormal events, not explicitly considered in ordinary design) (Starossek 2018). A robust structure is, therefore, less prone to disproportionate collapse, but not vice versa. Finally, a disproportionate collapse might not be *progressive*, as statically determinate structures will most likely collapse after the failure of a single component.

The main difference between design for resistance to disproportionate collapse in case of abnormal events and design for accidental situations (i.e. foreseen and quantifiable events as explosions or impacts) is that the latter assumes identified and quantified accidental actions, against which the structure is explicitly designed, so that a specified reliability level is reached, whereas the design for resistance to disproportionate collapse assumes events that cannot be easily quantified (e.g. man-made accidental or intentional events, extreme low-probability-high-consequences natural events, design or constructions errors, degradation).
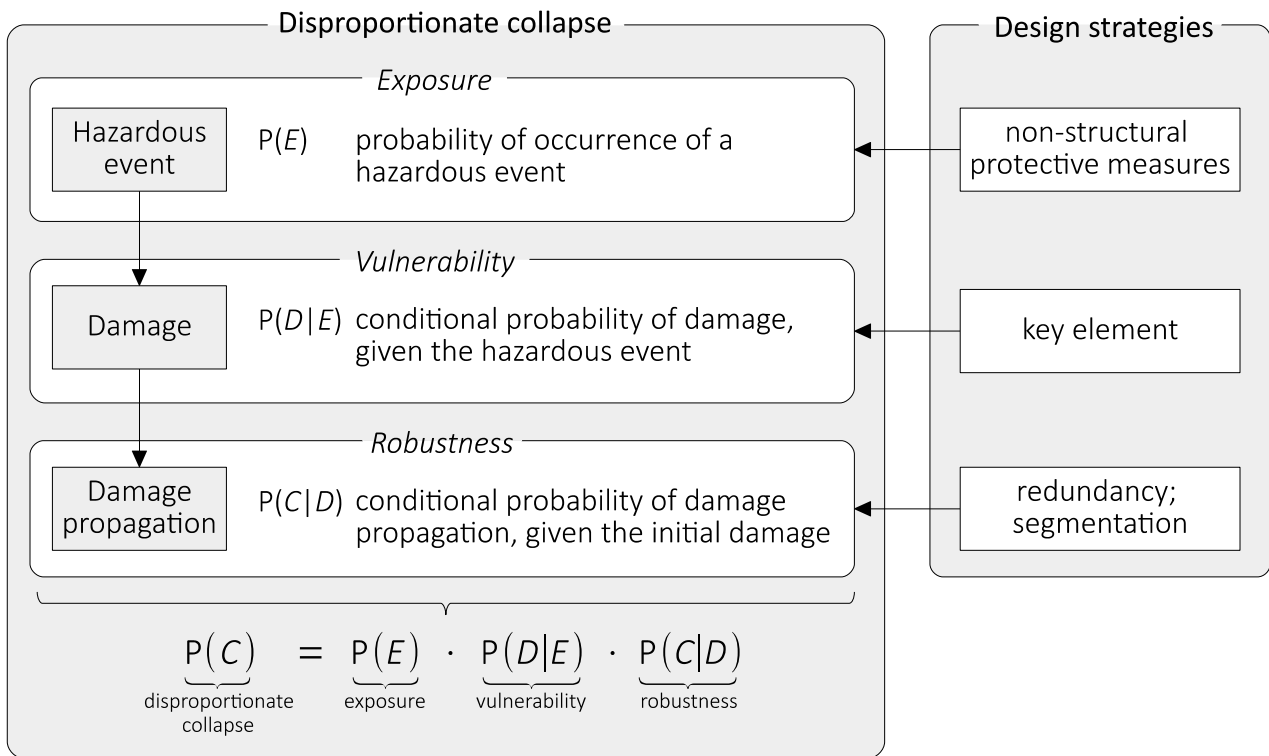
Figure 1. Disproportionate collapse prevention strategies, based on Starossek and Haberland (2010).

3   Design in accordance with the structural Eurocodes

3.1   Approach and shortcomings

The structural *Eurocodes* in their current and upcoming versions, as well as most current structural design codes, adopt a limit-state design approach, based on a probabilistic representation of the design parameters, in which the geometrical properties, the actions, and resistances are statistically determined so that predefined appropriate reliability levels are reached. EN 1990 *Eurocode 0* establishes the design principles, based mostly on the partial factor method, regarding structural safety, serviceability, robustness, durability, and sustainability. The actions and their values to be considered in the design are specified in EN 1991 *Eurocode 1*, and timber-specific aspects are addressed in EN 1995 *Eurocode 5*, namely regarding resistance of timber members and connections and their serviceability-related behaviour (Figure 2).
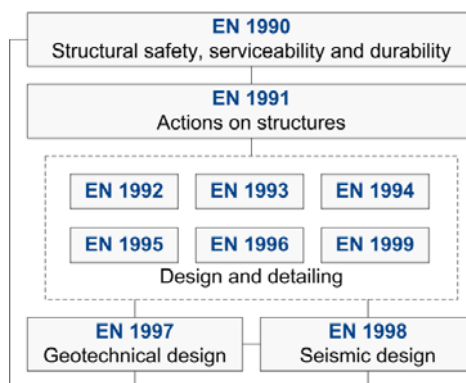

Figure 2. Current set of Structural Eurocodes *(https://eurocodes.jrc.ec.europa.eu/showpage.php?id=13).*

The main shortcoming of the Structural Eurocodes regarding resistance to disproportionate collapse is that they are based on the component behaviour (local) and not on the system behaviour (global), since probabilistic structural design is primarily concerned with component behaviour ("JCSS Probabilistic Model Code. Part I – Basis of design" 2001). Design verifications are made only on the local level, following an element-by-element approach, and it is assumed that the reliability of the structure is not much smaller than the reliability of each member or connection. However, the response of a structure to an initial local damage is dependent not only on the behaviour of its components in isolation, but on their arrangement and connectivity to the structure and the requirements for the reliability of the components should depend on the characteristics of the structure ("JCSS Probabilistic Model Code. Part I – Basis of design" 2001).

Another issue of the current approach regarding design for resistance to disproportionate collapse is the difficulty in dealing with extreme risks, i.e. low probability/high consequence events, such as a disproportionate collapse, due to the lack of statistical data (Starossek 2018). Strategies to enhance resistance to disproportionate collapse are "not generally associated with a target level of reliability as in structural member design against identified actions and could involve consideration of a conditional reliability" (prEN 1990:2019). Therefore, these events cannot easily be handled within the current reliability-based framework, even though target reliability levels have been set in the past for ultimate limit states corresponding to progressive collapse (Brynildsen 1975a; b).

Nevertheless, prEN 1990:2019 *Eurocode 0* recommends that structures "be designed to have an adequate level of robustness" and that "for most structures, design in accordance with the Eurocodes provides an adequate level of robustness without the need for any additional design measures to enhance structural robustness" (with *robustness* here being equivalent to *resistance to disproportionate collapse*, see Section 2). This statement might be based on the fact that not so many disproportionate collapses have been observed (Frühwald Hansson 2011) and that it has been traditionally accepted that "structural codes may consider these [progressive collapse] requirements satisfied if all other requirements can be fulfilled" (Brynildsen 1975a; b).

However, as mentioned before, it is difficult to judge the resistance of a structure to disproportionate collapse simply based on the individual behaviour of its elements and neglecting the structure's sensitivity to initial damage. Tests on a medium-rise multi-storey platform-frame building, with structural walls and floors constructed from small section timber studs and cladded with wood-based panels, showed that it had "significant inherent robustness and capacity to span over removed panels" (Milner et al. 1998; Enjily 2001; Grantham and Enjily 2004). But advanced mechanical simulations, which also took into account the variability of mechanical properties, of a medium-rise cross-laminated timber building showed that simple compliance with

building codes [i] (both the Eurocodes and the *National Building Code of Canada* and CSA O86-09:2010) led to a probability of disproportionate collapse as high as 32% after element removal (Bita et al. 2018).

3.2 Design criteria

prEN 1990:2019 *Eurocode 0* requires that structures are classified into five *consequence classes* that can be used to "choose design methods appropriate for enhancing robustness" (Tables 1 and 2), among other things. Due to cost-effectiveness considerations, it makes sense to link the level of requirements related to resistance to disproportionate collapse of a structure with its consequence class (e.g. from *no requirements* to *very high requirements*).

The specification of design requirements, namely hazard scenarios (e.g. sudden single or multiple-element failure) and performance objectives (e.g. acceptable extent of collapse as a percentage of floor area, volume, or costs), is not uniquely an engineering problem. It should be based on engineering advice, but must reflect the will of the owner and of the relevant authorities and different jurisdictions might have different requirements (prEN 1990:2019; Starossek 2018).

Table 1. Qualification of consequence classes (prEN 1990 *2019). Assigment of structures to consequences classes is a Nationally Determine Parameter (NDP), i.e. it can be defined at a national level by regulatory authorities in each Member State.*

Consequence class	Indicative qualification of consequences	
	Loss of human life or personal injury [a]	Economic, social or environmental consequences [a]
CC0 – Lowest	Very low	Insignificant
CC1 – Lower	Low	Small
CC2 – Normal	Medium	Considerable
CC3 – Higher	High	Very great
CC4 – Highest	Extreme	Huge

[a] The consequence class is chosen based on the more severe of these two columns.

3.3 Quantifying robustness

Various methods have been proposed to quantify robustness, mostly through deterministic, reliability, and risk-based robustness indexes (Sørensen 2011; Chen Yong-Liang et al. 2016). Besides in cases of collapses having occurred (i.e. in cases of forensic analyses) these indexes, however, are not easily determined (except maybe for deterministic-based indexes) and, as all single-value indexes that summarise complex systems, only reveal the susceptibility of the structure to disproportionate collapse to

---

[i] The building was not designed for earthquake resistance, only for a 1.0 kPa horizontal wind action. Explicit design for earthquake resistance could have indirectly increased the resistance to disproportionate collapse.

some extent. In addition, they are also mostly not applicable in ordinary design practice. Target reference values (e.g. like the target values for the reliability index β provided in prEN 1990:2019 *Eurocode 0*) against which the calculated indexes could be compared are also not available, making the indexes only useful for comparisons between not very dissimilar alternatives (i.e. same structure but different initial damage or different connectivity between elements).

4 Strategies against disproportionate collapse

Given that different structures are vulnerable to disproportionate collapse in different degrees, design for resistance to disproportionate collapse cannot be completely independent of the specificities of each project and should be considered in the early (i.e. conceptual) stages of the design process. For structures in lower consequence classes (Table 2), it should even be possible to achieve an adequate level of resistance to disproportionate collapse without any explicit design verifications. Nevertheless, even dismissing resistance to disproportionate collapse as not relevant in some circumstances should require an adequate justification from the designer. For structures in intermediate consequence classes, well-established prescriptive *indirect* design strategies without explicit consideration of hazard scenarios might be adequate (e.g. providing horizontal and/or vertical ties, or imposing failure modes with sufficient ductility in the connections [ii]). For structures in higher consequence classes, resistance to disproportionate collapse will very likely require more detailed analyses that include explicit *direct* design verifications for specific scenarios (e.g. element-removal analyses). This *direct* approach is more compatible with architectural complexity and design procedures that allow evaluating the global structural behaviour as a function of the behaviour of single elements can give valuable insights regarding resistance to disproportionate collapse of the structure. However, the required time, skill, and computational effort is greater than with the *indirect* approach. In any case, design for resistance to disproportionate collapse should not be interpreted as "simply applying rules" (as this could lead to these aspects being addressed too late in the design process, limiting the applicable strategies or entailing considerable costs), but rather to address design for resistance to disproportionate collapse in the conceptual design of the structures.

[ii] These two strategies might, in some cases, promote rather than prevent collapse progression (Munch-Andersen and Dietsch 2011; Starossek 2018).

Resistance to disproportionate collapse can be achieved at different levels (Figure 1), namely by:

- *choosing an adequate structural concept*

- *applying prescriptive design rules*;

- *preventing local failures* by

    – adopting protective measures (to reduce the extent or mitigate the *exposure* of the structure to abnormal events), or by

    – overdesigning key elements (to reduce their *vulnerability* and increase safety against initial failure); or by

- *assuming local failure and limiting the damage that follows through*

    – redundancy and/or segmentation (to increase the robustness, i.e. the insensitivity to initial damage)

Table 2. Indicative design methods for enhancing resistance to disproportinate collapse (prEN 1990:2019)

Consequence class	Design methods
CC1 – Lower	No design methods to provide enhanced robustness need be applied.

CC2 – Normal	When specified by the relevant authority or agreed for a specific project by the relevant parties, either:
	  a) for buildings: use of prescriptive design rules for horizontal ties to provide integrity and ductility; or
	  b) for buildings: use of prescriptive design rules for horizontal and vertical ties to provide integrity, ductility and alternative load paths; or
	  c) design of particular components as 'Key Elements'.

CC3 – Higher	When specified by the relevant authority or agreed for a specific project by the relevant parties, satisfy the requirements for CC2 appropriately adapted and in addition consider:
	  a) potential initial failure events;
	  b) propagation of failure;
	  c) resulting consequences;
	  d) risks, where appropriate.

4.1 Choosing an adequate structural concept

Choosing an adequate structural concept is as important for resistance to disproportionate collapse as it is for seismic design. Unlike the Eurocodes, the Swiss standard SIA 260:2013 *Basis of structural design* strongly emphasizes the importance of having an adequate *structural concept* together with clear assumptions regarding *basis of design*. The *structural concept* includes the chosen structural system, information on the most important dimensions, material properties and detailing, and the envisaged construction methods; the *basis of design* describes the hazard scenarios considered,

the requirements of structural safety, serviceability and durability (together with the measures needed to guarantee them), the assumed soil conditions, the important assumptions in the structural and analytical models, and the accepted risks. The extent and content of the *basis of design* are adapted to the importance of the structure and the associated hazards and environmental risks.

4.2   Applying prescriptive design rules

Prescriptive design rules are mostly based on providing resistance to disproportionate collapse through the creation of alternative load paths. They should be employed with caution, because in some cases they can promote rather than prevent collapse progression (Munch-Andersen and Dietsch 2011). Nevertheless, for structures of lower to normal consequence classes, the engineering effort of making multiple analyses assuming local failures might be excessive and well-established prescriptive design rules are probably better suited for these situations. The most common rules are based on providing tension ties (enabling catenary action) and ensuring ductility [iii] (Starossek 2018). The effectiveness of prescriptive design rules in increasing the resistance to disproportionate collapse is mostly unknown, but if their application is limited to structures in lower consequence classes, the consequences of them not working are limited.

Tying elements of a structure together is a strategy based on creating a statically indeterminate structure that is capable of allowing forces to follow alternative load paths in case of an abnormal event. Horizontal ties are intended to make beams or slabs able to span over a missing removed support and should be continuous across the building and around the perimeter (Hewson 2016). Vertical ties are intended to suspend elements that lost their support, by distributing their loads upwards and should be continuous over the height of the structure. Due to the limited load-carrying of timber connections with a small geometrical footprint, vertical ties might be difficult to materialise in timber structures (Arup 2011; Hewson 2016). For platform-frame buildings with structural walls and floors constructed from small section timber studs and cladded with timber-based panels, a suspended floor can be considered effectively anchored if it is in accordance with specified detailing rules and follows minimum nailing densities (IStructE/TRADA 2007; Mann et al. 2010).

Ensuring that the structure exhibits sufficient monotonic/static ductility is essential to allow the creation of alternative load paths under extensive deformations (e.g. the development of catenary action). Plastic strain hardening that occurs in steel parts in these circumstances might also provide additional load-carrying capacity (Knoll and Vogel 2009).

[iii] *Ductility* as the ability to accommodate large deformations without significant loss of strength capacity (Jorissen and Fragiacomo 2011).

4.3　Preventing local failures

Strategies based on *adopting protective measures* fall outside of the scope of Eurocode 5 and are not addressed in this paper. Strategies based on *overdesigning key elements* should be a last resort (Arup 2011; Hewson 2016; Huber et al. 2018), used only in cases where other alternatives are not viable or too costly. Design of key elements follows the common design procedure, even if the considered actions are anything but common, and since it can be done in accordance with the current rules in Eurocode 5 it is also not addressed in this paper.

4.4　Assuming local failure

4.4.1　Redundancy (alternative load paths)

The *redundancy* strategy is based on providing an alternative load path (ALP) for the forces not transmitted anymore through failed components. It is based on assessing the behaviour of the remaining structure after an initial damage. A commonly assumed initial damage is the notional removal of one (or several) components of the structure and a so-called *element-removal analysis* is then performed, with the objective of evaluating if the remaining structure is able to accommodate the damage.

There are various procedures available to estimate the extent of the initial damage to consider and the loads to take into account in element-removal analyses (Mann et al. 2010; Arup 2011; GSA 2016; UFC 4-023-03 2016). Dynamic effects from a sudden failure should be considered and maybe also additional loads originating from eventual debris. In any case, these aspects should be set by the relevant authorities or in agreement with relevant parties and it is not clear whether there is a need for specific rules for timber structures, maybe with the exception of specific structures, such as timber-frame walls.

The structural models to perform element-removal analysis need not be very advanced, even because a very complex mechanical model might be unreasonable given the uncertainties regarding the exposure and the variability of the mechanical properties of timber members and connections. In many cases, linear static analyses are performed in which the dynamic effects are considered through adequate dynamic amplification factors applied to the effects of static actions (Ellingwood et al. 2007; Arup 2011). This procedure can be applied iteratively to simulate progressive collapse. Since this procedure does not account for material or geometric non-linearities, its results should be very conservative. Models that include second-order effects and non-linear behaviour, namely of timber connections, do provide more realistic results, but there is currently no general method available to reliably derive displacement-load curves for any timber connection. A detailed description of available element-removal analysis methods for timber structures was presented by Huber et al. (2018).

4.4.2   Segmentation

Redundancy on its own might not be suitable to avoid disproportionate collapses. In the case of repetitive structures, systematic design or execution errors can compromise the ability of a structure to redistribute loads and lead to progressive collapses (Munch-Andersen and Dietsch 2011), as the alternative load paths are all affected by a common-cause failure. In these cases, *segmentation* can be an adequate design strategy. The objective of this strategy is to compartmentalise the structure in a way that collapse progression after an initial damage is halted at predefined locations, either through fuse-type elements or by having control joints at which the segments are physically separated.

Horizontal segmentation, in which each segment of the structure is disconnected from the neighbouring segments (or connected through components or connections with limited load-carrying capacity and ductility), is appropriate for structures that develop horizontally (e.g. bridges, industrial/sports halls, small/mid-rise buildings) (Munch-Andersen and Dietsch 2011), but not for tall structures, in which segmentation would create a series of parallel slender structures that would become even more unstable after the collapse of a segment (Starossek 2018). The notorious case of Ronan Point (Menzies and Moore 1985; Delatte 2006) is often portrayed as an example of disproportionate progressive collapse: an explosion blew out load-carrying concrete panels in one flat of a 23-storey concrete building and as a result there was a vertical progressive collapse of a whole corner of the building. However, the Ronan Point case can also be seen as an example of effective horizontal segmentation in a tall building. In structures with small height/length ratios, namely industrial/sports halls, common structural solutions with portal frames or trusses connected by simply supported purlins seem to be, to some degree, inherently segmented, since the ordinary connections between the purlins and the main members are far from being able to transfer the loading from a failing truss or frame to the adjacent ones, effectively limiting the extension of the collapse (Frühwald et al. 2007). However, in the case of continuous or lap-jointed purlin systems, a failed main member held by the continuous secondary structure could very significantly increase the loads in the remaining main members and lead to a collapse progressively (Dietsch 2011).

Vertical segmentation appropriate for medium/high-rise structures is more difficult to achieve, since making structural members able to resist the impact of a failing element would increase their weight, which in turn would increase impact actions and the weight of debris. Most common solutions for vertical segmentation rely on providing shock-absorbing zones with high energy dissipation capacity. In concrete buildings this zones can be materialised as unoccupied short storeys equipped with shock-absorbing devices, in the case of higher and/or heavier multi-storey vertical segments, or thicker slabs combined with shock-absorbing columns, in the case of single-storey vertical segments. Since timber structures are usually much lighter, the performance requirements for these segmentation boundaries should also be signifi-

cantly less demanding. Since up to now, there are not so many high-rise timber buildings, examples of vertical segmentation are scarce. However, the 14-storey timber building "Treet", in Norway, includes a paradigmatic example (Abrahamsen and Malo 2014): this building has two "power storeys" that carry a prefabricated concrete slab on top of which four levels of residential modules are stacked; these "power storeys" should be able to halt a progressive collapse of the stacked residential modules, limiting the extent of collapse.

5 Verification procedures in the 2nd generation EN 1995 *Eurocode 5*

5.1 Expectations and deliverables

In addition to discuss what can be provided by the 2nd generation EN 1995 *Eurocode 5* regarding resistance to disproportionate collapse, it is also important to establish what cannot be provided.

Eurocode 5 is not a textbook and therefore shall not provide guidance on how to set up an adequate structural model, but should provide, e.g., hints for the conceptual design of the timber structures, the mechanical properties that should be considered in the design and the assumptions under which these properties are valid (e.g. linear elastic analyses, linear relation between stress and strain until failure of individual members, cases where plasticity of members or connections may be accounted for). It shall also not set performance requirements (e.g. load combinations that a structure should be able to sustain, or maximum deformations), but provide ways to assess the performance (e.g. methods to determine load-carrying capacities, or stiffnesses).

Regarding resistance to disproportionate collapse, Eurocode 5 should not provide step-by-step analysis methods, because, as it was shown in the previous section, there is no single well-established and accepted procedure and the complexity of the analysis should fit its specific purposes. Eurocode 5 should, nevertheless, provide guidance regarding, e.g., what properties should be used in some analyses (e.g. element-removal analysis). Eurocode 5 should also not set performance requirements, as these should be "specified by the relevant authority or agreed for a specific project by the relevant parties" (prEN 1990:2019). However, guidance should be provided on how to assess the performance under the conditions of a disproportionate collapse, as it is done for seismic design, e.g. by providing adequate well-established verification methods.

Prescriptive design rules should be avoided, since their simple application does not imply that performance requirements are met (Starossek 2018). *Preventing local failures* by adopting protective measures also falls outside of the scope of Eurocode 5 and overdesigning key elements can be done within the existing framework, even if the design actions are arbitrarily determined instead of statistically assessed.

Finally, Eurocode 5 should focus on *direct design* methods (see Section 4) in which resistance to disproportionate collapse can be explicitly demonstrated for specified initial damages (e.g. loss of one or more columns) and performance requirements (e.g. acceptable extent of collapse as a percentage of floor area, volume, or costs). This can only be achieved for design strategies based on *assuming local failure* and limiting the damage that follows, namely *redundancy* (by providing alternative load paths) and/or segmentation.

As mentioned before, the design resistance to disproportionate collapse cannot simply be based on "applying rules"; choosing an adequate structural concept is as important for resistance to disproportionate collapse as it is for seismic design.

5.2   Draft clauses

The members of Working Group (WG) 10 *Basis of design and materials*, of the European standardisation Technical Committee CEN/TC 250/SC 5 *Eurocode 5* recently started a discussion on developing robustness-related[iv] clauses for the $2^{nd}-$generation Eurocode 5. The authors of this paper have started drafting these clauses and it is this first working draft that is presented in this paper. WG 10 agreed that provisions related to resistance to disproportionate collapse should follow the structure of prEN 1990:2019, namely very few general clauses in the section on Basis of design and an informative annex (i.e. compliance is voluntary) with more detailed provisions. Given the reasons presented in the previous Sections of this paper, the initial working draft is focused on *direct design* methods and presents design provisions for two strategies: *design for resistance to removal of load-carrying elements* (*redundancy* (alternative load paths) strategy) and; *design for segmentation using fuse elements* (*segmentation* strategy). The draft is based on the assumption that the design will be based on linear elastic analyses, as the other parts of Eurocode 5. Therefore, non-linear and dynamic effects have to be considered through adequate factors imposed on actions, resistances, and stiffnesses. It is not yet clear if enough data is available to derive all these factors, or if respective information is only available for specific types of structures or connections.

The design verifications for *resistance to removal of load-carrying elements* include two scenarios:

- *failure of a load-carrying element, including dynamic effects (accidental design situation); and*

- *resistance of the remaining structure, without the failed element (transient design situation).*

In the first scenario, the dynamic effects corresponding to the sudden failure of a load-carrying element are considered by applying a partial factor γ_E on the effects of

---

[iv] Robustness in the sense presented in Figure 1, i.e. insensitivity to initial damage.

actions. Different values have been proposed for such dynamic amplification factors. Grantham and Enjily (2004) propose a modification factor of 2.0 (for timber-frame walls), which is approximately two times the k_{mod} factor for the instantaneous load-duration class. Bita et al. (2018) state that for a 12-storey CLT building the forces from the dynamic simulation were about 1.5 times higher than the outcome from static analysis. According to Dietsch and Kreuzinger (2016), dynamic amplification fa tors due to brittle failures in shear-reinforced timber elements are between lower than 1.18. Stevens et al. (2011, 2015) present results that show a range of dynamic amplification factors from 1.20 to 1.85 for steel buildings and from 1.00 to 1.40 for concrete buildings. Hence, in the draft clauses a single provisional value of 1.5 was adopted, but it has to be discussed if different values should rather be chosen dependent on the type of structure.

The design verifications for *segmentation using fuse elements* consider:

- *limiting the upper value of the load-carrying capacity of fuse elements to a specified nominal action that the element should be allowed to carry; and*

- *limiting the over-strength of the fuse element to the design effects of the other combinations of actions considered in the design.*

The first verification is an explicit check of the fuse effect for specified nominal actions. The fuse elements are designed so that their resistance is lower than a specified nominal action. This nominal action can be specified by the relevant authority or agreed for a specific project by the relevant parties. The second verification is a safeguard to avoid the development of alternative load paths that could bypass the fuse effect, by limiting the over-strength of the fuse element to the effects of the other combinations of actions considered in the design. However, it is not clear yet if upper values of the load-carrying capacity of timber connections can be reliably estimated, if limitations on the stiffness of the sacrificial elements also be imposed, and if specific failure modes should be preferred for sacrificial elements.

6   Conclusions

Codification of resistance to disproportionate collapse of timber structures within the framework of the Eurocodes limits is not straightforward, in particular due to the lack of well-established design procedures.

Design strategies based on *direct design* methods, in which resistance to disproportionate collapse can be explicitly demonstrated for specified initial damages and performance requirements, are preferred. This can only be achieved for design strategies based on *assuming local failure* and limiting the damage that follows, namely *redundancy* by providing alternative load paths and/or *segmentation*.

Designing for robustness shall primarily be considered in the early stages of design, e.g. by choosing an adequate structural concept, materials, and detailing.

The discussion on how to proceed with the codification of robustness-related aspects in the 2nd-generation Eurocode 5 must also include an additional very important aspect that was not addressed in this paper, namely if the letter *C* in Figure 1 should be limited to disproportionate structural *collapse*, or if it should be extended to include any kind of disproportionate unfavourable *consequence* (e.g. too large deformations in multi-storey buildings as a result of high compressive perpendicular-to-the-grain stresses and/or large moisture content variations, extensive cracking due to a combination of perpendicular to the grain stresses with moisture gradients, severe durability issues due to the cumulative effect of unnoticed minor water leakages). This would lead to a much more general approach regarding design for robustness of timber structure (see draft clause R.2 (1) of the Annex).

Acknowledgements

7   References

Abrahamsen, R. B., and Malo, K. A. (2014). "Structural design and assembly of 'Treet' - a 14-storey timber residential building in Norway." *Proceedings of the World Conference on Timber Engineering 2014 (WCTE 2014)*, Quebec City, Canada, 8.

Arup. (2011). *Review of international research on structural robustness and disproportionate collapse*. Arup, 198.

Bita, H. M., Currie, N., and Tannert, T. (2018). "Disproportionate collapse analysis of mid-rise cross-laminated timber buildings." *Structure and Infrastructure Engineering*, 14(11), 1547–1560.

Brynildsen, O. (1975a). "Proposal for safety codes for load-carrying structures - code and recommendation concerning safety methods." *Meeting of Working Comisson W18 - Timber Structures*, CIB, Paris, France, 56.

Brynildsen, O. (1975b). "Comments to proposal for safety codes for load-carrying structures." *Meeting of Working Comisson W18 - Timber Structures*, CIB, Paris, France, 31.

Chen Yong-Liang, Huang Liang, Lu Yi-Qiu, Deng Lu, and Tan Hao-Zhi. (2016). "Assessment of structural robustness under different events according to vulnerability." *Journal of Performance of Constructed Facilities*, 30(5), 04016004.

CSA O86-09*. Engineering Design in Wood*. (2010). Canadian Standards Association, Ontario, Canada, 241.

Delatte, N. (2006). "Learning from failures." *Civil Engineering Practice*, 21(2), 21–38.

Dietsch, P. (2011). "Robustness of large-span timber roof structures — Structural aspects." *Engineering Structures*, Modelling the Performance of Timber Structures, 33(11), 3106–3112.

Dietsch, P., and Kreuzinger, H. (2016). "Dynamic effects in reinforced timber beams at time of timber fracture." *International Network on Timber Engineering Research (INTER) – Meeting Forty-Nine*, Graz, Austria, 401–404.

Ellingwood, B., Smilowitz, R., Dusenberry, D., Duthinh, D., Lew, H., and Carino, N. (2007). *Best Practices for Reducing the Potential for Progressive Collapse in Buildings | NIST*. National Institute of Standards and Technology (NIST), 194.

EN 1995-1-1:2004. *Eurocode 5: Design of timber structures – Part 1-1: General – Common rules and rules for buildings*. (2004). European Committee for Standardization (CEN), Brussels, 123.

Enjily, V. (2001). "The performance of timber structures, elements and components." *COST Action E24 Copenhagen Meeting*, COST Action E24, Denmark.

Frühwald, E., Serrano, E., Toratti, T., Emilsson, A., and Thelandersson, S. (2007). *Design of safe timber structures – How can we learn from structural failures in concrete, steel and timber?* Lund Institute of Technology, Lund University, Lund, Sweden, 228.

Frühwald Hansson, E. (2011). "Analysis of structural failures in timber structures: Typical causes for failure and failure modes." *Engineering Structures*, Modelling the Performance of Timber Structures, 33(11), 2978–2982.

Grantham, R., and Enjily, V. (2004). "UK Design Guidance for multi-storey timber frame buildings." *Proceedings of the 8th World Conference on Timber Engineering (WCTE2004)*, Lahti, Finland, 1001–1005.

GSA. (2016). *GSA Alternate path analysis and design guidelines for progressive collapse resistance (Revision 1)*. General Services Administration (GSA).

Hewson, N. (2016). *Robustness in structures*. Forest and Wood Products Australia.

Huber, J. A. J., Ekevad, M., Girhammar, U. A., and Berg, S. (2018). "Structural robustness and timber buildings – a review." *Wood Material Science & Engineering*.

IStructE/TRADA (Ed.). (2007). *Manual for the Design of Timber Building Structures to Eurocode 5*. IStructE / TRADA.

"JCSS Probabilistic Model Code. Part I – Basis of design." (2001). *JCSS Probabilistic Model Code*, Joint Committee on Structural Safety, 62.

Jorissen, A., and Fragiacomo, M. (2011). "General notes on ductility in timber structures." *Engineering Structures*, In Press, Corrected Proof.

Knoll, F., and Vogel, T. (2009). *Design for Robustness*. Structural Engineering Documents, International Association for Bridge and Structural Engineering (IABSE), Zurich, Switzerland.

Mann, A. P., Alexander, S. J., Carpenter, J. N., Cartz, J. P., Chryssanthopoulos, M., Harding, G. T., Jones, A. E. K., Kelly, P., Lewis, G., Thirumoolan, A., Tutt, J. N., and Cosgrove, T. C. (2010). *Practical guide to structural robustness and disproportionate collapse in buildings*. Institution of Structural Engineers.

Menzies, J. B., and Moore, F. A. (1985). *The Structure of Ronan Point and Other Taylor Woodrow-Anglian Buildings*. Building Research Establishment Report, Building Research Establishment (BRE), 85.

Milner, M., Edwards, S., Turnbull, D., and Enjily, V. (1998). "Verification of the robustness of a six-storey timber-frame building." *The Structural Engineer*, 76(16).

Munch-Andersen, J., and Dietsch, P. (2011). "Robustness of large-span timber roof structures – Two examples." *Engineering Structures*, Modelling the Performance of Timber Structures, 33(11), 3113–3117.

prEN 1990:2019*. Eurocode – Basis of structural and geotechnical design*. (2019). European Committee for Standardization (CEN), Brussels, 145.

SIA 260:2013. Basis of Structural Design. (2013). SIA, Zurich, Switzerland, 44.

Sørensen, J. D. (2011). "Framework for robustness assessment of timber structures." *Engineering Structures*, In Press, Corrected Proof.

Starossek, U. (2018). *Progressive collapse of structures*. ICE Publishing.

Starossek, U., and Haberland, M. (2010). "Disproportionate collapse: terminology and procedures." *Journal of Performance of Constructed Facilities*, 24(6), 519–528.

Stevens, D., Crowder, B., Sunshine, D., Marchand, K., Smilowitz, R., Williamson, E., and Waggoner, M. (2011). "DoD Research and Criteria for the Design of Buildings to Resist Progressive Collapse." *Journal of Structural Engineering*, 137(9), 870–880.

Stevens, D., Martin, E., Williamson, E., McKay, A., and Marchand, K. (2015). "Recent developments in progressive collapse design." Protection Engineering Consultants (PEC).

UFC 4-023-03. *Design of buildings to resist progressive collapse*. (2016). 4: Multi-Disciplinary And Facility-Specific Design, Departmentof Defense (DoD), 245.

ANNEX – Draft clauses regarding the design of timber structures for resistance to disproportionate collapse

(based on the internal WG 10 document CEN/TC 250/SC 5/WG 10/N 48)

Verbal forms

Requirements <REQ> convey objectively verifiable criteria to be fulfilled and from which no deviation is permitted if compliance with the document is to be claimed. Requirements are expressed using the verb "shall".

Recommendations <REC> convey a suggested possible choice or course of action deemed to be particularly suitable without necessarily mentioning or excluding others. In the negative form, a recommendation is the expression that a suggested possible choice or course of action is not preferred but it is not prohibited. Recommendations are expressed using the verb "should".

Permissions <PER> convey consent or liberty (or opportunity) to do something. Permissions are expressed using the verb "may".

Notes

NOTES are used to give additional information intended to assist the understanding or use of the text of document. Notes shall only contain statements of fact and the document shall be usable without the notes.

Section 4 Basis of design

4.1 Requirements

4.1.*x* Robustness

(1) <REQ> The provisions in prEN 1990:2019 regarding robustness shall be observed.

(2) <REC> An adequate level of robustness should be achieved through an adequate structural concept.

NOTE 1:   Robustness-related design verifications are dependent on the consequence class of the structure (see prEN 1990:2019 Annex A *Application rules* (normative)). More information may be given in the National annex.

NOTE 2:   Design procedures that allow evaluating the global structural behaviour as a function of the behaviour of single elements give valuable insights regarding resistance to disproportionate collapse.

NOTE 3:   Guidance on design of structures for resistance to disproportionate collapse is given in Annex R *Guidance for design of structures for resistance to disproportionate collapse* (informative).

Annex R (informative)

Guidance for design of structures for
resistance to disproportionate collapse

R.1 Use of this informative Annex

(1) This informative Annex provides additional guidance, to that given in Section 4.1.x, for enhancing the resistance to disproportionate collapse of timber structures.

NOTE 1:   Without an adequate choice of structural materials, their specification, structural concept, structural detailing, and quality management, compliance with the provisions given in this Annex might not be sufficient to ensure enhanced resistance to disproportionate collapse.

R.2 Scope and field of application

(1) The aim of designing for resistance to disproportionate collapse in accordance with this Annex is to prevent disproportionate consequences as a result of a hazardous event, such as the failure or collapse of a component or part of a structure.

NOTE 1:   General guidance on additional design measures to enhance structural robustness for buildings is given in Annex E of prEN 1990:2019.

NOTE 2:   Design for identified accidental actions should be undertaken in accordance with EN 1991. The distinction between designing for robustness in accordance with this Annex and designing for identified accidental actions in accordance with EN 1991 is described in prEN 1990:2019.

R.3 Design strategies for resistance to disproportionate collapse

R.3.1 General

(1) <PER> Strategies for designing structures for resistance to disproportionate collapse are listed in prEN 1990:2019 and include the following:

a) creation of alternative load paths:

- by providing sufficient ductility, deformation capacity, and redundancy to the structure; and/or

- applying prescriptive design rules, such as for tying;

b) segmentation of the structure into distinct parts, by means of one or more weaker components, so that each part is able to collapse independently without affecting the safety of the other parts.

NOTE: Strategies for designing for resistance to disproportionate collapse are not mutually exclusive and can be combined or used separately.

(3) <PER> The creation of alternative load paths within the structure may be achieved by designing for r*esistance to removal of load-carrying elements* (Section R.4).

(4) <PER> Segmentation of the structure may be achieved by designing *fuse elements* (Section R.5).

NOTE: A fuse element is a component of the structure that is expected to fail under certain damage scenarios, to halt a progressive collapse.

R.4 Design for resistance to removal of load-carrying elements

R.4.1 Principles of design

(1) <RCM> Design for resistance to removal of load-carrying elements should consider two design scenarios (see Table R.1):

— failure of a load-carrying element, including dynamic effects (accidental design situation); and

— remaining structure, without the failed element (transient design situation).

NOTE 1:   Regarding the classification of design situations, see Clause 5.2(3) of prEN 1990:2019.

NOTE 2:   Selection of element or elements to be removed and limitations on the extent of failure should be specified by the relevant authority or agreed for a specific project by the relevant parties.

Table R.1. Load-duration classes, combinations of actions, and partial factors on effects of actions, when designing for resistance to removal of load-carrying elements.

Design scenario	Load-duration class	Combination of actions	Partial factor on effects of actions [a),b)], γ_E
Failure of load-carrying element	Instantaneous	Combination of actions for accidental design situations	$\gamma_E = 1.5$
Structure without the removed element	Short-term		Not applicable (i.e. $\gamma_E = 1.0$)

[a)]   The partial factors on effects of actions consider the dynamic effects associated with an instantaneous element removal (see Section 8.3.2.3 of pr EN 1990:2019).

[b)]   The partial factor γ_E should only be applied to the effects of actions in the structural components that comprise the alternative load path, not to the entire structure (see Clause R.4.3.1.1(2)).

R.4.2 Structural analysis

R.4.2.1 Structural modelling

(1) <PER> The effects of actions may be determined from linear elastic analyses, provided that dynamic effects are adequately considered (see Clause R.4.3.1.1(1)).

R.4.3 Basic variables

R.4.3.1 Actions

R.4.3.1.1 Design values of actions

(1) <RCM> The actions due to a sudden failure of an element and/or due to the impact of collapsed elements should be taken into account.

(2) <PER> The dynamic effects corresponding to the sudden failure of a load-carrying element may be considered by applying the partial factor γ_E, given in Table R.1, on the effects of actions.

(3) <RCM> The partial factor on the effects of actions γ_E should only be applied in the structural components that comprise the alternative load path, not to the entire structure.

NOTE 1:   Regarding factors on effects of actions, see Section 8.3.2.3 of pr EN 1990:2019.

NOTE 2:   The partial factor on the effects of actions γ_E is an equivalent dynamic amplification factor to the effect of static actions.

R.4.3.1.2 Combination of actions

(1) <RCM> The combinations of actions given in Table R.1 should be used.

R.4.3.2 Material properties and resistances

R.4.3.2.1 Modification factors for strength, stiffness, and resistance

(1) <RCM> Actions should be assigned to the load‑duration classes in Table R.1. The corresponding values of the modification factor k_{mod} are given in Table *x*.

R.4.3.2.2 Resistance of timber connections

(1) <RCM> Timber connections should be designed to exhibit failure modes that provide an adequate level of ductility.

(1) <PER> Timber connections with dowel-type fasteners that are part of the alternative load path may be assumed to provide an adequate level of ductility if they are designed to exhibit:

— failure modes f), or k) (Figure 8.2 of EN 1995:2004) for timber-to-timber connections; and

— failure modes e), h), or m) (Figure 8.3 of EN 1995:2004) for steel-to-timber connections.

R.5 Design for segmentation using fuse elements

R.5.1 Principles of design for segmentation using fuse elements

(1) <RCM> Design for segmentation using fuse elements should consider:

— limiting the upper value of the resistance (load-carrying capacity) of fuse elements to a specified nominal action that the element should be allowed to carry (see Clause R.5.4(1); and

— limiting the over-strength of the fuse element to the design effects of the other combinations of actions considered in the design (see Clause R.5.4(2)).

NOTE 1: The first verification is an explicit check of the fuse effect for specified nominal actions: the fuse elements are designed so that their resistance is lower than a specified nominal action. This nominal action can be specified by the relevant authority or agreed for a specific project by the relevant parties.

NOTE 2: The second verification is a safeguard to avoid the development of alternative load paths that could circumvent the fuse effect, by limiting the over-strength of the fuse element to the effects of the other combinations of actions considered in the design.

NOTE 3: More than one vertical bracing system is required to ensure that the remaining parts of the structure are still stabilised after the failure of a main member.

(2) <RCM> The fuse elements must be timber connections designed to exhibit failure modes that are known to show reduced variability.

(3) <RCM> The selection of fuse elements should be made for specific damage scenarios, e.g. failure of a structural component or part of the structure.

NOTE : The definition of damage scenarios can be specified by the relevant authority or agreed for a specific project by the relevant parties.

R.5.2 Structural analysis

R.5.2.1 Structural modelling

(1) <PER> The effects of actions may be determined from linear elastic analyses, provided that the failure of fuse elements does not introduce significant dynamic effects.

NOTE : Dynamic effects can be due to a sudden failure of an element and/or due to the impact of collapsed elements.

R.5.3 Basic variables

R.5.3.1 Actions

R.5.3.1.1 Design values of actions

(1) <RCM> The actions due to a sudden failure of an element and/or due to the impact of collapsed elements should be taken into account.

R.5.3.1.2 Combination of actions

(1) <RCM> The combinations of actions given in Table R.2 should be used.

Table R.2. Load-duration classes and combinations of actions, when designing for segmentation using fuse elements.

Design scenario (verification of ULS in Section R.5.4)	Load-duration class	Combination of actions
Clause R.5.4(1)	Instantaneous	Combination of actions for accidental design situations
Clause R.5.4(2)		
Clause R.5.4(3)	Short-term	

R.5.3.2 Material properties and resistances

R.5.3.2.1 Modification factors for strength, stiffness, and resistance

(1) <RCM> Actions should be assigned to the load‑duration classes in Table R.2. The corresponding values of the modification factor k_{mod} are given in Table x.

R.5.3.2.2 Resistance of timber connections

(x)

R.5.4 Verification of ultimate limit states (ULS)

(1) <RCM> The upper value of the resistance (load-carrying capacity) $R_{d,up}$ of the fuse element should verify the inequality given by Formula R.1:

$$R_{d,up} \leq E_{nominal} \tag{R.1}$$

in which:

$R_{d,up}$ is the upper value of the design resistance (load-carrying capacity) of the fuse element;

$E_{nominal}$ maximum effect of a nominal action that the fuse element is allowed to carry.

NOTE: The maximum effect of a nominal action $E_{nominal}$ that the fuse element is allowed to carry can be specified by the relevant authority or agreed for a specific project by the relevant parties.

(2) <RCM> The resistance of a fuse element R_d to the design effects of the combinations of actions considered in the design, except for the action considered in the previous clause, should verify the inequality given by Formula R.2:

$$R_d \leq k \cdot E_d \tag{R.2}$$

in which:

R_d is the design resistance (load-carrying capacity) of the fuse element;
k is an over-strength factor;
E_d is a design effect of a combination of actions considered in the design.

NOTE: The recommended value of the over-strength factor k is (…).

Discussion

The paper was presented by P Palma

P Dietsch stated that the statement that typical hall structures are inherently segmented is not true as lap-jointed purlins can lead to considerable load-distribution. He mentioned that the post-tensioning of vertical systems could be connected to robustness in term of vertical ties. P Palma responded that 11 to 12 degree rotation might be a requirement for catenary action and agreed that vertical ties could be a good option.

K Voulpiotis commented that rocking wall systems with post tensioning would be very beneficial to robustness and resiliency. P Dietsch commented that stiffness of CLT cores using post tensioning to resist wind load would be a good application.

D Dolan commented that in the US seismic codes for timber systems featuring over-strength requirements might push designers to make high strength connections which could be brittle.

H Mpidi Bita commented that post-tensioned systems are good but still would need horizontal catenary actions. Also segmentation would imply damage was allowed. How to control and design for damage development would be critical for segmentation consideration. P Palma agreed.

H Daneshvar commented that progressive collapse consideration should follow the approaches of concrete and steel where conventional systems would be used and additional systems would be added for catenary action. He asked if progressive collapse has to be considered in building design in Europe. P Palma responded that this would not be mandated and there was not an actual guide but that a motherhood statement is given, stating that damage should be limited.

P Dietsch and H Mpidi Bita discussed the importance of segmentation for tall buildings. In wide and horizontal cases segmentation would be important. In tall timber it would be hard to achieve. P Palma said in Europe there is a large number of structures where progressive collapse considerations would be required. In US there are progressive collapse consideration requirements for government and military buildings. They are working on similar approaches for civilian buildings.

S Winter commented that it is necessary to give guidance so that progressive collapse situations are avoided. However with so many available systems, we must not make the design guidelines too strict. In addition, S Winter does not agree with the requirement of calculating probabilistic numbers as correct structural design has much larger effect.

Robustness in Tall Timber Buildings – An Improved Framework

Konstantinos Voulpiotis[1], Jochen Köhler[2], Robert Jockwer[3], Andrea Frangi[1]

[1] Chair of Timber Structures, Institute of Structural Engineering (IBK), Swiss Federal Institute of Technology (ETH) Zurich, Zurich, Switzerland

[2] Department of Structural Engineering, National Technical University of Norway (NTNU), Trondheim, Norway

[3] Division of Structural Engineering, Chalmers University of Technology, Gothenburg, Sweden

1 Introduction

The recent progress in timber engineering has made possible the construction of larger and more complex structures where timber has a primary structural role. Long span timber roofs, prestressed timber walls and frames, and tall timber buildings are becoming increasingly common.

Owing to timber's complex behaviour, such large structures present a number of challenges that engineers have not previously faced. The combination of light weight – relative to other common building materials such as steel and concrete – and low stiffness make serviceability criteria, in particular structural vibrations, difficult to satisfy. The inherent brittleness of timber for failure modes in tension and in shear make the redistribution of loads a challenging outcome to design for. In the large scale of tall timber structures, the effect of different parameters such as time (e.g. creep), moisture content, duration of load, and member size need to be understood in more detail.

One such challenge to address is structural robustness, or the ability of a structure to prevent adverse consequences that are disproportional to their origin. It is a desirable property that has received a lot of attention after famous collapses such as the Ronan Point building in London, in 1968 (Agarwal, et al., 2011). So far, research on structural robustness has focused primarily on concrete and steel structures, with only recent efforts focusing on timber structures, for example Mpidi Bita (2019), Huber, et al. (2018), Lyu, et al. (2018), and Sørensen, et al. (2010).

Consideration of robustness is not straightforward, due to the large number of variables and unknowns. There is no currently accepted "best practice" approach to consider robustness, but rather various methods which an engineer can consider to reduce the probability of disproportionate collapse of a structure. An overview of the methods is presented in the reports of COST Action TU0601 (2011), COST Action E55 (Sørensen, 2010) and the review of robustness by Arup (2011).

The different approaches to quantify and evaluate robustness can be summarized as follows:

- Risk approaches, where the risks of direct versus total (direct + indirect) consequences of an action are compared (Baker, et al., 2007), can be comprehensive methods to quantify robustness.
- Reliability approaches, where the probabilities of failure of the structure at the undamaged and damaged stages are compared (Sørensen, et al., 2010) can help with reducing the probabilities of failure, without the complex analysis of consequences.
- The most commonly used methods are deterministic, where the structural reaction of a building for assumed damage scenarios is modelled (Huber, et al., 2018). Despite there being numerous non-structural design methods to increase robustness, explicit consideration of the response of a structure to an abnormal event (e.g. column loss in a building) is the most common approach in practice (Starossek & Haberland, 2010).

When implementing the deterministic robustness approach in the design of a structure, direct and indirect methods exist (Huber, et al., 2018). Indirect methods aim to enhance a building's robustness without considering specific components or scenarios. Examples are tying some or all structural components together to enhance system performance, and providing redundancy at certain locations, or globally. Direct methods are applied for specific damage scenarios, for example a failed column due to an explosion. Examples are the Alternative Load Path Analysis (ALPA), designing key elements, and splitting the structure into different compartments to limit the spread of structural damage.

The above methods are studied in structures using analytical, experimental, or numerical analyses. The Finite Element Method (FEM) is most commonly used. The complexity of modelling can vary from simple, conservative linear static analyses, to complex, more accurate non-linear dynamic analyses. In addition, there are other methods available such as the Discrete Element Method (DEM), and the Applied Element Method (AEM) (Adam, et al., 2018).

A comprehensive overview of the structural robustness requirements in building codes is included in Adam et al. (2018) and Arup (2011). Although such requirements exist in most building codes, little help is offered to design structures accordingly. This is particularly problematic for timber structures, where specific considerations of

their potential brittleness are not explicitly reflected in the codes, with the exception of the Swiss design code SIA265 (2012), which provides additional robustness provisions regarding ductility.

2   Scale Approach

In order to study structural robustness, it is useful to define the event of "collapse" (or more general "indirect consequence") as a result of the events "damage" (or more general "direct consequence") and "exposure", see Figure 1.
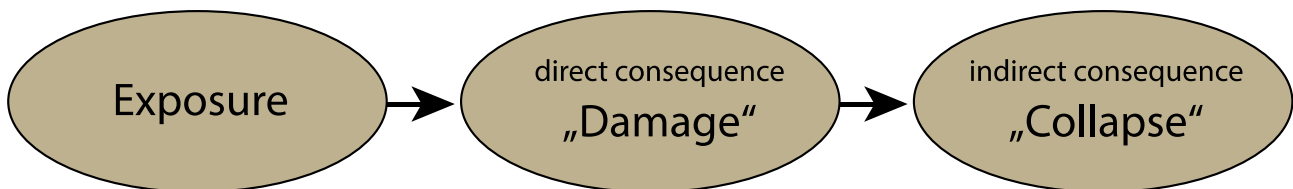

Figure 1: Structural collapse as a result of a sequence of events.

The probability of collapse can be formulated correspondingly, see e.g. (Starossek & Haberland, 2010).

$$\underset{\text{Probability of Collapse}}{\text{P}(C)} = \underset{\text{Exposure}}{\text{P}(E)} \times \underset{\text{Vulnerability}}{\text{P}(D|E)} \times \underset{\text{Robustness}}{\text{P}(C|D)} \qquad \text{Eq.1}$$

Robustness is related only to one of the three terms of the entire formulation, and is given by the conditional probability of a collapse C given a damage D which was caused by an exposure event E. This formulation explains well how component design (i.e. reducing vulnerability P($D|E$)) is reducing the collapse probability without increasing structural robustness – and component design is the strategy mainly followed in current design codes. In some cases, however, it is more economical for the engineer to control robustness for an effective reduction of the probability of collapse (Starossek & Haberland, 2010).

In the above formulation of the probability of collapse of a structure, "vulnerability" may refer to the components of the structure (e.g. beams, columns) and "robustness" may refer to the behaviour of the entire system of these components. For example, a building which has strengthened columns with a low probability of failure in the event of an explosion is said to have low vulnerability, and if it can redistribute loads from a failed column without collapsing, it is said to have high robustness.

It is however also possible to consider the robustness of a single element. For example, a column is said to have low vulnerability if its sub-components (e.g. web stiffeners, end connections) are unlikely to fail in a given exposure. Likewise, if any of these sub-components fail and the column survives, the column has high robustness.

The same can be applied to a connection and its parts (e.g. dowels). It becomes useful to consider a structure at multiple levels of the scale, while looking at robustness at each level separately. An example of a building is illustrated in Figure 2.
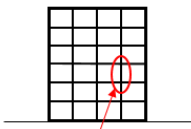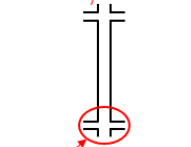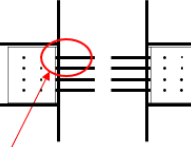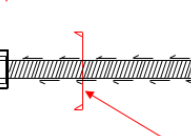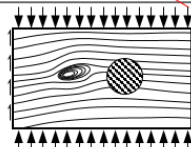
Level		Robustness of building	Robustness of components	Robustness of connections	Robustness of materials
System		**Robustness**			
Components		**Vulnerability**	**Robustness**		
Connections			**Vulnerability**	**Robustness**	
Connectors				**Vulnerability**	**Robustness**
Materials					**Vulnerability**

Figure 2: Robustness in a multi-level scale approach

Such a multi-level consideration of robustness is helpful to understand design methods such as the key elements: while indeed a key element does not increase the robustness of the entire structure (its removal will lead to disproportionate collapse), it can be designed in such a way to be robust in itself (low probability of failure of the key element), which translates to a low vulnerability on the level of the entire structure. Robustness of the key element is equivalent to the vulnerability of the structure, looked from a different perspective.

3   Proposed Framework

The interest of the structural engineer is to design a structure that has an acceptable overall probability of collapse. For given exposure, this can be achieved with an appropriate combination of high robustness and low vulnerability throughout the multiple levels of scale. A qualitative framework is presented in this section with an example. A quantitative example is presented in the following section.

3.1   Localised vs Systematic Exposures

It is important to first distinguish between two basic types of exposures to a structure: localised, where one or a small number of elements are affected (e.g. explosion near column), and systematic, where all or repeated elements are affected (e.g. design error affecting multiple connections). Current design strategies, for example structural tying, are aimed at localised exposures, but may be the cause of collapse in a systematic exposure scenario (part of the reason, for example, of the collapse of the Bad Reichenhall Arena, (Winter & Kreuzinger, 2008)).

This issue can be avoided if design methods for localised and systematic exposures address different levels of the building scale. An example of a tall timber building illustrates this in Figure 3.
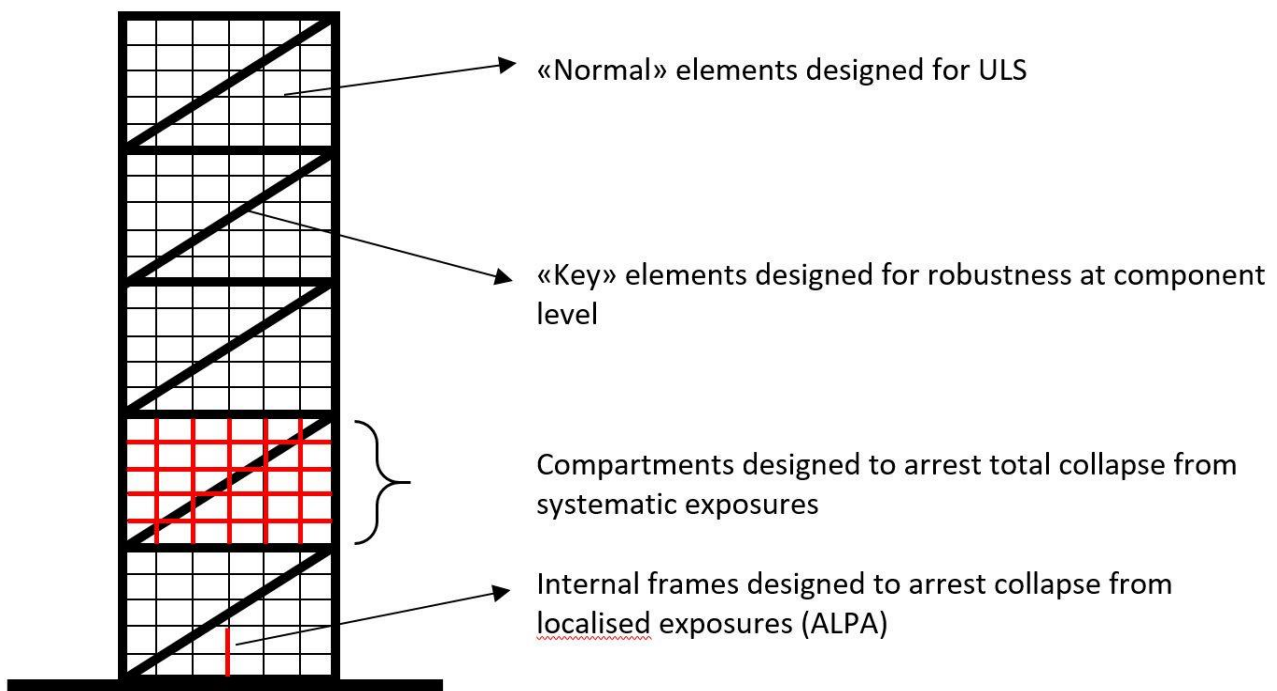

Figure 3: Example of tall timber building concept

In this example, compartments are formed by defining strong borders using key elements. These key elements are designed to have a high component robustness, such that their failure is acceptably unlikely for both localised and systematic exposures. A "normal" system of structural members is recommended to be contained within the compartments, whereby "normal" refers to the current expected qualities of a system that can develop alternative load paths, should local failure occur in one of its

members. If the building is exposed to a systematic error, this may cause the collapse of an entire system of structural members within its compartment. The failure will however be arrested by the key elements at the borders of the compartment, and the progressive collapse of the entire structure is prevented. Robustness for the entire building is provided with the combination of the robustness design in the component level (key elements forming compartments) and in the system level (internal redundancy of each compartment).

This complete collapse resistance approach can be seen in modern tall building design:

Figure 4: The Leadenhall Building, London, UK. ©Colin @Wikimedia Commons

Figure 5: Treet, Bergen, Norway. © BOB Norge

Particularly in modern skyscrapers, achieving new heights has required engineers to use advanced structural methods such as outriggers and mega frames. As engineers seek new heights in timber buildings, such advanced structural methods are already required for building heights of less than 100m, due to the lower strength and stiffness of timber as a material. A lot can be learnt from the design of supertall skyscrapers.

3.2   Complete Framework

The above example only serves to illustrate the general application of the multi-level scale approach for robustness. When considering tall timber buildings, or very tall buildings of any structural material, it is recommended to add the compartments as a distinct level in the scale. The complete scale with the design method for robustness on each level is shown in Figure 6.
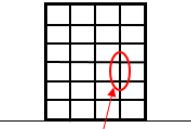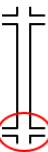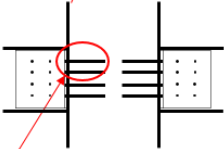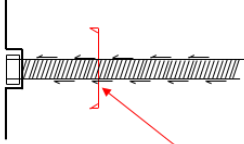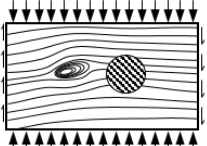
	Level	Design Method	Responsibility
Whole building		Compartmentalisation	Structural Engineer (Conceptual Design)
Compartments		Alternate Load Path Design	Structural Engineer (Conceptual Design)
Components		Key Element Design	Structural Engineer (Conceptual Design)
Connections		Robust Connection Design	Structural Engineer (Detailed Design)
Connectors		Key Connector Design	Supplier
Materials		Material Grading / Robust Manufacture	Supplier

Figure 6: Complete robustness approach for a tall (timber) building

The design of robust connections (for example those connecting the large key elements of a mega frame) using groups of connectors (e.g. dowels) and "key connectors" is not further discussed in this paper. The principles, however, remain the same.

In separating the different levels of the scale, it is important to recognise the different parties responsible for the design of robustness on each level as well as the different design methods. The responsibility list is not exhaustive; it shows that the structural engineer need not control every level of the scale. Conceptual design is a collaboration of engineers, architects, contractors, and many others.

The qualitative approach illustrates the principles of the proposed framework, which is material independent, but where the properties of timber would highly influence the conceptual design decision. In the next step, an attempt is made to quantify the robustness within this framework.

4 Quantification of Robustness

4.1 Formulation Including Consequences

In Equation 1, as presented by Starossek & Haberland (2010), the last term is defined as robustness, when in fact it represents the complement of robustness: reducing the probability of progressive collapse P($C|D$) corresponds to the increased robustness of a structure.

Equation 1 takes into account the probability that an event occurs and the probabilities of subsequent damage. To allow for a more complete picture, the risk of collapse must be evaluated. This includes the probabilities of the events together with their corresponding consequences. For the equation to cover the general case of structural safety, we recommend to replace the term "collapse" with "consequences". Following Baker et al. (2007), the expected consequences can be expressed as the sum of direct and indirect consequences:

$$\mathbb{E}[C] \quad = \quad \mathbb{E}[C_{Dir}] \quad + \quad \mathbb{E}[C_{Ind}] \qquad \text{Eq.2}$$

Expected Consequences   Expected Direct Consequences   Expected Indirect Consequences

From the definition the probability of collapse, the exposure and vulnerability of a structure are related to the direct consequences, whereas the indirect consequences are related to the robustness of the structure, given that damage has already occured. The terms in Equation 2 can therefore be broken down to express the expected consequences as follows:

$$\mathbb{E}[C] \; = \; \big(\mathrm{P}(E) \times \mathrm{P}(D|E)\big) \times C_{Dir} \; + \; \big(\mathrm{P}(E) \times \mathrm{P}(D|E) \times \mathrm{P}(C|D)\big) \times C_{Ind} \qquad \text{Eq.3}$$

The (dis)proportionality between direct and indirect consequences, which is the essence of the robustness definitions, can be quantified using a robustness index, which is the ratio of expected direct consequences and total expected consequences (Baker, et al., 2007). It must be noted that this index is independent of the exposure and vulnerability: it only considers the disproportionality of consequences.

$$I_{Rob} = \frac{\mathbb{E}[C_{Dir}]}{\mathbb{E}[C]} = \frac{\mathbb{E}[C_{Dir}]}{\mathbb{E}[C_{Dir}] + \mathbb{E}[C_{Ind}]} = \frac{C_{Dir}}{C_{Dir} + \mathrm{P}(C|D) \times C_{Ind}} \qquad \text{Eq.4}$$

4.2 Application to Simple Example

The above formulation is applied to a simple example of a continuous glulam beam with three supports, in the scenario of the loss of the middle support. Figure 7 shows the beam with a rectangular cross-section B x H of bending stiffness EI and two spans of length L in its undamaged state. A uniformly distributed load Q (floor load) and a point load F over the middle support are applied. The indicative bending moment diagram is shown in green.
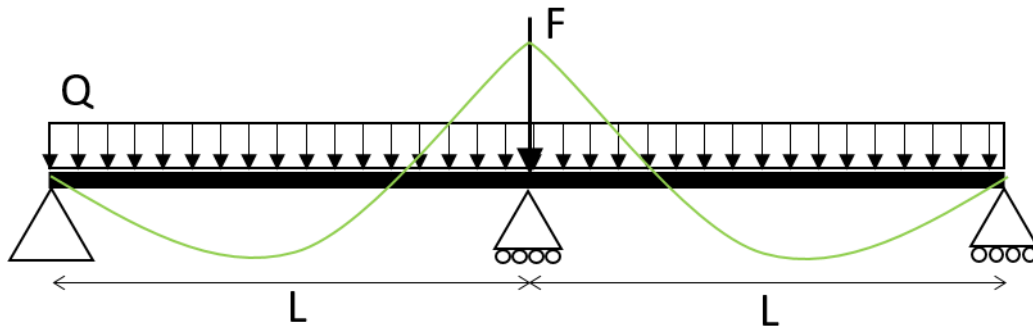
Figure 7: Illustration of continuous beam in its undamaged state

A Monte Carlo Simulation using an analytical limit state function of the bending stress was carried out in Matlab by modelling each variable using an appropriate distribution as shown in Table 1 below. The distribution type and coefficient of variation have been selected according to the JCSS (2006) and Baravalle (2017). The limit state function is the following:

$$G_{healthy} = R - \sigma = R - \frac{\frac{(B \times H \times \rho + Q) \times L^2}{8} \times \frac{H}{2}}{I} \qquad \text{Eq.5}$$

It is assumed that the supports are sufficiently stiff such that the maximum bending moment occurs over the middle support according to the continuous beam formulae. No other stresses are checked apart from bending in this simplified example that only illustrates the application of the robustness formulation of Equation 3.

Table 1: Variables for the Monte Carlo Simulation

Variable	Distribution	Mean	CoV
Beam height (H)	Lognormal	250 mm	5%
Beam width (B)	Lognormal	140 mm	5%
Density (ρ)	Normal	480 kg/m³	10%
Span (L)	Lognormal	4 m	1%
Imposed UD Load (Q)	Gumbel	5 kN/m	22%
Imposed Point Load (F)	Gumbel	15 kN	22%
Bending Strength (R)	Lognormal	24 N/mm²	15%

For $N = 10^6$ Monte Carlo simulations, the probability of failure for the continuous beam is approximately $P_f = 1.3 \times 10^{-5}$.

Now let us assume an exposure occurs (e.g. explosion) ($P(E) = 1$) that causes a 0.1% probability that the middle support is damaged ($P(D|E) = 0.001$), as shown in Figure 8:
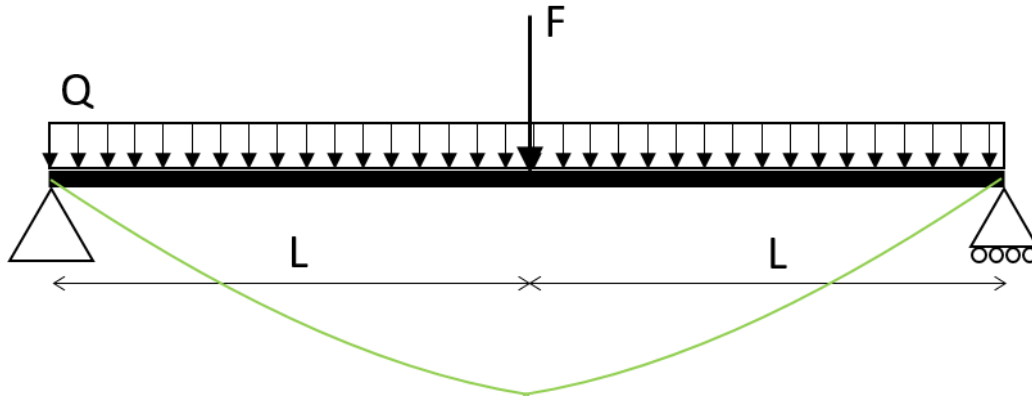
Figure 8: Illustration of continuous beam in its damaged state

At this damaged state, the beam is called to carry the loads in bending, and the maximum bending moment occurs at midspan, with the new limit state function being

$$G_{damaged} = R - \sigma = R - \frac{\left(\frac{(B \times H \times \rho + \psi_2 \times Q) \times L^2}{2} + \frac{\psi_2 \times F \times L}{2}\right) \times \frac{H}{2}}{I} \qquad \text{Eq.6}$$

where ψ_2 = 0.3 assuming a residential or office construction according to Eurocode 0 (2002) . The $N = 10^6$ Monte Carlo simulations return $P_{f,damaged}$ = 0.0318, which is several orders of magnitude higher than what is recommended for component design according to the JCSS (2001). For the scenario "loss of middle support", $P_{f,damaged} \equiv P(C|D)$, while the probability of losing that support in the first place is assumed as $P_{support\_loss} \equiv P(D|E)$ = 0.001.

We now need to evaluate the consequences to complete the calculation of the robustness index. For the assessment of the structural robustness index it is sufficient to estimate the relation between direct and indirect consequences. In the case of the presented example it is the relation between the consequences of the loss of the support and the consequences of the loss of the beam. The relation is assumed to be 1/100. Substituting all values into Equation 4 gives:

$$I_{Rob} = \frac{1}{1 + 0.0318 \times 100} = 0.239$$

which is rather low, meaning that a large proportion of the consequences of the loss of the middle support are indirect, corresponding to poor robustness. It is important to realise that this is considering robustness at the scale of the beam and that the probability of the loss of the middle support makes no difference in the robustness index calculated. This is where the multi-scale approach is useful.

Let us go one level lower in the scale and consider what happens to the middle support only. From the previous calculation we have already assumed the scenario conditional on the exposure event, i.e. $P(E)$ = 1. The exposure event causes failure of the support with $P(D|E)$ = 0.1%. The costs of this failure are $(C_{Dir} + C_{Ind})_{support} \equiv C_{Dir,beam}$ = 1. The probabilities are $P(C|D)_{support} \equiv P(D|E)_{beam}$ = 0.001, in line with Figure 2. Now we need to consider the initial (direct) consequences of the explosion. The support

may be designed such that damage given the explosion has a moderate probability ($P(D|E)_{support}$ = 0.1) and a low relative consequence ($C_{Dir,support}$ = 0.05) but the probability of complete loss of the column ($C_{Ind,support}$ = 0.95) is small ($P(C|D)_{support}$ = 0.001), therefore the support itself is robust. Substituting the terms in Equation 4 gives I_{Rob} = 0.981. Figure 9 illustrates the above more clearly.

P(E)	P(D|E)	P(C|D)	C_{Dir}	C_{Ind}	I_{Rob}
1	0.1	0.001	0.05	0.95	**0.981**

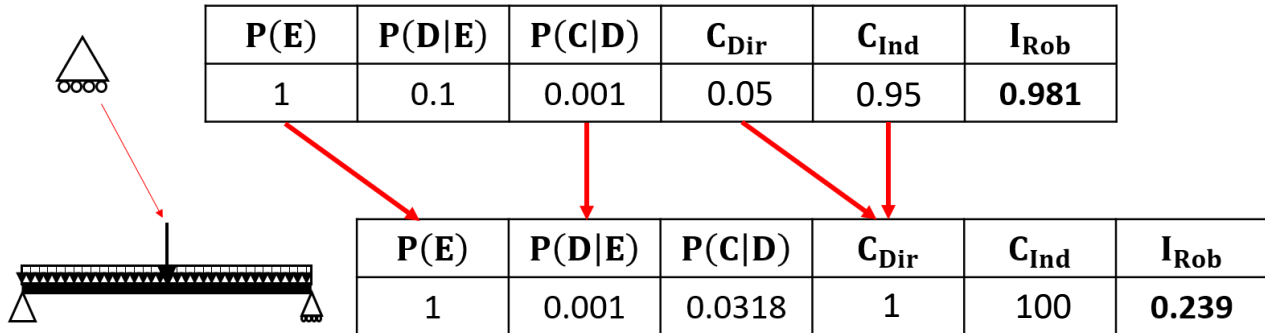| P(E)	P(D|E)	P(C|D)	C_{Dir}	C_{Ind}	I_{Rob}
1	0.001	0.0318	1	100	**0.239**

Figure 9: Illustration of scale approach and the robustness index for the beam example

This example raises the question of whether it is more economical to design for robustness on different scales to achieve the level of safety required.

4.3   Quantification Remarks

The example analysed in Section 4.2 is the application of the robustness index calculations and the scale approach in their simplest form. A more elaborate analysis (for example Finite Elements with consideration of nonlinearities and dynamics) shall ultimately replace the current analytical check for bending stress, to reflect the substantially more complex reality when larger structures are considered. However, despite the simplicity of the example, it illustrates some very important points with regard to structural robustness.

Another point to be raised is that the analyses are scenario-dependent. For a scenario-independent analysis one has to take $P(E)$ = $P(D|E)$ = 1 and consider only the sufficient reduction of $P(C|D)$, that is to increase robustness. The ability to do that in multiple levels of the scale becomes even more important to find the optimal solution.

Finally, a point should be made regarding the probabilities and consequence calculations: there are numerous underlying assumptions that can affect the results. These are discussed in more detail in the referenced probabilistic literature, for example JCSS (2001), Baravalle (2017), and Baker et al. (2007). In addition, it should be noted that the main findings of this paper are based on the relative changes between different scales and/or design scenarios. The observations and conclusions in this paper are therefore not sensitive to possible lack of precision in the assumptions.

5 Impact on Design Codes

Design codes regulate many of the design choices of structural engineers. As the size of timber structures increases and robustness becomes an increasingly complex topic of high importance, the future design codes should incorporate the topic of robustness in a simple but adequate way, to help practicing engineers consider it effectively in their designs.

Following the proposal of an improved robustness framework in the previous sections, the following recommendations are made regarding its inclusion in design codes. These recommendations consider only on the proposed robustness framework, and do not affect the existing provisions.

1. Make a clear distinction between the two types of consequences (localised and systematic).
2. Include robustness provisions that address different levels of the scale and not only the current definition of a system as a collection of building components (beams, columns, walls, floors).
3. The background calculations illustrated in the previous section can form the basis for evaluating and recommending different options to reduce the highest expected consequences, such that engineers can deterministically address robustness while achieving a target level of safety.

With more progress on the quantification of robustness, based on the example in Section 4, more specific code provisions can be recommended. In general, a more vivid discussion on how to increase robustness in structures and how to incorporate robustness in design codes is needed.

6 Conclusion

This paper presented an introduction into the current state-of-the-art for the topic of structural robustness, which is becoming increasingly important as we build larger and more complex timber structures, like tall timber buildings. An improved framework to design robust structures is proposed, based on:

• A distinction between localised and systematic exposures;
• A multi-level scale approach where measures to address the different types of exposures are considered at various levels and not just the building system alone.

This framework is qualitatively applied to a tall timber building example that combines key elements and ALPA to create compartments that ensure the structure's survival under both localised and systematic exposures.

The proposed framework includes consequences as well as probabilities for quantifying robustness. A simple example is used to demonstrate the application of the framework to a beam. It is seen that it is possible to quantify robustness at different levels of the scale. This distinction can be very useful for further calculations if the

cost of risk-reducing measures is accurately quantified. The current robustness approach is not looking at the building in a multi-level scale approach, but rather as a single system of components. The multi-level scale approach may be used to design solutions for safer structures that are not currently obvious.

Both qualitative and quantitative examples illustrate a more complete approach to considering the collapse resistance of all structures, with particular interest to tall buildings. Three recommendations are made for the potential application of the findings in a new generation building code that considers robustness holistically.

7 Acknowledgements

8   References

Adam, J. M., Parisi, F., Sagaseta, J. & Lu, X., 2018. Research and practice on progressive collapse and robustness of building structures in the 21st century. *Engineering Structures,* Volume 173, pp. 122-149.

Agarwal, J. et al., 2011. Robustness of Structures: Lessons from Failures. *Structural Engineering International,* Issue 1, pp. 105-111.

Anon., 2002. *Eurocode 0.* Brussels: CEN.

Arup, 2011. *Review of international research on structural robustness and disproportionate collapse.* London: Department for Communities and Local Government.

Baker, J. W., Schubert, M. & Faber, M. H., 2007. On the Assessment of Robustness. *Structural Safety,* Issue 30, pp. 253-267.

Baravalle, M., 2017. *Risk and Reliability Based Calibration of Structural Design Codes.* Trondheim: NTNU.

Canisius, G., 2011. *Structural Robustness Design For Practicing Engineers.* s.l.:COST TU0601.

Eurocode 0, 2002. *Basis of Structural Design (EN1990).* s.l.:s.n.

Huber, J., Ekevad, M., Girhammar, U. A. & Berg, S., 2018. Structural Robustness and Timber Buildings - A Review. *Wood Material Science & Engineering.*

JCSS, 2001. *Probabilistic Model Code: Part 1 - Basis of Design.* s.l.:JCSS.

JCSS, 2006. *Probabilistic Model Code: Part 3 - Resistance Models.* s.l.:JCSS.

Lyu, C. et al., 2018. *Progressive Collapse (Robustness) Behaviour of Mid-Rise Mass Timber Frame Buildings.* Seoul, WCTE.

Mpidi Bita, H., 2019. *Disproportionate Collapse Prevention Analyses for Mid-Rise Cross-Laminated Timber Platform-Type Buildings.* Vancouver: UBC.

SIA, 2012. *Swiss Standard 265: Timber Structures.* s.l.:s.n.

Sørensen, J. D., Dietsch, P., Kirkegaard, P. H. & Köhler, J., 2010. *Design for Robustness of Timber Structures.* Aachen: Shaker Verlag GmbH.

Starossek, U. & Haberland, M., 2010. Disproportionate Collapse: Terminology and Procedures. *Journal of Performance of Constructed Facilities,* 24(6), pp. 519-528.

Winter, S. & Kreuzinger, H., 2008. The Bad Reichenhall ice arena collapse and the necessary consequences for wide span timber structures.

Discussion

The paper was presented by K Voulpiotos

P Quenneville asked would you look at requiring reduction of forces. K Voulpiotis said this might be needed.

E Toumpanaki commented construction and site inspection would be another set of issues that would need consideration.

U Kuhlmann commented that connection to probability needed lots of assumptions that could influence results. A more deterministic approach would be preferred. The probabilistic method connected with cost would be even more problematic. Consequence in view of safety would be better . K Voulpiotis responded that component design is already based on probability in the background. He agreed that many assumptions were needed but the approach could be used to guide the conceptual design phase. Finally the concept of cost would be tied to safety and not to monetary values. U Kuhlmann responded that focus on consequence would be better than cost. R Jockwer agreed and they discussed the relationship between I_{Rob} vs C_{Ind}/C_{Dir} in terms of good and bad conceptual design for robustness.

P Dietsch discussed the proposed framework. What else would be needed in terms of robustness on the level of connections, components, and materials in addition to good design practice? E Voulpiotis agreed and said that if connectors were needed for robustness as a conceptual point, one would need to provide additional considerations to achieve this.

P Palma asked about the robustness index. How to assure that apples are not compared to pears, what kind of consequences would be needed for consideration and how a designer could determine this. E Voulpiotis responded that there are many I_{Rob} definitions and the I_{Rob} in this paper could be referenced to Baker's work as a relative term. P Palma said a better way is to simply state a building is safe if a certain index is reached.

H Daneshvar commented that the framework is not timber focus and how could you bring this toward timber. E Voulpiotis responded by discussing compartment design for timber as we are moving towards more tall timber structures. P Quenneville agreed that this work is completely material independent. E Voulpiotis responded that this is a valid concern but timber design might have different consequences per ductility, size effects etc. P Quenneville discussed cost or consequence for timber and mentioned that the structural concept will have a larger influence on robustness than the lower steps in the framewpork. E Voulpiotis responded that they will be working on this.

4 INTER Notes, Tacoma WA, USA 2019

Note 1   Ductility Factors of Timber Constructions Combined by Parts with Different Ductility Factor - T Tsuchimoto, T Miiyake

Note 2   Determination of Design Fires in Compartments with Combustible Structure – Modification of Existing Design Equations - J Schmid, R Fahrni, A Frangi, N Werther, D Brandon, A Just

Note 3   Timber Structures in the Cooling Phase – Additional Influence Factors - J Schmid, M Klippel, R Fahrni, A Frangi

Note 4   Behaviour of Cyclic Loaded Joint Made with Glued in Rod in Corner of CLT Frame - J Barbalic, V Rajcic, R Zarnic, N Perkovic

Note 5   Comparison of Cyclic Bending Test Methods for Self-tapping Screws – K Kobayashi

Ductility factors of timber constructions combined by parts with different ductility factor

Takahiro TSUCHIMOTO, Building Research Institute

Tatsuya MIYAKE, Nihon System Sekkei Co.ltd.

1 Introduction

In high seismic country Japan, the ultimate capacity of building over a certain scale must be design under the extremely rarely occurred earthquake. In other words, it need be verified that the applied load or stress on the members, horizontal elements and joints under the base shear of 1.0 is not over the ultimate capacities of them. However, the applied load or stress can be decreased depending on the abilities of deformation. The factor indicating how much they can be decreased is called as Ds and provided in the Notification of Ministry of Construction. The Notification has never shown the Ds of the structure combined by parts with different ductility factor. Then, the Ds of the timber constructions combined by parts with different ductility factor were studied analytically in this paper.

2 Analytical model and parametric study

From the past papers, the load-deformation relationships of the semi-rigid glulam frames, the shear walls, the brace systems and arch structure were picked up and modelled, as shown Figure 2.1. The vertical axis of it was normalised by the allowable capacity, Qa. The semi rigid glulam frame was assumed as 3 variation with high, medium and low capacity. The shear wall was distinguished between the plywood and gypsum board. The brace system was distinguished between the glulam jointed by the drift pins with steel plate and jointed by the bolts. The arch structure was distinguished between the curved glulam without joints and with some joints and straight glulam jointed by the drift pins. The ultimate capacity obtained by the bilinear model of the load-deformation relationships was defined as Qu. The Ds of alone structure is no other than Qa/Qu. The Ds of medium glulam frame, SW with plywood and gypsum board and brace jointed by DP and bolts were 0.37, 0.609, 0.707, 0.505 and 0.244, respectively.

The combinations with variable load-deformation relationships, as mentioned above, were applied to the structural model which the summation of allowable capacity, *Qa* is 1.0. The mixture ratio of the different load-deformation relationships were defined as *β*. The summation of the ultimate capacity of the different structure, *Qu* was varied from 0.2 to 0.75. The time history response analysis were con ducted to the structural model till the ultimate state.
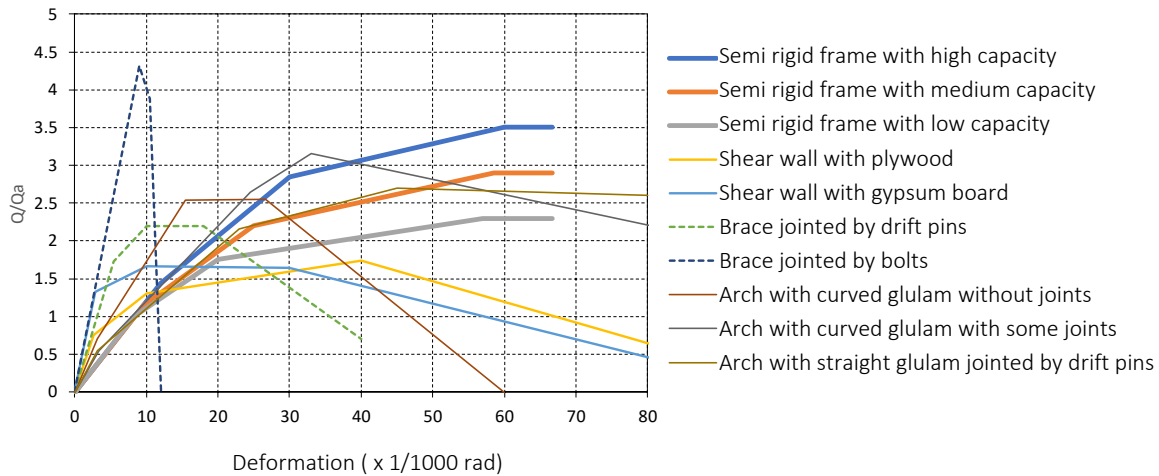

Figure 2.1. The picked up and modelled load-deformation relation ships.

3 Results

As a result of the parametric study, the response load-deformation relationships were obtained. When the maximum response deformation agreed with the ultimate deformation, the base shear was calculated by the results and defines as *Cu*. The *Cu* is no other than the ductility factor, *Ds* of combination structure after all. Some samples of *Ds* were shown in Table 3.1.

Table 3.1. Examples of ductility factor Ds obtained by the analysis.

Glulam frame with medium capacity combined with	Combination ratio *β*										
	0	0.1	0.2	0.3	0.4	0.5	0.6	0.7	0.8	0.9	1
SW with plywood	0.34	0.34	0.34	0.31	0.29	0.29	0.29	0.29	0.30	0.35	0.35
SW with gypsum B.	0.34	0.34	0.34	0.29	0.30	0.30	0.29	0.30	0.35	0.37	0.40
Brace jointed by DP	0.34	0.34	0.29	0.30	0.40	0.41	0.43	0.45	0.48	0.49	0.50
Brace jointed by bolts	0.34	0.29	0.29	0.52	acalculia						

4 Conclusions

The ductility factor of timber constructions combined by parts with different ductility factor need to adopt the higher one. However, the case of combination with shear wall had a possibility to decrease the ductility factor still more.

Determination of design fires in compartments with combustible structure – modification of existing design equations

Joachim Schmid, Reto Fahrni, Andrea Frangi, ETH Zurich, Switzerland

Norman Werther, TUM, Germany

Daniel Brandon, Alar Just, RISE, Sweden

Keywords: timber, physically based fire, Eurocode, fire load, heat release rate

1 Introduction

The determination of the fire development, i.e. the temperature-time curve, is an essential input for the fire design of structural elements when performance based design (PBD) is used. PBD uses the particular boundary conditions (i.e. geometry, openings, and fire load) of a compartment to define a relevant temperature development. This may be done according to EN 1991-1-2 Annex A or another method such as the corresponding German National Annex. Regardless the method, the consideration of the contribution of the structural fire load is required by EN 1991-1-2. The increase of the movable fire load by the structural fire load for timber corresponding a charring depth was mentioned by several authors (K. Leikanger -Friquin 2012, Brandon 2018, McNamee et al 2019). However, various approaches exist. This paper gives guidance about how to include the contribution of unprotected timber surfaces in the actual framework of EN 1995-1-2. Here, the estimation of the a) maximum heat release and b) the calculation of the fire load density are extended and c) the amount of heat released at the façade is given.

2 Background and state of the art

a. Available design models determine whether the fire is ventilation or fuel controlled. This because the burning rate of a solid is limited either by the availability of oxygen or the maximum production rate of combustible volatiles, i.e. surface-volume-share of the particular type of fire load; the minimum is decisive. Whenever the enclosure condition show low oxygen access but combustible volatiles are

created exceeding the required oxygen for the combustion, significant flaming at the façade exterior the compartment can be observed. Thus, all oxygen entering the compartment is consumed, a certain share of the combustion occurs exterior and the ventilation characteristics control the fire, i.e. a ventilation controlled fire.

b. The fire load density considers the available fire load per floor area depending on the occupancy of the compartment. No further guidance is given for the consideration of combustible surfaces, i.e. the heat release rate of structural timber with a low ratio volume to surface.

2.1   Limitation of available methods

This note focuses on the physically based fires in general and the parametric fire of EN 1991-1-2 in particular. In the method, an opening factor considers the compartment geometry including the opening. The opening height is a crucial variable as it allows the discharge of hot gases and the entry of oxygen. The parametric fire time-temperature curve can be considered as deformed in its height (modified temperature increase due to the thermal inertia) and length (depending on the availability of a fire load). For a timber structure, it would be conservative to assume that the structure represents an addition to the movable fire load. It seems scientifically more appropriate to consider the increase of the fire load using the charcoal depth. Recently, the iteration process required for the parametric fire design was described by Brandon et al. (2018). Verifying the approach with a series of large compartment experiments Brandon et al. introduced a combustion share of 0.7 to fit the measurements. With a deviating approach, McNamee et al. (2019) propose a combustion efficiency factor between 0.7 and 0.9 to fit their measurements.

3   Extended Eurocode Design

a) The floor related design value of the fire load density $q_{f,d}$ is currently defined:

$$q_{f,d} = q_{f,k} \cdot m \ \text{[MJ/m}^2\text{]}$$ (1a)

where

$q_{f,k}$ is the characteristic fire load density,

m is the combustion factor set to 0.8 for mainly cellulosic materials, thus also for timber. For the actual extension, the factors taking into account the fire activation risk and the different active firefighting measures are not included in Eq. (1a).

To consider combustible surfaces in the compartment Eq. (1a) should be extended to:

$$q_{f,d} = (q_{f,k} + q_{c,k}) \cdot m \ \text{[MJ/m}^2\text{]}$$ (1b)

where $q_{c,k}$ is the additional fire load due to the combustible structure which is set to:

$$q_{c,k} = A_c \cdot s \cdot \beta \cdot t \cdot \alpha / A_f \ \text{[MJ/m}^2\text{]}$$ (1c)

where

A_f is the floor area of the fire compartment, in m^2,

A_c is the area of the combustible surfaces, in m^2,

s is the specific heat release rate derived to s=0.13 $\frac{\text{MW}}{\text{m}^2}/\frac{\text{mm}}{\text{min}}$ based on a wood density of 450 kg/m^3 and the heat of combustion of wood 17.5 MJ/kg,

t is the relevant time of fire exposure, in sec (e.g. with temperatures higher than 300°C),

β is the charring rate, in mm/min.

Further, a correction factor α < 1 should be implemented to account for the combustion boundary conditions (reduced heat release of structural elements with a low ratio volume to surface in comparison to the movable fire load. Brandon (2018) proposed a combustion share factor of 0.7; however, a slightly different description of the heat release density was used. Conservatively, in Eq. (1c) α=1.0 can be used.

b) Correspondingly, the maximum heat release rate for fuel-controlled fires is defined:

$$Q_{\max,f,k} = HRR_f \cdot A_f + \textcolor{red}{HRR_{timber} \cdot A_c} \quad [\text{MW}] \tag{2a}$$

where HRR_{timber} is the heat release rate of timber for a certain charring rate:

$$HRR_{timber} = s \cdot \beta \quad [\text{MW/m}^2] \tag{2b}$$

The terminology in Equations (1) and (2) follows the design procedure of Eurocode and its content is based on straight forward physics. In contradiction to McNamee et al. (2019) a variable HRR for timber is proposed instead of a charring rate of 1.5 mm/min and the combustion factor is considered to be valid for the fire load irrespectively the source (movable or structural fire load). The factor α should be determined by calibration to experimental results and will be provided in the new Eurocode 5 replacing the version 2002.

4 References

Brandon D, Koji K, Hakkarainen T (2018): Performance based design for mass timber structures in fire Design - Calculation Example, COST FP1404 document N214-07. DOI 10.3929/ethz-b-000319459

McNamee, R, Zehfuss, J, Bartlett A, Heidari, M, Robert, F, Bisby, L (2019): Enclosure fire dynamics with a combustible ceiling, INTERFLAM 2019 proceedings, London.

Eurocode 1 (2002): Eurocode 1: Actions on structures - Part 1-2: General actions - Actions on structures exposed to fire. CEN. (EN 1991-1-2).

Eurocode 5 (2004): Design of timber structures - Part 1-2: General - Structural fire design. CEN. (EN 1995-1-2).

Timber structures in the cooling phase – additional influence factors

Joachim Schmid, Michael Klippel, Reto Fahrni, Andrea Frangi, ETH Zürich, Switzerland

Keywords: timber, fire dynamics, cooling phase, gas velocity, turbulence, oxygen, charring, char recession

1 Introduction

For more complex buildings, authorities and building owners tend to require an analytical or performance based design (PBD). Contrary to the traditional fire resistance design, using a standardised fire exposure (i.e. the EN/ISO standard fire and a verified time without collapse) the PBD requires structural survival of a realistic fire including the flashover and the cooling phase. Some design models for non-combustible structural elements exist while for timber elements further research is needed to provide tools for the holistic description of their behaviour in real fires.

Recent research showed that further variables influence the behaviour of timber members in the cooling phase. In this note, these variables are presented with preliminary results of a study performed at ETH Zürich.

2 Structural timber members in fires

The crucial factor for the description of the load-bearing capacity is the temperature profile within the solid. For short-term impact (a fire), the 300°C isotherm is considered as the marker between uncharred (virgin) wood and char. Besides the charring, the temperature profile within the uncharred section is crucial for its load-bearing capacity. Observing an about linear charring rate despite the logarithmic increase of a standard fire temperature, a significant importance is attributed to the insulating capability of the charcoal layer. Thus, reducing the charcoal layer may affect the temperature profile within the solid significantly. In the past, various authors have reported charcoal contraction describing a certain loss of char layer thickness. Schmid et al. (2018) could observe the effect of char recession under certain conditions in a

"fire tunnel" investigating the charring behaviour of timber under fire exposure varying the oxygen concentration and the gas velocity. Subsequent experimenting at ETH Zürich under conditions representative for the cooling phase of a fire and comparison to fire resistance tests in furnaces improved the understanding of timber in the cooling phase. While the total cross-section in fire resistance tests remains roughly constant (i.e. virgin wood thickness plus charcoal thickness equals the original thickness), the charcoal layer is consumed in the cooling phase under certain conditions.

The following external variables have impact on the charring behaviour in the cooling phase and subsequently the uncharred cross-section:

(1) irradiance heat flux to the surface,
(2) gas temperature,
(3) oxygen contact described by
   a. gas velocity,
   b. oxygen concentration,
   c. degree of turbulence;

Internal variables are the moisture content, density and wood species, which were not investigated in the current project.

3   Experiments at ETH

The novel experimental setup is capable to simulate realistic boundary conditions in fires up to 120 kW/m^2 (exposure level roughly corresponding to standard fire after one hour), 1 to 10 m/s gas velocity and degree of turbulence (high and moderate). In Table 1, the range of results are presented together with well-known values from standard fire resistance testing are given for comparison reasons.

Table 1: Test and experimental results (rounded values) of solid timber.

Variable	Standard fire resistance testing	Cooling phase experiments
Charring rate[1]	0.7 mm/min	0 to 2.5 mm/min
Char recession	0 to 5 mm[1]	0 to 1.5 mm/min

[1] 60 min testing

It is important to observe that results presented in Table 1 for charring and the char recession (rates) are not linearly correlated to one variable (1) to (3). E.g. while an increased gas velocity (gas with certain oxygen content and turbulence) induces a consumption of char (primarily resulting in heat generation and char consumption) the gas temperature decreases which is favourable with respect to the effect on the virgin wood section (i.e. the fire load is "moved").

4   Use of the results

The results aim mainly for the modelling of timber members in the cooling phase of a fire where a natural draft depending on the compartment geometry might elongate the cooling of the compartment when timber members are involved in the fire dynamics.

However, recently, requests by authorities to overlay the accidental case *fire* with *wind* were recognized by the authors. In general, the data obtained in this study might be used for this design scenario. However, the increased uncertainties by modelling the effects of the wind load in its entire characteristic (i.e. wind velocity, wind frequency, and its variation with increasing height above the ground) seem to provide challenging boundary conditions. Further experiments with respect to the topic in general and the recent "new scenario" seem to be essential.

5 References

Schmid, J., Santomaso, A., Brandon, D., Wickström, U., & Frangi, A. (2018). Timber under real fire conditions–the influence of oxygen content and gas velocity on the charring behavior. Journal of Structural Fire Engineering, 9(3), 222-236.

Eurocode 5 (2004): Design of timber structures - Part 1-2: General - Structural fire design. CEN. (EN 1995-1-2).

Behaviour of cyclic loaded joint made with glued in rod in corner of CLT frame

Barbalic, Jure - University of Zagreb, Faculty of Civil Engineering

Rajcic, Vlatka- University of Zagreb, Faculty of Civil Engineering

Zarnic, Roko - University of Ljubljana, Faculty of Civil and Geodetic Engineering

Perkovic, Nikola - University of Zagreb, Faculty of Civil Engineering

1 Introduction

During the design of structures in seismic areas, solution which provides increase of joint ductility and seismic capacity with minimal increase of structural mass is often required. Current research at the University of Zagreb, performed in cooperation with the University of Ljubljana, is leading to the development of hybrid panel made of CLT frame with high-ductility joints and laminated glass infill, which, in addition to strength and stiffness, is also characterized by high level of seismic energy dissipation. Although seismic behaviour of this element significantly depends on dimensions of individual panel segments, as well as on material physical characteristics, bearing capacity is predominantly defined by behaviour of girder-column joint. Previous research has determined the optimal type of joint – with glued-in rod. Further research, done under CSF project VETROLIGNUM (IP-2016-3811), is presented in paper. The main goal was to define how redistribution of internal forces and bending moments as well as stiffness of elements impact on bearing capacity and ductility of the joint. Samples with different rod diameters as well as with different position of column fixed restraint were tested under cyclic loading. Results are presented and discussed. Numerical and analytical model are presented as well as the model of the stiffness degradation.

2 Cyclic test on CLT frame corner

In this paper six difference samples were obtained, where two positions of fixed support were varied. The timber parts were made of CLT with lamellas of C24 grade and non-visible quality layer structure. All timber specimens (Figure 2.1.) were equal in cross section, 160 mm in heigh and 90 mm in width. Girders parts had length of 950 mm and columns parts length of 620 mm. Three types of threaded rods with strength grade 8.8 were varied: M10, M14 and M20, all with length of 320 mm. For bonding two-component epoxy based adhesive (EPOCON '88) by Croatian producer KGK was used. All tests were done in Structural Testing Laboratory within the Faculty of Civil Engineering in Zagreb, University of Zagreb. As the aim of this study was investigate the behaviour of glued-in rod joint in corner of horizontal loaded frame of the timber-glass panel, test protocol was focused on the same conditions of cyclic loading as used for panel testing. Both of sample variations were tested following the same procedure. The cyclic horizontal load protocol is composed of three sets of rules: definition of a yielding point (the Yasumura and Kawai (1997) procedure for timber shear wall), cyclic protocol EN 12512:2001 (1997) in the range of low displacement amplitudes (up to $2d_y$) and cyclic protocol ATC-24 in the range of high displacement amplitudes (over $2d_y$). Specimens of each type of joints were loaded by monotonous lateral loads until reaching a 20% drop of load bearing capacity to obtain the load-deformation curve which was used to determine the displacement at a yielding point (d_y). Although it is preferable to use only one test protocol, this combination proved more accurate results. However, with minor deviations at higher amplitudes (up to 15%), only the EN protocol can be used.
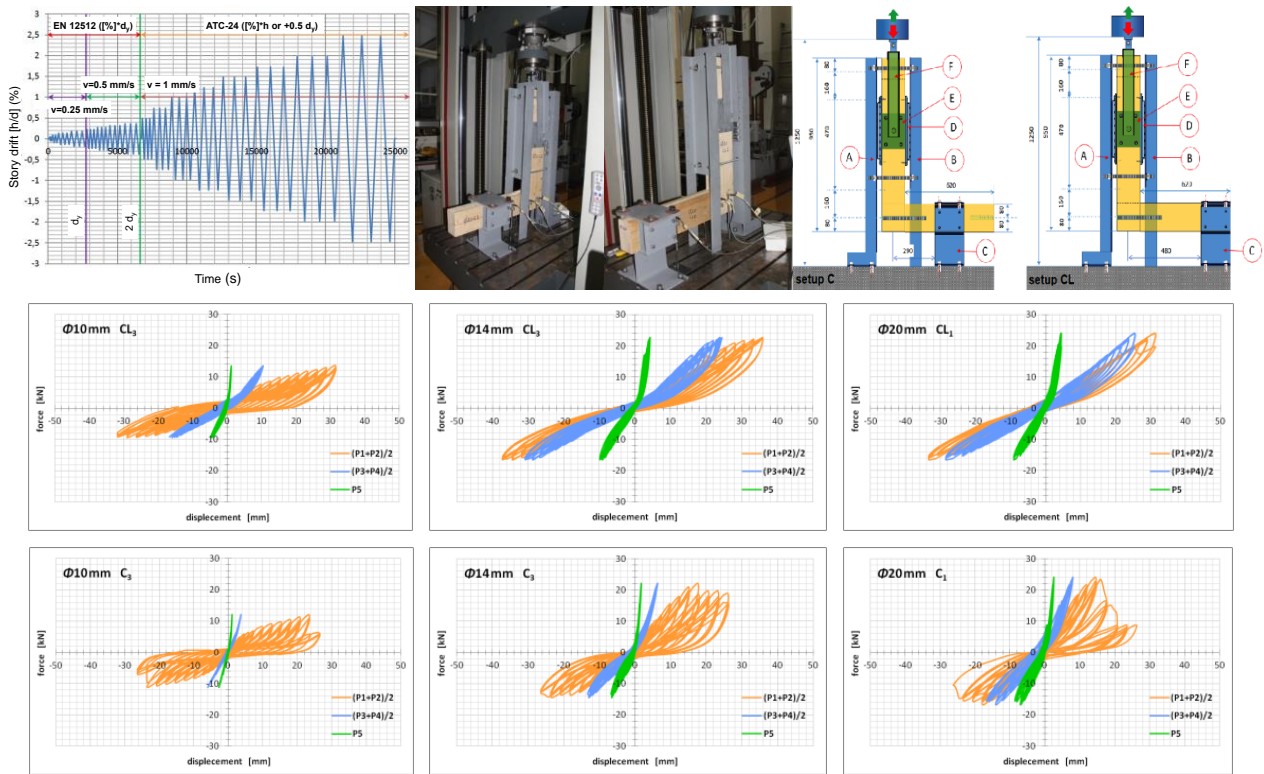
Figure 2.1. a) Test protocol b) Test setup c) Hysteresis behavior of joint.

Test shown that fracture of joint with M10 rod starts with yielding of rod in both timber members, where final failure happened due to additional tensile failure of rod (regardless of the boundary condition). Fracture of joint with M14 rod starts when the rod is yielding, forming a plastic hinge inside the column, where final failure happened by reaching the embedment strength of column element (regardless of the boundary condition). Fracture of joint with M20 rod starts when the rod is yielding, forming a plastic hinge inside the column or girder (depending of the boundary condition), where final failure happened by reaching the block shear capacity of central lamella (of column in CL sample or girder in C sample). Bearing capacity of the joint made with glued-in rod M14 is higher by 30% compared to the joint made with M10 rod as well as 10% lower in relation to the joint made with M20 rod. The best ratio of ductility and bearing capacity is shown in hysteresis curve of joint with M14 rod, so it can be concluded that joint with M14 glued-in rod in corner of timber frame is optimal in regular application.

3 Analytical and numerical model

In available literature there is not so many research involved in the moment resisting joints with glued-in rod. As a result, the behaviour of this type of joint at the stress and stiffness level is insufficiently defined. In the literature, there are available suggestions for design of directly pull-out loaded joint as well as for rigid joint made with two rods or two rod groups, where load distribution (tension and compression group) was clear. However, for the simultaneous action of axial and shear load, or for the semi rigid joint made with single rod, there is a lack of proposals. The first problem is the calculation of the stress distribution in the timber and rod in the connection region. This calculation is not trivial because of the heterogeneity of the connection region, in which different materials (timber and steel) are present. The discontinuity of the structure at the column-beam interface (only compressive stresses can be transmitted from timber to timber; the tensile stresses can be transmitted only in the rod), and the anisotropic behaviour of the timber, which is loaded parallel to the grain on one face and perpendicular to the grain on the other face at the column-beam interface. In the paper, analytical formulas are derived based on traditional mechanic theory (where only short-term analysis is given). Based on the neutral axis position, the bearing capacity and the stiffness of joint were determined (1, 2). Calibrated according to the tests results, there is also a proposal for the stiffness reduction (3), where Δ reached 20-30% The analytical model has shown a deviation of 10% in relation to the tests.

$$E_w \cdot b \cdot \frac{y^3}{6} + E_w \cdot b \cdot \left(-\frac{e_N}{2} + \frac{h}{4}\right) \cdot y^2 - E_s \cdot A_s \cdot e_N \cdot y + E_s \cdot A_s \cdot \frac{h}{2} \cdot e_N = \emptyset \tag{1}$$

$$K_C = \frac{1}{K_{CLTc,90}} + \frac{1}{K_{CLT,c0}} = K_T \cdot \left(\frac{h}{y} - 1\right) = \left(\frac{1}{K_{ser,GiR90}} + \frac{1}{K_{ser,GiR0}} + \frac{1}{K_R}\right) \cdot \left(\frac{h}{y} - 1\right) \tag{2}$$

$$\frac{K}{K_{ef}} = 0{,}67 \cdot \left(\frac{\Delta}{\Delta y_{80}}\right)^{-0{,}76} \tag{3}$$

The numerical model (Figure 3.1.) was made in the ANSYS software package, using the SOLID elements. Two criteria were used to define wood behaviour, first derived from the Hill's and second from the Tsai-Wu criteria for yielding. Hill's criterion was used for parts which are not in direct contact to steel rod or adhesive, respectively, for wooden parts in area of minor stresses. The numerical model has shown a deviation of 15% in relation to the tests and 10% in comparison to the analytical model.
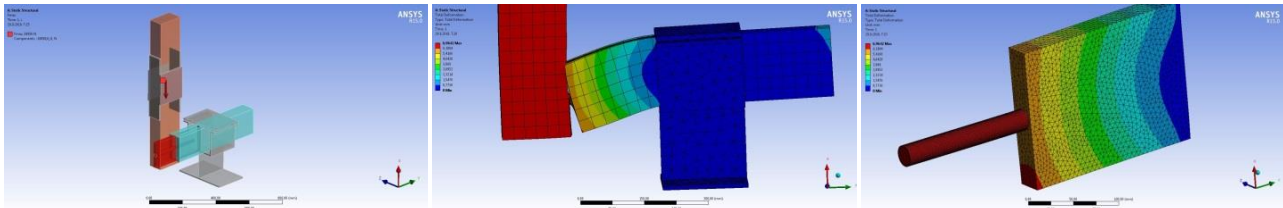

Figure 3.1. ANSYS numerical model of test setup.

4 Conclusion

For modelling the bearing capacity of semi rigid GiR joint, proposed model shown good results. The model also explains differences between embedding strengths depending on the angle between the hole axis and grain direction. Based on the estimation of material stiffness, model allows calculation of deformation in joints as well as a simple expression for stiffness degradation. The model is successfully verified and further proposed for the design of joints in CLT or GL frames. With known force redistribution given by the proposed model, expressions from European Design Guide (EN1995-1-1:2008), which provide background for calculation the bearing capacity of timber-to-timber connections, and, expressions from New Zealand (NZW 14085 SC: 2007) Design Guide, which provide verified good background for calculation the pull-out capacity of GiR connections, could be easily used to define final bearing capacity of such joint. Overall, the outcome of this study is seen as worthwhile for regulations on design of frame corner joints made with one or more glued in rods, even frame girder is under continuous or only lateral load.

5 References

Fragiacomo, M., Batchelar, M. (2012) Timber Frame Moment Joints with Glued-In Steel Rods I: Design. Journal of Structural Engineering, 138(6),789-801.

Steiger, R., Serrano, E., Stepinac, M., Rajcic, V., O'Neill, C., McPolin, D., Widmann, R. (2015). Strengthening of timber structures with glued-in rods. Construction and Building Materials, 97, 90-105.

Ehlbeck, J., Gerold, M. (1989) Ende Grain Connections with laterally Loaded Steel Bolts. CIB-W18A/22-7-1, 1-11.; Berlin, Germany.

Mori, T., Nakatani, M., Tesfamariam, S. (2015). Performance of Semirigid Timber Frame with Lagscrewbolt Connections: Experimen-tal, Analytical, and Numerical Model Results. International Journal of Advanced Structural Engineering, 7, 387-403.

European Committee for Standardization (CEN): Eurocode 5 (2004): Design of Timber Structures: Part 1-1 (EN 1995-1-1), Brussels, Belgium.

European Committee for Standardization (CEN): Timber Structures, Test Methods (2001): Cyclic Testing of Joints Made with Mechanical Fas-teners (EN 12512), Brussels, Belgium.

Applied Technology Council (ATC): Guidelines for Cyclic Seismic Testing of Components of Steel Structures (ATC-24) (1992), Redwood City, CA, USA.

Comparison of cyclic bending test methods for self-tapping screws

Kenji Kobayashi, Shizuoka University, Japan

Keywords: bending test, fatigue failure, self-tapping screw

1   Introduction

It has been pointed out that brittle failure occurs due to cyclic loading in the shear tests of the joints because of low cycle fatigue failure of the fastener (Kobayashi & Yasumura (2017), Nagase et al. (2018)). Therefore, it is important to confirm cyclic bending properties of the fasteners. However, there is no standard for the cyclic bending test method of the fasteners, and the influence of the difference in the test method on cyclic characteristics is uncertain. In this study, we performed cyclic bending tests for self-tapping screws using two types of loading apparatus, and test method and evaluation method are compared.

2   Test method

Self-tapping screw PX8-280 (Synegic co. ltd.) with a nominal diameter of 8 mm was used for the tests. The test was conducted with deformation angles ϑ = 15°, 22.5°, and 30°. The loading principle of two type of test apparatus – test A and test B – was based on EN409 (2009) and modified to enable cyclic loading. In any test, the distance between the fastener holders was 16 mm, which is twice the diameter d of the screw (d = 8 mm).

Figure 1. Loading apparatus of test A.

An outline of test A is shown in Figure 1. Test A is similar to the annex A.1 of EN409. Both side of the screw were fixed by clamps A and B. While the clamp B is rotated, the clamp A is kept almost horizontal. A load cell under a lever is used to measure bending moments. A linear guide is used at the bottom of the load cell so that the fastener holder and the arm can move freely in horizontal direction. The rotation angle of the clamp B was measured as bending deformation angle of the screw. The number of test specimens was 10 in each deformation angle.
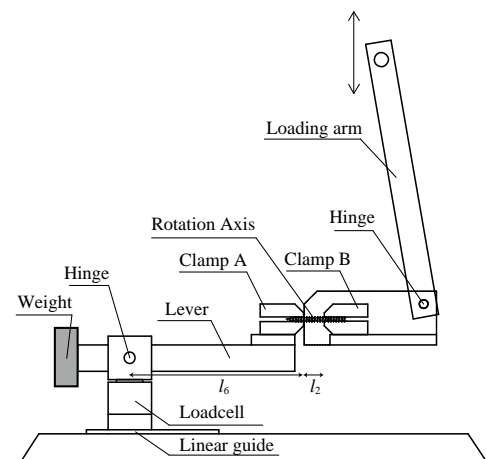
521

An outline of test B is shown in Figure 2. Four struts with bearings are attached to the left and right gears, respectively. The rotation angle of the gear was measured to obtain the bending deformation angle of the screw. A moment cell above the gear was used for measuring the moment. In addition, three types of fastener holders shown in Figure 3
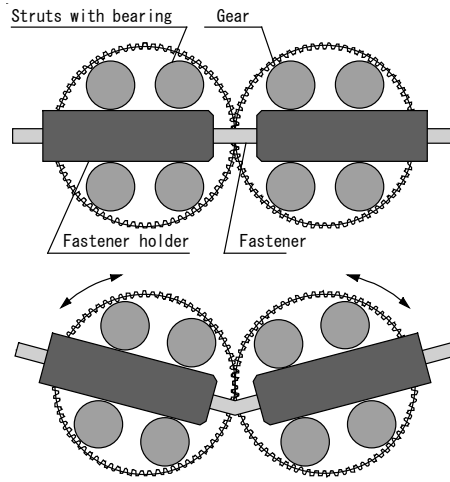

Figure 2. Loading apparatus of test B.

| Holder B1 · Not clamped · Inner diameter: 8.2mm |
| Holder B2 · Clamped perp. to loading direction |
| Holder B3 · Clamped parallel to loading direction |

Figure 3. Fastener holders.

were compared to verify the influence of the clamping condition. In test B1, a screw is inserted into the cylinder and not clamped. In test B2 and B3, screw was clamped by different ways. The numbers of test specimens were 4 in the test B1, and 6 the tests B2 and B3.

In both tests, the maximum moment M_{max}, peak moment (maximum moment in each cycle), and the number of repetitions $N_{f-0.8}$ and $N_{f-0.1}$ until the peak moment reached 80% or 10% of M_{max} were obtained from the cyclic test results. Figure 4 shows a method for calculating the plastic defor-

Figure 4. Plastic eformation angle.

mation angle. γ_{p-c} was obtained from the points (b, d) where the curve intersects the X axis. γ_{p-k} was obtained from the points (b', d') where the lines a-b' and c-d' have a gradient equal to initial stiffness K.
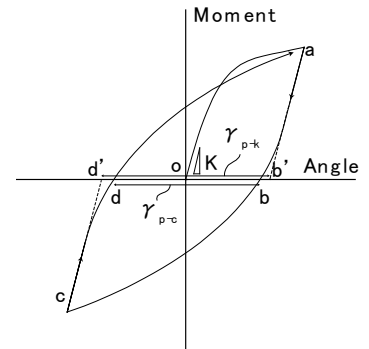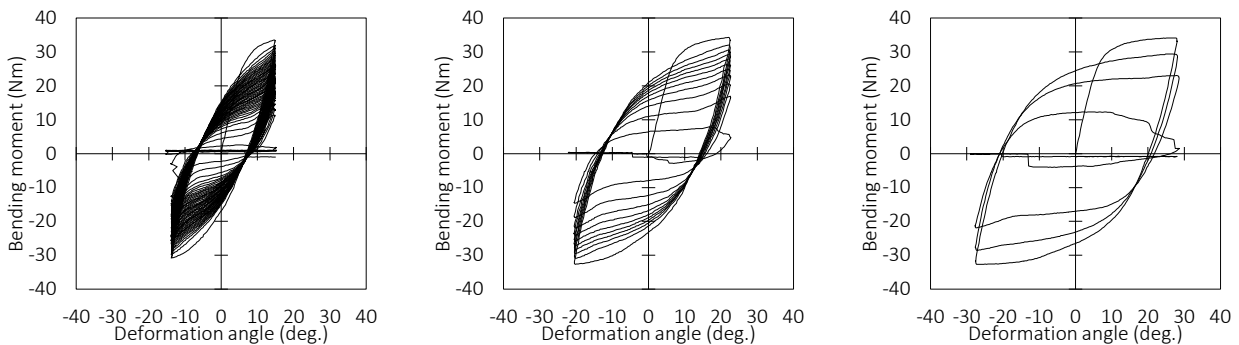
3   Test results

Examples of the moment-deformation angle curve obtained by cyclic bending tests

(a) A-15

(b) A-22.5
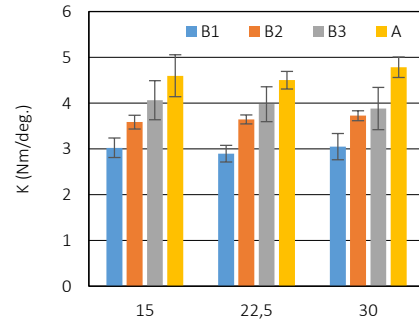
(c) A-30

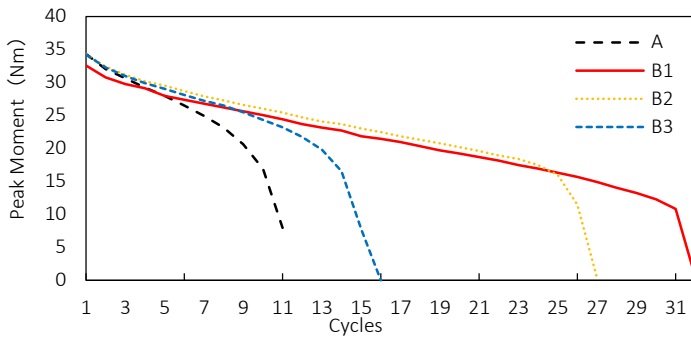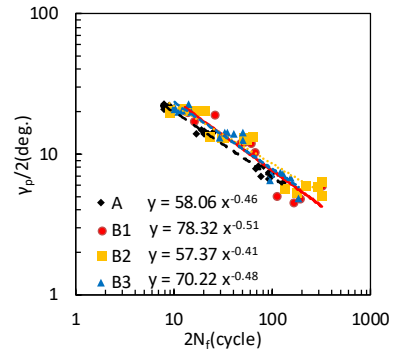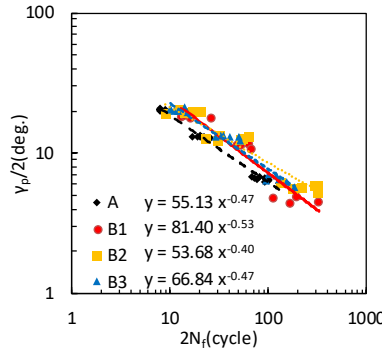Figure 5 Plastic deformation angle.

522

Figure 6 Relationship between cycles and peak moment

Figure 7. Initial stiffness.

are shown in Figure 5. As the deformation angle increased, the number of cycles to failure decreased. For the same deformation angle, the number of cycles to failure decreased in the order of B1> B2> B3> A (Figure 6). Since the initial stiffness is in the reverse order as shown in Figure 7, it is considered that the higher the degree of fixation of the clamp or the fastener holder, the higher the initial stiffness, and the greater the plastic deformation of the screw for the same deformation angle. Figure 8 shows the relationship between $N_{f-0.1}$ and γ_{p-c} or γ_{p-k}. In any condition, a linear relationship was shown on the logarithmic plots. By using the plastic deformation angle as a parameter, the plots of test B showed almost the same regression line regardless of the clamping conditions of the fastener holders. On the other hand, there was a slight difference between Test A and Test B. By using γ_{p-k} as the plastic deformation angle, they became a little bit closer.

(a) γ_{p-c} -$N_{f-0.1}$

(b) γ_{p-k} -$N_{f-0.1}$

Figure 8. Relationship between plastic deformation angle and cycles to failure.

4   Acknowledgement

5   References

EN 409 (2012): Timber Structures – Test methods – Determination of the yield moment of dowel type fasteners. CEN.

Kobayashi, K., Yasumura, M. (2017): Cyclic bending fatigue properties of dowel type fasteners. INTER 50-7-4, Kyoto, Japan.

Nagase, K., et al. (2018): Estimation of failure lifetime in plywood-to-timber joints with nails and screws under cyclic loading. Journal of wood science, DOI 10.1007/s10086-018-1742-8.

5 Peer review of papers for the INTER Proceedings

Experts involved:

The reviews are undertaken by long standing members of the INTER group which is a community of experts in the field of timber engineering.

Procedure of peer review

- Submission of manuscripts: all members of the INTER group attending the meeting receive the manuscripts of the papers at least four weeks before the meeting. Everyone is invited to read and review the manuscripts especially in their respective fields of competence and interest.

- Presentation of the paper during the meeting by the author

- Comments and recommendations of the experts, discussion of the paper

- Comments, discussion and recommendations of the experts are documented in the minutes of the meeting and are printed on the front page of each paper.

- Final acceptance of the paper for the proceedings with

  - no changes
  - minor changes
  - major changes
  - or reject

- Revised papers are to be sent to the editor of the proceedings and the chairman of the INTER group

- Editor and chairman check, whether the requested changes have been carried out.

6   Meetings and list of all CIB W18 and INTER Papers

CIB Meetings:

1	Princes Risborough, England; March 1973
2	Copenhagen, Denmark; October 1973
3	Delft, Netherlands; June 1974
4	Paris, France; February 1975
5	Karlsruhe, Federal Republic of Germany; October 1975
6	Aalborg, Denmark; June 1976
7	Stockholm, Sweden; February/March 1977
8	Brussels, Belgium; October 1977
9	Perth, Scotland; June 1978
10	Vancouver, Canada; August 1978
11	Vienna, Austria; March 1979
12	Bordeaux, France; October 1979
13	Otaniemi, Finland; June 1980
14	Warsaw, Poland; May 1981
15	Karlsruhe, Federal Republic of Germany; June 1982
16	Lillehammer, Norway; May/June 1983
17	Rapperswil, Switzerland; May 1984
18	Beit Oren, Israel; June 1985
19	Florence, Italy; September 1986
20	Dublin, Ireland; September 1987
21	Parksville, Canada; September 1988
22	Berlin, German Democratic Republic; September 1989
23	Lisbon, Portugal; September 1990
24	Oxford, United Kingdom; September 1991
25	Åhus, Sweden; August 1992
26	Athens, USA; August 1993
27	Sydney, Australia; July 1994
28	Copenhagen, Denmark; April 1995
29	Bordeaux, France; August 1996
30	Vancouver, Canada; August 1997
31	Savonlinna, Finland; August 1998
32	Graz, Austria; August 1999

33   Delft, The Netherlands; August 2000

34   Venice, Italy; August 2001

35   Kyoto, Japan; September 2002

36   Colorado, USA; August 2003

37   Edinburgh, Scotland; August 2004

38   Karlsruhe, Germany; August 2005

39   Florence, Italy; August 2006

40   Bled, Slovenia; August 2007

41   St. Andrews, Canada; August 2008

42   Dübendorf, Switzerland; August 2009

43   Nelson, New Zealand; August 2010

44   Alghero, Italy; August 2011

45   Växjö, Sweden; August 2012

46   Vancouver, Canada; August 2013

INTER Meetings:

47   Bath, United Kingdom; August 2014

48   Šibenik, Croatia; August 2015

49   Graz, Austria; August 2016

50   Kyoto, Japan; August 2017

51   Tallinn, Estonia; August 2018

52   Tacoma WA, USA; 2019

The titles of the CIB W 18 and INTER papers (starting from 2014) are included in the complete list of CIB/INTER papers: http://holz.vaka.kit.edu/392.php